Francisco Javier Rodríguez-Varela
Teko W. Napporn *Editors*

Advanced Electrocatalysts for Low-Temperature Fuel Cells

Springer

Advanced Electrocatalysts for Low-Temperature Fuel Cells

Francisco Javier Rodríguez-Varela
Teko W. Napporn
Editors

Advanced Electrocatalysts for Low-Temperature Fuel Cells

Springer

Editors
Francisco Javier Rodríguez-Varela
Cinvestav
Ramos Arizpe, Coahuila, Mexico

Teko W. Napporn
CNRS
French National Center for Scientific Research
Poitiers, France

ISBN 978-3-319-99018-7 ISBN 978-3-319-99019-4 (eBook)
https://doi.org/10.1007/978-3-319-99019-4

Library of Congress Control Number: 2018957465

This Springer imprint is published by the registered company Springer Nature Switzerland AG
The registered company address is: Gewerbestrasse 11, 6330 Cham, Switzerland

Contents

1 Introduction: Low-Temperature Fuel Cells 1
T. W. Napporn, A. Mokrini, and F. J. Rodríguez-Varela

2 Recent Advances on Electrocatalysts for PEM and AEM Fuel Cells 51
M. Roca-Ayats, S. Pérez-Rodríguez, G. García, and E. Pastor

3 Electrocatalysis of Alternative Liquid Fuels for PEM Direct Oxidation Fuel Cells 91
Ayan Mukherjee, Harikrishnan Narayanan, and Suddhasatwa Basu

4 Overview of Direct Liquid Oxidation Fuel Cells and its Application as Micro-Fuel Cells 129
R. Oliveira, J. Santander, and R. Rego

5 Application of Novel Carbonaceous Materials as Support for Fuel Cell Electrocatalysts 175
Abha Bharti and Gouri Cheruvally

6 Progress on the Functionalization of Carbon Nanostructures for Fuel Cell Electrocatalysts 215
X. Shi, K. Pérez-Salcedo, S. Hanif, R. Anwar, L. Cindrella, N. Iqbal, S. Jose, and A. M. Kannan

7 Non-Noble Metal Electrocatalysts for the Oxygen Reduction Reaction in Fuel Cells 235
I. L. Alonso-Lemus and M. Z. Figueroa-Torres

8 Non-Noble Metal as Catalysts for Alcohol Electro-oxidation Reaction 263
Samuel Dessources, Diego Xavier del Jesús González-Quijano, and Wilian Jesús Pech-Rodríguez

Index 291

About the Authors

I. L. Alonso-Lemus was born in Mexico City. She obtained her Ph.D. degree in Materials Science (2011) from Advanced Materials Research Center, in Chihuahua, México. From 2011 to 2013 she worked in the Bioengineering School at Monterrey Institute of Technology and Higher Education. She held postdoctoral position (2013–2014) in the Laboratory of Environment and Energy, Cancun Institute of Technology. She is a young researcher and currently works at Cinvestav-Saltillo. She has published 18 papers and is Secretary of the Mexican Hydrogen Society (2016–2018). Her research interests involve the development of electrochemical devices such as supercapacitors, batteries, and fuel cells as a sustainable alternative for power generation and storage. Recently, she has focused on the development of nanostructured carbon-based materials and biomass-derived carbons as non-noble metal electrocatalysts for the oxygen reduction reaction.

R. Anwar is currently pursuing master's in Energy Systems Engineering from USPCAS-E, NUST. He received his bachelor's degree in Chemical Engineering from the University of Engineering and Technology, Lahore, in 2015. His current research interests involve the development of low Pt catalyst for oxygen reduction reaction in polymer electrolyte fuel cell.

Suddhasatwa Basu completed Ph.D. in Chemical Engineering at Indian Institute of Science, Bangalore, and B. Tech in Chemical Engineering from Calcutta University. He is currently Director of CSIR-Institute of Minerals and Materials Technology, and prior to this he was Head of the Department of Chemical Engineering, IIT Delhi. He has vast work experience on development of energy materials and its application to energy conversion and storage devices, e.g., fuel cells, supercapacitor and battery, electrolyzer for hydrogen generation by water splitting, and CO_2 reduction to organics. He has published 144 manuscripts in high impact journals (with an H-index of 29), has 5 patents, and has transferred 2 technologies to various industries. He has been awarded with Fellow of National Academy of Science of India, Herdillia Award—Excellence in Basic Research in Chemical Engineering, and Dr. A. V. Rama Rao Foundation's Research Award in Chemical Engineering/Technology. He is Editor/Associate Editor/Editorial Board member of several international journals published by Wiley, Springer, Elsevier, and ACS.

Abha Bharti is a Ph.D. scholar at Vikram Sarabhai Space Centre (VSSC), Indian Space Research Organisation (ISRO), Thiruvananthapuram, India. She graduated from the University of Delhi with master's in Chemistry. Subsequently, she joined VSSC with the esteemed ISRO Fellowship for Ph.D. registered at Cochin University of Science and Technology. Her research work was supervised by Dr. Gouri C. at Lithium Ion and Fuel Cell Division of VSSC. The research was focused on the development of promising Pt-based cathode catalysts and their performance evaluation in a working proton exchange membrane fuel cell (PEMFC) to demonstrate their practical applicability. Abha has presented her work at numerous national and international conferences. She has received three best oral paper presentation awards and the prestigious Hydrogen Energy and Advanced Materials Scholar 2017 Award. Abha strives toward the development of sustainable energy technologies, and her research interests include nanomaterials and nanocomposites for energy application, PEMFCs, energy storage and conversion, and in situ electrochemical techniques.

Gouri Cheruvally is working as Consultant in Vikram Sarabhai Space Centre, Indian Space Research Organisation (ISRO), Thiruvananthapuram, India. She worked as Scientist in ISRO for 30 years and superannuated as Group Director. Dr. Gouri obtained master's and doctorate in Chemistry from the University of Kerala and postdoctorate from South Korea. Her research areas include polymeric adhesives and coatings, smart polymers and composites, electrochemical energy systems such as lithium-ion cell, fuel cell and nano-structured electrode-materials and electrolytes. Her publications comprise the book titled *Lithium Iron Phosphate: A Promising Cathode Active Material for Lithium Batteries* by Trans Tech Publications, Switzerland, 90 papers in international journals, 70 in international conferences, and 4 patents. Dr. Gouri received several accolades like ISRO Team Excellence Award, Kerala Academy of Science Fellowship, Materials Research Society of India Medal, and best paper awards in international conferences. She has supervised five Ph.D. students for their research work and is an active member of various professional bodies in Kerala.

L. Cindrella is Professor of Chemistry at the National Institute of Technology, Tiruchirappalli, India. Her research areas are fuel cell components, solar selective coatings, conducting polymers, energy materials, and computational modeling. She completed her Ph.D. degree in 1997 at Madurai Kamaraj University, India, specializing on solar selective coatings and convection suppression devices. She has guided 5 doctoral theses, 2 M.Phil. theses, and 56 M.Sc. projects. She has published 60 research articles in peer-reviewed international journals and an equal number of conference presentations. She has completed eight externally funded projects. Dr. Cindrella received the Technical Cooperation Training Fellowship (TCT) under UK-INDIA RECs project and specialized on "Chemical Storage of Solar Energy," at the University of Salford, England, 1997. She carried out the collaborative research on PEM fuel cell at Arizona State University (ASU), USA, in 2007, under the TEQIP, India program, and again as the Visiting Professor at ASU, USA, in 2009, under Global Inter-institutional Collaboration scheme, ASU, USA.

Samuel Dessources is a chemist and completed his postdoctorate in November 2017 at Cinvestav Unidad Saltillo (Mexico). He earned his bachelor's degree of Natural Sciences-Chemistry in 2010 at the State University of Haiti (UEH), master degree in Organic Chemistry in 2012, and Ph.D. in Electrochemistry at the Institute of Chemistry of Poitiers, Materials and Natural Resources IC2MP, University of Poitiers (France) in 2015. Samuel's research areas are focused on fuel cells, electrocatalysis, development of new energy materials, and use of alternative energies. He found a method for synthesis of well-dispersed core-shell nanoparticles which allowed to obtain high catalytic activity and high stability for the ethanol oxidation reaction (EOR).

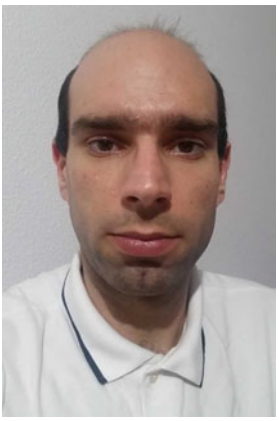

R. Oliveira is currently a research fellow in the University of Trás-os-Montes and Alto Douro at Chemistry Center of Vila Real (CQ-VR) in Vila Real, Portugal, where he performs research activities on ecofriendly catalysts for direct ethanol fuel cells, especially electrochemical experiments to evaluate Pd-based catalysts. He obtained master's degree in Chemical Engineering from the University of Akron in Ohio, USA, with a research thesis on natural corrosion inhibitors for carbon steel in ethanol media, always demonstrating a great interest in the electrochemistry field.

M. Z. Figueroa-Torres her main area of research is Materials Science and Nanomaterials. She obtained her Ph.D. degree in Materials Science from the Centro de Investigación en Materiales Avanzados S.C. Dr. Figueroa-Torres currently works as research-professor at the Universidad Autónoma de Nuevo León in the Civil Engineering Faculty. Her research interests include the synthesis and behavior of nanostructured and multifunctional materials with a focus on carbon materials, nanoparticles, and thin films for application on alternative energy devices and self-cleaned surfaces. Areas of work include the synthesis of materials from wastes, deposition of nanoparticles and thin-films by versatile and low temperature techniques.

G. García is a senior researcher at the University of La Laguna (Spain). He received his B.Sc. in Chemistry from the National University of Córdoba (Argentina); subsequently, he moved to Spain where he obtained his M.Sc. and European Ph.D. degrees in Chemistry and Chemical Engineering from the University of La Laguna (2007). After a short time working in the photovoltaic/solar industry, he spent postdoctoral internships at Leiden University (Netherlands) and at the Institute of Catalysis from the Spanish National Research Council, before he moved back to La Laguna in 2017. He was also a visiting researcher at the National University of Río Cuarto (Argentina), Sao Carlo Institute-USP (Brazil), University of the Republic

(Uruguay), Mannheim University of Applied Sciences (Germany), Consiglio Nazionale delle Ricerche-ITAE, University of Padova (Italy), and Pontifical Catholic University of Chile (Chile). His research interests are in fundamental and applied studies of (photo)electrochemical and (photo)electrocatalytic processes using a variety of conventional and nonconventional spectroelectrochemical techniques.

Diego Xavier del Jesús González-Quijano was born in 1983 in Yucatán (Mexico). He graduated in Electrical Engineering at Technological Institute of Merida (2006). He obtained his B.Sc. in Renewable Energy in 2011 from the Yucatan Scientific Research Center (CICY) and Ph.D. in Metallurgical and Ceramic Engineering (2016) from Center for Research and Advanced Studies (CINVESTAV-IPN) and was Postdoctoral Fellow (2016–2017) at Autonomous University of Nuevo León. He is Full Professor at Autonomous University of Aguascalientes (UAA). His research areas include nanomaterials, electrochemistry and nanocatalysts for fuel cells, perovskite solar cells materials, and hybrid energy systems.

S. Hanif is presently a Ph.D. candidate in US-Pakistan Center for Advanced Studies in Energy, Islamabad, Pakistan. Her research focuses on the metal organic framework (MOF)-derived electrocatalyst for oxygen reduction in proton exchange membrane fuel cells. She is doing her research work with Dr. AM Kannan in Batteries and Fuel Cells Lab, Arizona State University, USA.

N. Iqbal works as Associate Professor and Head of the Department Energy System Engineering at the USPCAS-E, National University of Sciences and Technology (NUST) since 2014. He obtained his Ph.D. in Chemistry from Institute of Applied Synthetic Chemistry, Vienna University of Technology, Austria. After Ph. D., Dr. Naseem Iqbal was a postdoctoral fellow at the Department of Chemistry, Norwegian University of Sciences and Technology (NTNU). He went as Exchange Faculty member to Arizona State University in spring 2016 and worked with Prof. Kannan (Fuel Cell and Batteries Lab). His research focuses in the following areas: MOF-based electrocatalyst for PEM fuel cell, electrode material for batteries, metal organic frameworks for gas adsorption application. Dr. Naseem Iqbal has authored and coauthored more than 30 refereed journal and conference publications and has given many talks and poster presentations in the area of catalysis. He also served as reviewer for various scientific publications.

S. Jose is Assistant Professor in School of Physics, Madurai Kamaraj University, India. After receiving her Ph.D. from Manonmaniam Sundaranar University, she joined Vickram College of Engineering in 2006. She moved to Madurai Kamaraj University in 2010. Sujin was awarded with Indo-US Raman Fellowship by UGC, New Delhi, and joined Ajayan Research Group, Rice University, USA, as a Postdoctoral Scientist in the year 2014–2015. She has published more than 60 articles in reputed scientific journals and has contributed chapters to books. She is currently working on the synthesis and optimization of various novel 2D and 3D innovative materials for energy storage solutions. She has close collaboration with Alternative Energy Materials Laboratory, ASU, USA, and with other international institutes which are actively involved in energy research. She received special appreciation from London Chemist David Bradley and was invited by ICTP, Trieste, to participate in NanoBioMed-2013. Recently, she was in ASU, USA, for a short spell as a visiting professor.

A. M. Kannan is a Professor in the Polytechnic School of the Ira A. Fulton Schools of Engineering at Arizona State University, USA, specializing in low temperature fuel cells, solar cells, and large-scale energy storage in batteries. He was Visiting Professor at Tampere University of Technology, Finland, Principal Scientist at the VTT Technical Research Center of Finland, and Distinguished Visiting Professor at Yuan Ze University, Taiwan. He has also been awarded a "Distinguished Chair" Fulbright Fellowship at the Aalto University, Finland, for 6 months. He possesses strong academic and professional experience, having also worked as Chief Scientist at Hoku Scientific Inc., Hawaii. Dr. A.M. Kannan has published extensively and presents regularly at international conferences on batteries and fuel cells. He serves as an Associate Editor of the *International Journal of Hydrogen Energy*, as well as on other editorial boards. He received his M.S. in Chemistry from Madurai Kamaraj University, India, in 1985, and completed his Ph.D. in 1990 at the Indian Institute of Science, India.

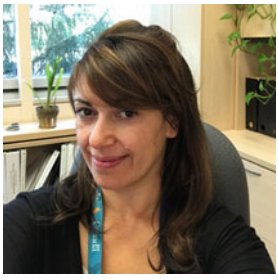

A. Mokrini is a Senior Research Officer and the lead of Materials for Energy Technologies team at the National Research Council of Canada. She obtained her Ph.D. from the Department of Chemical Engineering at the University of Barcelona in 1998, and an industrial master degree in Polymer Science and Engineering from the University Menendez Pelayo in Madrid in 2000. She was a postdoctoral fellow at the Consejo Superior de Investigaciones Cientificas (CSIC) in Madrid from 1999 to 2001. She joined NRC in 2003 as a research officer and is presently leading a team working on materials, components, testing protocols, and manufacturing processes development for clean electrochemical energy storage and generation systems such as proton exchange membranes fuel cells (PEMFC), and battery technologies.

Ayan Mukherjee obtained his M. Tech and Ph.D. in Material Science from the Department of Physics, National Institute of Technology Durgapur, India, and worked on the development of multiferroic material. Presently, he is working as a postdoctoral fellow in Fuel Cell Lab, Department of Chemical Engineering, Indian Institute of Technology Delhi, India. His main research interests concern development of different nanostructures and their electrochemical properties for energy conversion devices, electrocatalyst for low temperature fuel cell, water splitting, and photocatalysts. He has received senior research fellowship and research associateship from CSIR, Government of India, and national postdoctoral fellowship from SERB, Government of India.

T. W. Napporn is a tenured researcher of French National Center of Scientific Research (CNRS), working at the Poitiers Institute of Materials and Environmental chemistry (IC2MP). He received his master's degree in Applied Chemistry in 1991 and his Ph.D. in Electrochemistry in 1997 from the University of Poitiers (France). During his Ph.D. thesis, he developed anode materials for direct methanol fuel cell. After his Ph.D., he joined the Electrocatalysis Group at the University of Sao Paulo at Sao Carlos as a postdoctoral fellow and later in 1999, the Ecole Polytechnique de Montreal (Canada) as research associate. There, he had studied and developed the single chamber SOFC system in collaboration with Hydro-Quebec. Since 2008, he got a tenure position at CNRS for developing novel nanomaterials for electrocatalysis especially for application in energy conversion and storage systems. His recent research topics are focused on (1) morphology and size controlled nanomaterials as novel electrodes for fuel cell and water electrolyzer (acid and alkaline media); (2) oxygen reduction reaction and oxygen evolution reaction; and (3) full porous single chamber SOFC. Since September 2015, he is Adjunct Professor at the Chemistry of Hydrogen Energy Conversion Unit of the Institute of Advanced Science of Yokohama National University in Japan.

Harikrishnan Narayanan completed his B.Tech (2009) at Government Engineering College Calicut in Chemical Engineering and M.Tech (2012) at Indian Institute of Technology, Roorkee (IITR), India, in Chemical Engineering. He submitted Ph.D. thesis in 2018 on PEMFC diagnostics in the Department of Chemical Engineering, Indian Institute of Technology Delhi (IITD). His research interests are in fuel cells, electrolyzer, photoelectrochemical water splitting, and CO_2 conversion to valuable products.

E. Pastor is Professor at the University of La Laguna (Spain). She completed her bachelor's degree in Chemistry (1987) and Ph.D. (1992) at the University of La Laguna and spent post-doc stays at the University of Bonn and Jülich Research Center (Germany), University of Poitiers (France), and University of Sao Paulo (Brazil). Dr. Pastor is the Head of the Surface Science and Electrocatalysis Group, and her research has been focused on the preparation, physicochemical, and spectroelectrochemical characterization of catalysts for low temperature fuel cells (PEMFC, DAFC) and electrolyzers. She has been intensively involved in the application of on-line differential electrochemical mass spectrometry (DEMS) and Fourier transform infrared spectroscopy (FTIRS) to study the adsorption at the metal/electrolyte interface and the characterization of adsorbed species, as well as to the elucidation of structural effects in electrocatalysis.

Wilian Jesús Pech-Rodríguez is a Professor in the Polytechnic University of Victoria. Also, he is a member of the National System of Researchers of México. He received his master's degree from the Scientific Research Center of Yucatan in June 2011. In January 2016, he received his Ph.D. in Metallurgical and Ceramic Engineering from the Center for Research and Advanced Studies of the National Polytechnic Institute (CINVESTAV). His research interest is focused on the development of energy systems such as fuel cell and dye sensitized solar cell.

S. Pérez-Rodríguez received her B.Sc. in Chemical Engineering from the University of Zaragoza in 2009. In 2015, she defended her Ph.D. at the University of Zaragoza and the Carbochemistry Institute of the Spanish National Research Council (ICB-CSIC) under the supervision of Prof. Mª Jesús Lázaro (ICB-CSIC) and Prof. Elena Pastor (University of La Laguna, Spain). After a period focused on the design of graphene-based nanocomposites for energy-conversion devices at the ICB-CSIC, she joined the research group of Prof. Carmen Claver at the Chemistry Technologic Center of Catalonia (Spain) where she worked on the development of nanocatalysts for electrochemical biomass feedstock transformations. Currently, she is working at ICB-CSIC in the framework of a project on solar-assisted catalytic reforming. Her research interest includes the design of catalysts for electrochemical applications and the development of energy-conversion devices, such as CO_2 reduction, fuel cells, electrolyzers, or batteries.

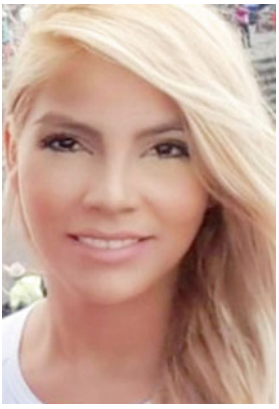

K. Pérez-Salcedo is currently a Ph.D. candidate in the Department of Renewal Energy at the Scientific Research Center of Yucatan (Merida, Mexico) under Dr. Beatriz Escobar's guidance. She received her Bachelor in Mechanical Engineering (2013) and master's degree in Materials Science and Energy (2016) from the Autonomous University of Carmen (Campeche, Mexico). Her current research focuses on metal-free electrocatalysts for alkaline oxygen reduction reaction.

R. Rego received her Ph.D. in Chemical Engineering from the Faculty of Engineering, University of Porto, Portugal, in 2006. She is currently a Professor at the Department of Chemistry, University of Trás-os-Montes e Alto Douro, Vila Real, Portugal. She was a visiting researcher in the Faculty of Chemistry, University of Barcelona, in Microelectronics Institute IMB-CNM (CSIC) in Spain, and in the Laboratory of New Materials for Electrochemistry and Energy of École

Polytechnique de Montréal (Canada). Her research have been focused on the applications of electrochemistry and advanced materials (catalysts, electrodes, carbon nanomaterials) to the development of different electrochemical devices including fuel cells, electrochromic devices, and electrochemical sensors.

Maria Roca-Ayats is currently a postdoctoral researcher at the Magnetism and Nanotechnology Group (NANOMAG) of the University of Santiago de Compostela. She holds a bachelor's degree in Chemistry from the University of Barcelona (2011) and a Ph.D. degree in Electrochemistry from the Autonomous University of Madrid (2016). She developed her Ph.D. on electrocatalysts for fuel cells and electrolyzers at the Institute of Catalysis (Spanish National Research Council, CSIC). During this period, she performed research internships at Brookhaven National Laboratory (USA), Max-Planck-Institut für Eisenforschung (Germany), and University of La Laguna (Spain). In 2017, she joined the Battery and Electrochemistry Laboratory (Karlsruhe Institute of Technology/BASF SE, Germany) as a postdoctoral fellow, where she performed research on the field of lithium-ion batteries.

F. J. Rodríguez-Varela completed his Ph.D. (2004) at École Polytechnique de Montréal. He joined the Centre for Research and Advanced Studies (Cinvestav Saltillo Campus) in 2006 and is Full Professor since 2009. He has been PI of several national and international research projects funded by Conacyt-Mexico. Dr. Rodríguez-Varela is former President of the Mexican Hydrogen Society (2012–2014) and General Coordinator of the National Network for Hydrogen Energy of Conacyt (2015). He is member of the scientific committee and Guest Editor of *Journal of New Materials for Electrochemical Systems*. He has been Guest Editor of *Journal of Applied Electrochemistry* and co-editor of two books in Spanish. Dr. Rodríguez-Varela has published about 60 works in international journals and 10 book chapters. He has guided 4 Ph.D. (3 in progress), 6 M.Sc. (4 in progress), and 6 undergraduate students. Dr. Rodríguez-Varela is member of the Electrochemical Society, International Society of Electrochemistry,

Materials Research Society, Sociedad Mexicana del Hidrógeno, Sociedad Mexicana de Electroquímica, and Sociedad Mexicana de Materiales. His research areas include novel nanomaterials, electrocatalysis, fuel cells, and hydrogen technologies.

J. Santander received the B.S. and Ph.D. degrees in Physics from the Autonomous University of Barcelona, Spain, in 1989 and 1996, respectively. He is currently a staff researcher at the Barcelona Microelectronics Institute IMB-CNM (CSIC). His main research areas are related to nano- and micro-systems fabrication technologies applied to the development of micro-fuel cell devices. Such micro-fuel cell must be able to be fabricated at the same time of the full micro-system by using the same fabrication technology in order to be integrated as the power source component of the micro-system. Recent research has been focused on passive, direct alcohol, alkaline micro-fuel cell devices.

X. Shi is currently a Ph.D. candidate in the Department of System Engineering at Arizona State University (2015 Fall) under Dr. Kannan's guidance. He received his bachelor's and master's degree in Mechanical Engineering at Tianjin University of Technology and New Jersey Institute of Technology, respectively. His research interests are decomposing MOF as support for the ORR catalyst for low temperature fuel cells, MnO_2 as ORR catalyst for AEMFC, and theoretical calculation for oxygen adsorption energy by using VASP.

Chapter 1
Introduction: Low-Temperature Fuel Cells

T. W. Napporn, A. Mokrini, and F. J. Rodríguez-Varela

Abstract This chapter describes the reactions occurring in low-temperature fuel cells, fuelled with from the most common H_2, to several organic molecules. The differences in the complexity of the anode reactions and their effect on the energy that may be generated from the fuel cells are discussed. It is established that, even though H_2/O_2 fuel cells are the most performing in terms of power density for large-demand systems, the use of liquid fuels is advantageous for several low-power applications. The performance of nanostructured anode and cathode catalysts in complete fuel cell systems is also covered. It is indicated that in alkaline media, some non-Pt nanocatalysts have a high catalytic activity, particularly for the ORR. Even more, the recent advances in polymer electrolyte membranes are shown, from the widely used commercial Nafion®, to the more recently developed anionic polymers for anion exchange membrane fuel cells. It is concluded that compatibility of composite and blend materials with the host ionomer is critical for the development of stable low-temperature fuel cells.

Keywords Proton exchange membrane fuel cells (PEMFC) · Anion exchange membrane fuel cells (AEMFC) · Perfluorosulfonic-acid membranes (PFSA) · Direct methanol AEMFCs (DM-AEMFCs) · Direct ethanol AEMFCs (DE-AEMFCs) · Direct ethylene Glycol AEMFCs (DEG-AEMFCs) · Direct glycerol AEMFCs (DG-AEMFCs) · Non-platinum group metal (PGM) · Perfluorinated PEMs · Nafion® membranes · Partially fluorinated PEMs · Hydrocarbon PEMs · Anion exchange

T. W. Napporn
Université de Poitiers, IC2MP UMR-CNRS 7285, Poitiers Cedex 9, France

A. Mokrini
NRC Automotive and Surface Transportation Research Center, Boucherville, QC, Canada

F. J. Rodríguez-Varela (✉)
Sustentabilidad de los Recursos Naturales y Energía, Cinvestav Unidad Saltillo, Ramos Arizpe, Mexico
e-mail: javier.varela@cinvestav.edu.mx

F. J. Rodríguez-Varela, T. W. Napporn (eds.), *Advanced Electrocatalysts for Low-Temperature Fuel Cells*, https://doi.org/10.1007/978-3-319-99019-4_1

membranes (AEMs) · Hydrogen oxidation reaction (HOR) · Tafel reaction · Heyrovsky reaction · Volmer reaction · Oxygen reduction reaction (ORR) · Rotating ring disk electrode (RRDE) · Koutecky–Levich plots

1.1 Introduction

Proton exchange membrane and anion exchange membrane fuel cells (PEMFC and AEMFC, respectively) have gained the attention of academic and industrial research groups, due to their capacity to generate high-power density at low temperatures. Ever since the advancements in the 1960s for space industry applications, both systems have experienced to an extent a technological development to reach near-commercialization status. This is particularly the case of PEMFCs, whose performance has been greatly improved by the use of the perfluorosulfonic acid membranes and the demonstration of high interfacial area gas diffusion electrodes at Los Alamos National Laboratories [1, 2]. The new electrode structure proposed in those studies has reduced the catalyst loading (i.e., Pt) by an order of magnitude [1]. PEMFC is a more advanced technology than AEMFC. However, fuel cells using anion exchange membrane are being studied with a significant interest in recent years due to the development of chemically stable alkaline polymers and the capability of using non-noble metals to catalyze the electrochemical reactions in basic media. The following sections introduce the electrochemical reactions taking place in AEMFCs working with hydrogen and liquid fuels. Also, the performance of several nanostructured electrocatalysts in complete fuel cell systems is shown. Moreover, the latest developments in membranes for PEM and AEM fuel cells are discussed.

1.2 Electrocatalytic Reactions in Anion Exchange Membrane Fuel Cells (AEMFCs)

In first half of the twentieth century, the research in alkaline fuel cells (AFCs) led this type of cell to be considered for several applications. Francis T. Bacon worked in the development of H_2/O_2 AFCs, which resulted in demonstrative programs of capacity up to 5 kW output [1–3]. AFC systems reached a status that allowed the technology to be considered for space applications [1]. However, disadvantages of AFCs included several restrictions, among them, the need to use fuels and oxidants free of CO_2 due to the risk of carbonation with KOH and NaOH [1, 4]. Also, the management of liquid-phase electrolytes has been a relevant issue in AFCs [5]. With the development of the polymer electrolyte membrane fuel cells (PEMFCs) based on Nafion®, the research on AFCs somehow decreased, particularly in the 1990s and early twenty-first century.

Over the past decade, however, AEMFCs have received increased attention of fuel cells science and technology research laboratories [6]. First of all, it is generally acknowledged that the kinetics of the electrochemical cathode reactions in alkaline media is faster compared to their acid counterpart (i.e., PEMFCs). Also, perhaps one the most attracting characteristics of AEMFCs is the possibility of using non-PGM (Pt group metals) or non-noble metal catalysts in anodes and cathodes to promote the hydrogen oxidation reaction (HOR) and the oxygen reduction reaction (ORR) [6–9]. Even more, regardless of its relatively low operation temperature, AEMFCs can also operate with liquid fuels as an alternative to hydrogen [10–14].

In fact, it has been reported that AEMFCs can operate with a CH_4 containing 5% H_2 [15]. In spite of the capability of using different fuels, attention must be paid to the purity of the oxidant, since as mentioned CO_2-containing air leads to carbonation by reacting with OH^- anions. The report by Dekel et al. indicates that bicarbonate (HCO_3^-) and carbonate (CO_3^{2-}) anions are formed, changing the anion composition of the anion exchange membrane [16]. Thus, the use of air as oxidant which may contain CO_2 decreases the cell performance [16, 17].

Nevertheless, the promoted attraction offered recently by AEMFCs can be attributed to the important advances in high-performance anion exchange membranes, even though one relevant issue is the ionomer stability [6, 18–20]. As pointed out by Varcoe et al., the first publication of the so-called alkaline membrane fuel cells (AMFCs) appeared in 2005 [18]. Ever since, the number of publications has clearly increased. Dekel has reported that the number of reports has overpassed 2000 in the 2013–2017 period (Fig. 1.1) [6]. Evidently, advances in the different components of AEMFCs other than membranes, including high performance and durable catalysts, will impulse the research and applications of this technology to new grounds.

In the following sections, the electrocatalytic reactions in AEMFCs fuelled with different fuels are given. The selection of fuels goes from H_2, to several of the most common C-containing fuels: methanol (CH_3OH), ethanol (C_2H_5OH), ethylene glycol ($C_2H_6O_2$), and glycerol ($C_3H_8O_3$). Each of the liquid fuels introduces cost and energetic advantages and disadvantages. But perhaps it is worth analyzing their use from a sustainability point of view, and therefore the feasibility of obtaining them from biomass resources.

1.2.1 H_2/O_2 AEMFCs

In terms of power density and catalyst durability, the most performing AEMFC is the H_2/O_2 cell. A power density of 1.4 W cm^{-2} has been reported by Varcoe et al., with the cell operating at 60 °C, equipped with an AEM based on radiation-grafted ethylene tetrafluoroethylene and PtRu/C (anode) and Pt/C (cathode) catalysts [21]. The same research group has reported the performance of an H_2/O_2 AEMFC with non-PGM cathode catalysts (1.0 mg_{Ag} cm^{-2}) having a power density above 1 W cm^{-2} [22]. The stability of H_2/O_2 AEMFCs has also been evaluated. Yu et al.

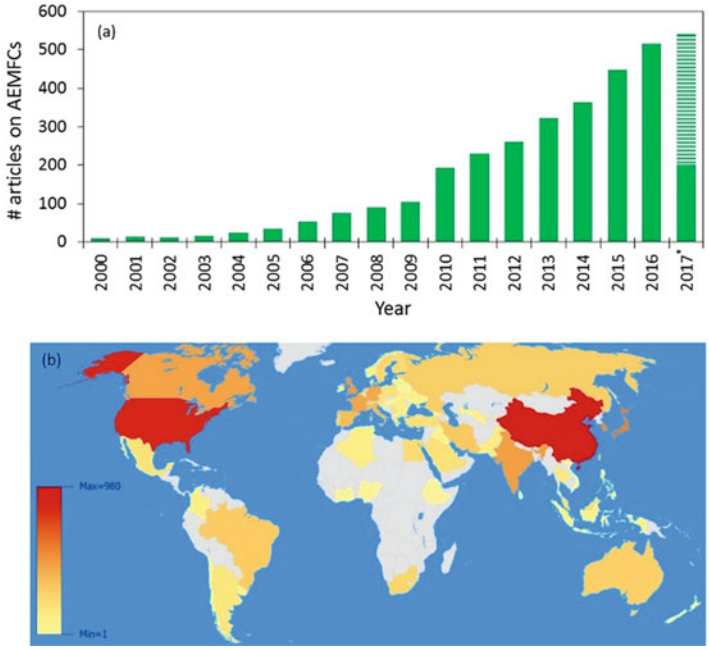

Fig. 1.1 (**a**) Reports published in the 2013–2017 period covering research on AEMFCs, (**b**) distribution by country of origin (reproduced from Ref. [6] with kind permission of © Elsevier)

have tested a cell for 500 h, with a decrease in cell voltage of 0.22 mV h^{-1}. The cell used quaternary ammonium SEBS as the ionomer [23].

In H_2/O_2 AEMFCs the electrochemical anode and cathode half-cell reactions, as well as the overall cell reaction, with their corresponding potentials at standard conditions are:

Anode reaction:

$$2H_2 + 4OH^- \rightarrow 4H_2O + 4e^-, E_a^o = 0.83 \text{ V vs.SHE} \tag{1.1}$$

Cathode reaction:

$$O_2 + 2H_2O + 4e^- \rightarrow 4OH^-, E_c^o = 0.40 \text{ V vs.SHE} \tag{1.2}$$

Overall:

$$2H_2 + O_2 \rightarrow 2H_2O, E_{\text{cell}} = 1.23 \text{ V} \tag{1.3}$$

H_2/O_2 AEMFCs are attractive from an economical point of view because of the feasibility of using non-PGM catalysts for the ORR and for the HOR [24]. However,

it should be mentioned that high performances have been reported when using catalysts such as Ir or Pd to promote the HOR either in half-cell experiments or in full AEMFC tests [25, 26].

1.2.2 Direct Methanol AEMFCs (DM-AEMFCs)

The enhanced kinetics of the methanol oxidation reaction (MOR) in 0.5 mol/l K_2CO_3 and 1 mol/l $KHCO_3$ electrolytes compared with a 0.5 mol/l H_2SO_4 solution, foreseen the use of CH_3OH in AEMFCs, has been discussed by Zhuang et al. [27]. By performing in-situ FTIR analysis, the authors concluded that methanol could be oxidized to CO_2 in those alkaline solutions. Scott and Hao have evaluated extensively a direct methanol alkaline fuel cell using Pt/C anode and cathode catalyst. The cell performance increased at higher temperatures (up to 60 °C). On the other hand, with the anion exchange membranes used, the crossover of methanol to the anode increased at higher fuel concentrations [28]. Kim et al. have reported the same effect in an air-breathing direct methanol fuel cell with anion exchange membrane when increasing the CH_3OH concentration from 7 to 10 M [29]. Even though it has been reported that AEMFCs fuelled with methanol are less performing compared to other liquid fuels [30], Bianchini et al. reported an enhanced performance of a direct methanol AEMFC at 60 °C with a Pd/MWCNT anode, compared to ethanol and glycerol [31].

In DM-AEMFCs the electrochemical reactions are:

Anode reaction:

$$CH_3OH + 6OH^- \rightarrow CO_2 + 5H_2O + 6e^-, E_a^o = -0.81 \text{ V vs.SHE} \quad (1.4)$$

Cathode reaction:

$$3/2O_2 + 3H_2O + 6e^- \rightarrow 6OH^-, E_c^o = 0.40 \text{ V vs.SHE} \quad (1.5)$$

Overall:

$$CH_3OH + 3/2O_2 \rightarrow CO_2 + 2H_2O, E_{\text{cell}} = 1.21 \text{ V} \quad (1.6)$$

1.2.3 Direct Ethanol AEMFCs (DE-AEMFCs)

The use of ethanol in fuel cells is of interest, since this organic molecule is considered a carbon neutral and sustainable fuel [32]. Even more, bioethanol from biomass has been used as the fuel in DE-AEMFCs, where a power density of ca. 90 mW cm^{-2} has been generated using a dealloyed PtCo/CNT anode

catalyst [33]. A power density of around 50 mW cm^{-2} has been obtained elsewhere using Pd-based catalysts at the anode fuelled with 1.0 mol L^{-1} ethanol +0.5 mol L^{-1} NaOH [34]. In their study, Fujiwara et al. have compared the performance of DEFCs equipped with anion and cation exchange membranes [35]. The power density generated with the AEM was about ten times higher, compared to the cationic counterpart. Nevertheless, due to the low OH^- conductivity of the membrane, 0.5 mol L^{-1} KOH had to be provided along with the 1.0 mol L^{-1} ethanol fuel at the anode in order to sustain a high performance. Recently, a passive DE-AEMFC stack delivering a peak power density of 38 mW cm^{-2} at room temperature, using PdNi/C anode catalysts and $FeCuN_4$/C cathode catalysts, has been demonstrated by Zhao and Li [36].

The electrochemical reactions in DE-AEMFCs are:

Anode reaction:

$$C_2H_5OH + 12OH^- \rightarrow 2CO_2 + 9H_2O + 12e^-, E_a^o = -0.74 \text{ V vs.SHE} \quad (1.7)$$

Cathode reaction:

$$3O_2 + 6H_2O + 12e^- \rightarrow 12OH^-, E_c^o = 0.40 \text{ V vs.SHE} \quad (1.8)$$

Overall:

$$C_2H_5OH + 3O_2 \rightarrow 2CO_2 + 3H_2O, E_{cell} = 1.14 \text{ V} \quad (1.9)$$

1.2.4 Direct Ethylene Glycol AEMFCs (DEG-AEMFCs)

Ethylene glycol (EG) has been used in fuel cells as a feasible alternative to replace methanol and ethanol. For this application, $C_2H_6O_2$ is safer to handle than methanol, is less toxic than methanol and ethanol, and its electron transfer rate is higher during oxidation than ethanol [37–39]. EG can also be produced from biomass and its partial selective oxidation in a DEG-AEMFC can generate valuable oxalic acid without CO_2 emissions [40]. The power density generated from a DEG-AEMFC at 60 °C has been shown to become higher by increasing the fuel concentration from 0.5 to 1.0, but decreases with 2 mol L^{-1} $C_2H_6O_2$ (with a KOH concentration of 1 mol L^{-1}) [39]. Such cell used an alkali-doped PBI membrane. Cremers et al. have compared the performance of DEG-AEMFCs equipped with KOH-doped PBI and a quaternary amine alkaline AEM, with the later generating a higher power density [41]. KOH-doped Nafion ® has also been used by Forbicini et al. in a DEG-AEMFC [42]. Evidently, DEG-AEMFCs equipped with several formulations of AEMs have been tested [43, 44]. It has been reported that the power density generated by

DEG-AEMFCs is higher than those of fuel cells fuelled with methanol, ethanol, and 1,2-propanediol, but slightly lower than in the case of glycerol [10, 44–46].

The electrochemical reactions in DEG-AEMFCs are:

Anode reaction:

$$C_2H_6O_2 + 10OH^- \rightarrow 2CO_2 + 8H_2O + 10e^-, E_a^o = -0.81 \text{ V vs.SHE} \quad (1.10)$$

Alternatively, the partial oxidation of EG to oxalate is [44]:

$$C_2H_6O_2 + 10OH^- \rightarrow (COO^-)_2 + 8H_2O + 8e^-, E_a^o = -0.81 \text{ V vs.SHE} \quad (1.11)$$

Cathode reaction:

$$5/2O_2 + 5H_2O + 10e^- \rightarrow 10OH^-, E_c^o = 0.40 \text{ V vs.SHE} \quad (1.12)$$

Overall:

$$C_2H_6O_2 + 5/2O_2 \rightarrow 2CO_2 + 3H_2O, E_{\text{cell}} = 1.21 \text{ V} \quad (1.13)$$

1.2.5 Direct Glycerol AEMFCs (DG-AEMFCs)

Glycerol has several advantages for fuel cell applications: it has a relatively low toxicity, high energy density, its crossover rate is low, and is relatively inexpensive [47, 48]. It is also a versatile fuel, since DG-AEMFCs have been operated as co-generators of electricity and valuable chemicals [49, 50]. Pt and Pd-based catalysts are normally used as anode catalysts in DG-AEMFCs [47, 48, 51–54]. However, Au-based nanomaterials have also shown a high catalytic activity for the oxidation of the molecule [49, 50, 55]. Li et al. have demonstrated a higher power density generated by a DG-AEMFC in the 50–80 °C temperature range with an Au/C anode (1.0 mol L^{-1} glycerol +2.0 mol L^{-1} KOH, Fe-Cu-N_4/C cathode), compared to a PEM DGFC at 90 °C (1.0 mol L^{-1} glycerol, PtRu/C anode, Pt/C cathode) [55]. It has been shown also that higher power density is generated from the DG-AEMFC, relative to DM and DEG-AEMFCs, with the same fuel concentration [55].

One more advantage of glycerol is that it can be used in its crude composition as obtained from the bio-diesel manufacturing industry, as reported by Li′s group [51, 54–56]. Crude glycerol is cheaper than refined glycerol, methanol, and ethanol [56]. Using 1.0 mol L^{-1} crude glycerol (+ 2.0 mol L^{-1} KOH), a DG-AEMFC generated a power density of ca. 40 mW cm^2 (anode: Au/C; cathode: Fe-Cu-N_4/C; AEM: A201, 28 mm, Tokuyama, 80 °C) [55].

The electrochemical reactions in DG-AEMFCs are shown below. According to some workers, the oxidation of glycerol in alkaline media may proceed through the formation of glycerate or tartronic acid [57, 58]. Following the tartronic acid route:

Anode reaction [58]:

$$C_3H_8O_3 + 8OH^- \rightarrow C_3H_4O_5 + 6H_2O + 8e^-, E_a^o = -0.77 \text{ V vs.SHE} \quad (1.14)$$

$$C_3H_4O_5 + 2OH^- \rightarrow (C_3H_2O_5)^{2-} + 2H_2O \quad (1.15)$$

Cathode reaction:

$$2O_2 + 4H_2O + 8e^- \rightarrow 8OH^-, E_c^o = 0.40 \text{ V vs.SHE} \quad (1.16)$$

Overall:

$$C_3H_8O_3 + 2O_2 + 2OH^- \rightarrow (C_3H_2O_5)^{2-} + 4H_2O, E_{cell} = 1.17 \text{ V} \quad (1.17)$$

1.2.6 AEMFCs Operating with Other Fuels

Other fuels have been evaluated at AEMFCs. For example, the reactions at direct borohydride (DB, Eqs. 1.18, 1.19, and 1.20) and direct formate (DF, Eqs. 1.21, 1.22, and 1.23) AEMFCs are [13, 59]:

For DB-AEMFCs:

Anode reaction:

$$BH_4^- + 8OH^- \rightarrow BO_2^- + 6H_2O + 8e^-, E_a^o = -1.24 \text{ V vs.SHE} \quad (1.18)$$

Cathode reaction:

$$O_2 + 2H_2O + 4e^- \rightarrow 4OH^-, E_c^o = 0.40 \text{ V vs.SHE} \quad (1.19)$$

Overall:

$$BH_4^- + 2O_2 \rightarrow BO_2^- + 2H_2O, E_{cell} = 1.64 \text{ V} \quad (1.20)$$

and

For DF-AEMFCs:

Anode reaction:

$$HCOO^- + 3OH^- \rightarrow CO_3^{2-} + 2H_2O + 2e^-, E_a^o = -1.05 \text{ V vs.SHE} \quad (1.21)$$

Cathode reaction:

$$1/2O_2 + H_2O + 2e^- \rightarrow 2OH^-, E_c^o = 0.40 \text{ V vs.SHE} \quad (1.22)$$

Overall:

$$HCOO^- + 1/2O_2 + OH^- \rightarrow CO_3^{2-} + 2H_2O, E_{cell} = 1.45 \text{ V} \quad (1.23)$$

Additionally, Ogumi et al. compared the performance of fuel cells fed with the polyalcohols, erythritol and xylitol, with those of ethylene glycol, glycerol, and methanol. It has been concluded that the higher power density is delivered by using ethylene glycol with the AEMFC operating at 323 K, with a Pt-Ru/C anode and Pt/C cathode [30].

1.3 Performance of Several Types of Nanostructured Anodes and Cathodes in AEMFCs

As discussed in Sect. 1.1, several fuels are being used in AEMFCs, from H_2 to organic molecules. Advantages and disadvantages of each of them seem to be clear. Higher power densities can be delivered by H_2/O_2 AEMFCs due to the high reactivity of the gaseous fuel. Also, the absence of C atoms avoids the need of C–C bonds cleavage and the formation of reaction intermediates such as CO_{ads} during the HOR. However, hydrogen is not freely available in nature and must be produced, mainly from hydrocarbons. Renewable hydrogen, i.e., from water electrolysis using solar or wind resources, is feasible, but still more expensive than natural gas reforming on a large-scale basis.

On the other hand, easier handling of the fuels compared to H_2 can be achieved with liquid molecules. Very important from a sustainability point of view, some of the organic fuels can be produced from biomass resources. Nevertheless, the power density obtained from AEMFCs is lower when fuelled with such liquid molecules relative to hydrogen [6]. Moreover, the operational problems caused by the cross-over phenomena remain in AEMFCs (to a less extent than in PEMFCs) using methanol, ethanol, or other liquid fuels. Therefore, the selection of nanostructured cathode catalysts is of high relevance to avoid depolarization losses caused by crossed fuel or reaction intermediates. As mentioned earlier, the kinetics of the ORR in alkaline media is faster than in acid electrolytes, allowing for the use of a number of high-performance cathodes, from Pt/C and Pd/C (and their alloys or composite materials with metal oxides), to non-PGM and metal-free nanocatalysts. Taking advantage of this variety that includes low-cost nanomaterials, AEMFCs may be a cheaper technology than PEMFCs.

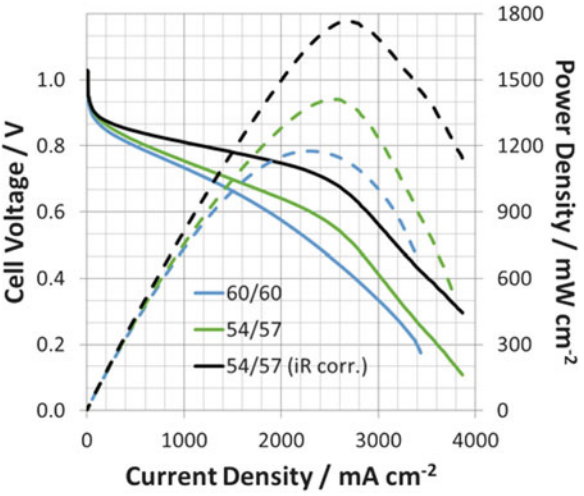

Fig. 1.2 Polarization curves of H_2/O_2 AEMFCs. Experimental conditions with 54/57 anode/cathode dew points: anode: 0.67 mg_{PtRu} cm^{-2} on 5% PTFE, cathode: 0.53 mg_{Pt} cm^{-2} on 5% PTFE GDL. Cell temperature: 60 °C (adapted from Ref. [21], reproduced with kind permission of © Elsevier)

Recent reports show the performance of AEMFCs under different operating conditions. Using a 0.53 mg_{Pt} cm^{-2} Pt/C cathode (40 wt. %), a power density of 1.4 W cm^{-2} has been delivered by a H_2/O_2 AEMFC operating at 60 °C (with an ETFE-g-VBCTMA membrane) as seen in Fig. 1.2 [21]. Power densities of 1.16 and 0.91 W cm^{-2} have been obtained from H_2/O_2 AEMFCs operating at 60 °C, with Pt/C cathodes, PtRu/C anodes, and RG-AEM(Cl^-) membranes [60]. The same group has reported a H_2/O_2 AEMFC delivering power densities of 1.1 and 0.699 W cm^{-2} using a non-Pt cathode (Ag/C, 1.0 mg_{Ag} cm^{-2}), operating with O_2 and CO_2-free air, respectively [22]. It has been reported by the authors that the Ag/C outperformed a Pt/C cathode with CO_2-free air at the cathode. Elsewhere, a peak power density of 1.0 W cm^{-2} has been reported with a H_2/O_2 AEMFC equipped with commercial Pt/C cathode and PtRu/C anode (metal loadings of 0.4 mg cm^{-2}) membrane of the aQAPS-Sx type and $T_{cell} = 60$ °C [61]. Also, a Pt-free H_2 (dry)/Air (<10 ppm CO_2) AEMFC operating at 73 °C delivered a power density of 0.5 W cm^{-2} (cathode: Ag, 3.0 mg_{Ag} cm^{-2}; anode: Pd/C-CeO_2) [26]. Moreover, a H_2 (dry)/Air (CO_2 free) AEMFC with a silver-based alloy (3.0 mg cm^{-2}) cathode and a Pd/Ni anode generated 0.4 W cm^{-2} power density at 73 °C [62].

It is therefore feasible to use non-Pt cathode catalysts and yet generate high-power densities not only from H_2/O_2 AEMFCs, but also from fuel cells using liquid fuels. Mesoporous Fe/N/C cathode catalysts with highly active Fe-Nx/C sites have been used in a H_2/O_2 AEMFC (A901 membrane, Tokuyama), exhibiting 40% higher power density (0.272 W cm^{-2}) than commercial Pt/C in single-cell tests with $T_{cell} = 50$ °C. The high performance of the non-Pt catalyst has been in part attributed to large pores in the mesoporous structure, which resulted in a high surface area and accessibility to the active sites [63]. Elsewhere, a H_2/O_2 AEMFC (membrane Tokuyama A201) containing a Fe-NMG (a type of Fe-N-C) cathode catalyst and Pt/C anode generated 0.218 W cm^{-2}, a higher value than 0.2 W cm^{-2} of a cell with Pt/C cathode and anode catalysts with $T_{cell} = 70$ °C (Fig. 1.3) [7]. A H_2/O_2 AEMFC

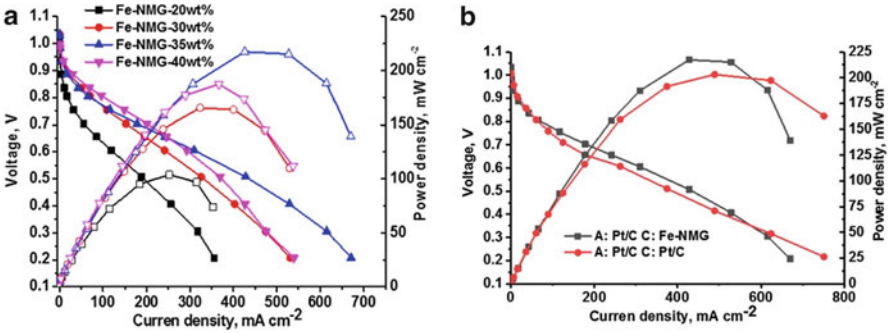

Fig. 1.3 Polarization curves of AEMFCs with (**a**) Fe-NMG cathodes at different ionomer concentration, (**b**) comparison of the performance of MEAs having Fe-NMG cathode and Pt/C anode catalysts, and Pt/C catalysts on both anode and cathode (reproduced from Ref. [7] with kind permission of © Elsevier)

composed of CoPPY/C-based cathodes and Ni-W-based anodes produced 0.04 W cm^{-2} at 60 °C, with a membrane of the xQAPS type [64].

Other types of AEMFCs have also reached a good development. It has been reported that a DM-AEMFC may produce 0.046 W cm^{-2} at 60 °C with Fe_2O_3/Mn_2O_3 (3:1) cathode and PtRu/C anode, and a polymer fiber membrane [65]. Elsewhere, a DM-AEMFC with MnO_2 cathode catalyst (membrane: Q-PVA/PECH; anode: PtRu/C) generates a maximum power density of 0.022 W cm^{-2} at 25 °C [66]. Using a similar cathode composition and a PVA/HAP membrane, an air-breathing DM-AEMFC has generated 0.011 W cm^{-2} at 25 °C (Ti-based anode with PtRu black) [67]. Recently, mesoporous 3D nitrogen-doped yolk-shelled carbon spheres have been used as cathodes in a DM-AEMFC, delivering 0.056 and 0.141 W cm^{-2} at 25 and 60 °C, respectively (polymer fiber membranes; PtRu anodes) [68].

Non-noble Fe-N-C catalyst has also been used in a DE-AEMFC, reaching a power density of 0.062 W cm^{-2} with 50 wt. % Nafion® content, Pt-Ru/C anode, and KOH-doped PBI membrane (T_{cell} = 90 °C) [8]. A higher power density (0.335 W cm^{-2}) has been generated by a DE-AEMFC equipped with a Fe-Co/C cathode, anode of the combined Pd/TNTA-web type, T_{cell} = 80 °C, and Tokuyama A201 membrane [45]. With these components, ethanol as the fuel outperformed the use of glycerol and ethylene glycol. Other fuels have been evaluated. For example, a DEG-AEMFC based on Fe-based cathode catalyst (Acta 4020, 3.0 $mg_{catalyst}$ cm^{-2}), PdAg/CNT anode (0.5 $mgPdcm^{-2}$), and a Tokuyama A901 membrane delivered a power density of 0.245 W cm^{-2} at 80 °C [46]. A DG-AEMFC (crude glycerol) generated 0.268 W cm^{-2} with a Fe–Cu–N_4/C cathode (Acta 4020, 3.0 mg catalyst cm^{-2}), PtCo/CNT anode (0.5 mg_{Pt} cm^{-2}), and a Tokuyama A901 membrane [52]. A Pt-free borohydride AEMFC delivered a 0.283 W cm^{-2} using $Co(OH)_2$-PPy-C cathode and anode catalysts and a co-impregnated PVA-AER membrane, with T_{cell} = 60 °C [12]. Table 1.1 summarized the components, conditions, and peak power densities delivered by several types of AEMFCs.

Table 1.1 Selected data of AEMFCs fuelled with H_2 and several organic molecules

AEMFC type	Fuel	Oxidant	Cathode	Anode	Membrane	T_{cell} (°C)	Peak power density (W cm^{-2})	Ref.
H_2/O_2	H_2	O_2	0.53 mg_{Pt} cm^{-2} Pt/C (40% wt. Pt/C)	0.67 mg_{PtRu} cm^{-2} (40% wt. Pt/C)	ETFE-based benzyltrimethylammonium-functionalized radiation-grafted alkaline AEM	60	1.40	[21]
H_2/O_2	H_2	O_2	0.4 mg_{Pt} cm^{-2} Pt/C	PtRu/C (50% mass Pt and 25% mass Ru) 0.40 mg_{Pt} cm^{-2} Pt loading	Benzyltrimethylammonium-type AEM	60	1.16	[60]
H_2/O_2	H_2	O_2	Ag/C (40 wt. % Ag, 1.0 mg_{Ag} cm^{-2}).	PtRu/C (50%wt Pt and 25%wt Ru) 0.4 mg_{Pt} cm^{-2}	ETFE-[poly(ethylene-co-tetrafluoroethylene)]-based radiation grafted (RG)	70	1.10	[22]
H_2/O_2	H_2	O_2	Pt/C (60 wt. %, 0.4 mg cm^{-2})	PtRu/C (60 wt. %, Ru atomic ratio: 20%, 0.4 mg cm^{-2})	Quaternary ammonia polysulfone (QAPS) with hydrophobic side chain backbone	60	1.00	[61]
H_2/O_2	H_2 (dry)	Air (<10 ppm CO_2)	Ag, 3.0 mg_{Ag} cm^{-2}	Pd/C-CeO_2, 50 wt. % CeO_2 and 50 wt. % Vulcan XC-72 carbon, Pd loading: 0.3 mg cm^{-2}.	Ion exchanged to hydroxyl form by soaking in NaOH	73	0.50	[26]
H_2/O_2	H_2 (dry)	Air (CO_2 free)	Silver-based alloy (3.0 mg cm^{-2})	Pd/Ni (1.5 mg cm^{-2} total metal loading, with 0.3 mg_{Pd} cm^{-2})	Quaternary ammonium-functionalized	73	0.40	[62]
H_2/O_2	H_2	O_2	m-FePhen-C (Fe/N/C with highly active Fe-Nx/C sites, 1.0 mg cm^{-2})	40 wt. % Pt/C, 0.5 mg cm^{-2} Pt loading	A901 membrane, Tokuyama	50	0.27	[63]

H_2/O_2	H_2	O_2	Fe-NMG (a type of Fe-N-C), 3.5 mg cm^{-2}	10 wt% Pt/C, 0.2 mg cm^{-2}	A201 membrane, Tokuyama	70	0.22	[7]
H_2/O_2	H_2	O_2	CoPPY/C based, 2 mg cm^{-2}	Ni-W, 17.5 mg cm^{-2}	Quaternary ammonium-functionalized	60	0.040	[64]
DM	4 M KOH + 5 M CH_3OH	O_2	Fe_2O_3/Mn_2O_3(3:1)	PtRu/C (60 wt. %, 5 mg cm^{-2})	Polymer fiber membrane	60	0.046	[65]
DM	4 M KOH + 2 M CH_3OH	Air	MnO_2/C catalyst mixed with BP2000 carbon black (MnO_2: BP2000 = 1:1)	PtRu/C (70 wt. % Pt: Ru = 1:1 at. ratio, 4 mg cm^{-2})	Quaternized poly(vinyl alcohol)/poly(epichlorohydrin)	25	0.022	[66]
DM	8 M KOH + 2 M CH_3OH	Air	MnO2/BP2000	PtRu/C (70 wt. % Pt: Ru = 1:1 at. ratio, 4 mg cm^{-2})	Poly(vinyl alcohol)/ hydroxyapatite	25	0.011	[67]
DM	4 M KOH + 5 M CH_3OH	O_2	Mesoporous 3D N-doped yolk-shelled carbon spheres (Fe-N-C)	PtRu	Polymer fiber membrane	60	0.141	[68]
DE	2 M KOH + 2 M C_2H_5OH	O_2	Fe-N-C (from Fe(II)-phthalocyanine)	Pt-Ru/C (45 wt. %, 1.33 mg cm^{-2})	KOH-doped PBI membrane	90	0.062	[8]
DE	2 M KOH + C_2H_5OH 10 wt. %	O_2	Fe-Co/C, 2 mg cm^{-2} (C = Ketjen Black EC 600 JD, 1.13 wt. % Fe and 1.71 wt. % Co)	Pd/TNTA-web type (6 mg_{Pd} cm^{-2}, Ti web as the electrode support)	A201 membrane, Tokuyama	80	0.335	[45]
DEG	6.0 M KOH + 3.0 M $C_2H_6O_2$	O_2	Fe-based cathode catalyst (Acta 4020, 3.0 $mg_{catalyst}$ cm^{-2})	PdAg/CNT anode (0.5 mg_{Pd} cm^{-2})	A901 membrane, Tokuyama	80	0.245	[46]
DG	6.0 M KOH + 3.0 M crude $C_3H_8O_3$ (88 wt. %)	O_2	Fe–Cu–N_4/C cathode (Acta 4020, 3.0 mg catalyst cm^{-2})	PtCo/CNT anode (0.5 mg_{Pt} cm^{-2})	A901 membrane, Tokuyama	80	0.268	[52]
DB	5 wt. % $NaBH_4$ + 10 wt. % NaOH	O_2	$Co(OH)_2$-PPy-BP (3 mg cm^{-2})	$Co(OH)_2$-PPy-BP (5 mg cm^{-2})	Co-impregnated poly(vinyl alcohol)-anion exchange resin composite membrane	60	0.283	[12]

1.4 Advances in Membranes for PEM and AEM Fuel Cells

Fuel cells using polymeric membranes as electrolytes are most promising fuel cell technologies to provide clean, efficient, and energy dense power sources. Acidic proton exchange membrane (PEM) and alkaline anion exchange membrane (AEM) for applications in low temperature polymer electrolyte fuel cells will be reviewed in this chapter. Technically, both PEMFCs and AEMFCs operate with hydrogen at the anode and oxygen or air at the cathode, however, as PEM and AEM electrolytes transport different ions: acidic proton H^+ and alkaline OH^-, respectively, the resulting electrochemical reactions occurring are unlike, resulting in very distinct ions and water transport properties during fuel cell operation.

As illustrated in Fig. 1.4a, in PEMFC and AEMFC ions and water are not transported in the same directions. Water is generated at the anode (twice as much as in a PEMFC, per electron), and consumed at the cathode in AEMFCs which is fundamentally different to what occurs in PEMFCs [6]. These differences provide each technology with advantages and challenges.

PEMFC is a mature technology capable of producing extremely high-power densities, with the required durability for automotive and stationary applications. It has already penetrated many demanding commercial markets (e.g., backup power, materials handling, automotive including cars, trucks, and buses). However, it still depends on the utilization of costly platinum group metal (PGM) catalysts, perfluorosulfonic acid (PFSA)-based electrolytes, and pure hydrogen.

As a consequence of the expected market growth, PEMFCs will experience ever greater demands on cost, performance, and durability. In general, alkaline media provides a less corrosive environment to the catalysts, and the ORR kinetics is more rapid in alkaline media than in acidic media (Fig. 1.4b) [69].

This could potentially facilitate, in the case of AEMFCs, the use of less expensive non-platinum group metal (PGM) catalysts which expands the parameter space for

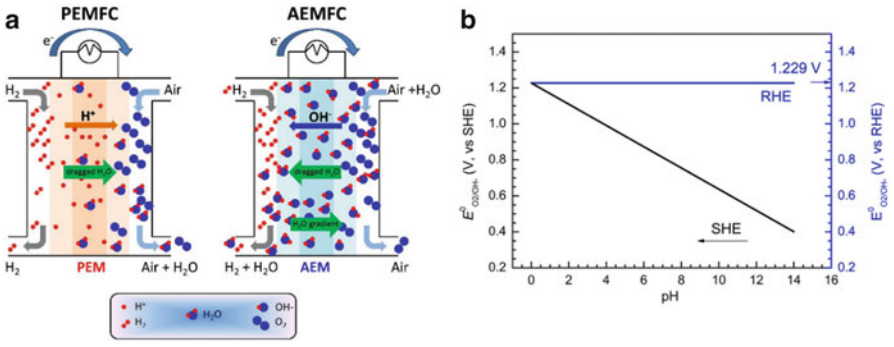

Fig. 1.4 (**a**) Schematic representation of an AEMFC as compared to a PEMFC (reproduced from Ref. [6] with kind permission of © Elsevier). (**b**) RHE scales with SHE of O_2/OH^- redox couple at different pH values of aqueous solutions (reproduced from Ref. [69] with kind permission of © Elsevier)

the discovery of highly selective catalysts with high stability in alkaline environments, and opens the possibility to consider hydrogen fuels containing substantial amounts of impurities. The foreseen cost reduction related to a possible free PGM catalysts fuel cell technology explains the resurgence of a large interest from industry and R&D community in AEM in the last decade. The following sections will introduce the state-of-the-art PEM and AEM and review recent development for both polymer electrolytes.

1.4.1 Proton Exchange Membranes (PEMs)

PEMs are solid polymer electrolyte membranes based on ionomers that contain fixed negative ionic functional groups, typically sulfonic acid (SO_3^-) and mobile positively charged cations, protons (H^+) in this case. PEMs are divided into three main categories: perfluorinated, semi-fluorinated, and hydrocarbon based.

Perfluorinated PEMs From a technology point of view, the development of perfluorinated sulfonic acid (PFSA)-based polymer membranes such as Nafion® has dominated due to their remarkable ion conductivity, low electronic conductivity, and chemical–mechanical durability compared to semi-fluorinated and hydrocarbon-based ionomer membranes. Still other properties such as water transport through diffusion and electro-osmosis, and the ability to fabricate high-performance membrane and membrane-electrode-assemblies (MEAs) are important when considering performance in operating system. However, researchers are actively working on alternatives to circumvent their high cost, limited use in low-temperature PEMs, and necessity of reinforcement to secure the required mechanical durability. Even after decades of research, Nafion® still stands as the state-of-the-art solid electrolyte for most PEMFC applications. Nafion® PFSA is a random copolymer developed in the late 1960s by Dupont composed of a non-ionic semi-crystalline polymer backbone of polytetrafluoroethylene (PTFE) and a randomly tethered long side chain with a pendant $SO3^-$ ionic group (sulfonic acid fluoride vinyl ether).

The different nature of the backbone and the covalently bonded pendant sulfonic groups results in a phase separation, as can be observed in Fig. 1.5a [70], which is enhanced by solvation upon hydration of the sulfonic groups to form water-swelled diffusion channels embedded in the hydrophobic matrix as revealed in Fig. 1.5b [71]. It is this phase-separated morphology between hydrophobic backbone and hydrophilic side chains that provides Nafion® its unique ion and water transport properties.

Most of fundamental research carried out on Nafion® membranes relates ionomer structure to properties (transport, physical, electrochemical, etc.) including computational work on mesoscale models and molecular dynamics (MD) simulations, with the objective of generating new synthetic approaches based on the fundamental understanding generated. Extremely extensive literature exists and was recently reviewed by Kusoglu et al. [72]. The reader is referred to the papers along with a

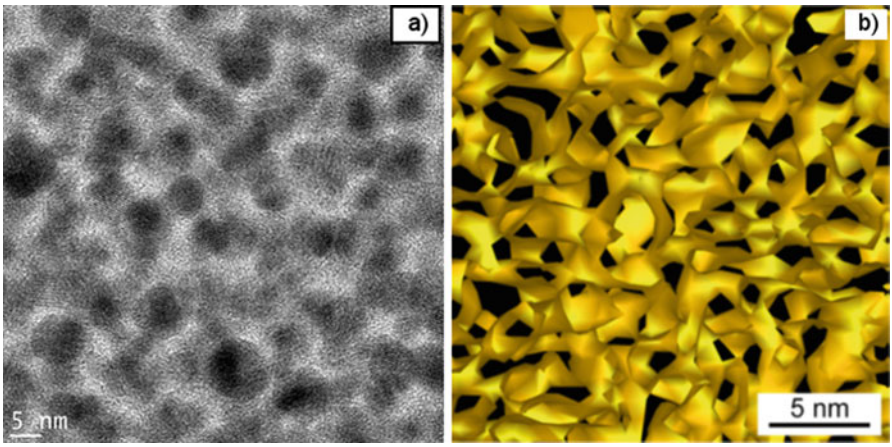

Fig. 1.5 (**a**) TEM on lead acetate stained Nafion® dry membranes. Ionic domains are dark (reproduced from Ref. [70] with kind permission of © The Electrochemical Society). (**b**) 3D reconstruction of the frozen hydrated cast Nafion membrane highlighting the spatial distribution of the hydrophilic domains in yellow (reproduced from Ref. [71] with kind permission of © The American Chemical Society)

number of other sources discussed. The most common synthetic approaches explored for new PFSA ionomers are based on the modification of either the backbone or side chain structure. The latest was mainly explored and generated several short side chain (SSC) ionomers, commercially available structures are illustrated in Fig. 1.6.

SSC-PFSA ionomers show higher structural crystallinity and increased glass transition temperature that translate to higher thermal stability compared to LSC-PFSA membranes. Furthermore, narrower ionic channels in SSC-PFSAs allow for improved water retention at low RH and lower gas crossover [73]. MD simulations suggest that shorter side chain ionomers have improved backbone flexibility, which enhances the proton dissociation and leads to higher conductivity [74, 75].

Modifications to the backbone length or distance between side chains resulted in smaller TFE repeat units and subsequently lower equivalent weight (EW) PFSAs. The EW being the mass of dry ionomer per mole of sulfonic acid groups, therefore lower EW ionomers show higher ion exchange capacity reaching IEC = 1.5 mmol/g for EW = 660 g/mol.

It was shown that due to the proximity of ionic groups in lower EW PFSAs, conduction mechanism may differ from LSC and may favor high temperature and low relative humidity operation, as supported by MD simulations [76]. Many studies intend to correlate side chain length and number of repeat units (or EW) to ionomers properties [77, 78]. There appears to exist a minimum backbone length or TFE repeat units $m = 3.5–5$ minimum for a PFSA to exhibit semi-crystallinity and the required packing order in the hydrophobic phase. Below this value, the ionomer exhibits a

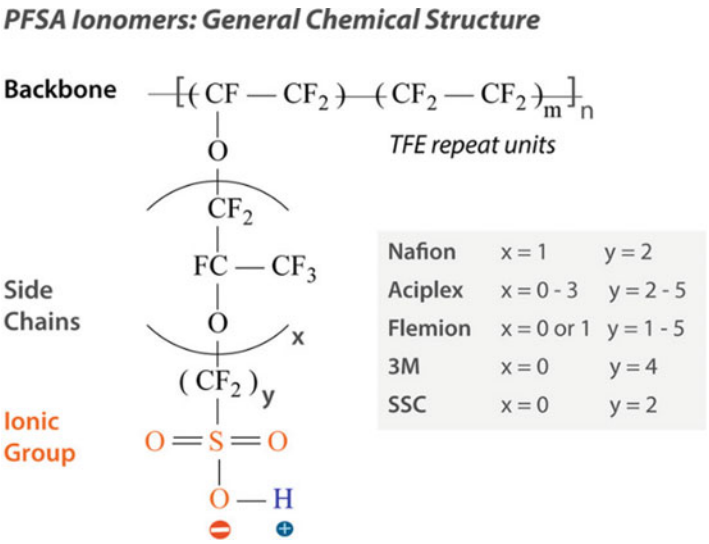

Fig. 1.6 PFSA ionomers general chemical structures (reproduced from Ref. [72] with kind permission of © The American Chemical Society)

gel-like behavior with weak stability, although with good proton transport properties. Studies reported minimum EW of 965 g/mol for Nafion® PFSA, 725 g/mol for 3 M PFSA, and 800 g/mol for Aquivion SSC-PFSA (previously Dow), which correspond to a minimum of 3–4 TFE units for all PFSAs [79–81].

PFSA ionomers offer a variety of PEMs which transport and mechanical durability among other properties, depend strongly on the TFE repeat units of fluorocarbon backbone, and the length of the sulfonic acid terminated side chains. The efforts to improve the transport functionalities and fuel cell performance are likely to compromise the mechanical durability and fuel cell longevity.

Besides increasing ionomers proton conductivity, another means to reduce proton resistance transport is to reduce membrane thickness, this strategy has led to the greatest improvement in PEMFC performance [82]. The advantages gained with this simple strategy include lower membrane resistance, improved hydration of the entire membrane, and lower material utilization and therefore, cost savings if we consider PFSA cost (e.g., 25 microns Nafion® 1100EW membranes cost vary between 1600 and 1300 US$/m^2 depending if reinforced or not). However, the extent to which a membrane can be thinned is limited, as gas crossover starts increasing, leading to increased voltage decay and earlier membranes failure.

PEMs manufacturing process could in some cases play an important role in compensating some of the mechanical weaknesses. Melt processes represent the best technologies to mass production of homogeneous thin polymer films at low cost. Besides eluding the serious safety and environmental concerns related to the mass production of membranes by solution-casting, melt processes provide a mechanical reinforcement through chain orientations following extrusion-stretching.

This structural reinforcement at a molecular level provides extruded PEM with the mechanical durability required for building robust and long-lasting PEM fuel cells, particularly for automotive applications. Mechanical degradation of three extensively studied model PFSA membranes was tested by Guittleman et al. [83] using humidity cycling tests: Nafion® NRE-211 (25 microns thick solution-cast membrane), Nafion® N111-IP (25 microns extruded membrane), and Gore-select® Series57 (18 micron e-PTFE reinforced three layers membrane). All membranes were made from LSC PFSA ionomer with EW = 1100, but prepared with different processes. Solution-cast membranes showed the shortest durability (4500 cycles), followed by e-PTFE-reinforced PEM (6000 cycles), extruded PEM has a significantly longer humidity cycling lifetime >20,000 cycles without failure. Significantly, even in model simulations, there appears to be a strong process-dependence of membrane morphology, indicating that structures produced by extrusion or solvent casting may be quite different, resulting in varied transport properties [76].

However, melt processing is only possible for ionomers that (1) possess the appropriate rheological properties to flow in the melt state and form uniform and mechanically sound thin membranes, and (2) are thermally stable at processing temperature. PFSA ionomers with sulfonic acid functional groups cannot be melt-processed as their melt processing temperature (>200 °C) is generally above sulfonic acid −SO3H groups degradation temperature. However, PFSA ionomers can be melt processed if the sulfonic acid functionality has been modified (i.e., sulfonyl fluoride precursor –SO_2F) or protected with additives to withstand melt processing high temperatures. In both cases a conversion of the membranes to the acidic form by hydrolysis or additive removal is required for operation in a fuel cell.

Extrusion by melt-casting, in the sulfonyl fluoride form followed by hydrolysis to convert to the sulfonic acid form, has been used to prepare proton exchange membranes, available commercially such as Nafion®N-117, Nafion®N-115, Nafion® N-1135, Nafion®N-112, and Nafion®111-IP with thicknesses of 183, 127, 89, 51, and 25 microns, respectively. These extruded membranes also suffer from anisotropy in their properties in general, generated by strong orientation in the machine direction that may cause a premature failure when submitted to humidity cycling in a fuel cell. Furthermore, the extrusion process by melt-casting does not allow the manufacturing of membranes thinner than 25 microns without compromising thickness uniformity.

It has been demonstrated that thermal stability of Nafion® PFSA ionomer is strongly dependent on the nature of the counterion associated with the fixed sulfonate site [84]. A number of small alkali metal and larger alkyl ammonium cation-exchanged Nafion® membranes were studied (e.g., sodium Na^+, potassium K^+, tetrabutylammonium TBA^+, tetramethylammonium TMA^+, tetradecylammonium $TDecA^+$) [85, 86]. It was found that Nafion® decomposition temperature is inversely dependent on the size of the exchanged cation, i.e., Nafion films show improved thermal stability as the size of the counter cation decreases. This inverse relationship of thermal stability with counterion size is strongly influenced by the strength of the sulfonate–counterion interaction. Most of the counterions investigated, even they

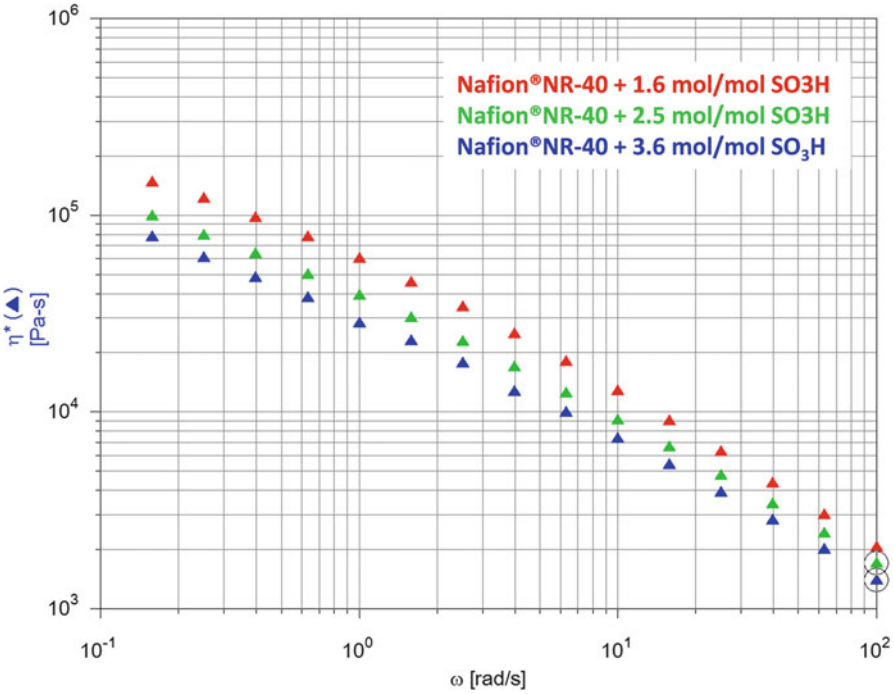

Fig. 1.7 Comparison of complex viscosity (η*) obtained from frequency sweep tests on Nafion® NR40 at 240 °C and different additive (1,2,4-triazole) content (from Ref. [89])

provided improved thermal stability of already processed membranes, do not allow for practical melt processing of PFSA ionomers.

Melt processing of LSC and SSC PFSAs in the acidic form using a series of heterocyclic azole molecules, i.e., benzimidazole, imidazole, and triazole, as additives was successfully investigated [87–89]. Figure 1.7 shows rheological data for Nafion® NR40 1000EW at 240 °C with different loading of 1,2,4-triazole, it shows the bifunctionality of the additive by neutralizing sulfonic acid groups on one hand, and acting as a plasticizer and aid-processing on the other. The complex viscosity is obviously reduced with increasing additive content.

Furthermore, PEMs were fabricated using an extrusion process based on melt-blowing of triazole neutralized Nafion® NR40 (EW = 1000). Some advantages of this process are (1) a better balance of mechanical properties than cast or extruded films because it is drawn in both the transverse and machine directions generating crystallinity in both directions, as a result mechanical properties of the thin film including tensile and flexural strength, and toughness are higher without e-PTFE reinforcement, (2) outstanding mechanical durability upon hydration and dehydration (>80,000 cycles) membranes swell preferentially in the thickness direction (Fig. 1.8 [89]) confirming that reduced in-plane swelling promotes long-term durability of the membrane electrode assembly (MEA) by constraining delamination of

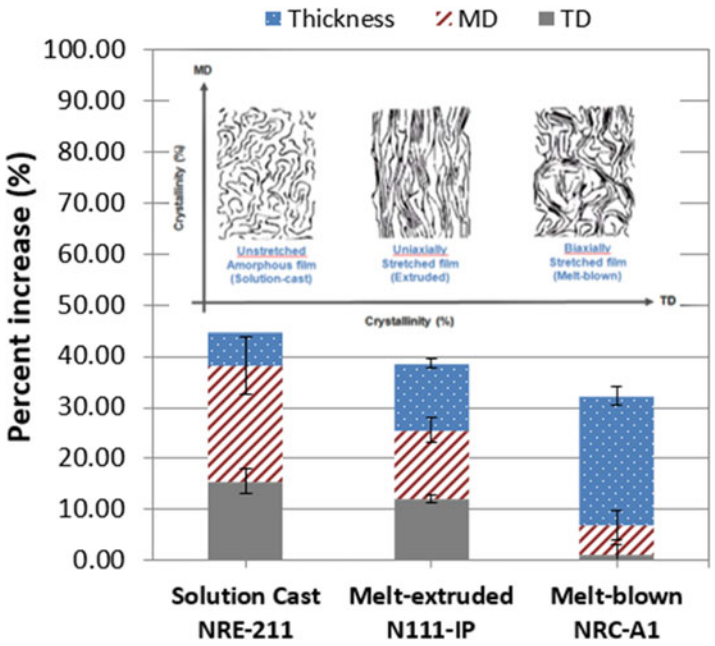

Fig. 1.8 Volume change for PEMs prepared with different processes as well as schematic representation of crystallinity evolution with processing. (From Ref. [89])

the catalyst layer from the membrane, (3) improved chemical durability; cumulative fluoride loss (CFL) was more than one order of magnitude lower than Nafion®NRE-211 reference; CFL = 160 mmol/cm^2 after 120 h (9.6 cycles) for the stack with Nafion®NRE-211 baseline and CFL = 5 mmol/cm2 after 162.5 h (13 cycles) for the five cell stack with triazole-Nafion®NR40 melt-blown membrane, and finally (4) PEM manufacturing cost is reduced 60–80% depending on annual production rates compared to e-PTFE reinforced solution-cast PEM.

Partially Fluorinated PEMs Non-fluorinated polystyrene sulfonic acid (PSSA) membranes were the first commercial polymer membranes developed in 1955 by GE [90] and were used in the first-ever operational PEMFC, the Grubb–Niedrach FC in the Gemini program. However, the system exhibited a short lifetime (<200 h) because of membrane poor stability and degradation under practical fuel cell operation, due to peroxide attacks on ternary benzylic hydrogen and the aromatic ring protons which results in IEC and conductivity loss, and membrane performance degradation. However, the very low cost of PSSA ionomer and its low fuel permeability originated the development of partially fluorinated PEM by substituting ternary hydrogen with fluorine resulting in more stable sulfonated poly(α,β,-β-trifluorostyrene) membranes developed by Ballard Advanced Materials as BAM3G membranes. These membranes contained sulfonated (α,β,-β-trifluorostyrene)- pendant groups and a perfluorinated backbone. Membrane

lifetime was strongly dependent upon equivalent weight and FC operating conditions, e.g., 3000 h operation time was achieved at 50 °C and low current density and only 500 h under practical FC conditions (higher current densities). A maximum operation time of 15,000 h was reported for pre-commercial BAM3G® [91, 92].

Radiation-induced grafting was largely investigated for the preparation of partially fluorinated polymers with styrene sulfonic acid (SSA) and modified SSA segments. Fluorinated polymers, such as polytetrafluoroethylene (PTFE), poly (tetrafluoroethylene-co-hexafluoropropylene) (FEP), poly(tetrafluoroethylene-co-perfluoropropyl vinyl ether) (PFA), polyvinylidenefluoride (PVDF), poly (vinylidenefluoride-co-hexafluoropropylene) (PVDF-co-HEP), poly(ethylene-tetrafluoroethylene) (ETFE), and polyvinylfluoride (PVF), were very stable and attractive skeleton structures for SSA-grafted membranes [93–99]. Such partially fluorinated grafted PEMs offered a substantially higher IECs with relatively moderate swelling because these membranes possessed isotropically connected ionic domains with high proton concentrations, PFEP-TFE-g-SSA membranes demonstrated proton conductivity up to 0.13 S/cm [100]. Unfortunately, these membranes exhibited substantially higher water absorption (up to 59 water molecules per SO_3 unit) than Nafion, which is a drawback as PEM materials. Another strategy to prepare SSA semi-fluorinated PEM was to blend polystyrene-based polymers with fluorinated polymers followed by post-sulfonation of styrene units [101, 102]. Polymer blending is one of the most effective methods to induce microphase separation. Despite all the strategies investigated, the applicability of partially fluorinated SSA-based membranes in PEMFCs is likely limited because the sulfonated styrene unit has a rather low oxidative stability even with fluorinated backbones or blends.

Poly(arylene perfluorocyclobutane) (PFCB), due to their particular thermal and chemical properties, are considered as high-performance partially fluorinated engineering materials for many applications [103–105]. The incorporation of proton-conducting groups in such macromolecular structures has been investigated for the development of PEM [106–110]. Various synthetic approaches were investigated and the most reported is based on the synthesis of functionalized bis-trifluorovinyl ether monomers, either in their sulfonic acid potassium salt form or as fluorosulfonyl analogues. Perfluorocyclobutyl (PFCB)-based blend PEM PFCB-based polymer blends comprising hydrophilic and hydrophobic polymers were prepared and characterized as PEM materials [109]. The hydrophobic polymers, BP-PFCB and SO_2-PFCB, were synthesized from the monomers 4,4′-bis(trifluorovinyloxy)-biphenyl 4,4′-sulfonyl-bis(trifluorovinyloxy)biphenyl, via a facile thermal polymerization. The hydrophilic blend component sBP-PFCB was prepared by the post-sulfonation of the BP-PFCB homopolymer using chlorosulfonic acid and thionyl chloride. The hydrophilic and hydrophobic components were combined in a common solvent obtaining transparent miscible membranes structurally stable with conductivities close to Nafion®.

Another PFCB copolymer developed through a collaboration between General Motors and Tetramer Technologies, LLC contains hydrophilic blocks of biphenyl vinyl ether (BPVE) with PFSA side chains and hydrophobic blocks of 1,1-bis

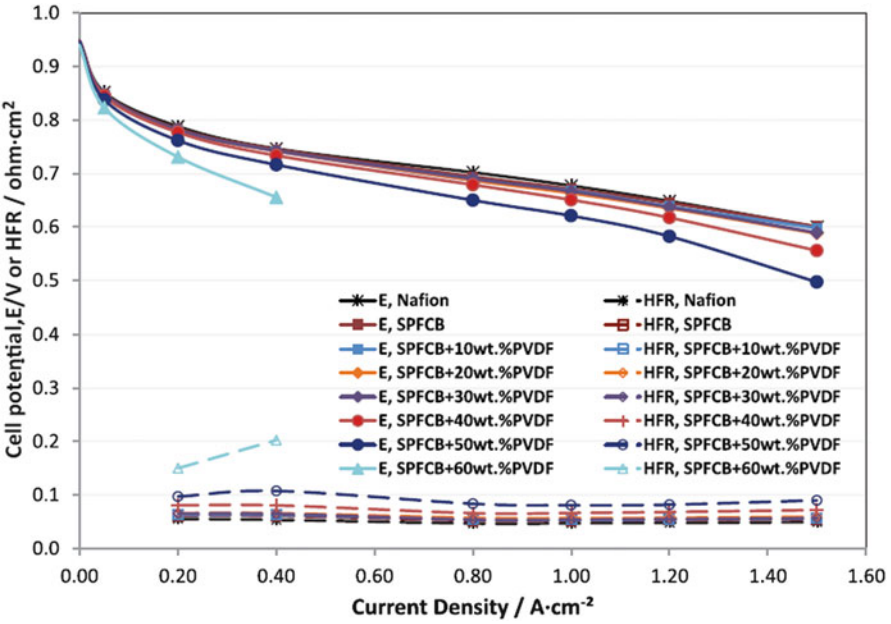

Fig. 1.9 Fuel cell polarization curves of MEAs containing SPFCB/PVDF blend membranes with various PVDF content (reproduced from Ref. [107] with kind permission of © Elsevier)

[4-[(trifluorovinyl)oxy]phenyl]hexafluoroisopropylidene (6F monomer) [107]. Proton exchange membranes based on SPFCB and SPFCB/PVDF blends with different PVDF contents (10–60 wt.%) were synthesized, fabricated, and characterized for fuel cell applications (Fig. 1.9) [107]. The composite SPFCB/PVDF membranes exhibit benefits of lower gas permeability and a higher ratio of conductivity to permeability compared to PFSA membranes for PVDF content <40 wt. %. In other work, e-PTFE-supported sPFCB membranes ran for over 3000 h in an accelerated durability test before ultimately failing due to chemical degradation [108]. This family of partially fluorinated PEMs based on SPFCB ionomer is probably one of the most promising alternatives to PFSA membranes because of the combination of good fuel cell performance, low gas permeance, and promising mechanical durability, as well as their relatively low projected cost.

Hydrocarbon PEMs Hydrocarbon-based PEMs are fluorine-free ion exchange membranes. This is probably the most investigated class of materials over the past few decades; they are of high interest because of their expected lower cost, intrinsically lower gas permeability, and higher glass transition temperatures compared to PFSA membranes. Most of hydrocarbon-based ionomers are sulfonated polymers and much of the research has focused on new (1) synthetic developments, (2) modification and functionalization of existing polymers, and (3) understanding of ionomers structures/properties relationship. Many publications covered extensive

reviews of all the strategies developed and the most relevant will be highlighted [111–114].

Hydrocarbon PEMs have been prepared from existing aromatic polymers and copolymers based on polystyrenes, polysulfones, polyimides, polyphosphazenes, polybenzimidazoles, poly(arylene-ether)s, poly(arylene sulfide)s, polyphenylenes, and many others. Polyarylene polymers and polymers containing phenyl pendant groups such as polystyrenes, as well as heterocyclic systems can be sulfonated by direct reaction with an appropriate sulfonating reagent. The most reactive sites for sulfonation depend on both the polymer structure and the directing effect of substituent groups. Simplicity and reproducibility were some of the advantages of polymers sulfonation, allowing for the possibility to generate different equivalent weights (EW) by controlling the reaction conditions. Most sulfonated polymers are thermally and mechanically stable up to 200 °C due to their more rigid polymer chain structure, and they have excellent fuel barrier properties, which lend themselves to PEM materials for low-temperature PEMFC applications. However, for a given IEC, sulfonated polymers generally have lower proton conductivities and higher dimensional swelling compared with PFSAs because of their lower acidity, lower hydrophobicity of polymer backbone, and weaker phase separation between hydrophilic and hydrophobic moieties, resulting in less effective microphase-separated morphology for water channel formation [113]. Furthermore, the starting polymers were originally developed for applications in environments different from those prevailing in a PEM fuel cell, i.e., temperature, relative humidity, pH, presence of radicals, etc. Under saturated vapor conditions, all materials (both sulfonated and non-sulfonated) show some decomposition between 150 and 200 °C, although the thermohydrolytic stability of the sulfonated polymers is always lower than that of the corresponding unmodified starting material, sulfonated polymers all show loss of sulfonic acid groups and hydrolysis of the functionalized units to some extent. Chemical stability of sulfonated polymers appears to be lower than PFSAs, particularly those with electron-rich structures containing ether linkages. As a general observation, sulfonated polyaromatic polymers are slightly more stable than sulfonated polyheterocyclic systems [111].

Sulfonated polymers can also be synthesized via various synthetic routes from diverse monomers to obtain a variety of structural architectures, e.g., random copolymer, block copolymer, grafted copolymer, and densely sulfonated or clustered copolymer. Synthetic routes provide the opportunity to have a better control of (1) the position and number of functional groups, which in turn define the ion exchange capacity and the morphology (hydrophobic/hydrophilic phase separation), and (2) the molecular weight to enhance durability which is more difficult to achieve with post-reaction on existing commercial polymers. The characteristics of functional groups such as position on the polymers chains (e.g., main chain, pendent unit, side chain, etc.), flexibility, and acidity or basicity are also important in the control of the final ionomer's morphology [112, 114]. The polymer backbone characteristics such as size, stiffness, hydrophobicity, and electron-withdrawing or -donating effects influence the hydrophobic domain structure.

Compared with random copolymers, block copolymers induce more ordered microphase-separated morphology because the different characteristics and length of each block induced phase separation. The chemical structure of hydrophobic sequences is one of the critical factors leading to phase separation. Furthermore, oligomer block lengths influenced the morphological features and interdomain distances. Longer block lengths induced clearer phase separation and increased domain sizes.

Various types of hydrocarbon-based ionomer membranes have been proposed for application in fuel cells, many studies reported ionic conductivities and even fuel cell performances higher than PFSAs, however, the issue of chemical and mechanical degradation of this class of ionomer membranes, especially under automotive operating conditions, has not been fully resolved at present. Shimizu et al. [115] reported recently on the chemical durability of two proton-conducting hydrocarbon polymer electrolyte membranes based on sulfonated benzophenone poly(arylene ether ketone) (SPK) and sulfonated phenylene poly(arylene ether ketone) (SPP) semiblock copolymers using accelerated OCV stress testing. Even if SPP-based fuel cell showed slower OCV decay compared to SPK, both hydrocarbon PEMs exhibited remarkable stability compared to Nafion®NRE211 baseline (Fig. 1.10.). They suggested that the lower hydrogen permeation in the cell led to a decreased

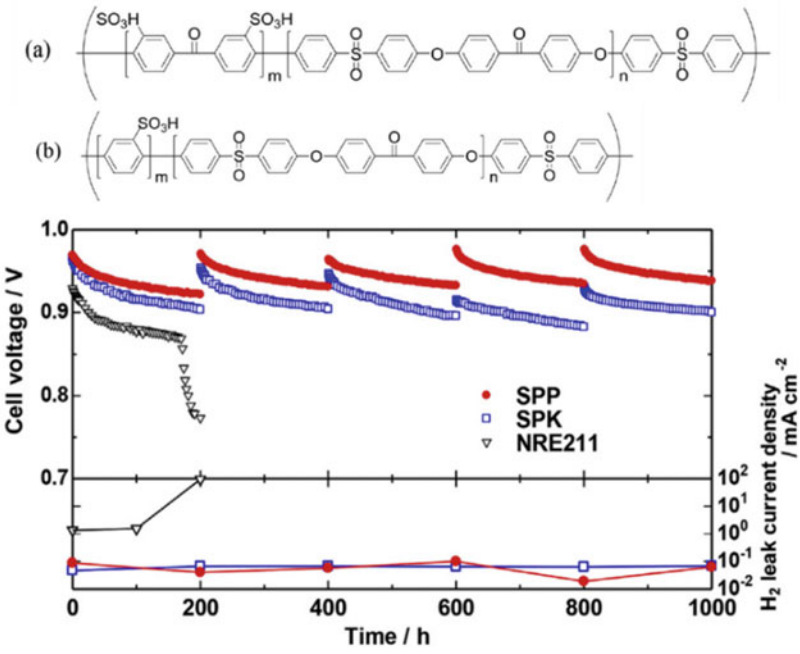

Fig. 1.10 Chemical structure of (**a**) sulfonated benzophenone poly(arylene ether ketone) (SPK) (**b**) sulfonated phenylene poly(arylene ether ketone) (SPP) semiblock copolymer, and cell voltage decay and hydrogen leak current density (reproduced from Ref. [115] with kind permission of © Elsevier)

production of oxidative radical species generated at the anode and led to a slowing of membrane degradation kinetics.

After decades of R&D and despite the progress made, the limitations related to the mechanical and chemical durability are still to be addressed for hydrocarbon PEMs to become suitable alternatives to perfluorinated fuel cell membranes, and simultaneous mitigation mechanisms for chemical and mechanical degradation should be mutually compatible. Gubbler et al. suggested that the shortcomings related to the mechanical durability should be solved using approaches that both reduce the membrane stress during humidity cycling and increase the strength at dry conditions, for instance, by minimizing in-plane swelling via clever multi-block copolymer architectures and lowering membrane stiffness by blending or copolymerizing with elastomeric polymers [108]. Membranes manufacturing process can also be an effective way for achieving low in-plane swelling when possible [89]. The approach effectively used for PFSA PEMs is to simultaneously reduce in-plane swelling and increase strength by using a relatively stiff porous e-PTFE polymer support. Radical induced chemical degradation will require a dedicated antioxidant strategy that needs to be self-sustaining over thousands of operating hours.

1.4.2 Anion Exchange Membranes (AEMs)

AEMs are solid polymer electrolyte membranes that contain fixed positive ionic groups, typically quaternary ammonium (QA) functional groups, and mobile negatively charged anions usually hydroxide (OH^-). As there are no typical membranes comparable to Nafion® used in PEMFCs, the development of an AEM equivalent to the well-established perfluorosulfonic acid proton exchange membranes (PEM) in their hydroxide form is hindered by several issues, the most reported are: (1) low intrinsic ionic conductivities; typical quaternary ammonium ionic groups in AEM are less dissociated than the typical sulfonic acid groups (pKa for sulfonic acid groups are typically -1 but for QA groups the related pKb values are around +4); [116] the diffusion coefficient of OH^- ions is twice less than that of H^+ (in bulk water), a higher concentration of OH^- ions is needed to achieve similar results, which in turn requires higher ion exchange capacity of the polymer. Achieving OH^- ion conductivity comparable to H^+ conductivity observed in PEMFCs becomes challenging without compromising mechanical properties due to excessive swelling, (2) the molecular structure of the membrane itself decomposes due to the presence of the highly nucleophilic OH^-. Decomposition typically starts at temperatures above $T = 60\ °C$ and leads to a reduction of ion exchange capacity (IEC), conductivity, and mechanical strength, and (3) the OH^- in AEMs is readily converted into carbonates when in contact with ambient CO_2 that precipitate irreversibly compromising electrodes porosity and fuel cell durability [117, 118].

The increased number of studies in the past few years indicates a growing interest in the research community, driven by the several advantages that AEMFC technology

might deliver over the currently commercialized proton exchange membrane fuel cells (PEMFCs) as mentioned at the beginning of this chapter. Improvements in the past decade show that newly developed AEMs have already reached high levels of conductivity, leading to satisfactory cell performance [6]. The most common, technologically relevant backbones reported are poly(arylene ethers) of various chemistries such as polysulfones (including cardo (polymer molecule with cyclic side groups whose one of the atoms belongs to the main polymer chain, phthalazinone, fluorenyl), poly(ether ketones), poly(ether imides), poly(ether oxadiazoles), polyphenylenes and poly-(phenylene oxides), polybenzimidazoles, poly(epichlorohydrins), unsaturated polypropylene and polyethylene, polystyrene, poly-(vinyl alcohol), poly(vinylbenzyl chloride), polyphosphazenes, perfluorinated, and based organic and inorganic hybrid types. Also, methods of preparation, including synthesis, radiation-grafting, plasma synthesis, pore-filling, electrospinning, and PTFE-reinforced types, have been reported [119]. The cationic functional-group chemistries that have been studied include (1) N-based groups, such as quaternary ammoniums (QA), heterocyclic systems (including imidazolium, benzimidazoliums, and pyridinium), guanidinium systems, (2) P-based types including stabilized phosphoniums, (3) sulfonium types, and (4) metal-based systems.

Although alternative cationic species from phosphonium or sulfonium groups have been shown to be less stable than QAs with similar substituents, some potentially viable highly sterically shielded phosphonium groups may be relevant, however, their synthesis is highly complex [120, 121] which is the reason why current research efforts mainly focus on QAs as anion exchanging groups.

Alkaline stability of many different QA groups was investigated by Marino et al. [118] for temperatures up to 160 °C and NaOH concentrations up to 10 mol/L with the aim to provide a basis for the selection of functional groups for AEMs. Most QAs exhibit unexpectedly high alkaline stability with the exception of aromatic cations. β-hydrogens are found to be far less susceptible to nucleophilic attack than previously suggested, whereas the presence of benzyl groups, nearby hetero-atoms, or other electron-withdrawing species promotes degradation reactions significantly. It is to remind that Hofmann elimination when β-hydrogens are present and direct nucleophilic attack by OH^- ion at the cationic site were for long time the most suggested AEM degradation mechanisms. Cyclic QAs proved to be exceptionally stable, with piperidinium-based cation featuring the highest half-life at the chosen conditions (Fig. 1.11).

Overall the degradation rate of quaternary ammonium (QA) groups increases dramatically both with OH^- concentration and temperature. It is important to mention that ex-situ alkali stability tests may not be necessarily representative of the AEMs stability in real fuel cell systems, where the membranes have to endure dehydration cycles [19] and might show reduced stability. This shows the importance of sufficient hydration of AEMs in alkaline fuel cells for achieving long durability.

A large number of AEMs have been synthesized using different combinations of polymer backbones and cationic functional groups for AEMFC. The results have been compiled over the last decade for different functional groups. An increasing

Table 1. Half-life of QA compounds at $T = 160\,^{\circ}C$ in 6 M NaOH with electron-withdrawing and electron-donating substituents compared to a neutral BTM, BTE, and the TMA benchmark (entries 1–5) and DABCO- (entries 6 and 7) and piperidinium-based QAs (entries 8 and 9) with and without a benzylic group.

Entry	QA	Abbreviation[a]	Half-life [h]
1		TMA	61.9
2		MBTM	16.6
3		BTM	4.18
4		BTE	0.68
5		NBTM	0.66
6		MAABCO	13.5
7		BAABCO	1.4
8		DMP	87.3
9		BMP	7.3

[a] TMA: tetramethylammonium; MBTM: 3-methoxy-benyzl trimethyl ammonium; BTM: benzyltrimethylammonium; BTE: benzyltriethylammonium; NBTM: 3-nitrobenyzltrimethylammonium; MAABCO: 1-methyl-4-aza-1-azonia-bicyclo[2.2.2]octane; BAABCO: 1-benzyl-4-aza-1-azonium-bicyclo[2.2.2]octane; DMP: *N,N*-dimethylpiperidinium; BMP: *N*-benzyl-*N*-methylpiperidinium.

Table 2. Half-lifes of BTM and various aromatic QA compounds at different temperatures in 6 M NaOH.

Entry	QA	Abbreviation[a]	Half-life [h]	*T* [°C]
1		BTM	4.18	160
2		PhTM	0.14	160
3		TMI	too short to measure	160
4	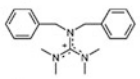	DTG	too short to measure	160
5		MOI	too short to measure	60
6	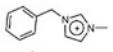	BMI	too short to measure	25
7		BP	too short to measure	25

[a] PhTM: phenyltrimethylammomnium; TMI: 1,2,3-trimethylimidazolium; DTG: 1,1-dibenzyl-2,2,3,3-tetramethylguaninidinium; MOI: 1-methyl-3-octylimidazolium; BMI: 1-benzyl-3-methylimidazolium; BP: *N*-benzylpyridinium.

Fig. 1.11 Half-life of quaternary ammonium (QA) compounds in 6 M NaOH (reproduced from Ref [118] with kind permission of © Elsevier)

number of studies succeeded to show good performance from cells made of improved materials developed for AEMFC technology. Pan et al. [19] made a comprehensive review and compiled fuel cell performance. Figure 1.12 shows performance and stability data for some of the best performing AEM.

The highest performance obtained was for AEM based on vinylbenzyl chloride (VBC) radiation grafted onto poly(ethylene-cotetrafluoroethylene) (ETFE) films followed by amination with trimethylamine that shows a very impressive peak power density of 1.4 W/cm^2. Nevertheless, and in spite of the many published reports with AEMFC performance test data, there are only a very few research studies reported in the literature of AEMFCs showing performance data of cells completely free of Pt (in both anode and cathode) and very few studies on cell performance stability which remains a challenge for the commercialization of AEMFC technology.

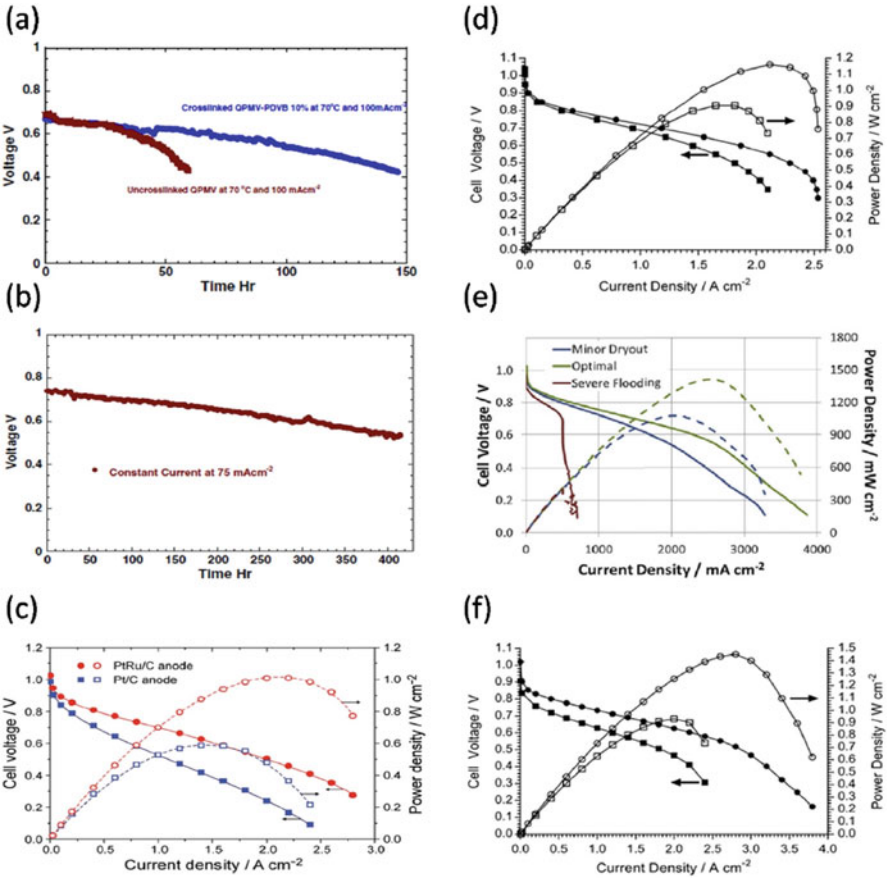

Fig. 1.12 Best performing H_2-AEMFCs from recent literature (reproduced from Ref [19], kind permission of © Elsevier). (**a**) Durability tests of uncrosslinked QPMV and 10% crosslinked QPMV-PDVBAAEM at 70 °C. (**b**) Durability test of 10% crosslinked AAEM at 50 °C [122]. (**c**) Cell performance of the AEMFC using the PtRu anode or Pt anode [61]. (**d**) Performance of H_2/O_2 AEMFC test data at 60 °C for E-R (squares) and E-6 (circles) using PtRu/C anodes and Pt/C cathodes and with no gas back-pressurization of the fully humidified gases [60]. (**e**) Performance of the AEMFC with different hypothesized distribution of water across the AEM and electrodes in an AEMFC [21]. (**f**) Performance of H_2/O_2 AEMFC at 80 °C with the LDPE-AEM with Pt/C (circles) or Ag/C (squares) as cathodes as well as PtRu/C anode [123]. (**a**, **b**, **e**: reproduced with kind permission of © Elsevier; **c**, **d**, **f**: reproduced with kind permission of © The Royal Society of Chemistry)

Finally, for all ionomers developed for PEM or AEM application, composite or blend membranes have been studied extensively in an attempt to compensate for some of the disadvantages of purely polymeric membranes. Functionalized or non-functionalized inorganic fillers have been incorporated to provide additional ions acceptor/donor sites, bind and retain water molecules at higher temperature, enhance ionic conductivity, improve mechanical properties, or have radical

scavenging effect to extend membranes lifetime. Polymer blending is also a promising method for inducing a microphase separation in membranes, controlling the swelling, and reinforcing mechanically the ionomer. In both cases compatibility of composite and blend materials with the host ionomer is critical.

1.5 Electrocatalytic Reactions in Proton Exchange Membrane (PEM) Fuel Cells

The operation of proton exchange membrane fuel cells (PEMFC) is based on the electrochemical reactions which occur at the interface "catalytic layer-electrolyte.". These reactions are the oxidation of the fuel at the anode and the reduction of the oxidant at the cathode. In practice, the electric efficiency of fuel cell depends on the current density j delivered by the cell. This efficiency is lower than that of the equilibrium reversible at $j = 0$ because of the irreversibility of the electrochemical reactions at the electrodes. Therefore, the cell voltage E_{cell} at $j \neq 0$ is expressed as follows:

$$E_{\text{cell}}(j) = E^{\circ}_{\text{eq}}(j = 0) - (|\eta_a| + |\eta_c| + R_e|j|) \tag{1.24}$$

where R_e is the cell resistance, $E^{\circ}_{\text{eq}}(j = 0)$, the cell voltage at $j = 0$, η_a and η_c are the overpotentials at the anode and the cathode, respectively.

It clearly appears that lower is the overpotential value better is the cell voltage. Therefore, progress in fuel cell is mostly focused on the decrease of the overpotential at the electrode and improves considerably the activity by developing new type of materials. In addition, the decrease of the electrode materials cost is a challenge since most of active materials are expensive noble metals mainly the platinum group metals.

Since this discovery, progress and improvements in this system were possible due to the innovations in various domains (nanotechnology, mechanical engineering, chemistry, electrochemistry, fluid management, etc.) which permitted to enhance substantially the performance of the cells. The last 30 years, the metal loading in the catalytic layer of PEMFCs has been divided by more 100. This improvement was due to the amazing progress in nanomaterials fabrication and also in the engineering of producing membrane electrodes assemblies (MEA). During the two last decays, various methods (chemical and physical) were adapted for elaborating very fine disseminated nanoparticles on the usual carbon support [124]. In addition, different types of carbon (such as carbon nanotubes, porous carbon, and recently graphene) were proposed as a support for nanocatalysts in order to avoid the corrosion and to improve the electron transfer observed on the usual carbon Vulcan XC 72 or 72R during the cell operation.

At the anode, various compounds can be used as fuel in PEMFCs. Up to date the operation conditions of the proton exchange membrane fuel cells have permitted to

investigate the hydrogen, formic acid, and various alcohols such as methanol, ethanol, glucose, hydrogen but also the formic acid and some alcohols.

1.5.1 Reactions of Fuel at the Anode of PEMFCs

1.5.1.1 Case of H_2

Hydrogen appears as the greenest fuel since its oxidation leads to water and heat. Under acidic environment, the H_2/O_2 fuel cell operates with the electrooxidation of H_2 at the anode and the oxygen reduction reaction at the cathode. It is well known that the kinetics of hydrogen oxidation reaction (HOR) is very fast mainly on platinum electrode. The half-cell reaction is as follows:

$$H_2 \rightarrow 2H^+ + 2e^- \qquad E^\circ = 0.000 \text{ V vs.SHE} \tag{1.25}$$

At the interface of the anode, the formed protons diffuse by migration through the polymer electrolyte membrane to the cathode where they react with the oxygen to produce water. In electrocatalysis, this reaction is taken as a model to explain mechanism of adsorption/desorption, diffusion, since it involves one electron per hydrogen atom. The overpotential η_a observed for the H_2 electrode is very small. Thereby, it can be approximated by the linear relationship with j as follows: $\eta_a = R_t j$, where R_t is called the charge transfer resistance [125].

Due to its presence at the anode of H_2/O_2 fuel cell, the HOR is deeply studied for understanding the different pathways when the reaction occurs on Pt electrodes. A pioneer work was done at the end of 1980s by Ticianelli et al. [126] with high metal loading (as 4 $mg_{Pt}\,cm^{-2}$) in a complete H_2/O_2 cell. Presently only few $\mu g_{Pt}\,cm^{-2}$ are enough to reach a highest cell performance [127, 128]. The study of HOR requires RDE measurements. Extensive study of this reaction was made by Croissant et al. [129] with different metal loadings from 0 to 0.3 $mg_{Pt}\,cm^{-2}$. These authors demonstrated the catalyst loading of 150 $\mu g\,cm^{-2}$ is the maximum value which below the evolution of the exchange current density is linear.

The reaction (1.25) can be expressed in three elementary reaction steps:

$$H_2 + \ 2\,Pt \leftrightarrow 2\,H_{ads} - Pt \qquad \text{Tafel reaction} \tag{1.26}$$

$$H_2 + Pt \leftrightarrow H_{ads} - Pt + H^+ + e^- \qquad \text{Heyrovsky reaction} \tag{1.27}$$

$$H_{ads} - Pt \leftrightarrow Pt + H^+ + e^- \qquad \text{Volmer reaction} \tag{1.28}$$

where H_{ads} is the adsorbed hydrogen atom as an adatom.

The dissociative adsorption of a hydrogen molecule is followed by two separate one-electron oxidations of the H_{ads} in the case of Tafel–Volmer pathway, while for the Heyrovsky–Volmer pathway, two one-electron oxidation occur. The first one is held simultaneously with chemisorption and the second one is the oxidation of H_{ads}.

To explain the HOR current behavior in the entire overpotential region relevant to the reaction, Wang et al. [130] have developed a dual-pathway kinetic equation which fits perfectly with the high surface electrocatalysts operating at 80 °C in fuel cells conditions.

Despite the simplicity of the HOR, efforts have been made for modelling the reaction, decreasing the amount of the Pt loading, or for elaborating new and very active catalyst tolerant for CO. Indeed, more than 80% of the hydrogen produced come from partial oxidation or steam reforming of hydrocarbons. Thereby, H_2 produced from this process contains traces of CO. CO is also one of intermediates from the oxidation of organic molecules (methanol, ethanol, etc.) on Pt electrode [131]. CO molecule strongly adsorbs on the Pt active sites and greatly decreases the performance of the Pt anode in fuel cell. Therefore the oxidation of CO is one of the mostly studied reactions in electrocatalysis due to the poisoning effect observed. Two approaches are possible to oxidize CO molecule on Pt electrode: (1) apply a high potential, or modify the structure and the composition of Pt in order to oxidize CO at very low potential. This second approach is suitable for the operation conditions of fuel cells. Considering Eq. (1.29), CO molecule requires an external oxygen for its complete oxidation in acid medium. Therefore, electrochemists added to Pt a second metal able to provide oxygenated species at very low potentials.

$$CO + H_2O \rightarrow CO_2 + 2H^+ + 2e^- \tag{1.29}$$

Figure 1.13 shows the effect of Ru and Sn added to platinum on the oxidation of CO. Pt-Sn electrode oxidizes CO at a potentials values 600 mV lower than that of Pt bulk electrode.

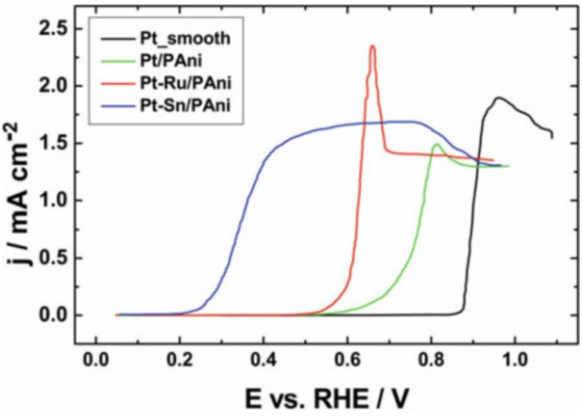

Fig. 1.13 Positive scan during the oxidation of CO on various Pt-based catalysts disseminated in a 0.5 µm thick of polyaniline film recorded in $HClO_4$ 0.1 moles L^{-1}, at room temperature and at 5 mV s^{-1}

1.5.1.2 Case of CH_3OH

The kinetics of alcohols oxidation on Pt in acid medium is low and leads to the formation of intermediates strongly adsorbed on the active sites. Therefore, the oxidation of some alcohols (i.e., methanol and ethanol) becomes the aim of several investigations in electrocatalysis.

For the some mobile applications of PEMFCs, H_2 is not suitable to hand and a liquid fuel appears the suitable solution. Therefore, organic fuels such as alcohols (i.e., methanol and ethanol) are proposed. However, the kinetics of their oxidation reactions is very slow because of the low operating temperature of the PEMFCs and the several steps involved. The oxidation of such alcohols occurs with very high overvoltages η_a (Fig. 1.14). Therefore, the challenges at the anode are to considerably decrease these overvoltages as indicated in Fig. 1.14.

The complete oxidation of methanol to CO_2 in acid medium is:

$$CH_3OH + H_2O \rightarrow CO_2 + 6\,H^+ + 6e^- \tag{1.30}$$

This oxidation is a six electrons transfer process which leads to several intermediates as extensively stated in the literature [131, 132]. During the oxidation of methanol on Pt catalysts, the cleavage of C–H bonds leads to the formation of the so-called formyl-like species $-(CHO)_{ads}$. This species can give $-CO_{ads}$, $-COOH_{ads}$, or directly CO_2. For oxidizing at low potential these three species to CO_2, or to avoid their formation, effective catalysts are needed. For promoting the oxidation of CH_3OH and its intermediates at low potential, other metals (Ru, Sn, Mo, Ni, Mo, etc.) are added to platinum to promote the formation of oxygenated species at low potentials [131–142]. Indeed, these metals can be oxidized at relatively low

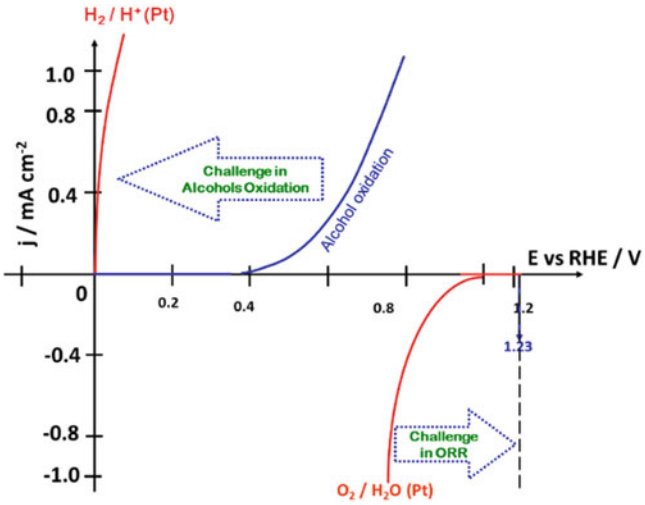

Fig. 1.14 Schematic drawing of the challenges at the electrodes of PEMFCs

potential. These materials activate and dissociate H_2O molecule while the organic molecule is adsorbed on Pt. Then a surface reaction involves the oxygenated species from the second metal and the organic adsorbed species will lead to the formation of CO_2. This surface reaction is known as a bifunctional mechanism which was suggested by Watanabe and Motoo [131, 143]. The structure, composition, and support of electrocatalyst are some parameters which are still studied for improving their performance towards the oxidation of methanol [132–146].

1.5.1.3 Case of CH_3CH_2OH

Ethanol is an attractive molecule which can be used directly in PEMFC system named direct ethanol fuel cell (DEFC). The complete oxidation of ethanol at the anode of DEFC is the following:

$$CH_3CH_2OH + 3H_2O \rightarrow 2CO_2 + 12\,H^+ + 12e^- \tag{1.31}$$

This reaction is complex since it involves theoretically 12 electrons transfer process which cannot be achieved in one step. The main challenge with this molecule is to break the C–C bond in order to complete the oxidation of challenge on this molecule is to the cleavage of the C–C bond. In reality, partial oxidation occurs leading to the two main products, the soluble acetaldehyde and the acetic acid. The reaction has been widely investigated mainly by in situ FTIR [147–149]. This technique permits to reveal the enhancement of catalysts. Up to now, Pt is the main element of electrode materials developed for the oxidation of ethanol. To avoid the partial oxidation pathway reactions, bi and trimetallic catalysts have been proposed [144, 147–183]. Pt-Sn/C is the electrode materials which exhibited high catalytic activity towards the oxidation of ethanol. However, a third element is required to improve the dehydrogenation reaction and also the cleavage of the C–C bond. The addition of Ni on PtRu/C and PtSn/C significantly increases the catalytic activity of these nanomaterials [177]. In the literature, various electrode materials have been proposed for the electrooxidation of ethanol, but few of them have a significant improvement compared to the platinum electrode. Effective electrocatalysts have to be developed.

1.5.1.4 Reaction at the Cathode: Oxygen Reduction Reaction (ORR)

The reaction which occurs at the cathode of all PEMFCs is the electrochemical reduction of molecular oxygen known as oxygen reduction reaction (ORR). In acid medium, the reaction is:

$$O_2 + 4H^+ + 4\,e^- \rightarrow 2H_2O \tag{1.32}$$

This reaction is complicated since it involves many intermediates which depend on the electrolyte, the nature, composition, and structure of electrode materials. The reduction of molecular oxygen in water involves four electrons. Damjanovic et al. [184] and later Wroblowa et al. [185] have made a pioneer investigation and suggested the mechanism explaining the different intermediates observed during the ORR. They pointed out the multi-electron transfer process and the main two-electron pathway which leads to the formation of hydrogen peroxide. According to the schematic drawing (Fig. 1.14), it appears that the ORR shows the sluggish reaction kinetics and the assessment of the intermediates is an important and key step for improving the catalytic performance of electrode materials. Several studies by rotating disk (RDE) and rotating ring disk (RRDE) electrodes have permitted to reach the kinetics parameters of the reaction on various catalysts [186–188]. The development of nanomaterials has permitted to improve the performance of the cathode materials due to their high surface to volume ratio. The most active material for ORR is platinum due to the bonding energy of some species like O and OH with its surface [189]. The RDE measurements are a useful technique for evaluating the electrocatalytic behavior of electrode materials for a reaction limited by the diffusion. It required three-electrode cell while for the RRDE, four electrodes system with a bi-potentiostat is required. Indeed, a part the reference and the counter electrodes, two working electrodes is needed. One (the disk) is the catalyst to be studied and the second (ring) to detect directly the amount of hydrogen peroxide produced during the reaction.

As ORR is limited by the diffusion, two conditions are needed to validate the Levich law: (1) the existence of a mass transport process that is the rate-determining step (rds), and (2) the reaction is of a first-order reaction with respect to the electro-reactive species (O_2). Afterwards, to apply the Koutecky–Levich equation, two conditions are required: (1) the existence of an electron transfer process that is the rate-determining step (rds), (2) the reaction is of a first-order reaction with respect to the electro-reactive species (O_2). The equations and the treatment of the data will not be exposed in this chapter. It is extensively detailed in the literature [188]. Figure 1.15 shows the polarization curves obtained for Pt and Pt-Cr/C catalysts in O_2 saturated acid medium and corresponding Tafel slopes. The polarization.

In respect to the four important criteria for using Levich and Koutecky–Levich equations, typical Koutecky–Levich plots are shown in Fig. 1.16.

As mentioned above the RRDE measurements permit to assess directly the H_2O_2 amount (Fig. 1.17). The fraction of hydrogen peroxide for the Pt-Cr/C is lower than that of Pt/C. The number of electrons involved is close to 4.

The ORR investigations by RRDE permit to assess the main parameters such as the number of electrons involved, the kinetic current density, the exchange current density, the limiting current density, and the Tafel slope in different potential regions. From the bulk materials to the dispersed nanoparticles, the ORR is a key reaction which still needs the development of new electrode materials [191, 192].

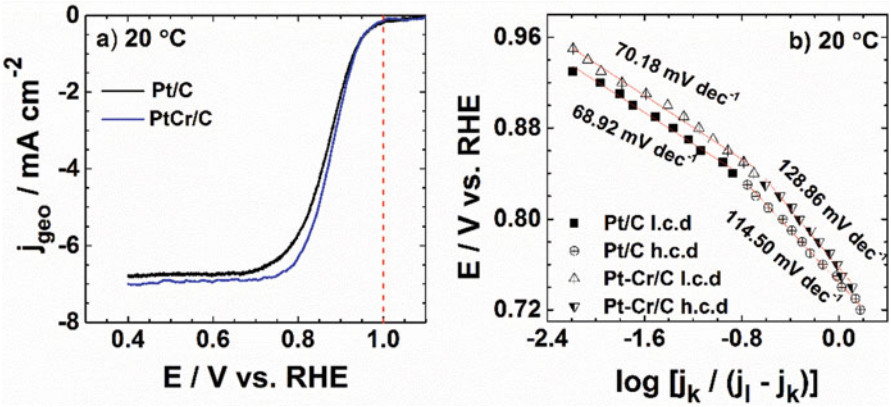

Fig. 1.15 RDE polarization curves of the Pt/C and PtCr/C electrocatalysts in a O_2-saturated 0.1 mol L^{-1} $HClO_4$ solution recorded at 1600 rpm, 5 mV s-1 and (**a**) 20 °C, (**b**) Tafel plots of oxygen reduction reaction on Pt/C and PtCr/C in 0.1 mol L^{-1} $HClO_4$ recorded at 5 mV s^{-1} and 20 °C for low current density (l.c.d) and high current density (h.c.d) region. Reproduced and adapted from Ref. [190] with kind permission of Elsevier©

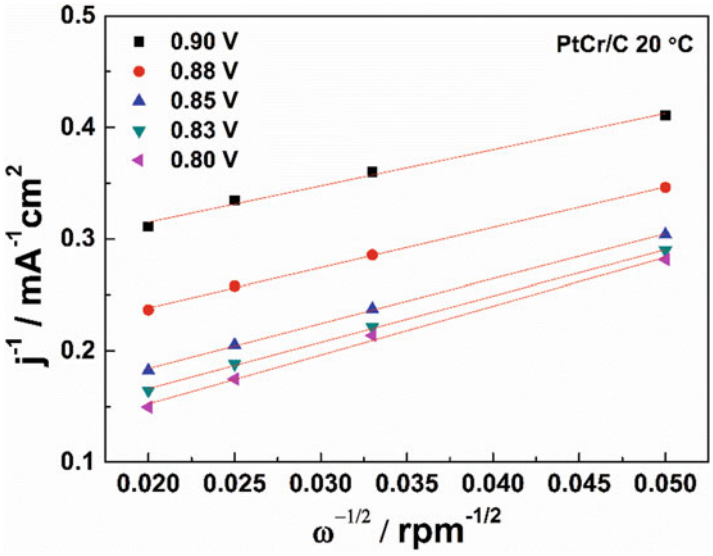

Fig. 1.16 Koutecky–Levich plots (inverse of the current density j versus inverse of the square root of rotation rate ω) of PtCr/C at 20 °C, in 0.1 mol L^{-1} $HClO_4$

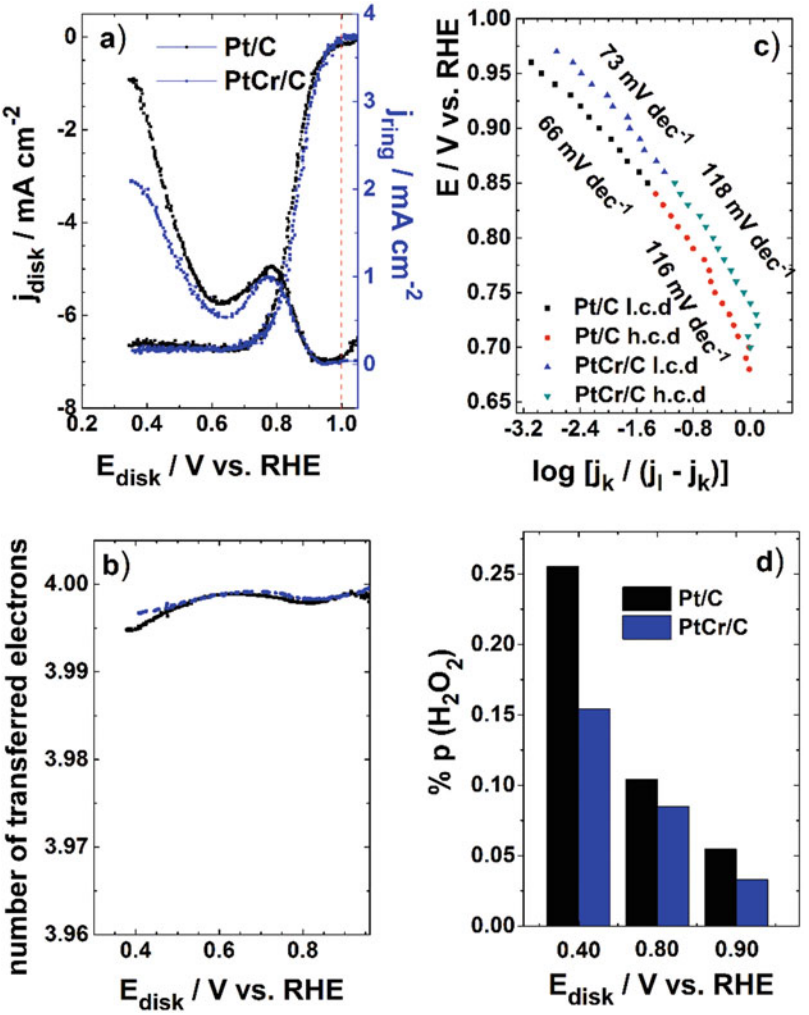

Fig. 1.17 Hydrodynamic voltammograms related to ORR for Pt/C and PtCr/C in a O_2-saturated 0.1 mol L^{-1} $HClO_4$ solution recorded at 5 mV s^{-1} and 1600 rpm. (**a**) Ring electrode and disk electrode current density, (**b**) average number of transferred electrons, (**c**) Tafel plots for low current density (l.c.d) and high current density (h.c.d) regions, and (**d**) fraction of peroxide from the oxygen reduction reaction detected on the ring electrode at 0.90, 0.80, and 0.40 V vs. RHE. From Ref. [190] with kind permission of Elsevier©

1.6 Performance of New Class of Electrode Materials for Proton Exchange Membrane (PEM) Fuel Cells

Both bottom up and top down approaches are used for developing new class of nanomaterials for fuel cell systems in order to considerably increase their performance and durability, but decrease considerably the metal loading. Therefore, oxide materials suggested a support for anode or cathode materials. Figure 1.18 shows three ceria-based anode catalysts prepared with different Pt contents of 0.6, 2, and 4 μg Pt/cm^2 of MEA (the samples denoted 0.6-Pt/Ce, 2-Pt/Ce, and 4-Pt/Ce), and the sputtered reference pure Pt film of 2 μg Pt/cm^2 (2-Pt), all deposited on the nGDL. In a H_2/O_2 fuel cell, the power density of an anode with 2 μg_{Pt} cm^{-2} on ceria is close to that of 2 mg of Pt [193]. The possibility of dividing by 1000 the Pt loading will permit to decrease considerably the cost of the electrodes.

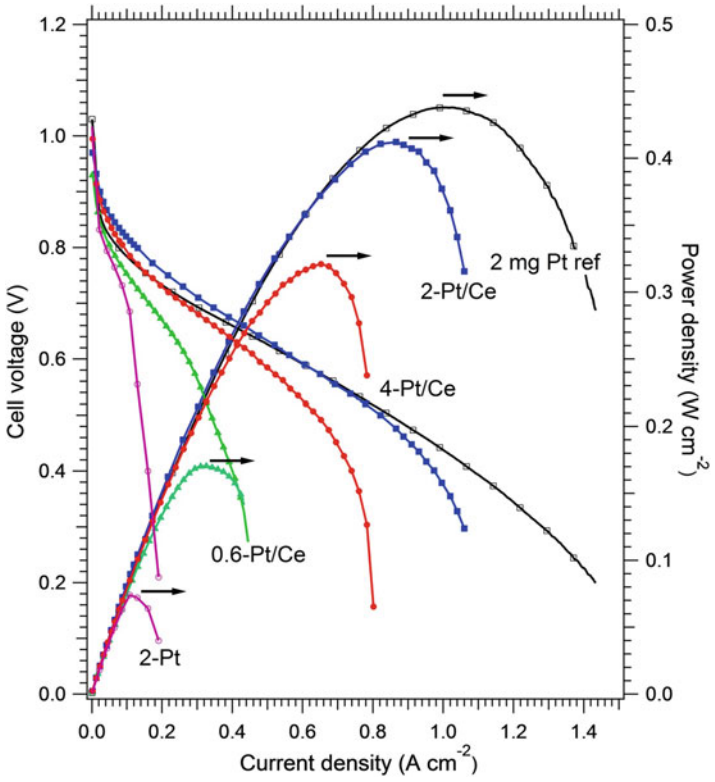

Fig. 1.18 The polarization *J–V* curves (left Y-axis) and the corresponding power density (right Y-axis) measured for the three ceria-based anode catalysts prepared with different Pt contents of 0.6, 2, and 4 μg Pt/cm^2 of MEA (the samples denoted 0.6-Pt/Ce, 2-Pt/Ce, and 4-Pt/Ce), and the sputtered reference pure Pt film of 2 μg Pt/cm^2 (2-Pt), all deposited on the nGDL. For comparison the data obtained on the commercial Pt/GDL catalyst (2 mg Pt ref) are added. From ref. [193] with kind permission of Elsevier©

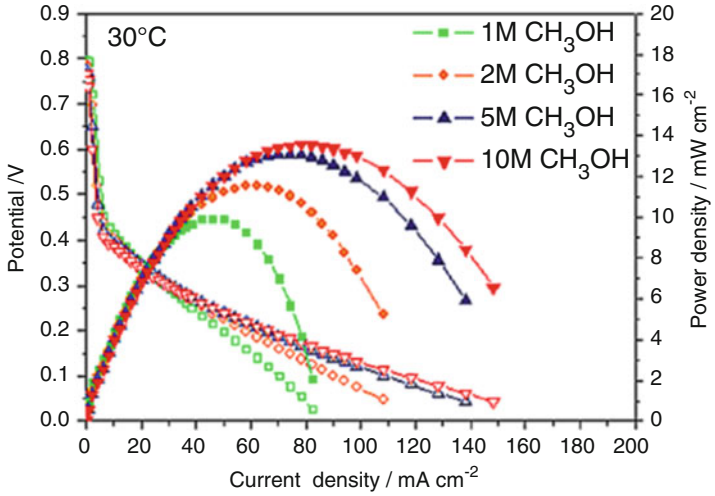

Fig. 1.19 Influence of methanol molarity on DMFC polarization (empty symbols) and power density (filled symbols) curves at 30 °C using the Fe-Nx-C-THT catalyst at the cathode (4.5–-0.2 mg cm^{-2}). Membrane: Nafion® 115. Anode: 1 mg_{PtRu} cm^{-2}. From Ref. [194] with kind permission of copyright Wiley

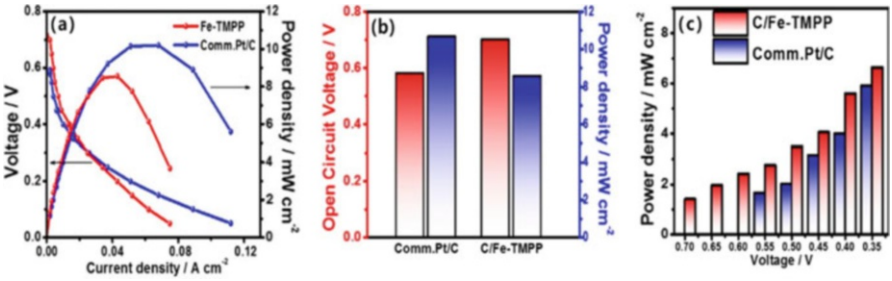

Fig. 1.20 (**a**) Polarization curves of the DEFCs with C/Fe-TMPP and Pt/C as cathode catalysts and PtRu as an anode catalyst supplied with 2 M EtOH and humidified O_2 gas at the anode and cathode, respectively, at 80 °C. (**b**) Comparison of OCVs and maximal power densities of the DEFCs with C/Fe-TMPP and Pt/C. (**c**) Comparison of power densities of the DEFCs with C/Fe-TMPP and Pt/C measured in the potential range of 0.70–0.35 V. From ref. [195] with kind permission of Copyright © 2018 American Chemical Society

One phenomenon which occurs in direct alcohol fuel cells is the crossover of the organic fuel to the cathode. Indeed, the presence of the fuel at the cathode leads to its deactivation. Therefore, cathode with high tolerance to the fuel is required. Figure 1.19 presents the polarization curves of DMFC using Fe-N-C-based catalyst as cathode.

Figure 1.20 shows the performance of a DEFC using a doped carbon nanostructure containing Fe. The DEFC supplied with high concentration of ethanol exhibited

high performance with this cathode. This performance can be attributed to ethanol tolerance in the oxygen reduction reaction [195].

1.7 Conclusion

The last 30 years, progresses have been made in the development of PEMFCs and AEMFCs. In terms of electrode materials, innovation in materials synthesis leads to the fabrication of new class of nanomaterials for anode and cathode of PEMFCs and AEMFCs. For the PEMFCs the metal loadings have been considerably decreased. Various noble metal-free cathodes are suggested for these fuel cells taking into account their tolerance to the liquid fuels such as alcohols and formic acid. For the DMFCs and DEFCs, effective anode nanomaterials are also suggested. AEMFCs are emerging due to the recent development of anion exchange membranes. These membranes offer the possibility to build compact alkaline fuel cells with low-cost materials.

Innovation in materials sciences, nanotechnology, and mechanical engineering is needed to develop powerful PEMFCs and AEMFCs that will be widely available for the world.

References

1. Perry ML, Fuller TF (2002) A historical perspective of fuel cell technology in the 20th century. J Electrochem Soc 149:S59–S67
2. Stone C, Morrison AE (2002) From curiosity to -power to change the world®. Solid State Ionics 152–153:1–13
3. Rodríguez-Varela FJ (2014) Fuel cells, components and systems for space technology applications. Recent Prog Space Technol 4:14–20
4. Gülzow E (2004) Alkaline fuel cells. Fuel Cells 4:251–255
5. https://www.energy.gov/sites/prod/files/2015/11/f27/fcto_fuel_cells_fact_sheet.pdf. Accessed 14 Apr 2018
6. Dekel DR (2018) Review of cell performance in anion exchange membrane fuel cells. J Power Sources 375:158–169
7. Hossen MM, Artyushkova K, Atanassov P, Serov A (2018) Synthesis and characterization of high performing Fe-N-C catalyst for oxygen reduction reaction (ORR) in alkaline exchange membrane fuel cells. J Power Sources 375:214–221
8. Osmieri L, Escudero-Cid R, Monteverde Videla AHA, Ocón P, Specchia S (2018) Application of a non-noble Fe-N-C catalyst for oxygen reduction reaction in an alkaline direct ethanol fuel cell. Renew Energy 115:226–237
9. Ratso S, Kruusenberg I, Käärik M, Kook M, Puust L, Saar R, Leis J, Tammeveski K (2018) Highly efficient transition metal and nitrogen co-doped carbide-derived carbon electrocatalysts for anion exchange membrane fuel cells. J Power Sources 375:233–243
10. Lenarda A, Bellini M, Marchionni A, Miller HA, Montini T, Melchionna M, Vizza F, Prato M, Fornasiero P (2018) Nanostructured carbon supported Pd-ceria as anode catalysts for anion exchange membrane fuel cells fed with polyalcohols. Inorg Chim Acta 470:213–220

11. Basumatary P, Konwar D, Soo Yoon Y (2018) A novel NiCu/ZnO@MWCNT anode employed in urea fuel cell to attain superior performances. Electrochim Acta 261:78–85
12. Qin H, Lin L, Chu W, Jiang W, He Y, Shi Q, Deng Y, Ji Z, Liu J, Tao S (2018) Introducing catalyst in alkaline membrane for improved performance direct borohydride fuel cells. J Power Sources 374:113–120
13. Miller HA, Ruggeri J, Marchionni A, Bellini M, Pagliaro MV, Bartoli C, Pucci A, Passaglia E, Vizza F (2018) Improving the energy efficiency of direct formate fuel cells with a Pd/C-CeO_2 anode catalyst and anion exchange ionomer in the catalyst layer. Energies 11:369–380
14. Muneeb O, Do E, Tran T, Boyd D, Huynh M, Ghosn G, Haan JL (2017) A direct ascorbate fuel cell with an anion exchange membrane. J Power Sources 351:74–78
15. Wagner K, Tiwari P, Swiegers GF, Wallace GG (2018) Alkaline fuel cells with novel gortex-based electrodes are powered remarkably efficiently by methane containing 5% hydrogen. Adv Energy Mater 8:1702285
16. Ziv N, Mustain WE, Dekel DR (2018) Review of ambient CO_2 effect on anion exchange membranes fuel cells. ChemSusChem 11:1–16
17. Piana M, Boccia M, Filpi A, Flammia E, Miller HA, Orsini M, Salusti F, Santiccioli S, Ciardelli F, Pucci A (2010) H_2/air alkaline membrane fuel cell performance and durability, using novel ionomer and non-platinum group metal cathode catalyst. J Power Sources 195:5875–5881
18. Slade RCT, Kizewski JP, Poynton SD, Zeng R, Varcoe JR (2013) Alkaline membrane fuel cells. In: Kreuer KD (ed) Selected entries from the encyclopedia of sustainability science and technology. Springer, New York, pp 9–29
19. Pan ZF, An L, Zhao TS, Tang ZK (2018) Advances and challenges in alkaline anion exchange membrane fuel cells. Prog Energy Combust Sci 66:141–175
20. Sun Z, Lin B, Feng Yan F (2018) Anion-exchange membranes for alkaline fuel-cell applications: the effects of cations. ChemSusChem 11:58–70
21. Omasta TJ, Wang L, Peng X, Lewis CA, Varcoe JR, Mustain WE (2018) Importance of balancing membrane and electrode water in anion exchange membrane fuel cells. J Power Sources 375:205–213
22. Wang L, Brink JJ, Varcoe JR (2017) The first anion-exchange membrane fuel cell to exceed 1 W cm^{-2} at 70 °C with a non-Pt-group (O_2) cathode. Chem Commun 53:11771–11773
23. Gao X, Yu H, Jia J, Hao J, Xie F, Chi J, Qin B, Fu L, Song W, Shao X (2017) High performance anion exchange ionomer for anion exchange membrane fuel cells. RSC Adv 7:19153–19161
24. Gottesfeld S, Dekel DR, Page M, Bae C, Yan Y, Zelenay P, Kim YS (2018) Anion exchange membrane fuel cells: current status and remaining challenges. J Power Sources 375:170–184
25. Strmcnik D, Uchimura M, Wang C, Subbaraman R, Danilovic N, van der Vliet D, Paulikas AP, Stamenkovic VR, Markovic NM (2013) Improving the hydrogen oxidation reaction rate by promotion of hydroxyl adsorption. Nat Chem 5:300–306
26. Miller HA, Lavacchi A, Vizza F, Marelli M, Di Benedetto F, D'Acapito F, Paska Y, Page M, Dekel DR (2016) A Pd/C-CeO_2 anode catalyst for high-performance platinum-free anion exchange membrane fuel cells. Angew Chem Int Ed Engl 55:6004–6007
27. Wang Y, Li L, Hu L, Zhuang L, Lu J, Xu B (2003) A feasibility analysis for alkaline membrane direct methanol fuel cell: thermodynamic disadvantages versus kinetic advantages. Electrochem Commun 5:662–666
28. Hao Yu E, Scott K (2004) Development of direct methanol alkaline fuel cells using anion exchange membranes. J Power Sources 137:248–256
29. Kim JH, Kim HK, Hwang KT, Lee JY (2010) Performance of air-breathing direct methanol fuel cell with anion-exchange membrane. Int J Hydrog Energy 35:768–773
30. Matsuoka K, Iriyama Y, Abe T, Matsuoka M, Ogumi Z (2005) Alkaline direct alcohol fuel cells using an anion exchange membrane. J Power Sources 150:27–31
31. Bambagioni V, Bianchini C, Marchionni A, Filippi J, Vizza F, Teddy J, Serp P, Zhiani M (2009) Pd and Pt–Ru anode electrocatalysts supported on multi-walled carbon nanotubes and

their use in passive and active direct alcohol fuel cells with an anion-exchange membrane (alcohol = methanol, ethanol, glycerol). J Power Sources 190:241–251
32. An L, Zhao TS (2017) Transport phenomena in alkaline direct ethanol fuel cells for sustainable energy production. J Power Sources 341:199–211
33. Wang F, Qiao J, Wu H, Qi J, Li W, Mao Z, Wang Z, Sun W, Rooney D, Sun K (2017) Bioethanol as a new sustainable fuel for anion exchange membrane fuel cells with carbon nanotube supported surface dealloyed PtCo nanocomposite anodes. Chem Eng J 317:623–631
34. Dutta A, Datta J (2012) Outstanding catalyst performance of PdAuNi nanoparticles for the anodic reaction in an alkaline direct ethanol (with anion-exchange membrane) fuel cell. J Phys Chem C 116:25677–22568
35. Fujiwara N, Siroma Z, Yamazaki S, Ioroi T, Senoh H, Yasuda K (2008) Direct ethanol fuel cells using an anion exchange membrane. J Power Sources 185:621–626
36. Li YS, Zhao TS (2016) A passive anion-exchange membrane direct ethanol fuel cell stack and its applications. Int J Hydrog Energy 41:20336–20342
37. Livshits V, Philosoph A, Peled E (2008) Direct ethylene glycol fuel-cell stack—study of oxidation intermediate products. J Power Sources 178:687–691
38. Demirci UB (2009) How green are the chemicals used as liquid fuels in direct liquid-feed fuel cells? Environ Int 35:626–631
39. An L, Zeng L, Zhao TS (2013) An alkaline direct ethylene glycol fuel cell with an alkali-doped polybenzimidazole membrane. Int J Hydrog Energy 38:10602–10606
40. Matsumoto T, Sadakiyo M, Lee Ooi M, Kitano S, Yamamoto T, Matsumura S, Kato K, Takeguchi T, Yamauchi M (2014) CO_2-free power generation on an iron group nanoalloy catalyst via selective oxidation of ethylene glycol to oxalic acid in alkaline media. Sci Rep 4:5620
41. Cremers C, Niedergesäß A, Jung F, Müller D, Tübke J (2011) Development of an alkaline anion exchange membrane direct ethylene glycol fuel cell stack. ECS Trans 41:1987–1996
42. de Souza LL, Neto AO, de O. Forbicini CALG (2017) Direct oxidation of ethylene glycol on PtSn/C for application in alkaline fuel cell. Int J Electrochem Sci 12:11855–11874
43. An L, Zhao TS, Shen SY, Wu QX, Chen R (2010) Performance of a direct ethylene glycol fuel cell with an anion-exchange membrane. Int J Hydrog Energy 35:4329–4335
44. An L, Chen R (2016) Recent progress in alkaline direct ethylene glycol fuel cells for sustainable energy production. J Power Sources 329:484–501
45. Chen Y, Bellini M, Bevilacqua M, Fornasiero P, Lavacchi A, Miller HA, Wang L, Vizza F (2015) Direct alcohol fuel cells: toward the power densities of hydrogen-fed proton exchange membrane fuel cells. ChemSusChem 8:524–533
46. Qi J, Benipal N, Liang C, Li W (2016) PdAg/CNT catalyzed alcohol oxidation reaction for high-performance anion exchange membrane direct alcohol fuel cell (alcohol = methanol, ethanol, ethylene glycol and glycerol). Appl Catal B Environ 199:494–503
47. Ottoni CA, Ramos CED, de Souza RFB, da Silva SG, Spinacé EV, Neto AO (2018) Glycerol and ethanol oxidation in alkaline medium using PtCu/C electrocatalysts. Int J Electrochem Sci 13:1893–1904
48. Ilie A, Simoes M, Baranton S, Coutanceau C, Martemianov S (2011) Influence of operational parameters and of catalytic materials on electrical performance of direct glycerol solid alkaline membrane fuel cells. J Power Sources 196:4965–4971
49. Xin L, Zhang Z, Wang Z, Li W (2012) Simultaneous generation of mesoxalic acid and electricity from glycerol on a gold anode catalyst in anion-exchange membrane fuel cells. ChemCatChem 4:1105–1114
50. Qi J, Xin L, Chadderdon DJ, Qiu Y, Jiang Y, Benipal N, Liang C, Li W (2014) Electrocatalytic selective oxidation of glycerol to tartronate on au/C anode catalysts in anion exchange membrane fuel cells with electricity cogeneration. Appl Catal B Environ 154–155:360–368
51. Qi J, Xin L, Zhang Z, Sun K, He H, Wang F, Chadderdon D, Qiu Y, Liang C, Li W (2013) Surface dealloyed PtCo nanoparticles supported on carbon nanotube: facile synthesis and

promising application for anion exchange membrane direct crude glycerol fuel cell. Green Chem 15:1133–1137
52. Zhiani M, Rostami H, Majidi S, Karami K (2013) Bis (dibenzylidene acetone) palladium (0) catalyst for glycerol oxidation in half cell and in alkaline direct glycerol fuel cell. Int J Hydrog Energy 38:5435–5441
53. Napoleão Geraldes A, da Silva DF, de Andrade e Silva LG, Spinacé EV, Neto AO, dos Santos MC (2015) Binary and ternary palladium based electrocatalysts for alkaline direct glycerol fuel cell. J Power Sources 293:823–830
54. Benipal N, Qi J, Liu Q, Li W (2017) Carbon nanotube supported PdAg nanoparticles for electrocatalytic oxidation of glycerol in anion exchange membrane fuel cells. Appl Catal B Environ 210:121–130
55. Zhang Z, Xin L, Li W (2012) Supported gold nanoparticles as anode catalyst for anion-exchange membrane-direct glycerol fuel cell (AEM-DGFC). Int J Hydrog Energy 37:9393–9401
56. Wang Z, Xin L, Zhao X, Qiu Y, Zhang Z, Baturina OA, Li W (2014) Carbon supported ag nanoparticles with different particle size as cathode catalysts for anion exchange membrane direct glycerol fuel cells. Renew Energy 62:556–562
57. Fashedemi OO, Miller HA, Marchionni A, Vizza F, Ozoemena KI (2015) Electro-oxidation of ethylene glycol and glycerol at palladium-decorated FeCo@Fe core–shell nanocatalysts for alkaline direct alcohol fuel cells: functionalized MWCNT supports and impact on product selectivity. J Mater Chem A 3:7145–7156
58. Han X, Chadderdon DJ, Qi J, Xin L, Li W, Zhou W (2014) Numerical analysis of anion-exchange membrane direct glycerol fuel cells under steady state and dynamic operations. Int J Hydrog Energy 39:19767–19779
59. Jamard R, Latour A, Salomon J, Capron P, Martinent-Beaumont A (2008) Study of fuel efficiency in a direct borohydride fuel cell. J Power Sources 176:287–292
60. Wang L, Magliocca E, Cunningham EL, Mustain WE, Poynton SD, Escudero-Cid R, Nasef MM, Ponce-González J, Bance-Souahli R, Slade RCT, Whelligan DK, Varcoe JR (2017) An optimised synthesis of high performance radiation-grafted anion-exchange membranes. Green Chem 19:831–843
61. Wang Y, Wang G, Li G, Huang B, Pan J, Liu Q, Han J, Xiao L, Lu J, Zhuang L (2015) Pt–Ru catalyzed hydrogen oxidation in alkaline media: oxophilic effect or electronic effect? Energy Environ Sci 8:177–181
62. Alesker M, Page M, Shviro M, Paska Y, Gershinsky G, Dekel DR, Zitoun D (2016) Palladium/nickel bifunctional electrocatalyst for hydrogen oxidation reaction in alkaline membrane fuel cell. J Power Sources 304:332–339
63. Mun Y, Kim MJ, Park SA, Lee E, Ye Y, Lee S, Kim YT, Kim S, Kim OH, Cho YH, Sung YE, Lee J (2018) Soft-template synthesis of mesoporous non-precious metal catalyst with Fe-Nx/C active sites for oxygen reduction reaction in fuel cells. Appl Catal B Environ 222:191–199
64. Hu Q, Li G, Pan J, Tan L, Lu J, Zhuang L (2013) Alkaline polymer electrolyte fuel cell with Ni-based anode and co-based cathode. Int J Hydrog Energy 38:16264–16268
65. Fang Y, Wang Y, Wang F, Shu C, Zhu J, Wu W (2018) Fe–Mn bimetallic oxides-catalyzed oxygen reduction reaction in alkaline direct methanol fuel cells. RSC Adv 8:8678–8687
66. Yang CC (2012) Alkaline direct methanol fuel cell based on a novel anion-exchange composite polymer membrane. J Appl Electrochem 42:305–317
67. Yang CC, Chiu SJ, Lin CT (2008) Electrochemical performance of an air-breathing direct methanol fuel cell using poly(vinyl alcohol)/hydroxyapatite composite polymer membrane. J Power Sources 177:40–49
68. Shu C, Song B, Wei X, Liu Y, Tan Q, Chong S, Chen YZ, Yang XD, Yang WH, Liu Y (2018) Mesoporous 3D nitrogen-doped yolk-shelled carbon spheres for direct methanol fuel cells with polymer fiber membranes. Carbon 129:613–620

69. Ge X, Sumboja A, Wuu D, An T, Li B, Thomas Goh FW, Andy Hor TS, Zong Y, Liu Z (2015) Oxygen reduction in alkaline media: from mechanisms to recent advances of catalysts. ACS Catal 5:4643–4667
70. Mokrini A, Raymond N, Theberge K, Robitaille L, Del Rio C, Ojeda MC, Garcia Escribano P, Acosta JL (2010) Properties of melt-extruded vs. solution-cast proton exchange membranes based on PFSA nanocomposites. ECS Trans 33:855–865
71. Allen FI, Comolli LR, Kusoglu A, Modestino MA, Minor AM, Weber AZ (2015) Morphology of hydrated as-cast nafion revealed through cryo electron tomography. ACS Macro Lett 4:1–5 (https://pubs.acs.org/doi/full/10.1021/mz500606h, further permissions should be directed to the ACS)
72. Kusoglu A, Weber AZ (2017) New insights into perfluorinated sulfonic-acid ionomers. Chem Rev 117:987–1104 (https://pubs.acs.org/doi/full/10.1021/acs.chemrev.6b00159, further permissions should be directed to the ACS)
73. Li J, Pan M, Tang H (2014) Understanding short-side-chain perfluorinated sulfonic acid and its application for high temperature polymer electrolyte membrane fuel cells. RSC Adv 4:3944–3965
74. Paddison SJ, Elliott JA (2006) The effects of backbone conformation on hydration and proton transfer in the short-side-chain perfluorosulfonic acid membrane. Solid State Ionics 177:2385–2390
75. Elliott JA, Paddison SJ (2007) Modelling of morphology and proton transport in PFSA membranes. Phys Chem Chem Phys 9:2602–2618
76. Tse YLS, Herring AM, Kim K, Voth GA (2013) Molecular dynamics simulations of proton transport in 3M and nafion perfluorosulfonic acid membranes. J Phys Chem C 117:8079–8091
77. Schaberg MS, Abulu JE, Haugen G, Emery MA, O'Conner SJ, Xiong PN, Hamrock S (2010) New multi acid side-chain ionomers for proton exchange membrane fuel cells. ECS Trans 33:627–633
78. Giffin GA, Haugen GM, Hamrock SJ, Di Noto V (2013) Interplay between structure and relaxations in perfluorosulfonic acid proton conducting membranes. J Am Chem Soc 135:822–834
79. Gierke TD, Munn GE, Wilson FC (1981) The morphology in nafion perfluorinated membrane products, as determined by wide-angle and small-angle X-ray studies. J Polym Sci Polym Phys 19:1687–1704
80. Tant MR, Darst KP, Lee KD, Martin CW (1989) Structure and properties of short-side-chain perfluorosulfonate ionomers. ACS Sym Ser 15:370–400
81. Moore RB, Martin CR (1989) Morphology and chemical- properties of the dow perfluorosulfonate ionomers. Macromolecules 22:3594–3599
82. Prater K (1990) The renaissance of the solid polymer fuel cell. J Power Sources 29:239–250
83. Gittleman CS, Coms FD, Lai YH (2012) Membrane durability: physical and chemical degradation. In: Mench MM, Kumbur EC, Veziroglu TN (eds) Polymer electrolyte fuel cell degradation. Elsevier, Oxford, pp 15–80
84. Feldheim DL, Lawson DR, Martin CR (1993) Influence of the sulfonate countercation on the thermal stability of nafion@ perfluorosulfonate membranes. J Polym Sci Polym Phys 31:953–957
85. Page KA, Cable KM, Moore RB (2005) Molecular origins of the thermal transitions and dynamic mechanical relaxations in perfluorosulfonate ionomers. Macromolecules 38:6472–6484
86. Page KA, Landis FA, Phillips AK, Moore RB (2006) SAXS analysis of the thermal relaxation of anisotropic morphologies in oriented nafion membranes. Macromolecules 39:3939–3946
87. Mokrini A (2014) Study of azoles as bifunctional additives for proton exchange membranes melt-processing from LSC and SSC perfluorosulfonic acid ionomers. ECS Trans 64:377–388
88. Mokrini A, Toupin M, Malek K (2016) Techno-economics of a new high throughput process for proton exchange membranes manufacturing. World Electric Vehicle J 8:431–442

89. Mokrini A (2017) Ion exchange membranes having low in-plane swelling. US Patent 9,941,538, 10 Apr 2018
90. Grubb WT (1955) Fuel cell. U.S. Patent 2,913,511, 17 Nov 1959
91. Basura VI, Chuy C, Beattie PD, Holdcroft S (2001) Effect of equivalent weight on electrochemical mass transport properties of oxygen in proton exchange membranes based on sulfonated α,β,β-trifluorostyrene (BAM®) and sulfonated styrene-(ethylene-butylene)-styrene triblock (DAIS-analytical) copolymers. J Electroanal Chem 501:77–88
92. Kraytsberg A, Ein-Eli Y (2014) Review of advanced materials for proton exchange membrane fuel cells. Energ Fuel 28:7303–7330
93. D'Agostino VF, Lee JY, Cook EH (1974) Trifluorostyrene sulfonic acid membranes. US Patent 4,012,303, 15 Mar 1977
94. Ding J, Chuy C, Holdcroft S (2002) Enhanced conductivity in morphologically controlled proton exchange membranes: synthesis of macromonomers by SFRP and their incorporation into graft polymers. Macromolecules 35:1348–1355
95. Ding J, Chuy C, Holdcroft SA (2001) A self-organized network of nanochannels enhances ion conductivity through polymer films. Chem Mater 13:2231–2233
96. Enomoto K, Takahashi S, Rohani R, Maekawa Y (2012) Synthesis of copolymer grafts containing sulfoalkyl and hydrophilic groups in polymer electrolyte membranes. J Membrane Sci 36:415–416
97. Gubler L, Gürsel SA, Scherer GG (2005) Radiation grafted membranes for polymer electrolyte fuel cells. Fuel Cells 5:317–335
98. Chen J, Septiani U, Asano M, Maekawa Y, Kubota H, Yoshida M (2007) Comparative study on the preparation and properties of radiation-grafted polymer electrolyte membranes based on fluoropolymer films. J Appl Polym Sci 103:1966–1972
99. Gubler L (2014) Polymer design strategies for radiation-grafted fuel cell membranes. Adv Energy Mater 4:1300827
100. Guzman-Garcia AG, Pintauro PN (1992) Analysis of radiation-grafted membranes for fuel cell electrolytes. J Appl Electrochem 22:204–214
101. Mokrini A, Huneault H, Gerard P (2006) Partially fluorinated proton exchange membranes based on thermoplastic elastomers compatibilized with methyl methacrylate based block copolymers. J Membrane Sci 283(1–2):74–83
102. Mokrini A, Huneault M (2006) Proton exchange membranes based on compatibilized polymer blends of PVDF and SEBS. J Power Sources 154:51–58
103. Babb DA (2002) Polymers from the thermal (2π+2π) cyclodimerization of fluorinated olefins. In: Hougham GG, Cassidy PE, Johns K, Davidson T (eds) Fluoropolymers. I. Synthesis. Kluwer Academic Publishers, New York, pp 25–50
104. Iacono ST, Budy SM, Jin J, Smith DW Jr (2007) Science and technology of perfluorocyclobutyl aryl ether polymers. J Polym Sci Pol Chem 45:5705–5721
105. Mujkic M, Iacono ST, Neilson AR, Smith DW Jr (2009) Recent optical applications of perfluorocyclobutyl aryl ether polymers. Macromol Symp 283−284:326–335
106. Perpall MW, Smith DW Jr, DesMarteau DD, Creager SE (2006) Alternative trifluorovinyl ether derived fluoropolymer membranes and functionalized carbon composite electrodes for fuel cells. Polym Rev 46:297–313
107. Jiang R, Fuller T, Brawn S, Gittleman C (2013) Perfluorocyclobutane and poly(vinylidene fluoride) blend membranes for fuel cells. Electrochim Acta 110:306–315
108. Gubler L, Nauser T, Coms FD, Lai YH, Gittleman CS (2018) Prospects for durable hydrocarbon-based fuel cell membranes. J Electrochem Soc 165:F3100–F3103
109. Kalaw GJD, Wahome JAN, Zhu Y, Balkus KJ Jr, Musselman IH, Yang DJ, Ferraris JP (2013) Perfluorocyclobutyl (PFCB)-based polymer blends for proton exchange membrane fuel cells (PEMFCs). J Membrane Sci 431:86–95
110. Marestin C, Thiry X, Rojo S, Chauveau E, Mercier R (2017) Synthesis of sulfonate ester and sulfonic acid-containing poly(arylene perfluorocyclobutane)s (PFCB) by direct copolymerization of a sulfonate ester-containing precursor. Polymer 108:179–192

111. Roziere J, Jones DJ (2003) Non-fluorinated polymer materials for proton exchange membranes fuel cells. Annu Rev Mater Res 33:503–555
112. Hickner MA, Ghassemi H, Kim YS, Einsla BR, McGrath JE (2004) Alternative polymer systems for proton exchange membranes (PEMs). Chem Rev 104(10):4587–4612
113. Page KA, Rowe BW (2012) An overview of polymer electrolyte membranes for fuel cell applications. In: Page KA, Soles CL, Runt J (eds) Polymers for energy storage and delivery. ACS Symposium Series, Washington, pp 145–164
114. Shin DW, Guiver MD, Lee YM (2017) Hydrocarbon-based polymer electrolyte membranes: importance of morphology on ion transport and membrane stability. Chem Rev 117:4759–4805
115. Shimizu R, Tsuji J, Sato N, Takano J, Itami S, Kusakabe M, Miyatake K, Iiyama A, Uchida M (2017) Durability and degradation analysis of hydrocarbon ionomer membranes in polymer electrolyte fuel cells accelerated stress evaluation. J Power Sources 367:63–71
116. Varcoe JR, Poynton SD, Slade RCT (2009) Alkaline anion-exchange membranes for low-temperature fuel cell application. In: Vielstich W, Lamm A, Gasteiger HA, Yokokawa H (eds) Handbook of fuel cells: fundamentals, technology and applications. Wiley, London, pp 323–335
117. Yanagi H, Fukuta K (2008) Anion exchange membrane and ionomer for alkaline membrane fuel cells (AMFCs). ECS Trans 16:257–262
118. Marino MG, Kreuer KD (2018) Alkaline stability of quaternary ammonium cations for alkaline fuel cell membranes and ionic liquids. ChemSusChem 8:513–523
119. Varcoe JR, Atanassov P, Dekel DR, Herring AM (2014) Anion-exchange membranes in electrochemical energy systems. Energy Environ Sci 7:3135–3191
120. Schwesinger R, Link R, Wenzl P, Kossek S, Keller M (2006) Extremely base-resistant organic phosphazenium cations. Chem Eur J 12:429–437
121. Noonan KJT, Hugar KM, Kostalik HA IV, Lobkovsky EB, Abruña HD, Coates GW (2012) Phosphonium-functionalized polyethylene: a new class of base-stable alkaline anion exchange membranes. J Am Chem Soc 134:18161–18164
122. Luo YT, Guo JC, Wang CS, Chu D (2012) Fuel cell durability enhancement by crosslinking alkaline anion exchange membrane electrolyte. Electrochem Commun 16:65–68
123. Wang LQ, Brink JJ, Liu Y, Herring AM, Ponce-Gonzalez J, Whelligan DK, Varcoe JR (2017) Non-fluorinated pre-irradiation-grafted (peroxidated) LDPE-based anion-exchange membranes with high performance and stability. Energy Environ Sci 10:2154–2167
124. Holade Y, Sahin N, Servat K, Napporn T, Kokoh K (2015) Recent advances in carbon supported metal nanoparticles preparation for oxygen reduction reaction in low temperature fuel cells. Catalysts 5:310
125. Bard AJ, Faulkner LR (2001) Electrochemical methods: fundamentals and applications, 2nd edn. Wiley, New York
126. Ticianelli EA, Derouin CR, Redondo A, Srinivasan S (1988) Methods to advance technology of proton exchange membrane fuel cells. J Electrochem Soc 135:2209–2214
127. Gasteiger HA, Panels JE, Yan SG (2004) Dependence of PEM fuel cell performance on catalyst loading. J Power Sources 127:162–171
128. Cavarroc M, Ennadjaoui A, Mougenot M, Brault P, Escalier R, Tessier Y, Durand J, Roualdes S, Sauvage T, Coutanceau C (2009) Performance of plasma sputtered fuel cell electrodes with ultra-low Pt loadings. Electrochem Commun 11:859–861
129. Croissant MJ, Napporn T, Léger JM, Lamy C (1998) Electrocatalytic oxidation of hydrogen at platinum-modified polyaniline electrodes. Electrochim Acta 43:2447–2457
130. Wang JX, Springer TE, Adzic RR (2006) Dual-pathway kinetic equation for the hydrogen oxidation reaction on Pt electrodes. J Electrochem Soc 153:A1732–A1740
131. Lamy C, Léger J-M, Srinivasan S (2001) Direct methanol fuel cells: from a twentieth century electrochemist's dream to a twenty-first century emerging technology. Kluwer Academic/ Plenum Publishers, New York

132. Velázquez-Palenzuela A, Centellas F, Garrido JA, Arias C, Rodríguez RM, Brillas E, Cabot P-L (2011) Kinetic analysis of carbon monoxide and methanol oxidation on high performance carbon-supported Pt–Ru electrocatalyst for direct methanol fuel cells. J Power Sources 196:3503–3512
133. Abida B, Chirchi L, Baranton S, Napporn TW, Morais C, Léger J-M, Ghorbel A (2013) Hydrogenotitanates nanotubes supported platinum anode for direct methanol fuel cell. J Power Sources 241:429–439
134. Brummel O, Waidhas F, Faisal F, Fiala R, Vorokhta M, Khalakhan I, Dubau M, Figueroba A, Kovacs G, Aleksandrov HA, Vayssilov GN, Kozlov SM, Neyman KM, Matolin V, Libuda J (2016) Stabilization of small platinum nanoparticles on Pt-CeO2 thin film electrocatalysts during methanol oxidation. J Phys Chem C 120:19723–19736
135. Cao J, Chen H, Zhang X, Zhang Y, Liu X (2018) Graphene-supported platinum/nickel phosphide electrocatalyst with improved activity and stability for methanol oxidation. RSC Adv 8:8228–8232
136. El Sawy EN, Birss VI (2018) Nanoengineered Ir-core@Pt-sheII nanoparticles with controlled Pt shell coverages for direct methanol electro-oxidation. ACS Appl Mater Interfaces 10:3459–3469
137. Jasim AM, Hoff SE, Xing Y (2018) Enhancing methanol electrooxidation activity using double oxide catalyst support of tin oxide clusters on doped titanium dioxides. Electrochim Acta 261:221–226
138. Kazemi R, Kiani A (2012) Deposition of palladium submonolayer on nanoporous gold film and investigation of its performance for the methanol electrooxidation reaction. Int J Hydrog Energy 37:4098–4106
139. Li Y, Gao W, Ci L, Wang C, Ajayan PM (2010) Catalytic performance of Pt nanoparticles on reduced graphene oxide for methanol electro-oxidation. Carbon 48:1124–1130
140. Ostroverkh A, Johanek V, Kus P, Sediva R, Matolin V (2016) Efficient ceria-platinum inverse catalyst for partial oxidation of methanol. Langmuir 32:6297–6309
141. Rednyk A, Johanek V, Khalakhan I, Dubau M, Vorokhta M, Matolin V (2016) Methanol oxidation on sputter-coated platinum oxide catalysts. Int J Hydrog Energy 41:265–275
142. Xie J, Zhang Q, Gu L, Xu S, Wang P, Liu J, Ding Y, Yao YF, Nan C, Zhao M, You Y, Zou Z (2016) Ruthenium–platinum core–shell nanocatalysts with substantially enhanced activity and durability towards methanol oxidation. Nano Energy 21:247–257
143. Watanabe M, Motoo S (1975) Electrocatalysis by ad-atoms: part II. Enhancement of the oxidation of methanol on platinum by ruthenium ad-atoms. J Electroanal Chem Interfacial Electrochem 60:267–273
144. Brueckner TM, Pickup PG (2017) Kinetics and stoichiometry of methanol and ethanol oxidation in multi-anode proton exchange membrane cells. J Electrochem Soc 164:F1172–F1178
145. Yuan W, Cheng Y, Shen PK, Li CM, Jiang SP (2015) Significance of wall number on the carbon nanotube support-promoted electrocatalytic activity of Pt NPs towards methanol/formic acid oxidation reactions in direct alcohol fuel cells. J Mater Chem A 3:1961–1971
146. Napporn WT, Laborde H, Léger JM, Lamy C (1996) Electro-oxidation of C1 molecules at Pt-based catalysts highly dispersed into a polymer matrix: effect of the method of preparation. J Electroanal Chem 404:153–159
147. Beyhan S, Uosaki K, Feliu JM, Herrero E (2013) Electrochemical and in situ FTIR studies of ethanol adsorption and oxidation on gold single crystal electrodes in alkaline. J Electroanal Chem 707:89–94
148. Delpeuch AB, Maillard F, Chatenet M, Soudant P, Cremers C (2016) Ethanol oxidation reaction (EOR) investigation on Pt/C, Rh/C, and Pt-based bi- and tri-metallic electrocatalysts: a DEMS and in situ FTIR study. Appl Catal B Environ 181:672–680
149. Pech-Rodriguez WJ, Gonzalez-Quijano D, Vargas-Gutierrez G, Morais C, Napporn TW, Rodriguez-Varela FJ (2017) Electrochemical and in situ FTIR study of the ethanol oxidation reaction on PtMo/C nanomaterials in alkaline media. Appl Catal B Environ 203:654–662

150. Almeida TS, Palma LM, Morais C, Kokoh KB, De Andrade AR (2013) Effect of adding a third metal to carbon-supported ptsn-based nanocatalysts for direct ethanol fuel cell in acidic medium. J Electrochem Soc 160:F965–F971
151. Beyhan S, Coutanceau C, Léger J-M, Napporn TW, Kadırgan F (2013) Promising anode candidates for direct ethanol fuel cell: carbon supported PtSn-based trimetallic catalysts prepared by Bönnemann method. Int J Hydrog Energy 38:6830–6841
152. Buso-Rogero C, Brimaud S, Solla-Gullon J, Vidal-Iglesias FJ, Herrero E, Behm RJ, Feliu JM (2016) Ethanol oxidation on shape-controlled platinum nanoparticles at different pHs: a combined in situ IR spectroscopy and online mass spectrometry study. J Electroanal Chem 763:116–124
153. Erini N, Krause P, Gliech M, Yang R, Huang Y, Strasser P (2015) Comparative assessment of synthetic strategies toward active platinum–rhodium–tin electrocatalysts for efficient ethanol electro-oxidation. J Power Sources 294:299–304
154. García-Rodríguez S, Somodi F, Borbáth I, Margitfalvi JL, Peña MA, Fierro JLG, Rojas S (2009) Controlled synthesis of Pt-Sn/C fuel cell catalysts with exclusive Sn–Pt interaction: application in CO and ethanol electrooxidation reactions. Appl Catal B Environ 91:83–91
155. Higuchi E, Takase T, Chiku M, Inoue H (2014) Preparation of ternary Pt/Rh/SnO2 anode catalysts for use in direct ethanol fuel cells and their electrocatalytic activity for ethanol oxidation reaction. J Power Sources 263:280–287
156. Ishitobi H, Ino Y, Nakagawa N (2017) Anode catalyst with enhanced ethanol electrooxidation activity by effective interaction between Pt-Sn-SiO2 for a direct ethanol fuel cell. Int J Hydrog Energy 42:26897–26904
157. Mahesh I, Jaithaliya R, Sarkar A (2017) Efficient electrooxidation of ethanol on bi@Pt/C nanoparticles: (i) effect of monolayer bi deposition on specific sites of Pt nanoparticle (ii) calculation of average number of e(−)s without help of chemical analysis. Electrochim Acta 258:933–941
158. Majlan EH, Rohendi D, Daud WRW, Husaini T, Haque MA (2018) Electrode for proton exchange membrane fuel cells: a review. Renew Sust Energ Rev 89:117–134
159. Pierozynski B (2012) On the ethanol electrooxidation reaction on catalytic surfaces of Pt in 0.1 M NaOH. Int J Electrochem Sci 7:4261–4271
160. Pierozynski B (2012) Electrooxidation of ethanol on PtRh and PtRu surfaces studied in 0.5 M H2SO4: relation to the behaviour at polycrystalline Pt. Int J Electrochem Sci 7:4488–4497
161. Pierozynski B (2012) Kinetic aspects of ethanol electrooxidation on catalytic surfaces of Pt in 0.5 M H2SO4. Int J Electrochem Sci 7:3327–3338
162. Purgato FLS, Pronier S, Olivi P, de Andrade AR, Leger JM, Tremiliosi-Filho G, Kokoh KB (2012) Direct ethanol fuel cell: electrochemical performance at 90 degrees C on Pt and PtSn/C electrocatalysts. J Power Sources 198:95–99
163. Rizo R, Sebastián D, Lázaro MJ, Pastor E (2017) On the design of Pt-Sn efficient catalyst for carbon monoxide and ethanol oxidation in acid and alkaline media. Appl Catal B Environ 200:246–254
164. Silva JCM, Parreira LS, De Souza RFB, Calegaro ML, Spinacé EV, Neto AO, Santos MC (2011) PtSn/C alloyed and non-alloyed materials: differences in the ethanol electro-oxidation reaction pathways. Appl Catal B Environ 110:141–147
165. Silva LC, Maia G, Passos RR, de Souza EA, Camara GA, Giz MJ (2013) Analysis of the selectivity of PtRh/C and PtRhSn/C to the formation of CO2 during ethanol electrooxidation. Electrochim Acta 112:612–619
166. Soares LA, Morais C, Napporn TW, Kokoh KB, Olivi P (2016) Beneficial effects of rhodium and tin oxide on carbon supported platinum catalysts for ethanol electrooxidation. J Power Sources 315:47–55
167. Xia XH, Liess HD, Iwasita T (1997) Early stages in the oxidation of ethanol at low index single crystal platinum electrodes. J Electroanal Chem 437:233–240

168. Yang YY, Ren J, Li QX, Zhou ZY, Sun SG, Cai WB (2014) Electrocatalysis of ethanol on a Pd electrode in alkaline media: an in situ attenuated total reflection surface-enhanced infrared absorption spectroscopy study. ACS Catal 4:798–803
169. Zhang Z, Xin L, Sun K, Li W (2011) Pd-Ni electrocatalysts for efficient ethanol oxidation reaction in alkaline electrolyte. Int J Hydrog Energy 36:12686–12697
170. Camara GA, de Lima RB, Iwasita T (2005) The influence of PtRu atomic composition on the yields of ethanol oxidation: a study by in situ FTIR spectroscopy. J Electroanal Chem 585:128–131
171. dos Anjos DM, Hahn F, Leger JM, Kokoh KB, Tremiliosi-Filho G (2008) Ethanol electrooxidation on Pt-Sn and Pt-Sn-W bulk alloys. J Braz Chem Soc 19:795–802
172. Garcia-Rodriguez S, Rojas S, Pena MA, Fierro JLG, Baranton S, Leger JM (2011) An FTIR study of Rh-PtSn/C catalysts for ethanol electrooxidation: effect of surface composition. Appl Catal B Environ 106:520–528
173. Kowal A, Gojkovic SL, Lee KS, Olszewski P, Sung YE (2009) Synthesis, characterization and electrocatalytic activity for ethanol oxidation of carbon supported Pt, Pt-Rh, Pt-SnO2 and Pt-Rh-SnO2 nanoclusters. Electrochem Commun 11:724–727
174. Lamy C, Rousseau S, Belgsir EM, Coutanceau C, Léger JM (2004) Recent progress in the direct ethanol fuel cell: development of new platinum–tin electrocatalysts. Electrochim Acta 49:3901–3908
175. Purgato FLS, Olivi P, Leger JM, de Andrade AR, Tremiliosi-Filho G, Gonzalez ER, Lamy C, Kokoh KB (2009) Activity of platinum-tin catalysts prepared by the Pechini-Adams method for the electrooxidation of ethanol. J Electroanal Chem 628:81–89
176. Purgato FLS, Pronier S, Olivi P, de Andrade AR, Léger JM, Tremiliosi-Filho G, Kokoh KB (2012) Direct ethanol fuel cell: electrochemical performance at 90°C on Pt and PtSn/C electrocatalysts. J Power Sources 198:95–99
177. Ribadeneira E, Hoyos BA (2008) Evaluation of Pt–Ru–Ni and Pt–Sn–Ni catalysts as anodes in direct ethanol fuel cells. J Power Sources 180:238–242
178. Ribeiro J, dos Anjos DM, Leger JM, Hahn F, Olivi P, de Andrade AR, Tremiliosi-Filho G, Kokoh KB (2008) Effect of W on PtSn/C catalysts for ethanol electrooxidation. J Appl Electrochem 38:653–662
179. Sen Gupta S, Datta J (2006) A comparative study on ethanol oxidation behavior at Pt and PtRh electrodeposits. J Electroanal Chem 594:65–72
180. Simoes FC, dos Anjos DM, Vigier F, Leger JM, Hahn F, Coutanceau C, Gonzalez ER, Tremiliosi-Filho G, de Andrade AR, Olivi P, Kokoh KB (2007) Electroactivity of tin modified platinum electrodes for ethanol electrooxidation. J Power Sources 167:1–10
181. Sun S, Halseid MC, Heinen M, Jusys Z, Behm RJ (2009) Ethanol electrooxidation on a carbon-supported Pt catalyst at elevated temperature and pressure: a high-temperature/high-pressure DEMS study. J Power Sources 190:2–13
182. Wang Z-B, Yin G-P, Zhang J, Sun Y-C, Shi P-F (2006) Investigation of ethanol electrooxidation on a Pt-Ru-Ni/C catalyst for a direct ethanol fuel cell. J Power Sources 160:37–43
183. Xu C, Shen P k, Liu Y (2007) Ethanol electrooxidation on Pt/C and Pd/C catalysts promoted with oxide. J Power Sources 164:527–531
184. Damjanovic A, Genshaw MA, Bockris JO, apos M (1966) Distinction between intermediates produced in main and side electrodic reactions. J Chem Phys 45:4057–4059
185. Wroblowa HS, Yen Chi P, Razumney G (1976) Electroreduction of oxygen: a new mechanistic criterion. J Electroanal Chem Interfacial Electrochem 69:195–201
186. Hsueh KL, Chin DT, Srinivasan S (1983) Electrode kinetics of oxygen reduction: a theoretical and experimental analysis of the rotating ring-disc electrode method. J Electroanal Chem Interfacial Electrochem 153:79–95
187. Schmidt TJ, Gasteiger HA, Stäb GD, Urban PM, Kolb DM, Behm RJ (1998) Characterization of high-surface-area electrocatalysts using a rotating disk electrode configuration. J Electrochem Soc 145:2354–2358

188. Coutanceau C, Croissant MJ, Napporn T, Lamy C (2000) Electrocatalytic reduction of dioxygen at platinum particles dispersed in a polyaniline film. Electrochim Acta 46:579–588
189. Lim D-H, Wilcox J (2012) Mechanisms of the oxygen reduction reaction on defective graphene-supported Pt nanoparticles from first-principles. J Phys Chem C 116:3653–3660
190. Sahin NE, Napporn TW, Dubau L, Kadirgan F, Leger JM, Kokoh KB (2017) Temperature-dependence of oxygen reduction activity on Pt/C and PtCr/C electrocatalysts synthesized from microwave-heated diethylene glycol method. Appl Catal B Environ 203:72–84
191. Huang Y, Wagner FT, Zhang JL, Jorne J (2014) Hydrogen adsorption on C-supported Pt and Pt-co shell-core nano-catalysts in proton exchange membrane fuel cells: entropic effects and catalytic activity. J Electrochem Soc 161:F653–F659
192. Asset T, Chattot R, Fontana M, Mercier-Guyon B, Job N, Dubau L, Maillard F (2018) A review on recent developments and prospects for the oxygen reduction reaction on hollow Pt-alloy nanoparticles. ChemPhysChem 19(13):1552–1567
193. Fiala R, Figueroba A, Bruix A, Vaclavu M, Rednyk A, Khalakhan I, Vorokhta M, Lavkova J, Illas F, Potin V, Matolinova I, Neyman KM, Matolin V (2016) High efficiency of Pt2+ – CeO2 novel thin film catalyst as anode for proton exchange membrane fuel cells. Appl Catal B Environ 197:262–270
194. David S, Alexey S, Kateryna A, Jonathan G, Plamen A, Aricò AS, Vincenzo B (2016) High performance and cost-effective direct methanol fuel cells: Fe-N-C methanol-tolerant oxygen reduction reaction catalysts. ChemSusChem 9:1986–1995
195. Ma K-B, Kwak D-H, Han S-B, Park H-S, Kim D-H, Won J-E, Kwon S-H, Kim M-C, Moon S-H, Park K-W (2018) Direct ethanol fuel cells with superior ethanol-tolerant nonprecious metal cathode catalysts for oxygen reduction reaction. ACS Sustain Chem Eng 6:7609–7618

Chapter 2
Recent Advances on Electrocatalysts for PEM and AEM Fuel Cells

M. Roca-Ayats, S. Pérez-Rodríguez, G. García, and E. Pastor

Abstract Herein, the general concepts of low-temperature fuel cells (LTFCs) are discussed, with special attention to proton exchange fuel cell (PEMFC) and anion exchange membrane fuel cell (AEMFC). LTFC has the potential to provide power to portable devices, transportation, and stationary sectors. With the aim to solve the principal catalytic problems at the anode and at the cathode of LTFCs, a fundamental study of the mechanism and kinetics of carbon monoxide and hydrogen oxidation as well as oxygen reduction on well-defined and practical catalysts in acidic and alkaline media is discussed. Consequently, the aim of the present work is not only to provide the new advances in the catalytic materials but also to understand the reactions occurring at fuel cell catalysts, which may help to improve the fabrication of novel electrodes in order to decrease the cost and to enhance the performance of LTFCs.

Keywords PEMFC · AEMFC · Catalyst · Electrocatalysis · Catalyst support · Active site · Stability · Degradation · HER · ORR · CO · Kinetic · Pt · Pd · Metal alloys · Metal oxides · Metal carbides · Metal nitrides · Core-shell · Nanoparticle

M. Roca-Ayats
Physical Chemistry Department, Faculty of Chemistry, University of Santiago de Compostela, Santiago de Compostela, Spain

S. Pérez-Rodríguez
Instituto de Carboquímica (CSIC), Zaragoza, Spain

G. García · E. Pastor (✉)
Instituto de Materiales y Nanotecnología, Departamento de Química, Universidad de La Laguna, Santa Cruz de Tenerife, Spain
e-mail: epastor@ull.es

F. J. Rodríguez-Varela, T. W. Napporn (eds.), *Advanced Electrocatalysts for Low-Temperature Fuel Cells*, https://doi.org/10.1007/978-3-319-99019-4_2

2.1 Introduction

Low-temperature fuel cells (LTFCs) have attracted great attention as a primary power source for electric devices and residential cogeneration units. LTFCs consist of two electrodes separated by an electrolyte medium (usually a membrane) that determines the type of LTFC, i.e., anion exchange membrane fuel cell (AEMFC) for LTFC working at high pH and proton exchange fuel cell (PEMFC) for LTFC running at low pH. Similar to the majority of fuel cells, LTFCs oxidized the fuel (hydrogen at LTFCs) at the anode, while oxygen is reduced at the cathode. The ions produced by these electrochemical reactions are transported through the electrolyte from one electrode to the other, while the electrons generated at the anode flow through an external circuit to the cathode. Accordingly, LTFCs usually reveal higher efficiency than systems operating on internal combustion since no combustion occurs and consequently there is not limitation by the Carnot cycle.

Despite the significant advantages of LTFCs as power sources, a real LTFC has several drawbacks, which decrease their working performance and increase their cost. In this regard, one of the most important issues to solve is that related to the anode and cathode electrodes for LTFCs, which usually employ platinum-based materials that are very active catalysts although their elevated cost, low abundance, and poor durability are a main obstacle in the development of LTFCs. Hence, it is very important to reduce the amount and optimize the use of this noble metal.

With this end in view, in this chapter the different anode and cathode nanomaterials for PEMFC and AEMFC are discussed and reviewed. The work focuses on precious metal-containing electrocatalysts with different structures such as alloys, metal–metal oxides, and core–shell nanostructures.

2.2 Hydrogen Oxidation Reaction

The electrochemical oxidation of hydrogen (HOR) takes place at the anode side of both acid (PEM) and alkaline (AEM) H_2–O_2 fuel cells. In these electrochemical devices, H_2 is used as fuel, and its stored chemical energy is efficiently transformed into electrical energy without emissions.

The overall reaction for HOR in acid electrolyte occurs following the reaction (2.1):

$$H_2 \rightarrow 2H^+ + 2e^- \tag{2.1}$$

while the product of the anodic reaction in alkaline media is water:

$$H_2 + 2OH^- \rightarrow 2H_2O + 2e^- \tag{2.2}$$

Besides to its importance in fuel cell technology, HOR (or its reverse, the hydrogen evolution reaction, HER) is a model reaction for the understanding of electrode kinetics and electrocatalysis and it has been extensively studied [1–6]. The mechanism of HOR in electrolyte solutions generally includes three sequential stages [1–5]:

1. Molecular hydrogen diffusion from the electrolyte to the electrode surface and posterior adsorption:

$$H_2 \rightarrow H_{2,\text{solv}} \rightarrow H_{2,\text{ad}} \tag{2.3}$$

2. Hydrogen dissociation/ionization through either the Tafel–Volmer sequence (2.4 and 2.7 or 2.8) or Heyrovsky–Volmer (2.5 or 2.6 and 2.7 or 2.8) route:

   Tafel:

$$H_{2,\text{ad}} \rightarrow 2H_{\text{ad}} \tag{2.4}$$

   Heyrovsky:

$$H_{2,\text{ad}} \rightarrow H_{\text{ad}} + H^+ + e^- \quad \text{(acidic media)} \tag{2.5}$$

$$H_{2,\text{ad}} + OH^- \rightarrow H_{\text{ad}} + H_2O + e^- \quad \text{(alkaline media)} \tag{2.6}$$

   Volmer:

$$H_{\text{ad}} \rightarrow H^+ + e^- \quad \text{(acidic media)} \tag{2.7}$$

$$H_{\text{ad}} + OH^- \rightarrow H_2O + e^- \quad \text{(alkaline media)} \tag{2.8}$$

3. Product desorption (H^+ and H_2O in acid and alkaline media, respectively) from electrode surface to the electrolyte.

The performance toward HOR depends strongly on the electrode material nature and the surface metallic arrangement [5]. In addition, the reaction is pH-dependent. Volcano curves have been obtained for HOR versus hydrogen binding energy (HBE) on different monometallic metals, in both acid [7] and base [8] electrolytes. These volcano-shaped curves suggest that metals which adsorb hydrogen neither too strongly nor too weakly develop highest activities. In acid media, the most active catalysts for hydrogen oxidation (placed on the top of the volcano plot) have been found to be Pt-group metals (including Pt, Ru, Pd, Ir, Os, and Rh) [7] due to their moderate HBE. Among these metals, Pt displays the highest exchange current density defined as the rate at which the reaction proceeds at the equilibrium potential (zero net current), and consequently, it is the most active metal for HOR. Much less research work has been made in the fundamental understanding of HOR in alkaline

solutions. Recently, Sheng et al. [8] showed that the exchange current density on monometallic surfaces in 0.1 M KOH can be also correlated with their HBE values via a volcano plot. Again, Pt presented the highest exchange current density in alkaline media confirming that it is the best catalyst for HOR under these conditions.

However, most Pt-group metals present an activity for HOR at least two order times lower in alkaline electrolyte than that developed in acid media, which is attributed to the interactions between oxygenated species and cations [3, 6]. Therefore, the use of Pt-based catalysts in AFM fuel cells will require high metal loadings at anode, and thus, it will represent a significant cost. In contrast, the fast HOR kinetics in acid media at Pt-group metals allows the ultralow Pt loading (~ 0.03 mgPt cm^2).

In addition to the high costs of the anode electrocatalysts, another key challenge facing the commercialization of PEM and AEM fuel cells is the susceptibility to carbon monoxide impurities. CO is the most common contaminant in hydrogen streams (from reformate processes) and it is preferentially and irreversibly adsorbed on Pt active sites, and consequently, blocking hydrogen adsorption and reducing the electrocatalytic activity. Even trace amounts of CO in the H_2 gas (as low as 10 ppm) are likely to dramatically decrease the fuel cell performance [9, 10].

CO electrooxidation takes place on Pt in acidic and alkaline media through the Langmuir–Hinshelwood mechanism; L–H [11–14]:

$$H_2O \rightarrow OH_{ad} + H^+ + e^- \tag{2.9}$$

$$CO_{ad} + OH_{ad} \rightarrow COOH_{ad} \tag{2.10}$$

$$COOH_{ad} \rightarrow CO_2 + H^+ + e^- \tag{2.11}$$

and in strong alkaline media, carbon dioxide undergoes a fast chemical conversion to carbonate, which can strongly block catalytic sites [11, 15]. Reaction (2.10) is a chemical reaction between adsorbed species that is suggested to be the rate-determining step (RDS) on Pt-based electrodes in the whole pH range because a Tafel slope value close to 60 mV dec^{-1} is frequently obtained.

In order to enhance the CO tolerance and to decrease the cost of the anode electrocatalysts, the use of bimetallic or trimetallic catalytic systems by allowing strategies of Pt with other metals (such as Ru, Sn, Rh, Mo, etc.), using core–shell architectures or modifying Pt with other metal oxides, has been proposed over the last decades [9, 16–19]. The mitigation of CO poisoning by alloying Pt is generally ascribed to one or both of these effects [20]:

1. *Bifunctional effect*, where CO electrooxidation is promoted by the formation of OH species on second metal sites:

$$M + H_2O \rightarrow M - OH + H^+ + e^- \tag{2.12}$$

$$M - OH + Pt - CO \rightarrow Pt + M + CO_2 + H^+ + e^- \quad (2.13)$$

2. *Electronic (ligand or promoted) effect*, where the added component (promoter) modifies the Pt electronic properties resulting in an improved Pt–H_2O (or Pt–OH in alkaline media) activation which may lead to a direct oxidation of CO on Pt sites or a weakening of the Pt–CO bond making easier CO oxidation.
3. *Morphological and structural effects*, where the composition, particle size, morphology, and structure of the catalyst modify the distribution of the Pt active sites, and thus, the reaction pathways and the activity may be varied. Furthermore, these factors affect the stability of the catalyst preventing their degradation during long-term operation.

Thus, Pt-based catalysts are the most conventionally used in fuel cell technology under different pH conditions. The catalyst active phase is usually dispersed on a carbon substrate. The use of a carbon support increases the electrochemically accessible active area, enhancing the electrochemical performance. Additionally, supported catalysts decrease the Pt loading, making them more attractive from an economical point of view.

This section reviews the main developments obtained in the field of CO-tolerant Pt-based catalysts for the HOR in acid solution. Additionally, a brief summary of some recent advances achieved using non-Pt catalysts is addressed.

2.2.1 *Electrode Materials for Hydrogen Oxidation Reaction in Acidic Media*

The HOR is extremely facile on Pt at low pH values, with an exchange current density of mA cm^{-2} at room temperature [4, 21]. In general, the HOR on Pt is around 10^5 to $l0^7$ times faster than oxygen reduction [22], which occurs at the cathode of a PEM fuel cell. Consequently, the anode potential is less than +0.1 V vs. RHE (reversible hydrogen electrode) when pure hydrogen is supplied at the anode at practical current densities, which is close to the standard reversible potential for this reaction (0.0 V vs. RHE) [5]. Additionally, Pt is stable under acidic environments. However, the main disadvantage of monometallic Pt electrodes in low pH electrolytes is the low CO tolerance that this metal displays even under trace impurities [9, 14], as mentioned before. In order to address this issue, other metals are incorporated in the Pt structure to increase the CO tolerance. The role of adding a second element into the structure of Pt is to mitigate CO poisoning via either the bifunctional mechanism or the ligand one or a combination of both effects. The bifunctional mechanism is explained by the improved oxidation of adsorbed CO on Pt in the presence of the second metal due to the formation of OH species at low potentials. Ligand effects are caused by the modification of the Pt structure, which weaken the CO adsorption and/or enhance the adsorption of oxygen-containing

species [9, 14]. Different catalytic systems based on Pt have been proposed, such as the use of binary/ternary alloys, Pt–metal oxides, core–shell structures, Pt catalysts modified with oxidative agents, etc.

Electrocatalysts based on other Pt-group metals or even non-Pt catalysts have been also proposed over the last decades [23–25]. However, these catalyst systems are out of the scope of this work. Further information about non-Pt electrodes for hydrogen oxidation can be found in Chap. 8 of this book or in other reviews [23–25].

This section describes the main results obtained in the development of CO-tolerant electrodes based on Pt for HOR during the last years. Additionally, non-Pt catalysts are also briefly introduced.

2.2.1.1 Pt-Based Alloys

The most commonly used strategy to avoid the strong CO poisoning is by alloying Pt with other metals, such as Ru [9, 17, 26–33], Sn [31, 34–36], Mo [27, 37–45], Pd [46, 47], Fe [44, 48, 49], Co [28, 32, 49], Ni [9], W [44], Ce [50], Re [51], Pb [52, 53], etc.

Among these bimetallic catalytic systems, Pt–Ru alloys are promising materials due to their high CO tolerance compared to Pt/C [9, 26–32]. Indeed, the CO oxidation occurs at potentials around 0.2 V more positive at PtRu/C than in monometallic Pt electrodes due to both bifunctional mechanism and electronic effects.

The performance of PtRu catalysts has been extensively studied using different compositions and particle sizes [9, 29–31]. $Pt_{0.5}Ru_{0.5}$ exhibits the best performance for CO oxidation since Pt and Ru atoms are adjacent to one another and well distributed on the catalyst surface (facilitating the bifunctional mechanism) [9, 54]. However, Koper and coworkers [29] reported that for HOR in the presence of CO traces, Ru with a monolayer of Pt might be more advantageous since this PtRu surface showed the weakest CO binding on the basis of their results of a periodic density-functional theory study of the adsorption of CO and OH on Pt, Ru, and PtRu alloys. In agreement with these results, Sato et al. [30] studied the effects of particle size and alloy composition for PtRu/C catalysts on the CO tolerance by in situ attenuated total reflection Fourier-transform infrared (ATR-FTIR) spectroscopy in 1% CO (H_2-balance)-saturated 0.1 M $HClO_4$. The highest CO-tolerant HOR activity was observed for the catalyst with a Pt-rich top surface and Ru-rich core (Pt_2Ru_3/C) and the lower particle size (2.6 nm).

Despite of the high performance of PtRu alloys, the stability of PtRu/C is unclear under long-term operation due to Ru dissolution [9, 55, 56]. Thus, the searching of a stable anodic catalyst with an enhanced CO-tolerant HOR activity is still a key challenge in PEM fuel cells. Additionally, potential oscillation due to the interactions of CO electrooxidation and adsorption reactions on the catalyst surface may decrease the performance of PtRu catalysts operating in PEMFC stacks [33].

A high activity for HOR and good performance for CO tolerance have been also shown at PtSn alloys due to the electronic and bifunnctional mechanism [31, 35, 36]. In contrast to PtRu electrodes, in this catalyst system CO binds only to Pt sites

and not to Sn, while hydroxyl groups have an energetic preference for Sn [36]. Despite of this low susceptibility to CO poisoning, PtSn catalysts shown generally a lower catalytic activity toward H_2/CO oxidation than the current state-of-the-art PtRu/C (1:1) electrodes [35]. However, Gasteiger et al. [57] obtained an improved performance for H_2 electrooxidation in the presence of CO on Pt_3Sn alloys (with a surface Sn amount ≈ 20 at.%) in 0.5 M H_2SO_4 at 62 °C by the rotating disk electrode (RDE) technique. Indeed, the onset potential for CO oxidation was 0.15 V lower compared to PtRu alloys. However, Pt–Sn alloys present the main disadvantage of the instability of the surface composition under anodic polarization.

Another alloy examined to enhance CO tolerance is PtMo, obtaining promising results for H_2/O_2 fuel cells [27, 38–43, 45]. For example, Mukerjee and coauthors [39] reported a significantly higher CO tolerance for PtMo/C (atomic ratio Pt: Mo = 3:1) compared to the most conventionally used Pt–Ru/C (1:1) in a PEM fuel cell operating at 85 °C with H_2/100 ppm CO. Additionally, low overpotential losses were observed on PtMo/C as the temperature (55–115 °C) and/or the CO concentration increased (5–100 ppm, balanced H_2) [39]. Again, the stability of Pt–Mo/C catalysts is a challenging issue [41]. Hassan et al. [41] studied the effect of heat treatment at several temperatures (from 400 to 700 °C) of a Pt–Mo/C (Pt: Mo = 60:40) on its HOR activity in the presence of CO. Interestingly, the highest activity was obtained on the catalyst treated at 600 °C (with a particle size around 17 nm). Additionally, a better stability was obtained on this catalyst as compared to the untreated electrode.

Other Pt-based bimetallic alloys (PtM/C; M = Fe, Ni, W, Pd, Pb, Ce, Co) have been also used obtaining a higher activity for H_2/CO electrooxidation than pure Pt [44, 46–50, 52, 53]. In this context, Ehteshami et al. [49] developed a comprehensive study of the performance for HOR in the presence of reformate impurities (CO and CO_2) for a series of carbon-supported Pt–M catalysts (M = = Ru, Mo, Fe, Co, Ni). PtMo/C presented the highest CO tolerance followed by PtRu/C, PtCo/C, PtFe/C, PtNi/C, and Pt/C. In contrast, the CO_2 tolerance decreased in the order: PtCo, PtNi > PtRu > PtFe > Pt > PtMo. By means of a combination of in situ X-ray absorption spectroscopy (XAS) measurements and FEFF8 code calculations, a correlation of CO and CO_2 tolerance trends with the electronic properties of catalysts was stated. The anode overpotential in the presence of CO_2 might be governed by the Pt electronic properties modified by the alloyed metal, whereas no such correlation was found for the anode overpotential in the presence of CO and Pt electronic properties. These results evidence the key role of Mo or Ru in the mitigation of CO poisoning via electronic and bifunctional mechanisms.

Finally, Pt-based ternary [49, 58–68] alloys have been also developed to improve the HOR activity in the presence of CO or the stability of the respective binary systems. Mukerjee and coworkers [49] reported an excellent reformate tolerance to both CO and CO_2 on a ternary alloy PtCoMo/C operating in the anode of a PEM fuel cell. This behavior was explained by the bifunctional mechanism ascribed to Mo and the ligand effect induced by Co simultaneously.

The combination of diverse thin layers of different bimetallic and ternary catalysts have been also used to enhance the CO tolerance and stability of anodic PEM

fuel cell catalysts [69, 70]. For example, Hassan et al. [69] studied the activity, stability, and CO tolerance of ternary and quaternary catalytic systems by combination of PtMo/C-PtFe/C, PtMo/C-PtRu/C, and PtMo/C-PtRu/C-PtFe/C. The resulting electrocatalysts (based on PtMoFe/C, PtMoRu/C, and PtMoRuFe/C) showed a higher performance for hydrogen oxidation in the presence of hydrogen containing 100 ppm CO compared to PtMo/C. Additionally, the stability was also improved in ternary/quaternary catalysts in comparison to the PtMo-based electrode.

2.2.1.2 Pt–Metal Oxide

Another strategy to mitigate CO poisoning is the addition of metal oxides to Pt structure [71–75]. In these metal–metal oxide interfaces, the oxide often becomes defective, contributing to the promotion effect and thus, enhancing the performance of Pt for HOR in the presence of CO. The role of metal oxides in Pt or PtRu structures as CO-tolerant catalysts for HOR has been studied by several authors [71–75].

Unsupported or carbon-supported Pt-WO_3 catalysts have been found to lighten the CO poisoning on Pt [71–75]. Cui et al. [71] studied mesoporous tungsten oxide with a low loading of Pt (7.5 wt.%) for hydrogen electrooxidation in the presence of CO. The catalyst was synthesized by a simple one-step casting approach using mesoporous silica as template. The resultant material presented an improved performance for HOR with a mass activity per gram of Pt three-fold higher than commercial Pt/C catalyst (20 wt.%, E-TEK) and with a better CO tolerance. Similarly, Lebedeva et al. [72] studied also the electrooxidation of both saturated CO adlayer and dissolved CO on $PtWO_3$/C. Cyclic voltammetry combined with online mass spectrometry studies showed that the onset shifted to more positive potentials in both cases (0.18 and 0.12 V vs RHE, respectively) compared to pure Pt. However, only a minor fraction of the adsorbed CO seems to be oxidized at low potentials and the major part was oxidized at potentials as high as that obtained for Pt/C. Additionally, reversible deactivation of $PtWO_3$/C material was observed upon a prolonged exposure to the CO-saturated solution in acid media [72].

Other catalysts based on the addition of W to platinum have been developed for the HOR [76]. In this context, Abruña and coworkers [76] designed an efficient and CO-tolerant anode catalyst based on Pt nanoparticles supported on $Ti_{0.7}W_{0.3}O_2$. Electrochemical studies by RDE technique showed that Pt/$Ti_{0.7}W_{0.3}O_2$ catalyst exhibited negligible overpotential for hydrogen oxidation (Fig. 2.1a, b). Levich plot slope (obtained from current–potential curves in the diffusion-limited potential at 0.25 V with different rotation rates) was 8.5×10^{-2} mA cm^{-2} $rpm^{-1/2}$ (Fig. 2.1c), similar to that obtained on Pt/C. Additionally, Pt/$Ti_{0.7}W_{0.3}O_2$ catalyst exhibited a lower potential for H_2 oxidation in the presence of CO compared to Pt/C and PtRu/C (Fig. 2.1d). In agreement with these results, differential electrochemical mass spectroemtry (DEMS) measurements evidenced that the onset potential for CO oxidation on Pt/$Ti_{0.7}W_{0.3}O_2$ was below 0.1 V (vs RHE), which might be due to a cocatalysis for CO oxidation by (Ti/W)O_2 [76].

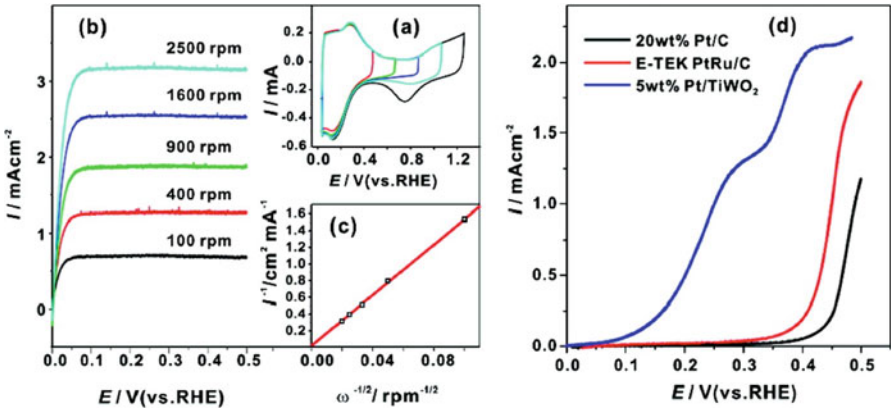

Fig. 2.1 (**a**) CV at 50 mV s^{-1} of $Pt/Ti_{0.7}W_{0.3}O_2$ (with 20 wt % C added) at different positive potentials limits in 0.1 M H_2SO_4 purged with N_2. (**b**) H_2 oxidation on $Pt/Ti_{0.7}W_{0.3}O_2$ (with 20 wt % C added) at RDE (1 mV s^{-1}) in 0.1 M H_2SO_4 base electrolyte saturated with H_2 at various rotation rates. (**c**) Levich plot from (**b**) in the diffusion-limited potential region at 0.25 V. (**d**) Polarization curves for H_2 oxidation on different catalysts in the presence of 2% CO at room temperature. Rotation rate, 1600 rpm; scan rate, 1 mV s^{-1}. From [76]

Ternary catalysts involving metal oxides have been also proposed as CO-tolerant catalysts for hydrogen electrooxidation, such as PtRu-MoO_x/C [77–79], PtRu-WO_3/C [80], or PtRu-SnO_x/C [75]. For example, Alcaide et al. [77] investigated ternary PtRu-MoOx/C catalysts anode materials for PEM fuel cells fed with H_2/CO mixtures at 80 °C. Two different Mo compositions were used (0.1 and 3.0 wt.%). Polarization curves demonstrated that the electrochemical activity for H_2 oxidation depends strongly on the Mo composition. A low Mo loading (0.1 wt.%) led to the highest CO tolerance, while an increase of the Mo composition (3 wt.%) decreased the activity of the PtRuMo catalyst, although CO poisoning was also decreased.

2.2.1.3 Core–Shell Architectures

Core–shell structures have been also used for CO-tolerant catalysts with high activity toward hydrogen oxidation [38, 48, 81–93]. An enhanced activity for both H_2 and CO electrooxidation has been found on core–shell architectures with Pt shells on various metal/metal oxide cores due to modifications of the electronic structure of Pt [38, 82, 87]. Additionally, a longer durability has been also evidenced in comparison to alloys containing the same metals since the Pt shell may act as protector of the non-noble metal core avoiding their dissolution [82, 87].

Ru@Pt core–shell materials presented a significant better performance and stability for CO tolerance in PEM fuel cell hydrogen than PtRu catalysts [87–89]. In this context, Zhang et al. [88] synthesized a novel PtRu catalyst consisting of a Ru-rich core and a Pt-rich shell by a two-step microwave irradiation approach. The CO tolerance of the HOR was tested using different CO concentrations (from 0 to

500 ppm). The core–shell nanoarchitecture developed a better electrocatalytic activity for HOR compared to Pt/C catalyst and with an improved CO tolerance in various CO concentrations. Similarly, Takimoto et al. [87] developed anodic catalysts for PEM fuel cells with a high performance combining the high utilization and activity of core@shell structures with the high surface area and stability of atomically thin nanosheets. Interestingly, a catalyst with a monolayer Ru-core and an average 1.5 monolayer Pt-shell supported on carbon displayed two times higher mass activity for the HOR in both pure H_2 and 300 ppm CO containing H_2 than benchmark Pt/C catalyst. Additionally, a better stability was developed under potential cycling [87]. Other authors have also obtained promising results using catalytic systems based on thin nanosheets [94, 95].

Eichhorn and coworkers [38] performed a comparative study of the activity for CO and H_2 oxidation on $Pt_{0.8}Mo_{0.2}$ and MoO_x@Pt core–shell nanoparticle electrocatalysts. RDE experiments exhibited that both structures present substantially higher CO tolerance than both PtRu alloy and Pt catalysts. Interestingly, the MoO_x@Pt core–shell nanocatalysts revealed the lowest onset H_2 oxidation potential (−0.14 V vs. SCE) and the diffusion-limited current was reached at 0.1 V in the base electrolyte (0.5 M H_2SO_4) in the presence of 1000 ppm of CO, which is far below that for Pt and PtRu. The great mitigation of CO poisoning on the core–shell architecture might result from the electronic effect of MoO_x core on the Pt shell [38].

However, due to the fast HOR kinetics in acid media, RDE measurements may lead to ambiguity in the results since removing H_2 mass-transport resistances is very challenging. Thus, the same authors tested the performance of PEMFC membrane electrode assemblies with $Pt_{0.8}Mo_{0.2}$ and MoO_x@Pt core–shell anode electrocatalysts and commercial Pt-based cathodes [81]. Polarization curves for the alloy system in H_2 containing 25–1000 ppm CO presented an improved CO tolerance than that obtained for PtRu catalysts. However, a lower performance was obtained on MoO_x@Pt nanoarchitecture compared to PtRu and $Pt_{0.8}Mo_{0.2}$ materials when the same total catalyst loading was used. They suggested that these results could be attributed to the presence of residual stabilizer from the core–shell nanoparticles synthesis, which blocks the catalyst–ionomer interfaces. Interestingly, MoO_x@Pt exhibited the highest electrochemical performance per gram of Pt for CO concentrations below 100 ppm [81].

Other core–shell structures have been proposed by the same research group obtaining promising results [48, 82, 83]. For example, a comparison of the electrocatalytic performance for CO/H_2 electrooxidation and stability of PtSn alloy, core–shell and intermetallic nanoparticles of the same composition and size, was performed in acidic electrolyte solutions (0.5 M H_2SO_4) [82]. The studies showed that PtSn intermetallic catalyst is significantly more stable and has superior performance relative to the PtSn alloy in acidic electrolyte solutions. Additionally, the intermetallic structure can be converted to a PtSn@Pt core–shell one by successive potential cycling in CO-saturated H_2SO_4 solutions, whereas the core–shell architecture is not formed from PtSn alloys. The PtSn@Pt and PtSn intermetallic nanocatalysts displayed a better CO tolerance than commercial PtRu and Pt (E-TEK) catalysts, as can be seen in Fig. 2.2.

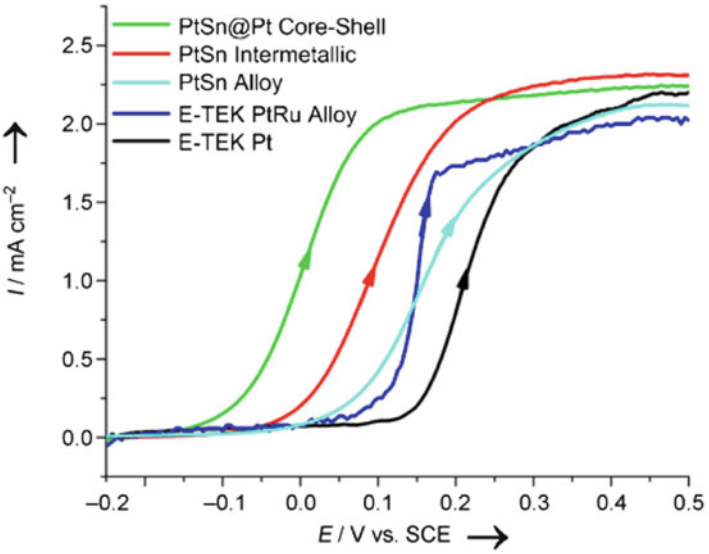

Fig. 2.2 Polarization curves for electrooxidation of CO/H_2 mixtures (1000 ppm CO, balance H_2) on different Pt–Sn catalysts and comparisons with E-TEK Pt and PtRu (all catalysts contain 30% total metal loading). Curves were recorded at 1 mVs^{-1} and 1600 rpm rotation rates in 0.5 M H_2SO_4 solution. From [82]

Additionally, core–shell nanoarchitectures offer an effective way to tune the electrocatalytic performance of catalysts. Interestingly, the shell thickness has been found to be a key role in the electrochemical activity for CO and H_2 electrooxidation [91]. Accordingly, Chen and coworkers [91] studied the electrochemical HOR of CO and H_2 on carbon-supported Ni@Pt core–shell catalysts (Ni@Pt/C) with different Pt coverages. They evidenced that both CO and H_2 oxidation were influenced by the Pt coverage. Indeed, the exchange current density (j_0) values for hydrogen oxidation of Ni@Pt/C catalysts decreased as the Pt coverage increased. At high Pt coverage, the value was the same than that obtained on Pt/C. This result was explained by the existence of nickel hydroxides and hydrogen spillover.

Other core–shell systems using nitrides as core [92] or shell [90] have been also developed. For example, Garg et al. [92] developed transition metal nitride core@noble-metal shell nanoparticles as CO-tolerant catalysts. In particular, they synthesized a Pt shell on titanium tungsten nitride core nanoparticles (Pt/TiWN). An increase in the CO tolerance was observed due to the modulation of the electronic structure of the Pt shell by the nitride core. On the other hand, bimetallic core@bimetallic shell structure has been also proposed [93]. Wang et al. [93] synthesized PtNi@PtRu/C catalysts with PtRu on the surface and PtNi in the core. A higher activity for CO electrooxidation was obtained on PtNi@PtRu/C than on PtNi/C, PtRu/C, and PtNiRu/C.

2.2.1.4 Pt/Transition Metal Carbides and Nitrides

Transition metal carbides have been also used as possible support for Pt [96–103]. Several works reported an enhancement of the electrochemical performance for hydrogen oxidation in the presence of CO using Pt/WC electrodes [104–106]. Ham et al. [105] synthesized a mesoporous tungsten carbide with a low Pt loading (7.5 wt.%) as effective CO-tolerant anode catalyst for hydrogen oxidation. The Pt/WC catalyst showed two times higher activity per gram of the precious metal than the benchmark Pt/C catalyst (E-TEK) with a high stability. On the other hand, Pt supported on *core–shell* Mo_{carb}-particles, with a reduced-Mo *core* (Mo_2C, MoO_2, and/or Mo^0) and an MoO_3-*shell* (2–3 nm), revealed an extraordinary CO tolerance revealing an onset potential of 0.065 V vs RHE for the CO oxidation reaction [102]. Recently was reported an enhanced catalytic activity toward CO electrooxidation on TiC- and TiCN-supported Pt materials induced by the amount of surface oxides at the Pt/support interface [97].

2.3 Oxygen Reduction Reaction

2.3.1 Introduction and Reaction Mechanism

The sluggish kinetics of the cathode side of the PEMFC is still the major challenge to overcome in order to be able to produce economically competitive devices [107]. The oxygen reduction reaction (ORR) is the reaction taking place at this electrode, and requires the utilization of high amounts of expensive catalysts, such as platinum-based materials, in order to overcome this sluggish kinetics [108]. This reaction is five times slower than the HOR in acid media and using platinum as a catalyst. Thus, a typical fuel cell with platinum catalyst at both anode and cathode contains 80–90% of this metal in the cathode side [108, 109]. However, the utilization of large amounts of scarce noble metals is not economically viable, and in this sense, the US Department of Energy (DoE) established a target for noble metal electrocatalysts of a maximum loading of 0.125 mg cm^{-2} and a mass activity of 0.44 mA g^{-1} to be achieved by 2020 [108, 110]. In order to achieve these requirements, the improvement and optimization of the cathode side electrocatalyst seems crucial [107]. That is why, the study of the oxygen reduction electrocatalysis has attracted a major interest in the last years and will most probably continue attracting interest in the years to come.

Research works in alkaline media attract more and more attention because the ORR kinetics is carried out in a more efficient manner than in acidic media [111, 112]. Hence, low-cost and abundant materials such as nickel, copper, and graphene-based catalysts can be employed [112–115]. However, several drawbacks such as the durability of the catalyst performance and the carbonation of the

electrolyte by the CO_2 present in the air that severly blocks active sites need to be solved [11, 111, 112].

The standar potential for the complete ORR (four-electron pathway) in alkaline media is 0.401 V:

$$O_2 + 2H_2O + 4e^- \longrightarrow 4OH^- \tag{2.14}$$

O_2 also may be reduced to peroxide ($E^0 = -0.076$ V) through the two-electron pathway:

$$O_2 + H_2O + 2e^- \longrightarrow HO_2^- + OH^- \tag{2.15}$$

that may be followed by further reduction ($E^0 = -0.878$ V):

$$HO_2^- + H_2O + 2e^- \longrightarrow 3OH^- \tag{2.16}$$

or by disproportionation:

$$2HO_2^- \longrightarrow 2OH^- + O_2 \tag{2.17}$$

On the other hand, the overall reaction taking place at the cathode in acidic solutions is the following:

$$O_2 + 4H^+ + 4e^- \longrightarrow 2H_2O \tag{2.18}$$

which possesses a standard potential of 1.229 V. However, the complete reduction of oxygen to water involves several elementary steps, pathways, and intermediates. Four electron and proton transfer steps and an O–O bond cleavage take place, and depending on the order in which each of this processes takes place, different reaction intermediates may form and several pathways may be possible. The elucidation of the oxygen reaction mechanism has not been straightforward, due, in part, to the difficulty to detect the different reaction intermediates by experimental techniques and to understand properly the kinetics data. However, nowadays it is extensively accepted that three main reaction pathways for the oxygen reduction coexist, depending on whether the O–O bond is broken before or after the different reduction steps. These are the so-called associative, dissociative, and peroxo pathways.

The first step is common in the three different pathways and corresponds with the chemical adsorption of oxygen. After that, different steps might happen. In the dissociative pathway, the O–O cleavage takes place just after the adsorption step, leading to the formation of two O_{ads} that are reduced to OH_{ads} and, finally, to water:

$$O_2 \longrightarrow O_{ads} + O_{ads} \tag{2.19}$$

$$O_{ads} + O_{ads} + 2(H^+ + e^-) \longrightarrow OH_{ads} + OH_{ads} \quad (2.20)$$

$$OH_{ads} + OH_{ads} + 2(H^+ + e^-) \longrightarrow 2H_2O \quad (2.21)$$

On the other hand, the adsorbed oxygen molecule may suffer a reduction step prior the O–O cleavage, leading to the formation of OOH_{ads}. In the associative mechanism, the O–O cleavage takes place after the formation of this intermediate and O_{ads} and OH_{ads} species are produced:

$$O_2 + (H^+ + e^-) \longrightarrow OOH_{ads} \quad (2.22)$$

$$OOH_{ads} \longrightarrow OH_{ads} + O_{ads} \quad (2.23)$$

$$O_{ads} + (H^+ + e^-) \longrightarrow OH_{ads} \quad (2.24)$$

$$OH_{ads} + OH_{ads} + 2(H^+ + e^-) \longrightarrow 2H_2O \quad (2.25)$$

The OOH_{ads} intermediate may be reduced prior to the O–O cleavage, leading to the formation of an $HOOH_{ads}$ species. This peroxo intermediate may dissociate into two OH_{ads}:

$$O_2 + (H^+ + e^-) \longrightarrow OOH_{ads} \quad (2.26)$$

$$OOH_{ads} + (H^+ + e^-) \longrightarrow HOOH_{ads} \quad (2.27)$$

$$HOOH_{ads} \longrightarrow OH_{ads} + OH_{ads} \quad (2.28)$$

Nonetheless, the $HOOH_{ads}$ species is likely to be desorbed in the form of hydrogen peroxide, reducing significantly the efficiency of the whole process, as only two electrons are exchanged instead of 4. Hydrogen peroxide is also an undesired side product due to its corrosive nature, which can endanger the stability of the fuel cell materials. Thus, electrocatalysts that favor the dissociative and associative pathways are desired. The prevalence of one pathway among the others depends on the electrocatalyst material and surface orientation, the oxygen coverage, and the potential, among others. For Pt (111) surfaces, which are expected to be the dominant on most platinum or platinum-based-alloyed nanoparticles, the associative mechanism has been reported to prevail [116, 117].

According to the Sabatier principle, the optimum catalyst may stabilize the intermediates of the reaction by adsorbing them with the adequate strength. Thus, one should expect to be able to design the perfect catalyst for the oxygen reduction reaction by optimizing the adsorption strengths of OOH_{ads}, OH_{ads}, and O_{ads}. However, as these three intermediates are bonded to the surface in a similar way, its adsorption energies are linked in a linear way. These are the so-called *scaling relationships* and imply that once one of the adsorption energies are defined, the other two will be determined [118]. As a consequence, it is possible to define the catalytic performance of the electrocatalyst for the ORR with only the adsorption energy of one of the three main intermediates and, thus, build volcano plots and

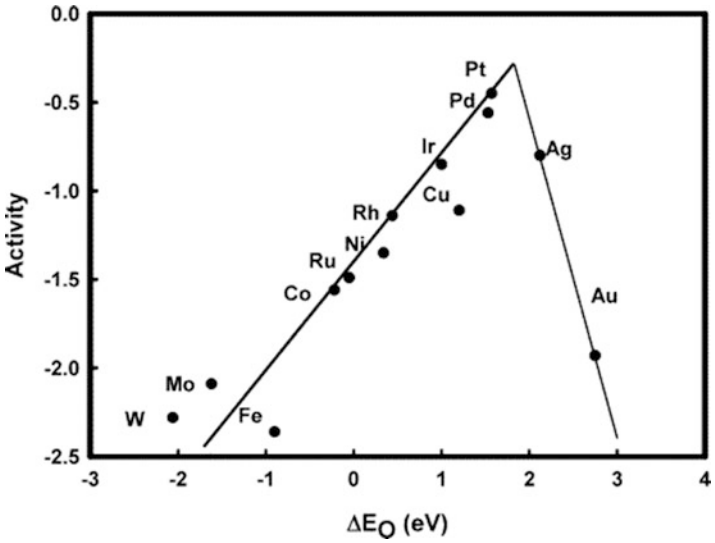

Fig. 2.3 Volcano plot showing the trend for the ORR activity as a function of the oxygen binding strenght. From [117]

predict the electrocatalyst performance of different materials in a straightforward way. However, the existence of these *scaling relationships* also implies that there will be always an overpotential for the ORR reaction, even for the best electrocatalyst. For instance, an electrocatalyst able to adsorb OOH_{ads} with an optimum strength will not optimally adsorb OH_{ads} due to the scaling, and therefore an overpotential associated to the last reaction step (OH_{ads} desorption as water) will happen [118, 119].

Figure 2.3 shows the volcano plot obtained by representing the ORR activity of different transition metals as a function of the oxygen adsorption strength.

The materials placed at the left side of the volcano plot adsorb oxygen intermediates too strong, which means that the reaction will be limited by the removal of OH_{ads} from the surface, while those at the right side are bonding the oxygen too weakly. Platinum is the material which is close to the top of the volcano, indicating that it will be the material displaying the minimum overpotential, and thus, with the higher catalytic activity. However, it is not placed at the very top of the volcano, and as a consequence, there is still margin to improve. Specifically, strategies to weaken the adsorption strength of the ORR intermediates in platinum surface by ≈0.1–0.2 eV are the desired to lead to the maximum of the volcano [116, 119, 120]. In the following section, the most successful strategies adopted during recent years will be reviewed.

2.3.2 *Strategies to Improve the Platinum Performance for the ORR*

Several strategies have been developed in order to optimize the absorption strength of platinum-based electrocatalysts. This adsorption strength depends on the electronic properties of the electrocatalyst and correlates with the distance between the d-band center and the Fermi level. When this distance is larger, the Pt–O becomes weaker. Thus, it is necessary to downshift the d-band center. This can be achieved by means of strategies such as a ligand effect or a contraction of the platinum lattice, which can be obtained by alloying, designing core–shell structures, or by a support effect, among others. Other strategies include the design of electrocatalyst with a suitable surface structure, such as preferentially oriented nanoparticles.

2.3.2.1 Morphological Effects on Platinum Electrocatalysts

Most of the electrocatalytic reactions are highly sensitive to the surface structure [121]. This means that the different surface orientations (e.g., (111), (110), and (100)) and morphologies (e.g., terrace, step, kink, and defect sites) deliver a significantly different catalytic activity. In the case of the ORR, this sensitivity is not that pronounced, and has been attributed to the differences on how the spectator species (i.e., anions in acid electrolyte and cations in alkaline electrolyte) interact with the catalytic surface. In this sense, major differences in the activity trends of the different surface orientations have been observed in diverse electrolytes. For electrolytes with non-adsorbing anions, such as $HClO_4$, the activity trend of the platinum basal planes has been reported to be: Pt(110) > Pt(111) > Pt (100) (Fig. 2.4) [122]. However, in sulfuric acid solution the activity trend changes to Pt(110) > Pt(100) > Pt (111) [123]. This knowledge on the different electrocatalytic performances of several platinum surface orientations, gained by means of the studies performed with single crystals, allowed a rational design in order to prepare catalyst with the most active surface orientation [124].

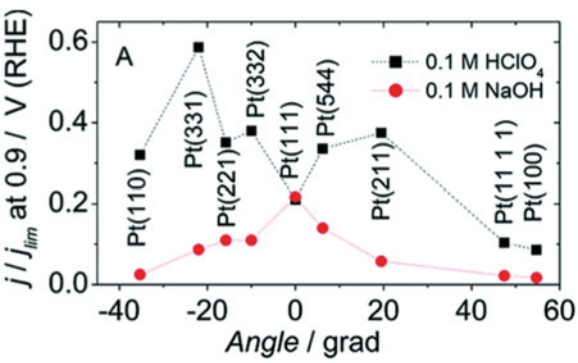

Fig. 2.4 ORR activities for single crystals with different orientation in acid and alkaline electrolytes. From [122]

Platinum nanoparticles usually present a combination of surfaces with (111) and (100) orientations. However, it is also possible to synthesize nanoparticles with cubic shape ((100) surface orientation) or octahedral and tetrahedral nanoparticles with (111) surface orientation, as well as nanoparticles with high index facets by applying a square-wave potential method [108, 124–128]. The ORR on nanoparticles with preferential surface orientation showed that those with a prevalence of (111) (octahedral shapes) were considerably more active than those with (100) (cubic nanoparticles) or with a combination of both basal planes (spherical nanoparticles) [129]. Furthermore, concave nanoparticles with high index orientation revealed great catalytic activity toward the ORR [127].

Regarding to the particle size, a similar effect was observed. Particles with small sizes present high quantity of defect sites on their surfaces. The last was expected to produce a particle size dependence on the ORR activity. Many groups have studied the effect of the particle size on the catalytic activity, obtaining some contradictory results [108, 130–133]. It was reported that the electrocatalytic specific activity of small nanoparticles (1–10 nm) increases as the size of the particles increases, correlating well with the amount of terraces present on the surface [131]. The specific activity was reported to increase with the particle size until c.a. 10 nm, for which the activity of bulk platinum was already achieved. The mass activity was reported to be maximum for particles around 3 nm [108, 130, 131]. However, other studies concluded that the electrocatalytic activity for small particles (1–5 nm) does not depend on the particle size, increasing only for larger sizes [132, 133]. It is noteworthy that similar activity–size trend was observed in acid and alkaline media [132].

2.3.2.2 Alloying

Alloying has been one of the first and most studied strategies to improve the platinum catalytic performance toward the ORR. The addition of a second metal, which is usually a less noble metal, has two main advantages: from one side, it decreases the price of the catalyst as the amount of platinum is reduced, and from the other side, the addition of the second metal enhances the catalytic performance by means of a shift of the d-band center. The presence of the secondary metal causes two main effects that contribute at the enhancement of the catalytic performance: a ligand effect and a contraction effect. The first one is a pure electronic effect, as the presence of the second metal generates modifications of the d-band occupancy that can downshift the d-center. In the other side, the contraction effect is a geometric effect due to the different size of the platinum and secondary atoms, which generates a modification of the interatomic distances on the surface [134]. With a proper selection of the second metal, it is possible to obtain alloys with the adequate modification (electronic vacancies and a geometric contraction) that can optimize the Pt–O adsorption strength, and thus, enhance the ORR.

Pt-Late Transition Metal Alloys

Several platinum-based alloys with metals such as Co, Fe, Cu, Ni, Ti, or Cr were tested during the last decade, obtaining specific activities at 0.9 V vs RHE several folds higher than those of bare platinum nanoparticles [135–144]. The experimental data obtained in these studies allowed building activity volcano plots for the different alloyed materials. The study of the 3-d metal series determined Pt_3Co and (111)-Pt_3Ni to be very close to the top of the volcano [144, 145]. In this sense, Markovic group reported a ten-fold higher activity on (111) Pt_3Ni catalyst than on Pt(111) surfaces.

During the last years, further effort has been put into the optimization of the morphological (e.g., size and shape) and compositional (e.g., nature of the composition and metal segregation) properties of the bimetallic nanoparticles in order to push up them to the top of the volcano plots. The effect of each of these parameters is not straightforward as in the case of the monometallic platinum nanoparticles, as may vary depending on the nature of the secondary metal, the synthesis method, or the annealing condition. As an example, optimum Pt:Ni ratio values of 2.5:1 [146] and 1.5:1 [147] were reported. For that reason, for further information and examples on the effect and optimization of each of these properties on the ORR electrocatalytic activity of bimetallic nanoparticles, the reader is referred to the following reviews [148–151]. In general, the optimization of several of these parameters allows a considerable increase of the ORR electrocatalytic activity. For instance, Cui et al. reported a 15 times higher activity for PtNi octahedral nanoparticles rather than for a conventional Pt/C catalyst [152].

More complex materials, such as ternary or quaternary alloys or doped binary alloys, have also been reported [153–157]. Huang et al. reported molybdenum surface-doped PtNi nanoparticles, obtaining significant improvements in the activity and stability [156]. Rh surface-doped PtNi nanoparticles were also reported to have an improved long-term performance, due to the suppression of shape modification over potential cycling [157].

The main drawback of this family of materials is their stability in acidic media, in which the alloyed nanoparticles become platinum rich due to a fast leaching of the non-noble metals [119]. The last leads to the formation of porous surfaces or even to major modification of the nanoparticles shapes. In order to avoid these phenomena, several strategies have been developed to form a stable platinum segregated surface region prior to the electrochemical testing:

1. Platinum-skin: consists on subjecting the alloys to a thermal annealing in order to generate platinum segregation that protect the bulk material. It has been reported that bimetallic alloys with a platinum-skin not only present a higher stability but also an enhanced electrochemical performance toward the ORR [144, 158, 159]. The last was ascribed to the decrease of the Pt–Pt distance on the temperature-induced segregated surface. A variation of this method consists to remove the non-noble metals from the surface of the alloy by acid washing followed by thermal annealing (Fig. 2.5) [160, 161]. Another alternative is to induce the noble metal segregation by carbon monoxide [162].

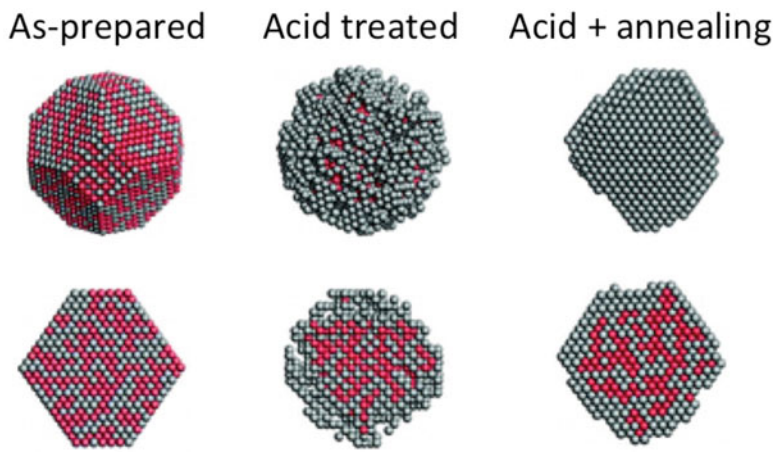

Fig. 2.5 Formation of a Pt-skin on a bimetallic catalyst by acid washing followed by thermal annealing. Adapted from [161]

2. Dealloying: the formation of a superficial platinum layer can also be achieved in a controlled way by electrochemical leaching of the non-noble metal in acid solutions. This technique was exhaustively employed by Strasser and coworkers for PtCu alloys and is achieved by cycling the electrocatalyst until a stable Pt-like cyclic voltamperogram is obtained, which indicates that most of the non-noble metal has leached from the surface [163]. More recently, this method has been successfully applied to other bimetallic alloys (PtCo, PtNi...) and trimetallic particles, and enhanced stability performances of these materials have been reported for three-electrode half-cells, as well as for PEMFC [164–166].

The dealloying and acid leaching phenomena can also be employed to produce highly porous materials with enhanced ORR activity following well-controlled processes [167–170]. In addition, it was proposed that this kind of materials may possess an improved stability due to its nanoscale curvature [171]. However, it was later demonstrated that the porous nanoarchitecture rapidly collapses along potentiodynamic cycles and therefore their stability is compromised [172].

Pushing the dealloying phenomena to an extreme, Chen et al. were able to synthesize hollow nanoparticles with a well-defined shape, called nanoframes [173]. In this case, they reported the synthesis of Pt_3Ni by the geometric evolution of $PtNi_3$ polyhedra ripened in chloroform or hexane at ambient condition for several weeks (Fig. 2.6). The nanoframes were annealed in order to form a Pt-skin surface [174] without losing their 3D-hollow structure. Mass activities 36-fold higher and specific activities 22-fold higher relative to a Pt/C catalyst were reported, which are among the highest ever reported. In addition, an enhanced performance toward the ORR after an accelerated stability test was reported. After this work, several binary and ternary alloy nanoframes with outstanding catalytic performance toward the ORR were published [175–178].

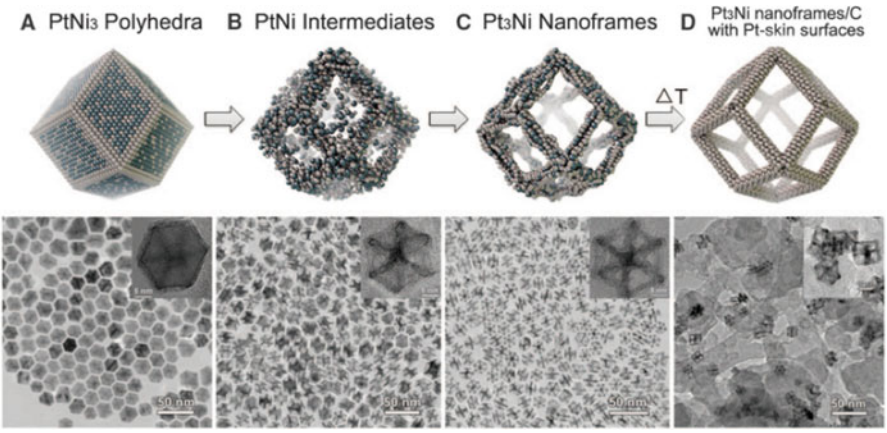

Fig. 2.6 Formation of a Pt-skin on a bimetallic catalyst by acid washing followed by thermal annealing. (**a**) $PtNi_3$ polyhedra. (**b**) PtNi Intermediates. (**c**) Pt_3Ni Nanoframes. (**d**) Pt_3Ni nanoframes/C with Pt-skin surfaces. From [173]

Pt-Early Transition Metal and Lanthanide Alloys

Greeeley and coworkers performed density-functional theory calculations in order to identify more active and stable alloys, and Pt_3Sc and Pt_3Y materials were identified as suitable candidates, which were later corroborated by experimental measurements. They reported a catalytic enhancement of 10 folds for polycrystalline Pt_3Y electrode compared to pure Pt [145]. The latter was also corroborated by carbon-supported Pt_3Sc and Pt_3Y catalysts [179, 180]. Hernandez-Fernandez and coworkers reported that the Y effect on the nanoparticles was purely a contraction effect. Lately, a similar effect was reported for a Pt_5La polycrystalline alloy, which opened the door to study the lanthanide series [181].

For Pt–lanthanide alloys, as the atomic size of Pt and the second metal is considerably different, the platinum atoms rearrange forming a surface Kagome-like layer after the acid leaching of the lanthanide (Fig. 2.7a). The Pt–Pt distance in these surfaces is considerably more compressed than for bare platinum of Pt-late transition metal alloys, and decreases progressively when we move from the left to the right in the periodic table, as a consequence of the lanthanides contraction. Thus, the Pt–O adsorption strength also decreases from the left to the right of the lanthanides series. In this way, a volcano plot is obtained, with the Pt_5Tb and Pt_5Gd placed very close to the top (Fig. 2.7b) [182]. The production of nanoparticles based on these alloys is not straightforward due to the standard potentials of the redox couples. However, an outstanding activity of 3.6 mA/mg_{Pt} for Pt_5Gd nanoparticles was reported, and it is among the highest ORR mass activities reported so far [182, 183].

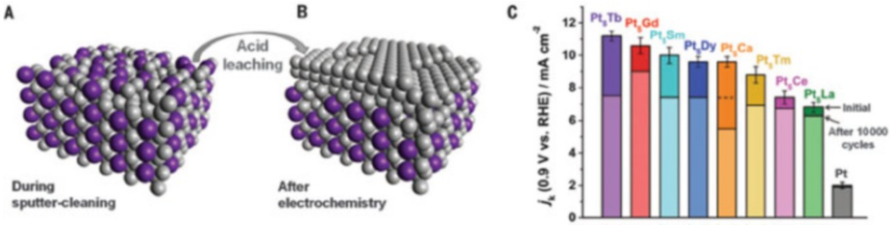

Fig. 2.7 Schematic views and electrocatalytic activity of the Pt–lanthanide series alloys. (**a**, **b**) show the tridemensional structure of the alloy before and after the acid leaching, respectively. (**c**) shows the specific activities of the different alloys before and after applying a 10,000-cycle stability test. From [182]

2.3.2.3 Core–Shell Structures

In order to decrease the price of the platinum-based electrocatalyst, an extensively used strategy has been the synthesis of core–shell nanoparticles, containing a thin platinum shell onto a less expensive core. In this way, most of the platinum is placed in the surface of the particles and thus, can be used [184].

Among the different strategies to prepare core–shell nanoparticles, the monolayer approach developed and extensively studied by the Adzic group has been the most successful one [185]. They developed a synthesis method to produce highly stable monolayers consisting in the platinum galvanic displacement of a copper monolayer produced by underpotential deposition (UPD) [185]. With this method, not only the totality of the platinum is on the surface but also the core may promote the catalytic activity of the shell by means of electronic and geometric (compression) effects. Palladium was identified as a good core to enhance the electrocatalytic activity of the platinum monolayer toward the ORR (Fig. 2.8). In recent years, the composition of the core has been optimized to further improve the monolayer activity. Some strategies that have been proved to be useful are the utilization of alloys as a core (which can also reduce the price) [186–189], well-defined nanoparticles (octahedral, tetrahedral, etc.) [190, 191], porous cores [192], and hollow nanoparticles cores to further optimize the compression degree of the monolayer [193].

Other synthesis methods have also been used to produce core–shell nanoparticles with different shell thicknesses. Among them, the direct chemical reduction of the platinum monolayer onto the cores seems to be one of the easiest for a long scale production [184]. Different solvents, capping, and reducing agents have been tested, allowing the design of methodologies that allow a precise control of the shell thicknesses [184, 194–199]. However, when employing this kind of synthesis protocols, one needs to make sure that a complete elimination of the organic compounds is achieved, as otherwise, they could block the electrocatalyst surface and hinder the activity.

Recently, core–shell nanoparticles using nitrides as cores have also been developed, showing outstanding stabilities [200]. Different carbides, nitrides, and oxides

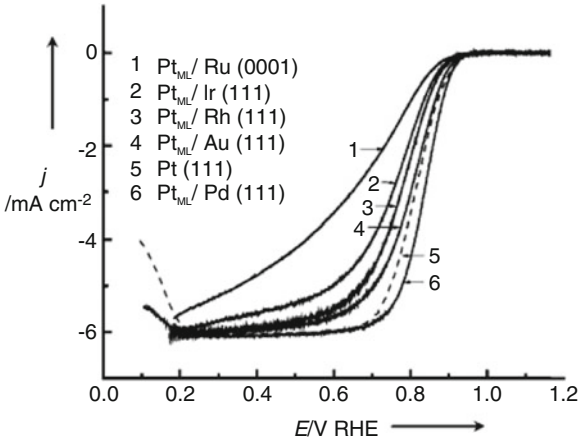

Fig. 2.8 Polarization curves for O_2 reduction on platinum monolayers (PtML) on Ru(0001), Ir (111), Rh(111), Au(111), and Pd(111) in a 0.1 m $HClO_4$. The rotation rate is 1600 rpm, and the sweep rate is 20 mVs^{-1}. From [185]

have also been reported to perform a promoting effect when used as electrocatalytic supports for platinum-based ORR electrocatalysts [201–205]. The effect of different carbonaceous supports will be discussed in Chap. 5 of the current book.

2.3.3 Non-Platinum Electrocatalysts

Due to the high price of platinum, a major effort has been placed in recent years to develop platinum-free electrocatalysts for the oxygen reduction reaction in acid media. Materials such as oxides, nitrides, carbonitrides, oxynitirides, and chalcogenides have been reported to deliver significant activities. Carbon-based materials with Fe/N/C and Co/N/C centers have also outstanding performances, as well as several metal-free carbon electrocatalysts [115, 195, 206]. The non-noble electrocatalyst for the ORR will be extensively reviewed in Chap. 7.

2.3.3.1 Palladium and Palladium-Alloy Catalysts

Palladium also delivers a high activity for the ORR. Actually, it is placed very close to platinum on the ORR volcano plot (Fig. 2.3). For that reason, the study of ORR on palladium-based electrocatalysts has also received some interest.

Despite the similarity of palladium to platinum, the (100) face has been reported to be the most active one for palladium surfaces [207]. This means that, for this metal, the preferred shape for the nanoparticles will be cubic. In this sense, several works reported an enhanced electrocatalytic activity of nanoparticles with this orientation rather than for bulk palladium or nanoparticles with other surface orientations [208–210]. As for platinum, several strategies such as alloying have been employed to enhance the electrocatalytic performance. Bimetallic alloys such as

Pd − M (M = Co, Fe, Ni, Cr, Mn, Ti, V, Sn, Cu, Ir, Ag, Rh, Au, Pt) have been reported as good candidates [211–213]. Strategies already discussed in the previous section such as dealloying, Pd-skins, monolayers, complex nanoarchitectures, or an enhancement effect of non-carbon supports have also been successfully implemented in order to improve the activity [214–219].

2.3.4 *Stability Issues*

In addition to the sluggish ORR kinetics on the electrocatalysts used at the cathode side of LTFCs, the stability of these electrocatalysts is also a main concern. The degradation and durability of the materials used as electrocatalyst, mainly those at the cathode side, have a huge impact on the performance of LTFCs. For that reason, during the last years, a lot of effort has been put into understanding the degradation mechanisms of the electrocatalyst under operation conditions [119, 220].

Several degradation mechanisms have been identified to take part at the electrocatalyst during the operation of LTFC, especially during the start up and shut down of the device, when sever potential jumps may occur [220]. The main degradation mechanisms are (Fig. 2.9):

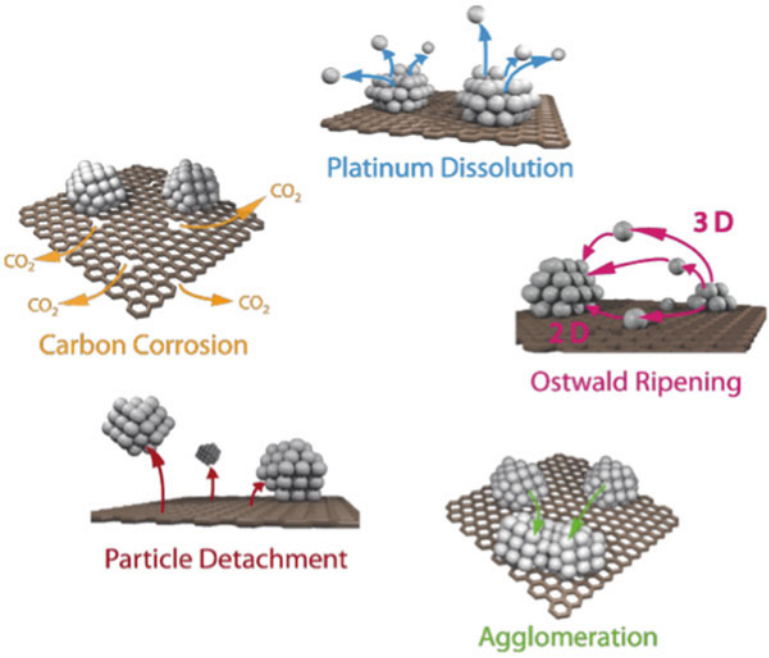

Fig. 2.9 Schematic representation of the main degradation mechanisms. From [222]

1. Metal dissolution: the dissolution of the metals contained in the electrocatalyst is a main issue as it supposes a lost in efficiency as well as the impossibility to recover the scarce and expensive noble metals.

   Platinum dissolution is known to be more prominent as smaller the nanoparticles are, due to an increase of the surface energy. The dissolution is also known to take place mainly during the cathodic process and is believed to be associated to the reduction of Pt–O-like species back to platinum (0). Even being considerably lower, the anodic dissolution during platinum oxidation is also not negligible [119, 221].

   For platinum-based alloys, the dissolution of the second metal is also a main issue. The dissolution of non-noble metals such as Cu, Ni, Co... is thermodynamically favored on the potential in which ORR takes place. This leads to a leaching of these metals out of the alloyed structure, and, thus, a progressive loss of the catalytic performance is attained. After an extensive dissolution of these metals, some porous platinum particles may be formed, while the dissolved cations may interact with the ionomer and hence slower diffusion and higher electric resistance are commonly observed [119, 220].
2. Ostwald ripening: as a consequence of platinum dissolution, the Ostwald ripening phenomena may take place. This process consists of the redeposition of the dissolved platinum from the smallest nanoparticles onto the bigger ones. Thus, it results on an increase of the nanoparticle size and a decrease of the mass activity, as a larger amount of platinum becomes inaccessible [119, 222].
3. Degradation of the catalyst support: the catalyst support also suffers from major corrosion problems under the operation condition of LTFC. Carbon corrosion to CO_2 is thermodynamically favorable above 0.2 V vs RHE but only kinetically relevant at higher potentials than 1.2 V. Main outcomes from the degradation of the catalyst support are the lower porosity that may hinder the mass transport and the generation of other degradation mechanisms such as the detachment and agglomeration of metal nanoparticles [119, 222].
4. Detachment of metal nanoparticles: metal nanoparticles may detach from the electrode as a consequence of the degradation of the catalyst support, and therefore the electric contact is lost and the overall efficiency drops [119, 222].
5. Agglomeration of metal nanoparticles: this process is a consequence of the support degradation, which leads to an increase of the nanoparticles size. When the support corrodes, it may shrink and allow different nanoparticles to enter in contact. Once this happens, the nanoparticles end up coalescing into bigger ones. A high mobility of the nanoparticles through the support also leads to agglomeration [119, 222].

2.4 Conclusions

In this chapter, the general concept of fuel cells was discussed, with special attention to low-temperature fuel cells (LTFCs) working in acid and alkaline media. LTFC is a very attractive technology and emerges to be one of the energy converting devices for the near future.

With the aim to solve the principal catalytic, durability, and cost problems at the anode and cathode of LTFCs, a fundamental and applied study of carbon monoxide and hydrogen oxidation as well as oxygen reduction reaction on platinum- and palladium-based nanomaterials in acidic electrolytes was considered and compared with the same reactions in alkaline media.

Then, mono-, bi-, and trimetallic catalysts involving alloys, core–shell nanoarchitectures, and transition metal oxides have been reviewed as effective electrocatatalysts for the oxidation of carbon monoxide and hydrogen as well as for the reduction of oxygen in acid and alkaline environments.

All the information revisoned and scrutinized here may help to improve the fabrication of novel catalysts in order to decrease the cost and enhance the performance of LTFCs, in such a way that LTFC commercialization will be real.

Acknowledgments The Spanish Ministry of Economy and Competitiveness (MINECO) has supported this work under project ENE2014-52158-C2-2R (cofunded by FEDER). G.G. acknowledges the Viera y Clavijo program (ACIISI & ULL) for financial support.

References

1. Tarasevich MR, Korchagin OV (2013) Electrocatalysis and pH (a review). Russ J Electrochem 49:600–618. https://doi.org/10.1134/S102319351307015X
2. Sheng W, Zhuang Z, Gao M, Zheng J, Chen JG, Yan Y (2015) Correlating hydrogen oxidation and evolution activity on platinum at different pH with measured hydrogen binding energy. Nat Commun 6:5848. https://doi.org/10.1038/ncomms6848
3. Zheng J, Sheng W, Zhuang Z, Xu B, Yan Y (2016) Universal dependence of hydrogen oxidation and evolution reaction activity of platinum-group metals on pH and hydrogen binding energy. Sci Adv 2(3):e1501602. https://doi.org/10.1126/sciadv.1501602
4. Sheng W, Gasteiger HA, Shao-Horn Y (2010) Hydrogen oxidation and evolution reaction kinetics on platinum: acid vs alkaline electrolytes. J Electrochem Soc 157:B1529–B1536
5. Marković NM (2010) The hydrogen electrode reaction and the electrooxidation of CO and H2/CO mixtures on well-characterized Pt and Pt-bimetallic surfaces. In: Handbook of fuel cells. Wiley, Chichester
6. García G (2017) Correlation between CO oxidation and H adsorption/desorption on Pt surfaces in a wide pH range: the role of alkali cations. ChemElectroChem 4:459–462. https://doi.org/10.1002/celc.201600731
7. Trasatti S (1972) Work function, electronegativity, and electrochemical behaviour of metals: III. Electrolytic hydrogen evolution in acid solutions. J Electroanal Chem Interfacial Electrochem 39:163–184. https://doi.org/10.1016/S0022-0728(72)80485-6

8. Sheng W, Myint M, Chen JG, Yan Y (2013) Correlating the hydrogen evolution reaction activity in alkaline electrolytes with the hydrogen binding energy on monometallic surfaces. Energy Environ Sci 6:1509. https://doi.org/10.1039/c3ee00045a
9. Ehteshami SMM, Chan SH (2013) A review of electrocatalysts with enhanced CO tolerance and stability for polymer electrolyte membarane fuel cells. Electrochim Acta 93:334–345. https://doi.org/10.1016/J.ELECTACTA.2013.01.086
10. Pedersen CM, Escudero-Escribano M, Velázquez-Palenzuela A, Christensen LH, Chorkendorff I, Stephens IEL (2015) Benchmarking Pt-based electrocatalysts for low temperature fuel cell reactions with the rotating disk electrode: oxygen reduction and hydrogen oxidation in the presence of CO (review article). Electrochim Acta 179:647–657. https://doi.org/10.1016/J.ELECTACTA.2015.03.176
11. García G, Koper MTM (2011) Carbon monoxide oxidation on Pt single crystal electrodes: understanding the catalysis for low temperature fuel cells. ChemPhysChem 12:2064–2072. https://doi.org/10.1002/cphc.201100247
12. García G, Koper MTM (2009) Mechanism of electro-oxidation of carbon monoxide on stepped platinum electrodes in alkaline media: a chronoamperometric and kinetic modeling study. Phys Chem Chem Phys 11:11437–11446. https://doi.org/10.1039/b914013a
13. Spendelow JS, Lu GQ, Kenis PJA, Wieckowski A (2004) Electrooxidation of adsorbed CO on Pt(1 1 1) and Pt(1 1 1)/Ru in alkaline media and comparison with results from acidic media. J Electroanal Chem 568:215–224. https://doi.org/10.1016/J.JELECHEM.2004.01.018
14. Lopes PP, Freitas KS, Ticianelli EA (2010) CO tolerance of PEMFC anodes: mechanisms and electrode designs. Electrocatalysis 1:200–212. https://doi.org/10.1007/s12678-010-0025-y
15. García G, Rodríguez P, Rosca V, Koper MTM (2009) Fourier transform infrared spectroscopy study of CO electro-oxidation on Pt(111) in alkaline media. Langmuir 25:13661–13666. https://doi.org/10.1021/la902251z
16. Asgardi J, Calderón JC, Alcaide F, Querejeta A, Calvillo L, Lázaro MJ, García G, Pastor E (2015) Carbon monoxide and ethanol oxidation on PtSn supported catalysts: effect of the nature of the carbon support and Pt:Sn composition. Appl Catal B Environ 168–169:33–41. https://doi.org/10.1016/j.apcatb.2014.12.003
17. Calderón JC, García G, Querejeta A, Alcaide F, Calvillo L, Lázaro MJ, Rodríguez JL, Pastor E (2015) Carbon monoxide and methanol oxidations on carbon nanofibers supported Pt–Ru electrodes at different temperatures. Electrochim Acta 186:359–368. https://doi.org/10.1016/j.electacta.2015.09.121
18. Rizo R, Lázaro MJMJ, Pastor E, García G (2016) Spectroelectrochemical study of carbon monoxide and ethanol oxidation on Pt/C, PtSn(3:1)/C and PtSn(1:1)/C catalysts. Molecules 21:1225. https://doi.org/10.3390/molecules21091225
19. Garcia G, Silva-Chong J, Guillen-Villafuerte O, Rodriguez J, Gonzalez E, Pastor E (2006) CO tolerant catalysts for PEM fuel cells: spectroelectrochemical studies. Catal Today 116:415–421. https://doi.org/10.1016/j.cattod.2006.05.069
20. Martínez Huerta MV, García G (2015) Fabrication of electro-catalytic nano-particles and applications to proton exchange membrane fuel cells. In: Leung DYC, Xuan J (eds) Micro & nano-engineering of fuel cells. CRC Press, London, pp 95–129
21. Maruyama J, Inaba M, Katakura K, Ogumi Z, Takehara Z (1998) Influence of Nafion® film on the kinetics of anodic hydrogen oxidation. J Electroanal Chem 447:201–209. https://doi.org/10.1016/S0022-0728(98)00004-7
22. Parthasarathy A, Martin CR, Srinivasan S (1991) Investigations of the O[sub 2] reduction reaction at the platinum/Nafion® interface using a solid-state electrochemical cell. J Electrochem Soc 138:916. https://doi.org/10.1149/1.2085747
23. Serov A, Kwak C (2009) Review of non-platinum anode catalysts for DMFC and PEMFC application. Appl Catal B Environ 90:313–320
24. Li H, Lee K, Zhang J (2008) Electrocatalytic H2 oxidation reaction. In: PEM fuel cell electrocatalysts and catalyst layers. Springer, London, pp 135–164

25. Wang T, Xie H, Chen M, D'Aloia A, Cho J, Wu G, Li Q (2017) Precious metal-free approach to hydrogen electrocatalysis for energy conversion: from mechanism understanding to catalyst design. Nano Energy 42:69–89. https://doi.org/10.1016/J.NANOEN.2017.10.045
26. Giorgi L, Pozio A, Bracchini C, Giorgi R, Turtù S (2001) H2 and H2/CO oxidation mechanism on Pt/C, Ru/C and Pt–Ru/C electrocatalysts. J Appl Electrochem 31:325–334. https://doi.org/10.1023/A:1017595920726
27. Pozio A, Giorgi L, Antolini E, Passalacqua E (2000) Electroxidation of H2 on Pt/C Pt–Ru/C and Pt–Mo/C anodes for polymer electrolyte fuel cell. Electrochim Acta 46:555–561. https://doi.org/10.1016/S0013-4686(00)00625-3
28. Uchida H, Izumi K, Watanabe M (2006) Temperature dependence of CO-tolerant hydrogen oxidation reaction activity at Pt, Pt−Co, and Pt−Ru electrodes. J Phys Chem B 110 (43):21924–21930. https://doi.org/10.1021/JP064190X
29. Koper MTM, Shubina TE, van Santen RA (2001) Periodic density functional study of CO and OH adsorption on Pt−Ru Alloy surfaces: implications for CO tolerant fuel cell catalysts. J Phys Chem B 106(3):686–692. https://doi.org/10.1021/JP0134188
30. Sato T, Okaya K, Kunimatsu K, Yano H, Watanabe M, Uchida H (2012) Effect of particle size and composition on CO-tolerance at Pt–Ru/C catalysts analyzed by in situ attenuated total reflection FTIR spectroscopy. ACS Catal 2:450–455. https://doi.org/10.1021/cs200550t
31. Camara GA, Ticianelli EA, Mukerjee S, Lee SJ, McBreen J (2002) The CO poisoning mechanism of the hydrogen oxidation reaction in proton exchange membrane fuel cells. J Electrochem Soc 149:A748. https://doi.org/10.1149/1.1473775
32. Wakisaka M, Mitsui S, Hirose Y, Kawashima K, Uchida H, Watanabe M (2006) Electronic structures of Pt−Co and Pt−Ru alloys for CO-tolerant anode catalysts in polymer electrolyte fuel cells studied by EC−XPS. J Phys Chem B 110(46):23489–23496. https://doi.org/10.1021/JP0653510
33. Chen C-Y, Huang K-P (2017) Performance and transient behavior of the kW-grade PEMFC stack with the PtRu catalyst under CO-contained diluted hydrogen. Int J Hydrog Energy 42:22250–22258. https://doi.org/10.1016/J.IJHYDENE.2017.06.037
34. Flórez-Montaño J, García G, Rodríguez JL, Pastor E, Cappellari P, Planes GA (2015) On the design of Pt based catalysts. Combining porous architecture with surface modification by Sn for electrocatalytic activity enhancement. J Power Sources 282:34–44. https://doi.org/10.1016/j.jpowsour.2015.02.018
35. Antolini E, Gonzalez ER (2010) The electro-oxidation of carbon monoxide, hydrogen/carbon monoxide and methanol in acid medium on Pt-Sn catalysts for low-temperature fuel cells: a comparative review of the effect of Pt-Sn structural characteristics. Electrochim Acta 56:1–14. https://doi.org/10.1016/J.ELECTACTA.2010.08.077
36. Shubina T, Koper MT (2002) Quantum-chemical calculations of CO and OH interacting with bimetallic surfaces. Electrochim Acta 47:3621–3628. https://doi.org/10.1016/S0013-4686(02)00332-8
37. Martínez-Huerta M, Tsiouvaras N, García G, Peña M, Pastor E, Rodriguez J, Fierro J (2013) Carbon-supported PtRuMo electrocatalysts for direct alcohol fuel cells. Catalysts 3:811–838. https://doi.org/10.3390/catal3040811
38. Liu Z, Hu JE, Wang Q, Gaskell K, Frenkel AI, Jackson GS, Eichhorn B (2009) PtMo alloy and MoO_x@Pt Core−shell nanoparticles as highly CO-tolerant electrocatalysts. J Am Chem Soc 131:6924–6925. https://doi.org/10.1021/ja901303d
39. Mukerjee S, Urian RC, Lee SJ, Ticianelli EA, McBreen J (2004) Electrocatalysis of CO tolerance by carbon-supported PtMo electrocatalysts in PEMFCs. J Electrochem Soc 151: A1094. https://doi.org/10.1149/1.1759363
40. Urian RC, Gullá AF, Mukerjee S (2003) Electrocatalysis of reformate tolerance in proton exchange membranes fuel cells: part I. J Electroanal Chem 554–555:307–324. https://doi.org/10.1016/S0022-0728(03)00241-9
41. Hassan A, Carreras A, Trincavelli J, Ticianelli EA (2014) Effect of heat treatment on the activity and stability of carbon supported PtMo alloy electrocatalysts for hydrogen oxidation in

proton exchange membrane fuel cells. J Power Sources 247:712–720. https://doi.org/10.1016/J.JPOWSOUR.2013.08.138
42. Hassan A, Iezzi RC, Ticianelli EA (2015) Activity and stability of molybdenum-containing dispersed Pt catalysts for CO tolerance in proton exchange membrane fuel cell anodes. ECS Trans 69:45–55. https://doi.org/10.1149/06917.0045ecst
43. Maya-Cornejo J, Garcia-Bernabé A, Compañ V (2018) Bimetallic Pt-M electrocatalysts supported on single-wall carbon nanotubes for hydrogen and methanol electrooxidation in fuel cells applications. Int J Hydrog Energy 43:872–884. https://doi.org/10.1016/J.IJHYDENE.2017.10.097
44. Pereira LGS, Paganin VA, Ticianelli EA (2009) Investigation of the CO tolerance mechanism at several Pt-based bimetallic anode electrocatalysts in a PEM fuel cell. Electrochim Acta 54:1992–1998. https://doi.org/10.1016/J.ELECTACTA.2008.07.003
45. Tarasevich MR, Bogdanovskaya VA, Grafov BM, Zagudaeva NM, Rybalka KV, Kapustin AV, Kolbanovskii YA (2005) Electrocatalytic properties of binary systems based on platinum and palladium in the reaction of oxidation of hydrogen poisoned by carbon monoxide. Russ J Electrochem 41:746–757. https://doi.org/10.1007/s11175-005-0134-8
46. Alcaide F, Álvarez G, Cabot PL, Miguel O, Querejeta A (2010) Performance of carbon-supported PtPd as catalyst for hydrogen oxidation in the anodes of proton exchange membrane fuel cells. Int J Hydrog Energy 35:11634–11641. https://doi.org/10.1016/J.IJHYDENE.2010.03.011
47. Papageorgopoulos DC, Keijzer M, Veldhuis JBJ, de Bruijn FA (2002) CO tolerance of Pd-rich platinum palladium carbon-supported electrocatalysts. J Electrochem Soc 149:A1400. https://doi.org/10.1149/1.1510131
48. Liu Z, Jackson GS, Eichhorn BW (2011) Tuning the CO-tolerance of Pt-Fe bimetallic nanoparticle electrocatalysts through architectural control. Energy Environ Sci 4:1900. https://doi.org/10.1039/c1ee01125a
49. Ehteshami SMM, Jia Q, Halder A, Chan SH, Mukerjee S (2013) The role of electronic properties of Pt and Pt alloys for enhanced reformate electro-oxidation in polymer electrolyte membrane fuel cells. Electrochim Acta 107:155–163. https://doi.org/10.1016/j.electacta.2013.06.026
50. Lin R, Cao C, Zhang H, Huang H, Ma J (2012) Electro-catalytic activity of enhanced CO tolerant cerium-promoted Pt/C catalyst for PEM fuel cell anode. Int J Hydrog Energy 37:4648–4656. https://doi.org/10.1016/J.IJHYDENE.2011.05.021
51. Grgur B, Markovic N, Ross P (1998) Electrooxidation of H2, CO and H2/CO mixtures on a well-characterized Pt–Re bulk alloy electrode and comparison with other Pt binary alloys. Electrochim Acta 43:3631–3635. https://doi.org/10.1016/S0013-4686(98)00120-0
52. Ranjan C, Hoffmann R, DiSalvo FJ, Abruña HD (2007) Electronic effects in CO chemisorption on Pt−Pb intermetallic surfaces: a theoretical study. J Phys Chem C 111 (46):17357–17369. https://doi.org/10.1021/JP0746603
53. de-los-Santos-Álvarez N, Alden LR, Rus E, Wang H, DiSalvo FJ, Abruña HD (2009) CO tolerance of ordered intermetallic phases. J Electroanal Chem 626:14–22. https://doi.org/10.1016/J.JELECHEM.2008.10.028
54. Wasmus S, Küwer A (1999) Methanol oxidation and direct methanol fuel cells: a selective review. J Electroanal Chem 461:14–31
55. Antolini E (2011) The problem of Ru dissolution from Pt–Ru catalysts during fuel cell operation: analysis and solutions. J Solid State Electrochem 15:455–472. https://doi.org/10.1007/s10008-010-1124-7
56. Hengge K, Gänsler T, Pizzutilo E, Heinzl C, Beetz M, Mayrhofer KJJ, Scheu C (2017) Accelerated fuel cell tests of anodic Pt/Ru catalyst via identical location TEM: new aspects of degradation behavior. Int J Hydrog Energy 42:25359–25371. https://doi.org/10.1016/J.IJHYDENE.2017.08.108

57. Gasteiger HA, Markovic NM, Ross PN (1995) Electrooxidation of CO and H2/CO mixtures on a well-characterized Pt3Sn electrode surface. J Phys Chem 99:8945–8949. https://doi.org/10.1021/j100022a002
58. Götz M, Wendt H (1998) Binary and ternary anode catalyst formulations including the elements W, Sn and Mo for PEMFCs operated on methanol or reformate gas. Electrochim Acta 43:3637–3644. https://doi.org/10.1016/S0013-4686(98)00121-2
59. Martínez-Huerta MV, Rojas S, Gómez de la Fuente JL, Terreros P, Peña MA, Fierro JLG (2006) Effect of Ni addition over PtRu/C based electrocatalysts for fuel cell applications. Appl Catal B Environ 69:75–84. https://doi.org/10.1016/j.apcatb.2006.05.020
60. Stevens DA, Rouleau JM, Mar RE, Atanasoski RT, Schmoeckel AK, Debe MK, Dahn JR (2007) Enhanced CO-tolerance of Pt–Ru–Mo hydrogen oxidation catalysts. J Electrochem Soc 154:B1211. https://doi.org/10.1149/1.2784188
61. Papageorgopoulos D, Keijzer M, de Bruijn F (2002) The inclusion of Mo, Nb and Ta in Pt and PtRu carbon supported electrocatalysts in the quest for improved CO tolerant PEMFC anodes. Electrochim Acta 48:197–204. https://doi.org/10.1016/S0013-4686(02)00602-3
62. Luo J, Kariuki N, Han L, Wang L, Zhong C-J, He T (2006) Preparation and characterization of carbon-supported PtVFe electrocatalysts. Electrochim Acta 51:4821–4827. https://doi.org/10.1016/J.ELECTACTA.2006.01.019
63. Kim HT, Yoo JS, Joh H-I, Kim H, Moon SH (2011) Properties of Pt-based electrocatalysts containing selectively deposited Sn as the anode for polymer electrolyte membrane fuel cells. Int J Hydrog Energy 36:1606–1612. https://doi.org/10.1016/J.IJHYDENE.2010.10.075
64. Liang Y, Zhang H, Zhong H, Zhu X, Tian Z, Xu D, Yi B (2006) Preparation and characterization of carbon-supported PtRuIr catalyst with excellent CO-tolerant performance for proton-exchange membrane fuel cells. J Catal 238:468–476. https://doi.org/10.1016/J.JCAT.2006.01.005
65. Antolini E (2007) Platinum-based ternary catalysts for low temperature fuel cells: part II. Electrochemical properties. Appl Catal B Environ 74:337–350. https://doi.org/10.1016/J.APCATB.2007.03.001
66. Antolini E (2007) Platinum-based ternary catalysts for low temperature fuel cells: part I. Preparation methods and structural characteristics. Appl Catal B Environ 74:324–336. https://doi.org/10.1016/J.APCATB.2007.03.002
67. Strasser P, Fan Q, Devenney M, Weinberg WH (2003) High throughput experimental and theoretical predictive screening of materials—a comparative study of search strategies for new fuel cell anode catalysts. J Phys Chem B 107(40):11013–11021. https://doi.org/10.1021/JP030508Z
68. Kim T, Kobayashi K, Take T, Nagai M (2012) Electronic modification effects induced by Fe in Pt-Ru-Fe ternary catalyst on the electrooxidation of CO/H_2; and methanol. J Oleo Sci 61:127–134. https://doi.org/10.5650/jos.61.127
69. Hassan A, Paganin VA, Ticianelli EA (2015) Effect of addition of Ru and/or Fe in the stability of PtMo/C electrocatalysts in proton exchange membrane fuel cells. Electrocatalysis 6:512–520. https://doi.org/10.1007/s12678-015-0269-7
70. Lu G, Cooper JS, McGinn PJ (2006) SECM characterization of Pt–Ru–WC and Pt–Ru–Co ternary thin film combinatorial libraries as anode electrocatalysts for PEMFC. J Power Sources 161:106–114. https://doi.org/10.1016/J.JPOWSOUR.2006.04.089
71. Cui X, Guo L, Cui F, He Q, Shi J (2009) Electrocatalytic activity and CO tolerance properties of mesostructured Pt/WO_3 composite as an anode catalyst for PEMFCs. J Phys Chem C 113:4134–4138. https://doi.org/10.1021/jp8079205
72. Lebedeva NP, Rosca V, Janssen GJM (2010) CO oxidation and CO2 reduction on carbon supported PtWO3 catalyst. Electrochim Acta 55:7659–7668. https://doi.org/10.1016/J.ELECTACTA.2009.12.041
73. Liu J, Jiang L (2018) Electrostatic self-assembly of Pt nanoparticles on hexagonal tungsten oxide as an active CO-tolerant hydrogen oxidation electrocatalyst. Int J Hydrog Energy 43:8944–8952. https://doi.org/10.1016/J.IJHYDENE.2018.03.131

74. Maillard F, Peyrelade E, Soldo-Olivier Y, Chatenet M, Chaînet E, Faure R (2007) Is carbon-supported Pt-WOx composite a CO-tolerant material? Electrochim Acta 52:1958–1967. https://doi.org/10.1016/J.ELECTACTA.2006.08.024
75. He C, Kunz HR, Fenton JM (2003) Electro-oxidation of hydrogen with carbon monoxide on Pt/Ru-based ternary catalysts. J Electrochem Soc 150:A1017. https://doi.org/10.1149/1.1583714
76. Wang D, Subban CV, Wang H, Rus E, DiSalvo FJ, Abruña HD (2010) Highly stable and CO-tolerant Pt/Ti $_{0.7}$ W $_{0.3}$ O $_{2}$ electrocatalyst for proton-exchange membrane fuel cells. J Am Chem Soc 132:10218–10220. https://doi.org/10.1021/ja102931d
77. Alcaide F, Álvarez G, Tsiouvaras N, Peña MA, Fierro JLG, Martínez-Huerta MV (2011) Electrooxidation of H2/CO on carbon-supported PtRu-MoOx nanoparticles for polymer electrolyte fuel cells. Int J Hydrog Energy 36:14590–14598. https://doi.org/10.1016/J.IJHYDENE.2011.08.037
78. Martínez-Huerta MV, Rodríguez JL, Tsiouvaras N, Peña MA, Fierro JLG, Pastor E (2008) Novel synthesis method of CO-tolerant PtRu−MoO $_{x}$ nanoparticles: structural characteristics and performance for methanol electrooxidation. Chem Mater 20:4249–4259. https://doi.org/10.1021/cm703047p
79. Tsiouvaras N, Martínez-Huerta MV, Moliner R, Lázaro MJ, Rodríguez JL, Pastor E, Peña MA, Fierro JLG (2009) CO tolerant PtRu–MoOx nanoparticles supported on carbon nanofibers for direct methanol fuel cells. J Power Sources 186:299–304. https://doi.org/10.1016/J.JPOWSOUR.2008.10.026
80. Chen KY, Sun Z, Tseung ACC (1999) Preparation and characterization of high-performance Pt-Ru/WO[sub 3]-C anode catalysts for the oxidation of impure hydrogen. Electrochem Solid-State Lett 3:10. https://doi.org/10.1149/1.1390943
81. Hu JE, Liu Z, Eichhorn BW, Jackson GS (2012) CO tolerance of nano-architectured Pt–Mo anode electrocatalysts for PEM fuel cells. Int J Hydrog Energy 37:11268–11275. https://doi.org/10.1016/J.IJHYDENE.2012.04.094
82. Liu Z, Jackson GS, Eichhorn BW (2010) PtSn intermetallic, core-shell, and alloy nanoparticles as CO-tolerant electrocatalysts for H_2 oxidation. Angew Chem Int Ed Engl 49:3173–3176. https://doi.org/10.1002/anie.200907019
83. Ochal P, Gomez de la Fuente JL, Tsypkin M, Seland F, Sunde S, Muthuswamy N, Rønning M, Chen D, Garcia S, Alayoglu S, Eichhorn B (2011) CO stripping as an electrochemical tool for characterization of Ru@Pt core-shell catalysts. J Electroanal Chem 655:140–146. https://doi.org/10.1016/J.JELECHEM.2011.02.027
84. Guo X, Fu Q, Ning Y, Wei M, Li M, Zhang S, Jiang Z, Bao X (2012) Ferrous centers confined on core–shell nanostructures for low-temperature CO oxidation. J Am Chem Soc 134:12350–12353. https://doi.org/10.1021/ja3038883
85. Kuai L, Geng B, Wang S, Sang Y (2012) A general and high-yield galvanic displacement approach to Au-M (M=Au, Pd, and Pt) core-shell nanostructures with porous shells and enhanced electrocatalytic performances. Chemistry 18:9423–9429. https://doi.org/10.1002/chem.201200893
86. Weber I, Solla-Gullón J, Brimaud S, Feliu JM, Jürgen Behm R (2017) Structure, surface chemistry and electrochemical de-alloying of bimetallic PtxAg100-x nanoparticles: quantifying the changes in the surface properties for adsorption and electrocatalytic transformation upon selective Ag removal. J Electroanal Chem 793:164–173. https://doi.org/10.1016/J.JELECHEM.2016.11.062
87. Takimoto D, Ohnishi T, Nutariya J, Shen Z, Ayato Y, Mochizuki D, Demortière A, Boulineau A, Sugimoto W (2017) Ru-core@Pt-shell nanosheet for fuel cell electrocatalysts with high activity and durability. J Catal 345:207–215. https://doi.org/10.1016/J.JCAT.2016.11.026
88. Zhang L, Kim J, Chen HM, Nan F, Dudeck K, Liu R-S, Botton GA, Zhang J (2011) A novel CO-tolerant PtRu core–shell structured electrocatalyst with Ru rich in core and Pt rich in shell

for hydrogen oxidation reaction and its implication in proton exchange membrane fuel cell. J Power Sources 196:9117–9123. https://doi.org/10.1016/J.JPOWSOUR.2011.05.020
89. Zhang L, Kim J, Zhang J, Nan F, Gauquelin N, Botton GA, He P, Bashyam R, Knights S (2013) Ti4O7 supported Ru@Pt core–shell catalyst for CO-tolerance in PEM fuel cell hydrogen oxidation reaction. Appl Energy 103:507–513. https://doi.org/10.1016/J.APENERGY.2012.10.017
90. Sun M, Lv Y, Song Y, Wu H, Wang G, Zhang H, Chen M, Fu Q, Bao X (2018) CO-tolerant PtRu@h-BN/C core–shell electrocatalysts for proton exchange membrane fuel cells. Appl Surf Sci 450:244–250. https://doi.org/10.1016/J.APSUSC.2018.04.170
91. Chen Y, Shi J, Chen S (2015) Small-molecule (CO, H_2) electro-oxidation as an electrochemical tool for characterization of Ni@Pt/C with different Pt coverages. J Phys Chem C 119:7138–7145. https://doi.org/10.1021/jp512283c
92. Garg A, Milina M, Ball M, Zanchet D, Hunt ST, Dumesic JA, Román-Leshkov Y (2017) Transition-metal nitride core@noble-metal shell nanoparticles as highly CO tolerant catalysts. Angew Chem Int Ed Engl 56:8828–8833. https://doi.org/10.1002/anie.201704632
93. Wang Q, Wang G, Tao H, Li Z, Han L (2017) Highly CO tolerant PtRu/PtNi/C catalyst for polymer electrolyte membrane fuel cell. RSC Adv 7:8453–8459. https://doi.org/10.1039/C6RA28198B
94. Nilekar AU, Sasaki K, Farberow CA, Adzic RR, Mavrikakis M (2011) Mixed-metal Pt monolayer electrocatalysts with improved CO tolerance. J Am Chem Soc 133:18574–18576. https://doi.org/10.1021/ja2072675
95. Shi G, Yano H, Tryk DA, Iiyama A, Uchida H (2017) Highly active, CO-tolerant, and robust hydrogen anode catalysts: Pt–M (M = Fe, Co, Ni) alloys with stabilized Pt-skin layers. ACS Catal 7:267–274. https://doi.org/10.1021/acscatal.6b02794
96. García G, Guillén-Villafuerte O, Rodríguez JL, Arévalo MC, Pastor E (2016) Electrocatalysis on metal carbide materials. Int J Hydrog Energy 41:19664–19673. https://doi.org/10.1016/j.ijhydene.2016.04.146
97. Roca-Ayats M, García G, Peña MA, Martínez-Huerta MV (2014) Titanium carbide and carbonitride electrocatalyst supports: modifying Pt-Ti interface properties by electrochemical potential cycling. J Mater Chem A 2(44):18786–18790. https://doi.org/10.1039/c4ta03782k
98. Roca-Ayats M, García G, Galante JL, Peña MA, Martínez-Huerta MV (2013) TiC, TiCN, and TiN supported Pt electrocatalysts for CO and methanol oxidation in acidic and alkaline media. J Phys Chem C 117:20769–20777. https://doi.org/10.1021/jp407260v
99. Roca-Ayats M, García G, Soler-Vicedo M, Pastor E, Lázaro MJ, Martínez-Huerta MV (2015) The role of Sn, Ru and Ir on the ethanol electrooxidation on Pt3M/TiCN electrocatalysts. Int J Hydrog Energy 40:14519–14528. https://doi.org/10.1016/j.ijhydene.2015.05.175
100. Guillén-Villafuerte O, García G, Rodríguez JL, Pastor E, Guil-López R, Nieto E, Fierro JLG (2013) Preliminary studies of the electrochemical performance of Pt/X@MoO_3/C (X = Mo_2C, MoO_2, Mo^0) catalysts for the anode of a DMFC: influence of the Pt loading and Mo-phase. Int J Hydrog Energy 38:7811–7821. https://doi.org/10.1016/j.ijhydene.2013.04.083
101. Guillén-Villafuerte O, García G, Guil-López R, Nieto E, Rodríguez JL, Fierro JLG, Pastor E (2013) Carbon monoxide and methanol oxidations on Pt/X@MoO_3/C (X = Mo_2C, MoO_2, Mo^0) electrodes at different temperatures. J Power Sources 231:163–172
102. Guillén-Villafuerte O, Guil-López R, Nieto E, García G, Rodríguez JL, Pastor E, Fierro JLG (2012) Electrocatalytic performance of different Mo-phases obtained during the preparation of innovative Pt-MoC catalysts for DMFC anode. Int J Hydrog Energy 37:7171–7179. https://doi.org/10.1016/j.ijhydene.2011.11.117
103. Alegre C, Calvillo L, Moliner R, González-Expósito JA, Guillén-Villafuerte O, Huerta MVM, Pastor E, Lázaro MJ (2011) Pt and PtRu electrocatalysts supported on carbon xerogels for direct methanol fuel cells. J Power Sources 196:4226–4235
104. Ganesan R, Ham DJ, Lee JS (2007) Platinized mesoporous tungsten carbide for electrochemical methanol oxidation. Electrochem Commun 9:2576–2579. https://doi.org/10.1016/J.ELECOM.2007.08.002

105. Ham DJ, Kim YK, Han SH, Lee JS (2008) Pt/WC as an anode catalyst for PEMFC: activity and CO tolerance. Catal Today 132:117–122. https://doi.org/10.1016/J.CATTOD.2007.12.076
106. Hara Y, Minami N, Itagaki H (2007) Synthesis and characterization of high-surface area tungsten carbides and application to electrocatalytic hydrogen oxidation. Appl Catal A Gen 323:86–93. https://doi.org/10.1016/J.APCATA.2007.02.011
107. Gasteiger HA, Kocha SS, Sompalli B, Wagner FT (2005) Activity benchmarks and requirements for Pt, Pt-alloy, and non-Pt oxygen reduction catalysts for PEMFCs. Appl Catal B Environ 56:9–35. https://doi.org/10.1016/j.apcatb.2004.06.021
108. Sui S, Wang X, Zhou X, Su Y, Riffat S, Liu C (2017) A comprehensive review of Pt electrocatalysts for the oxygen reduction reaction: nanostructure, activity, mechanism and carbon support in PEM fuel cells. J Mater Chem A 5:1808–1825. https://doi.org/10.1039/c6ta08580f
109. Debe MK (2012) Electrocatalyst approaches and challenges for automotive fuel cells. Nature 486:43
110. Office of Energy Efficiency & Renewable Energy. https://www.energy.gov/eere/fuelcells/doe-technical-targets-polymer-electrolyte-membrane-fuel-cell-components.
111. Antolini E, Gonzalez ER (2010) Alkaline direct alcohol fuel cells. J Power Sources 195:3431–3450. https://doi.org/10.1016/j.jpowsour.2009.11.145
112. Mora-Hernández JM, Luo Y, Alonso-Vante N (2016) What can we learn in electrocatalysis, from nanoparticulated precious and/or non-precious catalytic centers interacting with their support? Catalysts 6:145
113. Holade Y, Sahin NE, Servat K, Napporn TW, Kokoh KB (2015) Recent advances in carbon supported metal nanoparticles preparation for oxygen reduction reaction in low temperature fuel cells. Catalysts 5:310–348. https://doi.org/10.3390/catal5010310
114. Rivera LM, Fajardo S, Arévalo MC, García G, Pastor E (2017) S-and N-Doped graphene nanomaterials for the oxygen reduction reaction. Catalysts 7(9):278. https://doi.org/10.3390/catal7090278
115. Rivera LM, García G, Pastor E (2018) Novel graphene materials for the oxygen reduction reaction. Curr Opin Electrochem 9:233-239. https://doi.org/10.1016/j.coelec.2018.05.009
116. Kulkarni A, Siahrostami S, Patel A, Nørskov JK (2018) Understanding catalytic activity trends in the oxygen reduction reaction. Chem Rev 118:2302–2312. https://doi.org/10.1021/acs.chemrev.7b00488
117. Nørskov JK, Rossmeisl J, Logadottir A, Lindqvist L, Kitchin JR, Bligaard T, Jónsson H (2004) Origin of the overpotential for oxygen reduction at a fuel-cell cathode. J Phys Chem B 108:17886–17892. https://doi.org/10.1021/jp047349j
118. Calle-Vallejo F, Koper MTM (2012) First-principles computational electrochemistry: achievements and challenges. Electrochim Acta 84:3–11. https://doi.org/10.1016/j.electacta.2012.04.062
119. Katsounaros I, Cherevko S, Zeradjanin AR, Mayrhofer KJJ (2014) Oxygen electrochemistry as a cornerstone for sustainable energy conversion. Angew Chem Int Ed Engl 53:102–121. https://doi.org/10.1002/anie.201306588
120. Calle-Vallejo F, Koper MTM, Bandarenka AS (2013) Tailoring the catalytic activity of electrodes with monolayer amounts of foreign metals. Chem Soc Rev 42:5210–5230. https://doi.org/10.1039/c3cs60026b
121. Koper MTM (2011) Structure sensitivity and nanoscale effects in electrocatalysis. Nanoscale 3:2054–2073. https://doi.org/10.1039/c0nr00857e
122. Gomez-Marin AM, Rizo R, Feliu JM (2014) Oxygen reduction reaction at Pt single crystals: a critical overview. Cat Sci Technol 4:1685–1698. https://doi.org/10.1039/c3cy01049j
123. Markovic N, Gasteiger H, Ross PN (1997) Kinetics of oxygen reduction on Pt(hkl) electrodes: implications for the crystallite size effect with supported Pt electrocatalysts. J Electrochem Soc 144:1591–1597. https://doi.org/10.1149/1.1837646

124. Wang Y-J, Zhao N, Fang B, Li H, Bi XT, Wang H (2015) Carbon-supported Pt-based alloy electrocatalysts for the oxygen reduction reaction in polymer electrolyte membrane fuel cells: particle size, shape, and composition manipulation and their impact to activity. Chem Rev 115:3433–3467. https://doi.org/10.1021/cr500519c
125. Tian N, Zhou Z-Y, Sun S-G, Ding Y, Wang ZL (2007) Synthesis of tetrahexahedral platinum nanocrystals with high-index facets and high electro-oxidation activity. Science 316:732–735. https://doi.org/10.1126/science.1140484
126. Chen J, Lim B, Lee EP, Xia Y (2009) Shape-controlled synthesis of platinum nanocrystals for catalytic and electrocatalytic applications. Nano Today 4:81–95. https://doi.org/10.1016/j.nantod.2008.09.002
127. Yu T, Kim DY, Zhang H, Xia Y (2011) Platinum concave nanocubes with high-index facets and their enhanced activity for oxygen reduction reaction. Angew Chem Int Ed Engl 50:2773–2777. https://doi.org/10.1002/anie.201007859
128. Li M, Zhao Z, Cheng T, Fortunelli A, Chen C-Y, Yu R, Zhang Q, Gu L, Merinov B, Lin Z, Zhu E, Yu T, Jia Q, Guo J, Zhang L, Goddard WA, Huang Y, Duan X (2016) Ultrafine jagged platinum nanowires enable ultrahigh mass activity for the oxygen reduction reaction. Science 354(6318):1414–1419. https://doi.org/10.1126/science.aaf9050
129. Sánchez-Sánchez CM, Solla-Gullón J, Vidal-Iglesias FJ, Aldaz A, Montiel V, Herrero E (2010) Imaging structure sensitive catalysis on different shape-controlled platinum nanoparticles. J Am Chem Soc 132:5622–5624. https://doi.org/10.1021/ja100922h
130. Shao M, Peles A, Shoemaker K (2011) Electrocatalysis on platinum nanoparticles: particle size effect on oxygen reduction reaction activity. Nano Lett 11:3714–3719. https://doi.org/10.1021/nl2017459
131. Perez-Alonso FJ, McCarthy DN, Nierhoff A, Hernandez-Fernandez P, Strebel C, Stephens IEL, Nielsen JH, Chorkendorff I (2012) The effect of size on the oxygen electroreduction activity of mass-selected platinum nanoparticles. Angew Chem Int Ed Engl 51:4641–4643. https://doi.org/10.1002/anie.201200586
132. Nesselberger M, Ashton S, Meier JC, Katsounaros I, Mayrhofer KJJ, Arenz M (2011) The particle size effect on the oxygen reduction reaction activity of Pt catalysts: influence of electrolyte and relation to single crystal models. J Am Chem Soc 133:17428–17433. https://doi.org/10.1021/ja207016u
133. Yano H, Inukai J, Uchida H, Watanabe M, Babu PK, Kobayashi T, Chung JH, Oldfield E, Wieckowski A (2006) Particle-size effect of nanoscale platinum catalysts in oxygen reduction reaction: an electrochemical and 195Pt EC-NMR study. Phys Chem Chem Phys 8:4932–4939. https://doi.org/10.1039/b610573d
134. Mukerjee S, Srinivasan S, Soriaga MP, McBreen J (1995) Role of structural and electronic properties of Pt and Pt alloys on electrocatalysis of oxygen reduction: an in situ XANES and EXAFS investigation. J Electrochem Soc 142:1409–1422. https://doi.org/10.1149/1.2048590
135. Rivera Gavidia LM, García G, Celorrio V, Lázaro MJ, Pastor E (2016) Methanol tolerant Pt_2CrCo catalysts supported on ordered mesoporous carbon for the cathode of DMFC. Int J Hydrog Energy 41:19645–19655. https://doi.org/10.1016/j.ijhydene.2016.06.132
136. Antolini E, Salgado JRC, Santos LGRA, Garcia G, Ticianelli EA, Pastor E, Gonzalez ER (2006) Carbon supported Pt–Cr alloys as oxygen-reduction catalysts for direct methanol fuel cells. J Appl Electrochem 36:355–362. https://doi.org/10.1007/s10800-005-9072-0
137. Kang S, Kim J, Yoo S, Ryu H (2009) The synthesized 20% PtFe/C cathode catalyst for PEMFC by chemical reduction method. Geosystem Eng 12:43–46. https://doi.org/10.1080/12269328.2009.10541299
138. Matsumoto M, Yogi C, Arao M, Kuroki H, Tamaki T, Yamaguchi T, Imai H (2016) Oxygen reduction reaction mechanism of connected platinum-iron nanoparticle catalysts probed By EC-XPS. Meet Abstr MA2016-02:2384
139. Loukrakpam R, Luo J, He T, Chen Y, Xu Z, Njoki PN, Wanjala BN, Fang B, Mott D, Yin J, Klar J, Powell B, Zhong C-J (2011) Nanoengineered PtCo and PtNi Catalysts for oxygen

reduction reaction: an assessment of the structural and electrocatalytic properties. J Phys Chem C 115:1682–1694. https://doi.org/10.1021/jp109630n
140. Travitsky N, Ripenbein T, Golodnitsky D, Rosenberg Y, Burshtein L, Peled E (2006) Pt-, PtNi- and PtCo-supported catalysts for oxygen reduction in PEM fuel cells. J Power Sources 161:782–789. https://doi.org/10.1016/j.jpowsour.2006.05.035
141. Qian Y, Wen APA, Jiang Z, Hakim N, Saha MS, Mukerjee S (2008) PtM/C catalyst prepared using reverse micelle method for oxygen reduction reaction in PEM fuel cells. J Phys Chem C 112:1146–1157. https://doi.org/10.1021/jp074929i
142. Duan H, Hao Q, Xu C (2015) Hierarchical nanoporous PtTi alloy as highly active and durable electrocatalyst toward oxygen reduction reaction. J Power Sources 280:483–490. https://doi.org/10.1016/j.jpowsour.2015.01.136
143. Carpenter MK, Moylan TE, Kukreja RS, Atwan MH, Tessema MM (2012) Solvothermal synthesis of platinum alloy nanoparticles for oxygen reduction electrocatalysis. J Am Chem Soc 134:8535–8542. https://doi.org/10.1021/ja300756y
144. Stamenkovic VR, Mun BS, Arenz M, Mayrhofer KJJ, Lucas CA, Wang GF, Ross PN, Markovic NM (2007) Trends in electrocatalysis on extended and nanoscale Pt-bimetallic alloy surfaces. Nat Mater 6:241–247. https://doi.org/10.1038/nmat1840
145. Greeley J, Stephens IEL, Bondarenko AS, Johansson TP, Hansen HA, Jaramillo TF, Rossmeisl J, Chorkendorff I, Nørskov JK (2009) Alloys of platinum and early transition metals as oxygen reduction electrocatalysts. Nat Chem 1:552. https://doi.org/10.1038/nchem.367. https://www.nature.com/articles/nchem.367#supplementary-information
146. Choi SI, Xie S, Shao M, Lu N, Guerrero S, Odell JH, Park J, Wang J, Kim MJ, Xia Y (2014) Controlling the size and composition of nanosized Pt–Ni octahedra to optimize their catalytic activities toward the oxygen reduction reaction. ChemSusChem 7:1476–1483. https://doi.org/10.1002/cssc.201400051
147. Zhang C, Hwang SY, Trout A, Peng Z (2014) Solid-state chemistry-enabled scalable production of octahedral Pt–Ni alloy electrocatalyst for oxygen reduction reaction. J Am Chem Soc 136:7805–7808. https://doi.org/10.1021/ja501293x
148. Wang C, Markovic NM, Stamenkovic VR (2012) Advanced platinum alloy electrocatalysts for the oxygen reduction reaction. ACS Catal 2:891–898. https://doi.org/10.1021/cs3000792
149. Shaojun G, Sen Z, Shouheng S (2013) Tuning nanoparticle catalysis for the oxygen reduction reaction. Angew Chem Int Ed Engl 52:8526–8544. https://doi.org/10.1002/anie.201207186
150. Zhang C, Shen X, Pan Y, Peng Z (2017) A review of Pt-based electrocatalysts for oxygen reduction reaction. Front Energ 11:268–285. https://doi.org/10.1007/s11708-017-0466-6
151. Strasser P, Gliech M, Kuehl S, Moeller T (2018) Electrochemical processes on solid shaped nanoparticles with defined facets. Chem Soc Rev 47:715–735. https://doi.org/10.1039/c7cs00759k
152. Cui C, Gan L, Heggen M, Rudi S, Strasser P (2013) Compositional segregation in shaped Pt alloy nanoparticles and their structural behaviour during electrocatalysis. Nat Mater 12:765. https://doi.org/10.1038/nmat3668
153. Ammam M, Easton EB (2013) Oxygen reduction activity of binary PtMn/C, ternary PtMnX/C (X = Fe, Co, Ni, Cu, Mo and, Sn) and quaternary PtMnCuX/C (X = Fe, Co, Ni, and Sn) and PtMnMoX/C (X = Fe, Co, Ni, Cu and Sn) alloy catalysts. J Power Sources 236:311–320. https://doi.org/10.1016/j.jpowsour.2013.02.029
154. Nilekar AU, Xu Y, Zhang J, Vukmirovic MB, Sasaki K, Adzic RR, Mavrikakis M (2007) Bimetallic and ternary alloys for improved oxygen reduction catalysis. Top Catal 46:276–284. https://doi.org/10.1007/s11244-007-9001-z
155. Neyerlin KC, Srivastava R, Yu C, Strasser P (2009) Electrochemical activity and stability of dealloyed Pt–Cu and Pt–Cu–Co electrocatalysts for the oxygen reduction reaction (ORR). J Power Sources 186:261–267. https://doi.org/10.1016/j.jpowsour.2008.10.062
156. Huang X, Zhao Z, Cao L, Chen Y, Zhu E, Lin Z, Li M, Yan A, Zettl A, Wang YM, Duan X, Mueller T, Huang Y (2015) High-performance transition metal–doped Pt3Ni octahedra for oxygen reduction reaction. Science 348:1230–1234. https://doi.org/10.1126/science.aaa8765

157. Beermann V, Gocyla M, Willinger E, Rudi S, Heggen M, Dunin-Borkowski RE, Willinger M-G, Strasser P (2016) Rh-doped Pt–Ni octahedral nanoparticles: understanding the correlation between elemental distribution, oxygen reduction reaction, and shape stability. Nano Lett 16:1719–1725. https://doi.org/10.1021/acs.nanolett.5b04636
158. Beermann V, Gocyla M, Kühl S, Padgett E, Schmies H, Goerlin M, Erini N, Shviro M, Heggen M, Dunin-Borkowski RE, Muller DA, Strasser P (2017) Tuning the electrocatalytic oxygen reduction reaction activity and stability of shape-controlled Pt–Ni nanoparticles by thermal annealing – elucidating the surface atomic structural and compositional changes. J Am Chem Soc 139:16536–16547. https://doi.org/10.1021/jacs.7b06846
159. Wang D, Xin HL, Hovden R, Wang H, Yu Y, Muller DA, DiSalvo FJ, Abruña HD (2012) Structurally ordered intermetallic platinum–cobalt core–shell nanoparticles with enhanced activity and stability as oxygen reduction electrocatalysts. Nat Mater 12:81. https://doi.org/10.1038/nmat3458
160. Chen S, Ferreira PJ, Sheng W, Yabuuchi N, Allard LF, Shao-Horn Y (2008) Enhanced activity for oxygen reduction reaction on "Pt3Co" nanoparticles: direct evidence of percolated and sandwich-segregation structures. J Am Chem Soc 130:13818–13819. https://doi.org/10.1021/ja802513y
161. Wang C, Chi M, Li D, Strmcnik D, van der Vliet D, Wang G, Komanicky V, Chang K-C, Paulikas AP, Tripkovic D, Pearson J, More KL, Markovic NM, Stamenkovic VR (2011) Design and synthesis of bimetallic electrocatalyst with multilayered Pt-skin surfaces. J Am Chem Soc 133:14396–14403. https://doi.org/10.1021/ja2047655
162. Mayrhofer KJ, Juhart V, Hartl K, Hanzlik M, Arenz M (2009) Adsorbate-induced surface segregation for core–shell nanocatalysts. Angew Chem Int Ed Engl 48:3529–3531. https://doi.org/10.1002/anie.200806209
163. Yang R, Leisch J, Strasser P, Toney MF (2010) Structure of dealloyed PtCu3 thin films and catalytic activity for oxygen reduction. Chem Mater 22:4712–4720. https://doi.org/10.1021/cm101090p
164. Ratndeep S, Prasanna M, Nathan H, Peter S (2007) Efficient oxygen reduction fuel cell electrocatalysis on voltammetrically dealloyed Pt–Cu–Co nanoparticles. Angew Chem Int Ed Engl 46:8988–8991. https://doi.org/10.1002/anie.200703331
165. Han B, Carlton CE, Kongkanand A, Kukreja RS, Theobald BR, Gan L, O'Malley R, Strasser P, Wagner FT, Shao-Horn Y (2015) Record activity and stability of dealloyed bimetallic catalysts for proton exchange membrane fuel cells. Energy Environ Sci 8:258–266. https://doi.org/10.1039/c4ee02144d
166. Oezaslan M, Hasché F, Strasser P (2013) Pt-based core–shell catalyst architectures for oxygen fuel cell electrodes. J Phys Chem Lett 4:3273–3291. https://doi.org/10.1021/jz4014135
167. Benn EE, Gaskey B, Erlebacher JD (2017) Suppression of hydrogen evolution by oxygen reduction in nanoporous electrocatalysts. J Am Chem Soc 139:3663–3668. https://doi.org/10.1021/jacs.6b10855
168. Wang D, Zhao P, Li Y (2011) General preparation for Pt-based alloy nanoporous nanoparticles as potential nanocatalysts. Sci Rep 1:37. https://doi.org/10.1038/srep00037
169. Snyder J, Livi K, Erlebacher J (2013) Oxygen reduction reaction performance of [MTBD][beti]-encapsulated nanoporous NiPt alloy nanoparticles. Adv Funct Mater 23:5494–5501. https://doi.org/10.1002/adfm.201301144
170. Benn E, Uvegi H, Erlebacher J (2015) Characterization of nanoporous metal-ionic liquid composites for the electrochemical oxygen reduction reaction. J Electrochem Soc 162:H759–H766. https://doi.org/10.1149/2.0161510jes
171. McCue I, Snyder J, Li X, Chen Q, Sieradzki K, Erlebacher J (2012) Apparent inverse gibbs-thomson effect in dealloyed nanoporous nanoparticles. Phys Rev Lett 108:225503. https://doi.org/10.1103/PhysRevLett.108.225503
172. Baldizzone C, Gan L, Hodnik N, Keeley GP, Kostka A, Heggen M, Strasser P, Mayrhofer KJJ (2015) Stability of dealloyed porous Pt/Ni nanoparticles. ACS Catal 5:5000–5007. https://doi.org/10.1021/acscatal.5b01151

173. Chen C, Kang Y, Huo Z, Zhu Z, Huang W, Xin HL, Snyder JD, Li D, Herron JA, Mavrikakis M, Chi M, More KL, Li Y, Markovic NM, Somorjai GA, Yang P, Stamenkovic VR (2014) Highly crystalline multimetallic nanoframes with three-dimensional electrocatalytic surfaces. Science 343:1339–1343. https://doi.org/10.1126/science.1249061
174. Becknell N, Kang Y, Chen C, Resasco J, Kornienko N, Guo J, Markovic NM, Somorjai GA, Stamenkovic VR, Yang P (2015) Atomic structure of Pt3Ni nanoframe electrocatalysts by in Situ X-ray absorption spectroscopy. J Am Chem Soc 137:15817–15824. https://doi.org/10.1021/jacs.5b09639
175. Godínez-Salomón F, Mendoza-Cruz R, Arellano-Jimenez MJ, Jose-Yacaman M, Rhodes CP (2017) Metallic two-dimensional nanoframes: unsupported hierarchical nickel–platinum alloy nanoarchitectures with enhanced electrochemical oxygen reduction activity and stability. ACS Appl Mater Interfaces 9:18660–18674. https://doi.org/10.1021/acsami.7b00043
176. Han L, Liu H, Cui P, Peng Z, Zhang S, Yang J (2014) Alloy Cu3Pt nanoframes through the structure evolution in Cu-Pt nanoparticles with a core-shell construction. Sci Rep 4:6414. https://doi.org/10.1038/srep06414
177. Xiuhui S, Bin H, Xiaoneng C, Bin E, Yonggang F, Xiaoqing H (2018) Platinum–copper rhombic dodecahedral nanoframes with tunable channels as efficient bifunctional electrocatalysts for fuel-cell reactions. ChemCatChem 10:931–935. https://doi.org/10.1002/cctc.201701768
178. Taehyun K, Minki J, Young KH, Aram O, Jongsik P, Hionsuck B, Hoon JS, Kwangyeol L (2018) Vertex-reinforced PtCuCo ternary nanoframes as efficient and stable electrocatalysts for the oxygen reduction reaction and the methanol oxidation reaction. Adv Funct Mater 28:1706440. https://doi.org/10.1002/adfm.201706440
179. Hernandez-Fernandez P, Masini F, McCarthy DN, Strebel CE, Friebel D, Deiana D, Malacrida P, Nierhoff A, Bodin A, Wise AM, Nielsen JH, Hansen TW, Nilsson A, Stephens IEL, Chorkendorff I (2014) Mass-selected nanoparticles of PtxY as model catalysts for oxygen electroreduction. Nat Chem 6:732. https://doi.org/10.1038/nchem.2001
180. Jeon MK, McGinn PJ (2011) Carbon supported Pt–Y electrocatalysts for the oxygen reduction reaction. J Power Sources 196:1127–1131. https://doi.org/10.1016/j.jpowsour.2010.08.048
181. Stephens IEL, Bondarenko AS, Gronbjerg U, Rossmeisl J, Chorkendorff I (2012) Understanding the electrocatalysis of oxygen reduction on platinum and its alloys. Energy Environ Sci 5:6744–6762. https://doi.org/10.1039/c2ee03590a
182. Escudero-Escribano M, Malacrida P, Hansen MH, Vej-Hansen UG, Velázquez-Palenzuela A, Tripkovic V, Schiøtz J, Rossmeisl J, Stephens IEL, Chorkendorff I (2016) Tuning the activity of Pt alloy electrocatalysts by means of the lanthanide contraction. Science 352:73–76. https://doi.org/10.1126/science.aad8892
183. Velázquez-Palenzuela A, Masini F, Pedersen AF, Escudero-Escribano M, Deiana D, Malacrida P, Hansen TW, Friebel D, Nilsson A, Stephens IEL, Chorkendorff I (2015) The enhanced activity of mass-selected PtxGd nanoparticles for oxygen electroreduction. J Catal 328:297–307. https://doi.org/10.1016/j.jcat.2014.12.012
184. Jiang R, Tung S o, Tang Z, Li L, Ding L, Xi X, Liu Y, Zhang L, Zhang J (2018) A review of core-shell nanostructured electrocatalysts for oxygen reduction reaction. Energy Storage Mater 12:260–276. https://doi.org/10.1016/j.ensm.2017.11.005
185. Junliang Z, Vukmirovic MB, Ye X, Manos M, Adzic RR (2005) Controlling the catalytic activity of platinum-monolayer electrocatalysts for oxygen reduction with different substrates. Angew Chem 117:2170–2173. https://doi.org/10.1002/ange.200462335
186. Chen G, Kuttiyiel KA, Su D, Li M, Wang C-H, Buceta D, Du C, Gao Y, Yin G, Sasaki K, Vukmirovic MB, Adzic RR (2016) Oxygen reduction kinetics on Pt monolayer shell highly affected by the structure of bimetallic AuNi cores. Chem Mater 28:5274–5281. https://doi.org/10.1021/acs.chemmater.6b00500
187. Kuttiyiel KA, Choi Y, Sasaki K, Su D, Hwang S-M, Yim S-D, Yang T-H, Park G-G, Adzic RR (2016) Tuning electrocatalytic activity of Pt monolayer shell by bimetallic Ir-M (M=Fe,

Co, Ni or Cu) cores for the oxygen reduction reaction. Nano Energy 29:261–267. https://doi.org/10.1016/j.nanoen.2016.05.024
188. Nan H, Tian X, Yang L, Shu T, Song H, Liao S (2015) A platinum monolayer core-shell catalyst with a ternary alloy nanoparticle core and enhanced stability for the oxygen reduction reaction. J Nanomater 2015:11. https://doi.org/10.1155/2015/715474
189. Zhang L, Iyyamperumal R, Yancey DF, Crooks RM, Henkelman G (2013) Design of Pt-Shell nanoparticles with alloy cores for the oxygen reduction reaction. ACS Nano 7:9168–9172. https://doi.org/10.1021/nn403788a
190. Gong K, Choi Y, Vukmirovic MB, Liu P, Ma C, Su D, Adzic RR (2012) Tetrahedral palladium nanocrystals: a new support for platinum monolayer electrocatalysts with high activity and stability in the oxygen reduction reaction. Z Phys Chem 226:1025–1038. https://doi.org/10.1524/zpch.2012.0239
191. Shao M, He G, Peles A, Odell JH, Zeng J, Su D, Tao J, Yu T, Zhu Y, Xia Y (2013) Manipulating the oxygen reduction activity of platinum shells with shape-controlled palladium nanocrystal cores. Chem Commun 49:9030–9032. https://doi.org/10.1039/c3cc43276a
192. Shao M, Shoemaker K, Peles A, Kaneko K, Protsailo L (2010) Pt monolayer on porous Pd−Cu alloys as oxygen reduction electrocatalysts. J Am Chem Soc 132:9253–9255. https://doi.org/10.1021/ja101966a
193. Zhang Y, Ma C, Zhu Y, Si R, Cai Y, Wang JX, Adzic RR (2013) Hollow core supported Pt monolayer catalysts for oxygen reduction. Catal Today 202:50–54. https://doi.org/10.1016/j.cattod.2012.03.040
194. Choi R, Choi SI, Choi CH, Nam KM, Woo SI, Park JT, Han SW (2013) Designed synthesis of well-defined Pd@Pt Core–shell nanoparticles with controlled shell thickness as efficient oxygen reduction electrocatalysts. Chemistry 19:8190–8198. https://doi.org/10.1002/chem.201203834
195. Shao M, Chang Q, Dodelet J-P, Chenitz R (2016) Recent advances in electrocatalysts for oxygen reduction reaction. Chem Rev 116:3594–3657. https://doi.org/10.1021/acs.chemrev.5b00462
196. Guo S, Zhang S, Su D, Sun S (2013) Seed-mediated synthesis of core/shell FePtM/FePt (M = Pd, Au) nanowires and their electrocatalysis for oxygen reduction reaction. J Am Chem Soc 135:13879–13884. https://doi.org/10.1021/ja406091p
197. Wang X, Vara M, Luo M, Huang H, Ruditskiy A, Park J, Bao S, Liu J, Howe J, Chi M, Xie Z, Xia Y (2015) Pd@Pt core–shell concave decahedra: a class of catalysts for the oxygen reduction reaction with enhanced activity and durability. J Am Chem Soc 137:15036–15042. https://doi.org/10.1021/jacs.5b10059
198. Mazumder V, Chi M, More KL, Sun S (2010) Core/shell Pd/FePt nanoparticles as an active and durable catalyst for the oxygen reduction reaction. J Am Chem Soc 132:7848–7849. https://doi.org/10.1021/ja1024436
199. Zhang S, Hao Y, Su D, Doan-Nguyen VVT, Wu Y, Li J, Sun S, Murray CB (2014) Monodisperse core/shell Ni/FePt nanoparticles and their conversion to Ni/Pt to catalyze oxygen reduction. J Am Chem Soc 136:15921–15924. https://doi.org/10.1021/ja5099066
200. Tian X, Luo J, Nan H, Zou H, Chen R, Shu T, Li X, Li Y, Song H, Liao S, Adzic RR (2016) Transition metal nitride coated with atomic layers of Pt as a low-cost, highly stable electrocatalyst for the oxygen reduction reaction. J Am Chem Soc 138:1575–1583. https://doi.org/10.1021/jacs.5b11364
201. Liu Y, Kelly TG, Chen JG, Mustain WE (2013) Metal carbides as alternative electrocatalyst supports. ACS Catal 3:1184–1194. https://doi.org/10.1021/cs4001249
202. Huang S-Y, Ganesan P, Popov BN (2010) Electrocatalytic activity and stability of niobium-doped titanium oxide supported platinum catalyst for polymer electrolyte membrane fuel cells. Appl Catal B Environ 96:224–231. https://doi.org/10.1016/j.apcatb.2010.02.025
203. Baturina OA, Garsany Y, Zega TJ, Stroud RM, Schull T, Swider-Lyons KE (2008) Oxygen reduction reaction on platinum/tantalum oxide electrocatalysts for PEM fuel cells. J Electrochem Soc 155:B1314–B1321. https://doi.org/10.1149/1.2988730

204. Sungeun Y, Jiwhan K, Joo TY, Aloysius S, Hyunjoo L (2016) Single-atom catalyst of platinum supported on titanium nitride for selective electrochemical reactions. Angew Chem Int Ed Engl 55:2058–2062. https://doi.org/10.1002/anie.201509241
205. Alipour Moghadam Esfahani R, Rivera Gavidia LM, García G, Pastor E, Specchia S (2018) Highly active platinum supported on Mo-doped titanium nanotubes suboxide (Pt/TNTS-Mo) electrocatalyst for oxygen reduction reaction in PEMFC. Renew Energy 120:209–219. https://doi.org/10.1016/j.renene.2017.12.077
206. Gewirth AA, Varnell JA, DiAscro AM (2018) Nonprecious metal catalysts for oxygen reduction in heterogeneous aqueous systems. Chem Rev 118:2313–2339. https://doi.org/10.1021/acs.chemrev.7b00335
207. Kondo S, Nakamura M, Maki N, Hoshi N (2009) Active sites for the oxygen reduction reaction on the low and high index planes of palladium. J Phys Chem C 113:12625–12628. https://doi.org/10.1021/jp904278b
208. Shao M, Yu T, Odell JH, Jin M, Xia Y (2011) Structural dependence of oxygen reduction reaction on palladium nanocrystals. Chem Commun (Camb) 47:6566–6568. https://doi.org/10.1039/c1cc11004g
209. Erikson H, Sarapuu A, Tammeveski K, Solla-Gullón J, Feliu JM (2011) Enhanced electrocatalytic activity of cubic Pd nanoparticles towards the oxygen reduction reaction in acid media. Electrochem Commun 13:734–737. https://doi.org/10.1016/j.elecom.2011.04.024
210. Erikson H, Sarapuu A, Alexeyeva N, Tammeveski K, Solla-Gullón J, Feliu JM (2012) Electrochemical reduction of oxygen on palladium nanocubes in acid and alkaline solutions. Electrochim Acta 59:329–335. https://doi.org/10.1016/j.electacta.2011.10.074
211. Miguel L, Gavidia R, García G, Anaya D, Querejeta A, Alcaide F, Pastor E, Gavidia LMR, García G, Anaya D, Querejeta A, Alcaide F, Pastor E (2016) Carbon-supported Pt-free catalysts with high specificity and activity toward the oxygen reduction reaction in acidic medium. Appl Catal B Environ 184:12–19. https://doi.org/10.1016/j.apcatb.2015.11.021
212. Pires FI, Villullas HM (2012) Pd-based catalysts: influence of the second metal on their stability and oxygen reduction activity. Int J Hydrog Energy 37:17052–17059. https://doi.org/10.1016/j.ijhydene.2012.08.102
213. Savadogo O, Lee K, Oishi K, Mitsushima S, Kamiya N, Ota KI (2004) New palladium alloys catalyst for the oxygen reduction reaction in an acid medium. Electrochem Commun 6:105–109. https://doi.org/10.1016/j.elecom.2003.10.020
214. Shao MH, Huang T, Liu P, Zhang J, Sasaki K, Vukmirovic MB, Adzic RR (2006) Palladium monolayer and palladium alloy electrocatalysts for oxygen reduction. Langmuir 22:10409–10415. https://doi.org/10.1021/la0610553
215. Zhang L, Lee K, Zhang J (2007) The effect of heat treatment on nanoparticle size and ORR activity for carbon-supported Pd-Co alloy electrocatalysts. Electrochim Acta 52:3088–3094. https://doi.org/10.1016/j.electacta.2006.09.051
216. Yang R, Bian W, Strasser P, Toney MF (2013) Dealloyed PdCu3 thin film electrocatalysts for oxygen reduction reaction. J Power Sources 222:169–176. https://doi.org/10.1016/j.jpowsour.2012.08.064
217. Son J, Cho S, Lee C, Lee Y, Shim JH (2014) Spongelike nanoporous Pd and Pd/Au structures: facile synthesis and enhanced electrocatalytic activity. Langmuir 30:3579–3588. https://doi.org/10.1021/la4047947
218. Kwon K, Lee KH, Jin S, You DJ, Pak C (2011) Ceria-promoted oxygen reduction reaction in Pd-based electrocatalysts. Electrochem Commun 13:1067–1069. https://doi.org/10.1016/j.elecom.2011.06.036
219. Nie M, Zeng ZJ, He B, Li Q, Liu XW, Zheng CS (2014) Tungsten carbide promoted Au–Pd–Pt as methanol-tolerant electrocatalysts for oxygen reduction reaction. Mater Res Innov 18:255–258. https://doi.org/10.1179/1433075x13y.0000000189
220. Borup R, Meyers J, Pivovar B, Kim YS, Mukundan R, Garland N, Myers D, Wilson M, Garzon F, Wood D, Zelenay P, More K, Stroh K, Zawodzinski T, Boncella J, McGrath JE, Inaba M, Miyatake K, Hori M, Ota K, Ogumi Z, Miyata S, Nishikata A, Siroma Z,

Uchimoto Y, Yasuda K, Kimijima K, Iwashita N (2007) Scientific aspects of polymer electrolyte fuel cell durability and degradation. Chem Rev 107:3904–3951. https://doi.org/10.1021/cr0501821

221. Topalov AA, Cherevko S, Zeradjanin AR, Meier JC, Katsounaros I, Mayrhofer KJJ (2014) Towards a comprehensive understanding of platinum dissolution in acidic media. Chem Sci 5:631–638. https://doi.org/10.1039/c3sc52411f
222. Meier JC, Galeano C, Katsounaros I, Witte J, Bongard HJ, Topalov AA, Baldizzone C, Mezzavilla S, Schüth F, Mayrhofer KJJ (2014) Design criteria for stable Pt/C fuel cell catalysts. Beilstein J Nanotechnol 5:44–67. https://doi.org/10.3762/bjnano.5.5

Chapter 3
Electrocatalysis of Alternative Liquid Fuels for PEM Direct Oxidation Fuel Cells

Ayan Mukherjee, Harikrishnan Narayanan, and Suddhasatwa Basu

Abstract The direct oxidation of liquid fuels such as methanol, ethanol, ethylene glycol, formic acid and glycerol in fuel cell has attracted increasing interest as power source for portable applications in recent days. These fuels are economically and environmental friendly, exhibit high volumetric energy density, facile storing and handling as compared to hydrogen fuel. Based on their feeding directly and electro-oxidation process, these are termed as direct methanol fuel cell (DMFC), direct ethanol fuel cell (DEFC), direct ethylene glycol fuel cell (DEGFC), direct formic acid fuel cell (DFAFC) and direct glycerol fuel cell (DGEFC), which are discussed in the chapter. The oxidation reaction of these fuels at low temperature in acid electrolytes is discussed in detail. The various binary and ternary Pt-based catalysts which can ease the oxidation of these liquid fuels are presented with plausible reaction mechanism. The various parameters driving the fuel cell such as catalyst loading, fuel flow rates, operating temperature and the performance in terms of current–voltage characteristics, stability and durability of the fuel cells are discussed including the recent commercial development in the field. Authors also presented their view and further work required wherever deemed fit.

Keywords Fuel cell · Direct fuel cell · Renewable energy · Alternative liquid fuel · Electrochemistry · Methanol oxidation reaction · Ethanol oxidation reaction · Ethylene glycoloxidation reaction · Formic acid oxidation reaction · Glycerol oxidation reaction · Oxygen reduction reaction · Direct methanol fuel cell · Direct ethanol fuel cell · Direct ethylene glycol fuel cell · Direct formic acid fuel cell · Direct glycerol fuel cell · Catalyst · Proton exchange membrane · Anode material · Cathode material · Anode overpotentials · Fuel cross over · Power density · Current-voltage characteristics

A. Mukherjee · H. Narayanan
Department of Chemical Engineering, Indian Institute of Technology Delhi, New Delhi, India

S. Basu (✉)
Department of Chemical Engineering, Indian Institute of Technology Delhi, New Delhi, India

CSIR-Institute of Minerals and Materials Technology, Bhubaneswar, India
e-mail: sbasu@chemical.iitd.ac.in

F. J. Rodríguez-Varela, T. W. Napporn (eds.), *Advanced Electrocatalysts for Low-Temperature Fuel Cells*, https://doi.org/10.1007/978-3-319-99019-4_3

3.1 Introduction

In the current world scenario of climate change and increasing pollution, an alternative for fossil fuel-based energy source is required and need to be developed. Fuel cell is one of such clean energy source which converts chemical energy directly into electrical energy through redox reaction mechanism (oxidation at anode and reduction at cathode), thus increasing its fuel conversion efficiency. Proton exchange membrane fuel cell (PEMFC) is one of the conventional fuel cells, which uses hydrogen (H_2) as fuel at anode and oxygen (O_2) as oxidant at cathode [1]. Platinum (Pt) is used as catalyst for the redox reaction both at anode and cathode. H_2 undergoes oxidation reaction (HOR) at anode, producing H^+ ion and electrons (e^-), which moves to cathode through the proton-conducting polymer electrolytic membrane and outer circuit, respectively. At cathode, O_2 undergoes reduction reaction (ORR) with incoming H^+ and e^-, to produce water (H_2O). Equations (3.1) and (3.2) show HOR and ORR mechanism of a PEMFC.

$$H_2 \leftrightarrow 2H^+ + 2e^- \tag{3.1}$$

$$^1/_2O_2 + 2H^+ + 2e^- \leftrightarrow H_2O \tag{3.2}$$

PEMFCs can be further subcategorised based on the fuel used such as direct methanol fuel cell (DMFC), direct ethanol fuel cell (DEFC), direct formic acid fuel cell (DFAFC), direct ethylene glycol fuel cell (DEGFC) and direct glycerol fuel cell (DGEFC). They use Methanol, Ethanol, Formic Acid, Ethylene Glycol and Glycerol as fuel instead of pure H_2 at anode. One of the main advantages of using such liquid fuels is its ease to handle, transport and store, which is a big issue in case of H_2 as fuel. Apart from that, producing pure H_2 for fuel purpose from steam reforming of fossil fuels or electrolysis is an expensive process, as any form of impurity such as CO and SO_x in the fuel stream can cause deactivation of Pt catalyst eventually causing performance degradation of the cell. Another advantage of using such liquid fuels over H_2 is its compatibility and high theoretical gravimetric energy densities such as 6.1 $kWh.kg^{-1}$, 8 $kWh.kg^{-1}$, 5.3 $kWh.kg^{-1}$, 5.2 $kWh.kg^{-1}$ and 5 $kWh.kg^{-1}$ for Methanol, Ethanol, Formic Acid, Ethylene Glycol and Glycerol, respectively. Low operating temperature of such liquid fuel-based PEMFCs makes it convenient for applications like transportation, stationary, auxiliary power units and portable devices [2].

Even though the open circuit voltage (OCV) achieved in case of liquid fuels is comparable with that of H_2 as fuel [3], a minor drawback of using liquid fuels over H_2 in PEMFCs is fuel cross-over to cathode through the proton exchange membrane and slow liquid fuel oxidation kinetics. In order to overcome this issue, studies have been carried out on developing multimetallic (bi, tri) noble and non-noble electrocatalysts which focuses on reduction of oxidant rather than oxidisation of liquid fuels at cathode. One of such promising study is the formation of different carbon structures supporting nanomaterials.

3.2 Direct Methanol Fuel Cell (DMFC)

A direct methanol fuel cell (DMFC) is characterised by the conversion of chemical energy of the methanol fuel directly into usable electrical energy. Typically, in a DMFC using a polymer electrolytic membrane (PEM), methanol and water mixture is directly fed into the anode chamber which is oxidised to produce proton, electron and carbon dioxide. The proton permeates through the PEM to the cathode and the electron reaches the cathode through the external circuit. The electron, proton and oxygen react at the cathode chamber to produce water. The schematic of a DMFC is shown in Fig. 3.1. Practically, the oxidation of methanol proceeds through the formation of intermediate products such as carbon monoxide (CO), formaldehyde (HCHO) and formic acid (HCOOH) which are responsible for the sluggish kinetics of the methanol oxidation reaction (MOR) in the anode chamber.

The cell reaction that occurs in a DMFC using a PEM is as follows:

$$CH_3OH + H_2O \rightarrow CO_2 + 6H^+ + 6e^- \quad \text{(Anode)} \quad (E_a \sim 0.016 \text{ V vs.SHE}) \tag{3.3}$$

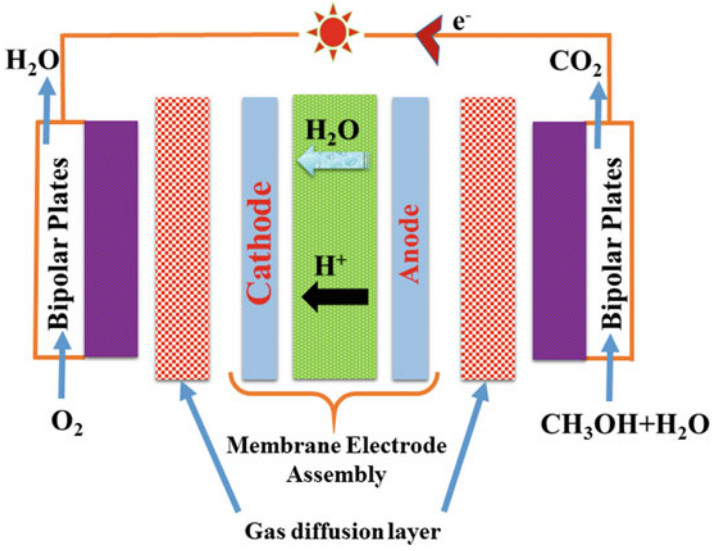

Fig. 3.1 Schematic representation of a typical direct methanol fuel cell

$$3/2O_2 + 6H^+ + 6e^- \rightarrow 3H_2O \qquad \text{(Cathode)} \quad (E_c \sim 1.229 \text{ V vs.SHE}) \quad (3.4)$$

$$CH_3OH + 3/2O_2 \rightarrow CO_2 + 2H_2O \qquad \text{(Overall)} \quad (E_0 \sim 1.21 \text{ V vs.SHE}) \quad (3.5)$$

Methanol can be produced easily from feedstock such as coal and natural gases through gasification and steam reforming processes. It can also be produced from renewable energy sources such as wood and agricultural wastes by thermochemical processes. A DMFC provides several fascinating advantages over hydrogen-fuelled polymer electrolytic membrane (PEM) fuel cell such as high theoretical gravimetric energy density (6.1 $kWh.kg^{-1}$), low exhaust, easy refilling and quick start-up at low temperature [2, 4]. Further, the commercialisation of H_2-fuelled PEM fuel cell is restricted severely due to on-board storage constraints and lack of H_2 distribution infrastructure and high cost of pure hydrogen [5, 6]. The on-board storage constraints are eliminated with the PEM fuel cell using methanol as fuel as it can be easily distributed using the existing setup of gasoline distribution with few alterations. However, the major constraints towards the commercialisation of DMFC is its significantly higher manufacturing cost as it uses platinum–ruthenium (Pt–Ru) for fuel oxidation at the anode and oxygen reduction at the cathode. Also, low efficiency, fuel crossover and low power density provides barriers for the deployment of DMFC technology in the portable power sources. The problems can be resolved by developing binary and ternary metal catalysts with various catalyst supports. The formation of various nanostructure catalysts in the nanometre regime can significantly improve the overall efficiency of DMFC.

3.2.1 Methanol Crossover

Methanol crossover is the most fundamental issue associated with any DMFC. In methanol crossover, methanol permeates from the anode chamber to the cathode chamber through the electrolytic membrane along with water separating the chambers. The high energy density in DMFC can be achieved by feeding the anode chamber with high concentrated methanol, but being small molecule it permeates through the electrolyte membrane, reacts with the oxygen in cathode chamber and provides mixed potential. This results in decrease in cathode potential, cathode depolarisation and low overall cell performance with chemical short circuit and self-discharge of methanol.

The methanol crossover can be reduced by lowering the methanol feed concentration, increasing the cell operating temperature and optimised catalyst loading at the anode. The electrolytic membrane plays a vital role in reducing the crossover. A perfluorinated ionomer membrane known as Nafion®, a DuPont product, is mostly used as an electrolyte membrane which includes a perfluoroalkyl side chain and perfluoroalkyl ether side chain with a sulfonic acid group at its end. The performance of Nafion® membrane can be improved by selective sealing of the water-rich

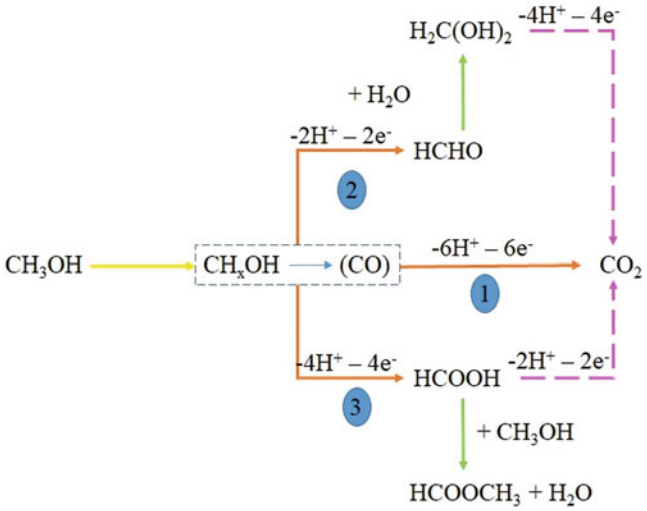

Fig. 3.2 Schematic representation of methanol oxidation reaction [8]

domains to suppress methanol crossover. Some proton-conducting membranes like polyetheretherketones, polyether imides, polybenzimidazoles, polyamides, polyphenylene sulphides and polyphenyquinoxalines provide superior performance than Nafion® membrane; however, their commercialisation is still restricted due to inferior stability.

3.2.2 Methanol Oxidation Reaction (MOR)

In 1988, Parsons and VanderNoot [7] studied the detailed oxidation of methanol in acidic medium. According to them, MOR follows: (a) electrosorption of methanol, (b) dissociation of methanol, (c) water adsorption and activation and (d) addition of oxygen to adsorbed carbon-containing intermediates to generate carbon dioxide. It is observed from Fig. 3.2 that the MOR proceeds through: (a) formation of CO (pathway 1), (b) formation of HCHO (pathway 2) and (c) formation of HCOOH (pathway 3).

The sluggish kinetics of MOR leads to poor DMFC performance. The problem can be solved by adjusting the methanol feed concentration, flow rate, efficient catalyst that ensures complete methanol oxidation, electrolytic membrane that ensures zero fuel crossover and non-Pt catalyst that ensures tolerance to methanol at the cathode.

3.2.3 Catalysts for Methanol Oxidation Reaction

Amongst various noble metal catalysts (Pt, Pd and Au), Pt is considered as most promising for MOR [9–16]. Han et al. [10] studied the MOR on Pt surface with dominant {100} face and observed that the {100} face favours the cleavage of C–C bond of methanol. The observation is also confirmed by Lee et al. [15], where the dominant {100} face provides large electrochemical active surface area for MOR. Further, they observed that the formation of various nanostructures of Pt (nanorods, nanotubes, nanocubes, etc.) can significantly improve the electrocatalytic methanol oxidation than the polycrystalline Pt. In another attempt, Tiwari et al. [11] prepared a two-dimensional (2D) continuous Pt island network for MOR and achieved improved performance due to increase in the surface area. They further observed that the performance and stability of MOR can be enhanced in 3D Pt nanoflowers than Pt thin film [12]. However, sluggish kinetics of MOR is achieved in pure Pt catalyst due to the irreversible absorption and subsequent formation of CO and carbonyl (CHO) intermediate species which limits the activity of the catalyst and restricts the commercialisation of DMFC. The poisonous intermediates can be removed when the Pt catalyst is alloyed with one or two other metals such as Ruthenium (Ru), Tin (Sn), Molybdenum (Mo), Cobalt (Co), Nickel (Ni), etc. The second metal facilitates the irreversible absorption of the poisoning intermediates by bifunctional mechanism and ligand effect.

Ren et al. [17] observed that PtRu catalyst exhibits excellent bifunctional mechanism for MOR at a lower potential with high current density (670 $mA.cm^{-2}$) and power density (400 $mW.cm^{-2}$). The intermediate CO and CHO adsorbed on the Pt surface oxidise at lower potential by active adsorbed hydroxyl ion (OH_{ads}) produced by Ru. The variation in the electronic structure of Pt and Ru could weaken the adsorption strength of CO_{ads} due to methanol dehydrogenation on Pt sites. Several other alternative binary catalysts such as PtSn [18, 19], PtMo [20, 21], PtW [20], PtOs [22] and PtMn [23] exhibit superior MOR activity than that of Pt alone. All these studies confirmed that the alloyed metal could produce OH species at lower electrode potential to remove the CO_{ads} species and facilitate the MOR. Rana et al. [24] prepared $Pd_{73}Pt_{27}$ nanowires using Te nanowires as sacrificial templates and studied the MOR. The $Pd_{73}Pt_{27}$ catalyst exhibits 10 times higher mass activity than commercial Pt/C with excellent stability (82.6% of its initial ECSA value after 4000 potential-cycles). The improved performance is attributed to the synergetic effect between Pt and Pd with dilution of Pt surface with Pd. On the other hand, PtSn exhibits both good [25] and poor [26] MOR performance. The controversy arises due the fact that when Sn adsorbed on the Pt surface it shows good activity, while when alloyed with Pt it exhibits poor activity. Ishikawa et al. [27] studied the density functional theory of dehydrogenation of methanol and water on Pt, Ru and bimetallic catalysts of Pt–M (M = Ru and Sn). They observed that the activity of Pt–M binary catalysts varies with the atomic ratio of Pt and M for MOR. The catalytic activity of MOR decreases with increasing Sn content due to the impedance property of Sn. Whereas the MOR is facile on Ru-rich surface due to ligand effect. Further,

Antolini et al. [28] observed that the catalytic activity of the PtRu is much higher than PtSn for methanol oxidation but its activity can be improved significantly by optimising the composition of the catalyst system. Habibi et al. [29] modified the electrode surface with poly(o-aminophenol) and then decorated with PtM (M = Ru, Sn) catalysts. The catalyst of PtSn showed current density of 150 $mA.cm^{-2}$, whereas PtRu showed current density of 125 $mA.cm^{-2}$ with superior stability in PtSn catalyst.

Tritsaris and Rossmeisl [30] estimated from density functional theory that although PtRu and PtSn are good catalysts for MOR; PtCu could also be a promising alternative because of having lower overpotential for MOR which was further confirmed by both theoretically and experimentally by Rossmeisl et al. [31]. They observed that MOR activity increases at lower potential when Cu atom is added to Pt (111) surface and the most effective PtCu catalysts will have three-atom ensembles of Cu (Cu_3Pt/Pt) which has similar activity to that of PtRu. Chiou et al. [32] studied the MOR using PtCu solid solution and observed that with increasing the Cu content from 5% to 20%, the peak current density increases from 130 $mA.mg_{Pt}^{-1}$ to 320 $mA.mg_{Pt}^{-1}$. However, further increase in the Cu content leads to the decrease in current density due to the formation of reductant Cu which blocks the active sites of the catalyst.

Maab and Nunes [33] studied the effect of Ti addition in Pt catalyst for electrocatalytic MOR and observed that $Pt_{25}Ti_{75}$/C catalyst exhibits much higher peak current density (128 $mA.mg_{Pt}^{-1}$) for MOR than $Pt_{50}Ti_{50}$/C (87.4 $mA.mg_{Pt}^{-1}$) and Pt/C (43 $mA.mg_{Pt}^{-1}$). Abe et al. [34] studied the MOR on atomically ordered and disordered Pt_3Ti nanoparticles. Both the ordered and disordered nanoparticles exhibit lower onset potential and CO adsorption affinity than pure Pt and PtRu catalyst. The atomically ordered nanoparticles showed higher current density than that of disordered Pt_3Ti, PtRu and Pt catalyst. Li et al. [35] studied the MOR using PtBi binary catalyst and compared with commercial PtRu catalyst and observed lower onset potential (0.4 V vs. NHE) and higher current density of 730 $mA.mg_{Pt}^{-1}$ than PtRu due to bifunctional mechanism and ligand effect.

Amongst all the binary catalyst PtRu exhibit best catalytic activity for MOR; however, the high cost of both Pt and Ru restricts the widespread application of the catalyst. Hence, the need of some alternative such as ternary, quaternary or multimetallic catalyst is utmost desired that can ease the MOR more efficiently than PtRu. In this regard, many ternary catalysts such as PtRuNi [36], PtRuMo [37, 38], PtRuSn [39], PtRuCo [40] and PtRuIr [41] are developed and found to exhibit 16 $A.g_{Pt}^{-1}$, 10.46 $A.cm^{-2}$, 100 $ma.mg_{Pt}^{-1}$, 100 $mA.cm^{-2}$ and 2.54 $A.cm^{-2}$, respectively.

Strasser et al. [42] studied the experimental and theoretical combinatorial and high-throughput screening method in multimetallic array catalyst consisting of PtRuM (M = Co, Ni, W). Out of 64 ternary catalysts tested at different permutation, PtRuCo is the best followed by PtRuNi, PtCoW and PtRu. Kakati et al. [38] studied the MOR using PtRuMo nanoparticle supported on multiwalled carbon nanotubes as catalyst and observed high electrochemical surface area (138 $m^2.g_{Pt}$) and mass activity (15 $A.g^{-1}{}_{Pt}$) than that of Pt and PtRu supported on multiwalled carbon

nanotubes. Zeng and Lee [43] reported that PtCoW/C catalyst exhibits better performance than Pt/C or PtRu for MOR and CO tolerance. The improved performance was attributed to the synergistic interactions where methanol dehydrogenation was initiated by CO, and removal of CO through the generation of oxygenated species. Welsch et al. [44] described the result of new elemental combinations with optical high-throughput screening method for various multimetallic catalysts used in MOR as shown in Fig. 3.3a–h. They have chosen $Pt_{30}X_aY_{(70\text{-}a)}$ type materials with XY combinations of the elements MnNi, Fe Ni, CoFe and Co Ni that showed a change in the fluorescence value during the measurement. For comparison of the MOR activity, the currents at 0.60 V (SHE) ($I_{0.6}$) and 0.80 V (SHE) ($I_{0.8}$) were normalised to the Pt content in each material which was measured in the 20th forward scan of each CV experiment. The two values ($I_{0.6}$ and $I_{0.8}$) were indicating the activity of the materials at low and high anode potentials. It is observed that the performance of the ternary catalysts such as PtTiZn, PtCoNi, PtMnNi and PtFeNi is superior than that of PtRu.

Further, several metal oxides such as RuO_2 [45], SnO_2 [46], TiO_2 [47], WO_3 [48, 49], MnO_2 [50, 51] and IrO_2 [52, 53] showed promising electrocatalytic activity towards MOR. The promotional effect between Pt and RuO_2 leads to excellent stability with mass activity of 0.4 $A.mg_{Pt}^{-1}$ in $PtRuO_2$ for MOR. The higher activity of the crystalline RuO_2 phase than that of metallic Ru towards CO oxidisation is ascribed by forming Ru–OH on the surface that lead to superior MOR activity [45]. $PtSnO_2$ exhibits higher MOR activity than Pt alone due to small deactivation loss after anodic activation and availability of active sites. In the presence of SnO_x, Pt is stabilised due to the formation of redox couple (Pt^0–Pt^{+2}, Pt^{+2}–Pt^{+4}) [54]. Zhao et al. [55] reported that $PtCo_3O_4$ exhibits better MOR activity than Pt electrode due to synergetic effect between Pt and Co_3O_4. The Co_3O_4 eases the oxidation of freshly chemisorbed species and provides active oxygen for removal of CO on the Pt surface effectively. They proposed that the adsorbed methanol on the Pt active site loses the methanolic proton to a basic oxide ion. The methoxy species, which is formed during the reaction get oxidatively decomposed to CO species and removed from the electrocatalyst surface by the reaction with Co_3O_4.

3.2.4 Performance of Direct Methanol Fuel Cell (DMFC)

Table 3.1 summarises the performance of various DMFC based on PEM. Surampudi et al. [56] developed a DMFC using liquid electrolyte. They achieved improved performance of 300 $mA.cm^{-2}$ current density at 0.5 V when the liquid alkali was replaced with solid electrolyte at 90 °C and optimum methanol fuel (2 M). Further, Shukla et al. [57] developed a vapour-fed DMFC that exhibits excellent stability for 8 h of operation with 75 $mA.cm^{-2}$ current density at 550 mV. In order to improve the performance of DMFC further, Jung et al. [58] made a systematic study on the dependence of performance on temperature and fuel feed. They achieved current density of 230 $mA.cm^{-2}$ at 0.5 V in a typical DMFC by optimising the operating

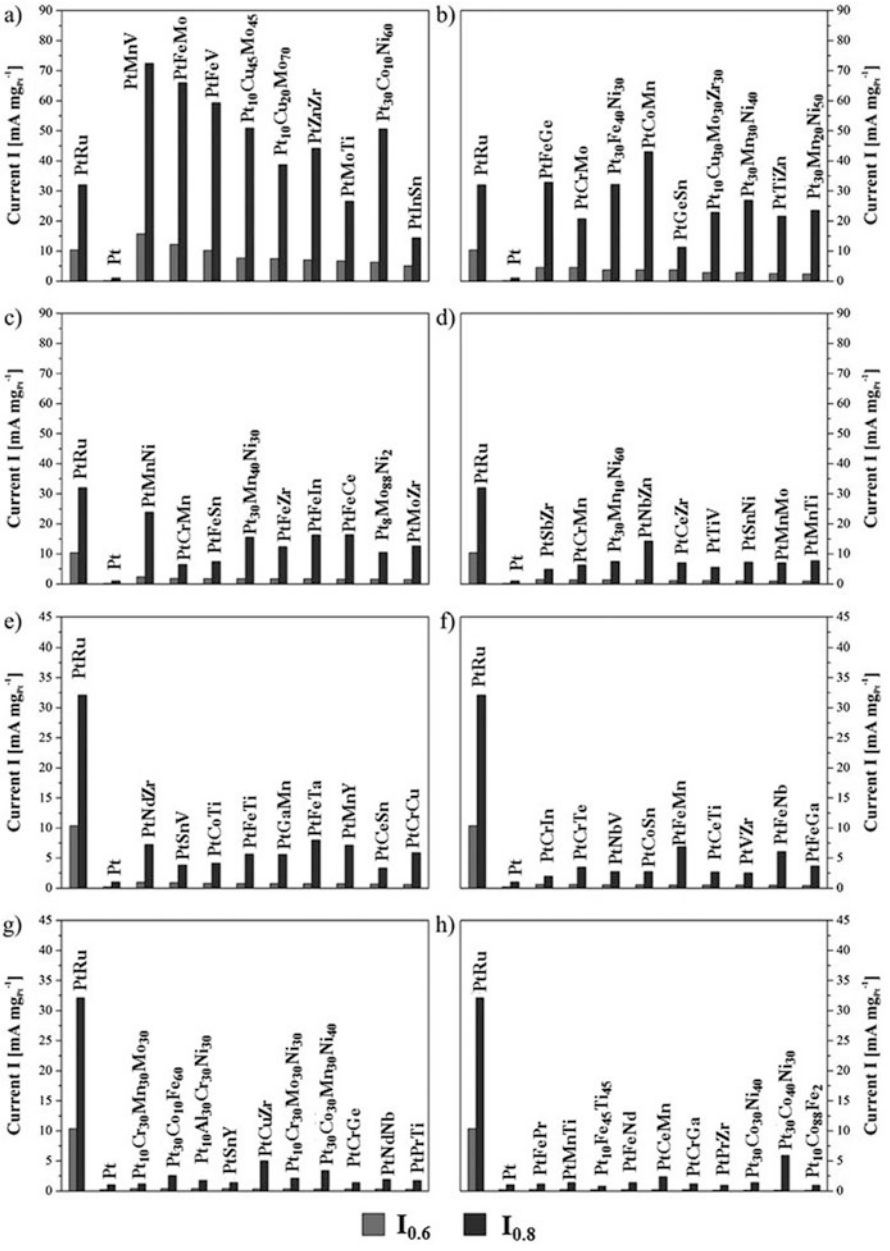

Fig. 3.3 (**a**–**h**) Comparative values of $I_{0.6}$ and $I_{0.8}$ (out of the twentieth forward scan) of various catalysts observed in CV experiments identified in high-throughput experiments [44]

Table 3.1 Performance comparison of various direct methanol fuel cell studies

Catalyst (loading mg.cm^{-2})	Methanol feed concentration/M	Membrane	Operating temperature/°C	Power density/ mW.cm^{-2}	Ref.
PtRu (4)	1	Nafion® 115	60	70	[62]
PtRu (3)	1	Hydrocarbon	80	110	[63]
PtRu (3)	2.5	Nafion® 117	90	260	[58]
PtRu (2.3)	1	Nafion® 112	130	390	[17]
PtRu/TiN (1)	1	Nafion® 115	40	32	[64]
PtRuCoP/C (2)	2	Nafion® 117	70	130	[65]
PtRu/CNT (4)	1	Nafion® 117	60	62	[66]
PtRu/CNT (4)	1	Nafion® 117	80	100	[66]
$PtNi_2P$/C (4)	1	Nafion® 117	60	65	[67]

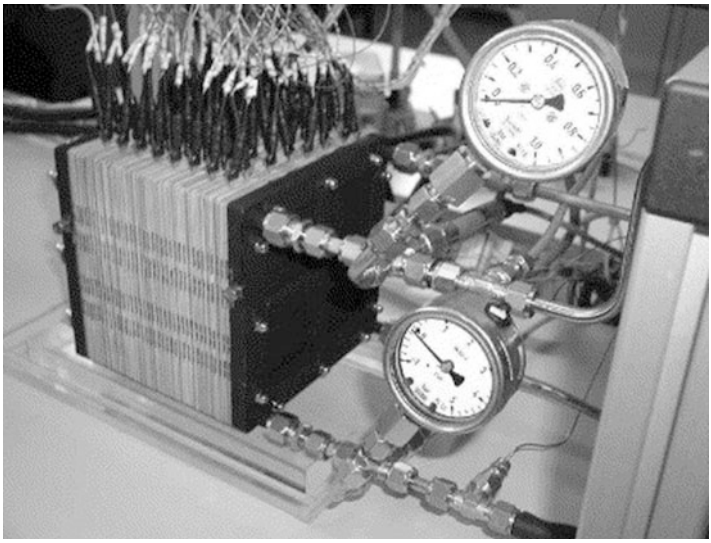

Fig. 3.4 A 500 W 71-cell direct methanol fuel cell stack [59]

temperature (60 °C–120 °C) and methanol feed (0.1 M to 4 M). The best MOR activity is achieved in a typical DMFC studied by Ren et al. [17] using PtRu as anode catalyst and perfluorosulfonic acid membranes operated at 130 °C. They observed peak power density of 390 mW.cm^{-2} due to high catalyst utilisations with optimal catalyst layer structures.

Towards the development of DMFC stack, Dillon et al. [2] designed a three cell stack starting with 3 cm^2 upto 60 cm^2 single cell. The stack produced 1.4 V at 0.1 A. cm^{-2} with total output power of 77 W. A 500 W 71-cell DMFC stack with an area of 144 cm^2 that utilised a 2-mm cell pitch (distance between two membrane electrode assemblies (MEAs)) is shown in Fig. 3.4 [59]. The assembled system contains a

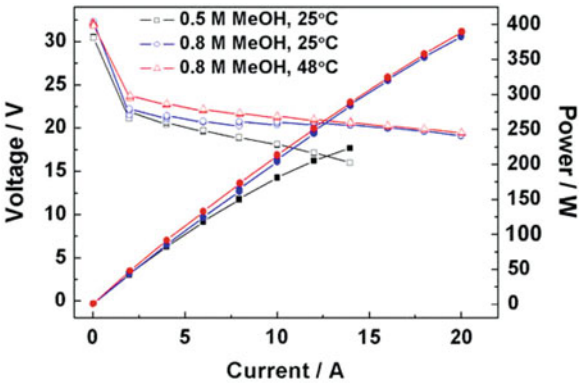

Fig. 3.5 Performance of 42-cell stack [61]

water/methanol reservoir, a heat exchanger, a pump and compressors as auxiliary components which are driven by the stack itself without any external power sources.

The characteristics of a 50-W DMFC stack were investigated by Kim et al. under various operating conditions including methanol concentration, fuel flow rate and the flow direction of the reactants [60]. The DMFC stack exhibit output power of 54 W (85 $mW.cm^{-2}$) and 98 W (158 $mW.cm^{-2}$) in air and oxygen, respectively, which increased to 20% when implementing a counter flow arrangement for the reactants. The performance of a 42-cell DMFC stack with active area of 138 cm^2 and output power of 400 W is shown in Fig. 3.5 [61]. A long-term operation coupled with performance restoration processes enables stable operation for 500 W with a voltage decay rate of 1.9 $\mu V.h^{-1}$.

3.3 Direct Ethanol Fuel Cell

Direct ethanol fuel cell (DEFC) utilises the chemical energy of the liquid ethanol and converts it into usable electrical energy to run power devices. In a typical DEFC, the anode chamber is fed directly with ethanol, whereas the cathode chamber is fed with oxygen. The electro-oxidation of ethanol at the anode chamber produces CO_2 and electrons. The schematic of a DEFC is shown in Fig. 3.6. The electrons travel through the external circuit from anode to cathode chamber to produce electrical energy to power devices [68, 69]. Ethanol possesses higher theoretical energy density (25 $MJ.kg^{-1}$) than methanol (22 $MJ.kg^{-1}$), non-toxic, cheap, having less crossover rate (bulkier than methanol) and easily available. Ethanol is produced from yeast through the fermentation of agricultural products, such as corn, sugar cane, maize, rice, etc. [70], thus it is renewable in nature. Ethanol also can be produced through steam reforming process of Naphtha (produced through the cracking of oil).

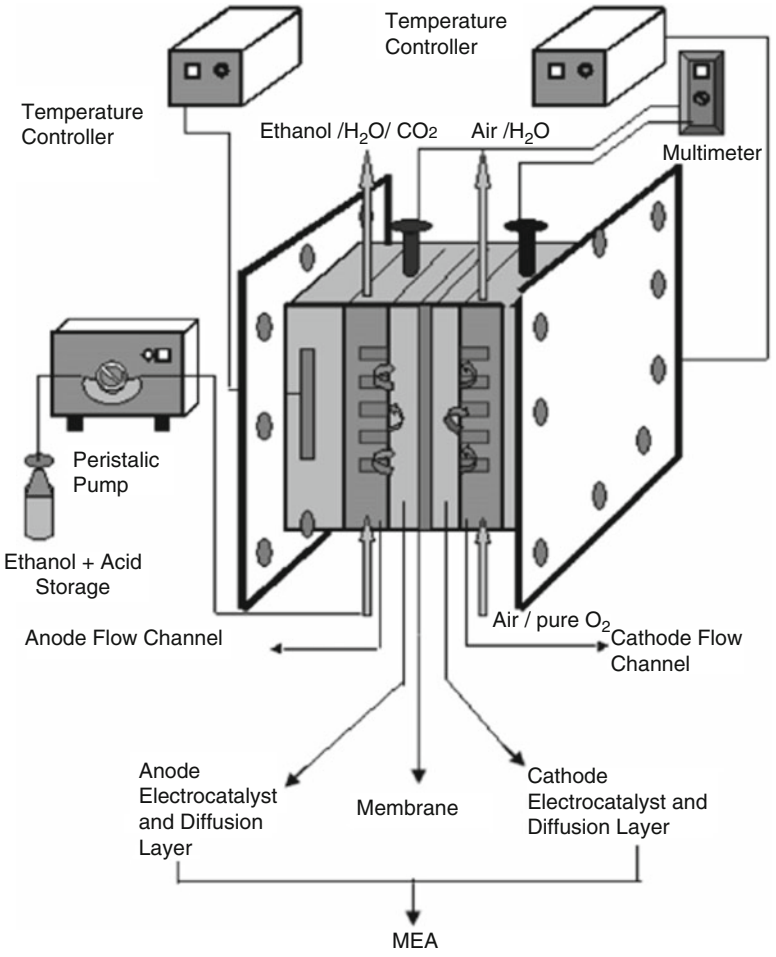

Fig. 3.6 Schematic of a typical direct ethanol fuel cell [71]

3.3.1 Ethanol Oxidation Reaction (EOR)

Generally, EOR is governed through multistep mechanism with the formation of several adsorbed reaction intermediates and by-products that leads to decrease in the performance of DEFC. A complete EOR using acidic electrolyte is proceeded through the cleavage of C–C bond and release of CO_2 molecules and 12 electrons per ethanol molecule. The anodic half-cell (EOR) reaction and cathodic half-cell reaction (ORR) is represented by:

Anode reaction:

$$CH_3CH_2OH + 3H_2O \rightarrow 2CO_2 + 12H^+ + 12e^- \quad (E_a \sim 0.09\ \text{V vs.SHE}) \quad (3.6)$$

Cathode reaction:

$$3O_2 + 12H^+ + 12e^- \rightarrow 6H_2O \quad (E_c \sim 1.23\ \text{V vs.SHE}) \quad (3.7)$$

Overall reaction:

$$CH_3CH_2OH + 3O_2 \rightarrow 2CO_2 + 3H_2O \quad (E_0 \sim 1.14\ \text{V vs.SHE}) \quad (3.8)$$

In order to achieve superior activity, the C–C and C–H bonds of ethanol need to be broken otherwise several intermediates which limits the EOR are formed according to:

$$CH_3CH_2OH \rightarrow CH_3CHO + 2H^+ + 2e^- \quad (3.9)$$

$$CH_3CH_2OH + H_2O \rightarrow CH_3CH(OH)_2 + 2H^+ + 2e^- \quad (3.10)$$

$$CH_3CH_2OH + H_2O \rightarrow CH_3CHOOH + 4H^+ + 4e^- \quad (3.11)$$

The partial oxidation of ethanol leads to acetaldehyde (Eq. (3.9)) or ethane, 1–1 diol (Eq. (3.10)) with the release of only two electrons and acetic acid (Eq. (3.11)) with the release of four electrons significantly decreasing the energy density.

The EOR is proceeded through either C1 or C2 pathway as shown in Fig. 3.7. The C1 pathway follows the cleavage of C–C bond either in C_2H_5OH or in CH_3CHO with the formation of CO_2 or CO_3^{2-}. The pathway C1 proceeds through breaking of C–C bond at lower potential, and results in adsorbed single carbon fragments. It is easy to break the C–C bond of acetaldehyde than that of ethanol. The C2 pathway takes place without breaking the C–C bond but cleavage of hydroxyl bond of ethanol with the formation of adsorbed ethoxy, followed by acetaldehyde (dehydrogenation process) and acetic acid (reaction with surface oxygenated species).

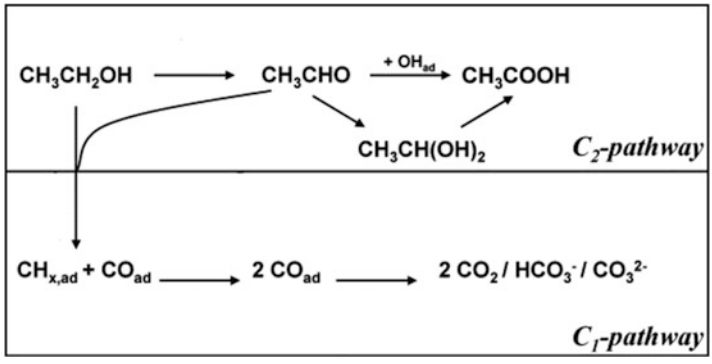

Fig. 3.7 Proposed reaction pathway for ethanol oxidation reaction [72]

3.3.2 Ethanol Crossover

Ethanol crossover is a serious issue that needs to be restricted to enhance the performance of DEFC based on PEM because it degrades the cathode performance severely. Similar to methanol, ethanol also has the tendency to diffuse through the PEM along with the H^+ ions. The diffused ethanol upon reaching the cathode chamber reacts with the O_2 and produces acetic acid. When the amount of acetic acid exceeds the O_2 in the cathode chamber, the acetic acid diffuses to the anode chamber and decreases the overall efficiency of DEFC. However, Verma and Basu [73] reported that the ethanol crossover rate in DEFC is much slower than methanol crossover in DMFC due to the fact that ethanol has lower permeability through the Nafion® membrane and slower electrochemical oxidation kinetics on the Pt/C cathode. The efficiency of the DEFC (δ) is related to current density according to:

$$\delta = \frac{i}{i + i_x} \tag{3.12}$$

where i is the current density of the DEFC, and i_x is the crossover current, which is not generated due to ethanol crossover. James and Pickup [74] reported that the ethanol crossover rate is directly proportional to the concentration of ethanol, temperature and current density [39]. Kontou et al. [75] observed that when the concentration of ethanol is beyond 4 M, it gives rise to a volcanic behaviour (solubility of ethanol and the swelling of the membrane) that increases the total crossover rate, diffusion and electroosmotic drag. Maab and Nunes [33] reported that the crossover issue can be overcome by using SPEEK (sulfonated poly(ether ether ketone)) membrane. They observed that the SPEEK membrane can be modified further to reduce the ethanol crossover. The membrane can be either coated with a carbon molecular sieves (CMS) layer or by using SPEEK/PI (polyimide) blends. The SPEEK/PI blends have shown better performance than CMS and Nafion® 117.

Beside the membrane, there are several parameters that govern the reaction kinetics of EOR such as temperature, concentration, pressure, catalyst and loading. The slow rate of EOR leads to voltage drop and reduction in power density. Hence, the parameters should be suitably handled and highly efficient catalyst should be prepared that can ease the ethanol oxidation easily.

3.3.3 Catalyst for Ethanol Oxidation Reaction (EOR)

The aim of catalyst research is to design and tune the activity by carefully controlling the composition and structural properties, up to the atomic level. The catalyst should facilitate the selective CO_2 formation with the transfer of 12 electrons per ethanol molecule, selectively provide surface site for C–C bond cleavage, and facilitate the bifunctional mechanism and ligand effect which promote the adsorption and activation of water to remove CO and CH_x species easily [76, 77].

Pt is widely used as anode catalyst in acidic medium for DEFC system. In low temperature, Pt usually oxidises ethanol completely to CO_2, in small amount because the active surface gets contaminated easily due to the adsorbed CO. The yield of CO_2 can be increased further by increasing the operating temperature due to the availability of more Pt surface active sites that increases in reactivity as the temperature increases. However, Zignani et al. [78] reported that the contamination rate increases with the increase in temperature making the active site unusable at faster rate. The implication is that the Pt surface is easily contaminated in any temperature, which might be restricted by alloying Pt with another metal (Ru, Sn, etc.) as the surface provides tolerance to contaminated intermediate species.

The most commonly used binary catalyst for EOR in acidic medium are PtRu and PtSn alloys due to bifunctional mechanism and ligand effect [79]. The presence of Ru and Sn facilitates the oxidation of the strongly adsorbed CO-containing species at a lower potential than pure Pt according to bifunctional mechanism and incorporation of Ru and Sn modifies the electronic structure of Pt that expedites the adsorption of oxygen-containing species, according to ligand effect.

Beyhan et al. [80] reported that PtSn/C (current density 150 $mA.mg_{pt}^{-1}$) exhibits superior activity for EOR in acidic medium than PtRu/C, PtPd/C, PtNi/C, PtRh/C and PtCo/C. Zhou et al. [81] further confirmed that the higher activity in PtSn/C is attributed due to the fact that Sn provides tolerance against poisoning of the surface active site. Research groups of Lamy [82–84] and Xin [81, 85–87] made an extensive study for EOR on PtRu/C catalyst. They reported controversial results on the content of Sn and degree of alloying between Pt and Sn. Lamy et al. [84] synthesised PtSn/C catalysts with Pt:Sn atomic ratios ranging from 90:10 to 50:50 and observed that the optimal composition of Sn varies in the range 10–20 atomic%. Conversely, Zhou et al. [81] observed that PtSn/C electrocatalysts with Pt:Sn molar ratios of 66:33, 60:40 and 50:50 showed superior electrocatalytic activity than 75:25 and 80:20 molar ratios, and observed that the optimal composition varies in the range 33–40 atomic%, depending on the operating conditions of DEFC. Jang et al. [88] compared the EOR on partially alloyed PtSn catalyst and quasi-non-alloyed PtSnO electrocatalyst and observed that the former exhibits superior activity. They inferred that the lattice parameters of Pt in SnOx have not been changed and SnOx in the presence of Pt nanoparticles could provide oxygen species easily to remove the CO-like species and facilitate the EOR. Colmenares et al. [89] reported that the prepared PtSn/C (3:1) catalyst demonstrates inferior activity than that of commercial catalyst of the same composition due to lower degree of alloying in prepared catalyst.

Other binary catalysts of PtM (M = W, Rh, Pd, Mo, Ti, Re, Ce) have shown improved performance towards EOR than Pt, but lower than that of PtSn and PtRu. Zhou et al. [51] observed superior EOR on Sn, Ru, Pd and W modified Pt and follows the order: PtSn/C > PtRu/C > PtW/C > PtPd/C > Pt/C. Dos Anjos et al. [90] reported superior EOR on PtMo catalyst over Pt. They observed that Pt alone had higher activity than PtMo (50:50) due to less availability of PtOH sites for oxidative removal of adsorbed CO and lower activity than PtMo (80:20) due to increase in the

electrode surface roughness caused by dissolution of Mo surface atoms or to an electronic modification of Pt.

It is well established from the previous studies that the activity of PtSn/C is superior than the others. Hence, to achieve further improvement in EOR, it was utmost desired to step towards ternary catalyst which can not only reduce the cost but suitably break the –CO and C–C bond of ethanol efficiently. Tayal et al. [91] added Re as the third element of PtSn ternary catalyst and observed that 20% Pt:5% Re:15% Sn can efficiently break the C–C bond of ethanol with higher EOR activity than other composition of ternary (20% Pt:10% Re:10% Sn) and binary (20% Pt:20% Sn, 20% Pt:20% Ru) catalyst. They also observed that PtIrSn/C exhibits superior EOR activity than PtSn/C and Pt/C electrocatalyst and follows the order PtIrSn/C (20% Pt, 5% Ir and 15% Sn by wt) > PtIrSn/C (20% Pt, 10% Ir and 10% Sn by wt) > PtSn/C (20% Pt and 20% Sn by wt) > PtIrSn/C (10% Pt, 15% Ir and 15% Sn by wt) > PtIr/C (20% Pt and 20% Ir by wt) > Pt/C (40% Pt by wt). Antolini et al. [92] prepared PtSn (1:1), PtSnRu (1:1:0.3, and 1:1:1) alloy catalyst and observed that PtSnRu (1:1:0.3) exhibits superior activity than the others because the ratios of non-alloyed Ru to non-alloyed Sn, which were 0.43 and 0.86 for PtSnRu (1:1:0.3) and PtSnRu (1:1:1), respectively, played the major role in electrochemical activity. The presence of Ru in the PtSnRu/C (1:1:0.3) catalyst had positive effect which was ascribed to the interactions between Sn and RuO_2. Rousseau et al. [93] studied the EOR at Pt, PtSn (90:10) and PtSnRu (86:10:4) in a single DEFC and observed that the addition of Ru to PtSn greatly enhanced the activity of the PtSnRu (86:10:4) than PtSn (90:10) and Pt alone. They further observed that acetic acid was the main oxidation product of EOR on PtSnRu and PtSn catalyst whereas acetaldehyde and carbon dioxide were the main product on Pt/C.

3.3.4 Performance of Direct Ethanol Fuel Cell (DEFC)

The performance of a DEFC depends mainly on the anode and cathode catalyst, fuel concentration, flow rate, catalyst loading, etc. Table 3.2 lists the performance of various catalysts on PEM-based DEFC. Several bimetallic PtX/C (X = Sn, Ni, Co, Rh, Pd) and trimetallic PtSnM/C (M = Ni, Co, Rh, Pd) catalysts had been tested in single-cell DEFC. The DEFC using PtSnNi/C (33 $mW.cm^{-2}$) and PtSnCo/C (35 $mW.cm^{-2}$) anode catalysts had significantly higher overall performance in terms of peak power density than the other catalysts [80].

Goel and Basu [101] studied the effect of various operating parameters such as operating temperature, fuel flow rate, ethanol concentration, etc. using Pt–Re–Sn (20:5:15)/C as anode catalyst. The performance of the DEFC was found to be increased by increasing the cell temperature and changing the support from carbon to multiwall carbon nanotube (MWCNT) to functionalised MWCNT (f-MWCNT) to mesoporous carbon nitrides (MCN). All these carbon structures exhibit excellent porosity and ease the catalysis. The peak power density of 52.4 $mW.cm^{-2}$ was achieved in a DEFC at 100 °C and 2 M ethanol. They further studied the effect of

Table 3.2 Performance of various direct ethanol fuel cells in acidic medium

Catalyst	Operating temperature/°C	Catalyst loading ($mg.cm^{-2}$)	Ethanol feed concentration/M	Power density/ $mW.cm^{-2}$	Ref.
40%PtIrSn/C	90	2	2	29	[94]
40%PtReSn/C	100	2	5	30.5	[91]
40%$Pt_{85}Sn_8W_7$/C	90	1	2	32	[95]
40%PtSnCo/C	90	2	1	35	[80]
40%$Pt_{80}Sn_{10}Ni_{10}$/C	80	2	2	46	[96]
40%PtReSn/f-MWCNT	100	2	2	52.4	[91]
40%PtRu/MCN	100	2	2	61.1	[97]
20%$Pt_{52}Ru_{48}$/C	80	3	2	62	[98]
70%$Pt_3Sn_1Ni_3$/C	90	2	1.5	70	[99]
40% PtSn/C	90	2	1.5	82	[100]

support material on the performance of DEFC using PtRu catalyst. The performance of DEFC on the basis of peak power density was found to be following the order PtRu/MCN > PtRu/f-MWCNTs > PtRu/MWCNTs > PtRu/Vulcan-XC. The PtRu/MCN exhibits highest power density of 61.1 mW cm^{-2} at 100 °C and 2 M ethanol [97]. Another breakthrough was achieved by Basu et al. [71] in the development of DEFC, when using low loading of PtRu/C anode catalyst (0.5 $mg.cm^{-2}$) and Ni mesh as current collector. They achieved power density of 15 $mW.cm^{-2}$ at 32 $mA.cm^{-2}$ current density from a single-cell DEFC. Zhu et al. [100] studied the effect of alloying degree in PtSn catalyst on the catalytic behaviour for EOR. They observed that PtSn/C catalyst with low alloying degree could enhance the yield of acetic acid, and high alloying degree promoted the entire activity for EOR and achieve power density of 82 $mW.cm^{-2}$ in a single cell as shown in Fig. 3.8.

Mathematical models on DEFCs have been developed that can predict the different fuel cell parameters such as overpotentials, electrolyte conductivity, performance losses, flow rate and reactant and product balance for improvement in the DEFC performance and scaling up issues [103, 104]. A typical DEFC prototype was developed by NDCP (Nanomaterial Discovery Corp. Power) (USA) with output power varying in the range 3–250 W and lifetime of more than 3700 h with a voltage decay rate of 40 μV/h for several portable applications.

3.4 Direct Ethylene Glycol Fuel Cell (DEGFC)

Direct ethylene glycol fuel cell (DEGFC) utilises the chemical energy of ethylene glycol to transform into useable electrical energy. Ethylene glycol has higher energy density (4.8 $Ah.ml^{-1}$) than methanol (4 $Ah.ml^{-1}$), non-toxic and easily available from renewable energy sources, which makes it promising fuel for next generation

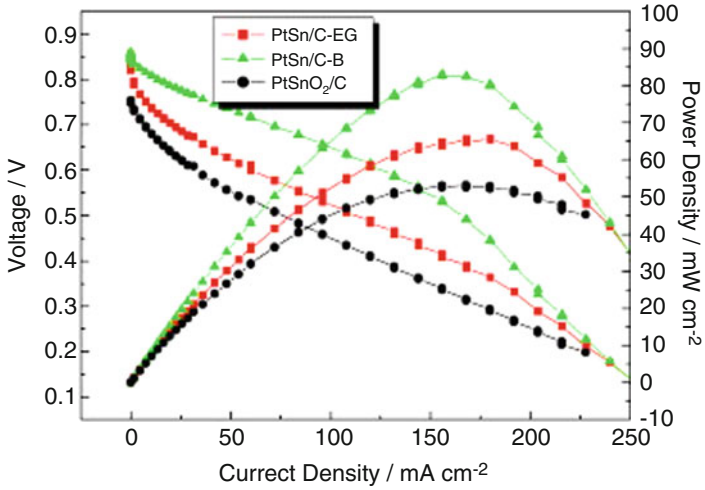

Fig. 3.8 Performance of various PtSn/C catalysts. PtSn/C–B catalyst displayed the highest alloying degree, and $PtSnO_2$/C catalyst had the lowest alloying degree [102]

fuel cell. It can also be produced economically from ethylene, which is available in shale gas in large quantity. It is facile to cease the C–C bond of ethylene glycol due to the presence of electronegative oxygen associated with both the C atoms.

3.4.1 Ethylene Glycol Oxidation Reaction

The partial oxidation product of EG is the oxalic acid with the transfer of eight electrons and the complete oxidation product is CO_2 with the transfer of ten electrons according to Eq. (3.13). Hence, the electron transfer rate is 80%, which is much higher than ethanol. DEGFC based on PEM operates at its highest efficiency at high temperature, usually greater than 110 °C.

$$(CH_2OH)_2 + 2H_2O \rightarrow 2CO_2 + 10H^+ + 10e^- \tag{3.13}$$

However, the incomplete oxidation of ethylene glycol produces several intermediate C2 products such as glycolaldehyde, glyoxal, glycolic acid, glyoxylic acid and oxalic acid [105] according to Fig. 3.9. To complete DEGFC operation, whereas Eq. (3.13) describes anode oxidation, the cathode reduction reaction remains the same as shown for ethanol, i.e., Eq. (3.7) and full stoichiometry balanced DEGFC is given by Eq. (3.14).

Wang et al. [102] observed that the consecutive oxidation of ethylene glycol and its intermediates follows 'desorption–re-adsorption–further oxidation' mechanism. They performed a series of experiments to observe the adsorption and oxidation

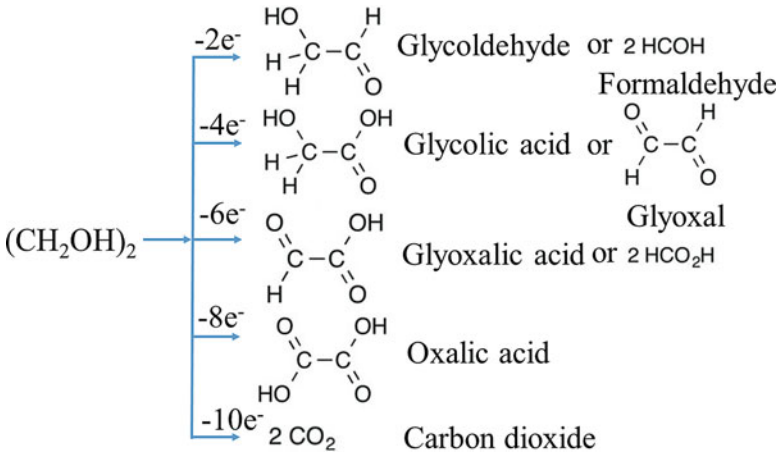

Fig. 3.9 Schematic of ethylene glycol oxidation

behaviour of ethylene glycol and its intermediates on the carbon-supported platinum surface in acidic media at room temperature. The efficiency for CO_2 formation from ethylene glycol is 6%, 14% for glycolaldehyde, glyoxal and glycolic acid and 35% for glyoxlaic acid. The intermediate products and CO_{ads} compete to block the active sites of the catalyst and restrict the adsorption of ethylene glycol further, thereby decreasing the fuel cell performance significantly.

3.4.2 Catalyst for Ethylene Glycol Oxidation Reaction (EGOR)

The mechanism of ethylene glycol oxidation with Pt catalysts at the anode side at room temperature in acidic medium suggests poor fuel utilisation and emission of large amount of poisonous intermediates that block the active site and lead to incomplete oxidation. Several approaches over the past few decades have been adopted to increase the efficiency and eliminate the undesirable intermediates. Increasing the Pt loading on the catalyst would increase the probability of re-adsorption of the intermediates on the surface and improve the performance, but the catalyst cost goes up significantly. The next solution is alloying Pt with other metals, e.g., Ru, Sn or others and reducing the cost with compromising on the efficiency of DEGFC.

Vielstich et al. [106] studied the influence of Pt:Ru ratio on the electrocatalytic activity of PtRu/C for EGOR. The activity increases significantly up to 40% Ru content due to the promotional effect between Pt and Ru. They observed that beside CO_2, glycolic and oxalic acid were the main oxidation products. Selvaraj et al. [107] deposited Pt and PtRu on surface-oxidised CNT and studied the oxidation of

ethylene glycol in acidic medium. They observed that PtRu/CNT catalyst with 12.62 mA.cm^{-2} current density exhibits superior performance than Pt/CNT (7.45 mA.cm^{-2}), which is ascribed to the promotion of CO_{ads} to CO_2 oxidation by the added ruthenium atoms. The probable mechanism of ethylene glycol oxidation on PtRu surface is:

$$(CH_2OH)_2 \rightarrow (CH_2OH)_{2(ads)} \rightarrow (:COH) + 2H_2O \rightarrow (HCOOH)_{ads} + 2H^+ + 2e^- \quad (3.14)$$

$$Pt(HCOOH)_{ads} \rightarrow Pt(CO)_{ads} + H_2O \quad (3.15)$$

$$Pt + H_2O \rightarrow Pt(OH)_{ads} \quad (3.16)$$

$$Pt(OH)_{ads} + Pt(CO)_{ads} \rightarrow Pt + CO_2 + H^+ \quad (3.17)$$

$$Ru + H_2O \rightarrow Ru(OH)_{ads} + H^+ + e^- \quad (3.18)$$

$$Ru(OH)_{ads} + Pt(CO)_{ads} \rightarrow Pt + Ru + CO_2 + H^+ + e^- \quad (3.19)$$

In order to improve the performance further, various trimetallic catalysts like PtRuW, PtRuNi and PtRuPd have been tested [106, 108, 109]. Amongst trimetallic catalysts for EGOR, Pt:Ru:W (1:1:1) exhibits superior EGOR (120 mA.cm^{-2}) than PtRu/Ti (80 mA.cm^{-2}) and PtRu/C (60 mA.cm^{-2}). The improved performance is ascribed to the transformation from W(VI) to W(IV) or from W(VI) to W(V) which renders the W sites active for the dissociative adsorption of water [108].

3.4.3 *Performance of Direct Ethylene Glycol Fuel Cell (DEGFC)*

There have been several reports on the performance of DEGFC based on PEM [106, 108] and nanoporous proton-conducting membrane (NP-PCM) [110, 111]. The Nafion® membrane is suitable for DEGFC, when it operates at low temperature but the reaction kinetics of ethylene glycol suggests higher operating temperature (< 80 °C) in order to restrict the poisonous intermediate formation. Vielstich et al. [106] studied the performance of a DEGFC using PtRu as anode catalyst, with Nafion®117 electrolytic membrane operated at 70 °C with 2 M ethylene glycol as fuel. They achieved a stable current density of 18 mA.cm^{-2} at a constant anode potential of 0.4 V for 1 h of operation. Chetty and Scott [108] tested a single-cell DEGFC using titanium mesh anode with the PtRuW/Ti as anode catalyst, with Nafion®117 electrolytic membrane at 90 °C with 1.0 M ethylene glycol solution and achieved peak power density of 15 mW.cm^{-2}, which was superior

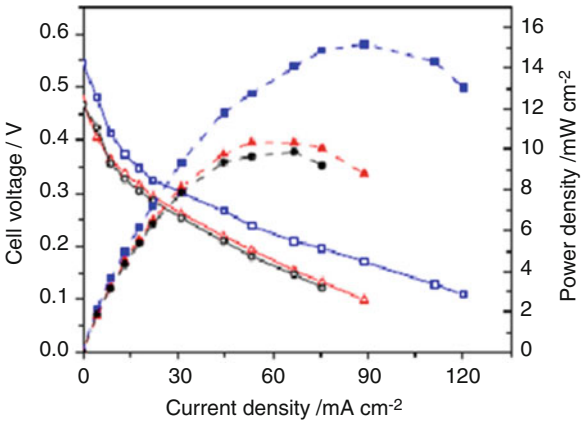

Fig. 3.10 Fuel cell performance of DEGFC using PtRu/C (black), PtRu/Ti (red) and PtRuW/Ti (blue) anode catalysts [108]

than that of the PtRu/Ti (10 mW.cm^{-2}) and PtRu/C (9 mW.cm^{-2}) catalysts as shown in Fig. 3.10.

Peled and his group studied the performance of DEGFC using NP-PCM as electrolytic membrane instead of Nafion®. They observed that the NP-PCM offers several advantages over the Nafion membrane such as: low cost, smaller pore, low crossover and higher conductivity. They prepared an NP-PCM using 28 wt.% poly (vinylidenedifluoride) (PVDF), and 12% SiO_2 and achieved maximum power densities of 320 mW cm^{-2} (at 0.32 V) at 130 °C. They assumed that the improvement is due to lower level of poisoning of the Pt catalyst by ethylene glycol and its oxidised species on the cathode side [110]. Further, Peled et al. [111] developed ten 10 cm^{-2} cells based on 2.2-mm bipolar plates as shown in Fig. 3.11. They achieved maximum power of 12 W (at 0.3 V cell^{-1}) at 80 °C in a DEGFC fresh stack fed with 0.5 M ethylene glycol with 1.7 M triflic acid solution at ambient dry air pressure.

3.5 Direct Formic Acid Fuel Cell

Formic acid when used as a fuel in proton exchange membrane fuel cell (PEMFC) has a higher output in terms of power density in comparison with methanol (DMFC)- and ethanol (DEFC)-based fuel cells. Other than power density, theoretical open circuit voltage (OCV) of direct formic acid fuel cell (DFAFC) is 1.48 V, which is way higher than methanol-powered (1.18 V) and H_2-powered (1.23 V) fuel cells. The main reason behind generation of such higher power output and OCV from DFAFC is its low fuel crossover, which eventually increases the electro-oxidation of the fuel at the anode. $HCOO^-$ group from formic acid and sulfuric group from nafion membrane repel each other, which causes decrease in fuel crossover. Apart from high rate of electro-oxidation and low fuel crossover of formic acid in DFAFC, non-toxicity, non-flammability and surplus availability make it more suitable and preferable as a fuel.

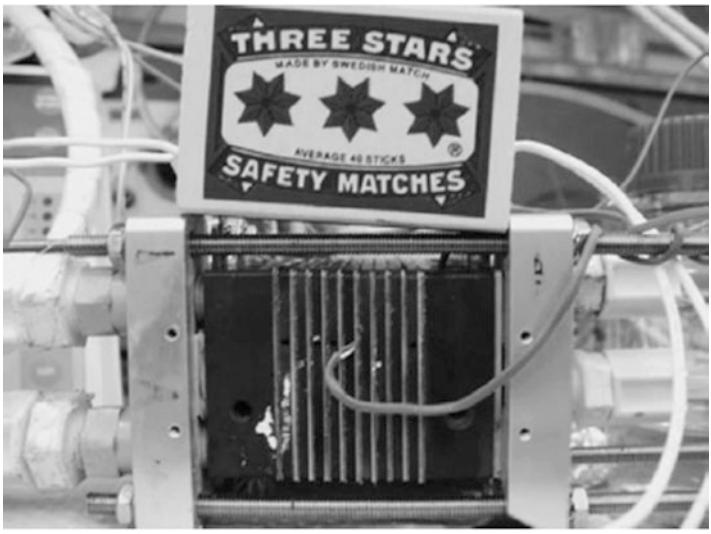

Fig. 3.11 A 10 (10 cm^2) cell direct ethylene glycol fuel cell stack [111]

3.5.1 Reaction Mechanism

Electro-oxidation of formic acid at anode of DFAFC can be described by two different reaction mechanisms: (1) dehydrogenation and (2) dehydration [112, 113]. Equation (3.20) shows the dehydrogenation mechanism of formic acid, where it undergoes electro-oxidation and releases CO_2, H^+ and two electrons as products. In dehydrogenation mechanism, the fuel conversion is higher by which an overall high cell efficiency is achieved. Dehydration mechanism is a two-step electro-oxidation mechanism as shown by Eqs. (3.21) and (3.22). In case of dehydration mechanism as shown by Eq. (3.21), adsorbed formic acid undergoes electro-oxidation and produces adsorbed CO species, which eventually blocks the catalytic active sites for further oxidation. The adsorbed CO further oxidises to CO_2 in the presence of OH molecule which is adsorbed on the catalyst surface as shown by Eq. (3.22).

$$HCOOH \rightarrow CO_2 + 2H^+ + 2e^- \quad \text{(Dehydrogenation)} \tag{3.20}$$

$$HCOOH \rightarrow CO_{ads} + H_2O \quad \text{(Dehydration)} \tag{3.21}$$

$$CO_{ads} + OH_{ads} \rightarrow CO_2 + H^+ + e^- \quad \text{(Dehydration)} \tag{3.22}$$

At the cathode side, O_2 undergoes reduction reaction as shown by Eq. (3.24). The anodic electro-oxidation, cathodic reduction and overall electrochemical reactions in a DFAFC are as follows:

At anode:

$$\mathrm{HCOOH} \rightarrow \mathrm{CO_2} + 2\mathrm{H^+} + 2\mathrm{e^-} \quad (E_0 = -0.25\ \mathrm{V\ vs\ SHE}) \tag{3.23}$$

At cathode:

$$^1/_2\mathrm{O_2} + 2\mathrm{H^+} + 2\mathrm{e^-} \rightarrow \mathrm{H_2O} \quad (E_0 = 1.23\ \mathrm{V\ vs\ SHE}) \tag{3.24}$$

Overall reaction:

$$\mathrm{HCOOH} + {}^1/_2\mathrm{O_2} \rightarrow \mathrm{CO_2} + \mathrm{H_2O} \quad (E_0 = 1.48\ \mathrm{V\ vs\ SHE}) \tag{3.25}$$

3.5.2 Catalyst for Formic Acid Electro–Oxidation

Major focus while developing electrocatalyst for formic acid oxidation (FAO) has always been to increase its electrocatalytic active surface area, durability and stability. Over the years, noble metal catalysts (Pt, Pd) have been the prime choice for FAO because of its good activity, but its susceptibility towards CO poisoning followed by loss in performance has paved way for improvement. Enhancement in activity along with stability can be achieved by providing better catalyst supports, developing multi (bi, tri) metallic alloy catalysts, causing morphological changes to existing noble metal catalyst or alteration in the present preparation techniques. The following sections discuss about various Pt- and Pd-based catalysts, multimetallic catalysts and performance-enhancing catalyst supports for FAO.

Pt has a good electrocatalytic activity towards FAO reaction, but its high cost and susceptibility towards CO poisoning makes it unaffordable to use in DFAFC for commercial purposes. Studies have shown that there is no significant difference in FAO kinetics on Pt/C and Pt catalyst, as carbon support in Pt/C provides high conductivity and good stability [113]. Layer-by-layer electrodeposition of Pt/C forms dendritic structure increasing the electrochemical active surface area (ECSA) and triple phase boundary (TPB), thus enhancing the performance [114]. Researchers have alloyed Pt with multi (bi, tri) noble and non-noble metals such as Pd, Ru, Au, Pb and Bi to overcome CO poisoning of Pt and increasing catalytic activity [115–121]. Pt–Pd alloy catalyst follows the dehydrogenation mechanism (Eq. (3.20)) for electro-oxidation of formic acid and produces CO_2 thus overcoming the issue of catalyst poisoning [117, 121]. In case of Pt–Ru alloy catalyst, formic acid electro-oxidation follows dehydration mechanism (Eqs. (3.21) and (3.22)) producing adsorbed CO on Pt, which oxidises to CO_2 by the adsorbed OH on Ru leaving Pt for further reaction [116, 117]. Au in Pt–Au successfully inhibits CO poisoning by blocking or occupying the adsorption sites of the Pt catalysts but eventually the performance of Pt–Au is very low as compared to Pt

or Pd [118]. Pt–Au NPs deposited on carbon support using ultrasonication technique in an atomic ratio of 32:68 (Pt:Au) has shown 153 times (14.5 A mg^{-1}) increase in FAO activity than that in Pt/C [120]. Pt–Pb showed better stability and enhanced activity than its counterparts like Pt, Pt–Ru and Pd due to better electronic interaction between Pt and Pb [115]. Pt nanoparticles along with Bi (Pt–Bi) has shown good catalytic performance irrespective of high levels of CO but performance still lags behind Pd [119]. Some of the trimetallic catalysts like $Pt_4PdCu_{0.4}$ [122] and MnO_x/Au/Pt [123] have shown 10.2, 67 times increase in activity than that for Pt/C, respectively, as the use of Cu and MnO_x promotes charge transfer and removal of adsorbed CO at a lower potential. Use of different supports like multiwalled carbon nanotubes (PdPtNi/MWCNTs), macrocycle composite (PtNi/N,N′-mono-8-quinolyl-o-phenylene diamine) and porous silicon (Pd/Pt/PS) other than carbon support increases the electrochemical active surface area, suppresses CO poisoning of Pt by providing other active sites for CO adsorption and follows dehydrogenation mechanism for FAO, respectively [124–126]. Nanostructured Cu_2O–Pt/GC catalyst follows 'Spill-over mechanism' where CO adsorbed on Pt migrates to Cu_2O and oxidises to CO_2 thus showing better CO tolerance than nano-Pt/GC [127].

It is well known that Pd-based catalyst can generate higher power density (at room temperature) compared to Pt-based catalyst but its higher cost and susceptibility towards CO poisoning makes it unaffordable to use in DFAFC. Researchers have alloyed Pd with other metals such as Co, CoP, Bi, Ir and Ni_2P in order to tackle CO poisoning by means of bifunctional, synergistic effects of the combinations [76, 128–133]. Bimetallic PdCo/PWA-C catalyst has shown an increase in activity and stability by 2.16 and 5.28 times than that of Pd/C [76]. Co in Pd–CoP/C and PdCo/PWA-C inhibits absorption of poisoning intermediates and provides oxidation sites at lower potentials [76, 130] whereas Bi induces better electronic transport between Bi and N in PdBi/N-graphene thus increasing its activity [131]. Ultrasonically prepared nanocrystal Pd_4Ir/graphene catalysts accounts for better stability even after 600 cycles of CV because of high ECSA (76.3 m^2 g^{-1}) and synergistic effect between Pd_4Ir and graphene [132]. Electrodeposited PdNPs (Pd nanoparticles) and IrNPs on glassy carbon electrodes as Ir/Pd/GC showed a –ve shift in onset potential and an increase in formic acid oxidation current and enhanced catalytic activity and stability shown by Ir/Pd/GC is attributed to the bifunctional mechanism of Ir on Pd [129]. Pd–Ni_2P/C has shown enhanced electrocatalytic activity, improved power density [128] and stability [134] due to the ability of Ni_2P to generate adsorbed OH species which can oxidise adsorbed CO to CO_2. Catalysts with a combination of Pd with metal oxides like ZrO_2 and MnO_x have demonstrated improved activity, stability and self-cleaning mechanism after CO poisoning [132, 135]. Apart from catalyst development, catalyst supports like MWCNTs, graphene, rGO, PWA-C, BN, TiO_2 NRs and Ni–B/C have also increased catalytic activity and ECSA of the catalyst thus providing a platform for Pd with better conductivity, and better charge transfer [76, 131, 132, 136–141]. Ni–B/C supports activate water molecules to generate OH species which oxides the adsorbed CO to CO_2. Mainly, bifunctional

effect between Pd and the support suppress formation and adsorption of CO intermediates promoting and dehydrogenation mechanism for FAO. Non-transition metals such as Sb, Sn and Bi alone have shown better stability under high levels of CO poisoning and durability under acidic conditions [7, 142, 143].

3.5.3 *Cell Configuration and Performance*

According to the cathode side arrangement, DFAFC can be classified into two types: Active DFAFCs and Air breathing DFAFCs. In DFAFCs, formic acid at the anode side can be supplied either as a batch or maintain continuous flow by using a liquid pump. For an active DFAFC, continuous supply of air/O_2 is provided through the cathode channel whereas in case of air breathing DFAFCs, the cathode electrode is directly exposed to atmosphere for air/O_2 [144]. A schematic representation of different components of DFAFC is shown in Fig. 3.12.

Some of the full DFAFC studies with Pt- and Pd-based electrocatalyst have shown good power density and activity. Anodes with dendritic Pt–Pd/C [121] and morphologically engineered Pt/C by electrodeposition technique [114] have shown a maximum power density of 49 mW cm^{-2} and 42 mW/cm^{-2}, respectively. PtNi/macrocycle composite anodes [124] have achieved 166 mW mg^{-1} maximum power density (w.r.t. mass of Pt). As already seen from half-cell studies, performance of Pd-based anodes in full cell is way better than Pt-based anodes. Studies have shown that tailoring with Pd NPs [145] and introducing Co with Pd [130] generates 245 mW cm^{-2} and 150 mW cm^{-2} as maximum power density, respectively. Introducing MWCNTs as support into Pd-based anodes such as Pd/MWCNTs and Pd–ZrO_2/MWCNTs has achieved a maximum power density of 119 mW mg^{-1} [136] and 55 mW mg^{-1} [146] (w.r.t. mass of Pd), respectively. Table 3.3 shows comparison of the performance of different anode catalysts for DFAFC and it can be

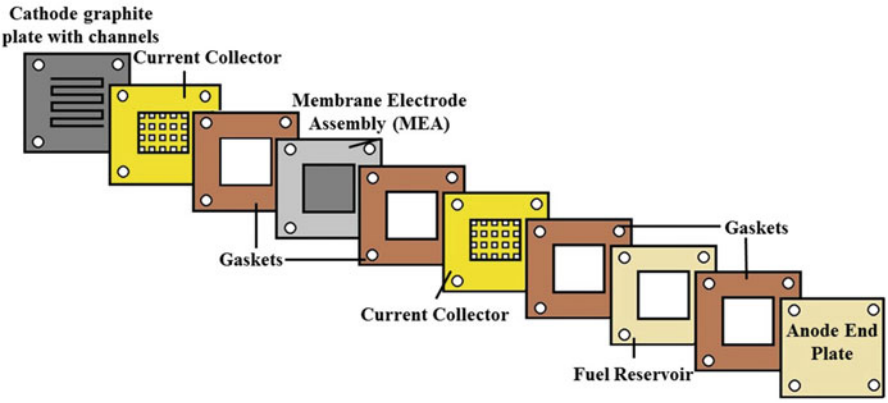

Fig. 3.12 Schematic of direct formic acid fuel cell

Table 3.3 Fuel and oxidant details and power density values for different anode catalysts in direct formic acid fuel cell

Anode catalyst	Fuel	Oxidant	Power density	Ref
Pt/C	3 M formic acid	Dry O_2	42 mW cm^{-2}	[114]
Pt–Pd dendrite/C	3 M formic acid	Dry O_2	49 mW cm^{-2}	[121]
Pt–Ni(mqph)	6 M formic acid	Humidified O_2	166 mW mg_{Pt}^{-1}	[124]
Pd black	5 M formic acid	O_2	245 mW cm^{-2}	[145]
Pd–CoP/C	3 M formic acid	O_2	150 mW cm^{-2}	[130]
Pd/MWCNTs	3 M formic acid	O_2	119 mW mg_{Pd}^{-1}	[136]
Pd–ZrO_2/MWCNTs	3 M formic acid	Air	55 mW mg_{Pd}^{-1}	[146]

seen that Pd–CoP/C gives the best power density even at a comparatively lower formic acid concentration. Further, Fuel Cell Research Centre at the Korea Institute of Science and Technology (KIST) developed a DFAFC hybrid power system with 15 MEA DFAFC stack for a laptop computer which can deliver 30 W power at 60 mW cm^{-2} current density.

3.6 Direct Glycerol Fuel Cell (DGEFC)

Glycerol being a polyol as a fuel is less toxic than other fuels such as methanol, ethanol, etc. and also has a comparatively good theoretical energy density (5 kWh. kg^{-1}). Investigators have shown that the activity and stability of electrocatalyst towards glycerol electro-oxidation reaction (GEOR) in an alkaline media [147–150] is much higher than the acidic media. Such difference in activity can be attributed to the lack of alkoxide formation and surface blocked by the anions in the acidic media [151]. Due to this reason, research on GEOR in acidic media is very limited and mainly focused on noble metal catalysts such as Pt, Au and Ru. It is essential to have a fundamental understanding of GEOR mechanism in order to overcome lack of activity and stability in acidic media. It is well understood that in a proton exchange membrane-based direct glycerol fuel cell (DGEFC), dilute solution of glycerol passed through the anode undergoes electro-oxidation (Eq. (3.26)), producing CO_2, H^+ and e^-, at cathode O_2 undergoes reduction reaction (ORR) (Eq. (3.27)) and overall reaction is given by Eq. (3.28).

$$C_3H_8O_3 + 3H_2O \rightarrow 3CO_2 + 14H^+ + 14e^- \tag{3.26}$$

$$3.5O_2 + 14H^+ + 14e^- \rightarrow 7H_2O \tag{3.27}$$

$$C_3H_8O_3 + 3.5O_2 \rightarrow 3CO_2 + 4H_2O \tag{3.28}$$

Direct pathway is mostly preferred (Eqs. (3.26) and (3.27)) for a better performance of a DGEFC, but research has shown that GEOR mechanism is very sensitive to electrocatalyst structure with regard to its selectivity and catalytic activity [152],

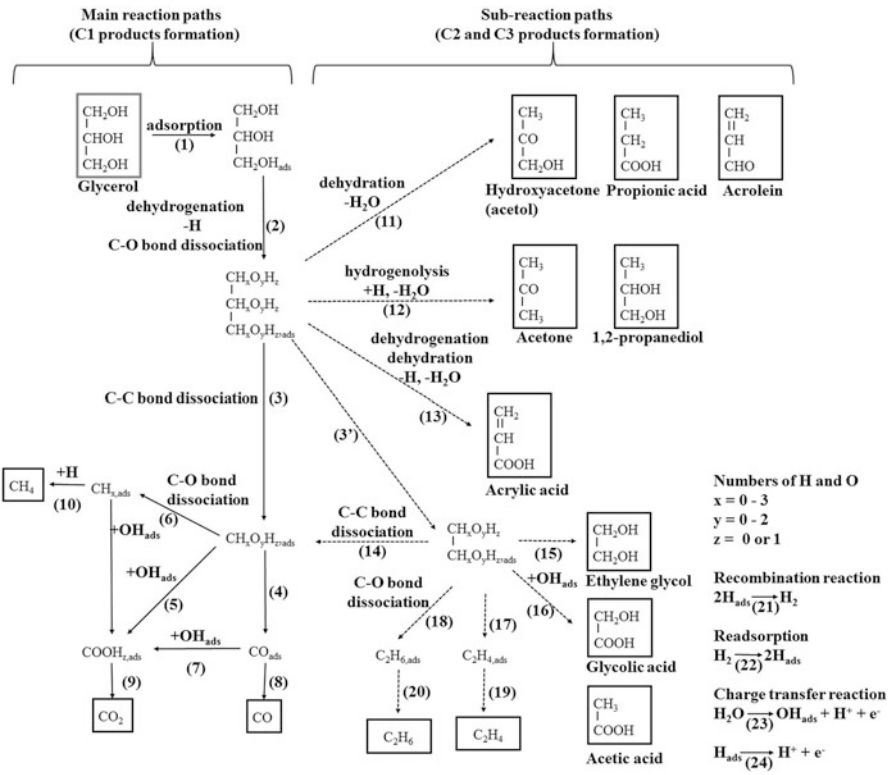

Fig. 3.13 Glycerol electro-oxidation reaction mechanism on a Pt/C electrode surface [153]

due to which various other GEOR pathways also exist (Fig. 3.13) [153]. It has been observed that different Pt surfaces like Pt (111), Pt (110) and Pt (100) produce different electro-oxidation products like formic acid, tartaric acid, glycolic acid, glyceraldehyde, etc. alongside CO_2 and H_2 through indirect pathways [152, 154, 155]. Pt (110) and Pt (100) surfaces is more entitled to produce CO_2 as it favours C–C–C bond breaking and it is observed that Pt (111) is less susceptible to poisoning [152]. Random defects created in Pt (111) surface modifies GEOR onset potential and produces C=O-based products [154]. DFT calculations show that glycerol binds with Pt (111) through 2 Pt–C bonds, whereas in case of Pt (100), a Pt = C bond adheres glycerol to Pt surface producing different products [155]. Experimental studies using Pt nanoparticles and polycrystalline Pt as GEOR electrocatalyst found that the steric effect between end $–CH_2OH$ group and central –CHOH group in glycerol and the favourability of $–CH_2OH$ group towards adsorbed OH species oxidises end $–CH_2OH$ group easily than central –CHOH group [156, 157]. It is also observed that rate of CO_2 formation from adsorbed CO increases at higher potentials even with a parallel reaction pathway [158, 159]. Alloy of PtRu supported on carbon (binary electrocatalyst) has shown an improvement in stability and a 40%

increase in the catalytic activity compared to Pt/C electrocatalyst due to the changes in the structure and electronic interaction brought by the incorporation of Ru [160]. In case of $Pb_x@Pt_y/C$ core–shell nanoparticles also, an improved electronic interaction and surface structure plays a role in increasing the catalyst activity [161]. For a ternary electrocatalyst such as Pt–Ru–TiO_2, ECSA increases three fold than PtRu when TiO_2 loading is about 50%. Other than CO and CO_2 as products, formation of intermediates like acetic acid is also observed with Pt–Ru–TiO_2 electrocatalyst [162]. Au is another electrocatalyst that has shown some catalytic activity towards GEOR other than Pt- and Pd-based electrocatalyst, but the reaction on polycrystalline Au surface very much depends on the pH value [151, 163].

3.7 Conclusions and Outlook

Direct oxidation fuel cells using proton exchange membrane are well known for the past few decades due to their wide variety of applications at low-temperature operation. The fuel cells efficiently convert the chemical energy of fuels (methanol, ethanol, ethylene glycol, formic acid and glycerol) into electricity and are named as direct methanol fuel cell, direct ethanol fuel cell, direct ethylene glycol fuel cell, direct formic acid fuel cell and direct glucose fuel cell based on the type of fuel used. The critical issues that restrict the widespread commercialisation of these fuel cells are cost of catalyst and electrolytic membrane, durability and performance at low temperature. This chapter describes the fuel oxidation mechanism at anode and cathode, working principle of the fuel cells and various operating conditions, catalyst loading, fuel flow rate and operating temperature, of these fuel cells. The use of fuels in direct fuel cell is very safe, economical and easy to handle and store due to their facile production from fossil fuel and renewable energy sources.

In a typical direct methanol fuel cell, methanol is oxidised directly to carbon dioxide with the release of six electrons. However, due to the sluggish kinetics of methanol oxidation reaction, several intermediates such as carbon monoxide, formic acid and formaldehyde are formed, which degrades the performance of direct methanol fuel cell to a large extent. Methanol crossover is another critical issue that reduces the cathode potential, cathode depolarisation with chemical short circuit, self-discharge of methanol and eventually degrades the performance of direct methanol fuel cell. Various binary and ternary catalysts based on noble and non-noble metals are developed which can facilitate the methanol oxidation reaction and improve the performance of direct methanol fuel cell. In this regard, PtRu and PtRuCoP/C catalysts exhibit superior performance than others for methanol oxidation reaction in direct methanol fuel cell. A 500 W 71-cell direct methanol fuel cell stack that utilised a 2-mm cell pitch and a 42-cell direct methanol fuel cell stack with active area of 138 cm^2 with output power of 400 W has been developed. Several electronics companies based on Japan and Korea (Toshiba, Hitachi, Fujitsu and Samsung) developed power backup system using direct methanol fuel cell. In direct

ethanol fuel cell, ethanol oxidation reaction is more complex than methanol oxidation reaction and governed by C–C bond cleavage of ethanol or acetaldehyde or cleavage of O–H bond of ethanol with the release of carbon dioxide and 12 electrons per ethanol molecule. Ethanol crossover is another critical issue that severely affects the direct ethanol fuel cell performance. The diffused ethanol upon reaching the cathode chamber reacts with the O_2 and produces acetic acid. When the amount of acetic acid exceeds the O_2 in the cathode chamber, the acetic acid diffuses to the anode chamber and decreases the overall efficiency of direct ethanol fuel cell. The crossover can be restricted by using sulfonated poly(ether ether ketone)/(polyimide) (SPEEK/PI) membrane and exhibit superior performance than Nafion®. It is noted that crossover in direct ethanol fuel cell is less than direct methanol fuel cell because ethanol is bulkier than methanol. Several binary and ternary metal-based catalysts which can ease the ethanol oxidation reaction are discussed in this chapter. PtSn/C (82 $mW.cm^{-2}$) and PtSnNi/C (70 $mW.cm^{-2}$) catalysts exhibit best performance than the others in proton exchange membrane-based direct ethanol fuel cell at low temperature. NDCP (Nanomaterial Discovery Corp.) Power (USA) developed DEFC prototype for many portable applications with output power in the range 3–250 W and lifetime of more than 3700 h with a voltage decay rate of 40 μV/h. The use of ethylene glycol directly into fuel cell, which is less volatile, high boiling point and high energy density than methanol is discussed. It is easy to break the C–C bond of ethylene glycol due to the presence of electronegative oxygen associated with both the C atoms. Pt:Ru:W (1:1:1) exhibit best EGOR than the others in proton exchange membrane-based direct ethylene glycol fuel cell. Nanoporous proton-conducting membrane exhibits better performance than Nafion® membrane. A ten 10 cm^{-2} cells exhibit maximum power of 12 W (at 0.3 V $cell^{-1}$) in a proton exchange membrane electrolyte-based direct ethylene glycol fuel cell. However, due to the complex oxidation mechanism of ethylene glycol in acidic medium leading to its degradation, it requires further study for the commercialisation of proton exchange membrane electrolyte-based direct ethylene glycol fuel cell. The various catalysts, e.g. Pt/C, PtPd/C, Pd–CoP/C and Pd/MWCNTs, for direct formic acid fuel cell are discussed. Pd-based catalyst demonstrates superior catalytic activity towards formic acid oxidation than Pt and exhibits power density of 245 $mW.cm^{-2}$ in a single-cell direct formic acid fuel cell based on proton exchange membrane electrolyte. A direct formic acid fuel cell hybrid power system for a laptop computer was developed by Fuel Cell Research Centre at the Korea Institute of Science and Technology (KIST) which can deliver 30 W power at 60 mW cm^{-2} current density with 15-membrane electrode assembly direct formic acid fuel cell stack. The various catalysts, e.g. Pt/C, PtRu/C and Pt–Ru–TiO_2, developed for glycerol oxidation reaction in acidic medium are discussed. The performance of direct glycerol fuel cell in acidic medium is inferior than in alkaline medium which demands further study for its commercialisation in acidic medium.

The performance of the proton exchange membrane-based fuel cell utilising methanol, ethanol, ethylene glycol, formic acid and glycerol as fuel can be improved further by the development of suitable anode catalyst with less amount of noble metal in binary and ternary form. Several non-noble metals such as Fe, Co, Ni, Sn,

etc. can be tried without compromising the fuel oxidation efficiency. Metal oxide framework, porous nanostructures and hierarchical microstructures which can provide better active surface area for fuel oxidation reaction can also be tried. Apart from the advanced catalysts development, catalyst supports such as functionalised multiwalled carbon nanotubes, functionalised graphene, carbon–nitrogen framework, nitrogen-doped ordered mesoporous carbon and nitrogen-doped carbon nanotubes play a vital role in stabilisation, improvement in durability and enhancement of catalytic activity. The catalysts with supports can reduce concentration polarisation in mass transport, provide high electrical conductivity and high chemical resistance tolerance to the acidic and oxidative environment to yield stable catalyst system. Last but not the least, new design of membrane electrode assembly, which provide higher ionic conductivity, lower fuel crossover, lower mass transfer resistance, accessibility of catalyst particles to fuel and oxidant, may lead to much improvement in performance of low-temperature direct hydrocarbon fuel cell.

References

1. Basu S (2007) Recent trends in fuel cell science and technology. Springer, New York
2. Dillon R, Srinivasan S, Aricò AS, Antonucci V (2004) International activities in DMFC R&D: status of technologies and potential applications. J Power Sources 127:112–126. https://doi.org/10.1016/j.jpowsour.2003.09.032
3. Wasmus S, Küver A (1999) Methanol oxidation and direct methanol fuel cells: a selective review. J Electroanal Chem 461:14–31. https://doi.org/10.1016/S0022-0728(98)00197-1
4. McNicol B, Rand DA, Williams K (1999) Direct methanol–air fuel cells for road transportation. J Power Sources 83:15–31. https://doi.org/10.1016/S0378-7753(99)00244-X
5. Ogden JM, Steinbugler MM, Kreutz TG (1999) Comparison of hydrogen, methanol and gasoline as fuels for fuel cell vehicles: implications for vehicle design and infrastructure development. J Power Sources 79:143–168. https://doi.org/10.1016/S0378-7753(99)00057-9
6. Armaroli N, Balzani V (2011) The hydrogen issue. ChemSusChem 4:21–36. https://doi.org/10.1002/cssc.201000182
7. Parsons R, VanderNoot T (1988) The oxidation of small organic molecules. J Electroanal Chem Interfacial Electrochem 257:9–45
8. Tiwari JN, Tiwari RN, Singh G, Kim KS (2013) Recent progress in the development of anode and cathode catalysts for direct methanol fuel cells. Nano Energy 2:553–578
9. Editor G, Russell A, Shen Y et al (2008) Electrocatalysis: theory and experiment at the interface. Phys Chem Chem Phys 10:3607. https://doi.org/10.1039/b808799g
10. Han SB, Song YJ, Lee JM et al (2008) Platinum nanocube catalysts for methanol and ethanol electrooxidation. Electrochem Commun 10:1044–1047. https://doi.org/10.1016/j.elecom.2008.04.034
11. Tiwari JN, Pan F-M, Tiwari RN, Nandi S (2008) Facile synthesis of continuous Pt island networks and their electrochemical properties for methanol electrooxidation. Chem Commun 48:6516. https://doi.org/10.1039/b813935k
12. Huang K, Yang X, Hua W et al (2009) Experimental evidence of a microwave non-thermal effect in electrolyte aqueous solutions. New J Chem 33:1486. https://doi.org/10.1039/b821970b
13. Alia SM, Zhang G, Kisailus D et al (2010) Porous platinum nanotubes for oxygen reduction and methanol oxidation reactions. Adv Funct Mater 20:3742–3746. https://doi.org/10.1002/adfm.201001035

14. He Y-B, Li G-R, Wang Z-L et al (2010) Pt nanorods aggregates with enhanced electrocatalytic activity toward methanol oxidation. J Phys Chem C 114:19175–19181. https://doi.org/10.1021/jp104991k
15. Lee Y-W, Han S-B, Kim D-Y, Park K-W (2011) Monodispersed platinum nanocubes for enhanced electrocatalytic properties in alcohol electrooxidation. Chem Commun 47:6296. https://doi.org/10.1039/c1cc10798d
16. Tiwari JN, Tiwari RN, Lin K (2011) Controlled synthesis and growth of perfect platinum nanocubes using a pair of low-resistivity fastened silicon wafers and their electrocatalytic properties. Nano Res 4:541–549. https://doi.org/10.1007/s12274-011-0110-4
17. Ren X, Wilson MS, Gottesfeld S (1996) High performance direct methanol polymer electrolyte fuel cells. J Electrochem Soc 143:L12–L15. https://doi.org/10.1149/1.1836375
18. Neto AO, Dias RR, Tusi MM et al (2007) Electro-oxidation of methanol and ethanol using PtRu/C, PtSn/C and PtSnRu/C electrocatalysts prepared by an alcohol-reduction process. J Power Sources 166:87–91. https://doi.org/10.1016/j.jpowsour.2006.12.088
19. Hassan HB (2009) Electrodeposited Pt and Pt-Sn nanoparticles on Ti as anodes for direct methanol fuel cells. J Fuel Chem Technol 37:346–354. https://doi.org/10.1016/S1872-5813(09)60024-4
20. Lee S-A, Park K-W, Choi J-H et al (2002) Nanoparticle synthesis and electrocatalytic activity of Pt alloys for direct methanol fuel cells. J Electrochem Soc 149:A1299. https://doi.org/10.1149/1.1502685
21. Morante-Catacora TY, Ishikawa Y, Cabrera CR (2008) Sequential electrodeposition of Mo at Pt and PtRu methanol oxidation catalyst particles on HOPG surfaces. J Electroanal Chem 621:103–112. https://doi.org/10.1016/j.jelechem.2008.04.029
22. Huang J, Yang H, Huang Q et al (2004) Methanol oxidation on carbon-supported Pt-Os bimetallic nanoparticle electrocatalysts. J Electrochem Soc 151:A1810. https://doi.org/10.1149/1.1804257
23. Kang Y, Murray CB (2010) Synthesis and electrocatalytic properties of cubic Mn - Pt nanocrystals (nanocubes). J Am Chem Soc 132:7568–7569. https://doi.org/10.1021/ja100705j
24. Rana M, Patil PK, Chhetri M et al (2016) Pd-Pt alloys nanowires as support-less electrocatalyst with high synergistic enhancement in efficiency for methanol oxidation in acidic medium. J Colloid Interface Sci 463:99–106. https://doi.org/10.1016/j.jcis.2015.10.042
25. Wei Z, Guo H, Tang Z (1996) Methanol electro-oxidation on platinum and platinum-tin alloy catalysts dispersed on active carbon. J Power Sources 58:239–242. https://doi.org/10.1016/S0378-7753(96)02389-0
26. Wang K, Gasteiger HA, Markovic NM, Ross PN (1996) On the reaction pathway for methanol and carbon monoxide electrooxidation on Pt-Sn alloy versus Pt-Ru alloy surfaces. Electrochim Acta 41:2587–2593. https://doi.org/10.1016/0013-4686(96)00079-5
27. Ishikawa Y, Liao MS, Cabrera CR (2000) Oxidation of methanol on platinum, ruthenium and mixed Pt-M metals (M = Ru, Sn): a theoretical study. Surf Sci 463:66–80. https://doi.org/10.1016/S0039-6028(00)00600-2
28. Antolini E, Gonzalez ER (2011) Effect of synthesis method and structural characteristics of Pt-Sn fuel cell catalysts on the electro-oxidation of CH3OH and CH 3CH2OH in acid medium. Catal Today 160:28–38. https://doi.org/10.1016/j.cattod.2010.07.018
29. Habibi B, Pournaghi-Azar MH, Abdolmohammad-Zadeh H, Razmi H (2009) Electrocatalytic oxidation of methanol on mono and bimetallic composite films: Pt and Pt-M (M = Ru, Ir and Sn) nano-particles in poly(o-aminophenol). Int J Hydrog Energy 34:2880–2892. https://doi.org/10.1016/j.ijhydene.2009.01.072
30. Tritsaris GA, Rossmeisl J (2012) Methanol oxidation on model elemental and bimetallic transition metal surfaces. J Phys Chem C 116:11980–11986. https://doi.org/10.1021/jp209506d
31. Rossmeisl J, Ferrin P, Tritsaris GA et al (2012) Bifunctional anode catalysts for direct methanol fuel cells. Energy Environ Sci 5:8335. https://doi.org/10.1039/c2ee21455e
32. Chiou YJ, Hsu HJ, Lin HM et al (2011) Synthesis and characterization of Cu-Pt/MWCNTs for use in electrocatalytic applications. Particuology 9:522–527. https://doi.org/10.1016/j.partic.2011.01.007

33. Maab H, Nunes SP (2010) Modified SPEEK membranes for direct ethanol fuel cell. J Power Sources 195:4036–4042. https://doi.org/10.1016/j.jpowsour.2010.01.005
34. Abe H, Matsumoto F, Alden LR et al (2008) Electrocatalytic performance of fuel oxidation by Pt 3 Ti nanoparticles. J Am Chem Soc 130:5452–5458
35. Li X, Chen G, Xie J et al (2010) An electrocatalyst for methanol oxidation in DMFC: PtBi/XC-72 with Pt solid-solution structure. J Electrochem Soc 157:B580. https://doi.org/10.1149/1.3309725
36. Ribeiro VA, Correa OV, Neto AO et al (2010) Preparation of PtRuNi/C electrocatalysts by an alcohol-reduction process for electro-oxidation of methanol. Appl Catal A Gen 372:162–166. https://doi.org/10.1016/j.apcata.2009.10.028
37. Zhen-Bo W, Peng-Jian Z, Ge-Ping Y (2009) Investigations of compositions and performance of PtRuMo/C ternary catalysts for methanol electrooxidation. Fuel Cells 9:106–113. https://doi.org/10.1002/fuce.200800096
38. Kakati N, Maiti J, Oh JY, Yoon YS (2011) Study of methanol oxidation of hydrothermally synthesized PtRuMo on multi wall carbon nanotubes. Appl Surf Sci 257:8433–8437. https://doi.org/10.1016/j.apsusc.2011.04.125
39. Yang LX, Allen RG, Scott K et al (2004) A comparative study of ptru and ptrusn thermally formed on titanium mesh for methanol electro-oxidation. J Power Sources 137:257–263. https://doi.org/10.1016/j.jpowsour.2004.06.028
40. Ioroi T, Yasuda K, Siroma Z et al (2003) Enhanced CO-tolerance of carbon-supported platinum and molybdenum oxide anode catalyst. J Electrochem Soc 150:A1225. https://doi.org/10.1149/1.1598211
41. Liao S, Holmes K-A, Tsaprailis H, Birss VI (2006) High performance PtRuIr catalysts supported on carbon nanotubes for the anodic oxidation of methanol. J Am Chem Soc 128:3504–3505. https://doi.org/10.1021/ja0578653
42. Strasser P, Fan Q, Devenney M, Weinberg WH (2003) High Throughput Experimental and Theoretical Predictive Screening of Materials − A Comparative Study of Search Strategies for New Fuel Cell Anode Catalysts. J Phys Chem B 107:11013–11021. https://doi.org/10.1021/jp030508z
43. Zeng J, Lee JY (2007) Ruthenium-free, carbon-supported cobalt and tungsten containing binary & ternary Pt catalysts for the anodes of direct methanol fuel cells. Int J Hydrog Energy 32:4389–4396. https://doi.org/10.1016/j.ijhydene.2007.03.012
44. Welsch FG, Stöwe K, Maier WF (2011) Fluorescence-based high throughput screening for noble metal-free and platinum-poor anode catalysts for the direct methanol fuel cell. ACS Comb Sci 13:518–529. https://doi.org/10.1021/co2000967
45. Huang SY, Chang CM, Wang KW, Yeh CT (2007) Promotion of platinum-ruthenium catalyst for electrooxidation of methanol by crystalline ruthenium dioxide. ChemPhysChem 8:1774–1777. https://doi.org/10.1002/cphc.200700238
46. Umverslty H (1992) Study of methanol electrooxidation. Electrochim Acta 37:1320
47. Hirakawa K, Inoue M, Abe T (2010) Methanol oxidation on carbon-supported Pt-Ru and TiO2 (Pt-Ru/TiO2/C) electrocatalyst prepared using polygonal barrel-sputtering method. Electrochim Acta 55:5874–5880. https://doi.org/10.1016/j.electacta.2010.05.038
48. Ganesan R, Lee JS (2006) An electrocatalyst for methanol oxidation based on tungsten trioxide microspheres and platinum. J Power Sources 157:217–221. https://doi.org/10.1016/j.jpowsour.2005.07.069
49. Tseung ACC, Chen KY (1997) Hydrogen spill-over effect on Pt/WO3 anode catalysts. Catal Today 38:439–443. https://doi.org/10.1016/S0920-5861(97)00053-9
50. Huang H, Chen Q, He M et al (2013) A ternary Pt/MnO 2/graphene nanohybrid with an ultrahigh electrocatalytic activity toward methanol oxidation. J Power Sources 239:189–195
51. Zhou C, Wang H, Peng F et al (2009) MnO2/CNT supported Pt and PtRu nanocatalysts for direct methanol fuel cells. Langmuir 25:7711–7717. https://doi.org/10.1021/la900250w
52. Baglio V, Sebastián D, D'Urso C et al (2014) Composite anode electrode based on iridium oxide promoter for direct methanol fuel cells. Electrochim Acta 128:304–310. https://doi.org/10.1016/j.electacta.2013.10.141

53. Baglio V, Amin RS, El-Khatib KM et al (2014) IrO2 as a promoter of Pt–Ru for methanol electro-oxidation. Phys Chem Chem Phys 16:10414. https://doi.org/10.1039/c4cp00466c
54. Katayama A (1980) Electrooxidation of methanol on a platinum-tin oxide catalyst. J Phys Chem 84:376–381. https://doi.org/10.1021/j100441a007
55. Zhao H, Zheng Z, Li J et al (2013) Substitute of expensive Pt with improved electro- catalytic performance and higher resistance to CO poisoning for methanol oxidation: the case of synergistic Pt-Co 3 O 4 nanocomposite. Nanomicro Lett 5:296–302. https://doi.org/10.5101/nml.v5i4.p296-302
56. Surampudi S, Narayanan SR, Vamos E et al (1994) Advances in direct oxidation methanol fuel cells. J Power Sources 47:377–385. https://doi.org/10.1016/0378-7753(94)87016-0
57. Shukla AK, Christensen PA, Hamnett A, Hogarth MP (1995) A vapour-feed direct-methanol fuel cell with proton-exchange membrane electrolyte. J Power Sources 55:87–91. https://doi.org/10.1016/0378-7753(94)02150-2
58. Jung DH, Lee CH, Kim CS, Shin DR (1998) Performance of a direct methanol polymer electrolyte fuel cell. J Power Sources 71:169–173. https://doi.org/10.1016/S0378-7753(97)02793-6
59. Dohle H, Schmitz H, Bewer T et al (2002) Development of a compact 500 W class direct methanol fuel cell stack. J Power Sources 106:313–322
60. Kim D, Lee J, Lim TH et al (2006) Operational characteristics of a 50 W DMFC stack. J Power Sources 155:203–212. https://doi.org/10.1016/j.jpowsour.2005.04.033
61. Joh HI, Hwang SY, Cho JH et al (2008) Development and characteristics of a 400 W-class direct methanol fuel cell stack. Int J Hydrog Energy 33:7153–7162. https://doi.org/10.1016/j.ijhydene.2008.08.016
62. Wang ZB, Rivera H, Wang XP et al (2008) Catalyst failure analysis of a direct methanol fuel cell membrane electrode assembly. J Power Sources 177:386–392. https://doi.org/10.1016/j.jpowsour.2007.11.070
63. Prabhuram J, Krishnan NN, Choi B et al (2010) Long-term durability test for direct methanol fuel cell made of hydrocarbon membrane. Int J Hydrog Energy 35:6924–6933. https://doi.org/10.1016/j.ijhydene.2010.04.025
64. Patel PP, Datta MK, Jampani PH et al (2015) High performance and durable nanostructured TiN supported Pt_{50}-Ru_{50} anode catalyst for direct methanol fuel cell (DMFC). J Power Sources 293:437–446. https://doi.org/10.1016/j.jpowsour.2015.05.051
65. Feng L, Li K, Chang J et al (2015) Nanostructured PtRu/C catalyst promoted by CoP as an efficient and robust anode catalyst in direct methanol fuel cells. Nano Energy 15:462–469. https://doi.org/10.1016/j.nanoen.2015.05.007
66. Jeng KT, Chien CC, Hsu NY et al (2006) Performance of direct methanol fuel cell using carbon nanotube-supported Pt-Ru anode catalyst with controlled composition. J Power Sources 160:97–104. https://doi.org/10.1016/j.jpowsour.2006.01.057
67. Chang J, Feng L, Liu C et al (2014) Ni 2 P enhances the activity and durability of Pt anode catalyst in direct methanol fuel cells. Energy Environ Sci 7:1628–1632
68. Verma A, Basu S (2005) Direct use of alcohols and sodium borohydride as fuel in an alkaline fuel cell. J Power Sources 145:282–285. https://doi.org/10.1016/j.jpowsour.2004.11.071
69. Verma A, Jha AK, Basu S (2005) Evaluation of an alkaline fuel cell for multifuel system. J Fuel Cell Sci Technol 2:234. https://doi.org/10.1115/1.2039955
70. Badwal SP, Giddey S, Kulkarni A et al (2015) Direct ethanol fuel cellls for transport and stationary applications - a comprehensive review. Appl Energy 145:80–103
71. Basu S, Agarwal A, Pramanik H (2008) Improvement in performance of a direct ethanol fuel cell: effect of sulfuric acid and Ni-mesh. Electrochem Commun 10:1254–1257. https://doi.org/10.1016/j.elecom.2008.05.042
72. Lai SCS, Kleijn SEF, Öztürk FTZ et al (2010) Effects of electrolyte pH and composition on the ethanol electro-oxidation reaction. Catal Today 154:92–104. https://doi.org/10.1016/j.cattod.2010.01.060

73. Verma A, Basu S (2007) Experimental evaluation and mathematical modeling of a direct alkaline fuel cell. J Power Sources 168:200–210. https://doi.org/10.1016/j.jpowsour.2007.02.069
74. James DD, Pickup PG (2010) Effects of crossover on product yields measured for direct ethanol fuel cells. Electrochim Acta 55:3824–3829. https://doi.org/10.1016/j.electacta.2010.02.007
75. Kontou S, Stergiopoulos V, Song S, Tsiakaras P (2007) Ethanol/water mixture permeation through a Nafion® based membrane electrode assembly. J Power Sources 171:1–7. https://doi.org/10.1016/j.jpowsour.2006.10.009
76. Tian Q, Chen W, Wu Y (2015) An effective PdCo/PWA-C anode catalyst for direct formic acid fuel cells. J Electrochem Soc 162:F165–F171. https://doi.org/10.1149/2.0901501jes
77. Kowal A, Li M, Shao M et al (2009) Ternary Pt/Rh/SnO2 electrocatalysts for oxidizing ethanol to CO2. Nat Mater 8:325–330. https://doi.org/10.1038/nmat2359
78. Zignani SC, Baglio V, Linares JJ et al (2013) Endurance study of a solid polymer electrolyte direct ethanol fuel cell based on a Pt-Sn anode catalyst. Int J Hydrog Energy 38:11576–11582. https://doi.org/10.1016/j.ijhydene.2013.04.162
79. Marković NM, Gasteiger HA, Ross PN Jr, Jiang X, Villegas I, Weaver MJ (1995) Electro-oxidation mechanism of methanol and formic acid on Pt-Ru alloy surfaces. Electrochim Acta 40:91–98
80. Beyhan S, Coutanceau C, Léger JM et al (2013) Promising anode candidates for direct ethanol fuel cell: carbon supported PtSn-based trimetallic catalysts prepared by Bönnemann method. Int J Hydrog Energy 38:6830–6841. https://doi.org/10.1016/j.ijhydene.2013.03.058
81. Zhou W, Zhou Z, Song S et al (2003) Pt based anode catalysts for direct ethanol fuel cells. Appl Catal B Environ 46:273–285. https://doi.org/10.1016/S0926-3373(03)00218-2
82. Vigier F, Coutanceau C, Hahn F et al (2004) On the mechanism of ethanol electro-oxidation on Pt and PtSn catalysts: electrochemical and in situ IR reflectance spectroscopy studies. J Electroanal Chem 563:81–89. https://doi.org/10.1016/j.jelechem.2003.08.019
83. Vigier F, Coutanceau C, Perrard A et al (2004) Development of anode catalysts for a direct ethanol fuel cell. J Appl Electrochem 34:439–446. https://doi.org/10.1023/B:JACH.0000016629.98535.ad
84. Lamy C, Rousseau S, Belgsir EM et al (2004) Recent progress in the direct ethanol fuel cell: development of new platinum-tin electrocatalysts. Electrochim Acta 49:3901–3908. https://doi.org/10.1016/j.electacta.2004.01.078
85. Jiang L, Zhou Z, Li W et al (2004) Effects of treatment in different atmosphere on Pt3Sn/C electrocatalysts for ethanol electro-oxidation. Energy Fuels 18:866–871. https://doi.org/10.1021/ef034073q
86. Jiang L, Sun G, Zhou Z et al (2004) Preparation and characterization of PtSn/C anode electrocatalysts for direct ethanol fuel cell. Catal Today 93–95:665–670. https://doi.org/10.1016/j.cattod.2004.06.029
87. Zhou WJ, Song SQ, Li WZ et al (2004) Pt-based anode catalysts for direct ethanol fuel cells. Solid State Ionics 175:797–803. https://doi.org/10.1016/j.ssi.2004.09.055
88. Jiang L, Sun G, Sun S et al (2005) Structure and chemical composition of supported Pt-Sn electrocatalysts for ethanol oxidation. Electrochim Acta 50:5384–5389. https://doi.org/10.1016/j.electacta.2005.03.018
89. Colmenares L, Wang H, Jusys Z et al (2006) Ethanol oxidation on novel, carbon supported Pt alloy catalysts-model studies under defined diffusion conditions. Electrochim Acta 52:221–233. https://doi.org/10.1016/j.electacta.2006.04.063
90. Dos Anjos DM, Kokoh KB, Léger JM et al (2006) Electrocatalytic oxidation of ethanol on Pt-Mo bimetallic electrodes in acid medium. J Appl Electrochem 36:1391–1397. https://doi.org/10.1007/s10800-006-9222-z
91. Tayal J, Rawat B, Basu S (2012) Effect of addition of rhenium to Pt-based anode catalysts in electro-oxidation of ethanol in direct ethanol PEM fuel cell. Int J Hydrog Energy 37:4597–4605. https://doi.org/10.1016/j.ijhydene.2011.05.188

92. Antolini E, Colmati F, Gonzalez ER (2007) Effect of Ru addition on the structural characteristics and the electrochemical activity for ethanol oxidation of carbon supported Pt-Sn alloy catalysts. Electrochem Commun 9:398–404. https://doi.org/10.1016/j.elecom.2006.10.012
93. Rousseau S, Coutanceau C, Lamy C, Léger JM (2006) Direct ethanol fuel cell (DEFC): electrical performances and reaction products distribution under operating conditions with different platinum-based anodes. J Power Sources 158:18–24. https://doi.org/10.1016/j.jpowsour.2005.08.027
94. Tayal J, Rawat B, Basu S (2011) Bi-metallic and tri-metallic PteSn/C, PteIr/C, PteIreSn/C catalysts for electro-oxidation of ethanol in direct ethanol fuel cell. Int J Hydrog Energy 36:14884–14897. https://doi.org/10.1016/j.ijhydene.2011.03.035
95. Ribeiro J, dos Anjos DM, Léger JM et al (2008) Effect of W on PtSn/C catalysts for ethanol electrooxidation. J Appl Electrochem 38:653–662. https://doi.org/10.1007/s10800-008-9484-8
96. Beyhan S, Léger J, Kadırgan F (2013) Pronounced synergetic effect of the nano-sized PtSnNi/C catalyst for ethanol oxidation in direct ethanol fuel cell. Appl Catal B 130–131:305–313. https://doi.org/10.1016/j.apcatb.2012.11.007
97. Goel J, Basu S (2014) Effect of support materials on the performance of direct ethanol fuel cell anode catalyst. Int J Hydrog Energy 39:15956–15966. https://doi.org/10.1016/j.ijhydene.2014.01.203
98. Liu Z, Yi X, Su X et al (2005) Preparation and characterization of Pt/C and Pt Ru/C electrocatalysts for direct ethanol fuel cells. J Power Source 149:1–7. https://doi.org/10.1016/j.jpowsour.2005.02.009
99. Mingyuan ZHU, Gongquan SUN, Huanqiao LI et al (2008) Effect of the Sn (II)/Sn (IV) redox couple on the activity of PtSn/C for ethanol electro-oxidation. Chin J Catal 29:765–770
100. Zhu M, Sun G, Xin Q (2009) Effect of alloying degree in PtSn catalyst on the catalytic behavior for ethanol electro-oxidation. Electrochim Acta 54:1511–1518. https://doi.org/10.1016/j.electacta.2008.09.035
101. Goel J, Basu S (2012) Pt-Re-Sn as metal catalysts for electro-oxidation of ethanol in direct ethanol fuel cell. Energy Procedia 28:66–77. https://doi.org/10.1016/j.egypro.2012.08.041
102. Wang H, Jusys Z, Behm RJ (2009) Adsorption and electrooxidation of ethylene glycol and its C2 oxidation products on a carbon-supported Pt catalyst: a quantitative DEMS study. Electrochim Acta 54:6484–6498. https://doi.org/10.1016/j.electacta.2009.05.097
103. Pramanik H, Basu S (2010) Chemical engineering and processing: process intensification modeling and experimental validation of overpotentials of a direct ethanol fuel cell. Chem Eng Process 49:634–641. https://doi.org/10.1016/j.cep.2009.10.015
104. Goel J, Basu S (2015) Mathematical modeling and experimental validation of direct ethanol fuel cell. Int J Hydrog Energy 40:14405–14415. https://doi.org/10.1016/j.ijhydene.2015.03.082
105. Leung LWH, Weaver MJ (1988) Real-time FTIR spectroscopy as a quantitative kinetic probe of competing electrooxidation pathways of small organic molecules. J Phys Chem 92:4019–4022. https://doi.org/10.1021/j100325a004
106. De Lima RB, Paganin V, Iwasita T, Vielstich W (2003) On the electrocatalysis of ethylene glycol oxidation. Electrochim Acta 49:85–91. https://doi.org/10.1016/j.electacta.2003.05.004
107. Selvaraj V, Vinoba M, Alagar M (2008) Electrocatalytic oxidation of ethylene glycol on Pt and Pt–Ru nanoparticles modified multi-walled carbon nanotubes. J Colloid Interface Sci 322:537–544. https://doi.org/10.1016/j.jcis.2008.02.069
108. Chetty R, Scott K (2007) Catalysed titanium mesh electrodes for ethylene glycol fuel cells. J Appl Electrochem 37:1077–1084. https://doi.org/10.1007/s10800-007-9358-5
109. Neto AO, Vasconcelos TRR, Da Silva RWRV et al (2005) Electro-oxidation of ethylene glycol on PtRu/C and PtSn/C electrocatalysts prepared by alcohol-reduction process. J Appl Electrochem 35:193–198. https://doi.org/10.1007/s10800-004-5824-5
110. Livshits V, Peled E (2006) Progress in the development of a high-power, direct ethylene glycol fuel cell (DEGFC). J Power Sources 161:1187–1191. https://doi.org/10.1016/j.jpowsour.2006.04.141

111. Livshits V, Philosoph M, Peled E (2008) Direct ethylene glycol fuel-cell stack—study of oxidation intermediate products. J Power Sources 178:687–691. https://doi.org/10.1016/j.jpowsour.2007.07.054
112. Larsen R, Ha S, Zakzeski J, Masel RI (2006) Unusually active palladium-based catalysts for the electrooxidation of formic acid. J Power Sources 157:78–84. https://doi.org/10.1016/j.jpowsour.2005.07.066
113. Gojkovic SL, Popovic KD, Olszewski P et al (2005) Kinetic study of formic acid oxidation on carbon-supported platinum electrocatalyst. J Electroanal Chem 581(581):294–302. https://doi.org/10.1016/j.jelechem.2005.05.002
114. Muthukumar V, Chetty R (2017) Morphological transformation of electrodeposited Pt and its electrocatalytic activity towards direct formic acid fuel cells. J Appl Electrochem 47:735–745. https://doi.org/10.1007/s10800-017-1076-z
115. Xia XH, Iwasita T (1993) Influence of underpotential deposited lead upon the oxidation of HCOOH in HCI04 at platinum electrodes. J Electrochem Soc 140:2559–2565
116. Ralph TR, Hards GA, Keating JE, Campbell SA, Wilkinson DP, Davis M, St-Pierre J, Johnson MC (1997) Low cost electrodes for proton exchange membrane fuel cells performance in single cells and Ballard stacks. J Electrochem Soc 144:3845–3857
117. Rice C, Ha S, Masel RI, Wieckowski A (2003) Catalysts for direct formic acid fuel cells. J Power Sources 115:229–235. https://doi.org/10.1016/S0378-7753(03)00026-0
118. Choi J, Jeong K, Dong Y et al (2006) Electro-oxidation of methanol and formic acid on PtRu and PtAu for direct liquid fuel cells. J Power Sources 163:71–75. https://doi.org/10.1016/j.jpowsour.2006.02.072
119. Uhm S, Lee HJ, Kwon Y, Lee J (2008) A stable and cost-effective anode catalyst structure for formic acid fuel cells. Angew Chem Int Ed Engl 120(52):10317–10320. https://doi.org/10.1002/ange.200803466
120. Fan H, Cheng M, Wang L et al (2018) Extraordinary electrocatalytic performance for formic acid oxidation by the synergistic effect of Pt and Au on carbon black. Nano Energy 48:1–9. https://doi.org/10.1016/j.nanoen.2018.03.018
121. Muthukumar V, Chetty R (2018) Electrodeposited Pt–Pd dendrite on carbon support as anode for direct formic acid fuel cells. Ionics. https://doi.org/10.1007/s11581-018-2526-2
122. Ye W, Chen S, Ye M et al (2017) Nano energy electrocatalysts for oxygen reduction reaction and formic acid oxidation. Nano Energy 39:532–538
123. Mohammad AM, Al-Akraa IM, El-Deab MS (2018) Superior electrocatalysis of formic acid electro-oxidation on a platinum, gold and manganese oxide nanoparticle-based ternary catalyst. Int J Hydrog Energy 43:139–149. https://doi.org/10.1016/j.ijhydene.2017.11.016
124. Wang J, Liu Y, Okada T (2016) Novel platinum-macrocycle composite catalysts for direct formic acid fuel cells. J Appl Electrochem 46:901–905. https://doi.org/10.1007/s10800-016-0975-8
125. Yashtulov NA, Patrikeev LN, Zenchenko VO et al (2016) Palladium–platinum–porous silicon nanocatalysts for fuel cells with direct formic acid oxidation. Nanotechnol Russ 11:562–568. https://doi.org/10.1134/S1995078016050207
126. Zhang JM, Wang RX, Nong RJ et al (2017) Hydrogen co-reduction synthesis of PdPtNi alloy nanoparticles on carbon nanotubes as enhanced catalyst for formic acid electrooxidation. Int J Hydrog Energy 42:7226–7234. https://doi.org/10.1016/j.ijhydene.2016.05.198
127. El-Nagar GA, Mohammad AM, El-Deab MS, El-Anadouli BE (2017) Propitious dendritic Cu2O-Pt nanostructured anodes for direct formic acid fuel cells. ACS Appl Mater Interfaces 9:19766–19772. https://doi.org/10.1021/acsami.7b01565
128. Chang J, Feng L, Liu C et al (2014) An effective Pd–Ni 2 P/C anode catalyst for direct formic acid fuel. Angew Chem Int Ed Engl 53:122–126
129. Al-akraa IM, Mohammad AM, El-deab MS, El-anadouli BE (2015) Advances in direct formic acid fuel cells: fabrication of efficient Ir/Pd nanocatalysts for formic acid electro-oxidation. Int J Electrochem Sci 10:3282–3290

130. Feng L, Chang J, Jiang K et al (2016) Nanostructured palladium catalyst poisoning depressed by cobalt phosphide in the electro-oxidation of formic acid for fuel cells. Nano Energy 30:355–361. https://doi.org/10.1016/j.nanoen.2016.10.023
131. Xu H, Yan B, Zhang K et al (2017) N-doped graphene-supported binary PdBi networks for formic acid oxidation. Appl Surf Sci 416:191–199. https://doi.org/10.1016/j.apsusc.2017.04.160
132. Zhang LY, Liu Z (2017) Graphene decorated with Pd 4 Ir nanocrystals: ultrasound-assisted synthesis, and application as a catalyst for oxidation of formic acid. J Colloid Interface Sci 505:783–788. https://doi.org/10.1016/j.jcis.2017.06.084
133. Wang S, Chang J, Xue H et al (2017) Catalytic stability study of a Pd-Ni_2 P/C catalyst for formic acid electrooxidation. ChemElectroChem 4:1243–1249. https://doi.org/10.1002/celc.201700051
134. Ishiyama K, Kosaka F, Shimada I et al (2015) Deactivation resistant PdeZrO2 supported on multiwall carbon nanotubes catalyst for direct formic acid fuel cells. Int J Hydrog Energy 40:16724–16733. https://doi.org/10.1016/j.jpowsour.2012.10.035
135. Al-Akraa IM (2017) Efficient electro-oxidation of formic acid at Pd-MnOx binary nanocatalyst: optimization of deposition strategy. Int J Hydrog Energy 42:4660–4666. https://doi.org/10.1016/j.ijhydene.2016.08.090
136. Lesiak B, Mazurkiewicz M, Malolepszy A et al (2016) Effect of the Pd/MWCNTs anode catalysts preparation methods on their morphology and activity in a direct formic acid fuel cell. Appl Surf Sci 387:929–937. https://doi.org/10.1016/j.apsusc.2016.06.152
137. Jiang S, Yi B, Zhao Q et al (2017) Palladium–nickel catalysts based on ordered titanium dioxide nanorod arrays with high catalytic performance for formic acid electro-oxidation. RSC Adv 7:11719–11723. https://doi.org/10.1039/C7RA00194K
138. Zuo L-X, Jiang L-P (2017) Electrocatalysis of the oxygen reduction reaction and the formic acid oxidation reaction on BN/Pd composites prepared sonochemically. J Electrochem Soc 164:H805–H811. https://doi.org/10.1149/2.1601712jes
139. He N, Gong Y, Yang Y et al (2017) ScienceDirect an effective Pd @ Ni-B/C anode catalyst for electro- oxidation of formic acid. Int J Hydrog Energy 43:3216–3222. https://doi.org/10.1016/j.ijhydene.2017.12.167
140. Ali H, Zaman S, Majeed I et al (2017) Porous carbon/rGO composite: an ideal support material of highly efficient palladium electrocatalysts for the formic acid oxidation reaction. ChemElectroChem 4:3126–3133. https://doi.org/10.1002/celc.201700879
141. Li H, Zhang Y, Wan Q et al (2018) Expanded graphite and carbon nanotube supported palladium nanoparticles for electrocatalytic oxidation of liquid fuels. Carbon 131:111–120. https://doi.org/10.1016/j.carbon.2018.01.093
142. Casado-rivera E, Volpe DJ, Alden L et al (2004) Electrocatalytic activity of ordered intermetallic phases for fuel cell applications. J Am Chem Soc 126:4043–4049. https://doi.org/10.1021/ja038497a
143. Lee JK, Jeon H, Uhm S, Lee J (2008) Influence of underpotentially deposited Sb onto Pt anode surface on the performance of direct formic acid fuel cells. Electrochim Acta 53:6089–6092. https://doi.org/10.1016/j.electacta.2008.02.089
144. Yu X, Pickup PG (2008) Recent advances in direct formic acid fuel cells (DFAFC). J Power Source 182:124–132. https://doi.org/10.1016/j.jpowsour.2008.03.075
145. Zainoodin AM, Tsujiguchi T, Masdar MS et al (2018) Performance of a direct formic acid fuel cell fabricated by ultrasonic spraying. Int J Hydrog Energy 43:6413–6420. https://doi.org/10.1016/j.ijhydene.2018.02.024
146. Malolepszy A, Mazurkiewicz M, Stobinski L et al (2015) Deactivation resistant Pd-ZrO2 supported on multiwall carbon nanotubes catalyst for direct formic acid fuel cells. Int J Hydrog Energy 40:16724–16733. https://doi.org/10.1016/j.ijhydene.2015.08.048
147. Bai Z, Shi M, Zhang Y et al (2016) Facile synthesis of silver@carbon nanocable-supported platinum nanoparticles as high-performing electrocatalysts for glycerol oxidation in direct glycerol fuel cells. Green Chem 18:386–391. https://doi.org/10.1039/C5GC01243K

148. Fashedemi OO, Ozoemena KI (2014) Comparative electrocatalytic oxidation of ethanol, ethylene glycol and glycerol in alkaline medium at Pd-decorated FeCo@Fe/C core-shell nanocatalysts. Electrochim Acta 128:279–286. https://doi.org/10.1016/j.electacta.2013.10.194
149. Lertthahan P, Yongprapat S, Therdthianwong A, Therdthianwong S (2017) Pt-modified Au/C catalysts for direct glycerol electro-oxidation in an alkaline medium. Int J Hydrog Energy 42:9202–9209. https://doi.org/10.1016/j.ijhydene.2016.05.120
150. Li Z-Y, Zhou J, Tang L-S et al (2018) Hydroxyl-rich ceria hydrate nanoparticles enhancing the alcohol electrooxidation performance of Pt catalysts. J Mater Chem A 6:2318–2326. https://doi.org/10.1039/C7TA09071D
151. de Souza NE, Gomes JF, Tremiliosi-Filho G (2017) Reactivity of 3-carbon-atom chain alcohols on gold electrode: a comparison to understand the glycerol electro-oxidation. J Electroanal Chem 800:106–113. https://doi.org/10.1016/j.jelechem.2016.08.019
152. Gomes JF, De Paula FBC, Gasparotto LHS, Tremiliosi-Filho G (2012) The influence of the Pt crystalline surface orientation on the glycerol electro-oxidation in acidic media. Electrochim Acta 76:88–93. https://doi.org/10.1016/j.electacta.2012.04.144
153. Ishiyama K, Kosaka F, Shimada I et al (2013) Glycerol electro-oxidation on a carbon-supported platinum catalyst at intermediate temperatures. J Power Sources 225:141–149. https://doi.org/10.1016/j.jpowsour.2012.10.035
154. Fernández PS, Tereshchuk P, Angelucci CA et al (2016) How do random superficial defects influence the electro-oxidation of glycerol on Pt(111) surfaces? Phys Chem Chem Phys 18:25582–25591. https://doi.org/10.1039/C6CP04768H
155. Garcia AC, Kolb MJ, Van Nierop Y Sanchez C et al (2016) Strong impact of platinum surface structure on primary and secondary alcohol oxidation during electro-oxidation of glycerol. ACS Catal 6:4491–4500. https://doi.org/10.1021/acscatal.6b00709
156. Fernández PS, Martins CA, Martins ME, Camara GA (2013) Electrooxidation of glycerol on platinum nanoparticles: deciphering how the position of each carbon affects the oxidation pathways. Electrochim Acta 112:686–691. https://doi.org/10.1016/j.electacta.2013.09.032
157. Fernández PS, Martins ME, Martins CA, Camara GA (2012) The electro-oxidation of isotopically labeled glycerol on platinum: new information on C-C bond cleavage and CO2production. Electrochem Commun 15:14–17. https://doi.org/10.1016/j.elecom.2011.11.013
158. Martins CA, Fernández PS, Troiani HE et al (2014) Ethanol vs. glycerol: understanding the lack of correlation between the oxidation currents and the production of CO2on Pt nanoparticles. J Electroanal Chem 717–718:231–236. https://doi.org/10.1016/j.jelechem.2014.01.027
159. Martins CA, Giz MJ, Camara GA (2011) Generation of carbon dioxide from glycerol: evidences of massive production on polycrystalline platinum. Electrochim Acta 56:4549–4553. https://doi.org/10.1016/j.electacta.2011.02.076
160. Kim Y, Kim HW, Lee S et al (2017) The role of ruthenium on carbon-supported PtRu catalysts for electrocatalytic glycerol oxidation under acidic conditions. ChemCatChem 9:1683–1690. https://doi.org/10.1002/cctc.201601325
161. Silva LSR, López-Suárez FE, Perez-Cadenas M et al (2016) Synthesis and characterization of highly active Pbx@Pty/C core-shell nanoparticles toward glycerol electrooxidation. Appl Catal B Environ 198:38–48. https://doi.org/10.1016/j.apcatb.2016.04.046
162. Hasa B, Kalamaras E, Papaioannou EI et al (2015) Effect of TiO2 loading on Pt-Ru catalysts during alcohol electrooxidation. Electrochim Acta 179:578–587. https://doi.org/10.1016/j.electacta.2015.04.104
163. Gomes JF, Tremiliosi-Filho G (2011) Spectroscopic studies of the glycerol electro-oxidation on polycrystalline Au and Pt surfaces in acidic and alkaline media. Electrocatalysis 2:96–105. https://doi.org/10.1007/s12678-011-0039-0

Chapter 4
Overview of Direct Liquid Oxidation Fuel Cells and its Application as Micro-Fuel Cells

R. Oliveira, J. Santander, and R. Rego

Abstract Direct liquid fuel cells (DLFCs) are a special type of FCs that generate power output through the electro-oxidation of liquid fuels easier to handle and store than the hydrogen gas used in traditional FCs, thus increasing the range of possible applications. As electronic devices continue to evolve at the macroscale (mobile phones, laptops) and at the micro-scale (micro-electromechanical systems, wearables, and implantable devices), micro-fuel cells (μFCs) are considered as a promising alternatives to batteries as power sources.

In this chapter, the development of low-temperature micro-direct liquid fuel cells (μDLFCs) operating with methanol, ethanol, formic acid, ethylene glycol, glycerol, or glucose as fuel is reviewed, covering structural design, membranes and catalysts used, and power output performance.

The key limitations for world-wide commercialization of μDLFCs include the fabrication process, water management, fuel crossover through the membranes, and the low activity/durability/selectivity of the catalysts. At present, the state-of-the-art power output is about 100, 58.0, 45.0, 30.3, 39.5, and 0.0063 mW cm^{-2} for methanol, ethanol, formic acid, ethylene glycol, glycerol, and glucose as fuel in μFCs, respectively.

Future research prospects in this field regarding each of these fuels are presented, confirming the μDLFC potential to replace traditional batteries in most portable applications.

R. Oliveira
CQ-VR, University of Trás-os-Montes e Alto Douro, Vila Real, Portugal

J. Santander
Instituto de Microelectrónica de Barcelona, IMB-CNM (CSIC), Campus UAB, Bellaterra (Barcelona), Spain

R. Rego (✉)
Chemistry Department and CQ-VR, University of Trás-os-Montes e Alto Douro, Vila Real, Portugal
e-mail: rrego@utad.pt

F. J. Rodríguez-Varela, T. W. Napporn (eds.), *Advanced Electrocatalysts for Low-Temperature Fuel Cells*, https://doi.org/10.1007/978-3-319-99019-4_4

Keywords Direct liquid fuel cells (DLFCs) · Micro-direct liquid fuel cells (μDLFCs) · Portable devices · DLFC designs · Micro and nano technologies (MNTs) · Passive or active μDLFCs · Catalysts · Electrodes · Membranes · Membraneless · Liquid fuels electro-oxidation · μDMFC · μDEFC · μDFAFC · μDEGFC · μDGlyFC · Implanted direct glucose fuel cell · μDGFC · Porous Pt electrodes · μDLFC power density output

4.1 Introduction

Fuel cells are direct chemical-to-electrical energy conversion systems which consist of an electrochemical cell to promote a fuel oxidation in the anode and a reduction reaction in the cathode, the oxygen reduction reaction (ORR). Concerning electrical power generation, it presents an intrinsic efficiency advantage over indirect systems, such as traditional internal combustion engines, which promote chemical-to-mechanical-to-electrical conversions, as each conversion step increases the overall energy loss. Its operation principle is similar to electrochemical batteries, but fuel cells can also be constantly supplied by external fuel sources instead of just relying in electrical recharging. A wide range of chemicals can be used as fuel, what makes fuel cell technology very adaptable for different applications [1].

In this chapter, the performance of different liquid fuels usable in fuel cells is explored considering its applicability to micro-fuel cell devices looking at its feasibility to power electronic devices. First, an overview of the different possibilities available as fabrication technologies is presented, arising the nano- and micro-technologies combination as the most promising scenario for the development of future micro-fuel cell devices. Then, this review will focus on oxidation reactions of the different fuels and its application in micro-fuel cells (structural design, membranes and catalysts used, and power output performance). Implantable micro-glucose fuel cells are also considered.

4.2 Overview of Fabrication Technologies for Micro-Fuel Cells

Micro-fuel cells are considered as a promising alternative to batteries to power small portable devices both at the mini- (mobile phones, laptops, etc.) and at the micro-scales (micro-electromechanical systems (MEMS), wearables, in-vivo implants, etc.) [2–4]. For such applications, easy to store liquid fuels are considered as the most appropriate alternatives, including methanol, ethanol, formic acid, ethylene glycol, glycerol, and glucose. This chapter focuses on micro-direct liquid fuel cells (μDLFC) devices.

In order to be implemented in the micro-scale, FCs must be designed in the simplest way, simplifying the added components usually found in standard size FCs to improve the performance of this electrochemical device, such as pumps or temperature control [5–8]. This principle guides research towards innovative new device architectures involving new materials that outperform traditional FC components [9–16]. In this way, typical architectures for micro-FCs are based in the use of microchannels driving liquid fuels by capillarity instead of pumping it through traditional bipolar plates. In this context, membraneless microfluidic FCs could be considered as an alternative architecture that permits omitting the ion conducting membrane at the cost of maintaining anode and cathode electrolytes in continuous movement in laminar flow regime, which prevents mixing of both electrolytes. The fluidic condition and the small amount of produced energy limit, in this case, the application of these devices to specialized environments (lab-on-a-chip, in vivo, etc.) [17–19]. Further development of the membraneless concept brings to the mixed-reactant membraneless FCs, which avoids the need for the anolyte and the catholyte to be separated by means of the use of tolerant electro-catalysts, so permitting a great amount of simplification in the fabrication of the final device [20].

There are many examples in the literature dealing with micro-FC devices fabricated using a great diversity of technologies. The first milestones in the development of micro-FCs were just the downscaling of the components made by the use of the traditional technologies used for standard size FCs, which lead to the fabrication of smaller devices useful for the study of the performance issues arising with small size and lack of auxiliary components. This context brought to alternative operation conditions for the FC, such as passive and air-breathing – avoiding ancillary devices like pumps or temperature controllers- [6, 7, 21] or higher fuel concentration [22], which imply controlling the crossover, managing the water production or using tolerant catalysts [23–25]. Gradually, different technologies were being adapted considering their advantages for miniaturization, i.e., the printed circuit technology [26]. As a result of this evolution, micro- and nanotechnologies (MNT) arise as a key element for the development of a new generation of micro-FCs as it is expected to be able to fulfill the requirements of further miniaturization, integration of new nanomaterials with tailored properties and, furthermore, economic benefits related when fabricating in large scale due to the batch micro-fabrication processes.

Among the new MNT-based materials it is worth mentioning porous silicon—which can be functionalized to be used as membrane [11, 13, 15] or as electrode [27]—or black silicon, a promising material to facilitate device integration [28]. MNT offer also interesting possibilities for the incorporation of catalysts to micro-FC devices. On the one hand, electrodeposition processes are commonly used in the MNT field, including sputtering, electroplating, or electroless processes, which have been used in some works on micro-FCs [28–31]. On the other hand, in the frame of nanotechnology recent advances, the development of carbon nanotube (CNT) growing techniques has open the possibility to incorporate this material as a catalyst support in micro-fabricated electrodes integrated in micro-fuel cell devices, so contributing to a better performance of the device with its unique mechanical and electrical properties [32, 33].

The implementation of micro-FCs can also profit from general strategies. In relation with catalyst development improvements, the use of an alkaline media improves the catalytic activity, which results in the development of the so-called alkaline anion exchange membrane micro-direct methanol fuel cells (AEM-μDMFCs), that can be considered as promising devices for further research as integrated power devices for the microsystems field (PowerMEMS) [34–40]. In this type of cells, it will be possible the use of non-Pt-based catalysts, obtaining a good performance at a lower cost. Moreover, the crossover of fuel to the cathode is reduced due to the opposite movement of the hydroxide anions. This effect, together with the use of a tolerant cathode catalyst, will permit the use of high concentration methanol solutions [25, 41–43], reinforcing the high energy density of this fuel in order to reduce the fuel reservoir volume of the micro-device.

Integration of different materials and components into a single MNT fabrication process is a very important issue for micro-FCs. In most of the reported works a dedicated packaging is needed to press together all the components of the FC, generally using extra plates with screws or rivets [5, 29, 44–46]. These auxiliary elements limit miniaturization and integration resulting in bulky devices. Although approaches based on the use of adhesives have been successfully explored towards the development of a planar device [47], these kind of adhesive materials are not fully compatible with MEMS technology. Alternative approaches focus on a more direct integration of components, i.e., incorporating micro-fabricated silicon current collectors with a fine silicon grid covered with a thin layer of electroplated noble metal catalysts, and at the same time a hybrid polymeric electrolyte membrane composed of a polydimethylsiloxane (PDMS) matrix that can be bonded to the silicon components by activating its surface with an oxygen plasma [16].

4.3 Direct Liquid Fuel Cell (DLFC) Designs

4.3.1 Proton Exchange Membrane Direct Liquid Fuel Cell (PEM-DLFC)

The predominant DLFC technology available uses a proton exchange membrane to separate the cathode and anode compartments, in order to avoid fuel and oxidant mixture. This design tries to prevent the oxygen reduction reaction (ORR) and fuel oxidation reaction from occurring simultaneously in the cathode, which would cause depolarization losses, reducing the cell performance. However, fuel crossover still occurs significantly through the main commercial PEMs, such as Nafion®, allowing it to reach the cathode surface. One strategy to mitigate this issue is to use less concentrated fuel solutions at the cost of decreasing the cell energy density and voltage output [48].

In order to increase the overall voltage output to the necessary values for most portable applications, it is necessary to connect these cells in a stack. Nonetheless,

the PEM-DLFC stack assembly demands several expensive parts such as the membrane, bipolar plates, clamping plates, current collectors, and gaskets, greatly increasing the stack cost [49].

Another important issue is water management, which can cause dangerous leakages to electronic devices. In the case of methanol, according to the methanol oxidation reaction (MOR) and ORR stoichiometry, for each oxidized methanol molecule, one water molecule is consumed in the anode and three are produced in the cathode, with an overall net production of two water molecules. Therefore, a system to remove excess water from the cell is necessary. Traditionally an active micropumping system could be used to purge part of the aqueous media in the cathode out of the cell, but this would cause a parasitic energy demand to run the cell, greatly reducing its overall energy output. Another alternative is to use a passive evaporation system where the heat generated by the cell is used to remove excess water by evaporation [48].

4.3.2 Membraneless Microfluidic Direct Liquid Fuel Cell (MF-DLFC)

It is possible to develop one-compartment FCs without a membrane and bipolar plates, significantly decreasing its cost. The fuel flow stream enters the cell through the compartment anode side and the oxidant flow stream through the cathode side. This system relies on the streams laminar flow behavior to avoid fuel and oxidant mixing before reaching the cell outlet. One issue with this cell configuration is the need to use an external pump to avoid mixing the two streams too quickly. Another important drawback to use this cell design in stacks is the need to perform oxidant and fuel separation in the cell outlet stream before it can enter another cell if a non-fuel-tolerant cathode catalyst is employed [49].

4.3.3 Mixed-Reactant Membraneless Direct Liquid Fuel Cell (MR-DLFC)

In order to avoid the need of pumps and separators, fuel and oxidant can be inserted in the FC together in a single stream, but selective catalysts must be used in the anode and cathode to ensure that the oxidation reaction occurs primarily in the anode and the ORR in the cathode. The fuel oxidation reaction is almost unaffected by the presence of oxygen, but the ORR is suppressed by the presence of liquid fuel [50].

For methanol-based FCs, methanol-tolerant non-precious metal cathode catalysts were previously studied, but despite the high selectivity towards ORR, they presented too low activity for practical applications when compared with traditional Pt-based catalysts [51]. A methanol-tolerant catalyst cathode consisting of Ag layer

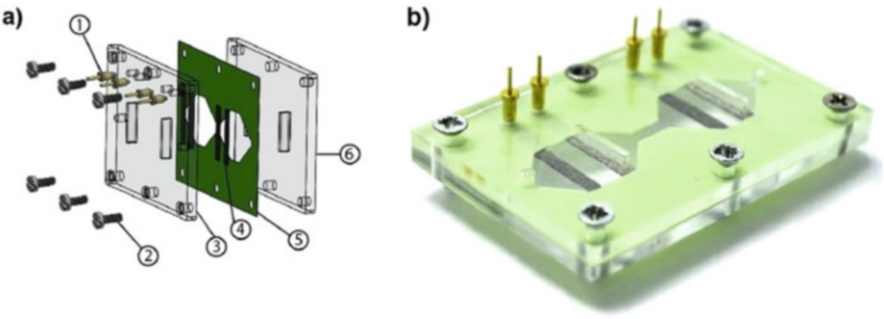

Fig. 4.1 (**a**) Schematic representation of the components and assembly of the microfluidic mixed-reactant μDMFC stack (1—Pogo pin, 2—Screw, 3—Top poly(methyl methacrylate) (PMMA) plate, 4—Porous electrodes, 5—Microchannel, and 6—Bottom PMMA plate) and (**b**) photograph of the stack. Reproduced with permission from Ref. [49], Copyright Elsevier, 2017

on top of Pt layer deposited on carbon paper was successfully tested to prevent the methanol molecules from reaching the Pt catalyst surface as the Ag layer is inert into the MOR and it blocks the passage of the greater methanol molecules and allows the smaller oxygen molecules to reach the Pt layer [52]. The mixed-reactant fuel cell (MR-FC) presents a higher volumetric power density, as it is more compact due to the simpler configuration. A schematic representation of the components and assembly of a MR-FC is shown in Fig. 4.1.

4.4 Oxygen Reduction Reaction (ORR)

As oxygen is readily present in the atmosphere, its reduction was, almost in all cases, used as the reduction reaction in the DLFC cathodes. The first FCs employed an active system to accelerate the oxygen transport to the cathode electrode, but as interest in the cell miniaturization increased, it became increasingly important to develop air-breathing μDLFC. This new design can be semi-passive or passive, relying on the natural diffusion and convection of oxygen to the cathode or both liquid fuel to the anode and oxygen to the cathode, respectively, that decreases the system complexity and eliminates the parasitic energy losses caused by pumps, blowers, and compressors necessary in an active system, allowing the development of more compact FCs. As an example, Fig. 4.2 displays a semi-passive air-breathing micro-direct methanol fuel cell (μDMFC) with an anode flow single-serpentine pattern [53].

Traditionally, Pt-based alloys were used as cathode catalysts and promoted high ORR activity, but they also presented a high cost and low selectivity towards ORR in the presence of fuels, especially alcohols, such as methanol. As in all FC types, the

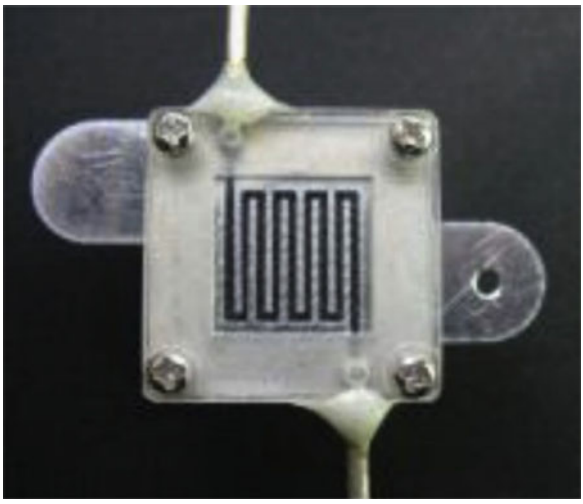

Fig. 4.2 Picture of the assembly of a semi-passive air-breathing μDMFC with an anode flow single-serpentine pattern. Reproduced with permission from Ref. [53], Copyright Elsevier, 2015

cathode is exposed, in some degree, to the fuel from the anode part, it is important to develop Pt free cathode catalysts with high ORR selectivity, avoiding the fuel oxidation reaction in the cathode [54].

4.5 Methanol Oxidation Reaction (MOR)

Methanol was one of the first considered liquid organic chemicals to replace hydrogen gas in FCs as it presents high theoretical energy density, lower cost, and it is easier to handle and store. Therefore, methanol electro-oxidation reaction kinetics and catalysis were extensively studied during the last decades. In this context, we will consider direct methanol fuel cells (DMFCs) together with their counterpart's micro-FCs. Several DMFC systems were successfully developed and most of them used Pt cathode and Pt-Ru anode electrodes, as it was shown that Pt promotes a high oxidation and reduction kinetics while Ru promotes a more complete methanol oxidation to carbon dioxide, decreasing the catalyst sites poisoning by carbon monoxide. However, methanol broad scale use in FCs still presents disadvantages as it is not a very available primary fuel, it is highly toxic and it is mostly produced from pollutant and non-renewable fossil fuels [55].

Catalyst cost still represents a major part of the total cost in micro-FCs production mainly because of Pt high cost; therefore, many researchers addressed this issue by developing strategies to keep high catalytic activity while decreasing Pt loading or replacing it with less expensive catalysts [56].

4.5.1 Catalysis in Acid Media

Vijh [57] studied the methanol electro-oxidation activity with pure metal catalysts, including several noble and non-noble metals, and verified that Pt promoted the best activity in acid media, while Pd presented insignificant activity. Bagotzki et al. [58] suggested that methanol electro-oxidation in Pt surface follows a reaction path consisted of methanol dehydrogenation with the formation of the following adsorbed species: $CH_2OH(x)$, $CHOH(xx)$, $COH(xxx)$, and $CO(x)$, where each (x) represents a bond with one Pt catalysts active site. $CO(x)$ can react with water molecules to form CO_2, while $CH_2OH(x)$ and $CHOH(xx)$ can lead to the formation of formaldehyde and formic acid, respectively, not promoting catalysts poisoning. However, $COH(xxx)$ reaction to CO_2 is slow, as it is strongly bonded to three adjacent active sites, slowly poisoning the catalysts. The use of Pt–Pd alloys, with a maximum of 33% Pd content, can mitigate the poisoning effect by decreasing the surface Pt active sites concentration. The presence of three adjacent sites becomes rarer, significantly decreasing the formation of $COH(xxx)$ in favor of the more active $CO(x)$, increasing the overall reaction rate and extending the catalyst durability. Higher Pd loadings are not desirable as its inactivity in acid media would significantly decrease the catalyst activity [59].

Nevertheless, it is possible to significantly decrease Pt loading by developing a catalysts design where Pt particles remain only present in a Pd catalyst surface. Wang et al. [60] developed highly ordered Pd–Pt core-shell nanowire arrays as catalysts with a very low Pt loading of 0.03 mg cm^{-2}, by coating a thin Pt film on the surface of Pd nanowire arrays. In acid media, this catalyst presented a Pt mass specific anodic peak current density of 756.7 mA mg^{-1}, which is much higher than traditional Pt and Pt–Ru catalysts. These results demonstrated that Pd can be used to significantly decrease Pt loadings and also increase catalytic activity in acid media. Its high activity is explained by synergetic effect between Pt and Pd in the methanol electro-oxidation mechanism and the higher oxophilicity of Pd than that of Pt.

4.5.2 Catalysis in Alkaline Media

Tripkovic et al. [61] demonstrated that the electrochemical oxidation of methanol is much higher in alkaline than in acid solutions, as it was verified at 60 °C and the low overpotential of 0.50 V; Pt and Pt_2Ru_3 catalysts were 30 and 20 times more active in alkaline than in acid media, respectively. This pH relation was attributed to the preferential adsorption of OH^- species in the active sites in alkaline media, which at low surface coverage promotes the complete oxidation of adsorbed carbon monoxide in the methanol oxidation mechanism, decreasing catalyst poisoning.

Demirci [62] compared theoretical results of the segregation energies and d-band center shifts for bimetallic alloys of Fe, Co, Ni, Cu, Ru, Rh, Pd, Ag, Ir, Pt, and Au. It is well known that Pt presents the best activity towards MOR among all single metal

catalysts, so bimetallic Pt-based alloys were compared to increase activity further and Pt–Ru was confirmed to be the most active Pt-based bimetallic catalyst, as Ru decreases catalyst poisoning by carbon monoxide and Pt strongly segregates to the surface, increasing its surface concentration and available active sites. Patel et al. [63] obtained higher anode catalytic activity for methanol oxidation with a $Pt_{50}Ru_{50}$ supported in a nanostructured titanium nitride (TiN) than in commercial Pt–Ru catalyst. The TiN supported catalyst presented a high electrochemical active surface area (ECSA) of 59 $m^2\ g^{-1}$ and a low charge transfer resistance of 16.8 $\Omega\ cm^2$, which allows a decrease in catalyst loading in DMFC. Alcaide et al. [64] verified the correlation between the unsupported Pt–Ru catalyst organic solvent polarity and the catalyst particles size and its layer performance as anode catalyst in DMFC, indicating that catalyst inks with more polar organic solvents develop smaller catalyst particles, increasing the active surface area and the overall DMFC performance. Therefore, Pt–Ru trimetallic catalysts activities were also studied and promising results were obtained with Mo, W, Co, Fe, Sn, and Ni, among others, indicating that the new developments also consider trimetallic catalysts.

Research on non-Pt anode catalysts for DMFC had recently focused in alkaline media and, in particular, AEM-DMFCs. Catalysts alloys based on several metals, such as Ir, Pd, Au, and Ru, were tested to replace Pt-based catalysts in alkaline media, but it still remains a challenge to obtain the same activity of Pt–Ru electrodes. Xu et al. [65] demonstrated that Pd presents much lower activity to methanol oxidation in alkaline media than Pt and it is not suitable for applications in micro-FCs as a single component catalyst. However, there are several promising Pd-based alloys that still require further investigations, such as Pd–Fe/C and Pd–Ni/C [66]. It was verified that, in the presence of Pd–Ni catalyst electrode in alkaline media, methanol is oxidized to carbonate, usually with the formation of formaldehyde in the catalyst surface [67].

4.5.3 Micro-Direct Methanol Fuel Cells (μDMFC)

Table 4.1 shows the experimental data available for passive μDMFCs, considering only the cells with active area smaller than 2.50 cm^2 and fuel and oxidant supplied passively through diffusion. However, it must be noticed that some of these FCs are just small cells made with traditional techniques not suitable for an effective miniaturization and mass production. In almost all cases, Pt-based catalysts were used, especially Pt–Ru/C in the anode and Pt/C in the cathode, but Verjulio et al. [40] developed a passive air-breathing AEM-μDMFCs with commercial Pt–Ru/C catalyst in the anode and a $CoSe_2$/C as cathode catalyst. A similar FC with commercial Pt/C cathode catalyst was used for comparison. The results have shown that, for low 1.0 and 3.0 M methanol concentrations, both FCs presented similar performances, but in high 7.0 M methanol concentration, the cell with $CoSe_2$/C cathode catalyst presented a much higher maximum power density of 1.2 mW cm^{-2} while the cell

Table 4.1 Passive micro-direct methanol fuel cells performance

Reference	Active area (cm^2)	P_{max} (mW cm^{-2})	T (°C)	[CH_3OH] (M)	Membrane	Anode	Cathode
[68]	1	16.2	30	4	CP-MEA[a]	Pt–Ru/C (4 mg cm^{-2})	Pt–Ru/C (2 mg cm^{-2})
[68]	1	23.2	30	6	CNT-MEA[b]	Pt–Ru/C (4 mg cm^{-2})	Pt–Ru/C (2 mg cm^{-2})
[69]	1	35	60	4	rGO-SSFF[c] Nafion® 117	–	Pt/C (4 mg cm^{-2})
[69]	1	31	60	3	CP-Nafion® 117	–	Pt/C (4 mg cm^{-2})
[69]	1	23.8	25	3	rGO-SSFF Nafion® 117	–	Pt/C (4 mg cm^{-2})
[69]	1	21.2	25	2	CP-Nafion® 117	–	Pt/C (4 mg cm^{-2})
[70]	1	5.5	–	2	Sulfo functionalized porous silicon membrane	Pt-Nanoflowers	Pt-Nanoflowers
[49]	0.015	1.2	22	5	Membraneless (2 cells stack)	Pt/CP (0.04 mg cm^{-2})	Ag–Pt/CP (0.04 mg cm^{-2})
[71]	2.25	19.2	25	3	Nafion® 117	Pt–Ru/CP (3 mg cm^{-2})	Pt/CPMPL[d] (0.5 mg cm^{-2})
[72]	2.25	29.3	25	4	Nafion® 117	Pt–Ru/CC[e] (4 mg cm^{-2})	Pt/CC (4 mg cm^{-2})
[39]	0.25	2.2	20	1	A201 (Tokuyama)	Pt–Ru/C (1:1 60 wt% of metal)	Pt/C (60 wt%)
[73]	0.48	19	50	1	Nafion® 117	Pt–Ru/CC (4 mg cm^{-2})	Pt/CC (2 mg cm^{-2})
[74]	1	20.8	25	7	rGO-SSFF/Nafion® 117	Pt–Ru/C (4 mg cm^{-2})	Pt/C (2 mg cm^{-2})
[74]	2	31.69	60	4	rGO-SSFF/Nafion® 117	Pt–Ru/C (4 mg cm^{-2})	Pt/C (2 mg cm^{-2})
[40]	0.25	1.2	22	7	A201 (Tokuyama)	Pt–Ru/C (1:1, 60 wt% of metal) (6 mg cm^{-2})	$CoSe_2$/C (20 wt% of metal) (1.5 mg cm^{-2})
[40]	0.25	0.6	22	3	A201 (Tokuyama)	Pt–Ru/C (1:1, 60 wt% of metal) (6 mg cm^{-2})	Pt/C (20 wt% of Pt) (1.5 mg cm^{-2})
[75]	1	18.3	20	2	Nafion® 117	Pt–Ru	Pt
[76]	1	46	40	3	CNT-MEA/Nafion® 117	Pt–Ru/C (4 mg cm^{-2})	Pt/C (2 mg cm^{-2})
[77]	1	40.9	25	4	Nafion® 117	–	–

[78]	0.6	10	25	2	PEM	Pt–Ru/C (4 mg cm^{-2})	Pt/C (4 mg cm^{-2})
[79]	0.071	15	25	5	Nafion® 117	Pt–Ru/C (1:1, 60 wt% PtRu) (2 mg cm^{-2})	FePc/C ((5 mg cm^{-2})[f]
[80]	1.44	34.2	25	2	Nafion® 117	Pt–Ru/C (1:1) (4 mg cm^{-2})	Pt/C (40 wt%) (4 mg cm^{-2})
[81]	1	2.2	25	4	Nafion® 117	Pt–Ru/C (1:1) (3 mg cm^{-2})	Pt/C (50 wt% Pt) (2 mg cm^{-2})
[81]	1	2.01	25	4	Nafion® 177 (6 cells stack)	Pt–Ru/C (1:1) (3 mg cm^{-2})	Pt/C (50 wt% Pt) (2 mg cm^{-2})
[82]	0.48	8.08	25	2	Nafion® 117	Pt–Ru/C (4 mg cm^{-2})	Pt/C (1.5 mg cm^{-2})
[83]	1.625	50	60	2	Nafion® 112	Pt–Ru (1:1) (4 mg cm^{-2})	Pt/C (40 wt% Pt) (1.3 mg cm^{-2} Pt)
[83]	1.625	16.5	25	2	Nafion® 112	Pt–Ru (1:1) (4 mg cm^{-2})	Pt/C (40 wt% Pt) (1.3 mg cm^{-2} Pt)
[84]	1	16.9	20	1	Nafion® 117 (4 cells stack)	Pt–Ru/C (4 mg cm^{-2})	Pt/C (2 mg cm^{-2})
[85]	1	15.39	25	2	Nafion® 117	–	–
[86]	–	85	60	2	–	–	–
[87]	1	0.031	25	2	Nafion® 117	Pt/C	Pt/C
[88]	0.44	100	25	1	Nafion® 117	Pt–Ru/C (1.5 mg cm^{-2})	Pt/C (1 mg cm^{-2})
[6]	0.25	10	25	4	Nafion® 117	Pt–Ru (4 mg cm^{-2})[g]	Pt (4 mg cm^{-2})[g]
[89]	–	2	25	3	Flemion tubes	Pt–Ru (6 mg cm^{-2})	Pt (6 mg cm^{-2})
[90]	1	38.9	60	2	CP-MEA/Nafion® 117	Pt–Ru/C	Pt/C (40 wt%) (2 mg cm^{-2})
[90]	1	42.4	60	3	SSFF-MEA/Nafion® 117	Pt–Ru/C	Pt/C (40 wt%) (2 mg cm^{-2})
[91]	1	21.2	25	2	CP-MEA/Nafion® 117	Pt–Ru/C (1:1, 60 wt%) (4 mg cm^{-2})	Pt/C
[91]	1	25.9	25	3	SSFF-MEA/Nafion® 117	Pt–Ru/C (1:1, 60 wt%) (4 mg cm^{-2})	Pt/C

(continued)

Table 4.1 (continued)

Reference	Active area (cm^2)	P_{max} (mW cm^{-2})	T (°C)	[CH_3OH] (M)	Membrane	Anode	Cathode
[12]	0.25	2.2	22	2	SU-8 membrane	Pt–Ru/C (1:1, 30 wt%) (1 mg cm^{-2})	Pt/C (40 wt%) (1 mg cm^{-2})
[12]	0.25	4.15	40	4	SU-8 membrane	Pt–Ru/C (1:1, 30 wt%) (1 mg cm^{-2})	Pt/C (40 wt%) (1 mg cm^{-2})

[a]Membrane electrode assembly with carbon paper as gas diffusion layer (GDL)
[b]Membrane electrode assembly with carbon nanotubes as GDL
[c]Reduced graphene oxide deposited in stainless steel fiber felt as GDL
[d]Carbon paper with microporous layer as GDL
[e]Carbon cloth with microporous layer as GDL
[f]Iron phthalocyanine based cathode
[g]E-TEK ELAT-supported

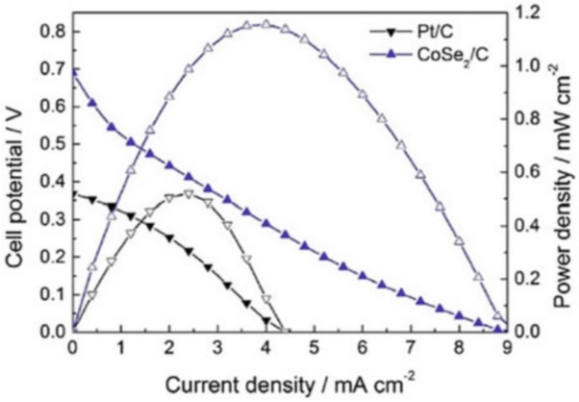

Fig. 4.3 AEM-μDMFC's performance comparison between Pt/C and $CoSe_2$/C cathodes with 7 mol L^{-1} methanol in 1 mol L^{-1} KOH. Reproduced with permission from Ref. [40], Copyright Elsevier, 2016

with Pt/C cathode catalyst presented only 0.50 mW cm^{-2} as it can be seen in Fig. 4.3. This suggests that $CoSe_2$/C is a high methanol-tolerant catalyst for ORR, allowing the use of higher methanol concentrations to increase power output.

Many researchers focused on the development of new membranes and diffusion layers for both acid and alkaline FCs, in order to obtain high ionic conductivity, low methanol crossover, and high oxygen transport to the cathode. The most employed membrane in acid media was commercial or modified Nafion® 117 (DuPont) [6, 69, 71–77, 79–82, 84, 85, 87, 88, 90, 91]. Lu et al. [83] used a modified Nafion® 112 (DuPont) membrane to decrease methanol crossover, achieving high power output with 2.0 M ethanol solution. The few researches with passive fuel cells in alkaline media adopted commercial A201® membranes (Tokuyama) [39, 40]. Carbon paper (CP) [49, 68, 69, 71, 90, 91], carbon nanotubes (CNTs) [68, 76], and modified stainless steel fiber felt (SSFF) [69, 74, 90, 91] were tested as gas diffusion layers, concluding that both CNT and SSFF promote higher cell power outputs than CP by increasing the oxygen transport to the cathode catalytic layer. Abrego-Martínez et al. [49] developed a two cells stack made of alkaline mixed-reactant membraneless μDMFCs with a methanol-tolerant Ag–Pt/CP cathode, obtaining similar output and durability to a separated reactants stack but with a much smaller cost and fabrication complexity. The stack achieved double open circuit potential and a 75% increase in power output, when compared with the single cell design, remaining stable for a period of at least 10 h, indicating that Ag–Pt catalyst is methanol-tolerant.

Verjulio et al. [39] developed a passive alkaline μDMFC with a very small active area of 0.25 cm^2 using conventional Pt–Ru and Pt catalysts for the anode and cathode, respectively. At ambient temperature and using a fuel solution of 1.0 M methanol and 4.0 M KOH, the maximum power density obtained was 2.2 mW cm^{-2}. Falcão et al. [71] tested several passive and active μDMFC with an active area of 2.25 cm^2 at ambient temperature. The optimum design was a passive cell with Nafion® 117 membrane, catalysts loadings of 3.0 mg cm^{-2} Pt–Ru at the anode and 0.5 mg cm^{-2} Pt at the cathode, and a 3.0 M methanol solution. The maximum

power density was 19.2 mW cm^{-2}, which is much higher than the power density achieved by Verjulio et al. [39], suggesting that, for Pt-based catalysts FCs, higher power densities are obtained in alkaline media and greater catalyst active area.

Qiao et al. [89] demonstrated a plating technique to create microtubular cathode electrodes, being suitable for micro-FCs mass production. In addition, Esquivel et al. [12] used SU-8 photoresist technology to develop a more compact μDMFC with very small 0.25 cm^2 active area, achieving a lower active area power density due to increased contact resistance, but a higher volumetric power density due to the significant decreased cell volume obtained. Therefore, this well-established fabrication technique is a promising approach to μDMFC mass production.

Table 4.2 displays the experimental results for active μDMFCs, including only the cells with active area smaller than 2.50 cm^2 and a fuel and/or oxidant active supply system. In all cases, Pt-based catalysts were used in both anode and cathode, especially Pt–Ru/C for MOR and Pt/C for ORR. No experimental data concerning alkaline active μDMFC were obtained in the literature. All FCs in Table 4.2 were operated in acid media. The most used membrane was commercial Nafion® 117 (DuPont) [53, 92–105], but Nafion® 115 (DuPont) [106–108] and Nafion® 112 (DuPont) [109] were also employed, mainly to decrease MEA's thickness while keeping low methanol crossover through its combination with improved carbon paper diffusion layers. Yuan et al. [53] developed a semi-active self-air-breathing μDMFC, using 1.0 M methanol solution at 1 mL min^{-1} flow rate, a catalyst active area of 0.64 cm^2, Pt–Ru/C anode catalyst and Pt/C cathode catalyst, both with 4.0 mg cm^{-2} loadings, obtaining at 20 °C and 60 °C the highest reported peak power densities of 50.6 mW cm^{-2} and 105.4 mW cm^{-2}, respectively. These results suggest that, for low fuel flow rates in active micro-FCs, the overall reaction rate is generally controlled by the methanol transport to the anode rather than the oxygen transport to the cathode, as the later can often passively diffuse to the cathode catalytic layer at a high enough rate.

D'Urso et al. [102] designed a co-planar active μDMFC with deposition of conventional Pt-based catalysts by a spray-coating technique, which allowed a fine control of the distance between anode and cathode layers. By increasing this distance, methanol crossover decreased but the overall cell impedance also increased significantly. Yuan et al. [95] studied the effect of the micro-scale aspects in the μDMFC power output and demonstrated, through experiments and simulations, that there is a direct correlation between the μDMFC scale size and its power density output. There is also a clear relation between the cell operation temperature and the overall power output, so Fang et al. [92] developed an active μDMFC with heat control. A micromethanol combustor with a control unit was used to keep the optimum cell temperature of 65 °C. Figure 4.4 shows a photograph of this integrated μDMFC with the control unit. The active cell power density was kept stable at 40.6 mW cm^{-2} during the whole experiment, while it was verified that a similar cell with no temperature control device kept at a room temperature of 65 °C quickly loses most of its power output within the first hour of operation, due to overheating, as it can be seen in Fig. 4.5. This indicates that cell temperature control is a key aspect when designing a μDMFC.

Table 4.2 Active micro-direct methanol fuel cells performance

Reference	Active area (cm^2)	P_{max} (mW cm^{-2})	T (°C)	[CH_3OH] (M)	Membrane	Anode	Cathode
[110]	0.64	96.7	60	1	–	–	–
[110]	0.64	49.8	20	1	–	–	–
[92]	1	40.6	65	2	Nafion® 117	Pt–Ru/C (40 wt% Pt 20 wt% Ru)	Pt/C (40 wt% Pt)
[106]	1.69	18.11	30	3	Nafion® 115	Pt–Ru/C (4.5 mg cm^{-2})	Pt/C (2.4 mg cm^{-2})
[93]	2.25	32	20	4	Nafion® 117	4 mg cm^{-2}	4 mg cm^{-2}
[111]	0.64	11.4	20	1	–	Pt–Ru/CP (4 mg cm^{-2})	Pt/CP (4 mg cm^{-2})
[94]	0.64	22	20	1	Nafion® 117	Pt–Ru (4 mg cm^{-2})	Pt (2 mg cm^{-2})
[107]	2.25	18.1	20	2	Nafion® 115	Pt–Ru (3 mg cm^{-2})	Pt (0.5 mg cm^{-2})
[95]	0.64	27.1	20	1	Nafion® 117	Pt–Ru (4 mg cm^{-2})	Pt (2 mg cm^{-2})
[53]	0.64	50.6	20	1	Nafion® 117	Pt–Ru/C (1:1) (4 mg cm^{-2})	Pt/C (4 mg cm^{-2})
[53]	0.64	105.4	60	1	Nafion® 117	Pt–Ru/C (1:1) (4 mg cm^{-2})	Pt/C (4 mg cm^{-2})
[96]	1	19	60	1	Nafion® 117	Pt–Ru/C (4 mg cm^{-2})	Pt/C (4 mg cm^{-2})
[96]	1	21.7	88	1	Nafion® 117	Pt–Ru/C (4 mg cm^{-2})	Pt/C (4 mg cm^{-2})
[97]	2.66	12.71	25	1	Nafion® 117 (2 cells stack)	Pt–Ru/C (4 mg cm^{-2})	Pt/C (1.5 mg cm^{-2})
[98]	2.25	20.29	25	6	Nafion® 117	–	–
[98]	2.25	86.92	25	2	Nafion® 117 (3 cells stack)	–	–
[99]	0.64	27.11	20	1	Nafion® 117	Pt–Ru/C (4 mg cm^{-2})	Pt/C (2 mg cm^{-2})
[100]	0.48	27.5	60	1	Nafion® 117 (8 cells stack)	Pt–Ru/C (1:1, 40 wt% Pt-Ru) (4 mg cm^{-2})	Pt/C (40 wt% Pt) (2 mg cm^{-2})
[101]	0.64	65.66	40	1.5	Nafion® 117	Pt–Ru/C (5 wt%) (4 mg cm^{-2})	Pt-Ru/C (5 wt%) (2 mg cm^{-2})
[101]	0.64	115	80	1.5	Nafion® 117	Pt–Ru/C (5 wt%) (4 mg/cm^{-2})	Pt-Ru/C (5 wt%) (2 mg/cm^{-2})

(continued)

Table 4.2 (continued)

Reference	Active area (cm^2)	P_{max} (mW cm^{-2})	T (°C)	[CH_3OH] (M)	Membrane	Anode	Cathode
[102]	–	1.3	25	2	Nafion® 117	Pt–Ru/C (85 wt%) (1 mg cm^{-2} Pt)	Pt/C (60 wt%) (0.25 mg cm^{-2} Pt)
[109]	2.25	22.74	20	5	Nafion® 112	Pt–Ru (1:1) (5 mg cm^{-2})[a]	Pt (5 mg cm^{-2})[a]
[86]	–	170	60	2	–	–	–
[108]	0.073	8	68	2	Nafion® 115	Pt–Ru/C (3.29 mg cm^{-2})	Pt/C (3.18 mg cm^{-2})
[112]	1	25	25	1	–	–	–
[112]	1	23.48	25	1	–	–	–
[113]	0.64	65.6	23	1	–	–	–
[103]	0.64	11.39	20	1	Nafion® 117	Pt–Ru/C (4 mg cm^{-2})	Pt/C (4 mg cm^{-2})
[114]	1	25	25	3%	Silicon based	–	–
[104]	0.11	0.5	25	1	Nafion® 117	Pt–Ru/C (1:1, 60 wt%) (2 mg cm^{-2})	Pt/C (60 wt%) (2 mg cm^{-2})
[105]	1	115.7	88	2	Nafion® 117	Pt–Ru/C (4:1) (4 mg cm^{-2} Pt)	Pt/C (4 mg cm^{-2})

[a]E-TEK-supported

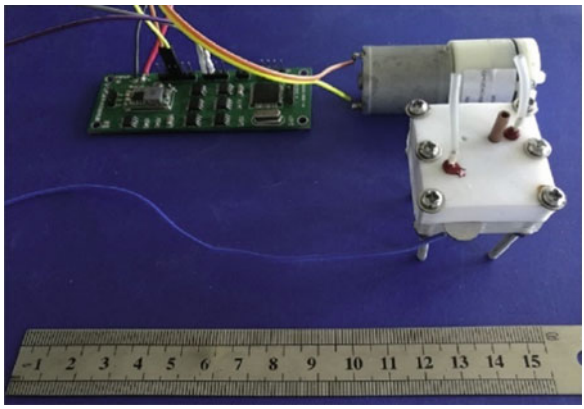

Fig. 4.4 The photograph of the integrated μDMFC unit with the control unit. Reproduced with permission from Ref. [92], Copyright Elsevier, 2016

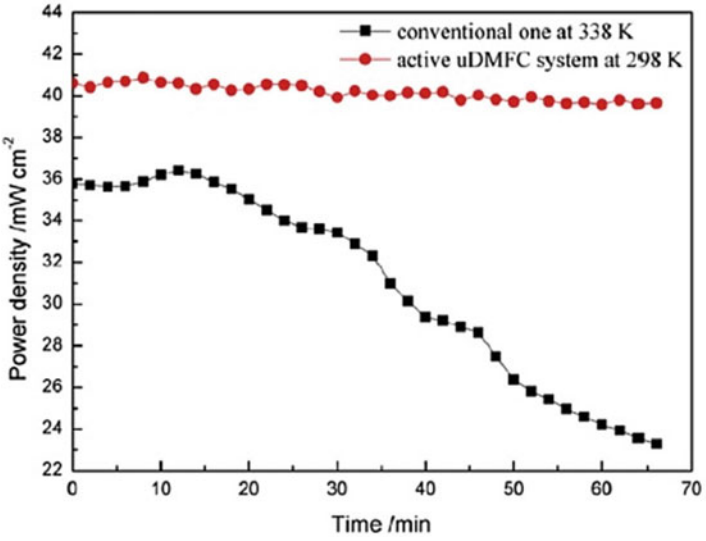

Fig. 4.5 Time-power profiles of the active μDMFC system with heat control and the conventional one without heat control kept at a room at 65 °C. Reproduced with permission from Ref. [92], Copyright Elsevier, 2016

4.6 Ethanol Oxidation Reaction (EOR)

Ethanol presents several advantages over methanol in FCs as it is less toxic, more intrinsically energetic, more readily available, and produced from more environmentally friendly biological renewable sources, such as sugarcane. Direct ethanol fuel cells (DEFCs) suffer much less alcohol crossover than DMFC as ethanol diffusion through the membranes is much slower due to its higher molecular size. However, ethanol oxidation kinetic is slower than in the case of methanol as it

presents a strong C–C bond that needs to be broken in order to achieve complete oxidation to carbon dioxide [115].

DEFCs can be divided into two major groups according to the membrane electrolyte assembly (MEA) type employed: PEM-DEFCs, which use acid electrolyte media and AEM-DEFCs, which use alkaline electrolyte media. It was also demonstrated that DEFC can be developed with alkaline media in the anode and acid media in the cathode, separated by a charger conducting membrane [116]. However, the kinetics of both EOR and ORR are slower in acid media than in alkaline, leading to smaller FC efficiencies. It was verified that alcohol crossover is higher in PEM-FCs than in AEM-FCs, as in the PEM case, the ionic flux through the membrane is from the anode to the cathode, facilitating the alcohol diffusion together, but in the AEM case, the ionic flux is from the cathode to the anode, decreasing the alcohol electro-osmotic drag. In addition, expensive Pt-based catalysts, such as Pt–Sn, need to be used in acid media FCs to achieve higher oxidation efficiencies, but catalysts based in less expensive metals, such as Pd, Ag, and Ni, can be more successfully used in alkaline media. Therefore, there is a growing research interest in the development of AEM-DEFCs [35].

Table 4.3 presents the experimental data available concerning the performance of passive μDEFCs. It was only considered the FCs which use natural diffusion to provide fuel and oxidant to both the anode and cathode, respectively, and with a catalyst active area smaller than 2.50 cm^2. Traditional Pt anode catalyst was only used in acid media [45]. Pt–Ru catalyst was used as anode catalysts in some studies that focus on the performance of new modified membranes [117, 118]. In most studies, alkaline electrolyte media were used with a focus on non-Pt electrodes.

Pd-based bimetallic alloys with Ni [38], Au [120], and Pt [122] were used as anode catalysts. Xu et al. [120] obtained high performance with Pd–Au/C as anode catalyst with the low 1.0 M ethanol concentration at room temperature. Additionally, Xu et al. [121] achieved an even higher performance with a physically mixed Pd_3Au cathode catalyst supported on carbon nanotubes (CNTs).

Tadanaga et al. [119] achieved a high peak power density using non-noble metal catalysts, Ni–Co for anode and Fe–Co for cathode. Several cathode catalysts based on Ag, Mn, and Pd were tested [38, 117, 118, 121]. Most studies used commercial AEM, such as A201 (Tokuyama). Composite polymer membranes based on poly (vinyl alcohol) were also tested but the results were not satisfactory [117, 118].

Table 4.4 contains the literature data about active μDEFCs, which generally presents a higher power output than passive cells. Only DEFCs with an active supply system to the anode and/or cathode and a catalyst active area smaller than 2.50 cm^2 were considered. Active μDEFCs with both Pt-based anode and cathode catalysts generally presented a lower performance than with non-Pt-based ones in both acid and alkaline media, as their smaller peak power output is obtained at a lower ethanol concentration due to its greater susceptibility to carbon monoxide poisoning [20, 105, 123–126].

In the case of the cells with Pd-based anode catalysts, there was an increase in maximum power output and ideal ethanol concentration, especially with Pd–Ni/C [116, 127–132, 134, 135]. Most of these cells used a commercial Fe–Co

Table 4.3 Passive micro-direct ethanol fuel cells performance

Reference	OCV (V)	Active area (cm^2)	P_{max} (mW cm^{-2})	J_{max} (mW cm^{-2})	T (°C)	[CH_3OH] (M)	[KOH] (M)	Membrane	Anode	Cathode
[38]	0.8	0.25	0.1	0.2	20	4	4	A201 (Tokuyama)	Pd–NiO/C (2 mg cm^{-2})	Ag/C (2 mg cm^{-2})
[119]	0.87	0.4	65	–	80	2.1	1.7	A202 (Tokuyama)	Ni–Co/CC	Fe–Co/Ni foam
[45]	0.26	1	8.1	–	23	8.5	–	Nafion® 115	Pt/porous silicon	Pt/porous silicon
[117]	–	1	10.74	37.38	25	2	8	PVA-HAP (1:2.5, 10 wt %)[a]	Pt–Ru/C (Ni foam) (4 mg cm^{-2})	MnO_2/C (3.63 mg cm^{-2})
[117]	–	1	7.56	20.28	25	2	8	PVA-HAP (1:2.5, 10 wt %)	Pt–Ru/C (CP) (4 mg cm^{-2})	MnO_2/C (3.63 mg cm^{-2})
[120]	–	1	57.5	167	25	1	1	A201 (Tokuyama)	Pd–Au/C (3:1, 30 wt%)	HYPERMECTM (1 mg cm^{-2})
[120]	–	1	56	179	25	1	1	A201 (Tokuyama)	Pd/C (30 wt%)	Non-Pt (1 mg cm^{-2})
[118]	0.853	1	8	35.68	25	2	4	PVA/TiO_2[b]	Pt–Ru/C (1:1, 70 wt%) (3.6 mg cm^{-2})	MnO_2/C
[121]	0.91	1	185	–	25	1	1	A201 (Tokuyama)	Non-Pt (Acta) (2 mg cm^{-2})	m-Pd_3Au/CNT (1 mg cm^{-2})[c]
[121]	0.86	1	136	–	25	1	1	A201 (Tokuyama)	Non-Pt (Acta) (2 mg cm^{-2})	Pd/CNT (1 mg cm^{-2})
[121]	0.82	1	101	–	25	1	1	A201 (Tokuyama)	Non-Pt (Acta) (2 mg cm^{-2})	Au/CNT (1 mg cm^{-2})
[122]	–	1	3.6	–	25	4	5	AEM	Pd–Pt/GA/NFP (1:1)[d]	Commercial Pt/C

[a]Poly(vinyl alcohol) hydroxyapatite composite polymer membrane
[b]Poly(vinyl alcohol)/titanium oxide composite polymer membrane
[c]Physically mixed Pd_3Au deposited on CNTs
[d]Graphene aerogel deposited on nickel foam plate

Table 4.4 Active micro-direct ethanol fuel cells performance

Reference	OCV (V)	Active area (cm^2)	P_{max} (mW cm^{-2})	J_{max} (mA cm^{-2})	T (°C)	[CH_3OH] (M)	[KOH] (M)	Membrane	Anode	Cathode
[127]	1.463	1	200	525	60	3	5	Nafion® 117	Pd–Ni/C (1 mg cm^{-2})	Au/NiCr (30 wt% Au) (1.2 mg cm^{-2})
[128]	–	1	130	1060	80	3	5	A201 (Tokuyama)	Pd–Ni/C-PTFE (2 mg cm^{-2} Pd)[a]	Fe–Co HYPERMEC K14
[128]	–	1	87	820	50	3	5	A201 (Tokuyama)	Pd–Ni/C-PTFE (2 mg cm^{-2} Pd)	Fe–Co HYPERMEC K14
[116]	1.6	1	240	270	60	3	5 M NaOH	Nafion® 117	Pd–Ni/C (1 mg cm^{-2})	Pt/C (60 wt%) (3.9 mg cm^{-2})
[129]	–	1	90	320	60	3	5 M NaOH	A201 (Tokuyama)	Pd–Ni/C (1 mg cm^{-2})	Fe–Co HYPERMEC K14 (1 mg cm^{-2})
[129]	–	1	100	270	60	3	5 M NaOH	Nafion® 211	Pd–Ni/C (1 mg cm^{-2})	Fe–Co HYPERMEC K14 (1 mg cm^{-2})
[123]	0.85	0.385	22.4	64	50	1	0.25	A201 (Tokuyama)	Commercial Pt–Ru (Alfa Aesar) (4 mg cm^{-2})	Pt/C (30 wt%) (1 mg cm^{-2})
[105]	0.722	1	35.3	–	88	2	–	Nafion® 117	Pt–Sn/C (1:1, 50 wt%) (4 mg cm^{-2} Pt)	Pt/C (60 wt%) (4 mg cm^{-2})
[124]	0.67	2	6	–	20	1	0.5	Nafion® 117	Pt–Ru/C (3 mg cm^{-2})	Pt/C (3 mg cm^{-2})
[124]	0.87	2	58	–	20	1	0.5	AEM (Tokuyama)	Pt–Ru/C (3 mg cm^{-2})	Pt/C (3 mg cm^{-2})
[125]	0.74	1	30	–	40	1	0.5 M NaOH	A-006 (Tokuyama)	Pt–Pd/PNVC-V_2O_5 (1 mg cm^{-2})[b]	Pt/C (1 mg cm^{-2})
[126]	–	2.25	27.5	92.5	90	3	–	Nafion® 117	Pt–Sn/C (3:1, 20 wt%) (1 mg cm^{-2})	Pt–Co/C (1:1, 10 wt%) (1 mg cm^{-2})
[130]	0.84	1	49	139	60	1	1	A201 (Tokuyama)	Pd_7IrNi_{12}/C (1 mg cm^{-2})	Fe–Co HYPERMEC K14

[130]	0.66	1	22	101	60	1	1	A201 (Tokuyama)	Pd/C (1 mg cm^{-2})	Fe–Co HYPERMEC K14
[130]	0.8	1	34	136	60	1	1	A201 (Tokuyama)	Pd_2Ni_3/C (1 mg cm^{-2})	Fe–Co HYPERMEC K14
[130]	0.7	1	29	103	60	1	1	A201 (Tokuyama)	Pd_7Ir/C (1 mg cm^{-2})	Fe–Co HYPERMEC K14
[130]	0.9	1	92	–	60	3	5	A201 (Tokuyama)	Pd_7IrNi_{12}/C (1 mg cm^{-2})	Fe–Co HYPERMEC K14
[130]	0.805	1	58.2	–	60	3	5	A201 (Tokuyama)	Pd/C (1 mg cm^{-2})	Fe–Co HYPERMEC K14
[130]	0.85	1	80	–	60	3	5	A201 (Tokuyama)	Pd_2Ni_3/C (1 mg cm^{-2})	Fe–Co HYPERMEC K14
[130]	0.86	1	71.9	–	60	3	5	A201 (Tokuyama)	Pd_7Ir/C (1 mg cm^{-2})	Fe–Co HYPERMEC K14
[20]	–	0.27	0.028	0.24	–	1	0.3	Membraneless	Pt/Graphite bar	PtAg/GCE[c]
[131]	0.9	1	130	–	60	3	5	A201 (Tokuyama)	Pd–Ni/C (1 mg cm^{-2})	Fe–Co HYPERMEC K14 (1 mg cm^{-2})
[131]	–	1	160	–	80	3	5	A201 (Tokuyama)	PdNi/C (1 mg cm^{-2})	Fe–Co HYPERMEC K14 (1 mg cm^{-2})
[132]	–	1	360	–	60	3	5 M NaOH	Nafion® 211	PdNi/C (1 mg cm^{-2})	Pt/C (60 wt%) (3.9 mg cm^{-2})
[133]	–	1	50	–	60	3	5	PVA-TMAPS (9:1)[d]	HYPERMECTM (2 mg cm^{-2})	HYPERMECTM (1 mg cm^{-2})
[133]	–	1	30	–	25	3	5	PVA-TMAPS (9:1)	HYPERMECTM (2 mg cm^{-2})	HYPERMECTM (1 mg cm^{-2})

(continued)

Table 4.4 (continued)

Reference	OCV (V)	Active area (cm^2)	P_{max} (mW cm^{-2})	J_{max} (mA cm^{-2})	T (°C)	[CH_3OH] (M)	[KOH] (M)	Membrane	Anode	Cathode
[134]	0.666	1	18	–	60	1	1	A201 (Tokuyama)	Pd/C (20 wt%) (1 mg cm^{-2} Pt)	Fe–Co HYPERMEC K14 (Acta)
[134]	0.812	1	40	–	100	1	1	A201 (Tokuyama)	Pd/C (20 wt%) (1 mg cm^{-2} Pt)	Fe–Co HYPERMEC K14
[135]	–	1	88	582	60	3	1	A201 (Tokuyama)	Pd–Ni/C-PTFE (2 mg cm^{-2})	Pd/C-PTFE (0.035 mg cm^{-2} Pt)

[a]Polytetrafluoroethylene
[b]Poly-vinyl carbazole crossed linked with V_2O_5 and embedded with Pt–Pd nano crystallites
[c]Glassy carbon electrode
[d]Poly (vinyl alcohol)/3-(trimethylammonium) propyl-functionalized silica hybrid membrane

HYPERMEC K14 (Acta) cathode catalyst, although high performance was also obtained with Au/NiCr [127] and Pt/C [116, 132] cathode catalysts.

Most studies employed commercial alkaline or acid membranes, especially A201 (Tokuyama) and Nafion® 117 (DuPont). Although, Wang et al. [133] developed and tested a hybrid membrane based on poly (vinyl alcohol)/3-(trimethylammonium) propyl-functionalized silica (PVA-TMAPS) with improved thermal stability and conductivity. An et al. [132] achieved the highest reported peak power density of 360 mW cm^{-2} at 60 °C in an alkaline-acid μDEFC with the very thin Nafion® 211 membrane (25 μm), 1 mg cm^{-2} Pd–Ni/C loading as anode catalyst and 3.9 mg cm^{-2} Pt/C loading as cathode catalyst. The fuel and oxidant used were a 3.0 M ethanol solution with 5.0 M NaOH and a 4.0 M H_2O_2 solution with 1.0 M H_2SO_4, respectively. However, ethanol crossover in this cell requires further investigation in order to verify the cell viability in the long term.

4.7 Formic Acid Oxidation Reaction (FAOR)

Formic acid presents a lower intrinsic energy density than methanol and ethanol, but its crossover through the FC membrane is significantly slower, which allows the use of higher fuel concentrations and thinner membranes, increasing the cell's volumetric power density output. As it is much less toxic than methanol, formic acid has been studied as a major substitute for methanol in FCs. In addition, it promotes a higher voltage in the cell, decreasing the number of single cells in series needed for practical applications. The most accepted formic acid electro-oxidation mechanism is called the dual pathway mechanism. The first pathway consists of a dehydrogenation reaction, generating CO_2 without CO as an intermediate. The second one is a dehydration reaction, which creates adsorbed CO molecules, poisoning the catalyst. Therefore, the anode catalyst selection should be made in order to favor the first pathway, avoiding the catalyst poisoning as much as possible [136].

Table 4.5 shows the available experimental data for micro-direct formic acid fuel cells (μDFAFCs), considering only the FCs with a catalytic active area smaller than 2.50 cm^2, regardless of the production technique used. In all cases, only PEM was employed, including Nafion® 112 [29, 137, 138], Nafion® 115 [139], Nafion® 117 [140, 141], Nafion® NRE 212 [142], and Flemion tubes [143] membranes. Gago et al. [25] developed a membraneless μDFAFC with a single stream entry containing both fuel and oxidant, relying in the $CoSe_2$ cathode catalyst with high selectivity towards ORR. Although the achieved peak power density was much lower than in the cells that use Pt-based cathode catalysts, the absence of Pt and a membrane greatly decreased the cell production cost, increasing its commercial viability. Therefore, the development of fuel-tolerant non-Pt cathode catalysts such as $CoSe_2$ is a major research interest. In addition, air-breathing membraneless microfluidic FCs were developed in order to increase the oxygen availability in the cathode surface, while employing two laminar flow streams to significantly prevent the formic acid from reaching the cathode electrode. Higher power densities at low

Table 4.5 Micro-direct formic acid fuel cells performance

References	Active area (cm^2)	P_{max} (mW cm^{-2})	T (°C)	[HCOOH] (M)	Membrane	Supply system	Anode	Cathode
[146]	0.0625	30	25	5	Nanoporous Si-MEA	Passive	Pd/C	Pt/C
[142]	2.5	26.53	50	10	NRE 212	Active in cathode	Pd/C (4 mg cm^{-2})	Pt/C (3 mg cm^{-2})
[137]	0.44	3	20	10	Nafion® 112	Active in cathode	Pt/Si-grid	Pt/Si-grid
[137]	0.44	10.1	20	10	Nafion® 112	Active in cathode	Pt–Pd (1:1)	Pt/Si-grid
[137]	0.44	20.6	20	10	Nafion® 112	Active in cathode	Pt–Pd-SD[a]	Pt/Si-grid
[137]	0.44	28	20	10	Nafion® 112	Active in cathode	Pd/Si-grid	Pt/Si-grid
[138]	0.44	21	20	10	Si-MEA-Nafion® 112	Active in cathode	Pt/Si (2.5 mg cm^{-2})	Pt/Si (2.5 mg cm^{-2})
[138]	0.44	30.7	20	10	Si-MEA-Nafion® 112	Active in cathode	Pd/Si (4 mg cm^{-2})	Pt/Si (2.5 mg cm^{-2})
[138]	0.44	33.1	20	5	Si-MEA-Nafion® 112	Active in cathode	Pd/Si (4 mg cm^{-2})	Pt/Si (2.5 mg cm^{-2})
[138]	0.44	9.1	20	10	Si-MEA-Nafion® 112	Passive	Pt/Si (2.5 mg cm^{-2})	Pt/Si (2.5 mg cm^{-2})
[138]	0.44	12.3	20	10	Si-MEA-Nafion® 112	Passive	Pd/Si (4 mg cm^{-2})	Pt/Si (2.5 mg cm^{-2})
[140]	1	33	20	10	Nafion® 117	Passive	PtRu/C (4 mg cm^{-2})	Pt/C HiSPECTM (12 mg cm^{-2})
[140]	1	16.6	20	1.8	Nafion® 117	Passive	PtRu/C (12 mg cm^{-2})	Pt/C HiSPECTM (12 mg cm^{-2})
[143]	–	4	20	5	Flemion tubes	Passive	Pd/C (2.5 mg cm^{-2})	Pt/C (6 mg cm^{-2})

[141]	–	45	20	5	Nafion® 117	Passive	Pd/C (40 wt%) (4 mg cm^{-2})	Pt/C (40 wt%) (4 mg cm^{-2})
[139]	1	13.6	20	10	Nafion® 115	Active	Pt–Ru/C	Pt/C
[29]	0.44	17	20	10	Nafion® 112	Active	Pt/C (2.5 mg cm^{-2})	Pt/C
[25]	1	1,04	25	10	Membraneless	Passive	Pd (10 mg cm^{-2})	$CoSe_2$/C (2 mg cm^{-2})
[144]	–	26	20	1	Membraneless	Active	Pd/C	Pt/C
[145]	0.9	14	25	3	Membraneless	Active	Pd/C (8 mg cm^{-2})	Pt/C

[a]Spontaneously deposited Pd on dendritic Pt

fuel concentrations than in most non-air-breathing cells were obtained, as it was shown that overall reaction rate is limited by the oxygen diffusion to the cathode surface [144, 145].

Both Pt [29, 137–140] and Pd [25, 137, 138, 141–146] were used as anode catalysts. However, Yeom et al. [138] demonstrated that Pd anode catalyst is much more active towards FAOR than Pt, encouraging the use of the Pd in more recent studies. As cathode catalyst, almost all groups used Pt as it presents the highest activity towards ORR although presenting a low selectivity, which makes fuel crossover a major concern. However, $CoSe_2$ was proposed as a cheap highly fuel-tolerant cathode catalyst to replace Pt [25]. The maximum power density was 45 mW cm^{-2}, which was obtained in a passive-micro-FC with Nafion® 117 membrane, operating with 5.0 M formic acid, Pd catalyst anode, and Pt catalyst cathode [141].

4.8 Ethylene Glycol Oxidation Reaction (EGOR)

Ethylene glycol is considered a less volatile substitute for ethanol in DLFCs [147]. As the C–C bond is much difficult to break at near ambient temperatures, ethanol oxidation is hardly complete in FCs, generating mostly acetate [127, 148]. Therefore, the actual electron transfer rate (ETR) is only 33% of the theoretical one considering complete oxidation to carbon dioxide. On the other hand, EGOR in FCs occurs mainly to oxalate, presenting a high 80% actual ETR [35, 149]. Matsuoka et al. [150] proposed a dual pathway mechanism for the electro-oxidation of ethylene glycol in alkaline media. One pathway is non-poisoning, leading to the formation of oxalate, which is stable in alkaline media. The other one promotes the ethylene glycol oxidation to adsorbed CO species with formate as an intermediate, poisoning the catalyst active sites, which can be mitigated by carefully selecting an adequate catalyst.

In addition, EG has the potential to be a major energy carrier as it can be electrochemically produced by using an external power source, which can be from renewable energy [151, 152]. These characteristics increased the research interest in the development of micro-direct ethylene glycol fuel cells (μDEGFCs).

Table 4.6 shows the available experimental data for μDEGFCs, considering only the FCs with a maximum 2.50 cm^2 active area, regardless of the FC fabrication technique used. In all these papers, the μDEGFCs were active with the EG and potassium hydroxide solution pumped at a constant flow rate to the anode. Most studies developed membraneless microfluidic FCs as a promising simple design for miniaturization in order to avoid the need of a membrane, achieving high performance at ambient temperature [153–155]. However, alkali-doped polybenzimidazole membrane (APM) [156] and a commercial AEM [157] were also tested at higher temperatures.

An et al. [156] developed a FC with Pd–Ni/C anode and Fe–Co cathode catalysts and an APM, achieving the highest peak power densities of 80 mW cm^{-2} at 60 °C

Table 4.6 Active micro-direct ethylene glycol fuel cells performance

References	Active area (cm^2)	P_{max} (mW cm^{-2})	T (°C)	[EG] (M)	[KOH] (M)	Membrane	Anode	Cathode
[156]	1	80[a]	60	1	7	APM[a]	Pd–Ni/C (1 mg cm^{-2})	Fe–Co HYPERMEC (1 mg cm^{-2})
[156]	1	112[a]	90	1	7	APM[a]	Pd–Ni/C (1 mg cm^{-2})	Fe–Co HYPERMEC (1 mg cm^{-2})[b]
[156]	1	92	90	1	7	APM[a]	Pd–Ni/C (1 mg cm^{-2})	Fe–Co HYPERMEC (1 mg cm^{-2})
[153]	0.07	1.6	20	2	0.3	Membraneless	Au–Pd/polyaniline (1:20)	–
[154]	0.02	19	20	0.1	0.3	Membraneless	Cu@Pd/C core@shell	Pt/C
[157]	1	67	60	1	7	AEM (28 μm)	Pd–Ni/C (2 mg cm^{-2})	Non-Pt HYPERMEC (1 mg cm^{-2})
[157]	1	35	60	1	1	AEM (28 μm)	Pd–Ni/C (2 mg cm^{-2})	Non-Pt HYPERMECTM (1 mg cm^{-2})
[155]	0.015	30.3	20	1.5	1	Membraneless	Pt/C/CP[c] (E-TEK 47%)	Pt/C/CP[c] (E-TEK 47%)
[155]	0.015	24	20	0.075	1	Membraneless	Pt/C/CP[c] (E-TEK 47%)	Pt/C/CP[c] (E-TEK 47%)

[a]Alkali-doped polybenzimidazole membrane
[b]Pure oxygen supplied to the anode
[c]Carbon paper

and 112 mW cm^{-2} at 90 °C. They showed that the best performance occurs with 1.0 M ethylene glycol and 7.0 M KOH solution as fuel. It must be noticed that these two results were obtained with pure oxygen supplied to the cathode, but a high power density of 92 mW cm^{-2} was also obtained at 90 °C with air supplied to the cathode. These achieved power densities are much higher than An et al. [157] obtained in the same conditions with a commercial AEM, suggesting that APM presents a better operation stability at high temperatures up to 100 °C. At ambient temperature (20 °C), the highest reported power density of 30.3 mW cm^{-2} was obtained in a 0.015 cm^2 microfluidic FC operating with ethylene glycol 1.5 M and KOH 1.0 M solution as fuel and Pt/C as both anode and cathode catalysts.

4.9 Glycerol Oxidation Reaction (GlyOR)

Glycerol is a non-toxic, non-flammable, and non-volatile compound already available in large quantities as a byproduct in biodiesel production. It has been regarded as a promising fuel for DLFCs due to its high intrinsic energy density and its ability to co-generate valuable chemicals otherwise costly to produce [158–161]. In addition, glycerol crossover rate through membranes is very low, especially if compared to methanol crossover [162]. Therefore, there is a research interest in the development of micro-direct glycerol fuel cells (μDGlyFC).

Table 4.7 displays the available experimental data for μDGlyFCs, considering only the FCs with a 2.50 cm^2 maximum active area, regardless of the fabrication technique used. In all studies, only active membraneless microfluidic FCs were tested. Cu deposited on Pd/C [154, 163], Cu deposited on Pt/C [163], Pd/C [164], Pd on multi-walled carbon nanotubes (MWCNTs) [164], and Pt/C [155] were used as anode catalysts while only Pt/C was employed as cathode catalyst. Martins et al. [155] verified that the FC peak power density decreases as the glycerol concentration is increased in the fuel inlet stream. This decreasing performance is caused by increasing flow viscosity, cell resistance, and limited mass transport as this fuel concentration increases. The highest reported peak power density is 39.5 mW cm^{-2} with the low 0.05 M glycerol concentration at ambient temperature, confirming that glycerol has the potential to be a cost-effective fuel for micro-FCs.

4.10 Glucose Oxidation Reaction (GOR)

Glucose sugar that powers human cells is one of the most interesting biomass fuels, because it is renewable, cheap, abundant, non-flammable, non-toxic, and can be easily handled and obtained. Its complete oxidation can produce very high energy density (4430 W h kg^{-1}). To access this energy glucose should be used as fuel of a direct glucose fuel cell (DGFC), where glucose is directly oxidized to generate electricity, similarly to DMFCs or DEFCs [165].

Table 4.7 Active micro-direct glycerol fuel cells performance

References	Active area (cm^2)	P_{max} (mW cm^{-2})	T (°C)	[Gly] (M)	[KOH] (M)	Anode	Cathode
[154]	0.02	20	25	0.1	0.3	Cu–Pd/C	Pt/C
[163]	0.02	17.4	25	5 vol %	0.3	Cu–Pd/C	Pt/C
[163]	0.02	23.2	25	5 vol %	0.3	Cu–Pt/C	Pt/C
[164]	0.45	0.51	30	0.1	0.3	Pd/C (30 wt% (1.3 mg cm^{-2} Pd)	Pt/C (0.54 mg cm^{-2})
[164]	0.45	0.7	30	0.1	0.3	Pd/MWCNT (12 wt%) (1.6 mg cm^{-2} Pd)[a]	Pt/C (0.54 mg cm^{-2})
[155]	0.015	39.5	25	0.05	1	Pt/C/CP[b]	Pt/C/CP[b]
[155]	0.015	38.7	25	0.1	1	Pt/C/CP[b]	Pt/C/CP[b]
[155]	0.015	29.8	25	0.5	1	Pt/C/CP[b]	Pt/C/CP[b]
[155]	0.015	25.2	25	1	1	Pt/C/CP[b]	Pt/C/CP[b]
[155]	0.015	24.4	25	2	1	Pt/C/CP[b]	Pt/C/CP[b]

[a]Multi-walled carbon nanotubes
[b]Carbon paper as diffusion layer

FCs based in glucose oxidation reaction (GOR) can be divided into three major groups: enzymatic, microbial, and abiotic FCs [166]. Enzymatic FCs use isolated enzymes as catalyst to the glucose oxidation, facilitating the glucose molecular bonds cleavage, and they were initially considered to supply energy to implantable devices but the enzymes activity tends to deteriorate too quickly for such applications. Microbial FCs use microorganisms to provide the enzymatic environment to catalyze the GOR, which is also a difficult strategy to sustain in the long term due to the cells colonies instability and the risk these microbes can present if exposed to the human organism in the case of implantable devices [167]. Abiotic catalyzed FCs use more conventional metallic catalysts, such as Pt, Au, Pd, and its alloys. Although the first two types were more studied in the past 20 years, there is a growing interest in the development of abiotic glucose-consuming micro-FCs due to its greater stability in the long term and operation safety [168]. Abiotic catalyzed DGFCs can take two forms, external and implantable. The external DGFCs can be used to power consumer electronics, miniature toys, kits and gadgets, portable military equipment, and other portable low-power devices [166].

Implantable μDGFCs are particularly interesting because of the abundance of oxygen and glucose in the body tissue and the possibility to generate a stable high continuous power output through the coupling of the GOR and ORR [169, 170]. The μDGFC could be used to operate devices, such as pacemakers, small valves for urinary bladder control, cochlear implants to treat profound deafness, deep brain stimulators to treat symptoms of Parkinson's disease, peripheral nerve stimulation for pain control, and arms and legs movement on paralyzed patients [169, 170]. This

makes the investigation on glucose electro-oxidation a very interesting research topic. This part of chapter will focus essentially on implantable μDGFCs.

The principle approach concept of μDGFCs goes back to the 1970s [171]. Current research is now focused on the development of: (1) new highly porous electrodes that can efficiently and selectively catalyze GOR and ORR in body; (2) membranes; (3) micro–nano cell fabrication; and (4) in vitro and in vivo tests.

Research on electrodes has been extremely active as demonstrated by the huge number of papers published in the literature. Pt and Au have been extensively used. However, Pt is non-selective and is poisoned by various components of blood and other physiological media, and Au requires a higher potential for GOR. At present, Au-, Pt-, and Pd-based bi- or tri-metallic catalysts, as well as non-noble metal compounds, have been found to exhibit catalytic activity with respect to GOR in alkaline media [172–175].

In the context of implantable devices, noble metal catalysts are considered to be favorable because they are biocompatible, allow the heat sterilization, and in contrast to enzymes are not subject to denaturation and loss of catalytic activity [176, 177].

An implantable μDGFC operates at near neutral pH, 37 °C, and where both reactants, i.e., glucose (3–5 mM) and oxygen (ca. 7%) are present, and consequently, the key for a good performance of μDGFCs is the use of both a glucose selective anode and an oxygen selective cathode.

Pt and tailored graphene materials particularly in flexible and miniaturized forms may be used as cathode catalysts [166, 178]. The simplicity with which tailored graphene materials can be produced by various low-cost large-scale methods, including the chemical vapor deposition, chemical reduction of graphite oxide, microwave plasma reaction, among others, suggests considerable cost-effective preparation of metal-free efficient graphene-based catalysts for ORR [179]. On the other hand, Do et al. [180] reported electrodes working as nanoporous oxygen selective cathodes prepared by depositing Pd thin films by e-beam evaporation on anodized aluminum oxide membrane substrates.

The anodes are essentially based on porous Pt or Pt alloys, fabricated by electro-deposition or from carbon-supported nanoparticles. If Pt-based catalysts are used, glucose is predominantly oxidized by a two electron transfer reaction to gluconic acid in an acid or neutral media [166]. Activated carbon with 5% Pt + 5% Bi [181] and, in particular, Raney-type catalysts, fabricated from Pt–Ni [170, 182], Zn [183, 184], and Al [169, 185] were used as anodes by many research teams. However, the use of Ni is not indicating for implantable electrodes because of its allergenic and carcinogenic properties [183].

Very recently, the Kerzenmacher's group have developed highly porous Pt anodes by cyclic or pulsed electrodeposition. It is based on the co-deposition of Pt and the less noble metal Cu, followed by a selective dissolution of Cu at an oxidizing potential. Upon repeated deposition/dissolution cycles or potentials, electrodes with high roughness factors were obtained [176, 186–188]. The pulsed electrodeposition process was also applied to prepare highly porous Pt–Cu electrodes with Pd, Ru, or Au [189]. Frei et al. [177] developed a highly porous Pt deposited onto a three-dimensional electrospun carbon fiber mat support. The GO anodes allow continuous

operation in horse serum during 30 days and 15 days in simulated tissue fluid at a current density of 7.2 ± 1.9 μA cm^{-2} and 0.061 ± 0.007 μA cm^{-2}, respectively. Also, this electrode showed an enhanced resistance towards poisoning by tissue fluids components [177].

In addition, Qazzazie et al. [190] fabricated Pt nanowires anchored on graphene-supported Pt nanoparticles. The anode's surface roughness was increased by factors up to 4000 to the geometrical surface area allowing maximized use of the Pt towards GO and efficient electron transfer between nanowires and the substrate. It is shown that the unique three-dimensional geometry of the nanostructures had a significant impact on their catalytic activity presenting short diffusional paths for slow glucose species and then, mass transport limitations are optimized leading to lower polarization losses.

Non-noble metal-based anodes, e.g., Cu–S has also been studied in 0.1 M phosphate buffer solution (pH 7.2) in the presence of 10^{-4} M glucose [191]. Table 4.8 summarizes the most important achievements of abiotic implantable μDGFCs.

Implantable μDGFC prototypes were first tested successfully in the 1970s in the subcutaneous tissue of dogs (2.2 μW cm^{-2}, OCV 0.65 V) for 30 days [168, 171]. However, no further development has been reported probably due to the strong involvement of industry and the introduction of lithium-iodine batteries for cardiac pacemakers in the mid-1970s [168]. In the last decade the implantable μDGFCs concept has gained growing attention, and a number of studies have been reported based on the optimization of the fuel cell power output.

Most of these works have been performed in idealized buffer systems with only glucose and oxygen present as reactants. Considering estimated physiological concentrations (phosphate-buffered saline (PBS) solution (pH 7.4), 3.0 mM glucose, 7.0% O_2 saturation), and in view of the reduced reactant supply due to tissue capsule formation maximum power densities of 3.3 ± 0.2 μW cm^{-2} [181], 2.2 ± 0.1 μW cm^{-2} for a single-layer fuel cell (SLFC) [192], 4.4 ± 0.2 μW cm^{-2} [184], 5.1 μW cm^{-2} [176, 186], and 6.3 ± 0.7 μW cm^{-2} have been reached [193]. This power density is sufficient to power, e.g., a cardiac pacemaker consuming 5–10 μW [176].

Rapoport et al. [169] reported power densities of up to 3.4 μW cm^{-2} steady-state power and up to 180 μW cm^{-2} peak power in PBS with 10 mM glucose and oxygen concentration is not given. The cerebrospinal fluid had also favorable conditions in terms of glucose and oxygen concentrations for implanted μDGFCs. The anode is a high-surface-area Raney nanostructured Pt–Al and the cathode is a network of single-walled carbon nanotubes embedded in a Nafion® film. The electrodes are separated by a Nafion® membrane.

When operate in stagnant conditions, the glucose/O_2 FC with Nafion® membrane using 7-nm Au nanowires (AuNWs) or 2-nm AuNWs as anode catalyst exhibits power output of 126 and 49.3 μW cm^{-2}, respectively, in 0.1 M PBS, 30 mM glucose, and O_2-bubling electrolyte [194], which is much higher that of a membraneless single compartment FC (16.2 μW cm^{-2}) [195].

Oncescu et al. [170, 182] developed μDGFCs without a separation membrane in order to improve glucose diffusion to the anode and reduce the thickness of the FC

Table 4.8 Most relevant abiotic implantable micro-direct glucose fuel cells performance

References	P_{max} ($\mu W\ cm^{-2}$)	[Glucose] (mM) or tissue	O_2 (%)	Membrane	Anode	Cathode
[165]	110	In vivo— subcutaneous neck layer brain of rat	(same)	–	Au–Zn dendrites-SPME[a]	(same)
[165]	290	In vitro— blood sample	In vitro—blood sample	Nafion® 115	Au–Zn dendrites	(same)
[169]	3.4/180	10	–	Nafion	Raney Pt–Al	SWCNT[b]
[170]	2.0	3	7	–	Raney Pt–Ni	Pt on membranes
[171]	2.2	In vivo—subcutaneous dog	(same)	–	–	Pt
[176]	5.1	3	7	Supor-450	Pt–Cu/Silicon	Pt/Silicon
[181]	3.3	3	7	Polyethersulfone	Activated carbon (5% Pt + 5% Bi)	Activated carbon
[182]	2.0	3	7	SLFC[c]	Raney Pt–Ni	Pt/CP
[184]	4.4	3	7	Porous	Raney Pt–Zn	Raney Pt
[186]	5.1	3	7	Silicon membrane	Pt–Cu	Pt/Silicon
[192]	2.2	3	7	SLFC[c]	Raney Pt–Zn	Raney Pt–Al
[193]	6.3	3	7	Supor-450	Pt–Cu	Pt–Cu/ silicon
[194]	126	30	Saturated	Nafion® 117	7 nm AuNWs[d]	Pt/C
[194]	49.3	30	Saturated	Nafion® 117	2 nm AuNWs[d]	Pt/C
[195]	16.2	5	–	Membraneless	Al/Au/ZnO	Pt rod
[196]	10	In vivo—venous blood	(same)	Mesoporous silica thin film	Pt/Si	RGO[e]
[196]	6	In vitro—blood sample	(same)	Mesoporous silica thin film	Pt/Si	RGO[e]

[a]Carbon screen-printed micro film electrodes
[b]Single-walled carbon nanotube mesh
[c]Single layer fuel cell
[d]Gold nanowires
[e]Reduced graphene oxide

and two designs, oxygen depletion and a SLFC. The anode was Pt–Ni Raney electrode. Under physiological concentrations similar to those described by Kerzenmacher's group [181] the peak power output of both FCs is ca. 2.0 μW cm^{-2}. A stacked FC unit of 12 SLFCs may provide a high volumetric power density (16 μW cm^{-2}).

Although a few attempts have been made recently to test in vivo implantable body glucose/O_2 FCs in pigs and rats [165, 196], the devices have not achieved commercialization yet.

One example is FCs with microelectrodes (polymer/Au–Zn dendrites with carbon screen-printed microfilm electrodes) which were implanted in the subcutaneous layer of the neck and brain of Wistar rats separately. The in vivo power density 0.11 μW cm^{-2} of the implantable FCs with Au–Zn dendrites was lower than that obtained for the in vitro blood sample (0.29 μW cm^{-2}), because of the different glucose concentrations. The microfilm FC implanted into the rat brain produced ca. 0.52 V continuously operating during 18 days [165].

Sharma et al. [196] assembled a μDGFC composed of mesoporous silica coated Pt anodes, polymer membrane and reduced graphene oxide pressed on stainless steel mesh was used as the cathode. The device was implanted into venous blood of a pig with power output of 10 μW cm^{-2}. In this case, the power density in vivo was higher than that of in vitro (6 μW cm^{-2}). Unfortunately, the total time of study was 12 min because the pig died.

4.11 Future Prospects

This study is a brief summary of the state of-up-to-date DLFCs. Portable applications for DLFCs are mainly focused on the market of portable power generators designed for light outdoor personal uses such as camping, light commercial applications such as portable signage and surveillance, power for emergency relief, consumer electronic devices, and military equipment. However, their cost and durability are yet to meet set targets.

μDMFC issues in need of attention include Pt and membranes high cost, the high methanol crossover rates, preventing the use of high concentration methanol solutions, and catalyst poisoning caused by adsorbed CO species produced during methanol electro-oxidation reaction. Therefore, future research may address these issues through the development of membraneless microfluidic micro-FCs, whose cheap and simple design are ideal for cost-effective micro-FCs mass production. In addition, the development of low-Pt trimetallic or Pt-free anode catalysts and methanol-tolerant cathode catalysts may further decrease the CO-poisoning effects and the efficiency losses caused by methanol crossover, respectively.

Aspects of AEMs stable and high-conductive development, acquisition of fundamental mechanism knowledge, and improvement on anode catalysts with high activity, durability, and selectivity are required. It must be noticed that no studies covering the development and performance of membraneless microfluidic μDEFCs

were found in the literature. Then an important topic in the future research it will be consider this design that has already been successfully tested for methanol. In addition, future work covering others oxidants sources in micro-FCs than atmospheric and dissolved oxygen gas, such as hydrogen peroxide, are important to increase the micro-FC's onset potential. Similarly, work on microfluidic μFACFs and AEM-μDEGFC is needed for its cost-effective large-scale commercialization.

Glycerol electro-oxidation mechanism is not yet fully understood, so further studies in this field could boost the development of better catalysts. Another important research topic will be the development of glycerol fuel additives in order to decrease the fuel viscosity and increase its conductivity. This approach would allow the use of more concentrated glycerol fuel solutions, increasing the fuel energy density. Finally, there is also a growing research interest in the development of multi-fuel μDLFC, as fuel mixtures can present synergetic effects to increase the FC power output [154, 155, 162].

Glucose FCs look very promising as a source of power for implanted devices because they could use glucose from body tissues as a source of power. Pioneering work by Drake and co-authors in the 1970s raised hopes that abiotic catalysts could oxidize glucose and reduce oxygen sufficiently to enable powering medical devices.

However, implanted μDGFCs are relatively new and still required a more complete understanding of the host to produce power in vivo. Both, the subcutaneous tissue and the cerebrospinal cavity are considered as body places for implantation. The amino acids and small organic molecules present at physiological concentration in simulated tissue fluid and simulated cerebrospinal fluid adsorb on the surface of Pt electrodes and reduce significantly their catalytic activity for GOR. However, even in the presence of poisoning compounds a residual GOR current remains. Then, the highest challenge for these FCs is to develop anode catalysts with very high specific surface, i.e., highly porous to increase the residual GOR current in the presence of endogenous amino acids [193, 197].

4.12 Acknowledgements

This work was supported by Fundação para a Ciência e a Tecnologia (FCT) (PTDC/CTM-NAN/0956/2014, POCI-01-0145-FEDER-016884, and UID/QUI/00616/2013) and UniRCell (SAICTPAC/0032/2015 and POCI-01-0145-FEDER-01642). R. Oliveira thanks FCT for UniRCell grant (BIM/UTAD/43/2017). J. Santander thanks the financial support of the Spanish project TEC2016-78284-C3-1/2-R (AEI/FEDER, UE).

References

1. Sadhasivam T, Dhanabalan K, Roh SH, Kim TH, Park KW, Jung S, Kurkuri MD, Jung HY (2017) A comprehensive review on unitized regenerative fuel cells: crucial challenges and developments. Int J Hydrog Energy 42:4415–4433. https://doi.org/10.1016/j.ijhydene.2016.10.140
2. Nguyen N-T, Chan SH (2006) Micromachined polymer electrolyte membrane and direct methanol fuel cells-a review. J Micromech Microeng 16:R1–R12. https://doi.org/10.1088/0960-1317/16/4/R01
3. Pichonat T, Gauthier-Manuel B (2007) Recent developments in MEMS-based miniature fuel cells. Microsyst Technol 13:1671–1678. https://doi.org/10.1007/s00542-006-0342-5
4. Sundarrajan S, Allakhverdiev SI, Ramakrishna S (2012) Progress and perspectives in micro direct methanol fuel cell. Int J Hydrog Energy 37:8765–8786. https://doi.org/10.1016/j.ijhydene.2011.12.017
5. Esquivel JP, Sabaté N, Santander J, Torres N, Cané C (2008) Fabrication and characterization of a passive silicon-based direct methanol fuel cell. Microsyst Technol 14:535–541. https://doi.org/10.1007/s00542-007-0451-9
6. Torres N, Santander J, Esquivel JP, Sabaté N, Figueras E, Ivanov P, Fonseca L, Gràcia I, Cané C (2008) Performance optimization of a passive silicon-based micro-direct methanol fuel cell. Sensors Actuators B Chem 132:540–544. https://doi.org/10.1016/j.snb.2007.11.035
7. Esquivel JP, Sabaté N, Santander J, Torres-Herrero N, Gràcia I, Ivanov P, Fonseca L, Cané C (2009) Influence of current collectors design on the performance of a silicon-based passive micro direct methanol fuel cell. J Power Sources 194:391–396. https://doi.org/10.1016/j.jpowsour.2009.04.065
8. Zhao TS, Chen R, Yang WW, Xu C (2009) Small direct methanol fuel cells with passive supply of reactants. J Power Sources 191:185–202. https://doi.org/10.1016/j.jpowsour.2009.02.033
9. Wang C, Waje M, Wang X, Tang JM, Haddon RC, Yan Y (2004) Proton exchange membrane fuel cells with carbon nanotube based electrodes. Nano Lett 4:345–348. https://doi.org/10.1021/nl034952p
10. Esquivel JP, Sabaté N, Tarancón A, Torres-Herrero N, Dávila D, Santander J, Gràcia I, Cané C (2009) Hybrid polymer electrolyte membrane for silicon-based micro fuel cells integration. J Micromech Microeng 19:65006 https://doi.org/10.1088/0960-1317/19/6/065006
11. Torres N, Duch M, Santander J, Sabaté N, Esquivel JP, Tarancón A, Cané C (2009) Porous silicon membrane for micro fuel cell applications. J New Mater Electrochem Syst 12:93–96
12. Esquivel JP, Senn T, Hernández-Fernández P, Santander J, Lörgen M, Rojas S, Löchel B, Cané C, Sabaté N (2010) Towards a compact SU-8 micro-direct methanol fuel cell. J Power Sources 195:8110–8115. https://doi.org/10.1016/j.jpowsour.2010.07.050
13. Moghaddam S, Pengwang E, Jiang Y-B, Garcia AR, Burnett DJ, Brinker CJ, Masel RI, Shannon MA (2010) An inorganic-organic proton exchange membrane for fuel cells with a controlled nanoscale pore structure. Nat Nanotechnol 5:230–236. https://doi.org/10.1038/nnano.2010.13
14. Xing X, Cherevko S, Chung CH (2011) Porous Pd films as effective ethanol oxidation electrocatalysts in alkaline medium. Mater Chem Phys 126:36–40. https://doi.org/10.1016/j.matchemphys.2010.12.027
15. Kouassi S, Gautier G, Thery J, Desplobain S, Borella M, Ventura L, Laurent JY (2012) Proton exchange membrane micro fuel cells on 3D porous silicon gas diffusion layers. J Power Sources 216:15–21. https://doi.org/10.1016/j.jpowsour.2012.05.046
16. Sabaté N, Esquivel JP, Santander J, Hauer JG, Verjulio RW, Gràcia I, Salleras M, Calaza C, Figueras E, Cané C, Fonseca L (2014) New approach for batch microfabrication of silicon-based micro fuel cells. Microsyst Technol 20:341–348. https://doi.org/10.1007/s00542-013-1781-4

17. Kjeang E, Djilali N, Sinton D (2009) Microfluidic fuel cells: a review. J Power Sources 186:353–369. https://doi.org/10.1016/j.jpowsour.2008.10.011
18. Zebda A, Renaud L, Cretin M, Pichot F, Innocent C, Ferrigno R, Tingry S (2009) A microfluidic glucose biofuel cell to generate micropower from enzymes at ambient temperature. Electrochem Commun 11:592–595. https://doi.org/10.1016/j.elecom.2008.12.036
19. Mousavi Ehteshami SM, Asadnia M, Tan SN, Chan SH (2016) Paper-based membraneless hydrogen peroxide fuel cell prepared by micro-fabrication. J Power Sources 301:392–395. https://doi.org/10.1016/j.jpowsour.2015.10.038
20. Abrego-Martínez JC, Wang Y, Mendoza-Huizar LH, Ledesma-Garcia J, Cuevas-Muñiz FM, Mohamedi M, Arriaga LG (2016) Mixed-reactant ethanol fuel cell using an electrochemically deposited Ag@Pt tolerant cathode. Int J Hydrog Energy 41:23417–23424. https://doi.org/10.1016/j.ijhydene.2016.09.032
21. Tang Y, Yuan W, Pan M, Tang B, Li Z, Wan Z (2010) Effects of structural aspects on the performance of a passive air-breathing direct methanol fuel cell. J Power Sources 195:5628–5636. https://doi.org/10.1016/j.jpowsour.2010.03.069
22. Li X, Faghri A, Xu C (2010) Structural optimization of the direct methanol fuel cell passively fed with a high-concentration methanol solution. J Power Sources 195:8202–8208. https://doi.org/10.1016/j.jpowsour.2010.06.041
23. Feng Y, Gago A, Timperman L, Alonso-Vante N (2011) Chalcogenide metal centers for oxygen reduction reaction: activity and tolerance. Electrochim Acta 56:1009–1022. https://doi.org/10.1016/j.electacta.2010.09.085
24. Zhao X, Yin M, Ma L, Liang L, Liu C, Liao J, Lu T, Xing W (2011) Recent advances in catalysts for direct methanol fuel cells. Energy Environ Sci 4:2736–2753. https://doi.org/10.1039/c1ee01307f
25. Gago AS, Gochi-Ponce Y, Feng YJ, Esquivel JP, Sabaté N, Santander J, Alonso-Vante N (2012) Tolerant chalcogenide cathodes of membraneless micro fuel cells. ChemSusChem 5:1488–1494. https://doi.org/10.1002/cssc.201200009
26. Weiland M, Wagner S, Hahn R, Reichl H (2013) Design and evaluation of a passive self-breathing micro fuel cell for autonomous portable applications. Int J Hydrog Energy 38:440–446. https://doi.org/10.1016/j.ijhydene.2012.09.117
27. Xiaowei L, Chunguang S, Yufeng Z, Wei W, Xuebin L, Ding T (2006) Application of MEMS technology to micro direct methanol fuel cell. Proceedings of the 1st IEEE International Conference on Nano/Micro Engineered and Molecular Systems, NEMS'06, pp 699–702
28. Scotti G, Kanninen P, Kallio T, Franssila S (2012) Integration of carbon felt gas diffusion layers in silicon micro fuel cells. J Micromech Microeng 22:94006. https://doi.org/10.1088/0960-1317/22/9/094006
29. Yeom J, Mozsgai GZ, Flachsbart BR, Choban ER, Asthana A, Shannon MA, Kenis PJA (2005) Microfabrication and characterization of a silicon-based millimeter scale, PEM fuel cell operating with hydrogen, methanol, or formic acid. Sensors Actuators B Chem 107:882–891. https://doi.org/10.1016/j.snb.2004.12.050
30. Chang CL, Chang TC, Ho WY, Hwang JJ, Wang DY (2006) Electrochemical performance of PEM fuel cell with Pt-Ru electro-catalyst layers deposited by sputtering. Surf Coat Technol 201:4442–4446. https://doi.org/10.1016/j.surfcoat.2006.08.036
31. Tang YH, Huang MJ, Shiao MH, Yang CR (2011) Fabrication of silicon nanopillar arrays and application on direct methanol fuel cell. Microelectron Eng 88:2580–2583. https://doi.org/10.1016/j.mee.2010.12.075
32. Jeng KT, Chien CC, Hsu NY, Yen SC, Chiou SD, Lin SH, Huang WM (2006) Performance of direct methanol fuel cell using carbon nanotube-supported Pt-Ru anode catalyst with controlled composition. J Power Sources 160:97–104. https://doi.org/10.1016/j.jpowsour.2006.01.057
33. Saha MS, Kundu A (2010) Functionalizing carbon nanotubes for proton exchange membrane fuel cells electrode. J Power Sources 195:6255–6261. https://doi.org/10.1016/j.jpowsour.2010.04.015

34. Varcoe JR, Slade RCT (2005) Prospects for alkaline anion-exchange membranes in low temperature fuel cells. Fuel Cells 5:187–200. https://doi.org/10.1002/fuce.200400045
35. Antolini E, Gonzalez ER (2010) Alkaline direct alcohol fuel cells. J Power Sources 195:3431–3450. https://doi.org/10.1016/j.jpowsour.2009.11.145
36. Yu EH, Wang X, Krewer U, Li L, Scott K (2012) Direct oxidation alkaline fuel cells: from materials to systems. Energy Environ Sci 5:5668–5680 https://doi.org/10.1039/C2EE02552C
37. Varcoe JR, Atanassov P, Dekel DR, Herring AM, Hickner MA, Kohl PA, Kucernak AR, Mustain WE, Nijmeijer K, Scott K, Xu T, Zhuang L (2014) Anion-exchange membranes in electrochemical energy systems. Energy Environ Sci 7:3135–3191. https://doi.org/10.1039/C4EE01303D
38. Verjulio RW, Alcaide F, Álvarez G, Sabaté N, Torres-Herrero N, Esquivel JP, Santander J (2013) A micro alkaline direct ethanol fuel cell with platinum-free catalysts. J Micromech Microeng 23:115006. https://doi.org/10.1088/0960-1317/23/11/115006
39. Verjulio RW, Santander J, Sabaté N, Esquivel JP, Torres-Herrero N, Habrioux A, Alonso-Vante N (2014) Fabrication and evaluation of a passive alkaline membrane micro direct methanol fuel cell. Int J Hydrog Energy 39:5406–5413. https://doi.org/10.1016/j.ijhydene.2013.12.014
40. Verjulio RW, Santander J, Ma J, Alonso-Vante N (2016) Selective CoSe/C cathode catalyst for passive air-breathing alkaline anion exchange membrane μ-direct methanol fuel cell (AEM-μDMFC). Int J Hydrog Energy 41:19595–19600 https://doi.org/10.1016/j.ijhydene.2016.01.132
41. Zhao TS, Yang WW, Chen R, Wu QX (2010) Towards operating direct methanol fuel cells with highly concentrated fuel. J Power Sources 195:3451–3462. https://doi.org/10.1016/j.jpowsour.2009.11.140
42. Li X, Faghri A (2013) Review and advances of direct methanol fuel cells (DMFCs) part I: design, fabrication, and testing with high concentration methanol solutions. J Power Sources 226:223–240. https://doi.org/10.1016/j.jpowsour.2012.10.061
43. Gago AS, Esquivel J-P, Sabate N, Santander J, Alonso-Vante N (2015) Comprehensive characterization and understanding of micro-fuel cells operating at high methanol concentrations. Beilstein J Nanotechnol 6:2000–2006 https://doi.org/10.3762/bjnano.6.203
44. Shimizu T, Momma T, Mohamedi M, Osaka T, Sarangapani S (2004) Design and fabrication of pumpless small direct methanol fuel cells for portable applications. J Power Sources 137:277–283. https://doi.org/10.1016/j.jpowsour.2004.06.008
45. Aravamudhan S, Rahman ARA, Bhansali S (2005) Porous silicon based orientation independent, self-priming micro direct ethanol fuel cell. Sensors Actuators A Phys 123–124:497–504. https://doi.org/10.1016/j.sna.2005.03.069
46. Chan SH, Nguyen N-T, Xia Z, Wu Z (2005) Development of a polymeric micro fuel cell containing laser-micromachined flow channels. J Micromech Microeng 15:231–236 https://doi.org/10.1088/0960-1317/15/1/032
47. Schmitz A, Tranitz M, Wagner S, Hahn R, Hebling C (2003) Planar self-breathing fuel cells. J Power Sources 118:162–171. https://doi.org/10.1016/S0378-7753(03)00080-6
48. Kamarudin SK, Achmad F, Daud WRW (2009) Overview on the application of direct methanol fuel cell (DMFC) for portable electronic devices. Int J Hydrog Energy 34:6902–6916. https://doi.org/10.1016/j.ijhydene.2009.06.013
49. Abrego-Martínez JC, Moreno-Zuria A, Cuevas-Muñiz FM, Arriaga LG, Sun S, Mohamedi M (2017) Design, fabrication and performance of a mixed-reactant membraneless micro direct methanol fuel cell stack. J Power Sources 371:10–17. https://doi.org/10.1016/j.jpowsour.2017.10.026
50. Kauranen PS, Skou E (1996) Mixed methanol oxidation/oxygen reduction currents on a carbon supported Pt catalyst. J Electroanal Chem 408:189–198. https://doi.org/10.1016/0022-0728(96)04515-9

51. Piela B, Olson TS, Atanassov P, Zelenay P (2010) Highly methanol-tolerant non-precious metal cathode catalysts for direct methanol fuel cell. Electrochim Acta 55:7615–7621. https://doi.org/10.1016/j.electacta.2009.11.085
52. Abrego-Martínez JC, Wang Y, Ledesma-García J, Cuevas-Muñiz FM, Arriaga LG, Mohamedi M (2017) A pulsed laser synthesis of nanostructured bi-layer platinum-silver catalyst for methanol-tolerant oxygen reduction reaction. Int J Hydrog Energy 42:28056–28062. https://doi.org/10.1016/j.ijhydene.2017.02.165
53. Yuan Z, Yang J, Zhang Y, Zhang X (2015) The optimization of air-breathing micro direct methanol fuel cell using response surface method. Energy 80:340–349. https://doi.org/10.1016/j.energy.2014.11.076
54. Falcão DS, Oliveira VB, Rangel CM, Pinto AMFR (2014) Review on micro-direct methanol fuel cells. Renew Sust Energ Rev 34:58–70. https://doi.org/10.1016/j.rser.2014.03.004
55. Lamy C, Lima A, LeRhun V, Delime F, Coutanceau C, Léger JM (2002) Recent advances in the development of direct alcohol fuel cells (DAFC). J Power Sources 105:283–296. https://doi.org/10.1016/s0378-7753(01)00954-5
56. Tiwari JN, Tiwari RN, Singh G, Kim KS (2013) Recent progress in the development of anode and cathode catalysts for direct methanol fuel cells. Nano Energy 2:553–578. https://doi.org/10.1016/j.nanoen.2013.06.009
57. Vijh AK (1975) Electrocatalysis of the anodic oxidation of methanol by metals. J Catal 37:410–415. https://doi.org/10.1016/0021-9517(75)90177-3
58. Bagotzky VS, Vassiliev YB, Khazova OA (1977) Generalized scheme of chemisorption, electrooxidation and electroreduction of simple organic compounds on platinum group metals. J Electroanal Chem 81:229–238. https://doi.org/10.1016/S0022-0728(77)80019-3
59. Antolini E (2009) Palladium in fuel cell catalysis. Energy Environ Sci 2:915–931. https://doi.org/10.1039/b820837a
60. Wang H, Xu C, Cheng F, Zhang M, Wang S, Jiang SP (2008) Pd/Pt core-shell nanowire arrays as highly effective electrocatalysts for methanol electrooxidation in direct methanol fuel cells. Electrochem Commun 10:1575–1578. https://doi.org/10.1016/j.elecom.2008.08.011
61. Tripkovic AV, Popovic KD, Grgur BN, Blizanac B, Ross PN, Markovi NM (2002) Methanol electrooxidation on supported Pt and PtRu catalysts in acid and alkaline solutions. Electrochim Acta 47:3707–3714. https://doi.org/10.1016/S0013-4686(02)00340-7
62. Demirci UB (2007) Theoretical means for searching bimetallic alloys as anode electrocatalysts for direct liquid-feed fuel cells. J Power Sources 173:11–18. https://doi.org/10.1016/j.jpowsour.2007.04.069
63. Patel PP, Datta MK, Jampani PH, Hong D, Poston JA, Manivannan A, Kumta PN (2015) High performance and durable nanostructured TiN supported Pt –Ru anode catalyst for direct methanol fuel cell (DMFC). J Power Sources 293:437–446. https://doi.org/10.1016/j.jpowsour.2015.05.051
64. Alcaide F, Álvarez G, Cabot PL, Genova-Koleva R, Grande HJ, Miguel O (2017) Effect of the solvent in the catalyst ink preparation on the properties and performance of unsupported PtRu catalyst layers in direct methanol fuel cells. Electrochim Acta 231:529–538. https://doi.org/10.1016/j.electacta.2017.02.127
65. Xu C, Cheng L, Shen P, Liu Y (2007) Methanol and ethanol electrooxidation on Pt and Pd supported on carbon microspheres in alkaline media. Electrochem Commun 9:997–1001. https://doi.org/10.1016/j.elecom.2006.12.003
66. Karim NA, Kamarudin SK (2013) An overview on non-platinum cathode catalysts for direct methanol fuel cell. Appl Energy 103:212–220. https://doi.org/10.1016/j.apenergy.2012.09.031
67. Mahajan A, Banik S, Roy PS, Chowdhury SR, Bhattacharya SK (2017) Kinetic parameters of anodic oxidation of methanol in alkali: effect of diameter of Pd nano-catalyst, composition of electrode and solution and mechanism of the reaction. Int J Hydrog Energy 42:21263–21278. https://doi.org/10.1016/j.ijhydene.2017.07.058

68. Deng H, Zhang Y, Zheng X, Li Y, Zhang X, Liu X (2015) A CNT (carbon nanotube) paper as cathode gas diffusion electrode for water management of passive μ-DMFC (micro-direct methanol fuel cell) with highly concentrated methanol. Energy 82:236–241. https://doi.org/10.1016/j.energy.2015.01.034
69. Xue R, Zhang Y, Liu X (2017) A novel cathode gas diffusion layer for water management of passive μ-DMFC. Energy 139:535–541 https://doi.org/10.1016/j.energy.2017.08.016
70. Wang M, Liu L, Wang X (2017) A novel proton exchange membrane based on sulfo functionalized porous silicon for monolithic integrated micro direct methanol fuel cells. Sensors Actuators B Chem 253:621–629. https://doi.org/10.1016/j.snb.2017.06.173
71. Falcão DS, Pereira JP, Rangel CM, Pinto AMFR (2015) Development and performance analysis of a metallic passive micro-direct methanol fuel cell for portable applications. Int J Hydrog Energy 40:5408–5415. https://doi.org/10.1016/j.ijhydene.2015.01.034
72. Falcão DS, Pereira JP, Pinto AMFR (2016) Effect of stainless steel meshes on the performance of passive micro direct methanol fuel cells. Int J Hydrog Energy 41:13859–13867. https://doi.org/10.1016/j.ijhydene.2016.05.059
73. Hsieh SS, Ho CC, Hung LC (2016) Performance tests of a double-passive μDMFC stack with parallel/dendrite flow field. Renew Energy 90:28–37. https://doi.org/10.1016/j.renene.2015.12.056
74. Zhang Y, Xue R, Zhang X, Song J, Liu X (2015) RGO deposited in stainless steel fiber felt as mass transfer barrier layer for μ-DMFC. Energy 91:1081–1086. https://doi.org/10.1016/j.energy.2015.09.026
75. Yuan Z, Zhang M, Zuo K, Ren Y (2018) The effect of gravity on inner transport and cell performance in passive micro direct methanol fuel cell. Energy 150:28–37 https://doi.org/10.1016/j.energy.2018.02.132
76. Deng H, Zhang Y, Li Y, Zhang X, Liu X (2013) A CNT-MEA compound structure of micro-direct methanol fuel cell for water management. Microelectron Eng 110:288–291. https://doi.org/10.1016/j.mee.2013.02.013
77. Deng H, Zhang X, Ma Z, Chen H, Sun Q, Zhang Y, Liu X (2014) A micro passive direct methanol fuel cell with high performance via plasma electrolytic oxidation on aluminum-based substrate. Energy 78:149–153. https://doi.org/10.1016/j.energy.2014.09.070
78. Zhou Y, Wang X, Guo X, Qiu X, Liu L (2012) A water collecting and recycling structure for silicon-based micro direct methanol fuel cells. Int J Hydrog Energy 37:967–976. https://doi.org/10.1016/j.ijhydene.2011.03.086
79. Baranton S, Coutanceau C, Léger JM, Roux C, Capron P (2005) Alternative cathodes based on iron phthalocyanine catalysts for mini- or micro-DMFC working at room temperature. Electrochim Acta 51:517–525. https://doi.org/10.1016/j.electacta.2005.05.010
80. Wang SJ, Huo WW, Zou ZQ, Qiao YJ, Yang H (2011) Computational simulation and experimental evaluation on anodic flow field structures of micro direct methanol fuel cells. Appl Therm Eng 31:2877–2884. https://doi.org/10.1016/j.applthermaleng.2011.05.013
81. Hashim N, Kamarudin SK, Daud WRW (2009) Design, fabrication and testing of a PMMA-based passive single-cell and a multi-cell stack micro-DMFC. Int J Hydrog Energy 34:8263–8269. https://doi.org/10.1016/j.ijhydene.2009.07.043
82. Zhang Q, Wang X, Zhong L, Zhou Y, Qiu X, Liu L (2009) Design, optimization and microfabrication of a micro-direct methanol fuel cell with microblocks in anode structure. Sensors Actuators A Phys 154:247–254. https://doi.org/10.1016/j.sna.2008.07.008
83. Lu GQ, Wang CY, Yen TJ, Zhang X (2004) Development and characterization of a silicon-based micro direct methanol fuel cell. Electrochim Acta 49:821–828. https://doi.org/10.1016/j.electacta.2003.09.036
84. Yuan Z, Zhang Y, Leng J, Gao Y, Liu X (2012) Development of a 4-cell air-breathing micro direct methanol fuel cell stack. J Power Sources 202:134–142. https://doi.org/10.1016/j.jpowsour.2011.10.090

85. Wang Z, Zhang X, Nie L, Zhang Y, Liu X (2014) Elimination of water flooding of cathode current collector of micro passive direct methanol fuel cell by superhydrophilic surface treatment. Appl Energy 126:107–112. https://doi.org/10.1016/j.apenergy.2014.03.029
86. Ghayor R, Shakeri M, Sedighi K, Farhadi M (2010) Experimental and numerical investigation on passive and active μDMFC. Int J Hydrog Energy 35:9329–9337 https://doi.org/10.1016/j.ijhydene.2009.09.066
87. Seo YH, Cho YH (2009) Micro direct methanol fuel cells and their stacks using a polymer electrolyte sandwiched by multi-window microcolumn electrodes. Sensors Actuators A Phys 150:87–96. https://doi.org/10.1016/j.sna.2008.12.009
88. Peng HC, Chen PH, Chen HW, Chieng CC, Yeh TK, Pan C, Tseng FG (2010) Passive cathodic water/air management device for micro-direct methanol fuel cells. J Power Sources 195:7349–7358. https://doi.org/10.1016/j.jpowsour.2010.05.007
89. Qiao H, Kunimatsu M, Okada T (2005) Pt catalyst configuration by a new plating process for a micro tubular DMFC cathode. J Power Sources 139:30–34. https://doi.org/10.1016/j.jpowsour.2004.07.003
90. Li Y, Zhang X, Nie L, Zhang Y, Liu X (2014) Stainless steel fiber felt as cathode diffusion backing and current collector for a micro direct methanol fuel cell with low methanol crossover. J Power Sources 245:520–528. https://doi.org/10.1016/j.jpowsour.2013.06.122
91. Xue R, Sang S, Jin H, Shen Q, Zhang Y, Liu X, Zhang X (2014) Stainless steel fiber felt as the anode diffusion backing and current collector for μ-DMFC. Microelectron Eng 119:159–163. https://doi.org/10.1016/j.mee.2014.02.006
92. Fang S, Zhang Y, Ma Z, Zou Y, Liu X (2016) Development of a micro direct methanol fuel cell with heat control. Energy 116:978–985. https://doi.org/10.1016/j.energy.2016.10.034
93. Falcão DS, Oliveira VB, Rangel CM, Pinto AMFR (2015) Experimental and modeling studies of a micro direct methanol fuel cell. Renew Energy 74:464–470. https://doi.org/10.1016/j.renene.2014.08.043
94. Yuan Z, Yang J, Zhang Y, Wang S, Xu T (2015) Mass transport optimization in the anode diffusion layer of a micro direct methanol fuel cell. Energy 93:599–605. https://doi.org/10.1016/j.energy.2015.09.067
95. Yuan Z, Yang J, Li X, Wang S (2016) The micro-scale analysis of the micro direct methanol fuel cell. Energy 100:10–17. https://doi.org/10.1016/j.energy.2016.01.057
96. Weinmueller C, Tautschnig G, Hotz N, Poulikakos D (2010) A flexible direct methanol micro-fuel cell based on a metalized, photosensitive polymer film. J Power Sources 195:3849–3857. https://doi.org/10.1016/j.jpowsour.2009.12.092
97. Zhong L, Wang X, Jiang Y, Zhang Q, Qiu X, Zhou Y, Liu L (2008) A micro-direct methanol fuel cell stack with optimized design and microfabrication. Sensors Actuators A Phys 143:70–76. https://doi.org/10.1016/j.sna.2007.06.045
98. Wang X, Zhu Y, Shen C, Zhou Y, Wu X, Liu L (2012) A novel assembly method using multi-layer bonding technique for micro direct methanol fuel cells and their stack. Sensors Actuators A Phys 188:246–254. https://doi.org/10.1016/j.sna.2012.02.007
99. Zhang Y, Zhang P, He H, Zhang B, Yuan Z, Liu X, Cui H (2011) A self-breathing metallic micro-direct methanol fuel cell with the improved cathode current collector. Int J Hydrog Energy 36:857–868. https://doi.org/10.1016/j.ijhydene.2010.10.039
100. Hsieh SS, Wu HC, Her BS (2012) Design, fabrication and characterization of micro-electro mechanical system based micro direct methanol fuel cell stacks. Sensors Actuators A Phys 187:57–66. https://doi.org/10.1016/j.sna.2012.08.026
101. Zhang B, Zhang Y, He H, Li J, Yuan Z, Na C, Liu X (2010) Development and performance analysis of a metallic micro-direct methanol fuel cell for high-performance applications. J Power Sources 195:7338–7348. https://doi.org/10.1016/j.jpowsour.2010.05.011
102. D'Urso C, Baglio V, Antonucci V, Aricò AS, Specchia S, Icardi UA, Saracco G, Spinella C, D'Arrigo G (2011) Development of a planar μDMFC operating at room temperature. Int J Hydrog Energy 36:8088–8093 https://doi.org/10.1016/j.ijhydene.2011.01.109

103. Deng H, Sang S, Zhang Y, Li Z, Liu X (2013) Investigations of silicon-based air-breathing micro direct methanol fuel cells with different anode flow fields. Microelectron Eng 111:180–184. https://doi.org/10.1016/j.mee.2013.03.143
104. Shen M, Walter S, Dovat L, Gijs MAM (2011) Planar micro-direct methanol fuel cell prototyped by rapid powder blasting. Microelectron Eng 88:1884–1886. https://doi.org/10.1016/j.mee.2010.12.079
105. Chu YH, Shul YG (2010) Combinatorial investigation of Pt-Ru-Sn alloys as an anode electrocatalysts for direct alcohol fuel cells. Int J Hydrog Energy 35:11261–11270. https://doi.org/10.1016/j.ijhydene.2010.07.062
106. Liang J, Luo Y, Zheng S, Wang D (2017) Enhance performance of micro direct methanol fuel cell by in situ CO removal using novel anode flow field with superhydrophobic degassing channels. J Power Sources 351:86–95 https://doi.org/10.1016/j.jpowsour.2017.03.099
107. Falcão DS, Silva RA, Rangel CM, AMFR P (2017) Performance of an active micro direct methanol fuel cell using reduced catalyst loading MEAs. Energies 10:1683 https://doi.org/10.3390/en10111683
108. Cha HY, Choi HG, Nam JD, Lee Y, Cho SM, Lee ES, Lee JK, Chung CH (2004) Fabrication of all-polymer micro-DMFCs using UV-sensitive photoresist. Electrochim Acta 50:795–799. https://doi.org/10.1016/j.electacta.2004.01.117
109. Lu Y, Reddy RG (2011) Effect of flow fields on the performance of micro-direct methanol fuel cells. Int J Hydrog Energy 36:822–829. https://doi.org/10.1016/j.ijhydene.2010.10.029
110. Yuan Z, Yang J, Li Z, Sun Y, Ye N, Shen H (2015) Analysis of CO transmission in a micro direct methanol fuel cell. Energy 83:496–502 https://doi.org/10.1016/j.energy.2015.02.053
111. Yang J, Yuan Z, Shen H, Li X, Di J, Mo J (2016) Influence of anode flow field on mass transport in a air-breathing micro direct methanol fuel cell. Proceedings of the 2016 IEEE 11th Conference on Industrial Electronics and Applications, ICIEA 2016, pp 1843–1846
112. Yuan Z, Zhang Y, Fu W, Wang Z, Zhang X, Liu X (2014) Hydrophilicity effect on micro-scale flow of μDMFC. Microelectron Eng 119:131–136 https://doi.org/10.1016/j.mee.2014.03.024
113. Yuan Z, Fu W, Zhao Y, Li Z, Zhang Y, Liu X (2013) Investigation of μDMFC (micro direct methanol fuel cell) with self-adaptive flow rate. Energy 55:1152–1158. https://doi.org/10.1016/j.energy.2013.03.056
114. Yao SC, Tang X, Hsieh CC, Alyousef Y, Vladimer M, Fedder GK, Amon CH (2006) Micro-electro-mechanical systems (MEMS)-based micro-scale direct methanol fuel cell development. Energy 31:636–649. https://doi.org/10.1016/j.energy.2005.10.016
115. Kamarudin MZF, Kamarudin SK, Masdar MS, Daud WRW (2013) Review: direct ethanol fuel cells. Int J Hydrog Energy 38:9438–9453. https://doi.org/10.1016/j.ijhydene.2012.07.059
116. An L, Zhao TS, Chen R, Wu QX (2011) A novel direct ethanol fuel cell with high power density. J Power Sources 196:6219–6222. https://doi.org/10.1016/j.jpowsour.2011.03.040
117. Yang CC, Lee YJ, Chiu SJ, Lee KT, Chien WC, Lin CT, Huang CA (2008) Preparation of a PVA/HAP composite polymer membrane for a direct ethanol fuel cell (DEFC). J Appl Electrochem 38:1329–1337 https://doi.org/10.1007/s10800-008-9563-x
118. Yang CC, Chiu SJ, Lee KT, Chien WC, Lin CT, Huang CA (2008) Study of poly(vinyl alcohol)/titanium oxide composite polymer membranes and their application on alkaline direct alcohol fuel cell. J Power Sources 184:44–51. https://doi.org/10.1016/j.jpowsour.2008.06.011
119. Tadanaga K, Furukawa Y, Hayashi A, Tatsumisago M (2010) Direct ethanol fuel cell using hydrotalcite clay as a hydroxide ion conductive electrolyte. Adv Mater 22:4401–4404. https://doi.org/10.1002/adma.201001766
120. Xu JB, Zhao TS, Shen SY, Li YS (2010) Stabilization of the palladium electrocatalyst with alloyed gold for ethanol oxidation. Int J Hydrog Energy 35:6490–6500. https://doi.org/10.1016/j.ijhydene.2010.04.016
121. Xu JB, Zhao TS, Li YS, Yang WW (2010) Synthesis and characterization of the Au-modified Pd cathode catalyst for alkaline direct ethanol fuel cells. Int J Hydrog Energy 35:9693–9700. https://doi.org/10.1016/j.ijhydene.2010.06.074

122. Tsang CHA, Leung DYC (2018) Use of Pd-Pt loaded graphene aerogel on nickel foam in direct ethanol fuel cell. Solid State Sci 75:21–26. https://doi.org/10.1016/j.solidstatesciences.2017.11.005
123. ÜnlÜ M, Abbott D, Ramaswamy N, Ren X, Mukerjee S, Kohl PA (2011) Analysis of double layer and adsorption effects at the alkaline polymer electrolyte-electrode interface. J Electrochem Soc 158:B1423–B1431 https://doi.org/10.1149/2.075111jes
124. Fujiwara N, Siroma Z, Yamazaki S, Ioroi T, Senoh H, Yasuda K (2008) Direct ethanol fuel cells using an anion exchange membrane. J Power Sources 185:621–626. https://doi.org/10.1016/j.jpowsour.2008.09.024
125. Datta J, Dutta A, Biswas M (2012) Enhancement of functional properties of PtPd nano catalyst in metal-polymer composite matrix: application in direct ethanol fuel cell. Electrochem Commun 20:56–59. https://doi.org/10.1016/j.elecom.2012.02.022
126. Varela FJR, Savadogo O (2009) Ethanol-tolerant Pt-alloy cathodes for direct ethanol fuel cell (DEFC) applications. Asia-Pacific J Chem Eng 4:17–24 https://doi.org/10.1002/apj.193
127. An L, Zhao TS, Xu JB (2011) A bi-functional cathode structure for alkaline-acid direct ethanol fuel cells. Int J Hydrog Energy 36:13089–13095. https://doi.org/10.1016/j.ijhydene.2011.07.025
128. Li YS, Zhao TS (2011) A high-performance integrated electrode for anion-exchange membrane direct ethanol fuel cells. Int J Hydrog Energy 36:7707–7713. https://doi.org/10.1016/j.ijhydene.2011.03.090
129. An L, Zhao TS (2011) An alkaline direct ethanol fuel cell with a cation exchange membrane. Energy Environ Sci 4:2213–2217 https://doi.org/10.1039/c1ee00002k
130. Shen S, Zhao TS, Xu J, Li Y (2011) High performance of a carbon supported ternary PdIrNi catalyst for ethanol electro-oxidation in anion-exchange membrane direct ethanol fuel cells. Energy Environ Sci 4:1428–1433. https://doi.org/10.1039/c0ee00579g
131. An L, Zhao TS, Zeng L, Yan XH (2014) Performance of an alkaline direct ethanol fuel cell with hydrogen peroxide as oxidant. Int J Hydrog Energy 39:2320–2324. https://doi.org/10.1016/j.ijhydene.2013.11.072
132. An L, Zhao TS (2011) Performance of an alkaline-acid direct ethanol fuel cell. Int J Hydrog Energy 36:9994–9999. https://doi.org/10.1016/j.ijhydene.2011.04.150
133. Wang ED, Zhao TS, Yang WW (2010) Poly (vinyl alcohol)/3-(trimethylammonium) propyl-functionalized silica hybrid membranes for alkaline direct ethanol fuel cells. Int J Hydrog Energy 35:2183–2189. https://doi.org/10.1016/j.ijhydene.2009.12.179
134. Shen SY, Zhao TS, Wu QX (2012) Product analysis of the ethanol oxidation reaction on palladium-based catalysts in an anion-exchange membrane fuel cell environment. Int J Hydrog Energy 37:575–582. https://doi.org/10.1016/j.ijhydene.2011.09.077
135. Li YS, Zhao TS (2012) Ultra-low catalyst loading cathode electrode for anion-exchange membrane fuel cells. Int J Hydrog Energy 37:15334–15338. https://doi.org/10.1016/j.ijhydene.2012.07.119
136. Yu X, Pickup PG (2008) Recent advances in direct formic acid fuel cells (DFAFC). J Power Sources 182:124–132. https://doi.org/10.1016/j.jpowsour.2008.03.075
137. Jayashree RS, Spendelow JS, Yeom J, Rastogi C, Shannon MA, Kenis PJA (2005) Characterization and application of electrodeposited Pt, Pt/Pd, and Pd catalyst structures for direct formic acid micro fuel cells. Electrochim Acta 50:4674–4682. https://doi.org/10.1016/j.electacta.2005.02.018
138. Yeom J, Jayashree RS, Rastogi C, Shannon MA, Kenis PJA (2006) Passive direct formic acid microfabricated fuel cells. J Power Sources 160:1058–1064. https://doi.org/10.1016/j.jpowsour.2006.02.066
139. Wang T, Zeng Y, Zhao Z, Guo H (2015) A micro direct formic acid fuel cell with PDMS fluid flow plates. Key Eng Mater 645–646:724–729 https://doi.org/10.4028/www.scientific.net/KEM.645-646.724
140. Ha S, Adams B, Masel RI (2004) A miniature air breathing direct formic acid fuel cell. J Power Sources 128:119–124. https://doi.org/10.1016/j.jpowsour.2003.09.071

141. Cai W, Liang L, Zhang Y, Xing W, Liu C (2013) Real contribution of formic acid in direct formic acid fuel cell: investigation of origin and guiding for micro-structure design. Int J Hydrog Energy 38:212–218 https://doi.org/10.1016/j.ijhydene.2012.09.155
142. Rejal SZ, Masdar MS, Kamarudin SK (2014) A parametric study of the direct formic acid fuel cell (DFAFC) performance and fuel crossover. Int J Hydrog Energy 39:10267–10274. https://doi.org/10.1016/j.ijhydene.2014.04.149
143. Qiao H, Shiroishi H, Okada T (2007) Passive micro tubular direct formic acid fuel cells (DFAFCs) with chemically assembled Pd anode nano-catalysts on polymer electrolytes. Electrochim Acta 53:59–65. https://doi.org/10.1016/j.electacta.2007.01.046
144. Jayashree RS, Gancs L, Choban ER, Primak A, Natarajan D, Markoski LJ, Kenis PJA (2005) Air-breathing laminar flow-based microfluidic fuel cell. J Am Chem Soc 127:16758–16759 https://doi.org/10.1021/ja054599k
145. Shaegh SAM, Nguyen NT, Chan SH (2012) Air-breathing microfluidic fuel cell with fuel reservoir. J Power Sources 209:312–317 https://doi.org/10.1016/j.jpowsour.2012.02.115
146. Chu KL, Gold S, Subramanian VR, Lu C, Shannon MA, Masel RI (2006) A nanoporous silicon membrane electrode assembly for on-chip micro fuel cell applications. J Microelectromech Syst 15:671–677 https://doi.org/10.1109/JMEMS.2006.872223
147. An L, Chen R (2016) Recent progress in alkaline direct ethylene glycol fuel cells for sustainable energy production. J Power Sources 329:484–501. https://doi.org/10.1016/j.jpowsour.2016.08.105
148. An L, Chai ZH, Zeng L, Tan P, Zhao TS (2013) Mathematical modeling of alkaline direct ethanol fuel cells. Int J Hydrog Energy 38:14067–14075. https://doi.org/10.1016/j.ijhydene.2013.08.080
149. Bianchini C, Shen PK (2009) Palladium-based electrocatalysts for alcohol oxidation in half cells and in direct alcohol fuel cells. Chem Rev 109:4183–4206. https://doi.org/10.1021/cr9000995
150. Matsuoka K, Iriyama Y, Abe T, Matsuoka M, Ogumi Z (2005) Electro-oxidation of methanol and ethylene glycol on platinum in alkaline solution: poisoning effects and product analysis. Electrochim Acta 51:1085–1090. https://doi.org/10.1016/j.electacta.2005.06.002
151. Ma S, Sadakiyo M, Luo R, Heima M, Yamauchi M, Kenis PJA (2016) One-step electrosynthesis of ethylene and ethanol from CO in an alkaline electrolyzer. J Power Sources 301:219–228 https://doi.org/10.1016/j.jpowsour.2015.09.124
152. Zheng MY, Wang AQ, Ji N, Pang JF, Wang XD, Zhang T (2010) Transition metal-tungsten bimetallic catalysts for the conversion of cellulose into ethylene glycol. ChemSusChem 3:63–66. https://doi.org/10.1002/cssc.200900197
153. Arjona N, Palacios A, Moreno-Zuria A, Guerra-Balcázar M, Ledesma-Garcia J, Arriaga LG (2014) AuPd/polyaniline as the anode in an ethylene glycol microfluidic fuel cell operated at room temperature. Chem Commun 50:8151–8153. https://doi.org/10.1039/c4cc03288h
154. Maya-Cornejo J, Ortiz-Ortega E, Álvarez-Contreras L, Arjona N, Guerra-Balcázar M, Ledesma-García J, Arriaga LG (2015) Copper–palladium core–shell as an anode in a multi-fuel membraneless nanofluidic fuel cell: toward a new era of small energy conversion devices. Chem Commun 51:2536–2539 https://doi.org/10.1039/c4cc08529a
155. Martins CA, Ibrahim OA, Pei P, Kjeang E (2018) Towards a fuel-flexible direct alcohol microfluidic fuel cell with flow-through porous electrodes: assessment of methanol, ethylene glycol and glycerol fuels. Electrochim Acta 271:537–543 https://doi.org/10.1016/j.electacta.2018.03.197
156. An L, Zeng L, Zhao TS (2013) An alkaline direct ethylene glycol fuel cell with an alkali-doped polybenzimidazole membrane. Int J Hydrog Energy 38:10602–10606. https://doi.org/10.1016/j.ijhydene.2013.06.042
157. An L, Zhao TS, Shen SY, Wu QX, Chen R (2010) Performance of a direct ethylene glycol fuel cell with an anion-exchange membrane. Int J Hydrog Energy 35:4329–4335. https://doi.org/10.1016/j.ijhydene.2010.02.009

158. Anitha M, Kamarudin SK, Kofli NT (2016) The potential of glycerol as a value-added commodity. Chem Eng J 295:119–130. https://doi.org/10.1016/j.cej.2016.03.012
159. Palma LM, Almeida TS, Morais C, Napporn TW, Kokoh KB, de Andrade AR (2017) Effect of the Co-catalyst on the selective electrooxidation of glycerol over ruthenium based nanomaterials. ChemElectroChem 4:39–45 https://doi.org/10.1002/celc.201600406
160. Simões M, Baranton S, Coutanceau C (2012) Electrochemical valorisation of glycerol. ChemSusChem 5:2106–2124. https://doi.org/10.1002/cssc.201200335
161. Kwon Y, Hersbach TJP, Koper MTM (2014) Electro-oxidation of glycerol on platinum modified by adatoms: activity and selectivity effects. Top Catal 57:1272–1276. https://doi.org/10.1007/s11244-014-0292-6
162. Livshits V, Peled E (2006) Progress in the development of a high-power, direct ethylene glycol fuel cell (DEGFC). J Power Sources 161:1187–1191. https://doi.org/10.1016/j.jpowsour.2006.04.141
163. Maya-Cornejo J, Guerra-Balcázar M, Arjona N, Álvarez-Contreras L, FJR V, Gurrola MP, Ledesma-García J, Arriaga LG (2016) Electrooxidation of crude glycerol as waste from biodiesel in a nanofluidic fuel cell using Cu@Pd/C and Cu@Pt/C. Fuel 183:195–205 https://doi.org/10.1016/j.fuel.2016.06.075
164. Dector A, Cuevas-Muñiz FM, Guerra-Balcázar M, Godínez LA, Ledesma-García J, Arriaga LG (2013) Glycerol oxidation in a microfluidic fuel cell using Pd/C and Pd/MWCNT anodes electrodes. Int J Hydrog Energy 38:12617–12622. https://doi.org/10.1016/j.ijhydene.2012.12.030
165. Noh HB, Naveen MH, Choi YJ, Choe ES, Shim YB (2015) Implantable nonenzymatic glucose/O micro film fuel cells assembled with hierarchical AuZn electrodes. Chem Commun 51:6659–6662 https://doi.org/10.1039/c5cc01567g
166. Santiago Ó, Navarro E, Raso MA, Leo TJ (2016) Review of implantable and external abiotically catalysed glucose fuel cells and the differences between their membranes and catalysts. Appl Energy 179:497–522. https://doi.org/10.1016/j.apenergy.2016.06.136
167. Santoro C, Arbizzani C, Erable B, Ieropoulos I (2017) Microbial fuel cells: from fundamentals to applications. A review. J Power Sources 356:225–244. https://doi.org/10.1016/j.jpowsour.2017.03.109
168. Kerzenmacher S, Ducrée J, Zengerle R, von Stetten F (2008) Energy harvesting by implantable abiotically catalyzed glucose fuel cells. J Power Sources 182:1–17. https://doi.org/10.1016/j.jpowsour.2008.03.031
169. Rapoport BI, Kedzierski JT, Sarpeshkar R (2012) A glucose fuel cell for implantable brain-machine interfaces. PLoS One 7:1–15. https://doi.org/10.1371/journal.pone.0038436
170. Oncescu V, Erickson D (2013) High volumetric power density, non-enzymatic, glucose fuel cells. Sci Rep 3:1226. https://doi.org/10.1038/srep01226
171. Drake RF, Messinger S, Matsuda S, Kusserow BK (1970) A tissue implantable fuel cell power supply. Trans Am Soc Artif Intern Organs 16:199–205
172. Jiang T, Yan L, Meng Y, Xiao M, Wu Z, Tsiakaras P, Song S (2015) Glucose electrooxidation in alkaline medium: performance enhancement of PdAu/C synthesized by NH modified pulse microwave assisted polyol method. Appl Catal B Environ 162:275–281 https://doi.org/10.1016/j.apcatb.2014.06.045
173. Mahoney EG, Sheng W, Cheng M, Lee KX, Yan Y, Chen JG (2016) Analyzing the electrooxidation of ethylene glycol and glucose over platinum-modified gold electrocatalysts in alkaline electrolyte using in-situ infrared spectroscopy. J Power Sources 305:89–96. https://doi.org/10.1016/j.jpowsour.2015.11.059
174. Brouzgou A, Song S, Tsiakaras P (2014) Carbon-supported PdSn and Pd Sn anodes for glucose electrooxidation in alkaline media. Appl Catal B Environ 158–159:209–216 https://doi.org/10.1016/j.apcatb.2014.03.051
175. Elouarzaki K, Le Goff A, Holzinger M, Thery J, Cosnier S (2012) Electrocatalytic oxidation of glucose by rhodium porphyrin-functionalized MWCNT electrodes: application to a fully

molecular catalyst-based glucose/O fuel cell. J Am Chem Soc 134:14078–14085 https://doi.org/10.1021/ja304589m
176. Kloke A, Köhler C, Zengerle R, Kerzenmacher S (2012) Porous platinum electrodes fabricated by cyclic electrodeposition of PtCu alloy: application to implantable glucose fuel cells. J Phys Chem C 116:19689–19698. https://doi.org/10.1021/jp306168t
177. Frei M, Erben J, Martin J, Zengerle R, Kerzenmacher S (2017) Nanofiber-deposited porous platinum enables glucose fuel cell anodes with high current density in body fluids. J Power Sources 362:168–173. https://doi.org/10.1016/j.jpowsour.2017.07.001
178. Hu C, Song L, Zhang Z, Chen N, Feng Z, Qu L (2015) Tailored graphene systems for unconventional applications in energy conversion and storage devices. Energy Environ Sci 8:31–54 https://doi.org/10.1039/c4ee02594f
179. Dai L, Chang DW, Baek J-B, Lu W (2012) Carbon nanomaterials for advanced energy conversion and storage. Small 8:1130–1166. https://doi.org/10.1002/smll.201101594
180. Do UP, Seland F, Maharbiz MM, Wang K, Johannesen Ø, Johannessen EA (2016) Thin film nanoporous electrodes for the selective catalysis of oxygen in abiotically catalysed micro glucose fuel cells. J Mater Sci 51:9095–9107. https://doi.org/10.1007/s10853-016-0162-7
181. Kerzenmacher S, Ducrée J, Zengerle R, von Stetten F (2008) An abiotically catalyzed glucose fuel cell for powering medical implants: reconstructed manufacturing protocol and analysis of performance. J Power Sources 182:66–75. https://doi.org/10.1016/j.jpowsour.2008.03.049
182. Oncescu V, Erickson D (2011) A microfabricated low cost enzyme-free glucose fuel cell for powering low-power implantable devices. J Power Sources 196:9169–9175. https://doi.org/10.1016/j.jpowsour.2011.06.100
183. Kerzenmacher S, Schroeder M, Brämer R, Zengerle R, von Stetten F (2010) Raney-platinum film electrodes for potentially implantable glucose fuel cells. Part 1: nickel-free glucose oxidation anodes. J Power Sources 195:6516–6523. https://doi.org/10.1016/j.jpowsour.2010.04.039
184. Kerzenmacher S, Kräling U, Metz T, Zengerle R, Von Stetten F (2011) A potentially implantable glucose fuel cell with Raney-platinum film electrodes for improved hydrolytic and oxidative stability. J Power Sources 196:1264–1272. https://doi.org/10.1016/j.jpowsour.2010.08.019
185. Kerzenmacher S, Kräling U, Schroeder M, Brämer R, Zengerle R, von Stetten F (2010) Raney-platinum film electrodes for potentially implantable glucose fuel cells. Part 2: glucose-tolerant oxygen reduction cathodes. J Power Sources 195:6524–6531. https://doi.org/10.1016/j.jpowsour.2010.04.049
186. Kloke A, Köhler C, Gerwig R, Zengerle R, Kerzenmacher S (2012) Cyclic electrodeposition of PtCu alloy: facile fabrication of highly porous platinum electrodes. Adv Mater 24:2916–2921. https://doi.org/10.1002/adma.201200806
187. Kloke A, Köhler C, Dryzga A, Gerwig R, Schumann K, Ade M, Zengerle R, Kerzenmacher S (2013) Fabrication of highly porous platinum by cyclic electrodeposition of PtCu alloys: how do process parameters affect morphology. J Electrochem Soc 160:D111–D118 https://doi.org/10.1149/2.001304jes
188. Köhler C, Kloke A, Drzyzga A, Zengerle R, Kerzenmacher S (2013) Fabrication of highly porous platinum electrodes for micro-scale applications by pulsed electrodeposition and dealloying. J Power Sources 242:255–263. https://doi.org/10.1016/j.jpowsour.2013.05.035
189. Frei M, Köhler C, Dietel L, Martin J, Wiedenmann F, Zengerle R, Kerzenmacher S (2018) Pulsed electro-deposition of highly porous Pt-alloys for use in methanol, formic acid, and glucose fuel cells. ChemElectroChem 5:1013–1023 https://doi.org/10.1002/celc.201800035
190. Qazzazie D, Yurchenko O, Urban S, Kieninger J, Urban G (2017) Platinum nanowires anchored on graphene-supported platinum nanoparticles as a highly active electrocatalyst towards glucose oxidation for fuel cell applications. Nanoscale 9:6436–6447 https://doi.org/10.1039/c7nr01391d

191. Yang YJ, Li W, Zi J (2013) Mechanistic study of glucose oxidation on copper sulfide modified glassy carbon electrode. Electrochem Commun 34:304–307. https://doi.org/10.1016/j.elecom.2013.07.012
192. Kloke A, Biller B, Krälling U, Kerzenmacher S, Zengerle R, Von Stetten F (2011) A single layer glucose fuel cell intended as power supplying coating for medical implants. Fuel Cells 11:316–326. https://doi.org/10.1002/fuce.201000114
193. Köhler C, Frei M, Zengerle R, Kerzenmacher S (2014) Performance loss of a Pt-based implantable glucose fuel cell in simulated tissue and cerebrospinal fluids. ChemElectroChem 1:1895–1900. https://doi.org/10.1002/celc.201402138
194. Yang L, Zhang Y, Chu M, Deng W, Tan Y, Ma M, Su X, Xie Q, Yao S (2014) Facile fabrication of network film electrodes with ultrathin Au nanowires for nonenzymatic glucose sensing and glucose/O_2 fuel cell. Biosens Bioelectron 52:105–110. https://doi.org/10.1016/j.bios.2013.08.038
195. Slaughter G, Sunday J (2014) A membraneless single compartment abiotic glucose fuel cell. J Power Sources 261:332–336. https://doi.org/10.1016/j.jpowsour.2014.03.090
196. Sharma T, Hu Y, Stoller M, Feldman M, Ruoff RS, Ferrari M, Zhang X (2011) Mesoporous silica as a membrane for ultra-thin implantable direct glucose fuel cells. Lab Chip 11:2460–2465. https://doi.org/10.1039/c1lc20119k
197. Köhler C, Bleck L, Frei M, Zengerle R, Kerzenmacher S (2015) Poisoning of highly porous platinum electrodes by amino acids and tissue fluid constituents. ChemElectroChem 2:1785–1793. https://doi.org/10.1002/celc.201500215

Chapter 5
Application of Novel Carbonaceous Materials as Support for Fuel Cell Electrocatalysts

Abha Bharti and Gouri Cheruvally

Abstract Low-temperature fuel cells are potential candidates in alternative energy industry due to their high energy efficiencies and near zero emissions. Typically, carbon supported Pt-based materials are used as electrocatalysts for anode and cathode reactions in low-temperature fuel cells. Carbon black (CB) is the most commonly employed support material for Pt-based electrocatalysts. However, CB materials suffer from significant drawbacks such as poor corrosion resistance and limited mass transport of fuels to active catalyst sites. As an alternative to conventional CB support materials, carbon structures such as graphene, ordered mesoporous carbon, and the so-called green carbon have been successfully used in recent years as supports for the dispersion of fuel cell catalyst nanoparticles. This chapter briefly describes the newly developed carbonaceous nanostructures and their applications in low-temperature fuel cells.

Keywords Low-temperature fuel cells · PEMFC · DMFC · Carbonaceous support materials · Pt electrocatalysts · Oxygen reduction reaction · Methanol oxidation reaction · Carbon black · Graphene · Ordered mesoporous carbon · Green carbon · Synthesis techniques · Nanoparticles dispersion · Hard template · Soft template · CVD · Biomass · Chemical reduction · Surface functionalization · Hybrid nanocomposites

5.1 Introduction

The twenty-first century has witnessed tremendous increase in global energy demand, consequent to depletion of fossil fuel reserves and serious climate concerns due to emission of greenhouse gases, which has directed mankind to switch to alternate "greener" and sustainable energy sources. Towards this, fuel cells with

A. Bharti · G. Cheruvally (✉)
Propellants, Polymers, Chemicals and Materials Entity, Vikram Sarabhai Space Centre, Thiruvananthapuram, Kerala, India

F. J. Rodríguez-Varela, T. W. Napporn (eds.), *Advanced Electrocatalysts for Low-Temperature Fuel Cells*, https://doi.org/10.1007/978-3-319-99019-4_5

high energy conversion efficiencies and near zero emissions have emerged as prospective alternate energy conversion devices for portable, mobile, and stationary power applications [1–3]. Fuel cells are electrochemical devices which are capable of converting chemical energy of "fuels" directly into electrical energy surpassing the intermediate stages of heat generation and mechanical work (Carnot's cycle), typical of conventional power generation methods. Thus, fuel cells are devoid of thermodynamic limitations of heat engines, and hence, are more efficient [4]. Low-temperature fuel cells, particularly proton exchange membrane fuel cells (PEMFCs) and direct methanol fuel cells (DMFCs) are considered the most effective and environmentally sustainable power sources because of their simple operation, high energy density, rapid start-up and shut-down cycle under ambient conditions, and high efficiency [5]. However, the effective commercialization of these classes of fuel cells is limited by the high usage of expensive Pt-based catalysts for electrochemical reactions at anode as well as cathode amounting to almost 27–43% of the cost of a fuel cell stack [6]. In addition, the sluggish kinetics of oxygen reduction reaction (ORR) at the cathode of both PEMFC and DMFC along with complex methanol oxidation reaction (MOR) and self-poisoning of Pt by intermediate products such as CO at anode in DMFC needs significant improvement for their wide scale applications. Furthermore, the methanol crossover from anode to cathode in DMFC hampers the ORR performance due to simultaneous methanol oxidation and oxygen reduction resulting in mixed potential losses at cathode. Hence, it is imperative to develop electrocatalysts with improved catalytic activities and lower Pt content to realize the real commercialization of fuel cells.

It is well known that significant enhancement in electrocatalytic activity can be achieved by dispersion of Pt-based catalysts on nanostructured support materials with additional advantage of reduced noble metal consumption [7, 8]. In this regard, a good catalyst support should have large surface area for dispersion of catalyst particles, good electrical conductivity, and high electrochemical stability [7]. Moreover, the nature of supporting materials and synergistic interactions between metal nanoparticles (NPs) and support greatly influence the catalyst performance [9, 10]. Hence, the selection of suitable supporting materials is vital for the development of fuel cell technology. The most commonly employed support materials for Pt-based catalysts in low-temperature fuel cells are carbonaceous materials, specifically carbon black (CB, Vulcan XC-72) because of its large surface area, high electronic conductivity, and easy availability [11]. However, CB suffers from severe disadvantages such as poor electrochemical stability/corrosion resistance and mass transport limitation due to the presence of micropores less than 1 nm which hinders fuel supply to the reactive sites limiting the catalytic activity. The large number of micropores also results in low accessible surface area for the deposition of metal NPs leading to a lower electrochemical surface area (ESA) and poor catalytic activity. Therefore, various alternatives to CB support materials are being searched extensively.

Recently, nanostructured carbon materials such as graphene [6], networked mesostructured porous carbon materials, specifically ordered mesoporous carbons (OMCs) [12], and green carbons, *i.e.*, the carbon derived from renewable resources

(biomass), have emerged as promising support materials for low-temperature fuel cells [13]. The higher catalytic activity of the Pt-based catalysts supported on these nanostructured carbon supports than that of the same catalysts supported on CBs has been ascribed to a combination of their unique structures and properties such as high surface area, good electronic conductivity, chemical stability, and synergistic metal–support interactions. This chapter presents an overview of synthesis techniques of graphene, OMCs, and green carbons together with the application of these newly developed carbonaceous structures as support materials for low-temperature fuel cells.

5.2 Graphene

Graphene is a single atom thin sheet of sp^2 hybridized, hexagonally arranged carbon atoms in a honeycomb lattice and derives its name from the combination of graphite and alkene [14]. This remarkable two-dimensional (2D) material has aroused tremendous interest for further pursuance because of its many unique properties such as high specific surface area (SSA, theoretical value of 2630 $m^2\ g^{-1}$), superior electronic conductivity (10^3–10^4 S m^{-1}), robust mechanical properties, excellent stability, fast electron transfer capabilities, and low manufacturing cost [15]. Considering these exceptional attributes, graphene is being explored as a promising support material for Pt-based catalysts in low-temperature fuel cells. The 2D planar structure of graphene provides high surface area for deposition of the catalyst NPs which can interact through both the edge planes and basal planes of the carbon sheets. The presence of strong metal–support interaction in this planar structure also improves the stability of the nanocatalysts which is highly desirable for long duration operation of fuel cells. Since its discovery in 2004, graphene has been studied as a support material for fuel cell catalyst and evidenced tremendous advancement in this area of research during the past decade. In this section, the synthesis methodologies developed for this wonder material and graphene supported nanocatalysts are summarized. In addition, the catalytic activity and durability of catalysts supported on graphene are compared with those of catalysts supported on the commonly used CBs.

5.2.1 Synthesis Techniques

The first graphene sheets were obtained by extracting monolayer sheets from the three-dimensional graphite using Scotch tape method in 2004 [16]. Since then, different approaches have been explored for the production of monolayer graphene sheets from graphite [17–21]. Out of these, three primary methods have been reported to be quite successful. These include: (1) mechanical exfoliation, (2) chemical vapor deposition (CVD) onto metal or Si substrates, and (3) chemical,

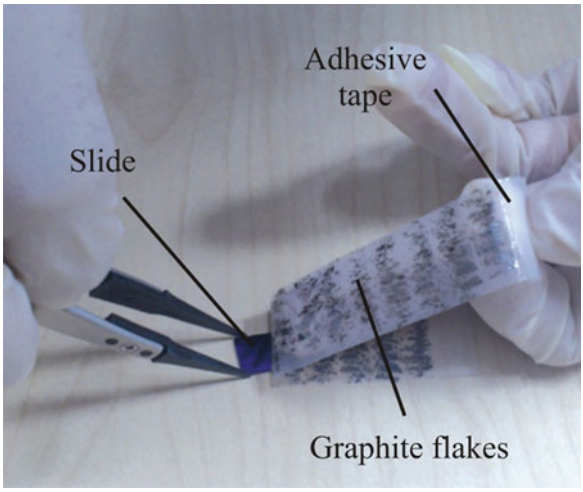

Fig. 5.1 Scotch tape procedure to get few-layer graphene. Reproduced with permission from Ref. [25], Copyright Nature, 2012

electrochemical, or thermal reduction of graphene oxide. Mechanical exfoliation is a top-down approach for preparing graphene with high carrier mobility (~10,000 cm^2 V^{-1} s^{-1}) and involves breaking apart of stacked layers of graphite to obtain single layer or few-layer sheets of graphene [22–24]. This micro-mechanical cleavage or more commonly, the scotch tape method, is quite straight-forward and requires no specialized equipment. The process typically involves placing of an adhesive tape onto the surface of graphite deposited on a silica slide and subsequently peeling it off to obtain thinner flakes (Fig. 5.1) [25, 26]. The whole process is repeated a number of times to obtain the desired graphene (single or few-layer) and is time consuming. Considering the inherent laborious process of this conventional micro-mechanical cleavage, Jayasena et al. introduced a novel lathe-like experimental setup utilizing ultra-sharp single crystal diamond wedge to cleave highly ordered pyrolytic graphite (HOPG) samples to produce few-layer graphene. Ultrasonic oscillations along the wedge assisted in cleaving HOPG for generating graphene flakes [27]. A modified scotch tape method-based exfoliation of natural graphite using three-roll mill machine with a polymer adhesive was reported by Chen et al. [28]. The employed polymer adhesive (polyvinyl chloride dissolved in dioctyl phthalate) has the same role as of tape adhesive in the original scotch tape method. The dispersion and exfoliation of graphite happen in the adhesive.

Graphene has been grown through CVD by high temperature pyrolysis of hydrocarbons using catalytic metals. CVD produces high quality graphene which can have high carrier mobility values, ~2000 to 4000 cm^2 V^{-1} s^{-1} [17]. The graphene growth via CVD can be categorized as proceeding either through surface catalyzed or segregation methods depending on the catalytic metal [21]. The solubility of the carbon containing species in the catalytic metal determines the dominant growth process. In surface catalyzed reactions, the decomposition of hydrocarbons occurs at metal surface and graphene growth is “self-limited” to monolayer. In the segregation method, the carbon dissolved in the bulk metal diffuses to the metal

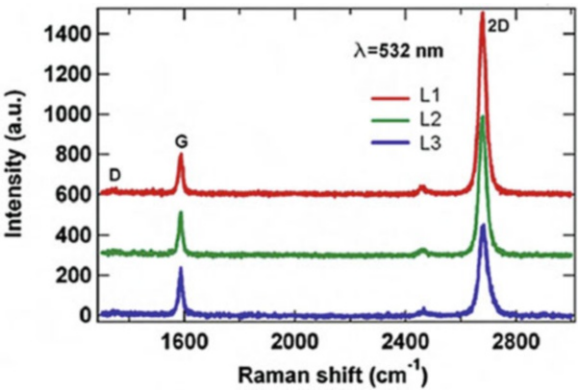

Fig. 5.2 Raman spectra of CVD graphene transferred to a Si/SiO_2 substrate. Reproduced with permission from Ref. [30], Copyright Elsevier, 2010

surface to produce graphene. CVD graphene growth is commonly performed using Cu and Ni catalysts [29]. Wu et al. reported wafer-scale synthesis of graphene on Cu foils by thermal CVD at a temperature of 1000 °C and under ambient pressure with methane as the precursor gas [30]. The Raman spectrum of graphene thus obtained (Fig. 5.2) showed I_{2D}/I_G ratio larger than 2, indicating formation of a monolayer. Van Nang et al. prepared few-layer graphene using Cu foil through inductively coupled plasma CVD within a duration of few seconds [31]. The authors demonstrated that the thickness of the graphene formed can be tuned by controlling the growth time and power of the plasma. Chae et al. reported synthesis of highly crystalline, large area graphene by CVD using poly-Ni substrate with C_2H_2/H_2 gas under optimized CVD conditions [32]. It was concluded that high temperature, short growth time, and an optimal gas mixing ratio were required to synthesize highly crystalline few-layer graphene.

Graphene can also be obtained via oxidation of graphite to graphene oxide which is based on many variations of the "Hummers method" invented by William Hummers in 1958 [33] and further reduction of graphene oxide to graphene. The Hummers method utilizes oxidation of graphite using powerful oxidizing agents and strong acids. The oxidation of the graphite results in an increase of interlayer spacing which facilitates the dispersion of graphene in appropriate solvents [23]. Also, the interlayer spacing is strongly dependent on the extent of oxidation of graphite and, hence, can be desirably tailored. The chemical oxidation of graphite produces graphene oxide which is further reduced through thermal, chemical, or electrochemical approach to get graphene. Iqbal and Abdala produced thermally reduced graphene (TRG) through thermal exfoliation of graphite oxide (GO) [34]. The oxidation of graphite was carried out through Staudenmaier method [35] using H_2SO_4, HNO_3, and potassium chlorate followed by rapid heating at 1000 °C in a tube furnace. TRG exhibited SSA of 210 $m^2\ g^{-1}$ and cumulative pore volume of 0.57 $cm^3\ g^{-1}$. The surface elemental composition analysis of TRG through X-ray photoelectron spectroscopy (XPS) revealed the presence of oxygen functional groups such as epoxy, hydroxyl, and carboxylic acid, which provides polar/hydrophilic nature to the graphene and assists in its dispersion in suitable solvents. In the

work of Choi et al., GO was first prepared by chemical oxidation of natural graphite with H_2SO_4, $K_2S_2O_8$, P_2O_5, and $KMnO_4$ [36]. The subsequent thermal exfoliation of GO at 830 °C under Ar atmosphere resulted in the formation of graphene nanosheets with surface oxygen functional groups (C–OH, C–O–C, and HO–C=O). A low-temperature hydrogen induced thermal exfoliation route was proposed by Kaniyoor et al. [37]. In contrast to conventional thermal exfoliation route, GO was exfoliated in the presence of hydrogen at a low temperature of 200 °C. Yan et al. also reported a low-temperature exfoliation method using $Mg(OH)_2$ nanosheets as template [38]. High surface area functionalized graphene nanosheets were obtained by heating the mixture of GO and $Mg(OH)_2$ at 300 °C for 2 h under N_2 atmosphere with a slow heating rate of 3 °C min^{-1}. Doping graphene with heteroatoms such as N, S, B, and P can effectively tune its electronic structure and other intrinsic properties which enhances its support characteristics [6, 39]. Sheng et al. reported synthesis of N-doped graphene through a facile, catalyst-free route by thermal annealing of GO and melamine (as nitrogen source) at 800 °C in a tubular furnace under Ar atmosphere [40]. Based on XPS analysis, a total of 10.1 wt.% of nitrogen was estimated in the graphene layers and the N 1s XPS spectrum showed that all nitrogen atoms were mostly in pyridine-like bonding configuration, which is known to improve electrocatalytic activity.

Utilizing chemical exfoliation of GO with hydrazine hydrate as reducing agent, Stankovich et al. prepared high surface area (466 $m^2 g^{-1}$) graphene nanosheets with good electrical conductivity (2×10^2 S m^{-1}) [41]. It was found that this reduction route resulted in the formation of unsaturated and conjugated carbon atoms which are responsible for imparting high electrical conductivity. Ramachandran et al. investigated the effect of concentration of reducing agent, $NaBH_4$ on synthesis, and properties of graphene from GO [42]. GO and $NaBH_4$ weight ratio was varied as 1:4, 1:8, 1:10, and 1:12 to prepare graphene by chemical exfoliation. Results demonstrated better reduction of GO and superior reduction of oxygen functional groups with the ratio of 1:10. Sridhar et al. employed a novel, microwave assisted chemical reduction approach to prepare graphene nanosheets [43]. In contrast to conventional chemical methods which utilize harsh oxidizers such as H_2SO_4/$KMnO_4$, here the reduction was carried out using eco-friendly chemicals (ammonium peroxy disulfate and hydrogen peroxide) and subsequent microwave irradiation resulted in rapid exfoliation of graphite. Wang et al. reported a low cost, scalable, and non-toxic green method for reduction of graphene oxide using green tea solution [44]. Chemical exfoliation of graphene oxide was achieved by utilizing the reducing capability and the aromatic rings of tea polyphenol (TP) in green tea. The strong interactions between the reduced graphene and the aromatic TPs imparted good dispersibility of the resultant graphene in both aqueous and a variety of organic solvents. The results also demonstrated efficient removal of the oxygen-containing groups in graphene oxide with TPs.

Electrochemical methods are also employed for the reduction of graphene oxide to remove the oxygen functionalities and improve the electronic properties of graphene formed. The electrochemical reduction of graphene oxide is typically carried out in a standard electrochemical cell with a non-hazardous aqueous

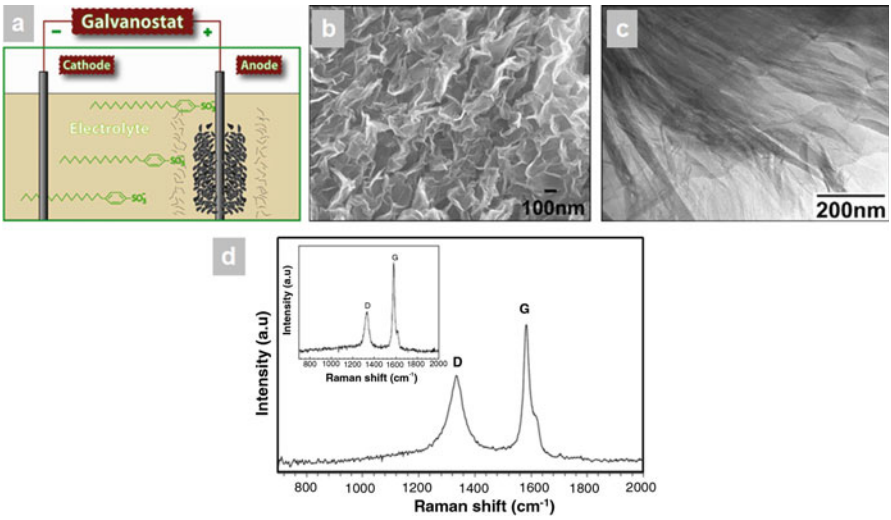

Fig. 5.3 (**a**) Experimental setup for synthesis of graphene via electrolytic exfoliation, (**b**) FESEM image of the bulk graphene powders, (**c**) TEM image of graphene sheets, and (**d**) Raman spectrum of the bulk graphene nanosheet powders. The inset is the Raman spectrum of the pristine graphite rod. Reproduced with permission from Ref. [47], Copyright Elsevier, 2009

electrolyte at room temperature with an applied potential [45]. The properties of the electrochemically reduced graphene oxide can be tuned by controlling the electrolysis parameters and electrolyte [46]. Wang et al. prepared graphene through electrolytic exfoliation of graphite using poly(sodium-4-styrenesulfonate) as an effective electrolyte [47]. A constant dc potential of 5 V was applied to two graphite rods placed in an electrolysis cell filled with the electrolyte and the electrolytic exfoliation continued for 4 h. The experimental setup is shown in Fig. 5.3a. The formation of monolayer graphene sheets and stacks containing a few-layer graphene sheets was confirmed through FESEM and TEM images (Fig. 5.3b, c, respectively). Furthermore, more intense G band as compared to D band was observed in the Raman spectrum shown in Fig. 5.3d indicating formation of graphene with a low defect content. Cooper et al. prepared few-layer graphene flakes of 2 nm thickness via the electrochemical intercalation of tetraalkylammonium cations into pristine graphite [48]. The electrochemical intercalation was carried out in a three electrode configuration with two types of working electrodes: HOPG and graphite rod. Tetramethylammonium perchlorate (TMA ClO_4), tetraethylammonium tetrafluoroborate (TEA BF_4), or tetrabutylammonium tetrafluoroborate (TBA BF_4) dissolved in 1-methyl-2-pyrrolidone were used as electrolytes. Significant electrode expansion had resulted with HOPD electrode than with graphite rod which was attributed to the high anisotropy of HOPG. It was also found that TBA was the most effective cation for HOPB electrode expansion, followed by TEA.

5.2.2 Application as Support and Dispersion of Metal Nanoparticles

Graphene is one of the most widely explored carbonaceous support materials for noble metal NPs. The hybrid nanocomposites of graphene with metal NPs are promising electrocatalysts for low-temperature fuel cells. The unique physicochemical properties of graphene such as 2D structure, high surface area with surface defects which acts as metal anchoring sites, and high electrical conductivity facilitate uniform dispersion of metal NPs onto its surface with strong metal–support interaction. This results in enhanced catalytic activity and durability of these hybrid electrocatalysts. The catalytic performance is significantly influenced by the size, composition, shape, and dispersion states of noble metal nanocrystals as well as their interactions with graphene support [6].

Metal NPs/graphene-based hybrid electrocatalysts are typically prepared by depositing metal precursors onto graphene-based support materials followed by their subsequent reduction adopting various methods [39]. Li et al. reported one pot synthesis of Pt nanoclusters with diameter of about 5–6 nm decorated graphene sheets via reduction of GO and Pt precursor with $NaBH_4$ [49]. The strong reducing agent facilitated in-situ reduction of reactants to form graphene and Pt-NPs and, thus, obtained Pt/Graphene nanocomposite. Compared to the conventional Pt/Vulcan catalyst, the Pt/Graphene nanocomposite demonstrated higher electrochemical surface area (ESA), better catalytic activity and stability for methanol oxidation. Jafri et al. used N-doped graphene (N-G) nano-platelets as support for Pt-NPs and studied their electrocatalytic properties. Graphene nano-platelets were synthesized by thermal exfoliation of GO and further treated in nitrogen plasma to produce nitrogen (3 at.%)-doped material [50]. Pt-NPs were dispersed on the support using the $NaBH_4$ reduction process to get the catalyst Pt/N–G. Membrane electrode assemblies (MEAs) fabricated using Pt/N–G and Pt/G as the ORR catalysts showed a maximum power density of 440 mW cm^{-2} and 390 mW cm^{-2}, respectively. The improved performance of Pt/N–G was attributed to the formation of pentagons and heptagons due to the incorporation of N in the C-backbone leading to increase in the conductivity of neighboring C atoms. In the work of Hsieh et al., Pt-NPs on graphene were formed from GO by two routes (one-step and two-step routes) [51]. For one-step route, a fixed weight of GO and a variable weight of $H_2PtCl_6{\cdot}6H_2O$ was used with ethylene glycol (EG) as the reducing agent. In the two-step route, the reduction of GO films was done initially to obtain graphene followed by deposition of Pt particles through EG reduction. The results showed that the Pt particles have smaller size and better distribution on the surface of graphene via two-step reduction route. The Pt/Graphene nanocomposites showed higher ESA (159.48 m^2 $g_{Pt}{}^{-1}$) and improved electrocatalytic activity towards the reduction of oxygen. The better results obtained were attributed to the very high Pt loading achieved and the small size of Pt-NPs dispersed uniformly on graphene nanosheets.

In recent years, microwave (MW) assisted processes have gained popularity to prepare metal NPs/graphene hybrids. MW irradiation offers homogeneous and rapid

heating which facilitates the formation of smaller and well-dispersed metal NPs [52, 53]. Zhao et al. fabricated a novel sandwich-structured graphene-Pt-graphene (G–P–G) catalyst through MW assisted polyol route using EG [54].The graphene support was first prepared by oxidation of graphite to GO by modified Hummers method. Subsequently, GO and Pt precursor were dispersed in EG/isopropyl alcohol solution (pH = 12) and subjected to continuous MW heating for 64 s which resulted in the formation of Pt-Graphene nanostructures. The sandwich G–P–G structures were formed by further addition of GO to Pt-Graphene dispersion followed by ultrasonic treatment and heating under Ar atmosphere at 140 °C for 1.5 h. Electrochemical results revealed superior MOR activity and stability with G–P–G catalyst which was attributed to facile metal support interaction due to anchoring of Pt-NPs between the two adjacent graphene sheets. Pt decorated, boron-doped graphene catalysts for ORR were prepared by Pullamsetty et al., following different chemical reduction methods by employing $NaBH_4$, EG, and mixture of $NaBH_4$ + EG (modified method) as reducing agent through conventional heating (CH) [55] as well as MW irradiation methods [56]. The study showed superior catalytic activity of boron-doped graphene-based catalysts prepared using the modified method following both CH and MW irradiation routes.

Oztuna et al. reported mesoporous graphene aerogel (GA) supported Pt-NPs prepared via supercritical deposition (SCD) using supercritical CO_2 ($scCO_2$), as ORR catalyst for PEMFC [57]. The Pt precursor was dissolved in $scCO_2$ and adsorbed onto GA at 35 °C and 10.7 MPa and was converted to its metal form under atmospheric pressure at different temperatures of 400 °C, 600 °C, and 800 °C. The effects of precursor conversion temperature on the structural properties of the composites and ORR activity were investigated. The results revealed that SCD helped to preserve the textural properties of the GA after the deposition of Pt-NPs, and Pt/GA converted at 600 °C exhibited an enhanced mass activity of 30.6 mA mg_{Pt}^{-1}, out-performing the mass activities reported in the literature for Pt/GA electrocatalysts prepared using conventional routes. Daş et al. investigated the effectiveness of two synthetic approaches: $scCO_2$ deposition and MW irradiation, to synthesize Pt-NPs uniformly dispersed on graphene nano-platelets (G) as catalyst support [58]. The study revealed formation of smaller Pt-NPs on G through $scCO_2$ deposition route (Pt/G2 1.5–1.6 nm) as compared to MW irradiation route (Pt/G1 3.1–3.4 nm). Pt/G2 catalyst exhibited higher ESA and fuel cell performance as compared to Pt/G1. The improved performance of the catalyst prepared via $scCO_2$ deposition route was attributed to the decrease in degree of agglomeration of Pt-NPs during the reduction process because of the higher interaction between adsorbed precursor ions and the graphene surface compared to the MW irradiation method. Pt/G2 also demonstrated higher corrosion resistance.

Electrochemical techniques have also been utilized for uniform dispersion of Pt-NPs on graphene-based support materials. Liu et al. utilized a "green" electrochemical approach to prepare nanocomposite films of Pt-NPs and graphene sheets [59]. First, expandable graphene oxide (EGO) support materials were prepared through modified Hummers and Offeman method using H_2SO_4, $KMnO_4$, and H_2O_2

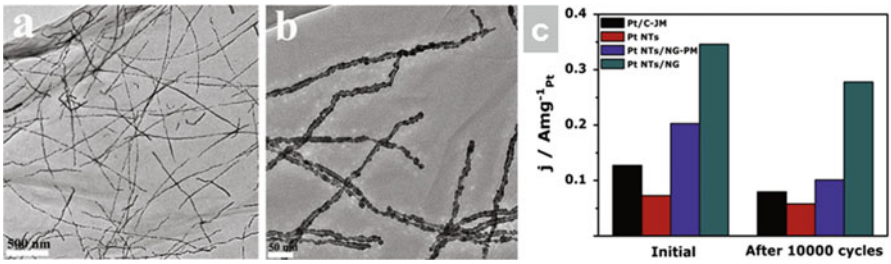

Fig.5.4 (**a**, **b**) TEM images of Pt NTs/NG catalyst and (**c**) mass activity of Pt-based catalysts before and after durability test. Reproduced with permission from Ref. [60], Copyright Elsevier, 2015

as oxidizing agents. Subsequently, electrophoretic deposition of EGO film on a conductive indium tin oxide surface was carried out at 150 V in constant potential mode. The deposited EGO film was in-situ electrochemically reduced using 0.1 M KCl to expandable graphene sheet (EGS). Finally, Pt-NPs were electrodeposited on the EGS film at a constant potential of −0.25 V for 1800 s in a mixed solution of 3 mM H_2PtCl_6 and 0.5 M H_2SO_4. Well-dispersed, uniform Pt-NPs with diameter of about 15 nm were distributed on EGS surface. Pt/EGS demonstrated better MOR activity than Pt-NPs deposited on glassy carbon. The improved electrocatalytic activity was attributed to the unique microstructure and surface topography of EGS and its synergistic interactions with the deposited Pt particles. Zhu et al. designed a strongly coupled Pt nanotubes/nitrogen-doped graphene (Pt NTs/NG) hybrid material utilizing galvanic replacement reaction between Te nanowires (NWs) and Pt precursors [60]. The Te NWs template resulted in the formation of one-dimensional (1D) tubular nanostructured Pt with an average diameter of 10.2 nm (Fig. 5.4a, b). The Pt NTs/NG demonstrated superior activity and durability towards ORR with a 2.7-fold improvement in mass activity (0.35 A mg^{-1} *vs.* 0.13 A mg^{-1}) as compared to commercial Pt/C catalyst. Pt NTs/NG catalyst also showed excellent durability characteristics and retained 88.9% of its initial activity after 10,000 cycles of accelerated durability tests (Fig. 5.4c).

Guo et al. fabricated 3D Pt on Pd bimetallic nanodendrites on graphene nanosheets (TP-BNGN) through a three step wet-chemical approach [61]. Poly(*N*-vinyl-2-pyrrolidone) (PVP) functionalized graphene was prepared first by ultrasonic exfoliation of GO with PVP solution followed by reduction with hydrazine and ammonia solution. In the next step, Pd NPs were deposited on PVP-functionalized graphene by HCOOH assisted chemical reduction. Finally, TP-BNGN catalyst was fabricated by mixing Pd NP/PVP-graphene with Pt precursor and subsequent metal reduction with ascorbic acid. The study demonstrated higher catalytic activity of TP-BNGNs than that of Pt/C (E-TEK) towards methanol electro-oxidation. The improved electrocatalytic activity was attributed to the three-dimensional (3D) bimetallic nanodendrites structure of Pt–Pd particles and their better dispersion on the graphene nanosheets with high surface area. Jafri et al. reported N-doped graphene as support for Pt-NPs that were synthesized using hydrothermal method and thermal solid state

method using two sources of nitrogen, ammonia and melamine, respectively [62]. The synthesized graphene-based catalysts were evaluated as ORR catalyst in both half-cell and full cell mode. In this work, MWCNT was used as a spacer and fuel cell results demonstrated enhanced performance with N-doped, graphene-based Pt catalyst prepared by hydrothermal method. This catalyst exhibited 1.5 times higher power density than commercial Pt/C catalyst (704 mW cm^{-2} *vs.* 460 mW cm^{-2}), establishing it as a promising cathode catalyst for PEMFC.

5.3 Ordered Mesoporous Carbons

Ordered mesoporous carbons (OMCs) belong to the family of carbon materials with pore size of 2–50 nm. OMCs are made up of periodically aligned arrays of mesopores with narrow pore size distribution forming a highly interconnected network. This novel carbonaceous material was discovered in the year 1999 by Ryoo et al. [63] and since then has witnessed a sudden upsurge of interest among the scientific community for its various applications, particularly in the field of energy storage and conversion [64]. Specifically, OMCs have garnered enormous attention as support materials for low-temperature fuel cells due to their unique properties such as high SSA, good electrical conductivity, large numbers of three dimensionally connected, mono-dispersed mesopores which facilitate diffusion of reactants, and by-products from the active sites contributing to catalysis [7, 65]. Additionally, they are also known to possess surface oxygen groups which are considered to improve the interaction between the metal catalyst and the carbon support allowing better dispersion; this also imparts better activity and durability. This section is focused on the synthesis methodology of OMCs, their suitability and application as support materials for low-temperature fuel cells.

5.3.1 Synthesis of OMCs

The story of OMCs started with the pioneering work of Ryoo et al. [63] where ordered mesoporous silica molecular sieve, Mobil Crystalline Matter/Mobil Composite Matter-48; MCM-48, was used as template along with sucrose as carbon source and sulfuric acid as the catalyst. The template was impregnated with the aqueous solution of sucrose and heated in the temperature range of 1073–1373 K under vacuum or inert atmosphere followed by conversion to carbon using sulfuric acid catalyst. Finally, the template was removed using aqueous solutions of NaOH and ethanol, which resulted in the formation of ordered porous carbon materials referred to as CKM-1. The authors demonstrated the applicability of this silica template-based synthetic route for large industrial applications. After 19 years of concerted efforts, significant development in the field of synthesis of these "unique" OMC materials has been realized [66–72] and OMCs with various mesostructures,

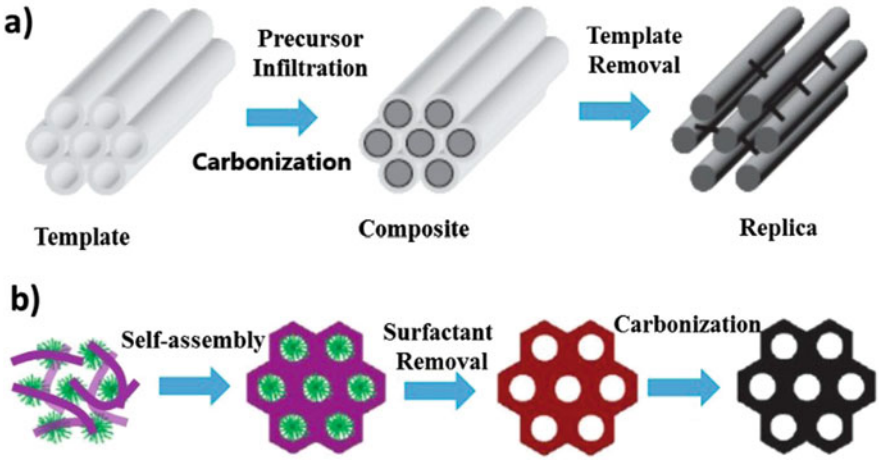

Fig. 5.5 Schematic comparing (**a**) hard template-based and (**b**) soft template-based synthesis strategies. Reproduced with permission from Ref. [64], Copyright Royal Society of Chemistry, 2017

pore diameters, particle morphologies, and framework microstructures are currently available. Typically, the methods of OMC synthesis can be broadly categorized into two: (1) hard-templating (impregnation and etching back) and (2) soft-templating (direct synthesis) as shown in Fig. 5.5a and b, respectively [12, 73]. Both these methods involve the formation of mesopores inside the counterpart bulk material [70, 74].

In the hard-templating strategy, mesoporous structures are created using preformed, ordered mesoporous solid template. This method is also called as nanocasting and involves infiltration of the pores of the template with suitable carbon precursor, its carbonization, followed by removal of the template creating mesostructures which are inverse replica of the mold as shown in Fig. 5.5a. It is vital that the employed hard template has 3D pore structure to aid in the formation of porous, interconnected carbon mesostructures after the removal of the template. It is also equally important that the carbonization of the carbon precursor is confined to the mesopores of the template to ensure the formation of replicated carbon structures. This can be achieved by the conversion of the carbon source to a cross-linked polymer before the carbonization process and can be facilitated by acid polymerization catalysts such as sulfuric acid at the surface of the ordered mesoporous template.

The commonly employed hard templates are silica-based ordered mesoporous structures such as MCM, Santa Barbara Amorphous (SBA), and hexagonal mesoporous silica (HMS) series [72, 75]. These templates favor the formation of highly ordered architecture of the mesopores but require stringent acid treatment process for the template removal which results in the loss of ordering of the material at the atomic scale hampering their intrinsic properties. Non-silica-based templates

such as MgO [76] have also been introduced which offer the advantage of the template removal following a milder acid treatment; however, these lack the uniformity of the mesopores as achieved with the silica templates. The carbon precursor also significantly influences the final morphology and properties of the formed OMC [77]. Carbon precursors with loose molecular structures such as sugar, sucrose, and furfuryl alcohol increase the framework shrinkage and result in the formation of higher SSA materials with dominance of micropores in the structural framework [63, 66, 71, 78]. On the other hand, carbon precursors with dense aromatic structures such as pitch, pyrene, polyacrylonitrile, and acenaphthene lead to the formation of replicated OMC with minimum framework shrinkage, high mechanical strength, and negligible microporosity [79–81]. It is noteworthy to mention here that the pore size and symmetric ordering of OMC are dependent on the solid template and not on the interaction between the carbon precursor and the template.

Jun et al. reported OMC designated as CKM-3 using SBA-15 as the template with sucrose as the carbon source and sulfuric acid as the carbonization catalyst [82]. This was the first report on the successful synthesis of OMC with retention of the structural symmetry of the silica template revealing similar diffraction peaks as that of the template. CKM-3 demonstrated similar characteristics as of CKM-1 such as high SSA of about 1500 $m^2\ g^{-1}$ and total pore volume of about 1.3 $cm^3\ g^{-1}$. However, CKM-3 exhibited larger pore size as compared to CKM-1 which is attributed to the thicker pore wall of SBA-15 as compared to MCM-48 template. Another commonly employed hard template is HMS which has a worm-hole structure and the OMCs synthesized with this template consist of interconnected network of carbon "worms" or "nanostrings" [83, 84]. In contrast to SBA-15, HMS is less costly to synthesize and has walls with twice the thickness resulting in the formation of OMCs with larger pore diameter [85, 86]. In the works of Banham et al. [85] and Li et al. [87], OMCs with HMS template were fabricated using sucrose, anthracene, and naphthalene as carbon precursors.

Silica spheres have also been utilized as template for synthesis of OMCs with 3D interconnected mesopores and macropores which have been proved beneficial for efficient mass transport of reactants and products in fuel cell electrochemical reactions. In the work of Lei et al., monodisperse SiO_2 particles with tunable diameter were prepared through the multi-step seed growth using hydrolysis and condensation of tetraethylorthosilicate (TEOS) in aqueous solution of ethanol and ammonia [88]. This resulted in the formation of colloidal solution of silica which acted as seed for subsequent growth of silica particles. The diameter of the silica particles was tuned during the seed growth by additionally injecting 2 ml TEOS into the seed solution at equal intervals of 6 h for total of 8 times. It was found that the diameter of the SiO_2 particles changes from 16.8 nm to 39 nm from first to eighth cycles of seed growth, respectively. The obtained silica particles were pressed into pellets to form the silica template and were mixed with aqueous solution of sucrose and sulfuric acid followed by carbonization at 850 °C in Ar atmosphere. Finally, porous carbon materials were obtained after the removal of the silica template using 20% HF for 12 h. The study revealed that the SSA and mesoporosity of the carbon materials increase with increase in the diameter of the silica particles. Zhang et al. prepared

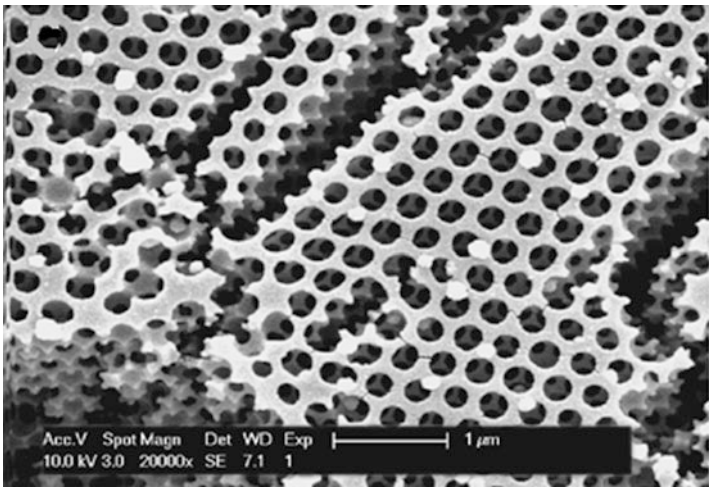

Fig. 5.6 Surface SEM image of hierarchically ordered porous carbon obtained using self-assembly of polymer latex and silica colloid. Reproduced with permission from Ref. [89], Copyright American Chemical Society, 2010

hierarchically ordered porous carbon utilizing silica particles as template through in-situ self-assembly approach of colloidal polymer spheres [89]. The self-assembly strategy of colloidal polymer and silica spheres to prepare hierarchically ordered porous carbons is simple and devoid of any additional infiltration process typical with traditional silica-based templates such as SBA. In this route, both the self-assembly of polymer spheres into the crystal template and the infiltration are completed in-situ in the same system and can be a suitable synthesis route for the mass production of hierarchically ordered porous carbon. In a typical synthesis, colloidal poly(methyl methacrylate-butyl acrylate-acrylic acid) [poly(MMA-BA-AA)] polymer latex (total solid content—15 wt.%) was mixed with colloidal silica, sucrose, and sulfuric acid. The obtained dispersion was solution cast on glass substrate and subjected to complete carbonization at 700 °C in N_2 to yield silica/carbon composite films which were etched using HF solution to form hierarchically ordered porous carbon as shown in Fig. 5.6.

Hollow mesoporous carbon spheres (HMCSs) with hollow core volume and low density are promising candidates for energy applications as compared to OMCs in other morphologies. Li et al. prepared HMCSs using hollow mesoporous aluminosilicate spheres (HMASs) [90]. HMCSs were fabricated through incipient-wetness impregnation method using furfuryl alcohol as the carbon source. The polymerization of furfuryl alcohol was catalyzed in-situ by aluminosilicate template and the final pyrolysis was carried out at 1273 K under N_2 flow. Subsequently, the aluminosilicate template was removed using a 5 wt.% aqueous solution of HF and drying at 373 K overnight to yield HMCSs with SSA of 1809 $m^2\ g^{-1}$ and total pore volume of about 1.01 $cm^3\ g^{-1}$. Gierszal and Jaroniec employed silica colloidal crystals (SCCs) as hard templates for synthesis of hollow core carbon spheres with large pore

volume (6 cm^3 g^{-1}) making them promising candidates for catalytic applications [91]. The porous carbon material was synthesized through incipient-wetness method by impregnating oxalic acid pre-treated SCCs template with solution of resorcinol and crotonaldehyde. The composite sample was subjected to a temperature-controlled polymerization to ensure uniform formation of polymeric film on the silica surface followed by carbonization under N_2 atmosphere at 900 °C for 2 h and removal of the template using diluted HF acid.

The hard-templating method is a highly versatile route for fabrication of OMCs which are negative replicates of the template and hence is widely adopted for construction of a variety of special morphologies such as nanotubes, nanostrings, nanospheres, and nanorods. However, the short-coming is that the various mesostructures are achieved through a chain of tedious multi-step processes at the expense of costly hard templates; thus, making this route incompetent for large scale production. In this regard, soft template synthesis approach comes in handy as instead of etching away the template, OMC can be directly synthesized by self-assembling of block copolymer surfactant and carbon precursor [92].

The soft template route basically involves assembly of carbon precursor and surfactants followed by the removal of the surfactant and subsequent carbonization forming OMCs with defined symmetry and pore size as represented in Fig. 5.5b. In this approach, the interaction between the surfactant and carbon sources drives the self-assembly of the soft template and determines the pore structure of the OMCs [93]. Hence, the direct synthesis route allows an easy adjustment of the structure, shape, and pore size of mesopores through fine tuning of the synthesis conditions such as temperature, ionic strength, pH, type of solvents, and the properties of the template molecules (e.g., hydrophobic/hydrophilic volume ratio) [94–96]. The carbon architectures fabricated through soft template route are more versatile and mechanically stable due to formation of interconnected continuous framework. The soft template route has thus emerged as a simple, flexible, and effective approach for large-scale synthesis of OMCs.

As the name suggests, soft template route employs "soft" molecules such as surfactants and amphiphilic block copolymers for realization of highly structured porous carbon materials [97]. The surfactants or amphiphiles consist of a hydrophilic head group and a hydrophobic tail which on hydrophobic interactions can assemble into discrete spherical, lamellar, or cylindrical structures at concentrations above their critical micelle concentration (CMC). Beyond CMC, these micelles undergo self-organization and aggregate to form diverse mesostructures. The aqueous surfactant assembly approach results in highly ordered mesostructures with well-controlled morphologies and tailored pore sizes. Utilizing this strategy, Zhang et al. prepared tailored mesostructured OMCs (FDU-16, FDU-15 and FDU-14) through organic–organic assembly of resols and triblock polymers [98]. In their work, phenol/formaldehyde resin was used as carbon precursor; whereas, Pluronic F127 and Pluronic P123 were used as triblock copolymer templates for the fabrication of FDU-16 and FDU-14, respectively. For the synthesis of FDU-15, an additional hydrocarbon was employed as swelling agent. The authors also demonstrated the usage of hydrocarbons (hexadecane and decane) to tune the pore size

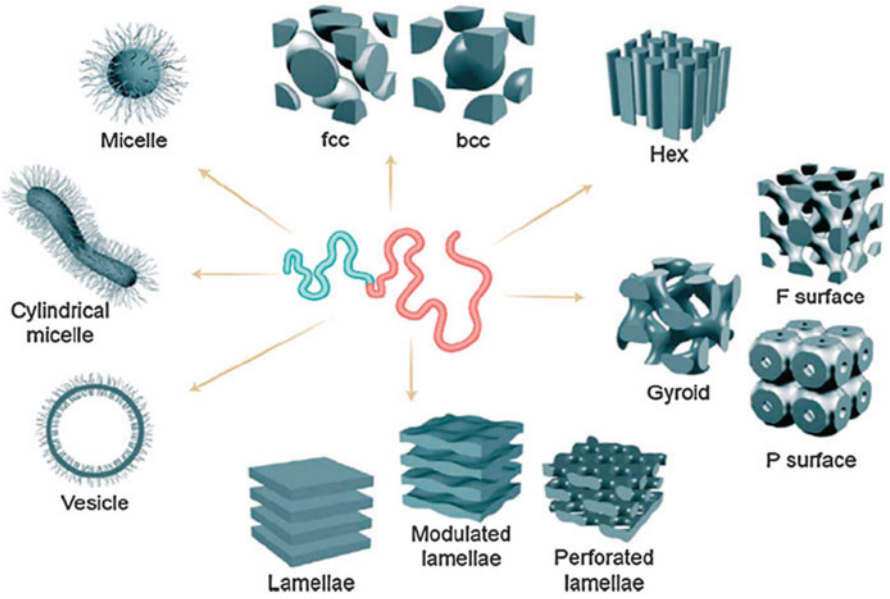

Fig. 5.7 Schematic representation of the various morphologies formed by block copolymers. Reproduced with permission from Ref. [74], Copyright Royal Society of Chemistry, 2012

(4.1–6.8 nm) of OMCs. Using a similar approach, Meng et al. tuned the mesostructures of OMCs from 2D hexagonal to 3D caged cubic and lamellar frameworks by modulating the mass ratio of the polymer precursors (resol) and amphiphilic Pluronic surfactants [99]. The Pluronic copolymers, particularly the triblock copolymers poly(ethylene oxide)-*b*-poly(propylene oxide)-*b*-poly(ethylene oxide) (PEO–PPO–PEO) (e.g., P123, F127, and F108), have been extensively utilized for the synthesis of OMCs with variable mesostructures. The success of this family of block polymers in achieving complex morphologies (Fig. 5.7) and tunable pore architectures is attributed to the microphase separation behavior of block copolymers facilitated by the opposite long-range repulsive and short-range attractive forces prevalent in the constituent blocks [100, 101].

Another commonly employed soft template strategy to prepare OMC materials is evaporation induced self-assembly (EISA) method. EISA approach involves the co-operative self-assembly of the templating agent and organic precursor through the evaporation of the solvent. It is a facile method and can be easily fine-tuned by adjusting synthesis conditions such as acidity of the reaction solution, surfactant, and phenol/template ratio [97, 102–104]. In the pioneering work of Meng et al., highly ordered mesoporous carbon frameworks were prepared using EISA method through organic–organic assembly of PEO-PPO-PEO triblock copolymers (Pluronic P123, F127, and F108) and resols (phenol-formaldehyde) with ethanol as the solvent [105]. They demonstrated synthesis of OMCs with diverse mesostructures such as hexagonal (FDU-16), cubic (FDU-15), bi-continuous cubic (FDU-14), and lamellar

by controlling the ratio of phenol/template and the PEO/PPO segment in triblock copolymer. The evaporation of ethanol assisted in the assembly of the organic precursor and template mainly through hydrogen bonding. Following a similar approach, Wang et al. prepared a functional composite of OMC/tungsten carbide (OMC/WC) with 2D hexagonal mesostructures using Pluronic F127 as a soft template, ammonium metatungstate as tungsten precursor, and phenol/formaldehyde resol as the carbon source through ethanol assisted evaporation [106]. In the works of Zhao et al., by employing ethanol assisted EISA strategy, OMC FDU-15 with different pore sizes (4.0–8.1 nm) was prepared using pore expanding agents, TEOS and decane [107]. This synthesis also utilized Pluronic F127 as a soft template and phenol/formaldehyde as the carbon source.

OMCs with large pores are highly desired as they offer the possibility of efficient loading of catalyst NPs without blocking the pore channels. It is well known that the hydrophobic volume of the template determines the pore size. Hence, block copolymers with long hydrophobic chains are promising candidates for fabrication of mesostructures with large pores. In this regard, Pluronic copolymers have restricted application due to limited short hydrophobic PPO blocks which lead to formation of mesoporous materials with pore size less than 12 nm without using any pore expanding agents such as 1,3,5-trimethylbenzene (TMB) [108, 109]. Another disadvantage associated with Pluronic family of block polymers is their low-temperature degradation (200–350 °C) even in inert atmosphere which gives rise to amorphous or semi-crystalline mesoporous structures. Considering these aspects, non-Pluronic copolymers such as poly(ethylene oxide)-*b*-polystyrene (PEO-*b*-PS), poly(2-vinylpyridine)-poly(isoprene) (P2VP-PI) and poly (4-vinylpyridine)-polystyrene(P4VP-PS) are adopted as promising templates to synthesize crystalline OMCs driven by strong hydrogen bonding interaction between the carbon precursor and the template [110]. These synthetic templates have longer rigid hydrophobic segments, higher carbon content, and stability as compared to their Pluronic counterparts. However, different from PEO-PPO-PEO block copolymers, non-Pluronic block copolymers have high molecular weight and hydrophobic segments which make them insoluble in water, and even with ethanol. Hence, synthesis of mesostructured materials using non-Pluronic copolymers as templates is mostly limited through the EISA approach [74, 97, 111, 112].

Comparing the hard template and soft template routes for preparation of OMCs, each has its own advantages and limitations [64, 97, 113]. Following hard template strategy, it is easier to obtain highly crystalline and graphitized OMCs; whereas, amorphous or semi-crystalline OMCs are obtained through soft template route. Also, soft template route offers a low cost, simple, and convenient methodology suitable for mass production of OMCs, while hard template approach is relatively complex, expensive, and time consuming, making it unsuitable for large-scale industrial production.

5.3.2 Surface Functionalization of OMCs

OMCs exhibit unique architectures and properties such as interconnected mesoporous structures, narrow pore size distribution, and high surface area which are highly desirable for application as support materials. However, the effective dispersion/anchoring of metal NPs into the mesoporous voids through the commonly employed "wet chemistry" approach is limited by the poor compatibility of hydrophobic carbon and hydrophilic solvents employed to dissolve the metal precursors [78, 114]. Hence, in order to achieve uniform and efficient dispersion of metal NPs, it is imperative to modify or functionalize the surface of OMCs with specific moieties, affinities, and reactivity [115, 116]. The surface modification or functionalization of OMCs renders surface functional groups which act as anchoring sites for metal catalysts and also aids in metal–support interaction which favorably enhances the activity and durability of the catalysts.

Surface functionalization of porous materials can be effectively achieved through introduction of oxygen-containing functional groups such as carboxylic, anhydride, phenolic, and carbonyl, which enhances the surface hydrophilicity of the carbon support aiding its dispersion in various solvents. Out of these, acid treatment is demonstrated to be an effective way of functionalization which makes the surface of carbon support act as site for metal catalysts and assist their anchoring. In the works of Guha et al. [117] and Salgado et al. [118], the surface of OMC support was modified using HNO_3 and the studies demonstrated strong dependence of the extent of functionalization on the catalytic activity of the supported metal electrocatalysts. However, the enhanced dispersibility of acid modified OMCs occurs at the expense of electrical conductivity and mechanical strength. In such a scenario, it is important to carefully select the acidic oxidation conditions such as type of oxidant, temperature, and treatment duration, since excessive oxidation leads to structural disintegration and subsequent dissolution of the carbon.

Surface modification of OMCs using heteroatoms such as nitrogen and sulfur has also been reported as an effective approach to tune their catalytic activity and stability. Perini et al. prepared nitrogen modified porous carbons using sucrose and ammonia as carbon and nitrogen source, respectively [119]. The study showed the effect of nitrogen defects on metal–support interactions and revealed that the nitrogen functional groups controlled the dimension and the dispersion of metal catalysts. In the work of Xiao et al., surface modification of CMK-3 with nitrogen doped carbon using polydopamine as the nitrogen source was attempted [120]. The results demonstrated formation of three phase interface areas with nitrogen modification of CMK-3 and higher electrochemical performance. Ji et al. utilized sulfur modified OMC which acted as metal trap because of its strong affinity towards noble metals due to soft acid–soft base interaction; this helped the effective dispersion of the catalyst particles [121]. Pt-based intermetallic nanocrystallites with sizes as low as 1.5 nm, which can be tuned up to ~3.5 nm, were formed with surface sulfur modified OMC supports.

Surface functionalization of OMCs can also be effectively achieved through charged species which assist in the improvement of synergistic interactions between metal catalysts and modified OMC supports. With positively charged cetyltrimethylammonium bromide (CTAB) surfactant, Zhou et al. modified the surface of OMC materials as support for Pt-NPs and demonstrated improvement in the wettability of OMCs with addition of CTAB resulting in better dispersion of Pt-NPs [122]. Li et al. functionalized OMCs with sodium dodecyl sulfate (SDS) followed by in-situ deposition of Pd NPs through MW assisted route. The electrostatic interaction between negatively charged SDS and positively charged Pd^{2+} facilitated the facile formation of the functional composite materials [123]. In the work of Zhang et al., positively charged, polyelectrolyte poly-(diallyldimethylammonium chloride) was used to wrap the OMCs which aided in facile anchorage of Pt-NPs through electrostatic interactions [124].

5.3.3 Application of OMCs as Support for Metal Catalysts

For the application as metal catalyst support for fuel cell, OMC materials offer several advantages compared to the traditional carbonaceous materials such as CB. Both OMC and CB support materials have high SSA to load the metal catalyst NPs and effectively reduce the expensive noble metal content. However, in the case of CB, metal particles get buried in the micropores making them inaccessible by the reactant fuels resulting in lower catalytic activity. In contrast, the mesoporous structure of OMCs effectively aids in mass transport of reactants and increases metal particle utilization thereby enhancing the mass activity of the catalysts. OMCs also exhibit higher chemical stability as compared to CBs. Furthermore, the structure, morphology, and physicochemical properties of OMCs can be easily customized by adjusting the synthesis conditions, template, type, and amount of carbon precursor and incorporation of heteroatoms.

Momčilović et al. employed OMC prepared through EISA method using resorcinol as the carbon precursor and Pluronic F127 as the soft template with ethanol/water as the solvent, as Pt catalyst support for HOR and ORR in acidic medium [125]. The kinetics of HOR and ORR on OMC supported Pt catalyst (Pt–OMC-SAM-800/3) was investigated using rotating disk electrode (RDE) voltammetry and the results showed reversible HOR kinetics and comparable ORR catalytic activity of Pt–OMC-SAM-800/3 with that of traditional carbon supported Pt electrocatalysts. Higher ORR and MOR catalytic activity was reported by Cao et al. with mesoporous carbon (MC) supported Pt catalysts as compared to Pt/XC72R and commercial Pt/C catalysts [126]. The improved electrocatalytic performance with Pt/MC was ascribed to the unique mesoporous structure of MCs and enhanced interaction between Pt-NPs and MCs. In the work of Xu et al., higher MOR and ORR activities along with stability were reported for Pt-NPs supported on ordered mesoporous carbon sphere (OMCS) array than Pt/CB and commercial Pt/C catalyst [127]. The enhanced performance of Pt/OMCS was attributed to the unique hierarchical structure of

OMCs supports with ordered macropores and mesopores which facilitated the mass transport of fuels and improved the dispersion of Pt particles. Joo et al. studied the effect of particle size of Pt-NPs supported on OMC on ORR and MOR activity [128]. Through a modified, sequential impregnation-reduction method, controlled Pt size from 2.7 to 6.7 nm was achieved. The study revealed volcano-type mass activity curve exhibiting the maximum activity at the Pt size of 3.3 nm for both ORR and MOR. In another work, Joo et al. investigated the effect of particle size of OMC support for Pt catalyst on ORR in DMFC [129]. They employed OMC with particle sizes of 100 nm, 300 nm, and 700 nm (OMC-100, OMC-300, and OMC-700) and deposited Pt-NPs of ~3 nm onto the supports. The electrochemical results revealed no significant influence of OMC particle size on ORR activity of the Pt/OMC catalysts. All the three catalysts exhibited similar catalyst utilization efficiency and ORR electrocatalytic activity.

Ahn et al. carried out studies to optimize the ionomer content in OMC supported Pt catalyst to achieve better PEMFC performance [130]. Electrodes with different ionomer content in the range of 5–30 wt.% were prepared as cathode and fabricated into MEA (MEA-5, MEA-10, MEA-15, MEA-20, and MEA-30) to assess their performance. The polarization curves with the fabricated MEA showed higher potential in the low current density region with increase in ionomer content due to their ability to form three phase boundaries. However, too much ionomer as in the case of MEA-30 resulted in poor performance due to strong hydrophilic interactions between H_2O and ionomer, restricting mass transport of reactants as well as the product, water. On the contrary, at higher current density, MEA with lower ionomer content demonstrated higher performance due to facile mass transport of product H_2O produced by electrochemical reactions. With Pt/OMCs as cathode catalysts for PEMFC, the highest ESA, Pt utilization, and cell voltage at high current density were obtained with MEA-10 containing 10 wt.% ionomer. Kim et al. studied the influence of three types of OMCs with different frameworks (CMK-3, CMK-3G, and CMK-5) as support materials for Pt on the ORR activity and durability [131]. These OMC materials were prepared using the same hard template SBA-15 and had similar hexagonal mesostructures, but with different carbon framework structures and degree of graphitization which significantly influenced their surface area, microporosity, and electrical conductivity. The authors showed a direct dependence of micropore volume of OMC supports to their catalytic activity and durability. The highest ORR activity was achieved with Pt/CMK-3G catalyst, and it was ascribed to the formation of crystalline Pt-NPs on the highly graphitic, crystalline CMK-3G framework which resulted in weaker adsorption of surface oxide and stronger interaction between the Pt particles and the support.

Surface functionalized OMC through nitric acid oxidative treatment was used as Pt catalyst support for DMFC by Calvillo et al. [132]. The introduced oxygen functional groups assisted in uniform dispersion of Pt particles and showed better MOR catalytic activity as compared to commercial Pt/C catalyst. Morales-Acosta et al. compared the influence of OMC, MWCNT, and Vulcan support materials on methanol, ethanol, and ethylene glycol electro-oxidation reaction (MOR, EOR, and EGOR, respectively) activity in direct alcohol fuel cells (DAFCs) [133]. The support

materials were pre-treated with HNO_3/H_2SO_4 solution before depositing Pt catalysts to modify their surface with oxygen-containing groups. It was found that the use of OMC enhances the catalytic activity towards the three reactions. It also exhibited higher electrochemical stability than the other two supports showing ESA loss of only 12% after 500 cycles of accelerated durability test (ADT). Samiee et al. proposed in-situ functionalization of OMC (CMK-3) with MWCNT following a two-step method [134]. In the first step, mesoporous carbon was functionalized with NiO following an impregnation route using the solution of nickelocene ($NiC_{10}H_{10}$) in ethanol. Subsequently, the Ni functionalized OMCs were utilized as substrate for deposition of MWCNT through CVD technique. It was found that the functionalization of CMK-3 with MWCNT resulted in partial damage of the mesoporous structure of OMCs; however, CMK-3 CNT supported Pt catalyst (CMK-3CNT20Pt) exhibited superior ORR catalytic activity and fuel cell performance compared to the industrial, 40 wt.% Pt/Vulcan catalyst.

Nsabimana et al. investigated the influence of boron-doped OMC support for Pt (Pt–BOMC) on MOR catalytic activity and compared the performance with undoped OMC supported Pt (Pt–OMC) and commercial Pt–C catalysts [135]. Pt–BOMC exhibited remarkably higher MOR catalytic activity than that of Pt–OMC and Pt–C catalysts; this was attributed to stronger Pt–support interactions attained with boron doping. Song et al. employed phosphorous doped OMCs supported Pt as anode catalyst in DMFC [136]. The study showed that addition of P enhances oxygen content of the support facilitating uniform dispersion of Pt-NPs with particle size of 3.5 ± 0.4 nm leading to higher ESA. Pt-based bi-metallic NPs have also been supported on OMCs and employed as catalyst materials in low-temperature fuel cells. Bruno et al. showed 15% higher peak power density with Pt–Ru/OMC anode catalyst over Vulcan supported catalyst, Pt–Ru/C [137]. Hung et al. synthesized core-shell Pt–M (M = Ru, Fe, and Mo) supported on OMCs and investigated them as anode catalyst for MOR in DMFC [138]. The bimetallic Pt–M NPs were well dispersed in the pore channels of the OMC support and showed superior MOR catalytic performance with remarkable tolerance to CO poisoning as compared to typical commercial PtRu/Vulcan XC72 anode catalyst.

5.4 Green Carbons

Carbon materials have made momentous impact in energy storage and conversion applications. Advanced functional carbonaceous materials are still being explored to achieve sustainable energy in the form of electrochemical power sources. Particularly, in low-temperature fuel cells, carbon materials play a vital role as supports and effectively assist in fuel cell catalysis as discussed in the previous sections. It is to be noted that preparation of most of carbonaceous supports such as graphene, carbon nanotubes (CNTs), carbon nanofibers (CNFs), CB, and activated carbons which are typically employed as catalyst supports involves tedious synthesis procedures, complicated apparatus, usage of metal catalysts, high temperature processing and

are most often derived from expensive fossil fuel-based precursors making them undesirable for sustainable energy production [139–143]. In such a scenario, the realization of sustainable energy through application of these carbonaceous materials in fuel cells sounds "misnomer." Hence, the development of "green carbon" through environmentally benign and economically sustainable way gains utmost significance and urgency for their applications in fuel cells. Considering these aspects, this section discusses biomass derived novel carbons as viable support materials for fuel cell catalysts. The methodology involved in anchoring of diverse NPs onto these "green carbon" is also discussed at the end of this section for better understanding of the overall process involved in the preparation of "green carbon"-based catalysts for low-temperature fuel cells.

5.4.1 Biomass as Source of Novel Carbons

Mother Nature provides limitless renewable biomass source which can be effectively converted to valuable "green carbon" through viable, environmentally and economically sustainable approaches. Biomass sources are readily available, accessible, and recyclable across planet Earth. They also offer a wide variety and structural diversity for fabrication of novel carbons with fine-tuned chemical structure and morphology for the targeted application.

Plants (lignocelluloses) are one of the most common and readily available sources of biomass. Lignocellulose is the main structural constituent of the cell walls in woody and non-woody plants. They are composed of cellulose, hemicellulose, and lignin which act as source of carbon. Glucose, the building block of cellulose, is a cheap and facile source of carbon. Using glucose as carbon precursor, Falco et al. prepared functionalized carbon materials through hydrothermal carbonization (HTC) [144]. The authors showed significant influence of processing temperature and time on glucose derived carbon particle diameter and size distribution. They also showed that, through proper control of processing conditions, the final chemical structure of carbon can also be tuned from oxygen rich carbonaceous polyfuran to carbonaceous network with extensive aromatic domains. Using borax (sodium borate) mediated hydrothermal approach with glucose as carbon source, Fellinger et al. prepared hierarchically structured carbon aerogels [145]. The experimental results demonstrated that the sugar:borax ratio controlled the primary carbon NP size; whereas, their spinodal destabilization resulted in the controlled aggregation of carbonaceous particles leading to the formation of monoliths. Liu et al. prepared porous carbon structures and carbon sheets with glucose precursor through molten salt process using different oxysalts ($KNmO_x$; Nm = H, B, C, N, P, S, Cl), dissolved in the LiCl/KCl solvent [146]. The type of oxysalt employed significantly influenced the morphology, surface area, microporosity, and pore volume of the resultant carbons.

Sucrose is another naturally renewable bio-resource and is effectively utilized for sustainable generation of advanced functional materials. Sucrose has been the most

popular carbon precursor for fabrication of OMCs. Xiao et al. fabricated OMCs with selective morphologies using SBA-15 and sucrose as template and carbon precursor, respectively, by simply controlling the infiltration processing conditions [147]. Ting et al. synthesized OMCs with hexagonal mesostructures through organic–inorganic self-assembly of sucrose, Pluronic P127 and TEOS in acidic conditions [148]. The structural properties of the developed high surface area carbon materials (1225 $m^2\ g^{-1}$) were tailored by adjusting the reaction parameters and compositions. Sivadas et al. prepared nitrogen enriched mesoporous carbon through simple heating and KOH activation process utilizing sucrose (carbon source) and urea (nitrogen source) [149]. By adjusting the amount of sucrose, carbon, and KOH, mesoporous carbons with different N content were prepared with high SSA and pore volume. Hierarchically porous carbon monoliths with SSA and pore volume up to 1426 $m^2\ g^{-1}$ and 3.097 $cm^3\ g^{-1}$, respectively, were also prepared by Yu et al. using sucrose and amino-functionalized monolithic NH_2–SiO_2 through hydrothermal nanocasting strategy [150]. Yu et al. prepared biomass derived carbon materials through HTC of carbohydrate precursors (xylose, glucose, sucrose, and starch) and concluded that the porosity of the developed carbon functional materials was highly dependent on thermal treatment temperature [151].

Cellulose derivatives are also promising raw materials for preparing carbonaceous materials due to their naturally ubiquitous abundance, inherent non-toxicity, and 1D nanostructures [152, 153]. Celluloses are comprised of only C, H, and O atom; hence, co-doping with one or more heteroatoms is generally carried out to achieve carbon materials with superior properties. N-doped carbon nanosheets with high SSA (~1362.36 $m^2\ g^{-1}$) and large pore volume (~3.36 $cm^3\ g^{-1}$) were prepared by direct pyrolysis of cellulose/urea [154]. 3D porous networked Fe and P co-doped CNFs with large surface area were derived by carbonizing bacterial cellulose (BC) [155]. Similarly, by direct pyrolysis and subsequent ammonia activation of BC, networked nitrogen doped CNF aerogel was fabricated with high density of N-containing active sites (5.8 at.%) and high SSA (916 $m^2\ g^{-1}$) [156]. Lai et al. also prepared nitrogen doped CNF network by a single step carbonization process; here the BCs were coated with polyaniline as the nitrogen source to produce 3D porous network [157]. Mulyadi et al. prepared hybrid 3D carbon nanomaterials, N,P-doped carbon with N,S-doped CNF using cellulose nanofibril precursors [158]. High surface area carbon aerogels with interconnected nanostructures were also prepared using BC pellicles as biomass source [159, 160]. Sun et al. prepared networked carbonaceous nanofibers through direct pyrolysis of BC pellicles under nitrogen atmosphere [161]. Using 3D nanostructured BC pellicles as biomass precursor, Wu et al. fabricated a highly electrochemically active nanocomposities of Mo_2C NPs embedded within BC derived carbonaceous framework [162].

Chitosan (CS) is the second most naturally abundant nitrogen-containing biopolymer after cellulose and has been successfully employed as biomass precursor for realizing advanced functional carbonaceous materials. Rybarczyk et al. prepared highly porous activated carbon material by pyrolysis of chitosan with $ZnCl_2$/LiCl salt mixture [163]. The resulting CS derived carbon materials showed SSA of

1317.97 $m^2 g^{-1}$ with total nitrogen content of 6.5%. Nitrogen enriched (ca. 6–7 wt. %) micro/mesoporous activated carbon materials were prepared by Kucinska et al. utilizing CS and $ZnCl_2$ as activating agent via oxygen-free carbonization [164]. The surface area, pore volume, and pore size distribution of the carbons were tailored by tuning the CS–$ZnCl_2$ ratio in the precursor. Following a similar $ZnCl_2$ assisted carbonization and activation process, Wang et al. also prepared hierarchical macro/microporous N-doped carbon materials with large surface area [165]. Jiang et al. produced N-doped porous carbon materials through a simple template carbonization process using carboxymethyl chitosan and $Zn(NO_3)_2 \cdot 6H_2O$ as the carbon/nitrogen source and template, respectively. The effect of two direct synthesis methods, *viz.* solution-phase and solid-phase, on physicochemical properties of the obtained carbon materials was thoroughly investigated in a study which demonstrated formation of N-doped (2.06 at.%) porous carbons with higher surface area (1956 $m^2 g^{-1}$) and larger pore volume (1.48 $cm^3 g^{-1}$) with solution-phase method.

Novel carbonaceous materials can also be prepared using green plants as carbon precursors. Chen et al. prepared N-doped nanoporous carbon nanosheets (NCS) using a wetland plant, cattail through a facile hydrothermal treatment and subsequent post-treatment in ammonia gas [166]. The prepared NCS materials exhibited microporous structure with high surface area (898 $m^2 g^{-1}$) and high content of nitrogen (9.1 at.%). Liu et al. obtained nitrogen self-doped porous carbon through simple pyrolysis of water hyacinth at controlled temperatures (600–800 °C) with $ZnCl_2$ as an activation reagent [167]. The obtained porous carbon showed surface area up to 1199.3 $m^2 g^{-1}$ and nitrogen content of 5.02 at.%. It was found that different forms of nitrogen (pyridinic, pyrrolic, and graphitic) were incorporated into the carbon molecular skeleton. Through carbonization of natural cotton and subsequent activation with KOH in nitrogen atmosphere, Cheng et al. prepared high surface area carbon aerogel fiber with good electronic conductivity (~860 S m^{-1}) [168]. It was found that depending on the amount of KOH employed during the activation process, the SSA of the carbon aerogel varied from 1536 to 2436 $m^2 g^{-1}$ without any significant change in the electrical conductivity. Using low cost corn husk [169] and mushroom [170] as biomass carbon resource, hierarchically porous carbon was reported through direct pyrolysis and activation process with KOH and H_3PO_4/KOH, respectively.

Animal biomasses are attractive sources for production of functional carbon materials and offer additional advantage of waste management from livestock which are quite challenging. Chicken and pig poultry industries are sources of abundant waste animal biomass. By carbonizing chicken [171] and pig bones [172], high surface area (560–770 $m^2 g^{-1}$) N-doped porous carbon materials were successfully synthesized. Chicken feathers also served as economical and sustainable bio-source for preparation of N,S-co-doped porous carbon materials [173]. Pig skin was used as green source to prepare high surface area (2799 $m^2 g^{-1}$) N-doped porous carbon with $CaCO_3$ as activating agent [174]. Using porcine blood, a series of nitrogen-doped carbon nanospheres were prepared at different pyrolysis temperatures, and it was found that higher percentage of planar N species resulted in excellent electrochemical activity [175]. Fish bio-wastes are considered as excellent

raw materials for preparation of porous nitrogen enriched carbonaceous materials. Wang et al. fabricated porous N-doped carbon material through a simple pyrolysis of fish bone followed by acidic treatment [176]; whereas, Guo et al. prepared N-doped porous carbon network by fish-scale pyrolysis and subsequent activation by $ZnCl_2$ [177]. Eggs are natural biological materials rich with protein and cholesterols. Furthermore, they are also cheap source of heteroatoms such as N, S, and P alleviating the need of external doping agents making them suitable alternative carbon precursors to obtain in-situ heteroatom doped porous carbon materials. Egg derived heteroatom doped mesoporous carbons with large surface area and high pore volume have been reported through spray drying process [178] and carbonization with graphical carbon nitride which acted as template, N source, and swelling agent [179]. Heteroatom doped mesoporous carbons were also prepared by a single step facile pyrolyzing process [180]. Apart from the poultry-based bio-waste, human hairs are another widely available organic waste and being rich in heteroatoms (N,S) can serve as low cost scrap materials to fabricate valuable porous carbon materials. N,S co-doped porous carbon materials with large surface area and high porosity were developed through a simple approach comprised of degradation of human hair followed by carbonization and subsequent activation/graphitization process [181–183].

5.4.2 New Family of Green Carbon Supports

Biomass derived advanced "green carbon" materials typically have a large surface area with beneficial porous structures which facilitate efficient mass transportation of reactants and products [184, 185]. Furthermore, many biomass precursors contain abundant heteroatoms, which can directly serve as doping agents to create catalytically active sites [186, 187]. Also, the conductive carbon framework can enable the efficient electron transfer for electrochemical reactions. Hence, biomass derived green carbons are promising support materials for low-temperature fuel cell catalysts. In the work of Zhou et al., nitrogen containing mesoporous carbon (CS) with high surface area (516.6 $m^2\ g^{-1}$) and total pore volume (0.45 $cm^3\ g^{-1}$) was derived from carbonizing soybeans [188]. CS was employed as support for Pt-NPs for electro-oxidation of methanol and the catalytic performance was compared with Pt supported on Vulcan carbon XC-72. Compared with traditional carbon support, Pt/CS showed higher methanol oxidation onset potential and 1.5 times higher peak oxidation current (Fig. 5.8a) along with higher durability as shown by chronoamperometric results (Fig. 5.8b). The enhanced performance of Pt/CS was ascribed to more active sites for methanol oxidation with CS supports as compared to Vulcan XC-72 and unique dendritic morphology of Pt-NPs. In another work of Zhang et al., okara-derived carbon (ODC) was prepared by carbonizing okara at 800 °C under N_2 atmosphere and was employed as support for Pt-NPs for MOR [189]. The electrochemical results revealed higher electrocatalytic activity and resistance to CO poisoning of Pt/ODC than Pt/C catalyst. This improved MOR electrocatalytic performance of Pt/ODC was attributed to the high degree of

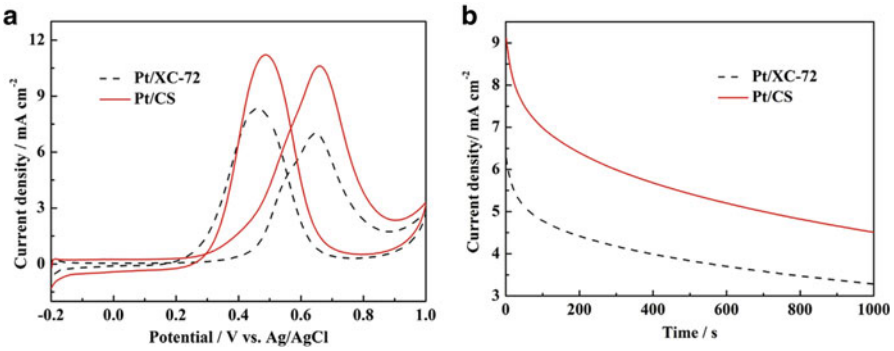

Fig. 5.8 (**a**) CV plots at scan rate of 50 mV $s^{-1}$and (**b**) chronoamperometric curves of Pt/CS and Pt/XC-72 electrodes in N_2-saturated 0.5 mol L^{-1} H_2SO_4 + 0.5 mol L^{-1} CH_3OH. Reproduced with permission from Ref. [188], Copyright Elsevier, 2014

graphitization and multi-grain interfaces with ODC supports which are conducive for favorable formation of more catalytically active sites. Pt-NPs supported on chitosan-carbon black derived N-doped carbon material (Pt/NC) were investigated for MOR and the performance was compared with commercial Pt/C and home-made Pt/C catalysts [190]. Pt/NC demonstrated better MOR electrocatalytic activity and stability than the commercial catalysts which was attributed to synergistic metal–support interactions.

Yan et al. explored mesoporous bowl-like carbons (BLCs) as support for Pt-NPs [191]. BLCs were prepared using glucose as carbon source and solid core mesoporous shell silica spheres as template. A regular bowl shaped mesoporous structured carbon as shown in Fig. 5.9 was obtained after the etching process with HF. The derived mesostructured carbons exhibited high surface area (1108.3 m^2 g^{-1}) and large pore volume (2.7 cm^3 g^{-1}) which are highly desirable for uniform and stable dispersion of Pt-NPs. Moreover, the mesopores of BLCs assist in mass transfer of reactants and products during catalytic reactions. BLC supported Pt catalyst (Pt/BNC) were evaluated for MOR and ORR activity. For a meaningful comparison, MOR and ORR activity of commercial Pt/C (TKK) was also evaluated. Pt/BLC demonstrated 2.6 times (1846 mA mg_{Pt}^{-1} *vs.* 723 mA mg_{Pt}^{-1}) and 1.6 times (180.6 mA mg_{Pt}^{-1} *vs.* 114.2 mA mg_{Pt}^{-1}) higher catalytic activity for methanol oxidation and oxygen reduction, respectively, than that of TKK. Furthermore, Pt/BLC also exhibited higher stability for ORR and lost only 6.9% of its catalytic activity in contrast to 18.9% loss by TKK catalyst after 10,000 potential cycles which was ascribed to stable attachment of Pt-NPs on mesoporous BLC support and consequent stronger force of physical interaction. Using soluble sucrose as precursor, ultrathin carbon layer (UTCL) stabilized Pt-NPs were reported by Cheng et al. [192]. The starch stabilized Pt-NPs in the colloidal state were further supported on Vulcan XC-72R carbon followed by pyrolysis at 350 °C for 10 min under Ar atmosphere forming UTCL (≈0.58 nm) around Pt-NPs. Thus fabricated Pt/UTCL-C catalyst displayed comparable ORR activity (mass activity, 112.5 A g^{-1} vs. 116.2 A g^{-1})

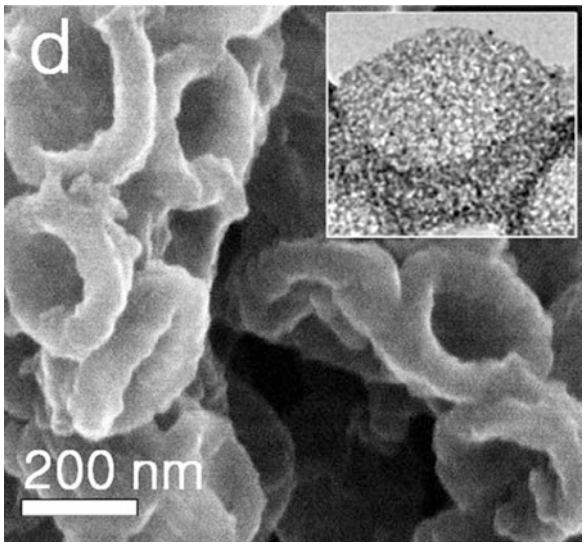

Fig. 5.9 SEM image of the BLCs showing regular bowl shape. Inset shows TEM images showing mesoporous structure of BLCs. Reproduced with permission from Ref. [191], Copyright Elsevier, 2013

as of commercial Pt/C which was also heat treated in an identical manner. However, Pt/UTCL-C catalyst demonstrated excellent stability with 40% loss of mass activity after 10,000 cycles of accelerated electrochemical aging tests as compared to 69% loss shown by conventional Pt/C catalyst. The superior stability of the former catalyst was attributed to UTCL around the catalyst particles that hindered migration and agglomeration of Pt-NPs and their detachment from the support. Liu et al. used pig bone derived hierarchical porous carbon (HPC) as support material for Pt electrocatalysts [193]. HPCs were prepared by carbonizing, activation by KOH, and acid treatment of the pig bones. The resulting nitrogen self-doped HPC exhibited high surface area (2157 $m^2\ g^{-1}$) with three-dimensional open macropore structure. HPC supported Pt exhibited larger ESA (Pt/HPC = 117.3 $m^2\ g^{-1}$) than that of carbon black supported Pt-NP catalyst (Pt/Vulcan XC-72 = 66.7 $m^2\ g^{-1}$), suggesting higher Pt utilization by the former catalyst owing to their open macroporous structure and nitrogen atoms. Compared with Pt/Vulcan XC-72, Pt/HPC also displayed higher ORR catalytic activity and stability. The enhanced performance was attributed to hierarchical porous structures, large surface area, and large amount of micropores and nitrogen-doped surface state of HPC which facilitated the mass transportation and improved the catalytic activity of Pt-NPs.

5.4.3 Anchorage of Nanoparticles on Green Carbons

In contrast to conventional CB support materials, biomass derived mesoporous carbon materials are fabricated through low cost routes utilizing renewable resources and also offer added advantage of uniform and stable dispersion of metal NPs by

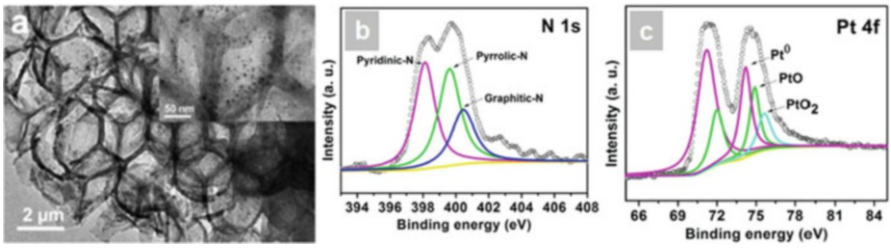

Fig. 5.10 (**a**) TEM images, (**b**) XPS N 1s spectra, and (**c**) XPS Pt 4f spectra of Pt-N/C PMCs. Reproduced with permission from Ref. [194], Copyright Elsevier, 2017

virtue of self-doped heteroatoms which create anchoring sites for deposition of NPs. Hence, biomass derived mesostructured porous carbon supported Pt-based catalysts exhibit improved electrocatalytic activity and stability than conventional Pt/C catalyst.

Cheng et al. used 3D N-doped porous microspherical cavities derived from self-polymerization of polydopamine (PDA) and polystyrene microspheres (PS) as support materials [194]. Pt-NPs were decorated onto the mesoporous support through in-situ reduction of Pt precursor (K_2PtCl_6) on the surface of PDA followed by carbonization process. Pt-NPs with average diameter of 1.9 ± 0.5 nm were deposited onto the support Fig. 5.10a) and the catalyst showed high percentage of metallic Pt, pyridinic N (39.2%), and graphitic N (22.6%) in the resulting Pt–N/C catalysts as shown by XPS results (Fig. 5.10b, c). The electrochemical results proved enhanced ORR catalytic activity, stability of Pt–N/C PMCs, and remarkable methanol tolerance as compared to Pt/C catalysts. The improved electrocatalytic performance was attributed to the combined effect of higher content of metallic Pt (Pt^0), active pyridinic and graphitic along with the porous structure of the support that facilitated mass transport of reactant and electrolyte to the active sites. In the work of Wang et al., hard carbon spherules (HCS) derived from hydrothermal carbonization of sugar were used as support [195]. Pt-NPs were deposited onto the support following two reduction methods involving reduction of the Pt precursor with $Na_2S_2O_4$ in aqueous solution (Pt/HCS1) or EG (Pt/HCS2). It was found that reduction conditions of Pt precursor influenced the size and aggregation of the Pt particles and subsequently their catalytic activity. High and well-dispersed Pt-NPs with average diameter of 5 nm were obtained with EG reduction method. Pt/HCS2 also exhibited 9.5 times higher electrocatalytic activity than Pt/Vulcan XC-72 catalyst which was attributed to uniform dispersion of the Pt-NPs and better electrode–electrolyte contact. Fe-doped porous graphitic carbon nanostructure (GCN) derived from filter paper was used as Pt support by Afraz et al. [196]. Pt-NPs were electrochemically deposited onto glassy carbon electrode modified with GCN support (Pt–NP/GCN) through potentiostatic double-pulse technique using 0.5 mM H_2PtCl_6 in de-aerated KNO_3 solution. Pt–NP/GCN displayed higher methanol oxidation current density than commercial Pt/C electrode. The improved electrocatalytic performance was attributed to synergistic metal–support interaction and iron oxide impurity of GCNs.

Biomass derived support materials for Pt were also prepared by pyrolyzing silkworm cocoon with ferric chloride as activator [197]. Thus, obtained cocoon-derived activated carbon (AC) with high surface area (756 $m^2\ g^{-1}$) and narrow pore size distribution (3.6 nm). Pt particles were deposited onto the AC support (N–Pt/AC) through hydrothermal route using sodium citrate and ethylene glycol. N–Pt/AC demonstrated higher activity towards MOR as compared to Pt/C catalyst in terms of higher ESA (98.3 $m^2\ g_{Pt}{}^{-1}$ *vs.* 46.3 $m^2\ g_{Pt}{}^{-1}$) and better CO tolerance. The enhanced performance of N–Pt/AC catalyst was attributed to the multi-grained Pt structure formed as a result of cocoon-derived AC. Lobos et al. utilized biochar produced by pyrolysis of untreated and phosphoric acid treated cellulose as support materials for Cu–Ru@Pt core-shell NPs [198]. The tri-metallic NPs were deposited onto the support through a two-step procedure. Cu–Ru NPs were deposited first onto the carbonaceous materials using $NaBH_4$ reduction of the precursor salts in a weight ratio of 3:1. Finally, the Cu–Ru@Pt core-shell NPs were obtained by galvanic replacement reaction of Cu^{2+} by Pt^{4+} ions. It was found that phosphoric acid treatment modified the carbonaceous support and significantly influenced catalytic activity through surface defect sites (metal–support interaction). Cu–Ru@Pt supported onto the phosphoric acid treated biochar exhibited high ESA and MOR activity with turnover number value of 0.151 mol $site^{-1}\ s^{-1}$ at 0.5 V.

5.5 Conclusions and Outlook

Electrocatalyst support materials significantly influence the performance of low-temperature fuel cells. This chapter briefly discussed the newly developed carbonaceous nanostructures such as graphene, OMCs, and green carbon as alternatives to conventional CB support materials in low-temperature fuel cells. Graphene is a fascinating 2D material and has exceptional properties such as high surface area, high conductivity, and unique graphitized basal plane which favorably assist in the improvement of catalytic activity and durability of supported nanocatalysts. The novel properties of OMCs such as high surface area and large amount of mesopores facilitate high metal dispersion and good reactant flux rendering it a highly suitable electrocatalyst support for fuel cells. Moreover, the defects and functional groups present on the surface of OMCs act as sites for deposition of metal nanocatalysts and metal–support interaction resulting in improved activity and durability of OMC-based hybrid catalysts. Biomass offers sustainable and renewable resources for derivation of novel "green carbon" materials as electrocatalyst support materials. Most often, biomass derived carbon materials are self-heteroatom doped which favorably enhance the electrocatalytic activity. Though significant advances have been made in the synthesis of graphene, OMCs, and green carbon, it is vital to develop simpler, more effective, and low cost procedure for their mass production. Furthermore, most of the electrocatalytic and stability measurements with newly developed carbonaceous nanostructures are carried out in half-cell mode (RDE) with acidic/alkaline electrolytes which are not true representation of their actual

performance in fuel cell. Hence, it is essential to evaluate their performance in-situ in working fuel cell under operating conditions to validate their practical applicability. It is certain that continued concerted research in this exciting field of new carbonaceous materials will help to alleviate the limitations of low-temperature fuel cells and result in enhanced performance for wide scale commercial applications.

Acknowledgments The authors gratefully acknowledge Director, VSSC and Deputy Director, PCM, VSSC for granting permission to publish this work.

References

1. Wang Y, Chen KS, Mishler J, Cho SC, Adroher XC (2011) A review of polymer electrolyte membrane fuel cells: technology, applications, and needs on fundamental research. Appl Energy 88(4):981–1007
2. Sharaf OZ, Orhan MF (2014) An overview of fuel cell technology: fundamentals and applications. Renew Sust Energ Rev 32:810–853
3. Wilberforce T, Alaswad A, Palumbo A, Dassisti M, Olabi AG (2016) Advances in stationary and portable fuel cell applications. Int J Hydrog Energy 41(37):16509–16522
4. O'Hayre R, Cha S-W, Prinz FB, Colella W (2016) Fuel cell fundamentals. Wiley, Hoboken
5. Dicks AL, Rand DAJ (2018) Fuel cell systems explained. Wiley, New York
6. Liu M, Zhang R, Chen W (2014) Graphene-supported nanoelectrocatalysts for fuel cells: synthesis, properties, and applications. Chem Rev 114(10):5117–5160
7. Sharma S, Pollet BG (2012) Support materials for PEMFC and DMFC electrocatalysts—a review. J Power Sources 208:96–119
8. Basri S, Kamarudin SK, Daud WRW, Yaakub Z (2010) Nanocatalyst for direct methanol fuel cell (DMFC). Int J Hydrog Energy 35(15):7957–7970
9. Huang H, Wang X (2014) Recent progress on carbon-based support materials for electrocatalysts of direct methanol fuel cells. J Mater Chem A 2(18):6266–6291
10. Bharti A, Cheruvally G (2017) Influence of various carbon nano-forms as supports for Pt catalyst on proton exchange membrane fuel cell performance. J Power Sources 360:196–205
11. Yuan X, Ding X-L, Wang C-Y, Ma Z-F (2013) Use of polypyrrole in catalysts for low temperature fuel cells. Energy Environ Sci 6(4):1105–1124
12. Xu JB, Zhao TS (2013) Mesoporous carbon with uniquely combined electrochemical and mass transport characteristics for polymer electrolyte membrane fuel cells. RSC Adv 3 (1):16–24
13. Antolini E (2016) Nitrogen-doped carbons by sustainable N-and C-containing natural resources as nonprecious catalysts and catalyst supports for low temperature fuel cells. Renew Sust Energ Rev 58:34–51
14. Dhakate SR, Chauhan N, Sharma S, Tawale J, Singh S, Sahare PD, Mathur RB (2011) An approach to produce single and double layer graphene from re-exfoliation of expanded graphite. Carbon 49(6):1946–1954
15. Qu L, Liu Y, Baek J-B, Dai L (2010) Nitrogen-doped graphene as efficient metal-free electrocatalyst for oxygen reduction in fuel cells. ACS Nano 4(3):1321–1326
16. Novoselov KS, Geim AK, Morozov SV, Jiang D, Zhang Y, Dubonos SV, Grigorieva IV, Firsov AA (2004) Electric field effect in atomically thin carbon films. Science 306 (5696):666–669
17. Yin PT, Shah S, Chhowalla M, Lee K-B (2015) Design, synthesis, and characterization of graphene–nanoparticle hybrid materials for bioapplications. Chem Rev 115(7):2483–2531

18. Randviir EP, Brownson DAC, Banks CE (2014) A decade of graphene research: production, applications and outlook. Mater Today 17(9):426–432
19. Zhong YL, Tian Z, Simon GP, Li D (2015) Scalable production of graphene via wet chemistry: progress and challenges. Mater Today 18(2):73–78
20. Avouris P, Dimitrakopoulos C (2012) Graphene: synthesis and applications. Mater Today 15 (3):86–97
21. Edwards RS, Coleman KS (2013) Graphene synthesis: relationship to applications. Nanoscale 5(1):38–51
22. Selvakumar D, Tripathi SK, Singh R, Nasim M (2007) Solvo-thermal preparation of cadmium telluride nanoparticles from a novel single source molecular precursor. Chem Lett 37(1):34–35
23. Das S, Sudhagar P, Kang YS, Choi W (2014) Graphene synthesis and application for solar cells. J Mater Res 29(3):299–319
24. Yi M, Shen Z (2015) A review on mechanical exfoliation for the scalable production of graphene. J Mater Chem A 3(22):11700–11715
25. Van Noorden R (2012) Production: beyond sticky tape. Nature 483:S32. https://doi.org/10.1038/483S32a
26. Dresselhaus MS, Dresselhaus G (2002) Intercalation compounds of graphite. Adv Phys 51 (1):1–186
27. Jayasena B, Subbiah S (2011) A novel mechanical cleavage method for synthesizing few-layer graphenes. Nanoscale Res Lett 6(1):95
28. Chen J, Duan M, Chen G (2012) Continuous mechanical exfoliation of graphene sheets via three-roll mill. J Mater Chem 22(37):19625–19628
29. Muñoz R, Gómez-Aleixandre C (2013) Review of CVD synthesis of graphene. Chem Vap Depos 19:297–322
30. Wu W, Liu Z, Jauregui LA, Yu Q, Pillai R, Cao H, Bao J, Chen YP, Pei S-S (2010) Wafer-scale synthesis of graphene by chemical vapor deposition and its application in hydrogen sensing. Sensor Actuat B Chem 150(1):296–300
31. Van Nang L, Kim E-T (2012) Controllable synthesis of high-quality graphene using inductively-coupled plasma chemical vapor deposition. J Electrochem Soc 159(4):K93–K96
32. Chae SJ, Güneş F, Kim KK, Kim ES, Han GH, Kim SM, Shin HJ, Yoon SM, Choi JY, Park MH (2009) Synthesis of large-area graphene layers on poly-nickel substrate by chemical vapor deposition: wrinkle formation. Adv Mater 21(22):2328–2333
33. Hummers WS Jr, Offeman RE (1958) Preparation of graphitic oxide. J Am Chem Soc 80 (6):1339–1339
34. Iqbal MZ, Abdala AA (2013) Thermally reduced graphene: synthesis, characterization and dye removal applications. RSC Adv 3(46):24455–24464
35. Staudenmaier L (1898) Verfahren zur darstellung der graphitsäure. Eur J Inorg Chem 31 (2):1481–1487
36. Choi SM, Seo MH, Kim HJ, Kim WB (2011) Synthesis of surface-functionalized graphene nanosheets with high Pt-loadings and their applications to methanol electrooxidation. Carbon 49(3):904–909
37. Kaniyoor A, Baby TT, Ramaprabhu S (2010) Graphene synthesis via hydrogen induced low temperature exfoliation of graphite oxide. J Mater Chem 20(39):8467–8469
38. Yan J, Wang Q, Wei T, Jiang L, Zhang M, Jing X, Fan Z (2014) Template-assisted low temperature synthesis of functionalized graphene for ultrahigh volumetric performance supercapacitors. ACS Nano 8(5):4720–4729
39. Antolini E (2012) Graphene as a new carbon support for low-temperature fuel cell catalysts. Appl Catal B Environ 123:52–68
40. Sheng Z-H, Shao L, Chen J-J, Bao W-J, Wang F-B, Xia X-H (2011) Catalyst-free synthesis of nitrogen-doped graphene via thermal annealing graphite oxide with melamine and its excellent electrocatalysis. ACS Nano 5(6):4350–4358

41. Stankovich S, Dikin DA, Piner RD, Kohlhaas KA, Kleinhammes A, Jia Y, Wu Y, Nguyen ST, Ruoff RS (2007) Synthesis of graphene-based nanosheets via chemical reduction of exfoliated graphite oxide. Carbon 45(7):1558–1565
42. Ramachandran R, Saranya M, Velmurugan V, Raghupathy BPC, Jeong SK, Grace AN (2015) Effect of reducing agent on graphene synthesis and its influence on charge storage towards supercapacitor applications. Appl Energy 153:22–31
43. Sridhar V, Jeon J-H, Oh I-K (2010) Synthesis of graphene nano-sheets using eco-friendly chemicals and microwave radiation. Carbon 48(10):2953–2957
44. Wang Y, Shi Z, Yin J (2011) Facile synthesis of soluble graphene via a green reduction of graphene oxide in tea solution and its biocomposites. ACS Appl Mater Interfaces 3 (4):1127–1133
45. Toh SY, Loh KS, Kamarudin SK, Daud WRW (2014) Graphene production via electrochemical reduction of graphene oxide: synthesis and characterisation. Chem Eng J 251:422–434
46. Alanyalıoğlu M, Segura JJ, Oro-Sole J, Casan-Pastor N (2012) The synthesis of graphene sheets with controlled thickness and order using surfactant-assisted electrochemical processes. Carbon 50(1):142–152
47. Wang G, Wang B, Park J, Wang Y, Sun B, Yao J (2009) Highly efficient and large-scale synthesis of graphene by electrolytic exfoliation. Carbon 47(14):3242–3246
48. Cooper AJ, Wilson NR, Kinloch IA, Dryfe RAW (2014) Single stage electrochemical exfoliation method for the production of few-layer graphene via intercalation of tetraalkylammonium cations. Carbon 66:340–350
49. Li Y, Tang L, Li J (2009) Preparation and electrochemical performance for methanol oxidation of Pt/graphene nanocomposites. Electrochem Commun 11(4):846–849
50. Jafri RI, Rajalakshmi N, Ramaprabhu S (2010) Nitrogen doped graphene nanoplatelets as catalyst support for oxygen reduction reaction in proton exchange membrane fuel cell. J Mater Chem 20(34):7114–7117
51. Hsieh SH, Hsu MC, Liu WL, Chen WJ (2013) Study of Pt catalyst on graphene and its application to fuel cell. Appl Surf Sci 277:223–230
52. Galema SA (1997) Microwave chemistry. Chem Soc Rev 26(3):233–238
53. Bharti A, Cheruvally G, Muliankeezhu S (2017) Microwave assisted, facile synthesis of Pt/CNT catalyst for proton exchange membrane fuel cell application. Int J Hydrog Energy 42(16):11622–11631
54. Zhao L, Wang Z-B, Li J-L, Zhang J-J, Sui X-L, Zhang L-M (2015) A newly-designed sandwich-structured graphene–Pt–graphene catalyst with improved electrocatalytic performance for fuel cells. J Mater Chem A 3(10):5313–5320
55. Pullamsetty A, Sundara R (2016) Investigation of catalytic activity towards oxygen reduction reaction of Pt dispersed on boron doped graphene in acid medium. J Colloid Interface Sci 479:260–270
56. Pullamsetty A, Subbiah M, Sundara R (2015) Platinum on boron doped graphene as cathode electrocatalyst for proton exchange membrane fuel cells. Int J Hydrog Energy 40 (32):10251–10261
57. Oztuna FES, Barim SB, Bozbag SE, Yu H, Aindow M, Unal U, Erkey C (2017) Graphene aerogel supported Pt electrocatalysts for oxygen reduction reaction by supercritical deposition. Electrochim Acta 250:174–184
58. Daş E, Gürsel SA, Şanli LI, Yurtcan AB (2016) Comparison of two different catalyst preparation methods for graphene nanoplatelets supported platinum catalysts. Int J Hydrog Energy 41(23):9755–9761
59. Liu S, Wang J, Zeng J, Ou J, Li Z, Liu X, Yang S (2010) "Green" electrochemical synthesis of Pt/graphene sheet nanocomposite film and its electrocatalytic property. J Power Sources 195 (15):4628–4633
60. Zhu J, Xiao M, Zhao X, Liu C, Ge J, Xing W (2015) Strongly coupled Pt nanotubes/N-doped graphene as highly active and durable electrocatalysts for oxygen reduction reaction. Nano Energy 13:318–326

61. Guo S, Dong S, Wang E (2009) Three-dimensional Pt-on-Pd bimetallic nanodendrites supported on graphene nanosheet: facile synthesis and used as an advanced nanoelectrocatalyst for methanol oxidation. ACS Nano 4(1):547–555
62. Jafri RI, Rajalakshmi N, Dhathathreyan KS, Ramaprabhu S (2015) Nitrogen doped graphene prepared by hydrothermal and thermal solid state methods as catalyst supports for fuel cell. Int J Hydrog Energy 40(12):4337–4348
63. Ryoo R, Joo SH, Jun S (1999) Synthesis of highly ordered carbon molecular sieves via template-mediated structural transformation. J Phys Chem B 103(37):7743–7746
64. Eftekhari A, Fan Z (2017) Ordered mesoporous carbon and its applications for electrochemical energy storage and conversion. Mater Chem Front 1(6):1001–1027
65. Ambrosio EP, Francia C, Manzoli M, Penazzi N, Spinelli P (2008) Platinum catalyst supported on mesoporous carbon for PEMFC. Int J Hydrog Energy 33(12):3142–3145
66. Ryoo R, Joo SH, Kruk M, Jaroniec M (2001) Ordered mesoporous carbons. Adv Mater 13 (9):677–681
67. Ryoo R, Joo SH (2004) Nanostructured carbon materials synthesized from mesoporous silica crystals by replication. Stud Surf Sci Catal 148:241–260
68. Lee J, Han S, Hyeon T (2004) Synthesis of new nanoporous carbon materials using nano-structured silica materials as templates. J Mater Chem 14(4):478–486
69. Yang H, Zhao D (2005) Synthesis of replica mesostructures by the nanocasting strategy. J Mater Chem 15(12):1217–1231
70. Lu AH, Schüth F (2006) Nanocasting: a versatile strategy for creating nanostructured porous materials. Adv Mater 18(14):1793–1805
71. Lee J, Kim J, Hyeon T (2006) Recent progress in the synthesis of porous carbon materials. Adv Mater 18(16):2073–2094
72. Chang H, Joo SH, Pak C (2007) Synthesis and characterization of mesoporous carbon for fuel cell applications. J Mater Chem 17(30):3078–3088
73. Xu W, Wu Z, Tao S (2016) Recent progress in electrocatalysts with mesoporous structures for application in polymer electrolyte membrane fuel cells. J Mater Chem A 4(42):16272–16287
74. Deng Y, Wei J, Sun Z, Zhao D (2013) Large-pore ordered mesoporous materials templated from non-Pluronic amphiphilic block copolymers. Chem Soc Rev 42(9):4054–4070
75. Antolini E (2009) Carbon supports for low-temperature fuel cell catalysts. Appl Catal B Environ 88(1–2):1–24
76. Morishita T, Tsumura T, Toyoda M, Przepiórski J, Morawski AW, Konno H, Inagaki M (2010) A review of the control of pore structure in MgO-templated nanoporous carbons. Carbon 48(10):2690–2707
77. Liang C, Li Z, Dai S (2008) Mesoporous carbon materials: synthesis and modification. Angew Chem Int Ed Engl 47(20):3696–3717
78. Joo SH, Choi SJ, Oh I, Kwak J, Liu Z, Terasaki O, Ryoo R (2001) Ordered nanoporous arrays of carbon supporting high dispersions of platinum nanoparticles. Nature 412(6843):169
79. Li Z, Jaroniec M (2001) Colloidal imprinting: a novel approach to the synthesis of mesoporous carbons. J Am Chem Soc 123(37):9208–9209
80. Li Z, Jaroniec M (2001) Silica gel-templated mesoporous carbons prepared from mesophase pitch and polyacrylonitrile. Carbon 39(13):2080–2082
81. Li Z, Jaroniec M (2003) Synthesis and adsorption properties of colloid-imprinted carbons with surface and volume mesoporosity. Chem Mater 15(6):1327–1333
82. Jun S, Joo SH, Ryoo R, Kruk M, Jaroniec M, Liu Z, Ohsuna T, Terasaki O (2000) Synthesis of new, nanoporous carbon with hexagonally ordered mesostructure. J Am Chem Soc 122 (43):10712–10713
83. Banham D, Feng F, Burt J, Alsrayheen E, Birss V (2010) Bimodal, templated mesoporous carbons for capacitor applications. Carbon 48(4):1056–1063
84. Kim CH, Lee D-K, Pinnavaia TJ (2004) Graphitic mesostructured carbon prepared from aromatic precursors. Langmuir 20(13):5157–5159

85. Banham D, Feng F, Pei K, Ye S, Birss V (2013) Effect of carbon support nanostructure on the oxygen reduction activity of Pt/C catalysts. J Mater Chem A 1(8):2812–2820
86. Zhai Y, Wan Y, Cheng Y, Shi Y, Zhang F, Tu B, Zhao D (2008) The influence of carbon source on the wall structure of ordered mesoporous carbons. J Porous Mater 15(5):601–611
87. Li X, Forouzandeh F, Fürstenhaupt T, Banham D, Feng F, Ye S, Kwok DY, Birss V (2018) New insights into the surface properties of hard-templated ordered mesoporous carbons. Carbon 127:707–717
88. Lei Z, Xiao Y, Dang L, Lu M, You W (2006) Fabrication of ultra-large mesoporous carbon with tunable pore size by monodisperse silica particles derived from seed growth process. Microporous Mesoporous Mater 96(1–3):127–134
89. Zhang S, Chen L, Zhou S, Zhao D, Wu L (2010) Facile synthesis of hierarchically ordered porous carbon via in situ self-assembly of colloidal polymer and silica spheres and its use as a catalyst support. Chem Mater 22(11):3433–3440
90. Li Y, Yang Y, Shi J, Ruan M (2008) Synthesis and characterization of hollow mesoporous carbon spheres with a highly ordered bicontinuous cubic mesostructure. Microporous Mesoporous Mater 112(1–3):597–602
91. Gierszal KP, Jaroniec M (2006) Carbons with extremely large volume of uniform mesopores synthesized by carbonization of phenolic resin film formed on colloidal silica template. J Am Chem Soc 128(31):10026–10027
92. Chuenchom L, Kraehnert R, Smarsly BM (2012) Recent progress in soft-templating of porous carbon materials. Soft Matter 8(42):10801–10812
93. Wang Q, Zhang W, Mu Y, Zhong L, Meng Y, Sun Y (2014) Synthesis of ordered mesoporous carbons with tunable pore size by varying carbon precursors via soft-template method. Microporous Mesoporous Mater 197:109–115
94. de Aa Soler-Illia GJ, Crepaldi EL, Grosso D, Sanchez C (2003) Block copolymer-templated mesoporous oxides. Curr Opin Colloid Interface Sci 8(1):109–126
95. Wan Y, Zhao D (2007) On the controllable soft-templating approach to mesoporous silicates. Chem Rev 107(7):2821–2860
96. Wan Y, Shi Y, Zhao D (2007) Supramolecular aggregates as templates: ordered mesoporous polymers and carbons. Chem Mater 20(3):932–945
97. Ma T-Y, Liu L, Yuan Z-Y (2013) Direct synthesis of ordered mesoporous carbons. Chem Soc Rev 42(9):3977–4003
98. Zhang F, Meng Y, Gu D, Yan Y, Chen Z, Tu B, Zhao D (2006) An aqueous cooperative assembly route to synthesize ordered mesoporous carbons with controlled structures and morphology. Chem Mater 18(22):5279–5288
99. Meng Y, Gu D, Zhang F, Shi Y, Yang H, Li Z, Yu C, Tu B, Zhao D (2005) Ordered mesoporous polymers and homologous carbon frameworks: amphiphilic surfactant templating and direct transformation. Angew Chem Int Ed Engl 117(43):7215–7221
100. Hillmyer MA, Bates FS, Almdal K, Mortensen K, Ryan AJ, Fairclough JPA (1996) Complex phase behavior in solvent-free nonionic surfactants. Science 271(5251):976–978
101. Bucknall DG, Anderson HL (2003) Polymers get organized. Science 302(5652):1904–1905
102. Sanchez C, Boissiere C, Grosso D, Laberty C, Nicole L (2008) Design, synthesis, and properties of inorganic and hybrid thin films having periodically organized nanoporosity. Chem Mater 20(3):682–737
103. Liang C, Hong K, Guiochon GA, Mays JW, Dai S (2004) Synthesis of a large-scale highly ordered porous carbon film by self-assembly of block copolymers. Angew Chem Int Ed Engl 43(43):5785–5789
104. Tanaka S, Nishiyama N, Egashira Y, Ueyama K (2005) Synthesis of ordered mesoporous carbons with channel structure from an organic–organic nanocomposite. Chem Commun (16):2125–2127
105. Meng Y, Gu D, Zhang F, Shi Y, Cheng L, Feng D, Wu Z, Chen Z, Wan Y, Stein A (2006) A family of highly ordered mesoporous polymer resin and carbon structures from organic–organic self-assembly. Chem Mater 18(18):4447–4464

106. Wang Y, He C, Brouzgou A, Liang Y, Fu R, Wu D, Tsiakaras P, Song S (2012) A facile soft-template synthesis of ordered mesoporous carbon/tungsten carbide composites with high surface area for methanol electrooxidation. J Power Sources 200:8–13
107. Zhao G, Zhao TS, Xu J, Lin Z, Yan X (2017) Impact of pore size of ordered mesoporous carbon FDU-15-supported platinum catalysts on oxygen reduction reaction. Int J Hydrog Energy 42(5):3325–3334
108. Wan Y, Shi Y, Zhao D (2007) Designed synthesis of mesoporous solids via nonionic-surfactant-templating approach. Chem Commun (9):897–926
109. Yu C, Fan J, Tian B, Stucky GD, Zhao D (2003) Synthesis of mesoporous silica from commercial poly (ethylene oxide)/poly (butylene oxide) copolymers: toward the rational design of ordered mesoporous materials. J Phys Chem B 107(48):13368–13375
110. Wan Y, Shi Y, Zhao D (2008) Ordered mesoporous polymers and carbon molecular sieves. Chem Mater 20:932–945
111. Deng Y, Yu T, Wan Y, Shi Y, Meng Y, Gu D, Zhang L, Huang Y, Liu C, Wu X (2007) Ordered mesoporous silicas and carbons with large accessible pores templated from amphiphilic diblock copolymer poly (ethylene oxide)-b-polystyrene. J Am Chem Soc 129 (6):1690–1697
112. Deng Y, Liu C, Gu D, Yu T, Tu B, Zhao D (2008) Thick wall mesoporous carbons with a large pore structure templated from a weakly hydrophobic PEO–PMMA diblock copolymer. J Mater Chem 18(1):91–97
113. Li W, Liu J, Zhao D (2016) Mesoporous materials for energy conversion and storage devices. Nat Rev Mater 1(6):16023
114. Liu H, Song C, Zhang L, Zhang J, Wang H, Wilkinson DP (2006) A review of anode catalysis in the direct methanol fuel cell. J Power Sources 155(2):95–110
115. Shen W, Li Z, Liu Y (2008) Surface chemical functional groups modification of porous carbon. Recent Pat Chem Eng 1(1):27–40
116. Tang J, Liu J, Torad NL, Kimura T, Yamauchi Y (2014) Tailored design of functional nanoporous carbon materials toward fuel cell applications. Nano Today 9(3):305–323
117. Guha A, Lu W, Zawodzinski TA Jr, Schiraldi DA (2007) Surface-modified carbons as platinum catalyst support for PEM fuel cells. Carbon 45(7):1506–1517
118. Salgado JRC, Quintana JJ, Calvillo L, Lázaro MJ, Cabot PL, Esparbé I, Pastor E (2008) Carbon monoxide and methanol oxidation at platinum catalysts supported on ordered mesoporous carbon: the influence of functionalization of the support. Phys Chem Chem Phys 10(45):6796–6806
119. Perini L, Durante C, Favaro M, Perazzolo V, Agnoli S, Schneider O, Granozzi G, Gennaro A (2015) Metal–support interaction in platinum and palladium nanoparticles loaded on nitrogen-doped mesoporous carbon for oxygen reduction reaction. ACS Appl Mater Interfaces 7 (2):1170–1179
120. Xiao C, Chen X, Fan Z, Liang J, Zhang B, Ding S (2016) Surface-nitrogen-rich ordered mesoporous carbon as an efficient metal-free electrocatalyst for oxygen reduction reaction. Nanotechnology 27(44):445402
121. Ji X, Lee KT, Holden R, Zhang L, Zhang J, Botton GA, Couillard M, Nazar LF (2010) Nanocrystalline intermetallics on mesoporous carbon for direct formic acid fuel cell anodes. Nat Chem 2(4):286
122. Zhou J-H, He J-P, Ji Y-J, Dang W-J, Liu X-L, Zhao G-W, Zhang C-X, Zhao J-S, Fu Q-B, Hu H-P (2007) CTAB assisted microwave synthesis of ordered mesoporous carbon supported Pt nanoparticles for hydrogen electro-oxidation. Electrochim Acta 52(14):4691–4695
123. Li F, Wang H, Zhao X, Li B, Zhang Y (2016) Microwave-assisted route for the preparation of Pd anchored on surfactant functionalized ordered mesoporous carbon and its electrochemical applications. RSC Adv 6(75):70810–70815
124. Zhang Y, Bo X, Luhana C, Guo L (2011) Preparation and electrocatalytic application of high dispersed Pt nanoparticles/ordered mesoporous carbon composites. Electrochim Acta 56 (17):5849–5854

125. Momčilović M, Stojmenović M, Gavrilov N, Pašti I, Mentus S, Babić B (2014) Complex electrochemical investigation of ordered mesoporous carbon synthesized by soft-templating method: charge storage and electrocatalytical or Pt-electrocatalyst supporting behavior. Electrochim Acta 125:606–614
126. Cao J, Chen Z, Xu J, Wang W, Chen Z (2013) Mesoporous carbon synthesized from dual colloidal silica/block copolymer template approach as the support of platinum nanoparticles for direct methanol fuel cells. Electrochim Acta 88:184–192
127. Zhang C, Xu L, Shan N, Sun T, Chen J, Yan Y (2014) Enhanced electrocatalytic activity and durability of Pt particles supported on ordered mesoporous carbon spheres. ACS Catal 4 (6):1926–1930
128. Joo SH, Kwon K, You DJ, Pak C, Chang H, Kim JM (2009) Preparation of high loading Pt nanoparticles on ordered mesoporous carbon with a controlled Pt size and its effects on oxygen reduction and methanol oxidation reactions. Electrochim Acta 54(24):5746–5753
129. Joo SH, Lee HI, You DJ, Kwon K, Kim JH, Choi YS, Kang M, Kim JM, Pak C, Chang H (2008) Ordered mesoporous carbons with controlled particle sizes as catalyst supports for direct methanol fuel cell cathodes. Carbon 46(15):2034–2045
130. Ahn C-Y, Cheon J-Y, Joo S-H, Kim J (2013) Effects of ionomer content on Pt catalyst/ordered mesoporous carbon support in polymer electrolyte membrane fuel cells. J Power Sources 222:477–482
131. Kim N-I, Cheon JY, Kim JH, Seong J, Park J-Y, Joo SH, Kwon K (2014) Impact of framework structure of ordered mesoporous carbons on the performance of supported Pt catalysts for oxygen reduction reaction. Carbon 72:354–364
132. Calvillo L, Lázaro MJ, García-Bordejé E, Moliner R, Cabot PL, Esparbé I, Pastor E, Quintana JJ (2007) Platinum supported on functionalized ordered mesoporous carbon as electrocatalyst for direct methanol fuel cells. J Power Sources 169(1):59–64
133. Morales-Acosta D, Rodríguez-Varela FJ, Benavides R (2016) Template-free synthesis of ordered mesoporous carbon: application as support of highly active Pt nanoparticles for the oxidation of organic fuels. Int J Hydrog Energy 41(5):3387–3398
134. Samiee L, Shoghi F, Maghsodi A (2014) In situ functionalisation of mesoporous carbon electrodes with carbon nanotubes for proton exchange membrane fuel-cell application. Mater Chem Phys 143(3):1228–1235
135. Nsabimana A, Bo X, Zhang Y, Li M, Han C, Guo L (2014) Electrochemical properties of boron-doped ordered mesoporous carbon as electrocatalyst and Pt catalyst support. J Colloid Interface Sci 428:133–140
136. Song P, Zhu L, Bo X, Wang A, Wang G, Guo L (2014) Pt nanoparticles incorporated into phosphorus-doped ordered mesoporous carbons: enhanced catalytic activity for methanol electrooxidation. Electrochim Acta 127:307–314
137. Bruno MM, Petruccelli MA, Viva FA, Corti HR (2013) Mesoporous carbon supported PtRu as anode catalyst for direct methanol fuel cell: polarization measurements and electrochemical impedance analysis of mass transport. Int J Hydrog Energy 38(10):4116–4123
138. Hung C-T, Liou Z-H, Veerakumar P, Wu P-H, Liu T-C, Liu S-B (2016) Ordered mesoporous carbon supported bifunctional PtM (M= Ru, Fe, Mo) electrocatalysts for a fuel cell anode. Chin J Catal 37(1):43–53
139. Volotskova O, Levchenko I, Shashurin A, Raitses Y, Ostrikov K, Keidar M (2010) Single-step synthesis and magnetic separation of graphene and carbon nanotubes in arc discharge plasmas. Nanoscale 2(10):2281–2285
140. Li X, Cai W, An J, Kim S, Nah J, Yang D, Piner R, Velamakanni A, Jung I, Tutuc E (2009) Large-area synthesis of high-quality and uniform graphene films on copper foils. Science 324 (5932):1312–1314
141. Titirici M-M, White RJ, Falco C, Sevilla M (2012) Black perspectives for a green future: hydrothermal carbons for environment protection and energy storage. Energy Environ Sci 5 (5):6796–6822

142. Wei L, Sevilla M, Fuertes AB, Mokaya R, Yushin G (2011) Hydrothermal carbonization of abundant renewable natural organic chemicals for high-performance supercapacitor electrodes. Adv Energy Mater 1(3):356–361
143. Liu W-J, Jiang H, Yu H-Q (2015) Development of biochar-based functional materials: toward a sustainable platform carbon material. Chem Rev 115(22):12251–12285
144. Falco C, Baccile N, Titirici M-M (2011) Morphological and structural differences between glucose, cellulose and lignocellulosic biomass derived hydrothermal carbons. Green Chem 13 (11):3273–3281
145. Fellinger TP, White RJ, Titirici MM, Antonietti M (2012) Borax-mediated formation of carbon aerogels from glucose. Adv Funct Mater 22(15):3254–3260
146. Liu X, Antonietti M (2014) Molten salt activation for synthesis of porous carbon nanostructures and carbon sheets. Carbon 69:460–466
147. Xiao Y, Dong H, Lei B, Qiu H, Liu Y, Zheng M (2015) Ordered mesoporous carbons with fiber-and rod-like morphologies for supercapacitor electrode materials. Mater Lett 138:37–40
148. Ting C-C, Wu H-Y, Vetrivel S, Saikia D, Pan Y-C, Fey GTK, Kao H-M (2010) A one-pot route to synthesize highly ordered mesoporous carbons and silicas through organic–inorganic self-assembly of triblock copolymer, sucrose and silica. Microporous Mesoporous Mater 128 (1–3):1–11
149. Sivadas DL, Vijayan S, Rajeev R, Ninan KN, Prabhakaran K (2016) Nitrogen-enriched microporous carbon derived from sucrose and urea with superior CO_2 capture performance. Carbon 109:7–18
150. Yu L, Brun N, Sakaushi K, Eckert J, Titirici MM (2013) Hydrothermal nanocasting: synthesis of hierarchically porous carbon monoliths and their application in lithium–sulfur batteries. Carbon 61:245–253
151. Yu L, Falco C, Weber J, White RJ, Howe JY, Titirici M-M (2012) Carbohydrate-derived hydrothermal carbons: a thorough characterization study. Langmuir 28(33):12373–12383
152. Wu Z-Y, Liang H-W, Chen L-F, Hu B-C, Yu S-H (2015) Bacterial cellulose: a robust platform for design of three dimensional carbon-based functional nanomaterials. Acc Chem Res 49 (1):96–105
153. Klemm D, Kramer F, Moritz S, Lindström T, Ankerfors M, Gray D, Dorris A (2011) Nanocelluloses: a new family of nature-based materials. Angew Chem Int Ed Engl 50 (24):5438–5466
154. Liu Q, Chen C, Pan F, Zhang J (2015) Highly efficient oxygen reduction on porous nitrogen-doped nanocarbons directly synthesized from cellulose nanocrystals and urea. Electrochim Acta 170:234–241
155. Li S, Xu W, Cheng P, Luo J, Zhou D, Li J, Li R, Yuan D (2017) Bacterial cellulose derived iron and phosphorus co-doped carbon nanofibers as an efficient oxygen reduction reaction electrocatalysts. Synth Met 223:137–144
156. Liang H-W, Wu Z-Y, Chen L-F, Li C, Yu S-H (2015) Bacterial cellulose derived nitrogen-doped carbon nanofiber aerogel: an efficient metal-free oxygen reduction electrocatalyst for zinc-air battery. Nano Energy 11:366–376
157. Lai F, Miao YE, Zuo L, Lu H, Huang Y, Liu T (2016) Biomass-derived nitrogen-doped carbon nanofiber network: a facile template for decoration of ultrathin nickel-cobalt layered double hydroxide nanosheets as high-performance asymmetric supercapacitor electrode. Small 12 (24):3235–3244
158. Mulyadi A, Zhang Z, Dutzer M, Liu W, Deng Y (2017) Facile approach for synthesis of doped carbon electrocatalyst from cellulose nanofibrils toward high-performance metal-free oxygen reduction and hydrogen evolution. Nano Energy 32:336–346
159. Wu Z-Y, Liang H-W, Li C, Hu B-C, Xu X-X, Wang Q, Chen J-F, Yu S-H (2014) Dyeing bacterial cellulose pellicles for energetic heteroatom doped carbon nanofiber aerogels. Nano Res 7(12):1861–1872
160. Zu G, Shen J, Zou L, Wang F, Wang X, Zhang Y, Yao X (2016) Nanocellulose-derived highly porous carbon aerogels for supercapacitors. Carbon 99:203–211

161. Sun Y, Wang X, Ding C, Cheng W, Chen C, Hayat T, Alsaedi A, Hu J, Wang X (2016) Direct synthesis of bacteria-derived carbonaceous nanofibers as a highly efficient material for radionuclides elimination. ACS Sustain Chem Eng 4(9):4608–4616
162. Wu Z-Y, Hu B-C, Wu P, Liang H-W, Yu Z-L, Lin Y, Zheng Y-R, Li Z, Yu S-H (2016) Mo 2 C nanoparticles embedded within bacterial cellulose-derived 3D N-doped carbon nanofiber networks for efficient hydrogen evolution. NPG Asia Mater 8(7):e288
163. Rybarczyk MK, Gontarek E, Lieder M, Titirici M-M (2018) Salt melt synthesis of curved nitrogen-doped carbon nanostructures: ORR kinetics boost. Appl Surf Sci 435:543–551
164. Kucinska A, Golembiewski R, Lukaszewicz JP (2014) Synthesis of N-rich activated carbons from chitosan by chemical activation. Sci Adv Mater 6(2):290–297
165. Wang Y-Y, Hou B-H, Lü H-Y, Wan F, Wang J, Wu X-L (2015) Porous N-doped carbon material derived from prolific chitosan biomass as a high-performance electrode for energy storage. RSC Adv 5(118):97427–97434
166. Chen P, Wang L-K, Wang G, Gao M-R, Ge J, Yuan W-J, Shen Y-H, Xie A-J, Yu S-H (2014) Nitrogen-doped nanoporous carbon nanosheets derived from plant biomass: an efficient catalyst for oxygen reduction reaction. Energy Environ Sci 7(12):4095–4103
167. Liu X, Zhou Y, Zhou W, Li L, Huang S, Chen S (2015) Biomass-derived nitrogen self-doped porous carbon as effective metal-free catalysts for oxygen reduction reaction. Nanoscale 7 (14):6136–6142
168. Cheng P, Li T, Yu H, Zhi L, Liu Z, Lei Z (2016) Biomass-derived carbon fiber aerogel as a binder-free electrode for high-rate supercapacitors. J Phys Chem C 120(4):2079–2086
169. Song S, Ma F, Wu G, Ma D, Geng W, Wan J (2015) Facile self-templating large scale preparation of biomass-derived 3D hierarchical porous carbon for advanced supercapacitors. J Mater Chem A 3(35):18154–18162
170. Cheng P, Gao S, Zang P, Yang X, Bai Y, Xu H, Liu Z, Lei Z (2015) Hierarchically porous carbon by activation of shiitake mushroom for capacitive energy storage. Carbon 93:315–324
171. Song H, Li H, Wang H, Key J, Ji S, Mao X, Wang R (2014) Chicken bone-derived N-doped porous carbon materials as an oxygen reduction electrocatalyst. Electrochim Acta 147:520–526
172. Wang R, Wang K, Wang Z, Song H, Wang H, Ji S (2015) Pig bones derived N-doped carbon with multi-level pores as electrocatalyst for oxygen reduction. J Power Sources 297:295–301
173. Fang Y, Wang H, Yu H, Peng F (2016) From chicken feather to nitrogen and sulfur co-doped large surface bio-carbon flocs: an efficient electrocatalyst for oxygen reduction reaction. Electrochim Acta 213:273–282
174. Gao A, Guo N, Yan M, Li M, Wang F, Yang R (2018) Hierarchical porous carbon activated by $CaCO_3$ from pigskin collagen for CO_2 and H_2 adsorption. Microporous Mesoporous Mater 260:172–179
175. Guo C, Liao W, Li Z, Chen C (2015) Exploration of the catalytically active site structures of animal biomass-modified on cheap carbon nanospheres for oxygen reduction reaction with high activity, stability and methanol-tolerant performance in alkaline medium. Carbon 85:279–288
176. Wang H, Wang K, Song H, Li H, Ji S, Wang Z, Li S, Wang R (2015) N-doped porous carbon material made from fish-bones and its highly electrocatalytic performance in the oxygen reduction reaction. RSC Adv 5(60):48965–48970
177. Guo C, Hu R, Liao W, Li Z, Sun L, Shi D, Li Y, Chen C (2017) Protein-enriched fish "biowaste" converted to three-dimensional porous carbon nano-network for advanced oxygen reduction electrocatalysis. Electrochim Acta 236:228–238
178. Wu H, Geng J, Ge H, Guo Z, Wang Y, Zheng G (2016) Egg-derived mesoporous carbon microspheres as bifunctional oxygen evolution and oxygen reduction electrocatalysts. Adv Energy Mater 6(20):1600794, 1–8
179. Lu Y, Zhu N, Yin F, Yang T, Wu P, Dang Z, Liu M, Wei X (2017) Biomass-derived heteroatoms-doped mesoporous carbon for efficient oxygen reduction in microbial fuel cells. Biosens Bioelectron 98:350–356

180. Shao Z, Zhang W, An D, Zhang G, Wang Y (2015) Pyrolyzed egg yolk as an efficient bifunctional electrocatalyst for oxygen reduction and evolution reactions. RSC Adv 5 (118):97508–97511
181. Chaudhari KN, Song MY, Yu JS (2014) Transforming hair into heteroatom-doped carbon with high surface area. Small 10(13):2625–2636
182. Zhao Z-Q, Xiao P-W, Zhao L, Liu Y, Han B-H (2015) Human hair-derived nitrogen and sulfur co-doped porous carbon materials for gas adsorption. RSC Adv 5(90):73980–73988
183. Liu X, Zhou W, Yang L, Li L, Zhang Z, Ke Y, Chen S (2015) Correction: nitrogen and sulfur co-doped porous carbon derived from human hair as highly efficient metal-free electrocatalysts for hydrogen evolution reactions. J Mater Chem A 3(18):10135–10135
184. Ding W, Li L, Xiong K, Wang Y, Li W, Nie Y, Chen S, Qi X, Wei Z (2015) Shape fixing via salt recrystallization: a morphology-controlled approach to convert nanostructured polymer to carbon nanomaterial as a highly active catalyst for oxygen reduction reaction. J Am Chem Soc 137(16):5414–5420
185. Liang J, Du X, Gibson C, Du XW, Qiao SZ (2013) N-doped graphene natively grown on hierarchical ordered porous carbon for enhanced oxygen reduction. Adv Mater 25 (43):6226–6231
186. Gong X, Liu S, Ouyang C, Strasser P, Yang R (2015) Nitrogen-and phosphorus-doped biocarbon with enhanced electrocatalytic activity for oxygen reduction. ACS Catal 5 (2):920–927
187. Ye D, Wang L, Zhang R, Liu B, Wang Y, Kong J (2015) Facile preparation of N-doped mesocellular graphene foam from sludge flocs for highly efficient oxygen reduction reaction. J Mater Chem A 3(29):15171–15176
188. Zhou T, Wang H, Ji S, Linkov V, Wang R (2014) Soybean-derived mesoporous carbon as an effective catalyst support for electrooxidation of methanol. J Power Sources 248:427–433
189. Zhou T, Wang H, Ji S, Feng H, Wang R (2014) Synthesis of mesoporous carbon from okara and application as electrocatalyst support. Fuel Cells 14(2):296–302
190. Zhao X, Zhu J, Liang L, Li C, Liu C, Liao J, Xing W (2014) Biomass-derived N-doped carbon and its application in electrocatalysis. Appl Catal B Environ 154–155:177–182
191. Yan Z, Zhang M, Xie J, Wang H, Wei W (2013) Smaller Pt particles supported on mesoporous bowl-like carbon for highly efficient and stable methanol oxidation and oxygen reduction reaction. J Power Sources 243:48–53
192. Cheng K, Kou Z, Zhang J, Jiang M, Wu H, Hu L, Yang X, Pan M, Mu S (2015) Ultrathin carbon layer stabilized metal catalysts towards oxygen reduction. J Mater Chem A 3 (26):14007–14014
193. Liu H, Cao Y, Wang F, Zhang W, Huang Y (2014) Pig bone derived hierarchical porous carbon-supported platinum nanoparticles with superior electrocatalytic activity towards oxygen reduction reaction. Electroanalysis 26(8):1831–1839
194. Cheng Y, Lu H, Zhang K, Yang F, Dai W, Liu C, Dong H, Zhang X (2018) Fabricating Pt-decorated three dimensional N-doped carbon porous microspherical cavity catalyst for advanced oxygen reduction reaction. Carbon 128:38–45
195. Yang R, Qiu X, Zhang H, Li J, Zhu W, Wang Z, Huang X, Chen L (2005) Monodispersed hard carbon spherules as a catalyst support for the electrooxidation of methanol. Carbon 43 (1):11–16
196. Afraz A, Rafati AA, Hajian A, Khoshnood M (2015) Electrodeposition of Pt nanoparticles on new porous graphitic carbon nanostructures prepared from biomass for fuel cell and methanol sensing applications. Electrocatalysis 6(2):220–228
197. Yang H, Wang H, Ji S, Ma Y, Linkov V, Wang R (2014) Nanostructured Pt supported on cocoon-derived carbon as an efficient electrocatalyst for methanol oxidation. J Solid State Chem 18(6):1503–1512
198. Lobos MLN, Sieben JM, Comignani V, Duarte M, Volpe MA, Moyano EL (2016) Biochar from pyrolysis of cellulose: an alternative catalyst support for the electro-oxidation of methanol. Int J Hydrog Energy 41(25):10695–10706

Chapter 6
Progress on the Functionalization of Carbon Nanostructures for Fuel Cell Electrocatalysts

X. Shi, K. Pérez-Salcedo, S. Hanif, R. Anwar, L. Cindrella, N. Iqbal, S. Jose, and A. M. Kannan

Abstract Carbon supports are functionalized with −COOH, −OH, $-NH_2$, surfactants, and polyelectrolytes to efficiently attach and disperse metal nanoparticles on their surface influencing the catalytic activity of fuel cell electrocatalysts. This chapter discusses different methods which have been applied for carbon support surface modifications, from chemical covalent to physical non-covalent functionalization. In the covalent method, different oxidizing agents and nitrogen-containing precursors are commonly used to anchor functional groups on carbon surface. On the other hand, in the non-covalent functionalization method different surfactants and polyelectrolytes act as capping agents and anchoring sites to help disperse and attach metal nanoparticles. With the help of surface functionalization, both electrocatalyst and fuel cell performance are improved.

X. Shi · A. M. Kannan (✉)
Fuel Cell Lab, The Polytechnic School, Ira A. Fulton Schools of Engineering, Arizona State University, Mesa, AZ, USA
e-mail: amk@asu.edu

K. Pérez-Salcedo
Centro de Investigación Científica de Yucatán, Carretera Sierra Papacal – Chuburná Puerto, Mérida, Yucatán, Mexico

S. Hanif · R. Anwar
Fuel Cell Lab, The Polytechnic School, Ira A. Fulton Schools of Engineering, Arizona State University, Mesa, AZ, USA

USPCAS-E, National University of Sciences and Technology, Islamabad, Pakistan

L. Cindrella
Department of Chemistry, National Institute of Technology, Tiruchirappalli, India

N. Iqbal
USPCAS-E, National University of Sciences and Technology, Islamabad, Pakistan

S. Jose
Advanced Materials Lab, School of Physics, Madurai Kamaraj University, Madurai, India

F. J. Rodríguez-Varela, T. W. Napporn (eds.), *Advanced Electrocatalysts for Low-Temperature Fuel Cells*, https://doi.org/10.1007/978-3-319-99019-4_6

Keywords Carbon support electrocatalysts · Covalent functionalization · Carboxylic · Hydroxyl · Nitrogen · Non-covalent functionalization · Defects · Surfactant · Polyelectrolyte · Anchoring · Metal dispersion · ORR · MOR · PEM · AFC

6.1 Introduction

Direct electrochemical conversion of chemical energy of fuel to electrical energy without any mechanical movement leads to increased fuel conversion efficiency. Fuel cells are one of the most efficient systems, not limited by the thermodynamic constraints imposed by Carnot efficiency [1, 2]. The electrolyte employed in the fuel cells determines the range of operating temperature and physicochemical properties of the other cell components (catalysts, electrodes, interconnectors, and current collectors) [3]. For example, a proton-exchange membrane fuel cell (PEMFC) is typically operated below 100 °C and hence could be a potential system for automotive applications. In contrast, the molten carbonate or solid oxide electrolyte-based fuel cells require much higher temperatures (>800 °C) making them slow to start up but ideal for continuous power generation. The PEMFCs are being accepted as promising power sources for automotive, stationary, and portable applications due to their higher power densities compared to other fuel cell types [4, 5]. While low-temperature fuel cells are better suited for periodic ON–OFF usage patterns, the slow electrochemical kinetics at low temperature require the use of catalysts to achieve the type of performance required for typical transportation applications. The heart of the PEMFC system is the membrane-electrode assembly (MEA) consisting of a proton conducting membrane with anode and cathode catalyst layers (CL) and gas diffusion layers (GDL) in contact with each of the CLs. Figure 6.1 illustrates the schematic of an MEA configuration and its main components including the gas diffusion layers, electrocatalyst layers, and polymer electrolyte membrane. The

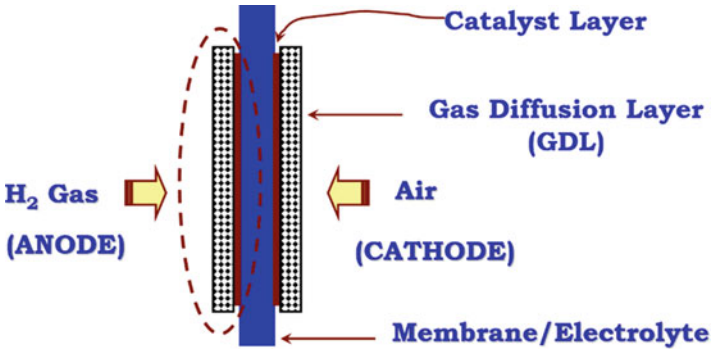

Fig. 6.1 Schematic configuration of membrane electrodes assembly

hydrogen oxidation reaction (HOR) occurs at the anode catalyst layer, while the oxygen reduction reaction (ORR) takes place at the cathode catalyst layer. Protons generated at the anode are transported through a humidified electrolyte membrane and they combine with pure oxygen (or oxygen from air) at the cathode to form water and heat. As seen in Fig. 6.1, the electrolyte is sandwiched with the electrocatalyst and GDL layers and the assembly is generally referred to as a membrane electrode assembly (MEA). The GDL is a crucial component in the PEMFC and hence an enormous amount of research and development is being carried out by educational institutions as well as commercial organizations. Membranes with ionic groups that are ionized by water, like perfluorinated sulfonic acid ionomers, need to be hydrated in order to maintain high proton conductivity and ensure adequate fuel cell performance with access to optimum amount of reactants.

Generally, the low catalyst activity and mass transportation, mainly at the cathode, limit the power density values in PEMFCs. To date, efforts in improving the PEMFC performance have been focused through maximizing catalyst utilization by decreasing the catalyst nanoparticles (NPs) on the carbon support, dispersing the platinum NPs on the support uniformly, and also by enhancing proton transport using a polymer electrolyte within the catalyst layer [6–8]. With an objective to lower the cost, other electrocatalysts such as metal porphyrins, metal oxides, and ruthenium-based chalcogenides have been pursued in the literature over the years; however, their electrocatalytic activities are generally inferior to that of pure platinum [9–11]. Therefore, a major breakthrough is desired to achieve superior performance and durability demanded for commercial viability of PEMFCs.

Significant progress has been made in the PEMFC development with increase in stack conversion efficiency and reduction in the overall system cost, from 1960s. However, there are several technical barriers related to hydrogen generation, storage, and distribution, such as system cost, fuel cell reliability, durability, etc., which remain the major challenges for PEMFCs. Electrocatalysts such as platinum or other highly active materials play a critical role in the cost and durability of PEMFCs [12]. With the Pt-based anode and cathode catalysts used in PEMFCs, the cost of the electrocatalysts accounts for 35–42% of the total cost of the PEMFC stacks [13]. Furthermore, the sensitivity of Pt-based catalysts to contamination, carbon corrosion, and nanoparticle agglomeration has shifted the technical burden to a high purity hydrogen supply and the development of advanced support materials. A flurry of publication in the literature highlights the various approaches in developing different Pt-based nanocatalyst support materials to improve performance as well as durability [14]. The major objective of this review is to examine recent development on carbon supports to enhance electrocatalytic properties and electrochemical performance to promote the use of cost-effective catalyst in PEM and alkaline fuel cells. In particular, this chapter discusses advanced carbon-based supports for electrocatalysts through various functionalizations for low-temperature fuel cells.

In general, carbon-based materials with the unique characteristics of thermal, optical, mechanical, chemical, and electrical properties are highly suitable for establishing covalent and non-covalent bonds with organic molecules when the functionalization is carried out. During functionalization, functional groups such

as −COOH, −OH, −H, =O, −N, and −F form covalent bonding with various carbon-based materials. Non-covalent bonding can be physical interactions as like Van der Waals interaction, ion–ion interaction, ion–dipole interaction, hydrogen bonding, dipole–dipole interaction, dipole-induced dipole interaction, or London forces. Carbon materials are mainly used in low-temperature fuel cell applications as catalyst support due to their higher surface area/porosity, electronic conductivity, and oxidative stability. Acetylene black and Ketjenblack are used as support materials in low-temperature fuel cells for the improvement of catalyst activity and stability from the very beginning [15, 16].

In general, metal NPs can be dispersed on to the carbon support through impregnation or colloidal methods. McBreen and coworkers studied extensively the Pt dispersion on five different carbon supports (Regal 600R, Vulcan XC-72, Monarch 1300, Mogul L, and CSX98) by colloidal method and came up with the conclusion that Regal 600R and Vulcan XC-72 have higher Pt dispersion [17].

Even though the carbon blacks have high surface area, the micropores in them limit fuel supply, so the catalytic activity decreases. So, mesoporous carbons with high surface area have effective dispersion of Pt with pore size greater than 20 nm. There are other types of nonconventional carbon materials including CNTs, carbon aerogels, carbon nanohorns, ordered mesoporous carbons, carbon nanocoils, graphene, carbon nanofibers, and carbon quantum dots. These are of great interest because of their improved electrical and mechanical properties, as well as versatile pore size distribution [14].

Generally, carbon blacks are activated and functionalized before being used as catalyst support to enhance the metal dispersion and catalytic activity. Usually, carbon blacks are activated by either chemical or physical activation. The activation of carbon blacks defines the catalyst activity. Carbon blacks can be activated with oxidants like HNO_3, H_2O_2, O_2, or O_3 which introduce different functional groups like carboxylic, lactonic, or etheric groups, on their surfaces [18]. All types of oxidative treatments are for the enhancement of Pt dispersion on the carbon blacks. Sepulveda-Escribano et al. revealed that the presence of oxygen functional groups provides the anchoring sites for $[Pt(NH_3)_4]^{2+}$ but they do not have effect on the retention of Pt NPs on the support when H_2PtCl_6 is used as precursor [19].

The activity and performance of an electrocatalyst deeply depend on the type of carbon support because the catalyst–support interaction plays a crucial role in electrocatalytic performance. CNTs are considered the best carbon support so far. Pt NPs could not be dispersed on CNTs because of their inert nature, so they need to be functionalized for efficient dispersion of Pt NPs on CNTs. Functionalization is basically the surface structure modification by adding different functional groups and defects on to the surface. These defects provide the anchoring sites for Pt NPs. Covalent and non-covalent functionalization are the two main types of carbon support functionalization methods.

In the covalent functionalization, CNTs are treated chemically with acids (HNO_3 or H_2SO_4) to create the anchoring sites on the surface. On the other hand, CNTs are physically treated with surfactants, polymers, and other capping agents in the non-covalent functionalization process. Although the covalent functionalization

improves the dispersion of Pt NPs, but it also causes damage to the CNTs structure which ultimately decreases the electrocatalyst performance stability. On the other side, the non-covalent functionalization prevents the structural damage of CNTs along with the efficient dispersion of Pt NPs which improves the electrocatalyst activity and stability [20].

6.2 Covalent Functionalization

6.2.1 =O, −OH, −COOH Functionalization

Chemical behavior and surface morphology of various carbon supports can be altered by the addition of different functional groups on their surfaces in a process called surface modification. It can be covalent or non-covalent based on the nature of bonding between carbon support and functional group. Surface modification provides an enabling environment for the good dispersion of catalyst nanoparticles by improving the interaction between the support and catalyst [21].

The most extensively used functionalization technique is the oxidation of carbon support using strong oxidizing agents such as sulfuric acid, nitric acid, hydrogen peroxide, and hydrofluoric acid thus creating different oxygen functional groups. This treatment introduces hydrophilic groups such as hydroxyl (–OH), carboxyl (–COOH), and carbonyl (>C=O) groups to the surface of carbon support. These groups act as active sites for the deposition of metal/Pt NPs which results in homogeneous distribution of NPs enhancing the electrocatalytic activity and stability of metal/Pt NPs on covalently functionalized CNTs as compared to the Pt NPs on spherical carbon [22] but causing permanent damage to the structure of CNTs [23].

In 2010, Hernández-Fernández et al. subjected MWCNTs to the strong acid treatment to be used as a support for the Pt metal NPs incorporation. Due to the increased number of Pt adsorption sites, they showed superior electrochemical performance for ORR in a proton-exchange membrane fuel cell. The maximum power density for Pt NPs dispersed on acid-treated MWCNTs was higher (490 mW.cm^{-2}) than Pt NPs supported on untreated carbon (450 mW.cm^{-2}) [22].

In 2011, Salgado and coworkers studied the activity of Pt catalyst supported on functionalized carbon using sulfuric acid and nitric acid. Compared to the untreated carbon, acid-treated carbon showed improved electrochemical performance for methanol oxidation. The synergistic effect between the surface functional groups carboxyl (−COOH), hydroxyl (-OH), and carbonyl (>C=O) groups created by the acid treatment and the Pt metal NPs resulted an efficient electrocatalyst for methanol oxidation [24].

The performance of the electrocatalysts depends on the support properties such as surface area, porosity, nanoparticle size, electric conductivity, etc. The influence of functionalization of carbon nanofibers on the electrochemical performance of the electrocatalyst was studied by Sebastián et al. [25]. In their work, carbon nanofibers were modified by introduction of oxygenated groups on their surface by oxidizing in

acid medium. By this method, Pt NPs supported on functionalized carbon nanofibers exhibited two times higher current density towards methanol electrooxidation than commercial untreated Pt/C catalyst [25]. Another study showed significantly higher MOR performance using Pt NPs (3.5 nm) supported on acid-functionalized carbon with homogeneous catalyst distribution, as evident from the TEM images [26]. Recently, Kim et al. have reported the performance of carbon black (CB) treated by mild HCl and HNO_3 (0.5 M) at 80 °C for 12 h. FTIR spectrum showed an additional peak at 1740 cm^{-1} for treated sample corresponding to the C=O vibration. The XPS C1s spectrum results in graphitized carbon, C–O, and C=O at 284.6 eV, 286.0 eV, and 289.0 eV, respectively. The Pt NPs were reduced and dispersed on the treated and untreated samples. The oxygenated carbon showed smaller Pt NPs size and higher electrochemical surface area (ECSA); however, the durability of treated carbon support was inferior as compared to untreated CB [27]. CNF and three different grades of amorphous carbon (SX Ultra, Cat SX Plus Cat, and DLC Supra 50 from Norit Inc. Marshall TX) were treated with concentrated 7 M HNO_3 at 120 °C for 16 h with a mixture of concentrated H_2SO_4 and HNO_3 with 1:1 ratio at 120 °C for 4 h. The mixture of H_2SO_4 and HNO_3 gives severer environment to functionalize the carbon support and the amorphous carbon started to dissolve into the acid mixture. From XPS O1s analysis, 5% atomic ratio of oxygen was observed to be present in the 7 M HNO_3 treated CNF sample and 21.4% atomic ratio of oxygen atoms when treated with H_2SO_4 and HNO_3. The surface area decreased from 1300, 1100, and 2090 $m^2\ g^{-1}$ to 928, 881, and 913 $m^2\ g^{-1}$ of SX Ultra, Cat SX Plus Cat, and DLC Supra 50, respectively. The pH values of those four kinds of carbon were from alkaline/neutral to acidic ~2–3 after 7 M HNO_3 treatment and the functional group was proposed to be −COOH. The Pt NPs were anchored and dispersed by refluxing in ethylene glycol (EG), with average particle size around 3 nm [28].

Table 6.1 discusses the covalent modification of different types of carbon supports using strong oxidants such as sulfuric acid and nitric acid which are commonly used for the modification of carbon supports. These modifications lead to improved catalytic performance in methanol oxidation reaction (MOR) and ORR. The enhanced catalytic properties can be attributed to homogeneous dispersion of metal NPs on the support aided by the presence of surface functional groups.

Functional groups like C–O, C=O, and −COOH can also be introduced on to the CNTs surface by plasma treatment. Depending on the plasma precursor gas, the functional group of carbon surface can be varied. With O_2/Ar plasma, the oxygen-containing functional groups like C–O, C=O, and HO–C=O can be introduced on to the carbon nanotube surface. The surface of CNTs contains sp^2 hybridization (C=C) which is active and can be easily attacked by the plasma forming two free radicals. First, the feeding plasma containing active O atoms react with the free radicals to form C–O, and then C–O is stabilized by the hydrogen atom to form C–OH. The hydrogen atoms can be introduced during the synthesis phase of MWCNTs or via atmosphere absorption as shown in Fig. 6.2a. Oxygen radicals can be generated and these can undergo an intramolecular reaction with C–C bonds forming new C=O bonds, as presented in Fig. 6.2b. Two more radicals can be generated from C=O site

Table 6.1 Covalent functionalization of carbon supports

No.	Carbon type	Functionalization method/agent	Size (nm)/ catalyst	Catalytic performance	Reference
1.	Vulcan carbon (VC)	Heating HNO_3 + H_2SO_4 (3:1 v/v)	3.51 (Pt)	18 $mA.cm^{-2}$ (MOR vs Ag/AgCl)	[26]
2.	Graphene oxide	Mixing GO + 2 amino ethanethiol (1:1)	10 (Pt/Au)	0.95 $mA.cm^{-2}$ (MOR vs RHE)	[29]
3.	MWCNT	Dispersion Nitrobenzene	2.9 (Pt)	0.62 $mA.cm^{-2}$ (MOR vs RHE)	[30]
4.	Vulcan XC-72R	Heating HNO_3 + H_2SO_4 (1:1 v/v)	7.4 (Pt)	1 $mA.cm^{-2}$ (MOR vs RHE)	[24]
5.	MWCNT	Reflux HNO_3	– (Pt)	6.2 $mA.cm^{-2}$ (MOR vs Ag/AgCl)	[31]
6.	MWCNT	Heating HNO_3 + H_2SO_4	5.2 (Pt)	490 $mW.cm^{-2}$ (PEMFC)	[22]
7.	Carbon Nano Fibers	Stirring HNO_3 + H_2SO_4 (1:1 v/v)	5.4 (Pt)	1.71 $mA.cm^{-2}$ (MOR vs RHE)	[25]
8.	MWCNT	Ultrasonication HNO_3 + H_2SO_4 (2:3 w/w)	5.5 (PtRu)	–	[32]
9.	CNTs	Dispersion H_2O_2; Reflux HNO_3 + H_2SO_4	3 (Pt)	120 $mW.cm^{-2}$ (PEMFC)	[33]

by dissociating C–C bond, and the two free radicals will react with active O atom to form O–C=O like in step one. The HO–C=O can be finally obtained with proton stabilization (Fig. 6.2c). Interestingly, with the help of plasma, the carboxyl group can internally transfer to lactone groups, see Fig. 6.2d [34].

6.2.2 Nitrogen Functionalization

Metal NPs supported on the carbon materials surface tend to aggregate, and therefore modification of carbon materials plays an important role in improving platinum (Pt) performance. Recent studies suggest that carbon-based catalyst support materials can be systematically doped with nitrogen to create strong, beneficial catalyst–support interactions which substantially enhance catalyst activity and stability. Nitrogen functionalities in the carbon lattice act as "tethers" which can improve dispersion of the Pt NPs and provide resistance to NP agglomeration [35] altering the electron donating character of the support, which in turn impacts the binding of the catalyst to the support [36].

The most widely used methods to prepare nitrogen-modified carbon nanomaterials are chemical vapor deposition (CVD), thermal treatment and plasma treatment. Data suggest that nitrogen functional groups introduced into a carbon support appear to influence at least three aspects of the catalyst–support system:

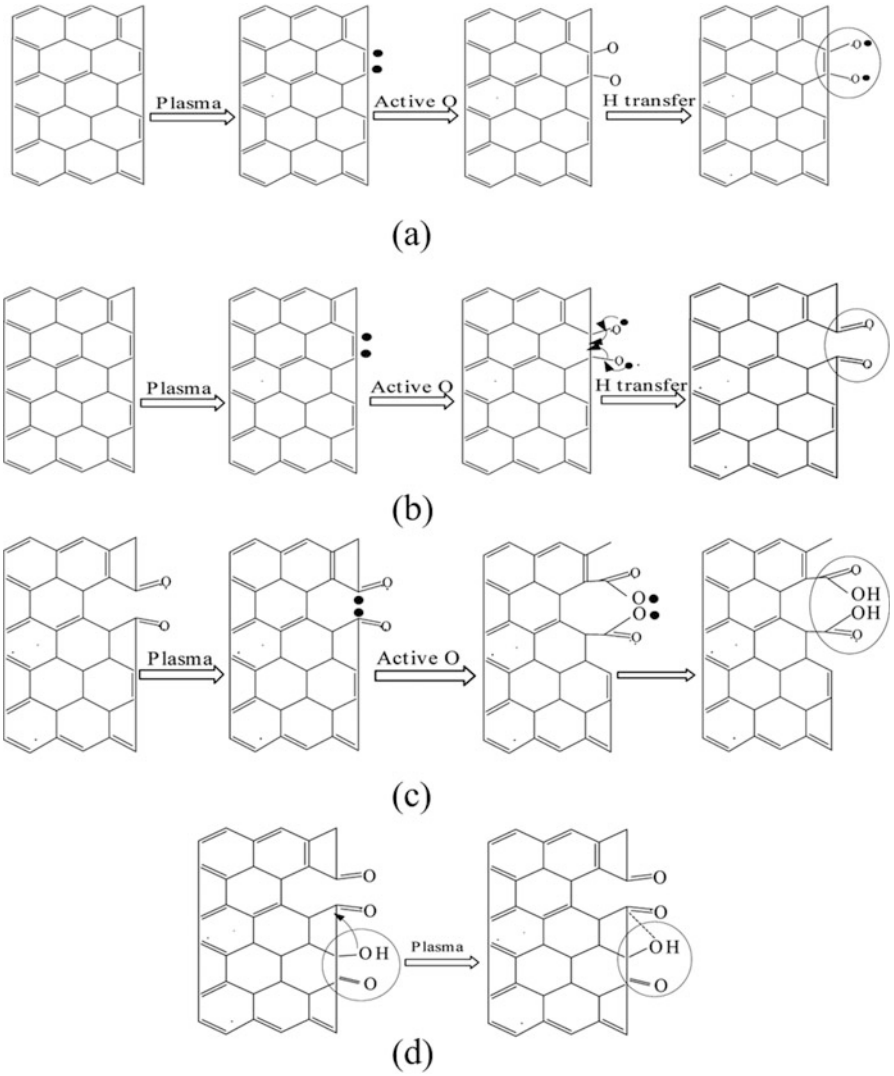

Fig. 6.2 Possible mechanism of MWCNT oxidation by Ar/O_2 plasma: (**a**) generation of C–O bonds; (**b**) generation of C=O bonds; (**c**) generation of O–C=O bonds; and (**d**) transfer between carboxyl and lactone. Reprinted (adapted) with permission from [34] Copyright American Chemical Society

(1) modified nucleation and growth kinetics during catalyst NP deposition, which results in smaller catalyst NPs size and increased catalyst particle dispersion, (2) increased support–catalyst chemical binding (or "tethering"), which results in enhanced durability, and (3) catalyst NP electronic structure modification, which

enhances intrinsic catalytic activity [36]. These improvements are due to nitrogen species in the C–N-containing materials as reported [37].

C–N-containing materials indicate the presence of multiple nitrogen-containing species, including pyridinic, pyrrolic, graphitic (quaternary), and oxide forms. In particular, pyridinic nitrogen has sometimes been linked to improved performance, although there is some debate as to whether the pyridinic nitrogen plays an active role or whether it serves simply as a marker of total degree of carbon edge-plane defects, which are themselves active, a direct correlation between pyridinic nitrogen content and the number of reducing sites has also been observed. It is speculated that these pyridinic edge sites may provide stronger interaction between the Pt and the support, thus inhibiting agglomeration of the noble nanophase [36]. In general terms, Pt catalysts should benefit most strongly from the addition of graphitic and pyridinic types of nitrogen. For instance, the stability of PtRu catalysts could most likely be improved by the addition of graphitic N and a well balanced mix of pyrrolic and pyridinic N, where pyridinic N improves stability of Pt in Ru_2Pt_2 and pyrrolic N improves stability of both Pt in Ru_2Pt_2 and Ru in Pt_2Ru_2 [38]. These combinations will promote a low Pt loading for the optimal performance of fuel cell and its cost effective commercialization.

The low loading of Pt on nitrogen-doped carbon nanocapsules (Pt/NCNC) by ORR (acidic media) in PEMFCs has been reported by Shanmugan et al. Their deconvoluted high-resolution N1s spectra showed the presence of pyridinic, pyrrolic, and graphitic type nitrogen which played an important role in dispersion and stabilization of Pt NPs. Specifically, the uniform dispersion of Pt NPs is attributed to the high amount of graphitic nitrogen doping that improved the Pt/NCNC performance which exhibited 2.7 times higher activity than commercial Pt/C electrocatalyst. This can be attributed to the existence of pyridinic type nitrogen (27.6%) and surface nitrogen content (7.1 wt.%) [39]. Platinum NPs supported on N-doped graphene nanosheets (NDGN) have been reported as catalyst for cathodic oxygen reduction reaction in low-temperature fuel cells by Jukk et al. In their work, NDGN were synthesized by chemical reduction of hexachloroplatinic acid. Smaller Pt NPs were identified when ethylene glycol was used as reducing agent. NDGN showed a high dispersion of Pt NPs due to strong interaction of Pt with nitrogen functionalities [40]. Also, as C–N bond occurs mostly at the edges and defects of the graphite sheets, vertically aligned carbon nanofibers which expose large amounts of edge-plane graphite seemed optimal for study, so Zhang and coworkers synthesized N-doped carbon nanofiber (CNF)-supported Pt catalysts by an approach combined of plasma-enhanced chemical vapor deposition and in situ plasma activation that introduced nitrogen functionalities into the carbon network preserving the graphitic structure of the carbon support. Their results showed that NH_3 plasma modification creates pyridinic nitrogen functionalities, while N_2 plasma modification increases the percentage of pyrrolic nitrogen in the carbon network. The plasma-modified CNF supports possessed higher percentage of Pt in the Pt/CNF electrode because the adsorption between Pt and the carbon support resulted in strong Pt–C bondings and electron transfers from Pt atoms or Pt clusters towards the carbon support, leading to the relatively positive charge states of Pt. Also, N-modified Pt/CNF electrodes show

higher methanol electrooxidation activities than pristine Pt/CNF electrodes. Finally, their Pt/CNF–NH_3 electrode with small Pt particle size and high percentage of pyridinic nitrogen exhibits the highest Pt utilization, electrochemical activity, and poisoning-resistance ability [41]. Regarding ORR, high nitrogen contents are expected to be favorable for enhanced ORR activity; however, too high N content might be disadvantageous for ORR because of the interruption of the π–π electron conjugation thus leading to low electronic conductivity [40].

On the activity of Pt/C catalyst system for methanol oxidation reaction, N-doped highly oriented pyrolytic graphite (HOPG) provides increased agglomeration resistance, significantly enhanced intrinsic catalyst activity, promotes nucleation during the electrochemical deposition process yielding smaller average Pt NPs size and a narrower particle size distribution due to intrinsic chemical interaction effects which enhance the overlying Pt NP activity and stability. Zhou and his coworkers proposed that the polar nitrogen functional groups on N-doped HOPG surface intensify the electron withdrawing effect against Pt; the resulting decreased electron density of Pt should then facilitate the oxidation of methanol, thus leading to the higher intrinsic catalyst activity observed in this system [35].

Finally, regarding precious metals, recently, biomass-derived nitrogen-doped carbons (NDC) have been investigated as fuel cell catalyst supports. Various catalysts, such as Pt, PtRuIr, and Pd, were supported on biomass-derived NDCs, and their structural characteristics and catalytic activity were compared with that of the same catalysts supported on conventional Pt/C. Generally, compared with carbon black supported electrocatalysts, the biomass-derived NDC supported catalysts showed larger electrochemical active surface area and enhanced catalytic activity for methanol and ethanol oxidation as well as for oxygen reduction than Pt/C [42].

Non-precious NPs supported onto carbon have been also studied by Shi and colleagues who synthesized nitrogen-doped graphene by hydrothermal method and then used it to support Cu catalysts for dimethyl carbonate synthesis via the oxidative carbonylation of methanol. They found that the lone pair electrons provided by nitrogen atoms can result in polarity that enhances the insertion of the copper ions into the nitrogen-doped graphene nanosheets during the impregnation process. So, the catalytic performance of Cu/NG catalysts was mainly depending on the nitrogen doping effects, which resulted in enhanced metal support interaction and the high degree of dispersion of active Cu NPs [43].

Simple approaches have been explored also for preparing nitrogen-doped carbons supported non-precious catalysts for ORR in alkaline media. Ghanbarlou et al. investigated the electrocatalytic properties of nitrogen-doped graphene (NDG) and metal (Fe, Co, and Fe–Co) NPs supported on NDG and they studied the response of their materials towards ORR in alkaline media (0.1 M KOH). By XPS, they found that the amount of nitrogen incorporated into the nitrogen-doped graphene was 4%. So, the best performance was showed by cobalt NPs supported on NDG (Co/NG) which showed more positive ORR peak potential (−0.33 V) and also exhibited good stability compared with commercial Pt/C for ORR in alkaline media. This improvement in electrocatalytic activity was attributed to the presence of more electroactive sites after the precipitation of metal NPs [44].

6.3 Non-covalent Functionalization

6.3.1 Surface Defects

Non-covalent functionalization of carbon material by metal NPs is possible due to interactions between metal and carbon vacancies. In CNTs, the collision of an energetic particle with carbon atoms results in the formation of a vacancy (single or multiple) and a number of primary knock on atoms which, if their energy is high enough, can leave the nanotube or displace other atoms within [45].

CNTs are recognized as a promising alternative carbon support material for fuel cell electrocatalysts due to their higher electrical conductivities, low impurities, high catalyst loading efficiency, and higher durability as compared to carbon black. However, CNTs are inert materials that are difficult to disperse in solution due to high Van der Waals energy [46]. As-synthesized pristine CNTs form bundled structures and are difficult to solubilize/disperse in solvents and it is difficult to attach metal NPs homogeneously onto the surfaces of CNTs. Therefore, the primary step in the utilization of CNTs for basic studies and material applications was to develop a surface modification method to exfoliate bundled CNTs and solubilize/disperse them in solvents. Typically, using strong acid chemical treatment, the CNT surfaces are oxidized to form hydrophilic groups, such as –COOH and –OH groups, and the obtained CNTs can be dispersed in water [47]. Noble or rare metal NPs such as Pt, Au, Pd, Ag, Rh, Ru, and Ni can be directly deposited onto the surface of CNTs by Van der Waals force when their salts were reduced in the presence of CNTs [48]. Nucleation and growth of metal NPs directly on the surface of CNTs is the mostly used method to prepare metal NPs/CNTs catalysts [49]. Also, defects are usually introduced in CNT by oxidation pretreatment of the CNT using nitric acid, H_2O_2, or other reactants. The treatment is necessary to obtain a good dispersion of the metal NPs. These methods, in fact, create different surface functional groups (lactone, pyran, carboxylic, anhydride, quinone, phenol, and furan), although several of these groups have a low thermal stability.

The presence of defects, enhancing the amount of surface functional groups on CNT, influences various aspects: (1) the efficiency of three-phase boundary and thus the transport of protons to or from the active metal NPs, (2) the resistance of electron transfer, and (3) the tolerance of the catalyst to CO poisoning attributed to carbon functional groups in close contact with very small Pt NPs favoring the reactivation of Pt sites poisoned by CO [50].

6.3.2 Surfactant-Based Non-Covalent Functionalizing Carbon Support

The surfactants are long chain amphiphilic molecules that consist of hydrophilic heads and hydrophobic tails. They can be categorized by four kinds of hydrophilic

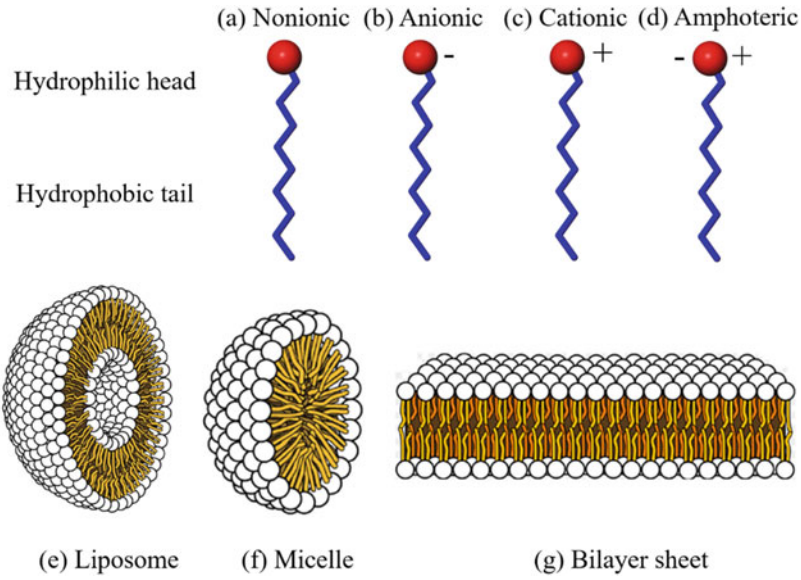

Fig. 6.3 Schematic of surfactant and aggregations, (**a**) nonionic, (**b**) anionic, (**c**) cationic, (**d**) Zwitterionic (amphoteric), (**e**) liposome, (**f**) micelle, and (**g**) bilayer sheet

heads, namely nonionic (Fig. 6.3a), anionic (Fig. 6.3b), cationic (Fig. 6.3c), and Zwitterionic (amphoteric), as seen in Fig. 6.3d. The surfactant contains anionic heads such as sulfate, sulfonate, phosphate esters, and carboxylates. Some cationic head groups are pH dependent, e.g., amines will become positively charged when pH < 10, while others are permanently charged, like quaternary ammonium salts. Zwitterionic (amphoteric) surfactant has both cation and anion in the hydrophilic heads. For instance, primary, secondary, tertiary amines or quaternary ammonium ions can be positively charged while the sulfonates can be negatively charged. Nonionic surfactants have covalently bonded oxygen-containing hydrophilic groups attached on the hydrophobic tails. When the carbon materials are dispersed, the hydrophobic tails will aggregate and adsorb onto them due to the repulsion force of solvent molecules forming spherical liposome (Fig. 6.3e), spherical micelles (Fig. 6.3f), or lipid bilayers (Fig. 6.3g). As a consequence, the hydrophilic head will be attracted by the liquid molecules so that aggregates could be dispersed into the liquid phase. And, its shape will depend on the balance in size between the head and the tail.

CNT has been made by warping the graphene sheet to a closed tube; in the graphitic plane surface of CNT, the *p*-orbital of one CNT will interact with *p*-orbital of another CNT to form a π–π stacking interaction. The Van der Waals force keeps the CNTs in bundled form and hard to disperse it in the solvent. These agglomerated CNTs will prevent Pt NP dispersing also difficult to make uniform MEA. Usually, the ionic surfactant is preferable to disperse CNTs in water media and nonionic surfactant is proposed to be better when organic solvent is used. So, the mechanism

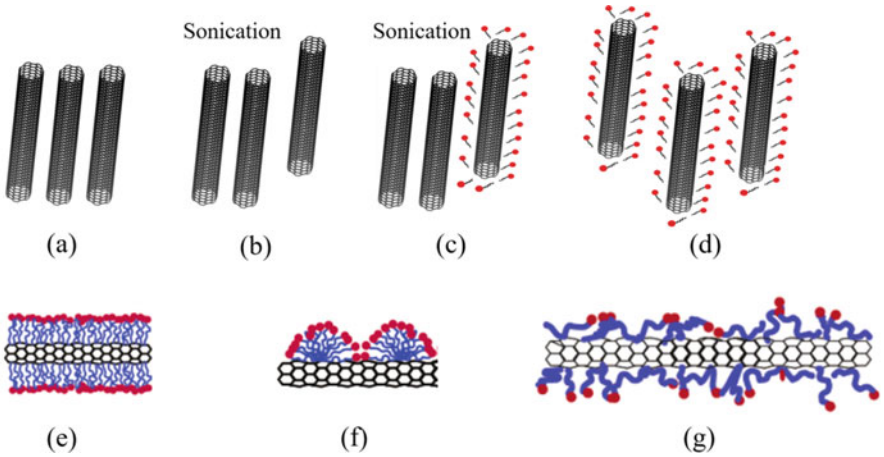

Fig. 6.4 Schematically showing the mechanism of isolating CNTs bundle by ultrasonication (**a**) CNTs bundle, (**b**) single CNT separated by soni-cation, (**c**) surfactant adsorption on isolated CNT, (**d**) dispersed CNTs with help of surfactant and the possible way of CNTs-surfactant inter-actions (**e**) cylindrical micelles, (**f**) hemimicelles and (**g**) random adsorption

of MWCNT isolation with the aid of ultrasonication and surfactant was proposed. The role of ultrasonication is to provide a local shear force to break the π–π interaction at the bundle end. Once the gap is formed, the surfactant would diffuse, adsorb, and ultimately separate the MWCNT from the bundle [51].

Sodium dodecyl sulfate (SDS) is an anionic surfactant which consists of a 12-carbon tail attached to a sulfate group. The CNT bundles are exfoliated during sonication for stabilizing the dispersion by SDS adsorption (Fig. 6.4a–d). It is reported that the CNTs–SDS dispersion could be stable for several months with critical micelles forming concentration of ~0.2 wt% SDS [52]. The CNTs–surfactant interaction could be visualized through cylindrical micelles (Fig. 6.4e), hemimicelles (Fig. 6.4f), or randomly adsorbed surfactant on CNTs (Fig. 6.4g). In particular, with the critical micelles forming concentration of ~ 0.2 wt. % SDS, there is a formation of CNTs–SDS randomly adsorbed on CNTs (Fig. 6.4g) [53]. Dodecyl-benzene sodium sulfonate (NaDDBS) is also an anionic surfactant with sulfonate group and has been widely reported for dispersion of CNTs. The benzene ring inside the NaDDBS is believed to have π–π interaction with CNTs leading to higher adsorption ratio of surfactant [54]. The π–π interaction does not limit the benzene ring, and naphthenic (saturated rings) groups also provide good surfactant to nanotube affinity. Both ring structures in the head or tail are playing an important role in dispersing CNTs. Naphthalene group (two fused rings) hydrophobic tail has more effective adsorption than benzene, due to this reason, sodium diisopropyl naphthalene sulfonate (Aerosol OS surfactant) shows better dispersion compared to the NaDDBS as evidenced from UV-Vis spectrum [55]. Nonionic surfactant Tween-60 and Tween-80 (polyethylene oxide (20) sorbitan monostearate and monooleate, respectively) have been studied to disperse CNTs. The higher dispersion of Tween-80 is due to the

unsaturated bond in the tail [56]. The SWCNTs dispersion in heavy water with an optimum surfactant octyl-phenol-ethoxylate amount of 0.004 g/mol (Triton X-100) and the mechanism involved has been discussed in detail [57].

With the help of the surfactant, the Pt NPs can be easily anchored on to the carbon materials. In 2005, Lee et al. deposited Pt on SDS-modified graphite nanofibers (GN), MWCNT, and SWCNT for MOR. During the refluxing, 1-dodecanol was gradually released from SDS to reduce Pt ions. The Pt sizes of Pt/GN, Pt/MWCNT, and Pt/SWCNT were 1.6, 1.87, and 1.87 nm, respectively. The MOR performance improved with the increasing carbon material diameter [58]. Another research reported Pt on SDS-modified MWCNT prepared by urea assisted ethylene glycol refluxing, and the material showed superior fuel cell performance compared to the Vulcan XC-72. With the modification of SDS, more anchor sites were generated on the outer surface of MWCNT for Pt (IV) ions, and with the help of ethylene glycol, the platinum was homogeneously distributed within the MWCNT support [59]. Also, Silva-Carrillo et al. reported hexadecyltrimethylammonium bromide (CTAB)-modified MWCNTs to prepare Pt/MWCNT. In their work, Pt ions were reduced in hexane, heptane, and octane with CTAB-functionalized MWCNT; the heptane medium reduced platinum had the best ORR performance [60]. In 2015, an anion conducting surfactant quaternary ammonia poly (2, 6-dimethyl-1, 4-phenylene oxide) (QAPPO) was used to functionalize the reduced graphene oxide (rGO). In this work, TEM picture showed that the Pt on the QAPPO-treated rGO was around 2.46 nm compared to 3.95 nm on the rGO without treating. The AFC performance showed that QAPPO-treated sample had peak power density of 264.8 $mW.cm^{-2}$ at 60 °C which is 30% higher than the AFC MEA made by Pt/rGO. The QAPPO-coated rGO could stabilize the Pt precursor by electrostatic interactions which led to uniformly distributed Pt NPs [61]. In another report, Kannan and coworkers have also reported SDS-modified MWCNTs as support for Pt NPs for PEMFC application. SDS concentrations along with multiple reducing agents were investigated extensively. Pt NPs supported on SDS micelle encapsulated MWCNTs have been reported to show peak power density of 950 $mW.cm^{-2}$ using Nafion-212 [62].

6.3.3 *Polymer-Based Non-Covalent Functionalizing Carbon Support*

Non-covalent functionalization is considered better as compared to covalent functionalization because it allows the attachment of polyelectrolytes through CH–π, π–π staking, or hydrophobic interactions, creating effective active locations for the uniform dispersion of Pt-based electrocatalyst or NPs along with the preservation of the structural integrity and intrinsic electronic properties of CNTs. As published, various agents such as surfactants, aromatic compounds, polyelectrolytes, or polymers can be employed for non-covalent functionalization of carbon materials [63]. For example, polypyrrole (PPY), poly diallyldimethylammonium chloride

Table 6.2 Non-covalent functionalization of carbon supports

No.	Carbon type	Functionalization method/ agent	Size (nm)/ catalyst	Catalytic performance (mA. mg^{-1})	Reference
1.	MWCNTs	Microwave/poly (ethyleneimine)	2.5 (PtRu)	680	[71]
2.	CNTs	Electrostatic adsorption/ polyaniline	3.6 (Pt)	–	[72]
3.	CNTs	Sonication/chitosan	3 (PtRu)	230	[73]
4.	CNTs	Microwave/poly(allylamine hydrochloride)	1.5 (Pt)	300	[70]
5.	CNTs	Microwave/poly(sodium 4-styrenesulfonate)	1.5 (Pt)	400	[70]
6.	CNTs	Microwave/poly(acrylic acid)	1.5 (Pt)	800	[70]
7.	MWCNTs	Refluxing/ polybenzimidazole	4.0 (Pt)	470	[74]
8.	MWCNTs	Refluxing/poly (diallyldimethylammonium chloride)	1.8 (Pt)	480	[75]
9.	MWCNTs	Microwave/1-Aminopyrene	2.0 (PtRu)	300	[75]
10.	Carbon nanofibers	Microwave/polyvinyl pyrrolidone	1.8 (Pt)	250	[76]

(PDDA), polyethylenimine (PEI), phenanthroline, polyaniline (PANI), 1-aminopyrene (1-AP or AP), hydroxyquinoline, and tetrahydrofuran (THF) have been used to functionalize CNTs as electrocatalyst supports. Table 6.2 summarizes the functionalization methods using different polyelectrolytes and their MOR performances. Non-covalent functionalization with polyelectrolytes or solvents can significantly increase the distribution and electrocatalytic activities of Pt and Pt-based alloy NPs on to the surface of graphene and CNTs towards ORR and MOR [64].

Since CNTs are 1D nanostructures made up of single/multiple layers of graphene sheets, many types of small polymers/molecules with a π–π conjugated structure can make complexes with CNTs through π–π interaction. The type of polymers with widespread π–π conjugated backbone is called conjugated polymers. The conjugated polymers–CNTs composite has been reported to show synergistic properties such as enhanced mechanical strength, stability, and electrical conductivity [65].

The non-covalent π–π interaction of conjugated polymer with the CNTs has been studied extensively; for example, the polypyridinium salts were prepared and employed to form π–π and cationic–π interactions with SWCNTs [66]. Lee et al. synthesized an amphiphilic molecule oligothiophene-terminated polyethylene glycol (TN-PEG) and evaluated its ability to homogenously disperse and to provide long-term stability of CNTs in water through π–π interactions [67].

Non-covalent functionalization through CH–π interaction has also been used for functionalizing CNTs for the dispersion of CNTs by Xu et al. The MWCNTs were

functionalized with hyperbranched polyethylene (HBPE) in organic solvents like chloroform and tetrahydrofuran (THF) and examined using electron microscopic studies to confirm the uniform dispersion. The homogenous dispersion has been reported to be due to CH–π interactions between hyperbranched structure of HBPE and MWCNT sidewalls [68].

When Pt NPs are supported on CNTs functionalized by the polyelectrolytes, there is a shift in the binding energy of Pt NPs. This shift might be positive or negative and may cause the change in the electron density of Pt NPs. Tsukuda and coworkers have shown that the polyvinylpyrrolidone acts as electron donor (polyanion) for Pt NPs decreasing binding energy and increasing electron density around them [69]. Similar behavior has been observed for poly(sodium 4-styrenesulfonate) (PSS) and polyacrylic acid, and the results show a downshift of the d-band center of Pt NPs weakening the chemisorption with oxygen-containing functional groups like −OH and −CO. On the other hand, there are polyelectrolytes that are electron acceptor or polycations like poly(diallyldimethylammonium chloride) (PDDA) and poly (allylamine hydrochloride) (PAH) which are responsible for positive shift in binding energy of Pt NPs. According to d-band theory, Pt + PDDA and Pt + PSS have higher oxygen adsorption energy than Pt + PAA and Pt + PSS. The oxygen adsorption energy can be an indicator for catalytic activity; the stronger it is the more difficult to remove −CO and −OH from Pt thus lowering the MOR and ORR performance. As seen in Table 6.2, the MOR performance is the best for PAA compared to all other polyelectrolytes [70].

References

1. Schell A, Peng H, Tran D, Stamos E, Lin C-C, Kim MJ (2005) Modelling and control strategy development for fuel cell electric vehicles. Annu Rev Control 29:159–168. https://doi.org/10.1016/j.arcontrol.2005.02.001
2. EG&G Technical Services, Inc (2004) Fuel cell handbook. Fuel Cell 7 Edition:1–352. https://doi.org/10.1002/zaac.200300050
3. Singhal SC (2007) Solid oxide fuel cells. Electrochem Soc Interface 16:41
4. Service RF (2002) Fuel cells. Shrinking fuel cells promise power in your pocket. Science 296:1222. https://doi.org/10.1126/science.296.5571.1222
5. Springer TE, Zawodzinski TA, Gottesfeld S (1991) Polymer electrolyte fuel cell model. J Electrochem Soc 138:2334–2342. https://doi.org/10.1149/1.2085971
6. Mathias MF, Makharia R, Gasteiger HA, Conley JJ, Fuller TJ, Gittleman CJ, Kocha SS, Miller DP, Mittelsteadt CK, Xie T (2005) Two fuel cell cars in every garage. Electrochem Soc Interface 14:24–35
7. Gasteiger HA, Kocha SS, Sompalli B, Wagner FT (2005) Activity benchmarks and requirements for Pt, Pt-alloy, and non-Pt oxygen reduction catalysts for PEMFCs. Appl Catal B Environ 56:9–35. https://doi.org/10.1016/j.apcatb.2004.06.021
8. Wang C, Waje M, Wang X, Tang JM, Haddon RC, Yan Y (2004) Proton exchange membrane fuel cells with carbon nanotube based electrodes. Nano Lett 4:345–348. https://doi.org/10.1021/nl034952p

9. Thompson SD, Jordan LR, Forsyth M (2001) Platinum electrodeposition for polymer electrolyte membrane fuel cells. Electrochim Acta 46:1657–1663. https://doi.org/10.1016/S0013-4686(00)00767-2
10. Sun X, Li R, Villers D, Dodelet JP, Desilets S (2003) Composite electrodes made of Pt nanoparticles deposited on carbon nanotubes grown on fuel cell backings. Chem Phys Lett 379:99–104. https://doi.org/10.1016/j.cplett.2003.08.021
11. Yasuda K, Nishimura Y (2003) The deposition of ultrafine platinum particles on carbon black by surface ion exchange—increase in loading amount. Mater Chem Phys 82:921–928. https://doi.org/10.1016/j.matchemphys.2003.08.020
12. Bashyam R, Zelenay P (2006) A class of non-precious metal composite catalysts for fuel cells. Nature 443:63. https://doi.org/10.1038/nature05118
13. Debe MK (2012) Electrocatalyst approaches and challenges for automotive fuel cells. Nature 486:43. https://doi.org/10.1038/nature11115
14. Antolini E (2009) Carbon supports for low-temperature fuel cell catalysts. Appl Catal B Environ 88:1–24. https://doi.org/10.1016/j.apcatb.2008.09.030
15. Jaouen F, Marcotte S, Dodelet JP, Lindbergh G (2003) Oxygen reduction catalysts for polymer electrolyte fuel cells from the pyrolysis of iron acetate adsorbed on various carbon supports. J Phys Chem B 107:1376–1386. https://doi.org/10.1021/jp021634q
16. Wei Z, Guo H, Tang Z (1994) Pretreatment of acetylene black: influence on electrochemical behaviour. J Power Sources 52:123–127. https://doi.org/10.1016/0378-7753(94)01949-5
17. McBreen J, Olender H, Srinivasan S, Kordesch KV (1981) Carbon supports for phosphoric acid fuel cell electrocatalysts: alternative materials and methods of evaluation. J Appl Electrochem 11:787–796. https://doi.org/10.1007/BF00615184
18. Kameron DS (1990) Carbons as support for precious metal catalyst. Catal Today 7:113–137. https://doi.org/10.1016/0920-5861(90)85012-D
19. Sepúlveda-Escribano A, Coloma F, Rodríguez-Reinoso F (1998) Platinum catalysts supported on carbon blacks with different surface chemical properties. Appl Catal A Gen 173:247–257. https://doi.org/10.1016/S0926-860X(98)00183-5
20. Wang S, Jiang SP, White TJ, Wang X (2010) Synthesis of Pt and Pd nanosheaths on multiwalled carbon nanotubes as potential electrocatalysts of low temperature fuel cells. Electrochim Acta 55:7652–7658. https://doi.org/10.1016/j.electacta.2009.09.003
21. Eitan A, Jiang K, Dukes D, Andrews R, Schadler LS (2003) Surface modification of multiwalled carbon nanotubes: toward the tailoring of the interface in polymer composites. Chem Mater 15:3198–3201. https://doi.org/10.1021/cm020975d
22. Hernández-fernández P, Montiel M, Ocón P, De JLG, García-rodríguez S, Rojas S, Fierro JLG (2010) Functionalization of multi-walled carbon nanotubes and application as supports for electrocatalysts in proton-exchange membrane fuel cell. Appl Catal B 99:343–352. https://doi.org/10.1016/j.apcatb.2010.07.005
23. Stamatin SN, Borghei M, Dhiman R, Andersen SM, Ruiz V, Kauppinen E, Skou EM (2015) Activity and stability studies of platinized multi-walled carbon nanotubes as fuel cell electrocatalysts. Appl Catal B Environ 162:289–299. https://doi.org/10.1016/j.apcatb.2014.07.005
24. Salgado JRC, Duarte RG, Ilharco LM, Botelho do Rego AM, Ferraria AM, Ferreira MGS (2011) Effect of functionalized carbon as Pt electrocatalyst support on the methanol oxidation reaction. Appl Catal B Environ 102:496–504. https://doi.org/10.1016/j.apcatb.2010.12.031
25. Sebastián D, Calderón JC, González-Expósito JA, Pastor E, Martínez-Huerta MV, Suelves I, Moliner R, Lázaro MJ (2010) Influence of carbon nanofiber properties as electrocatalyst support on the electrochemical performance for PEM fuel cells. Int J Hydrog Energy 35:9934–9942. https://doi.org/10.1016/j.ijhydene.2009.12.004
26. Eris S, Daşdelen Z, Sen F (2018) Investigation of electrocatalytic activity and stability of Pt@f-VC catalyst prepared by in-situ synthesis for methanol electrooxidation. Int J Hydrog Energy 43:385–390. https://doi.org/10.1016/j.ijhydene.2017.11.063

27. Kim JH, Cheon JY, Shin TJ, Park JY, Joo SH (2016) Effect of surface oxygen functionalization of carbon support on the activity and durability of Pt/C catalysts for the oxygen reduction reaction. Carbon 101:449–457. https://doi.org/10.1016/j.carbon.2016.02.014
28. Guha A, Lu W, Zawodzinski TA, Schiraldi DA (2007) Surface-modified carbons as platinum catalyst support for PEM fuel cells. Carbon 45:1506–1517. https://doi.org/10.1016/j.carbon.2007.03.023
29. Yola ML, Eren T, Atar N, Saral H, Ermiş I (2016) Direct-methanol fuel cell based on functionalized graphene oxide with mono-metallic and bi-metallic nanoparticles: electrochemical performances of nanomaterials for methanol oxidation. Electroanalysis 28:570–579. https://doi.org/10.1002/elan.201500381
30. Tao L, Dou S, Ma Z, Wang S (2015) Platinum nanoparticles supported on nitrobenzene-functionalized multiwalled carbon nanotube as efficient electrocatalysts for methanol oxidation reaction. Electrochim Acta 157:46–53. https://doi.org/10.1016/j.electacta.2015.01.054
31. Hoa LQ, Vestergaard MC, Yoshikawa H, Saito M, Tamiya E (2011) Functionalized multi-walled carbon nanotubes as supporting matrix for enhanced ethanol oxidation on Pt-based catalysts. Electrochem Commun 13:746–749. https://doi.org/10.1016/j.elecom.2011.03.041
32. Yang C, Wang D, Hu X, Dai C, Zhang L (2008) Preparation and characterization of multi-walled carbon nanotube (MWCNTs)-supported Pt-Ru catalyst for methanol electrooxidation. J Alloys Compd 448:109–115. https://doi.org/10.1016/j.jallcom.2006.10.030
33. Xu C, Chen J, Cui Y, Han Q, Choo H, Liaw PK, Wu D (2006) Influence of the surface treatment on the deposition of platinum nanoparticles on the carbon nanotubes. Adv Eng Mater 8:73–77. https://doi.org/10.1002/adem.200500179
34. Chen C, Ogino A, Wang X, Nagatsu M (2011) Oxygen functionalization of multiwall carbon nanotubes by Ar/H_2O plasma treatment. Diam Relat Mater 20:153–156. https://doi.org/10.1021/jp9012015
35. Zhou Y, Pasquarelli R, Holme T, Berry J, Ginley D, O'Hayre R (2009) Improving PEM fuel cell catalyst activity and durability using nitrogen-doped carbon supports: observations from model Pt/HOPG systems. J Mater Chem 19:7830. https://doi.org/10.1039/b910924b
36. Zhou Y, Neyerlin K, Olson TS, Pylypenko S, Bult J, Dinh HN, Gennett T, Shao Z, O'Hayre R (2010) Enhancement of Pt and Pt-alloy fuel cell catalyst activity and durability via nitrogen-modified carbon supports. Energy Environ Sci 3:1437. https://doi.org/10.1039/c003710a
37. Escobar B, Pérez-Salcedo KY, Alonso-Lemus IL, Pacheco D, Barbosa R (2017) N-doped porous carbon from Sargassum spp. as metal-free electrocatalysts for oxygen reduction reaction in alkaline media. Int J Hydrog Energy 42(51):30274–30283. https://doi.org/10.1016/j.ijhydene.2017.06.240
38. Pylypenko S, Borisevich A, More KL, Corpuz AR, Holme T, Dameron AA, Olson TS, Dinh HN, Gennett T, O'Hayre R (2013) Nitrogen: unraveling the secret to stable carbon-supported Pt-alloy electrocatalysts. Energy Environ Sci 6:2957. https://doi.org/10.1039/c3ee40189h
39. Shanmugam S, Sanetuntikul J, Momma T, Osaka T (2014) Enhanced oxygen reduction activities of pt supported on nitrogen-doped carbon nanocapsules. Electrochim Acta 137:41–48. https://doi.org/10.1016/j.electacta.2014.05.145
40. Jukk K, Kongi N, Tarre A, Rosental A, Treshchalov AB, Kozlova J, Ritslaid P, Matisen L, Sammelselg V, Tammeveski K (2014) Electrochemical oxygen reduction behaviour of platinum nanoparticles supported on multi-walled carbon nanotube/titanium dioxide composites. J Electroanal Chem 735:68–76. https://doi.org/10.1016/j.jelechem.2014.10.008
41. Zhang C, Hu J, Zhang X, Wang X, Meng Y (2015) Certain nitrogen functionalities on carbon nanofiber support for improving platinum performance. Catal Today 256:193–202. https://doi.org/10.1016/j.cattod.2015.01.026
42. Antolini E (2016) Nitrogen-doped carbons by sustainable N- and C-containing natural resources as nonprecious catalysts and catalyst supports for low temperature fuel cells. Renew Sust Energ Rev 58:34–51. https://doi.org/10.1016/j.rser.2015.12.330
43. Shi R, Zhao J, Liu S, Sun W, Li H, Hao P, Li Z, Ren J (2018) Nitrogen-doped graphene supported copper catalysts for methanol oxidative carbonylation: enhancement of catalytic

activity and stability by nitrogen species. Carbon 130:185–195. https://doi.org/10.1016/j.carbon.2018.01.011
44. Ghanbarlou H, Rowshanzamir S, Kazeminasab B, Parnian MJ (2014) Non-precious metal nanoparticles supported on nitrogen-doped graphene as a promising catalyst for oxygen reduction reaction: synthesis, characterization and electrocatalytic performance. J Power Sources 273:981–989. https://doi.org/10.1016/j.jpowsour.2014.10.001
45. Corti HR, Gonzalez ER (2014) Direct alcohol fuel cells: materials, performance, durability and applications. Springer, New York
46. Sudirman S, Indriyati I, Adi WA, Yudianti R, Budianto E (2017) Structural analysis of platinum nanoparticles on carbon nanotube surface as electrocatalyst system. Int J Chem 9:60. https://doi.org/10.5539/ijc.v9n2p60
47. Fujigaya T, Nakashima N (2013) Fuel cell electrocatalyst using polybenzimidazole-modified carbon nanotubes as support materials. Adv Mater 25:1666–1681. https://doi.org/10.1002/adma.201204461
48. Meng L, Fu C, Lu Q (2009) Advanced technology for functionalization of carbon nanotubes. Prog Nat Sci 19:801–810. https://doi.org/10.1016/j.pnsc.2008.08.011
49. Jiang Z, Jiang Z-J (2011) Carbon nanotubes supported metal nanoparticles for the applications in proton exchange membrane fuel cells (PEMFCs). Carbon Nanotub Growth Appl. https://doi.org/10.5772/16565
50. Centi G, Gangeri M, Fiorello M, Perathoner S, Amadou J, Bégin D, Ledoux MJ, Pham-Huu C, Schuster ME, Su DS, Tessonnier JP, Schlögl R (2009) The role of mechanically induced defects in carbon nanotubes to modify the properties of electrodes for PEM fuel cell. Catal Today 147:287–299. https://doi.org/10.1016/j.cattod.2009.07.080
51. Vaisman L, Wagner HD, Marom G (2006) The role of surfactants in dispersion of carbon nanotubes. Adv Colloid Interf Sci 128–130:37–46. https://doi.org/10.1016/j.cis.2006.11.007
52. Yurekli K, Mitchell CA, Krishnamoorti R (2004) Small-angle neutron scattering from surfactant-assisted aqueous dispersions of carbon nanotubes. J Am Chem Soc 126:9902–9903. https://doi.org/10.1021/ja047451u
53. Yu J, Grossiord N, Koning CE, Loos J (2007) Controlling the dispersion of multi-wall carbon nanotubes in aqueous surfactant solution. Carbon 45:618–623. https://doi.org/10.1016/j.carbon.2006.10.010
54. Kim IT, Nunnery GA, Jacob K, Schwartz J, Liu X, Tannenbaum R (2010) Synthesis, characterization, and alignment of magnetic carbon nanotubes tethered with maghemite nanoparticles. J Phys Chem C 114:6944–6951. https://doi.org/10.1021/jp9118925
55. Tan Y, Resasco DE (2005) Dispersion of single-walled carbon nanotubes of narrow diameter distribution. J Phys Chem B 109:14454–14460. https://doi.org/10.1021/jp052217r
56. Vaisman L, Marom G, Wagner HD (2006) Dispersions of surface-modified carbon nanotubes in water-soluble and water-insoluble polymers. Adv Funct Mater 16:357–363. https://doi.org/10.1002/adfm.200500142
57. Wang H, Zhou W, Ho DL, Winey KI, Fischer JE, Glinka CJ, Hobbie EK (2004) Dispersing single-walled carbon nanotubes with surfactants: a small angle neutron scattering study. Nano Lett 4:1789–1793. https://doi.org/10.1021/nl048969z
58. Lee CL, Ju YC, Chou PT, Huang YC, Kuo LC, Oung JC (2005) Preparation of Pt nanoparticles on carbon nanotubes and graphite nanofibers via self-regulated reduction of surfactants and their application as electrochemical catalyst. Electrochem Commun 7:453–458. https://doi.org/10.1016/j.elecom.2005.01.016
59. Fang B, Kim M-S, Kim JH, Song MY, Wang Y-J, Wang H, Wilkinson DP, Yu J-S (2011) High Pt loading on functionalized multiwall carbon nanotubes as a highly efficient cathode electrocatalyst for proton exchange membrane fuel cells. J Mater Chem 21:8066. https://doi.org/10.1039/c1jm10847f
60. Silva-carrillo C, Reynoso-soto EA, Félix-navarro RM, Lin-ho SW, Díaz-rivera A, Paraguay-delgado F, Chávez-carvayar JÁ, Alonso-núñez G, Mar R (2016) Organic solvent ' s effect in the

deposition of platinum particles on MWCNTs for oxygen reduction reaction. J Nanomater 2016:5783920. https://doi.org/10.1155/2016/5783920
61. Zeng L, Zhao TS, An L, Zhao G, Yan XH, Jung CY (2015) Graphene-supported platinum catalyst prepared with ionomer as surfactant for anion exchange membrane fuel cells. J Power Sources 275:506–515. https://doi.org/10.1016/j.jpowsour.2014.11.021
62. Lin JF, Mason CW, Adame A, Liu X, Peng XH, Kannan AM (2010) Synthesis of Pt nanocatalyst with micelle-encapsulated multi-walled carbon nanotubes as support for proton exchange membrane fuel cells. Electrochim Acta 55:6496–6500. https://doi.org/10.1016/j.electacta.2010.06.032
63. Yuan W, Lu S, Xiang Y, Jiang SP (2014) Pt-based nanoparticles on non-covalent functionalized carbon nanotubes as effective electrocatalysts for proton exchange membrane fuel cells. RSC Adv 4:46265–46284. https://doi.org/10.1039/C4RA05120C
64. Cheng Y, Xu C, Shen PK, Jiang SP (2014) Effect of nitrogen-containing functionalization on the electrocatalytic activity of PtRu nanoparticles supported on carbon nanotubes for direct methanol fuel cells. Appl Catal B Environ 158–159:140–149. https://doi.org/10.1016/j.apcatb.2014.04.017
65. Tuncel D (2011) Nanoscale. Nanoscale 3:3545
66. Jo TS, Han H, Ma L, Bhowmik PK (2011) Dispersion of single-walled carbon nanotubes with poly(pyridinium salt)s. Polym Chem 2:1953. https://doi.org/10.1039/c1py00212k
67. Uk J, Huh J, Hyeong K, Park C, Jo WH (2007) Aqueous suspension of carbon nanotubes via non-covalent functionalization with oligothiophene-terminated poly (ethylene glycol). Carbon 45:1051–1057. https://doi.org/10.1016/j.carbon.2006.12.017
68. Xu L, Ye Z, Cui Q, Gu Z (2010) Noncovalent nonspecific functionalization and solubilization of multi-walled carbon nanotubes at high concentrations with a hyperbranched polyethylene. Macromol Chem Phys 210:2194–2202. https://doi.org/10.1002/macp.200900460
69. Tsunoyama H, Ichikuni N (2009) Effect of electronic structures of au clusters stabilized by poly (N-vinyl-2-pyrrolidone) on aerobic oxidation catalysis. J Am Chem Soc 131(20):7086–7093. https://doi.org/10.1021/ja810045y
70. Wang S, Yang F, Jiang SP, Chen S, Wang X (2010) Tuning the electrocatalytic activity of Pt nanoparticles on carbon nanotubes via surface functionalization. Electrochem Commun 12:1646–1649. https://doi.org/10.1016/j.elecom.2010.09.017
71. Cheng Y, Jiang SP (2013) Electrochimica Acta Highly effective and CO-tolerant PtRu electrocatalysts supported on poly (ethyleneimine) functionalized carbon nanotubes for direct methanol fuel cells. Electrochim Acta 99:124–132. https://doi.org/10.1016/j.electacta.2013.03.081
72. Shi L, Liang R-P, Qiu J-D (2012) Controllable deposition of platinum nanoparticles on polyaniline-functionalized carbon nanotubes. J Mater Chem 22:17196. https://doi.org/10.1039/c2jm31859h
73. Cui Z, Li M, Ping S (2011) PtRu catalysts supported on heteropolyacid and chitosan functionalized carbon nanotubes for methanol oxidation reaction of fuel cells. Phys Chem Chem Phys 13(36):16349–16357. https://doi.org/10.1039/c1cp21271k
74. Okamoto M, Fujigaya T, Nakashima N (2009) Design of an assembly of poly(benzimidazole), carbon nanotubes, and Pt nanoparticles for a fuel-cell electrocatalyst with an ideal interfacial nanostructure. Small 5:735–740. https://doi.org/10.1002/smll.200801742
75. Wang S, Jiang SP, Wang X (2008) Polyelectrolyte functionalized carbon nanotubes as a support for noble metal electrocatalysts and their activity for methanol oxidation. Nanotechnology 19 (26):265601. https://doi.org/10.1088/0957-4484/19/26/265601
76. Yu LH, Kuo CH, Yeh CT (2007) Poly(vinylpyrrolidone)-modified graphite carbon nanofibers as promising supports for PtRu catalysts in direct methanol fuel cells. J Am Chem Soc 129:9999–10010. https://doi.org/10.1021/ja072367a

Chapter 7
Non-Noble Metal Electrocatalysts for the Oxygen Reduction Reaction in Fuel Cells

I. L. Alonso-Lemus and M. Z. Figueroa-Torres

Abstract Low temperature fuel cells are promising and sustainable alternative in energy generation. However, their large-scale production have been limited due at high-cost and scarce electrocatalysts based commonly in noble metals. Development of non-noble electrocatalysts has become intensive in recent years. A wide variety of materials as perovskite-type, spinel-type oxides, tungsten carbides, and heteroatom-doped carbons has been explored as alternative electrocatalysts to platinum. They have demonstrated promising electrocatalytic activity toward the oxygen reduction reaction (ORR) in alkaline electrolytes. However, these electrocatalysts are not favorable using strong acid electrolytes. Moreover, transition metal macrocycles show activity performance close to those of Pt-based electrocatalysts in acid media. In this chapter, we present the most recent developments regarding non-noble metal electrocatalyst, starting with a review of some basic electrochemistry concepts and some techniques commonly used to evaluate their performance. Then, materials used as non-noble metal electrocatalyst are presented which are divided into two groups: (1) the most promising non-noble metal electrocatalysts used in acid electrolytes and (2) in alkaline media. Finally, the conclusions and futures perspective are mentioned for these materials that should be considered as the future electrocatalysts for sustainable large-scale fuel cell commercialization.

Keywords Oxygen reduction reaction · Metal-free electrocatalysts · Transition metal chalcogenide · Transition metal macrocycles · Transition metal nitride · Transition metal carbide · Perovskites · Spinel oxide · Heteroatom-doped carbon · Biomass · Nitrogen precursor · Heteroatom precursor · Koutecky-Levich · 4 electron pathway · 2 electron pathway · Alkaline media · Acid media · Non-noble metal electrocatalysts · Rotating-ring disk electrode · Rotating disk electrode

I. L. Alonso-Lemus (✉)
CONACyT, Sustentabilidad de los Recursos Naturales y Energía, CINVESTAV Unidad Saltillo, Parque Industrial Saltillo-Ramos Arizpe 25900, Ramos Arizpe, Coahuila, Mexico

M. Z. Figueroa-Torres
Universidad Autónoma de Nuevo León, Facultad de Ingeniería Civil, Ciudad Universitaria. 66455, San Nicolás de los Garza, Nuevo León, Mexico

F. J. Rodríguez-Varela, T. W. Napporn (eds.), *Advanced Electrocatalysts for Low-Temperature Fuel Cells*, https://doi.org/10.1007/978-3-319-99019-4_7

7.1 Introduction

The oxygen reduction reaction (ORR) plays a key role in several important processes such as energy conversion, gas sensors, and biology. In energy conversion systems as fuel cells and metal–air batteries, the ORR takes place in the cathode of the device. This reaction is a complex electrochemical process, that is involving multi-electron transfer, which occurs mainly by two pathways: the direct 4-electron reduction pathway and the 2-electron reduction pathway. Additionally, 1-electron reduction pathway can also occur in nonaqueous aprotic solvents and/or in alkaline solutions.

Moreover, the ORR kinetics is very slow; for this reason, to speed up its kinetics a cathode ORR catalyst is needed. Platinum (Pt)-based catalysts are the most used in low temperature fuel cells. However, it is known that Pt-based catalysts are too expensive for making viable the large-scale commercialization of fuel cells. Extensive research over the past several decades has focused on developing alternative catalysts, including non-noble metal catalysts [1].

In this chapter, the most recent advances in the development of non-noble metal catalysts are reviewed. In the first section, we focus on the ORR background information, including the reaction kinetics and mechanisms in acid and alkaline media of the most studied ORR catalysts: platinum, followed by the conventional techniques for electrochemical measurements. The following sections address the wide variety of non-noble metal catalysts that have been developed in recent years, which were classified into two major groups: non-noble catalysts for proton exchange membrane fuel cells (PEMFCs), including direct methanol fuel cells (DMFCs) and non-noble metal catalysts for anion exchange membrane fuel cells anion exchange fuel cells (AEMFC).

Catalysts for PEMFCs include transition metal macrocyclic compounds, transition metal chalcogenides, metal nitrides, oxynitrides, and carbonitrides. On the other hand, catalysts for AEMFC include perovskite, transition metal oxides with spinel structure, and heteroatom-doped carbon materials. The chemical structure of each group of electrocatalysts and the reaction mechanisms proposed for the ORR are discussed in detail in Sects. 7.3 and 7.4 of this chapter.

Finally, a comparison between the catalysts used in acid and basic medium is elucidated, where we discuss from our perspective, what are the biggest challenges and the major areas of opportunity offered by this line of research in the near future.

7.2 Fundamentals of the ORR

The mechanism by which the ORR is carried out currently is complicated to explain, and this depends mainly on the naturalness of the catalyst, surface structure of electrode and the electrolyte. The reaction mechanisms according to the type of

Table 7.1 ORR in different electrolytes and their thermodynamic potential [2]

Electrolyte	Pathway	Reactions	Thermodynamic electrode potential vs. NHE (V)
Acidic	$4e^-$	$O_2 + 4H^+ + 4e^- \rightarrow 2H_2O$	1.299
	$2e^-$	$O_2 + 2H^+ + 2e^- \rightarrow H_2O_2$	0.70
		$H_2O_2 + 2H^+ + 2e^- \rightarrow 2H_2O$	1.76
Alkaline	$4e^-$	$O_2 + 2H_2O + 4e^- \rightarrow 4HO^-$	0.401
	$2e^-$	$O_2 + H_2O + 2e^- \rightarrow HO^- + HO_2^-$	−0.065
		$HO_2^- + H_2O + 2e^- \rightarrow 3HO^-$	0.867
Nonaqueous aprotic solvents	$1e^-$	$O_2 + e^- \rightarrow O_2^-$	[a]
		$O_2^- + e^- \rightarrow O_2^{2-}$	[a]

[a]The thermodynamic potential of this reaction strongly depends on the solvent used

electrolyte in the ORR has been summarized in Table 7.1. In electrochemical devices such as fuel cells and metal–air batteries, the 4-electron pathway is highly desirable.

The kinetics of the reactions presented in Table 7.1 depends on two factors: (1) the rate of the electrons that are transferred from the electrode to the reactant species and vice versa, and (2) the rate of mass transport on the surface of the electrode to displace the reaction products and feed on the reactant species.

The mass transport is relatively easy to control through the design of the cell and the selection of the materials for the fuel cell construction, while the electrons transfer is more complicated. The model of Julius Tafel (classic model) for the electrons transfer relates the reaction rate constant with the molecular structure of the reactants and the characteristics of the reaction medium [3]. However, the theory proposed by Gerischer is more suitable in electrochemical systems because it realizes the nanoscopic aspects with voltage–current variable [4]. This theory is based on determining the energy density states and their occupation in the electrode and the reactant species, associating the probability of tunneling between the electrode and the redox species.

Several studies about electron transfer have been performed by physicists [5, 6]. The main problem of electron transfer in solution is the highly polarizable environment in which transfer processes are carried out. The "polaron" theory has been discussed based on electron and hole conduction in semiconductors. The electron transfer occurs between one occupied quantum state and one quantum vacant state. During the ORR, the electron is transferred from the active site (occupied quantum state) to the oxygen molecule (vacant quantum state). In this case, the electrons in the electrode are studied according to the Sommerfeld–Drude model, while the electrons of the redox pair are treated as ions in solution.

In order to understand the fundamental about the effect of structure and properties of the non-noble metal electrocatalysts, several theoretical studies have been

developed [7]. Ab initio is considered a useful tool to calculate adsorption geometry, energy, the dissociation energy barrier, reversible potential, activation energy, and potential-dependent properties for elementary electron transfer steps [8]. In summary, the theoretical models have contributed greatly to the knowledge of the electrocatalytic systems and are considered a helpful tool for further development in this area.

Experimental studies are also widely used in the determination of some kinetical parameters of the ORR. The most frequently used techniques for the kinetic studies for the ORR are rotating disk electrode (RDE) and rotating-ring disk electrode (RRDE) . The ORR pathway is determined by RDE, and the number of electrons transferred is commonly calculated from the Koutecky–Levich plot [9], where the inverse of the kinetic current ($1/i_k$) is plotted versus the inverse of the square root of the rotation speed ($1/\omega^{1/2}$) according with the Koutecky–Levich Eq. (7.1):

$$\frac{1}{i} = \frac{1}{i_k} + \frac{1}{i_L} = \frac{1}{i_k} + \frac{1}{0.62\mathrm{nFAD}^{2/3}\mathrm{Cv}^{-1/6}w^{1/2}} \tag{7.1}$$

where i_k is the kinetic current for the ORR, i_L is the mass transport limiting current, n is the number of electrons per oxygen molecule for the ORR, F is the Faraday constant, A is the geometrical area of electrode, C is the saturation concentration for oxygen in water, D is the aqueous binary diffusion coefficient of oxygen, ν is the kinematic viscosity of the solution, and ω is the rotation rate.

Additionally, $1/0.62\mathrm{nFAD}^{2/3}\mathrm{Cv}^{-1/6}$ can be determined when calculating the Koutecky–Levich slope [10]. However, the Koutecky–Levich method was developed more than 50 years ago, under the assumptions of elementary reactions [11]. This method is not very useful with some of the recently developed nanostructured 3D electrocatalysts in alkaline electrolytes. Koutecky–Levich plots are often not linear and the electron number (n) sometimes exceeds the theoretical limits. It is highly desirable that the estimation of n, which is a very important indicator of the performance of an electrocatalyst, should preferably be performed with the RRDE technique. This technique allows the detection of intermediate compounds as H_2O_2 during the ORR, where n and the peroxide hydrogen percent are calculated from RRDE data using Eqs. (7.2) and (7.3) [12]:

$$n = \frac{4i_D}{i_D + i_R/N} \tag{7.2}$$

$$\%\mathrm{H_2O_2} = \frac{200i_R/N}{i_D + i_R/N} \tag{7.3}$$

where i_D is the reduction current density at the disc, i_R is the oxidation current density at the ring, and N is the collection efficiency of the RRDE.

The polarization curves that are typically obtained from the RRDE data are shown in Fig. 7.1a, where the current registers by the disk at several rotations rates are plotted. The ring current is several orders of magnitude smaller than the current of the disk (Fig. 7.1b). The plots of the Figs. 7.1c, d have been obtained from

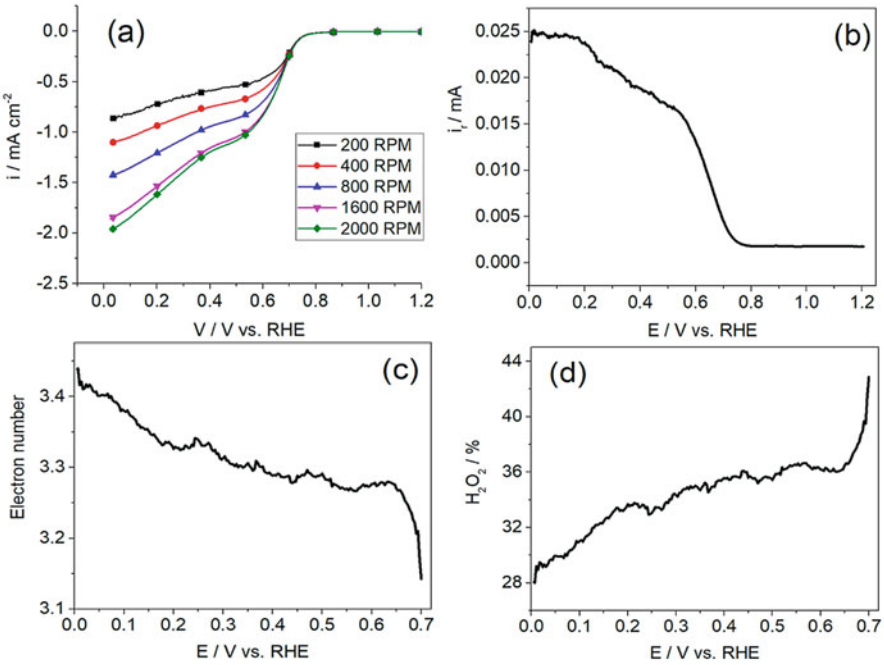

Fig. 7.1 Typical plots obtained from RDDE technique: (**a**) potential-current curves collected by the disk, (**b**) potential-current curve collected in the ring, (**c**) electron number n calculated from Eq. (7.2), and (**d**) H_2O_2% calculated from Eq. (7.3)

polarization curves data using the Eqs. (7.2) and (7.3). The number of electrons and the percentage of hydrogen peroxide can be calculated at different potentials. Thus, it is appreciated that *n* is not a constant value in the potential window of this test, as is assumed in Koutecky–Levich method; therefore, RDDE technique has important advantages to calculate *n*. In a study conducted by Zhou and coworkers [13], the authors suggest that it is preferable to use an electrode with Au ring instead of Pt, in addition to proposing an interesting methodology to calibrate the N value (efficiency of collection).

Many of the experimental and theoretical methods proposed currently base their models on Pt-based electrocatalysts to explain the electron transfer and pathway for the ORR. However, these models have not been so useful when trying to explain these two parameters in non-noble metal electrocatalysts. Therefore, it has been necessary to propose new models and mechanisms according to the nature and properties of each material.

In the following sections, two main groups of non-noble metal electrocatalysts are presented, highlighting some of their most important properties in relation to the ORR performance.

7.3 Electrocatalysts for ORR in Acid Media

7.3.1 Transition Metal Macrocycles

In recent years, transition metals macrocycles (TMM) are studied as alternative of Pt-based electrocatalyst, due they have a good catalytic activity for ORR in acid electrolytes. These materials are large molecules composed of a transition metal bound to a complex ligand. There are several reports in the literature about TMM that have been studied for the ORR. Some of these studies considered the use of noble transition metals such as Pd, Pt, or Ru [12]. However, in this chapter we will focus only on TMM with non-noble metals in their chemical structure.

The TMM with better performances and a remarkable electrocatalytic activity for the ORR are Fe- and Co- macrocyclic complex. Moreover, other TMM studied, although with less attractive performances, include transition metals such as Mo [14], Ni [15, 16], Cu [17, 18], Zn [16], Mn [19], V [16] and Ti [20].

Regarding the complex ligands, they play an important role maintaining stable the metal in the electrode surface and serving as active site. The chelating group composed of four nitrogen atoms (N_4) that coordinate with the metal ion for the TMM formation. Phthalocyanine (Pc) and porphyrin (PP) are the most used ligands complex in the literature. The structural formulas of the TMM with a Pc and PP ligands complex are shown in Fig. 7.2.

The reaction mechanism that takes place to carry out the ORR in these materials is still unclear. Several results from electrochemical studies suggest that electronic transfer occurs with the combination of 2- and 4-electron pathway. Some authors suggest that ORR involves a modified redox reaction [21, 22], where the first step involves the adsorption of O_2 on the metal ion located in the center of the TMM forming and oxygen–catalyst adduct. Subsequently, electrons are released and

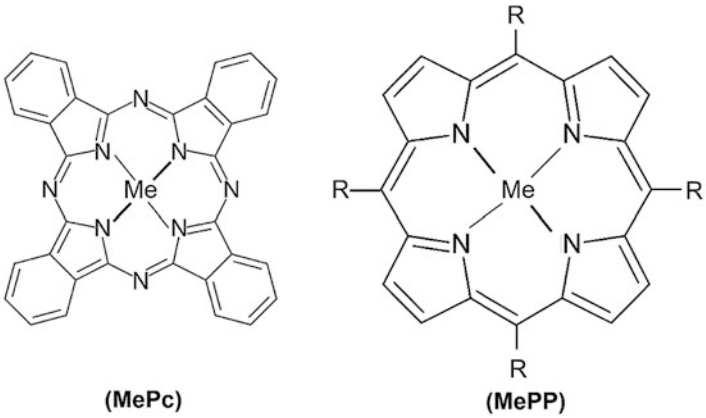

Fig. 7.2 Structural formula of TMM of the most reported ligands complex: phthalocyanine (Pc) and porphyrin (PP), Me = Transition metal ion and R = substituents

transferred from the metal ion to the bond of the oxygen molecule. The adduct undergoes further reductions forming intermediate spices like hydrogen peroxide or water. The reduced N_4-chelates will be regenerated to complete the cycle (Eqs. (7.4), (7.5), (7.6), and (7.7)).

$$XMe^{2+} + O_2 \rightarrow \left(XMe^{\delta+} \ldots {O_2}^{\delta-}\right) \tag{7.4}$$

$$\left(XMe^{\delta+} \ldots {O_2}^{\delta-}\right) + H^+ \rightarrow \left(XMe^{3+} \ldots O_2H\right)^+ \tag{7.5}$$

$$\left(XMe^{3+} \ldots O_2H\right)^+ + H^+ + e^- \rightarrow XMe + \text{intermediates (peroxide)} \tag{7.6}$$

$$H_2O_2 + XMe \rightarrow H_2O + 1/2\ O_2 \tag{7.7}$$

On the other hand, several factors have been identified that have a direct effect on the ORR activity such as the transition metal, the complex ligand, the heat treatment, and the support used.

The central transition metal defines largely the electron transfer pathway by which the ORR is carried out. It has been shown that most TMM with Fe reduce by direct 4-electron pathway, while TMM with Co generate peroxide as an intermediate product through the 2-electron pathway. However, Co complexes have shown more electrochemical stability than Fe complexes. Moreover, the formation of dimetal face-to-face macrocycles is another interesting alternative. An electrocatalyst with two Co centers face-to-face can provide two adsorption sites for O_2 molecule instead of one site promoting the 4-electron transfer process [23]. In addition, the advantage of combining two different metal centers with porphyrins complex ligand has been studied [16], resulting electrocatalysts with much greater activity and stability for ORR than electrocatalysts with a metal center only.

Furthermore, the complex ligand also plays an important role in the ORR. The majority complexes with Fe and Co have ORR activity, and their catalytic activity is attributed to the inductive and mesomeric effects of the ligand to the central metal ion [24]. Some of the N_4 chelate complexes evaluated for the ORR are tetracarboxyphthalocyanine (TcPc), tetramethoxyphenylporphyrin (TMPP), tetraphenylporphyrin (TPP), tetrasulfophthalocyanine (TSP), phthalocyanine (Pc), and dibenzotetraazaannulene (TAA).

The N_4 chelate complexes have their optimal catalytic activity when are subjected to heat treatments in a temperature range of 500–700 °C [16]. At temperatures below 500 °C, the catalytic activity is usually reduced by half, while at too high temperatures the active sites Me–N_4 are destroyed and lose their active nature [17]. Then, the effect of the heat treatment has a direct effect on the catalytic activity; however, it does not have a significant effect on the catalytic stability [12].

Jaouen et al. [25] suggest that the catalytic activity of Fe–N_4/C and FeN_2/C electrocatalysts depends directly on the type of carbon material in which they are supported. Specific surface area and pore size distribution are determining factors in the performance for the ORR. Although the most important factor is the nitrogen content in these materials, the higher it is, the higher is the density of the catalytic

sites. In terms of electrochemical parameters, the TMM performances report onset potentials in a range of 600–800 mV vs. RHE in strong acid electrolytes and current densities like the Pt-based electrocatalysts [26–29].

The ORR activity of TMMs has recently been evaluated in alkaline electrolytes; however, these results are not discussed in this review. If the reader is interested in this topic, there are several reviews that we recommend [30, 31].

The future research directions for the TMM as non-noble metal electrocatalyst request exploring new materials that optimize the catalytic activity and stability, may be optimizing the heat treatments in order to introduce more nitrogen active sites, using novel carbon supports with high surface areas and tunable pore sizes. Finally, the fundamental understanding of the reaction mechanisms involved in the ORR is necessary.

7.3.2 Transition Metal Chalcogenides

The pioneers in the development of transition metal chalcogenides (TMC) as non-noble metal alternative electrocatalysts are Alonso-Vante and Tributsch, publishing the first report three decades ago [32]. The TMC have a cluster structure with a repeating crystal lattice, the so-called Chevrel phase. The metal ion in the center is surrounded by several nonmetal ions. There are binary compounds with a basic formula Me_xX_y, where Me is a transition metal and X is chalcogen (e.g., S, Se, or Te). There are also ternary compounds with basic formula $MoM^1{}_xX_y$, where M^1 is an intercalated metal guest ion and the so-called pseudobinary compounds such as $MoM^2{}_xX_y$, where M^2 is a metal ion which replaces the Mo in the octahedral M^2 cluster.

Extensive studies have focused on Me_6X_8 and $MoM^2{}_xX_8$ pseudobinary compounds, due to their high current density and relative and comparatively close onset potential to platinum reported for the ORR. The reaction mechanism for an oxygen molecule in acid medium is proposed by Alonso-Vante [33]:

$$\bullet + O_2 \rightarrow \bullet - O_{2ads} \tag{7.8}$$

$$\bullet - O_{2ads} + (H^+ + e^-) \rightarrow \bullet - O_{ads} + H_2O \tag{7.9}$$

$$\bullet - O_{ads} + (H^+ + e^-) \rightarrow \bullet - OH_{ads} \tag{7.10}$$

$$\bullet - OH_{ads} + (H^+ + e^-) \rightarrow \bullet + H_2O \tag{7.11}$$

where the active site localized on the electrode surface is •, and an oxygen molecule adsorbed on an active site is $\bullet{-}O_2$. The ORR takes place with the transition metal d-states. For example, for the TMC $Mo_4Ru_2Se_8$, the catalytic center is the ruthenium atoms. For this material, the cluster serve as electrons reservoirs that adsorb oxygen molecules which favored the formation of water via 4-electron pathway. On the other hand, a change of volume occurs during the transfer process, which favors the

breaking bond O=O, and this last theory has been confirmed using nanodivided chalcogenide materials [34–37].

The carbonyl chemical route is the synthesis method most used to obtain TMC with Chevrel phase clusters. Ru_xSe_y electrocatalysts contain Ru *hpc* core cluster whose surface is coordinated to selenium atoms [34, 38–40], which preset a promising activity toward ORR and good methanol tolerance. Additionally, they can reduce oxygen by the 4-electron pathway.

Binary TMC containing Ru, Ir, Co, Fe, and Ni have shown high activity for the ORR [41–46], while the ternary Ru-Mo-Se TMC with Chevrel phase has been widely studied in this application [47]. Ru-based chalcogenides show high catalytic activity and good stability toward ORR in acid media. However, this noble metal and other such Ir-, Pt-, and Rh-based chalcogenides are not feasible for large-scale commercialization of PEMFC.

Regarding non-noble metal chalcogenide electrocatalysts, these have been reported since 1970. Combination of TMC consisting in Co_xS_y have high density current (958–2150 mA/m^2 at 5 0.0–0.6 V vs. RHE), good chemical stability, and an open circuit potential (OCP) $\approx$ 0.83 V vs. RHE [48], while the binary TMC containing Ti, W, Ta, Mo, and Cr bound to S atoms are shown the lowest current densities (> 1 mA/m^2 at 0.6 V vs. RHE). Furthermore, cobalt selenides supported on carbon ($Co_{1-x}Se/C$) exhibit significant ORR current compared with Co, Se, and carbon. The OCP in acid medium for these electrocatalysts is of 0.78 V vs. RHE [49]. In another research, Feng and coworkers investigated the ORR activity of $CoSe_2/C$; in this work, chalcogenide nanoparticles show an OCP of 0.81 V vs. RHE, and the electron transfer process involves about 3.5 electrons and the production of H_2O_2 between 15 and 30% (higher than the requirement below 5%) [50]. Although, one of the best performing TMCs is the pseudobinary compound $CoNiS_2$ with spinel structure and an OCP of 0.89 V vs. RHE.

Some theoretical studies have been carried out with the objective of clarifying the reaction mechanisms involved in the ORR. Sidik and Anderson conducted a study using the Vienna ab initio simulation package (VASP). They propose a mechanism of a TMC type Co_9S_8 with pentlandite structure, where the oxygen molecule can be adsorbed in a cobalt site or a sulfur site. In this work, they calculated the theoretical overpotentials between 0.74 and 0.89 V, which are higher compared to the overpotentials calculated for cobalt selenides with the same approach (0.22 V) [51].

There is still a long way to go to explore all the alternatives of TMC as non-noble metal electrocatalysts. The main challenges that they present are to improve their catalytic activity, which is still below that of Pt-based electrocatalyst. In addition, it is necessary to propose synthesis methods that are more environment friendly, using green solvents, for example. Finally, it is worth mentioning that in recent years there has not been an important development of TMC evaluated in acid medium; and that as with other types of materials such as TMM, the interest has focused on evaluating these materials in an alkaline medium.

7.3.3 Transition Metal Nitrides and Carbides

Transition metal nitrides (TMeN) and carbides (TMeC) have physical properties such as high melting point, high electrical conductivity, and chemical stability as well. These features make them excellent candidates as electrocatalysts to operate under the hostile conditions in the cathode of the fuel cells. The TMeC and TMeN are considered as "interstitial allows" [52] formed between transition metals of groups IVB-VIB and nitrogen or carbon atoms (see Table 7.2). Moreover, these materials are usually unstable with most of the metals of groups VIIB and VIIIB, mainly noble metals. An exception is the Fe, which can form iron carbides/nitrides (Fe_3C and Fe_3N), and Co and Ni, which can form nitrides such as Co_3N and Ni_3N, respectively.

TMeC and TMeN often have unit cells such as face-centered cubic (fcc), hexagon close-packed (hcp), and hexagonal simple, which are usually formed by the small carbon or nitrogen atoms occupying interstitial positions (Fig. 7.3) [53]. The intercalation of the nitrogen/carbon atoms in the metal lattice causes an expansion, which would be broadening the metal d-band. These contractions in the d-band produce a greater density of states (DOS). This redistribution of DOS could give to the carbides and nitrides electronic properties analogous to the noble metals [54]. However, theoretical models and catalytic mechanisms are still under discussion.

Despite the similarities in the electronic structure of carbides and nitrides compared to noble metals, their electrochemical activity toward the ORR is still low. The

Table 7.2 Transition metal carbides/nitrides and their formula regarding their position in the periodic table

	Group		
	IVB	VB	VIB
Carbides	TiC_{1-x}	VC_{1-x}	Cr_3C_2
	ZrC_{1-x}	NbC_{1-x}	Mo_2C
	HfC_{1-x}	TaC_{1-x}	WC
Nitrides	TiN	VN_{1-x}	Cr_3N_2
	ZrN_{1-x}	NbN_{1-x}	Mo_2N
	HfN_{1-x}	TaN_{1-x}	WN

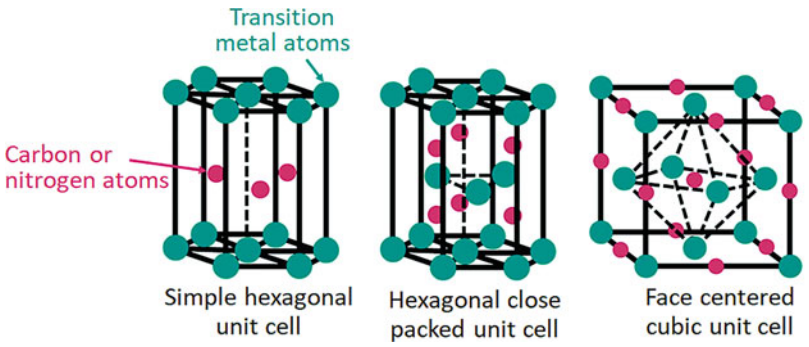

Fig. 7.3 Common unit cells of the TMeN and TMeC

WC, for example, is unstable at potentials over 0.6 V vs. RHE [55]. To improve its stability at higher potentials, Lee and coworkers synthesized the compound $W_{42}Ta_{24}C_{34}$, which is more stable in acid corrosive environments than WC and has an onset potential 350 mV higher than pure WC [56]. In other research, the addition of Ta to nickel carbide ($Ni_{33}Ta_{41}C_{26}$) had an effect like the mentioned above, where Ta improves the stability and onset potential of the electrocatalysts for the ORR; however, Ta_2O_5 is formed, which is a problem due that this oxide is an electrical insulation [57].

Recently, it was reported Fe_3C as novel non-noble metal electrocatalyst with high onset potential (0.92 V vs. RHE) and good stability in strong acid electrolytes [58]. Moreover, ternary Fe/N/C has been considered one of the most promising candidates for their high ORR activity [59–61]. The synergistic effect between Fe and N supported on carbon matrix promotes the ORR and is relatively stable in acidic media. Lui and coworkers [62] developed core shell Fe_2N/C structures from seaweed biomass, in which the nitride is the core and nitrogen-doped amorphous carbon is the shell. The ORR performance shows a high onset potential of 0.93 V vs. RHE in 1 M $HClO_4$ electrolyte, good tolerance to methanol, and an electron transfer number of 3.85.

Furthermore, monometallic (δ-MoN, Mo_5N_6, and Mo_2N) and bimetallic ($Co_{0.6}Mo_{1.4}N_2$) molybdenum nitrides exhibit catalytic activity with a modest onset potential of 0.71 V vs. RHE and electron transfer mechanism of 4-electron at potential lower than 0.5 V [63].

The reaction mechanisms of the ORR are not clear yet; however, it is evident that the synergy that occurs between Fe–C–N improves the catalytic activity. Thus, materials based on these elements are the most promising electrocatalysts to replace noble metal-based catalyst operating in acid media. Recently, Sun and coworkers achieve a comparative study between Fe_3C, Fe_2N, and Fe–N_4/C moieties. The highest catalytic activity of Fe–N_4/C moieties has an onset potential of 0.879 V vs. RHE. However, the formation of moieties is not easy to obtain. On the other hand, the catalytic activity of iron nitride/carbide is lower than moieties and they are unstable in acid media due to their possible dissolution [64].

7.4 Electrocatalysts for ORR in Alkaline Media

7.4.1 Perovskite-Type Oxides

Oxides with perovskite or closely related structures play an important role in the development of effective earth-abundant and low-cost electrocatalysts for renewable energy storage and conversion systems. Perovskite oxides obtain their name from the structure of the mineral calcium titanium oxide ($CaTiO_3$) discovered in 1839 [65].

Commonly, perovskites have the general chemical formula ABO_3, where A is a rare-earth, alkaline earth, or a mix of both cations and B is one or more transition metal cations [66, 67]. The ideal cubic perovskite lattice is shown in Fig. 7.4a, b. It

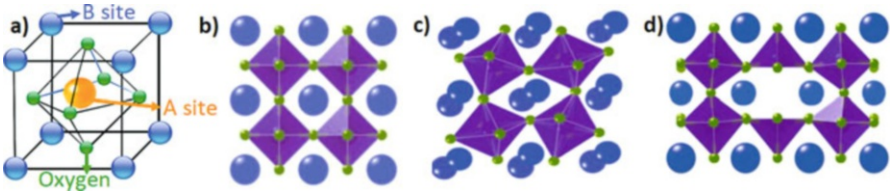

Fig. 7.4 (**a**, **b**) Ideal cubic perovskite unit cell. (**c**) Distorted perovskite structure and (**d**) perovskite structure with partial B-site substitution

consists of A cations located at the corners of the cube, which are 12-fold coordinated by oxygen. While cations at the B site are in the center, octahedrally coordinated with oxygen ions in the face-centered positions. The A site cation is slightly larger than B cation. The structure is commonly visualized as a three-dimensional network of regular corner-linked BO6 octahedra, where all B–O–B angles are 180°.

However, the wide variety of substitutions in the A and B sites lead to structural distortion and/or oxygen vacancies (δ) that can be related to the A and B ionic radii and electronic configuration of the metal ions. The degree of deviation from the ideal cubic perovskite can be quantified using the Goldschmidt tolerance factor (*t*) [68]. It relates how much strain can tolerate the lattice before it deforms. Thus, the perovskite-type structure is usually obtained in the range of $0.75 \leq t \leq 1.0$, for the ideal perovskite structure $t = 1$. The limiting values of t may differ depending upon the set of ionic radii employed [69]. As t decreases from 1 (A cations are too small), the perovskite structure deforms to orthorhombic or rhombohedral structures. When t is higher than 1 (A cations are very large), the structure of the perovskite is no longer cubic leading to a so-called hexagonal perovskite. In which, the octahedra share faces instead of corners modifying the M-O bond distances as well as making possible interactions between transition metals (Fig. 7.4c) [66, 69].

Moreover, it is possible to make partial substitutions of the A or B sites giving the formation of quaternary oxides or double perovskite. Where the cations in the A or B site are two different elements with strongly differing sizes $(A_xA'_y)BO_3$, $A(B_xB'_y)O_3$ where $x + y = 1$ or a complex perovskite $(A_xA'_y)(B_xB'_y)O_3$. These oxides result in a complex structure array and oxygen vacancies are frequently presented. Some of these oxides are known as perovskite-like oxides, see Fig. 7.4d. Interestingly, there is a relation between the structural distortions and oxygen vacancies (or oxygen nonstoichiometry δ) to the rise of important properties in the perovskite oxides. Thus, their physicochemical properties can be systematically tuned by carefully selecting the A or B cation and adjusting the stoichiometry [66, 69]. Up to now, many perovskite-type oxides and perovskite-like oxides have been generated and investigated as electrocatalysts for the ORR. They have shown promising electrocatalytic activity and stability in alkaline solutions due to their high electrical conductivity and outstanding catalytic behavior [66, 70, 71].

It was reported in the literature that for the ORR attractive electrocatalytic performance has been reported for perovskites containing in the A-site La, Nd, Ca, Sm, Li, Ba, and Sr ions and good chemical stability is obtained when Co, Fe, Mn, Ni,

and Cu ions were used at the B-site [66]. Among perovskite oxides, the lanthanum-based oxides have been recognized as one of the most promising electrocatalysts for the ORR. This type of oxides has high electrical conductivity at room temperature and significant stability against anodic oxidation in alkaline solution. Sunarso et al. [70] studied the electrocatalytic tendency of B-site substitution by the trivalent 3d transition metal ions such as Ni, Co, Fe, Mn, and Cr in $LaBO_3$ perovskite using a 0.1M KOH solution. The $LaCoO_3$ showed the largest ORR current density and the most positive onset potential followed by Mn, Fe, Ni, and Cr. Similar results were reported by Suntivich et al. [72] and Celorrio et al. [71] confirming that Co and Mn cations at the B-site presented the best performance for the ORR on $LaBO_3$ (B = Cr, Co, Fe, Mn, and Ni) nanoparticles. For these La systems, the ORR followed a close four-electron pathway.

Partial substitutions of the B site and stoichiometry on the electrocatalytic activity were studied by Larsson and Johansson [73] in $LaMn_xCu_yO_3$, $LaMn_xCr_yO_3$, and $LaMn_xNi_yO_3$ where $x = 0.1$–0.9 using 6 M KOH solution. They tried to find a relation with the current density and the magnetic moment of the superoxide ion O^{2-} due to that the rate determining step in alkaline media involves the adsorption of the ion at the surface. However, they did not find a linear trend between the measurements. It is also known that for many perovskites charge ordering effects lead to charge disproportionation, but complementary spectroscopic experiments are required to understand the effect. Suntivich et al. [72] concluded that Mn is a more active element than Ni in the La oxides perovskites with partial substitution at the B-site.

The effect of A-site substitution on the ORR in an $AMnO_3$ was systematically varied using several lanthanoids and yttrium [74]. It was reported that the electrocatalytic activity is higher as the ionic radius of the lanthanide increases being in the order of La > Pr > Nd > Sm > Gd > Y > Dy > Yb. Partial substitutions at the A-site have been also studied for the system $AMnO_3$ using cations such as: $A = La_XCa_{1-x}$ where $X = 0.36, 0.4, 0.5, 0.6, 0.81$ [72, 75, 76]. $A = La_{1-x}Sr_x$, where $X = 0.1, 0.2, 0.33, 0.4, 0.5, 0.7, 0.8$ [77, 78]. In all studies, the best performance was obtained around 0.4 of the divalent A-site cation, which promotes the maximum oxidation state of Mn increasing the electron transfer number close to four. A similar tendency was obtained for the $Pr_{1-x}Ca_xMnO_3$ perovskite where the maximum current density was obtained when $x = 0.4$ [79].

Another important factor in the design of perovskite oxides for the ORR is the effect of oxygen stoichiometry. Several authors have reported that the appropriated amount of oxygen ion vacancies (δ) enhanced the electrocatalytic activity. Takeda et al. [80] found that for the $SrFeO_{3-\delta}$, the samples with $0.24 < \delta < 0.29$ showed the best activity. However, a slight dependence was observed in $SrCoO_{3-\delta}$. Du et al. [81] studied the effect of oxygen vacancies in the range of $0 < \delta \leq 0.5$ for the $CaMnO_{3-\delta}$, and the higher electroactivity was obtained when δ is close to 0.5 and average Mn valence close to 3.5. The improvement in the catalytic activity of the ORR is due to an rise electrical conductivity generated by the oxygen defects which facilitated the oxygen activation. The absence of too much oxygen will result in the formation of less conductive and poorly active perovskite oxide and the loss of perovskite structure.

Moreover, for the electrocatalytic measurements, perovskite oxides are usually mixed with carbon forming an electrocatalytic layer. It has been reported that the use of carbon disperses the oxide particles, electrically connects the particles, and enhances the electroactivity acting as cocatalyst in some cases. To investigate the effect of the amount of carbon in the electrocatalyst layer, Poux et al. [82] evaluated the electrocatalytic activity for the ORR on electrodes containing perovskite alone ($LaCoO_3$ and $La_{0.8}Sr_{0.2}MnO_3$), carbon alone, and both perovskite and carbon. They concluded that the presence of carbon electrocatalyzes the reduction of O_2 into OH^- as intermediate, which can react to ultimately result in a $4e^-$ ORR to water. Mixing it with perovskites improves the electrical contact between the oxide particles increasing the number of accessible active sites on the oxide surface for the reduction of the OH^{2-}.

Significant progress has been made over the last decades in understanding the electrocatalytic activity and stability of perovskite oxides for the ORR. The flexibility in the oxidation states leads to the formation of redox coupes, unique electronic properties, defective structure for oxygen vacancies or excess, and cation ordering resulting in distortion-free channels of oxygen vacancies and enhanced mobility of oxygen ions, which facilitate their bifunctional electrocatalytic activity for the oxygen reduction and oxygen evolution reactions. However, they can only be used in alkaline media, thus the long-term stability still being an issue to overcome. The formation of hydrogen peroxide during the ORR process can attack the electrocatalysts damaging their actives sites. Moreover, the structures of such active sites are not well understood. More research is necessary with emphasis on the activity–stability improvement. Further efforts are also required to understand the dependence of carbon supports and perovskites to catalyze the ORR or the use of other types of cocatalysts for engineering optimization proposes and fuel cell commercialization.

7.4.2 Spinel-Type Oxides

Spinel-type oxides are an interesting class of compounds that have been identified as promising candidates and alternatives to noble metal electrocatalysts. These oxides are also bifunctional electrocatalysts of the ORR and OER (oxygen evolution reaction) in alkaline media [83]. Spinel oxides with general formula AB_2O_4 are a very large family of compounds with the same crystal structure as the mineral $MgAl_2O_4$. The spinel structure can be described as a face-centered cubic close-packed array of O^{2-} ions, with tetrahedrally A^{2+} and octahedrally B^{3+} coordinated metal cations, see Fig. 7.5 [84]. Tetrahedral interstices are usually smaller than the octahedral; thus, cations with smaller ionic radii occupy the A-sites, while the larger cations occupy the B-sites. Moreover, to keep the valence balance, cation A can be in the $+2$ or $+$ 4 oxidation states and the corresponding cation B can be in the $+3$ or $+$ 2 oxidation states.

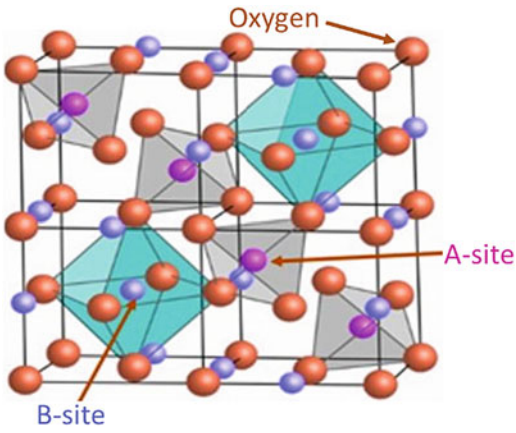

Fig. 7.5 Unit cell of ideal spinel-type oxide structure

The variations in distribution of cations in the A and B sites cause marked changes in some of the physical properties. For these oxides, several researches have been done to identify the active site and defect features, and understand the composition-dependent activities and intentional substitution of cations or dopants to enhance the electrocatalytic activity for the ORR [85–87]. Spinel oxides with cations on the B-site such as Co, Mn, and Fe are among the most active for the ORR. Many spinel oxides have been synthesized using cations in the A-site such as Co, Ni, Mn, Li, Zn, Cu, and Fe [83, 87].

In general, these compounds exhibit comparable electrocatalytic activities than precious metal-based electrocatalysts, high corrosion resistance, and easy availability. However, their low electrical conductivity and large particle size have limited their electrocatalytic performance and long-term stability. Numerous researches have been conducted to enhance their performance by controlling composition, designing nonstoichiometric oxides, creating defects, nanostructured characteristics, and using carbon nanomaterials as supports [87–90].

The synthesis of nonstoichiometric compounds and the creation of oxygen defects optimize the electronic structures of spinel, produce more active sites for molecular adsorption of oxygen, and reduce the reaction energy barriers. To examine the effect of M^{2+} substitution, Mn, Fe, Co, and Cu were used as cations in the nonstoichiometric $MFe_{3-x}O_4$. It was demonstrated that the most active spinel for ORR was $MnFe_{3-x}O_4$ followed by $Co_xFe_{3-x}O_4$, $CuxFe_{3-x}O_4$, and Fe_3O_4 [91]. Recently, Wei et al. [83] reported an increasing activity for $MnCo_2O_4$ with the reduction from $Mn^{3.7+}$ to $Mn^{3.2+}$ showing that the band gap occupancy of the active cation in the octahedral site is the activity descriptor for ORR, consolidating the role of electron orbital filling in metal oxide electrocatalysts.

Spinel with nanostructured characteristics as nanoparticles, nanoneedles, nanopetals, core-shell arrays, or porous structures have been prepared to improve their ORR properties. Zhu et al. [91] have been reported that $MnFe_2O_4$ nanoparticles (around 10 nm) with catalytic activity towards ORR comparable with the commercial Pt-based electrocatalyts in alkaline solution. The mesoporous nanostructured

MFe_2O_4 (M = Co, Mn, Ni) oxides exhibited excellent performance as bifunctional electrocatalysts for ORR and OER; the $CoFe_2O_4$ and $NiFe_2O_4$ exhibited higher OER activity than $MnFe_2O_4$ [89]. Recently, Bhandary et al. [92] synthesized $MnFe_2O_4$ nanopetals on porous carbon paper, and reported that electrocatalytic activity for the ORR (onset potential of 1.6 V vs RHE and higher current density of 11.5 mA/cm^2 at 2.0 V vs RHE reference electrode) was better than those other earlier reported spinel electrocatalysts and comparable to those spinel oxides supported on graphene or carbon nanotubes.

Carbon substrates are used to improve the electrical conductivity and adsorption capability by increasing the number of active sites. A high ORR electrocatalytic performance and durability was reported in a zinc ferrite/reduced graphene oxide ($ZnFe_2O_4$/rGO) with 69.8 wt.% of electrocatalyst, which follows a four-electron transfer mechanism in alkaline media [90].

7.4.3 Heteroatom-Doped Carbon Materials

Carbon materials are most widely used as electrodes in several energy devices such as fuel cell, batteries, and supercapacitors. In addition, they are frequently used as supports for many of the materials that have been mentioned in the previous sections. Certainly, this group of materials is one of the most promising for the performance of the ORR. Its boom began in 2009, when Dai et al. [93] reported that carbon nanotubes doped with nitrogen had high catalytic activity for the ORR in alkaline solution.

Basically, heteroatom-doped carbons are materials formed mainly by carbon atoms (<80% wt.), where doping consists in substituting a carbon atom with a heteroatom (N, S, B, P, etc.). The incorporation of one type of heteroatom into the carbon lattice generates a charge delocalization in the adjacent carbons, which promotes the formation of catalytic sites [94–96]. Additionally, the electronegativity and size of the doping atom has a determining influence on the electronic modulation of the electrocatalysts [97]. Moreover, it has been reported that the incorporation of dual-doped or more types of heteroatoms into carbon materials favors the formation of active sites, and usually have greater activity than its counterpart with a single heteroatom, and in some cases better catalytic activity than Pt/C [98–101]. In addition, most of these electrocatalysts have shown greater stability than Pt/C [102].

Nitrogen-doped carbons are probably the metal-free electrocatalysts most studied in the last decade [103–106]. Nitrogen–carbon bonds (N–C) can be identified relatively easily by X-ray photoelectron spectroscopy (XPS). Figure 7.6 shows the main N–C bonds in relation to their binding energy. This classification considers five types of N–C bonds commonly identified as pyridinic (N1), amine (N2), pyrrolic (N3), graphitic (N4), and pyridine-N-oxide (N5). Usually, several authors do not report the amine bond (N2, ≈399.4 eV); however, it has been reported that N2 bond is important to explain the evolution of carbon functionalities during pyrolysis treatments, to which carbon materials are usually subjected [107].

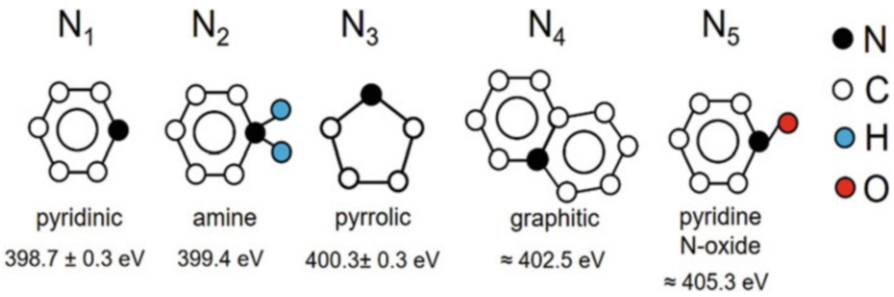

Fig. 7.6 Commonly nitrogen–carbon bonds identified by XPS in nitrogen-doped carbon materials

N-C type bond has a direct influence on the electrochemical performance of the electrocatalyst. Several studies suggest that N1 and N4 bonds favor the ORR [108]. However, the reaction mechanisms have not yet been fully elucidated. Conversely, it is currently a challenge to clarify these mechanisms and validate them experimentally and theoretically. Theoretical methods based on the density functional theory (DFT) have been widely used to propose some mechanisms. Some hybrid methods such as B3LYP-DFT and Car–Parrinello molecular dynamic simulation have also been employed [109, 110]. It should be noted that the theoretical studies proposed recently have been developed for nanostructured carbon materials such as carbon nanotubes and graphene doped with nitrogen.

Zhang and Xia [111] reported a theoretical study, where they justify how the ORR takes place for 4-electron pathway in N-doped graphene, and this reaction did not arise in pristine graphene, due mainly to pristine graphene does not have electroactive sites. Additionally, they observe that when introducing hydrogen atoms at the edges of the carbon lattice, the sequential reactions for the ORR energetically can occur. One of these reactions involves the formation of the chemical bond O–C between the oxygen of the medium and one carbon of the graphene. The O–O bond breaks up forming water molecules. For each step of the reaction, the energy of the system decreases, which indicates that the reaction by 4-electron pathway is spontaneous and possible. The active catalytic sites depend on the distribution of the density of the spin and the distribution of the atomic charge. The substitution of nitrogen atoms generates a pair of free electrons that modifies the distribution of the atomic charge in graphene. According to this study, carbon atoms with high spin densities are the electrocatalytically most active sites. As can be expected, N–C bond type has influence in the charge distribution of the carbon atoms adjacent to where the nitrogen doping atom is located. The dopant or heteroatom that is introduced into the carbon lattice not only causes changes in the distribution of electronic charge, it also causes defects such as bending and breaking of C–C bonds in the lattice.

The catalytic activity toward ORR for N-doped carbon materials is close to Pt/C electrocatalyst; however, the cost of these metal-free electrocatalysts is considerably lower, which opens the possibility of large-scale production of the fuel cells. Many reports show that N-doped carbons have onset potential in a range of 0.75 to

0.86 V vs. RHE. For example, partially exfoliated N-CNT has onset potential of 0.77 V [112]. Moreover, N-doped graphene synthetized by resin-based methodology has an onset potential 60 mV lower than Pt/C, comparable activity but higher durability than Pt/C, and 3.9 electron transfer number at −0.2 V [113]. Other authors have obtained N-doped graphene with promising performance, and most of them agree that these metal-free electrocatalysts have comparable ORR activity with Pt/C, higher long-term stability and resistance to crossover than Pt/C [103, 114–116].

Besides nitrogen, nanostructured carbon materials as carbon nanotubes (CNT), graphene, mesoporous ordered carbons (MOC), carbon aerogels, and carbon nanofibers (CNF) have been doped with heteroatoms such as sulfur [117–119], boron [120–122], phosphorous [123, 124], silicon [125], and halogens [126, 127].

Table 7.3 summarizes several heteroatom-doped nanostructured carbons evaluated as metal-free electrocatalysts in alkaline electrolyte, the range of binding energy in which they are usually identified by XPS, the type of bond formed between heteroatom-carbon and other elements that usually are present, and their onset potential according to recent reports. It should be noted that for comparative purposes, it is best to report the onset potential vs. the reversible hydrogen electrode (RHE), because the pH of the electrolyte is adjusted.

Table 7.3 Chemical structure of some heteroatom-doped carbon nanostructured electrocatalysts and their electrochemical activity toward the ORR

Heteroatom	Energy binding (eV)	Formed bonds	Onset potential	Reference
Si 2p	100–105	SiO_2 C–Si–O Si–C	−0.2 V vs. Ag/AgCl in 0.1 M KHO	[125]
P 2p	132–137	P–C P–O P=O	−0.2 V vs. Hg/Hg_2Cl_2 in 0.1 M KOH	[123]
S 2p	161–172	C–S–C R–SO_2 RO_2–S–S–R	0.69 V vs. RHE 0.88 V vs. RHE 0.86 V vs. RHE 0.96 V vs. RHE 0.80 V vs. RHE	[128] [129] [130] [131] [132]
B 1s	186–194	B_2O_3 CBO_2 C_2BO B–C sp^2 B_4C	0.83 V vs. RHE −0.14 V vs. Ag/AgCl in 0.1 M KOH	[122] [121]
I 3d	617–632	I2 I–C	≈ −0.1 V vs. Ag/AgCl in 0.1 M KOH	[127]
F 1s	681–690	Ionic C–F Semi-ionic C–F Covalent C–F	≈ −0.15 V vs. SCE in 0.1 M KOH ≈ −0.13 V vs. SCE in 0.1 M KOH	[133] [126]

It can be seen that heteroatom-doped nanostructured carbon shows promising performances toward the ORR. However, nanostructured carbon materials currently have several drawbacks: (1) the chemical reagents used in the processes to obtain them, generally they are of high purity and high costs, which in many cases are hazardous for the health and the environment; (2) although sophisticated technologies or equipment are used in synthesis processes, even large-scale production remains a challenge in order to obtain high quality materials [134].

The most recent research has a clear tendency: to use natural sources of carbon and heteroatoms as raw materials instead of expensive reagents that are commonly hazardous chemicals, mainly motivated by economic and environmental reasons [135]. In addition, several investigations have been carried out proposing less inexpensive methodologies to obtain nanostructured carbon materials and increase the large-scale production [134, 135]. The use of biomass as a carbon and heteroatom source to obtain metal-free electrocatalysts is economically and environmentally attractive. This alternative has recently been explored; biomass-derived electrocatalysts have performance for the ORR higher than heteroatom-doped nanostructured carbons, and in some cases higher than Pt/C. Most of the biomass waste is usually used as an energy source through direct combustion and gasification processes, among others. However, the possibility of taking advantage of biomass residues for the manufacture of carbon materials used in electrochemical devices is very attractive. In addition, the technology to obtain them is inexpensive [136–138]. The above, then, also represents an alternative for the exploitation of several biomass wastes generated in large quantities and that are currently disposed in landfills or are left open.

Food and several biomass wastes such as urban, forest, vegetable, and animal wastes have been used as raw materials in obtaining metal-free electrocatalysts. Most biomass-derived carbons are synthetized by pyrolysis and/or hydrothermal carbonization treatments. Their electrochemical performances are very attractive; for example, egg [139], soybeans [140], amaranth [141], soy milk [142], and honey [143] have been used as raw materials in obtaining metal-free electrocatalysts and evaluated in the ORR.

However, the use of food in obtaining carbon could have serious food implications globally. Plant and forest wastes such as tree leaves [144], vegetables skin [128], luffa [145], and algae [146, 147] have also been explored to obtain metal-free electrocatalysts. As far as animal waste is concerned, carbons have been obtained from human hair [148], human urine [149], leather [137, 138], bones, and pig blood [150, 151]. Generally, the electrochemical performance of these materials in an alkaline media is comparable to that of Pt/C, due to their high surface areas, and high current densities are usually reported. However, it is still a challenge to improve the onset potential.

7.5 Conclusions

Throughout the last decade, a wide variety of materials have been studied as non-noble metal electrocatalysts, each family of materials have advantages and disadvantages over Pt/C. However, to have electrocatalysts with the most favorable properties for ORR, it is necessary to use several types of materials to enhance their properties. On the other hand, carbon materials have been used as a support and as metal-free electrocatalysts, they are very versatile materials, of great abundance and therefore of low cost. Prospects indicate that heteroatom-doped carbon materials in combination with transition metals such as Fe or Co could be a very promising option for the substitution of noble metals in fuel cell cathodes.

Now, environmentally the use of biomass waste as raw material for producing metal-free electrocatalysts would be very attractive. The main advantage of these materials is that they have a heterogeneous chemical composition, which includes metals that can function as active sites for the ORR. There is still a long way to go to develop a material with the properties to replace the noble metals; however, the use of non-noble metal electrocatalysts is a research area that is developing rapidly. Last, but not least, it must be considered that for the development of new non-noble metal electrocatalysts it is necessary to implement methodologies that have a low environmental impact; in addition, the process must be easily scalable to cover market demand and that its production involves the use of technologies of easy implementation.

Acknowledgment The authors would like to thank to the Mexican Council for Science and Technology (CONACyT) for financial support grant CB-2015-250632.

References

1. Shao M, Chang Q, Dodelet J-P, Chenitz R (2016) Recent advances in electrocatalysts for oxygen reduction reaction. Chem Rev 116:3594–3657
2. Zhang L, Zhang J, Wilkinson DP, Wang H (2006) Progress in preparation of non-noble electrocatalysts for PEM fuel cell reactions. J Power Sources 156:171–182
3. Allen J, Bard LRF (2000) Electrochemical methods: fundamentals and applications, 2nd edn. Wiley, New York
4. Gerischer H (1997) Principles of electrochemistry. In: Gellings PJ, Bouwmeester HJM (eds) The CRC handbook of solid state electrochemistry, 1st edn. CRC Press, Boca Raton, p 656
5. Adzic R, Gong K (2017) Platinum-monolayer oxygen-reduction electrocatalysts: present status and future prospects. In: Mirking MV, Amemiya S (eds) Nanoelectrochemistry, 1st edn. CRC Press, Pittsburgh, pp 125–144
6. Soldano GJ, Schmickler W, Juarez MF, Quaino P, Santos E (2017) Electron transfer in nanoelectrochemical systems. In: Mirking MV, Amemiya S (eds) Nanoelectrochemistry, 1st edn. CRC Press, Pittsburgh, pp 3–28
7. Dy E, Shi Z (2014) Theoretical modeling of non-noble metal electrocatalysts for acid and alkaline PEM fuel cells. In: Chen Z, Dodelet J, Dodelet JZ (eds) Non-noble metal fuel cell catalysts. Wiley, Weinheim, pp 205–242

8. Shi Z, Zhang J, Liu ZS, Wang H, Wilkinson DP (2006) Current status of ab initio quantum chemistry study for oxygen electroreduction on fuel cell catalysts. Electrochim Acta 51:1905–1916
9. Koutecky J, Levich BG (1958) The application of the rotating disc electrode to studies of kinetic and catalytic processes. Zhurnal Fiz Khimii 32:1565–1575
10. Zhang HJ, Yuan X, Sun L, Zeng X, Jiang QZ, Shao Z, Ma ZF (2010) Pyrolyzed CoN4-chelate as an electrocatalyst for oxygen reduction reaction in acid media. Int J Hydrog Energy 35:2900–2903
11. Frumkin A, Nekrasov L, Levich B, Ivanov J (1959) Die anwendung der rotierenden scheibenelektrode mit einem ringe zur untersuchung von zwischenprodukten elektrochemischer reaktionen. J Electroanal Chem 1:84–90
12. Song C, Zhang J (2008) Electrocatalytic oxygen reduction reaction. In: Zhang J (ed) PEM fuel cell electrocatalysts and catalyst layers: fundamentals and applications. Springer, London, pp 89–134
13. Zhou R, Zheng Y, Jaroniec M, Qiao S-Z (2016) Determination of the electron transfer number for the oxygen reduction reaction: from theory to experiment. ACS Catal 6:4720–4728
14. Xia D, Liu S, Wang Z, Chen G, Zhang L, Zhang L, Hui S (Rob), Zhang J (2008) Methanol-tolerant MoN electrocatalyst synthesized through heat treatment of molybdenum tetraphenylporphyrin for four-electron oxygen reduction reaction. J Power Sources 177:296–302
15. Behret H, Binder H, Sandstede G, Scherer GG (1981) On the mechanism of electrocatalytic oxygen reduction at metal chelates. J Electroanal Chem Interfacial Electrochem 117:29–42
16. Chu D, Jiang R (2002) Novel electrocatalysts for direct methanol fuel cells. Solid State Ionics 148:591–599
17. Ding L, Xin Q, Dai X, Zhang J, Qiao J (2013) Evaluation of carbon-supported copper phthalocyanine (CuPc/C) as a cathode catalyst for fuel cells using Nafion as an electrolyte. Ionics (Kiel) 19:1415–1422
18. Reis RM, Valim RB, Rocha RS, Lima AS, Castro PS, Bertotti M, Lanza MRV (2014) The use of copper and cobalt phthalocyanines as electrocatalysts for the oxygen reduction reaction in acid medium. Electrochim Acta 139:1–6
19. Domínguez C, Pérez-Alonso FJ, Abdel Salam M, Gómez De La Fuente JL, Al-Thabaiti SA, Basahel SN, Peña MA, Fierro JLG, Rojas S (2014) Effect of transition metal (M: Fe, Co or Mn) for the oxygen reduction reaction with non-precious metal catalysts in acid medium. Int J Hydrog Energy 39:5309–5318
20. Demir F, Erdoğmuş A, Koca A (2013) Oxygen reduction reaction catalyzed with titanyl phthalocyanines in nonaqueous and aqueous media. Phys Chem Chem Phys 15:15926
21. Beck F (1977) The redox mechanism of the chelate-catalysed oxygen cathode. J Appl Electrochem 7:239–245
22. Zagal JH (1992) Metallophthalocyanines as catalysts in electrochemical reactions. Coord Chem Rev 119:89–136
23. Coliman JP, Denisevich P, Konai Y, Marrocco M, Koval C, Anson FC (1980) Electrode catalysis of the four-electron reduction of oxygen to water by dicobalt face-to-face porphyrins. J Am Chem Soc 102:6027–6036
24. Li J, Wu X, Yuan R, Lin H, Yu R (1994) Cobalt phthalocyanine derivatives as neutral carriers for nitrite-sensitive poly(vinyl chloride) membrane electrodes. Analyst 119:1363
25. Jaouen F, Marcotte S, Dodelet JP, Lindbergh G (2003) Oxygen reduction catalysts for polymer electrolyte fuel cells from the pyrolysis of iron acetate adsorbed on various carbon supports. J Phys Chem B 107:1376–1386
26. Baranton S, Coutanceau C, Garnier E, Léger J-M (2006) How does α-FePc catalysts dispersed onto high specific surface carbon support work towards oxygen reduction reaction (orr)? J Electroanal Chem 590:100–110

27. Faubert G, Côté R, Guay D, Dodelet JP, Dénès G, Poleunis C, Bertrand P (1998) Activation and characterization of Fe-based catalysts for the reduction of oxygen in polymer electrolyte fuel cells. Electrochim Acta 43:1969–1984
28. Sirk AHC, Ampbell SA, Birss VI (2005) Oxygen reduction by sol derived [Co, N, C, O]-based catalysts for use in proton exchange membrane fuel cells. Electrochem Solid-State Lett 8:A104
29. Alves MCM, Tourillon G (1996) Influence of complexation processes on the catalytic properties of some polymer-based cobalt compounds for oxygen electroreduction. J Phys Chem 100:7566–7572
30. Liu Y, Yue X, Li K, Qiao J, Wilkinson DP, Zhang J (2016) PEM fuel cell electrocatalysts based on transition metal macrocyclic compounds. Coord Chem Rev 315:153–177
31. Masa J, Ozoemena K, Schuhmann W, Zagal JH (2012) Oxygen reduction reaction using N_4-metallomacrocyclic catalysts: fundamentals on rational catalyst design. J Porphyr Phthalocyanines 16:761–784
32. Vante NA, Tributsch H (1986) Energy conversion catalysis using semiconducting transition metal cluster compounds. Nature 323:431–432
33. Alonso-Vante N, Fieber-Erdmann M, Rossner H, Holub-Krappe E, Giorgetti C, Tadjeddine A, Dartyge E, Fontaine A, Frahm R (1997) The catalytic centre of transition metal chalcogenides vis-à-vis the oxygen reduction reaction: an in situ electrochemical EXAFS study. J Phys IV 7: C2-887–C2-889
34. Colmenares L, Jusys Z, Behm RJ (2007) Activity, selectivity, and methanol tolerance of Se-modified Ru/C cathode catalysts. J Phys Chem C 111:1273–1283
35. Malakhov IV, Nikitenko SG, Savinova ER, Kochubey DI, Alonso-Vante N (2002) In situ EXAFS study to probe active centers of ru chalcogenide electrocatalysts during oxygen reduction reaction. J Phys Chem B 106:1670–1676
36. Alonso-Vante N, Malakhov I, Nikitenko S, Savinova E, Kochubey D (2002) The structure analysis of the active centers of Ru-containing electrocatalysts for the oxygen reduction. An in situ EXAFS study. Electrochim Acta 47:3807–3814
37. Alonso-Vante N, Borthen P, Fieber-Erdmann M, Strehblow H-H, Holub-Krappe E (2000) An in situ grazing incidence X-ray absorption study of ultra thin RuxSey cluster-like electrocatalyst layers. Electrochim Acta 45:4227–4236
38. Liu G, Zhang H, Hu J (2007) Novel synthesis of a highly active carbon-supported $Ru_{85}Se_{15}$ chalcogenide catalyst for the oxygen reduction reaction. Electrochem Commun 9:2643–2648
39. Zehl G, Schmithals G, Hoell A, Haas S, Hartnig C, Dorbandt I, Bogdanoff P, Fiechter S (2007) On the structure of carbon-supported selenium-modified ruthenium nanoparticles as electrocatalysts for oxygen reduction in fuel cells. Angew Chem Int Ed Engl 46:7311–7314
40. Delacôte C, Bonakdarpour A, Johnston CM, Zelenay P, Wieckowski A (2009) Aqueous-based synthesis of ruthenium–selenium catalyst for oxygen reduction reaction. Faraday Discuss 140:269–281
41. Feng Y, Alonso-Vante N (2008) Nonprecious metal catalysts for the molecular oxygen-reduction reaction. Phys Status Solidi 245:1792–1806
42. Alonso-Vante N (2011) 5 structure and reactivity of transition metal chalcogenides toward the molecular oxygen reduction reaction. In: Vayenas CG (ed) Interfacial phenomena in electrocatalysis. Springer, New York, pp 255–300
43. Satoshi Kaneco BV, Funasaka K (2006) Photo/electrochemistry and photobiology in the environment energy and fuel. Research Signpost, Trivandrum
44. Feng Y, Gago A, Timperman L, Alonso-Vante N (2011) Chalcogenide metal centers for oxygen reduction reaction: activity and tolerance. Electrochim Acta 56:1009–1022
45. Lee J-W, Popov BN (2007) Ruthenium-based electrocatalysts for oxygen reduction reaction-a review. J Solid State Electrochem 11:1355–1364
46. Gao M-R, Jiang J, Yu S-H (2012) Solution-based synthesis and design of late transition metal chalcogenide materials for oxygen reduction reaction (ORR). Small 8:13–27
47. Alonso-Vante N (2003) Vielstich W, Lamm A, Gasteiger HA (eds) Handbook of fuel cells: fundamentals, technology, and applications, 2nd edn. Wiley, New York, pp 534–543

48. Lee K, Alonso-Vante N, Zhang J (2014) Transition metal chalcogenides for oxygen reduction electrocatalysts in PEM fuel cells. In: Non-noble metal fuel cell catalysts. Wiley, Weinheim, pp 157–182
49. Susac D, Sode A, Zhu L, Wong PC, Teo M, Bizzotto D, Mitchell KAR, Parsons RR, Campbell SA (2006) A methodology for investigating new nonprecious metal catalysts for PEM fuel cells. J Phys Chem B 110:10762–10770
50. Feng Y, He T, Alonso-Vante N (2009) Oxygen reduction reaction on carbon-supported $CoSe_2$ nanoparticles in an acidic medium. Electrochim Acta 54:5252–5256
51. Sidik RA, Anderson AB (2006) Co_9S_8 as a catalyst for electroreduction of O_2: quantum chemistry predictions. J Phys Chem B 110:936–941
52. Toth L (1971) Transition metal carbides and nitrides, 1st edn. Academic Press, New York
53. Oyama ST (1996) The chemistry of transition metal carbides and nitrides. Springer, Dordrecht
54. Dong S, Chen X, Zhang X, Cui G (2013) Nanostructured transition metal nitrides for energy storage and fuel cells. Coord Chem Rev 257:1946–1956
55. Zellner MB, Chen JG (2005) Surface science and electrochemical studies of WC and W2C PVD films as potential electrocatalysts. Catal Today 99:299–307
56. Lee K, Ishihara A, Mitsushima S, Kamiya N, Ota K (2004) Stability and electrocatalytic activity for oxygen reduction in WC + Ta catalyst. Electrochim Acta 49:3479–3485
57. McIntyre DR, Vossen A, Wilde JR, Burstein GT (2002) Electrocatalytic properties of a nickel–tantalum–carbon alloy in an acidic electrolyte. J Power Sources 108:1–7
58. Hu Y, Jensen JO, Zhang W, Cleemann LN, Xing W, Bjerrum NJ, Li Q (2014) Hollow spheres of iron carbide nanoparticles encased in graphitic layers as oxygen reduction catalysts. Angew Chem Int Ed Engl 53:3749–3749
59. Jiang Y, Lu Y, Lv X, Han D, Zhang Q, Niu L, Chen W (2013) Enhanced catalytic performance of Pt-free iron phthalocyanine by graphene support for efficient oxygen reduction reaction. ACS Catal 3:1263–1271
60. Liang J, Zhou RF, Chen XM, Tang YH, Qiao SZ (2014) Fe-N decorated hybrids of CNTs grown on hierarchically porous carbon for high-performance oxygen reduction. Adv Mater 26:6074–6079
61. Zhou D, Yang L, Yu L, Kong J, Yao X, Liu W, Xu Z, Lu X (2015) Fe/N/C hollow nanospheres by Fe(III)-dopamine complexation-assisted one-pot doping as nonprecious-metal electrocatalysts for oxygen reduction. Nanoscale 7:1501–1509
62. Liu L, Yang X, Ma N, Liu H, Xia Y, Chen C, Yang D, Yao X (2016) Scalable and cost-effective synthesis of highly efficient Fe 2 N-based oxygen reduction catalyst derived from seaweed biomass. Small 12:1295–1301
63. Cao B, Neuefeind JC, Adzic RR, Khalifah PG (2015) Molybdenum nitrides as oxygen reduction reaction catalysts: structural and electrochemical studies. Inorg Chem 54:2128–2136
64. Sun T, Jiang Y, Wu Q, Du L, Zhang Z, Yang L, Wang X, Hu Z (2017) Is iron nitride or carbide highly active for oxygen reduction reaction in acidic medium? Cat Sci Technol 7:51–55
65. Smith AJ, Welch AJE (1960) Some mixed metal oxides of perovskite structure. Acta Crystallogr 13:653–656
66. Risch M (2017) Perovskite electrocatalysts for the oxygen reduction reaction in alkaline media. Catalysts 7:154
67. Zhu Y, Zhou W, Yu J, Chen Y, Liu M, Shao Z (2016) Enhancing electrocatalytic activity of perovskite oxides by tuning cation deficiency for oxygen reduction and evolution reactions. Chem Mater 28:1691–1697
68. Goldschmidt VM (1926) Die Gesetze der Krystallochemie. Naturwissenschaften 14:477–485
69. Ramadass N (1978) ABO3-type oxides—their structure and properties—a bird's eye view. Mater Sci Eng 36:231–239
70. Sunarso J, Torriero AAJ, Zhou W, Howlett PC, Forsyth M (2012) Oxygen reduction reaction activity of La-based perovskite oxides in alkaline medium: a thin-film rotating ring-disk electrode study. J Phys Chem C 116:5827–5834

71. Celorrio V, Dann E, Calvillo L, Morgan DJ, Hall SR, Fermin DJ (2016) Oxygen reduction at carbon-supported lanthanides: therole of the B-site. ChemElectroChem 3:283–291
72. Suntivich J, Gasteiger HA, Yabuuchi N, Nakanishi H, Goodenough JB, Shao-Horn Y (2011) Design principles for oxygen-reduction activity on perovskite oxide catalysts for fuel cells and metal-air batteries. Nat Chem 3:546–550
73. Larsson R, Johansson LY (1990) On the catalytic properties of mixed oxides for the electrochemical reduction of oxygen. J Power Sources 32:253–260
74. Hyodo T, Hayashi M, Miura N, Yamazoe N (1996) Catalytic activities of rare-earth manganites for cathodic reduction of oxygen in alkaline solution. J Electrochem Soc 143:L266–L267
75. Yuan X-Z, Li X, Qu W, Ivey DG, Wang H (2011) Electrocatalytic activity of non-stoichiometric perovskites toward oxygen reduction reaction in alkaline electrolytes. ECS Trans 35:11–20
76. Celorrio V, Calvillo L, Dann E, Granozzi G, Aguadero A, Kramer D, Russell AE, Fermín DJ (2016) Oxygen reduction reaction at $La_xCa_{1-x}MnO_3$ nanostructures: interplay between A-site segregation and B-site valency. Cat Sci Technol 6:7231–7238
77. Stoerzinger KA, Lü W, Li C, Ariando VT, Shao-Horn Y (2015) Highly active epitaxial $La_{(1-x)}Sr_xMnO_3$ surfaces for the oxygen reduction reaction: role of charge transfer. J Phys Chem Lett 6:1435–1440
78. Tulloch J, Donne SW (2009) Activity of perovskite $La_{1-x}Sr_xMnO_3$ catalysts towards oxygen reduction in alkaline electrolytes. J Power Sources 188:359–366
79. Hyodo T, Hayashi M, Mitsutake S, Miura N, Yamazoe N (1997) Praseodymium-calcium manganites ($Pr_{1-x}Ca_xMnO_3$) as electrode catalyst for oxygen reduction in alkaline solution. J Appl Electrochem 27:745–746
80. Takeda Y, Kanno R, Kondo T, Yamamoto O, Taguchi H, Shimada M, Koizumi M (1982) Properties of $SrMO_{3-\delta}$ (M=Fe, Co) as oxygen electrodes in alkaline solution. J Appl Electrochem 12:275–280
81. Du J, Zhang T, Cheng F, Chu W, Wu Z, Chen J (2014) Nonstoichiometric perovskite $CaMnO_{3-\delta}$ for oxygen electrocatalysis with high activity. Inorg Chem 53:9106–9114
82. Poux T, Bonnefont A, Kéranguéven G, Tsirlina GA, Savinova ER (2014) Electrocatalytic oxygen reduction reaction on perovskite oxides: series versus direct pathway. ChemPhysChem 15:2108–2120
83. Wei C, Feng Z, Scherer GG, Barber J, Shao-Horn Y, Xu ZJ (2017) Cations in octahedral sites: a descriptor for oxygen electrocatalysis on transition-metal spinels. Adv Mater 29:1–8
84. Verwey EJW, Heilmann EL (1947) Physical properties and cation arrangement of oxides with spinel structures I. Cation Arrangement in Spinels. J Chem Phys 15:174–180
85. Chakrapani K, Bendt G, Hajiyani H, Lunkenbein T, Greiner MT, Masliuk L, Salamon S, Landers J, Schlögl R, Wende H, Pentcheva R, Schulz S, Behrens M (2018) The role of composition of uniform and highly dispersed cobalt vanadium iron spinel nanocrystals for oxygen electrocatalysis. ACS Catal 8:1259–1267
86. Zhou Y, Xi S, Wang J, Sun S, Wei C, Feng Z, Du Y, Xu ZJ (2018) Revealing the dominant chemistry for oxygen reduction reaction on small oxide nanoparticles. ACS Catal 8:673–677
87. Zhao Q, Yan Z, Chen C, Chen J (2017) Spinels: controlled preparation, oxygen reduction/evolution reaction application, and beyond. Chem Rev 117:10121–10211
88. Chen D, Chen C, Baiyee ZM, Shao Z, Ciucci F (2015) Nonstoichiometric oxides as low-cost and highly-efficient oxygen reduction/evolution catalysts for low-temperature electrochemical devices. Chem Rev 115:9869–9921
89. Si C, Zhang Y, Zhang C, Gao H, Ma W, Lv L, Zhang Z (2017) Mesoporous nanostructured spinel-type MFe_2O_4 (M = Co, Mn, Ni) oxides as efficient bi-functional electrocatalysts towards oxygen reduction and oxygen evolution. Electrochim Acta 245:829–838
90. Hong W, Li L, Xue R, Xu X, Wang H, Zhou J, Zhao H, Song Y, Liu Y, Gao J (2017) One-pot hydrothermal synthesis of Zinc ferrite/reduced graphene oxide as an efficient electrocatalyst for oxygen reduction reaction. J Colloid Interface Sci 485:175–182

91. Zhu H, Zhang S, Huang Y-X, Wu L, Sun S (2013) Monodisperse $M_xFe_{3-x}O_4$ (M = Fe, Cu, Co, Mn) nanoparticles and their electrocatalysis for oxygen reduction reaction. Nano Lett 13:2947–2951
92. Bhandary N, Ingole PP, Basu S (2018) Electrosynthesis of Mn-Fe oxide nanopetals on carbon paper as bi-functional electrocatalyst for oxygen reduction and oxygen evolution reaction. Int J Hydrog Energy 43:3165–3171
93. Gong K, Du F, Xia Z, Durstock M, Dai L (2009) Nitrogen-doped carbon nanotube arrays with high electrocatalytic activity for oxygen reduction. Science 323:760–764
94. Liu M, Zhang R, Chen W (2014) Graphene-supported nanoelectrocatalysts for fuel cells: synthesis, properties, and applications. Chem Rev 114:5117–5160
95. Lin Z, Waller GH, Liu Y, Liu M, Wong C (2013) 3D nitrogen-doped graphene prepared by pyrolysis of graphene oxide with polypyrrole for electrocatalysis of oxygen reduction reaction. Nano Energy 2:241–248
96. Wang H, Maiyalagan T, Wang X (2012) Review on recent progress in nitrogen-doped graphene: synthesis, characterization, and its potential applications. ACS Catal 2:781–794
97. Liang Y, Wang H, Diao P, Chang W, Hong G, Li Y, Gong M, Xie L, Zhou J, Wang J, Regier TZ, Wei F, Dai H (2012) Oxygen reduction electrocatalyst based on strongly coupled cobalt oxide nanocrystals and carbon nanotubes. J Am Chem Soc 134:15849–15857
98. Nie R, Bo X, Luhana C, Nsabimana A, Guo L (2014) Simultaneous formation of nitrogen and sulfur-doped carbon nanotubes-mesoporous carbon and its electrocatalytic activity for oxygen reduction reaction. Int J Hydrog Energy 39:12597–12603
99. Liang J, Jiao Y, Jaroniec M, Qiao SZ (2012) Sulfur and nitrogen dual-doped mesoporous graphene electrocatalyst for oxygen reduction with synergistically enhanced performance. Angew Chem Int Ed Engl 124:11664–11668
100. Nasini UB, Gopal Bairi V, Kumar Ramasahayam S, Bourdo SE, Viswanathan T, Shaikh AU (2014) Oxygen reduction reaction studies of phosphorus and nitrogen co-doped mesoporous carbon synthesized via microwave technique. ChemElectroChem 1:573–579
101. Choi CH, Chung MW, Park SH, Woo SI (2013) Additional doping of phosphorus and/or sulfur into nitrogen-doped carbon for efficient oxygen reduction reaction in acidic media. Phys Chem Chem Phys 15:1802–1805
102. Wang S, Zhang L, Xia Z, Roy A, Chang DW, Baek J-B, Dai L (2012) BCN graphene as efficient metal-free electrocatalyst for the oxygen reduction reaction. Angew Chem Int Ed Engl 51:4209–4212
103. Shao Y, Zhang S, Engelhard MH, Li G, Shao G, Wang Y, Liu J, Aksay IA, Lin Y (2010) Nitrogen-doped graphene and its electrochemical applications. J Mater Chem 20:7491
104. Geng D, Chen Y, Chen Y, Li Y, Li R, Sun X, Ye S, Knights S (2011) High oxygen-reduction activity and durability of nitrogen-doped graphene. Energy Environ Sci 4:760
105. Carrillo-Rodríguez JC, Alonso-Lemus IL, Siller-Ceniceros AA, Martínez GE, Pizá-Ruiz P, Vargas-Gutiérrez G, Rodríguez-Varela FJ (2017) Easy synthesis of N-doped graphene by milling exfoliation with electrocatalytic activity towards the Oxygen Reduction Reaction (ORR). Int J Hydrog Energy 42:30383–30388
106. Alonso-Lemus IL, Figueroa-Torres MZ, García-Hernández AB, Escobar-Morales B, Rodríguez-Varela FJ, Fuentes AF, Lardizabal-Gutierrez D, Quintana-Owen P (2017) Low-cost sonochemical synthesis of nitrogen-doped graphene metal-free electrocatalyst for the oxygen reduction reaction in alkaline media. Int J Hydrog Energy 42(21):30330–30338
107. Pels JR, Kapteijn F, Moulijn JA, Zhu Q, Thomas KM (1995) Evolution of nitrogen functionalities in carbonaceous materials during pyrolysis. Carbon 33:1641–1653
108. Yan L, Yu J, Houston J, Flores N, Luo H (2017) Biomass derived porous nitrogen doped carbon for electrochemical devices. Green Energy Environ 2:84–99
109. Yang S, Zhao G-L, Khosravi E (2010) First principles studies of nitrogen doped carbon nanotubes for dioxygen reduction. J Phys Chem C 114:3371–3375
110. Reda M, Hansen HA, Vegge T (2018) DFT study of stabilization effects on N-doped graphene for ORR catalysis. Catal Today 312:118–125

111. Zhang L, Xia Z (2011) Mechanisms of oxygen reduction reaction on nitrogen-doped graphene for fuel cells. J Phys Chem C 115:11170–11176
112. Yu H, Shang L, Bian T, Shi R, Waterhouse GIN, Zhao Y, Zhou C, Wu L-Z, Tung C-H, Zhang T (2016) Nitrogen-doped porous carbon nanosheets templated from g-C3N4 as metal-free electrocatalysts for efficient oxygen reduction reaction. Adv Mater 28:5080–5086
113. He C, Li Z, Cai M, Cai M, Wang J-Q, Tian Z, Zhang X, Shen PK (2013) A strategy for mass production of self-assembled nitrogen-doped graphene as catalytic materials. J Mater Chem A 1:1401–1406
114. Luo Z, Lim S, Tian Z, Shang J, Lai L, MacDonald B, Fu C, Shen Z, Yu T, Lin J (2011) Pyridinic N doped graphene: synthesis, electronic structure, and electrocatalytic property. J Mater Chem 21:8038
115. Feng L, Chen Y, Chen L (2011) Easy-to-operate and low-temperature synthesis of gram-scale nitrogen-doped graphene and its application as cathode catalyst in microbial fuel cells. ACS Nano 5:9611–9618
116. Deng D, Pan X, Yu L, Cui Y, Jiang Y, Qi J, Li W-X, Fu Q, Ma X, Xue Q, Sun G, Bao X (2011) Toward N-doped graphene via solvothermal synthesis. Chem Mater 23:1188–1193
117. Tavakol H, Keshavarzipour F (2016) A sulfur doped carbon nanotube as a potential catalyst for the oxygen reduction reaction. RSC Adv 6:63084–63090
118. Zhang L, Niu J, Li M, Xia Z (2014) Catalytic mechanisms of sulfur-doped graphene as efficient oxygen reduction reaction catalysts for fuel cells. J Phys Chem C 118:3545–3553
119. Seredych M, László K, Bandosz TJ (2015) Sulfur-doped carbon aerogel as a metal-free oxygen reduction catalyst. ChemCatChem 7:2924–2931
120. Wang L, Dong H, Guo Z, Zhang L, Hou T, Li Y (2016) Potential application of novel boron-doped graphene nanoribbon as oxygen reduction reaction catalyst. J Phys Chem C 120:17427–17434
121. Su J, Cao X, Wu J, Jin C, Tian J-H, Yang R (2016) One-pot synthesis of boron-doped ordered mesoporous carbons as efficient electrocatalysts for the oxygen reduction reaction. RSC Adv 6:24728–24737
122. Lin Y, Zhu Y, Zhang B, Kim YA, Endo M, Su DS (2015) Boron-doped onion-like carbon with enriched substitutional boron: the relationship between electronic properties and catalytic performance. J Mater Chem A 3:21805–21814
123. Guo M, Huang J, Kong X, Peng H, Shui H, Qian F, Zhu L, Zhu W, Zhang Q (2016) Hydrothermal synthesis of porous phosphorus-doped carbon nanotubes and their use in the oxygen reduction reaction and lithium-sulfur batteries. New Carbon Mater 31:352–362
124. Zhang X, Lu Z, Fu Z, Tang Y, Ma D, Yang Z (2015) The mechanisms of oxygen reduction reaction on phosphorus doped graphene: a first-principles study. J Power Sources 276:222–229
125. Liu Z, Fu X, Li M, Wang F, Wang Q, Kang G, Peng F (2015) Novel silicon-doped, silicon and nitrogen-codoped carbon nanomaterials with high activity for the oxygen reduction reaction in alkaline medium. J Mater Chem A 3:3289–3293
126. Sun X, Zhang Y, Song P, Pan J, Zhuang L, Xu W, Xing W (2013) Fluorine-doped carbon blacks: highly efficient metal-free electrocatalysts for oxygen reduction reaction. ACS Catal 3:1726–1729
127. Yao Z, Nie H, Yang Z, Zhou X, Liu Z, Huang S (2012) Catalyst-free synthesis of iodine-doped graphenevia a facile thermal annealing process and its use for electrocatalytic oxygen reduction in an alkaline medium. Chem Commun 48:1027–1029
128. Mena-Durán CJ, Alonso-Lemus IL, Quintana P, Barbosa R, Ordoñez LC, Escobar B (2018) Preparation of metal-free electrocatalysts from cassava residues for the oxygen reduction reaction: a sulfur functionalization approach. Int J Hydrog Energy 43:3172–3179
129. Yang S, Mao X, Cao Z, Yin Y, Wang Z, Shi M, Dong H (2018) Onion-derived N, S self-doped carbon materials as highly efficient metal-free electrocatalysts for the oxygen reduction reaction. Appl Surf Sci 427:626–634

130. Sun Y, Wu J, Tian J, Jin C, Yang R (2015) Sulfur-doped carbon spheres as efficient metal-free electrocatalysts for oxygen reduction reaction. Electrochim Acta 178:806–812
131. Yang Z, Yao Z, Li G, Fang G, Nie H, Liu Z, Zhou X, Chen X, Huang S (2012) Sulfur-doped graphene as an efficient metal-free cathode catalyst for oxygen reduction. ACS Nano 6:205–211
132. Inamdar S, Choi H-S, Wang P, Song MY, Yu J-S (2013) Sulfur-containing carbon by flame synthesis as efficient metal-free electrocatalyst for oxygen reduction reaction. Electrochem Commun 30:9–12
133. Sun X, Song P, Zhang Y, Liu C, Xu W, Xing W (2013) A class of high performance metal-free oxygen reduction electrocatalysts based on cheap carbon blacks. Sci Rep 3:2505
134. Li Y, Chopra N (2015) Progress in large-scale production of graphene. Part 2: vapor methods. JOM 67:44–52
135. Luque R (2013) Producing fuels and fine chemicals from biomass using nanomaterials, 1st edn. CRC Press, Boca Raton
136. Antolini E (2016) Nitrogen-doped carbons by sustainable N- and C-containing natural resources as nonprecious catalysts and catalyst supports for low temperature fuel cells. Renew Sust Energ Rev 58:34–51
137. Alonso-Lemus IL, Rodriguez-Varela FJ, Figueroa-Torres MZ, Sanchez-Castro ME, Hernandez-Ramírez A, Lardizabal-Gutierrez D, Quintana-Owen P (2016) Novel self-nitrogen-doped porous carbon from waste leather as highly active metal-free electrocatalyst for the ORR. Int J Hydrog Energy 41:23409–23416
138. Lardizabal-Guitierrez D, González-Quijano D, Bartolo-Pérez P, Escobar-Morales B, Rodríguez-Varela FJ, Alonso-Lemus IL (2016) Communication—synthesis of self-doped metal-free electrocatalysts from waste leather with high ORR activity. J Electrochem Soc 163:H15–H17
139. Zhang J, Wu S, Chen X, Pan M, Mu S (2014) Egg derived nitrogen-self-doped carbon/carbon nanotube hybrids as noble-metal-free catalysts for oxygen reduction. J Power Sources 271:522–529
140. Liu F, Peng H, Qiao X, Fu Z, Huang P, Liao S (2014) High-performance doped carbon electrocatalyst derived from soybean biomass and promoted by zinc chloride. Int J Hydrog Energy 39:10128–10134
141. Gao S, Geng K, Liu H, Wei X, Zhang M, Wang P, Wang J (2015) Transforming organic-rich amaranthus waste into nitrogen-doped carbon with superior performance of the oxygen reduction reaction. Energy Environ Sci 8:221–229
142. Zhai Y, Zhu C, Wang E, Dong S (2014) Energetic carbon-based hybrids: green and facile synthesis from soy milk and extraordinary electrocatalytic activity towards ORR. Nanoscale 6:2964
143. Lu J, Bo X, Wang H, Guo L (2013) Nitrogen-doped ordered mesoporous carbons synthesized from honey as metal-free catalyst for oxygen reduction reaction. Electrochim Acta 108:10–16
144. Pan F, Cao Z, Zhao Q, Liang H, Zhang J (2014) Nitrogen-doped porous carbon nanosheets made from biomass as highly active electrocatalyst for oxygen reduction reaction. J Power Sources 272:8–15
145. Li J, Wang S, Ren Y, Ren Z, Qiu Y, Yu J (2014) Nitrogen-doped activated carbon with micrometer-scale channels derived from luffa sponge fibers as electrocatalysts for oxygen reduction reaction with high stability in acidic media. Electrochim Acta 149:56–64
146. Escobar B, Pérez-Salcedo KY, Alonso-Lemus IL, Pacheco D, Barbosa R (2017) N-doped porous carbon from Sargassum spp. as metal-free electrocatalysts for oxygen reduction reaction in alkaline media. Int J Hydrog Energy 42(51):30274–30283
147. Song MY, Park HY, Yang D-S, Bhattacharjya D, Yu J-S (2014) Seaweed-derived heteroatom-doped highly porous carbon as an electrocatalyst for the oxygen reduction reaction. ChemSusChem 7:1755–1763
148. Chaudhari KN, Song MY, Yu JS (2014) Transforming hair into heteroatom-doped carbon with high surface area. Small 10:2625–2636

149. Chaudhari NK, Song MY, Yu J-S (2015) Heteroatom-doped highly porous carbon from human urine. Sci Rep 4:5221
150. Wang R, Wang K, Wang Z, Song H, Wang H, Ji S (2015) Pig bones derived N-doped carbon with multi-level pores as electrocatalyst for oxygen reduction. J Power Sources 297:295–301
151. Guo C-Z, Chen C-G, Luo Z-L (2014) A novel nitrogen-containing electrocatalyst for oxygen reduction reaction from blood protein pyrolysis. J Power Sources 245:841–845

Chapter 8
Non-Noble Metal as Catalysts for Alcohol Electro-oxidation Reaction

Samuel Dessources, Diego Xavier del Jesús González-Quijano, and Wilian Jesús Pech-Rodríguez

Abstract This chapter describes the use of non-noble metals as catalysts in DAFCs, and their catalytic activity and stability with different liquid fuels in acid and alkaline media. Section "Methanol Oxidation Reaction (MOR) on Nickel-Based Anodes" of the chapter aims to describe the methanol oxidation reaction (MOR) on non-noble metal catalysts containing Ni, Sn, Co, and Cu. In addition, the effect of the methanol concentration for this reaction and that of the method of synthesis on these catalysts is revised. In section "Ethanol Oxidation Reaction (EOR) on Non-noble Metals", the ethanol oxidation reaction (EOR) is studied for anodes based on Ni, Ir, and Co. Also, a new non-noble catalyst called HYPERMEC is reported for the EOR. This catalyst has shown a better oxidation reaction activity, which is carried out without the formation of acetate. It also shows higher tolerance to the CO poisoning than Pt-based catalysts. Furthermore, the ethylene glycol oxidation reaction (EGOR) in alkaline media for this catalyst is reported and summarized in section "Ethylene Glycol Oxidation (EGOR) in Alkaline Media" of this chapter. This information will be helpful in providing the catalytic activity reported to date of these non-noble metal catalysts, and to understand their catalytic behavior.

Keywords Non-noble catalysts · Ethylene glycol · Ethanol · Solid alkaline fuel cells · PEMFC · Nickel-base anodes · Cobalt-base anodes · Iridium-base anodes · HYPERMEC · Alkaline media · Acid media · MOR · EOR · EGOR · DAFC · DMFC · Synthesis · Alloy · Plurimetalic · Core-shell

S. Dessources (✉)
Sustentabilidad de los Recursos Naturales y Energía, Cinvestav Unidad Saltillo, Parque Industrial Ramos Arizpe, Ramos Arizpe, Coahuila, Mexico

D. X. del Jesús González-Quijano
Departamento de Ingeniería Biomédica, Centro de Ciencias de la Ingeniería, Universidad Autónoma de Aguascalientes Campus Sur, Aguascalientes, Aguascalientes, Mexico

W. J. Pech-Rodríguez
Universidad Politécnica de Victoria, Parque Científico y Tecnológico de Tamaulipas, Ciudad Victoria, Tamaulipas, Mexico

F. J. Rodríguez-Varela, T. W. Napporn (eds.), *Advanced Electrocatalysts for Low-Temperature Fuel Cells*, https://doi.org/10.1007/978-3-319-99019-4_8

8.1 Introduction

The liquid fossil fuels have been used as main source of energy in industrialized countries for the past decades, leading to their depletion and shortage and resulting in the need to develop new energy sources [1]. Hence, the development of sustainable, clean, efficient, and reliable energy sources to provide the required energy for industrial and home applications is a great challenge because of the growing energy consumption. Several technologies have been developed to face up this challenge such as solar, hydroelectric, wind, and photovoltaic energy sources [2].

However, the most promising energy sources are the technologies based on fuel cells. Because of the ability to convert the chemical energy into electrical energy with higher efficiencies and lower pollution than conventional systems, fuel cells can be used in mobile or stationary applications [3]. Particularly, the proton exchange membrane (PEM) fuel cell has attracted attention, additionally to the abovementioned advantages, because of its high energy density obtained from compact-size-devices at low operating temperature and can be used with a wide variety of fuels [4].

Figure 8.1 shows the basic structure of the PEM fuel cell (hereafter abbreviated as PEMFC) that consists of two electrodes, anode and cathode, separated by a solid polymer electrolyte. Each of the electrodes contain a catalyst that allows the

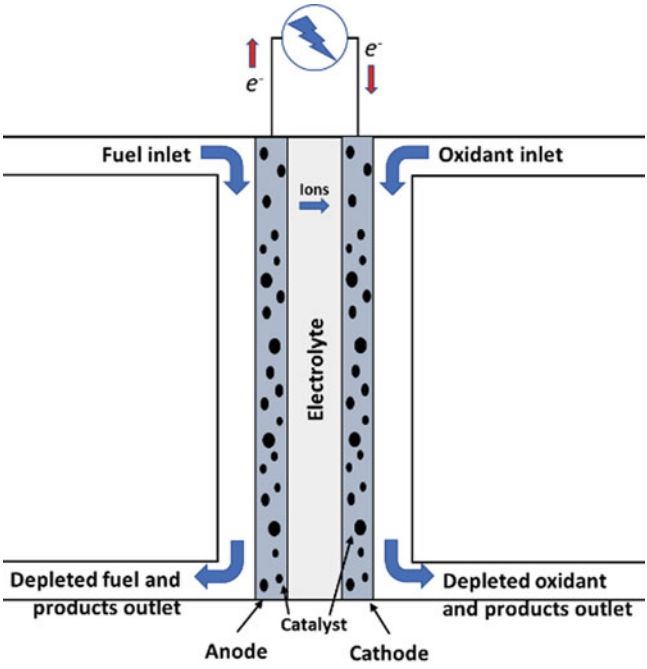

Fig. 8.1 Schematic representation of the basic elements of a PEMFC

oxidation and reduction reactions of the fuels and oxidant, respectively, and the polymer electrolyte assures the ion exchange [5].

The production of electricity occurs when an external electrical device is connected to the fuel cell and as soon the fuel is fed into the cell at the anode and the oxidant at the cathode; the catalyst at the anode oxidizes the fuel producing protons and electrons [6]. Then, the protons cross through the electrolyte and the electrons travel by an external electric circuit that can be utilized to produce electrical work; the protons and electrons recombine at the cathode and the unused fuel, products, and byproducts formed are expelled on the corresponding outlet-side [7]. This process will continue while continuing the supply of fuel and oxidant.

Traditionally, hydrogen has been used as fuel for PEMFC, but some problems related to its storage, transportation, and distribution have caused the necessity to replace it with liquid fuels such as alcohols [8]. Fuel cells that utilize these liquid fuels to produce energy are generally known as direct alcohol fuel cell (DAFC) and the most common liquid fuels that can be used are methanol, ethanol, or ethylene glycol [4, 8].

8.1.1 Methanol

This alcohol can be obtained biologically or from other sources such as the wood pyrolysis or by low-pressure processes that use natural gas and hydrogen. The alcohols obtained from biological sources are known as bioalcohols (e.g., biomethanol). However, no matter how it is produced there is no chemical or physical difference between them [1]. Methanol has one carbon atom (C1) in its structure, its energy density is 6.1 kWh kg^{-1} and is one of the liquid fuels used in the study of the oxidation on PEMFC using platinum groups metals [9].

The reaction bellow indicates the complete reaction in a direct methanol fuel cell:

$$CH_3OH + 3/2\ O_2 \rightarrow CO_2 + 2H_2O \tag{8.1}$$

This reaction leads to a standard reversible potential of 1.21 V [10]. However, due to the formation of byproducts and intermediates during the oxidation of the fuel a higher potential is required to carry out a complete oxidation; achieved by reducing the anodic potential and increasing the cathodic potential [10].

8.1.2 Ethanol

Ethanol can be obtained from the chemical modification of ethylene and from the biological degradation of high sugar content feedstocks and grains such as sugar cane, sugar beets, switch grass, corn, and barley and the remaining product can be used as food for livestock. It is a flammable and volatile colorless liquid with

psychoactive properties, used in thermometers, alcoholic beverages, and as gasoline additive in the USA and Brazil [1].

Ethanol has an energy density of 8.01 kWh kg^{-1} and a standard reversible potential of 1.145 V, which is obtained from the complete reaction in a direct ethanol fuel cell [4]:

$$C_2H_5OH + 3/2\ O_2 \rightarrow 2CO_2 + 3H_2O \tag{8.2}$$

However, its oxidation, likewise methanol, produces byproducts and intermediates that adsorb onto platinum-catalysts surface decreasing its catalytic activity, also called poisoning effect [11].

8.1.3 Ethylene Glycol

Ethylene glycol is one of the liquid fuels most recently studied for fuel cells. Obtained from the chemical modification of the ethylene oxide [12], it is an odorless, colorless, sweet-tasting, viscous liquid with moderate toxicity [6]. Mainly used as raw material to produce polyester fibers and for antifreeze additives. Has an energy density of 5.29 kWh kg^{-1} [4]. Its complete oxidation in a fuel cell produces 1.22 V:

$$C_2H_6O_2 + 5/2\ O_2 \rightarrow 2CO_2 + 3H_2O \tag{8.3}$$

The oxidation of the ethylene glycol is more complex than that of ethanol and methanol, because of the formation of some incomplete oxidation products such as glyoxylic acid, glyoxal, glycolic acid, glycolaldehyde, and oxalic acid [13]. Despite that these alcohols are an excellent energy source for DAFCs due to their energy density, easy storage, and transportation, their electrooxidation still needs to be improved, mainly to avoid the poisoning effect produced by the intermediates and byproducts formed during the reaction.

8.1.4 Non-Noble Metals as Catalysts for Alcohol Electrooxidation Reaction

The early PEMFCs were very expensive devices because of the high platinum loadings required to oxidize the fuel [14]. After several years of research, the materials and design of the PEMFCs were improved; particularly, the catalyst loading was reduced by using carbon powders and nanoparticles [14]. Another way to reduce or avoid the platinum loading is the use of non-noble metals into the preparation of pluri-metallic catalysts, which have shown a better electrocatalytic

performance and higher tolerance to the poisoning effect than the platinum catalyst in acid and alkaline media [15–19].

8.2 Methanol Oxidation Reaction (MOR) on Nickel-Based Anodes

One of the first non-precious metals proposed to be used for alcohol electro-oxidation was Ni [20, 21]. In the 19th century, relevant works were published by Fleischmann's group where they studied the oxidation of different organic compounds at passivated nickel electrodes in aqueous alkaline solution [20, 22]. After that, several works focused on Ni-based materials as catalysts for alcohols have been published [21]. In recent years, considerable interest has been paid in direct methanol fuel cells (DMFC) because methanol has low molecular weight, high energy density (6.1 kWh kg^{-1}), and low operating temperature and it is easy to handle [23]. It is well known that Ni has benefits as catalyst due to its surface properties and demonstrated activity towards methanol oxidation. Planar nickel electrodes show poor catalytic activity; therefore, nanoparticle structures with high dispersion are necessary, with the aim to improve methanol oxidation. On these regards, Taraszewska and coworkers demonstrated the activity of electrodeposited Ni nanoparticles for methanol oxidation by using electrochemical measurements [24]. The cyclic voltammetry (CV) measurements conducted by this research group, in 0.01 mol L^{-1} NaOH and 0.05 mol L^{-1} methanol at a scan rate of 50 mV s^{-1}, reveal a peak near 0.68 V vs SHE attributed to methanol oxidation at the Ni-modified electrode.

To enhance the catalytic activity of Ni materials, different approaches have been considered. For example, Ni was impregnated in a Silicate Zeolite structure to obtain a 2 wt. % of Ni into the Si matrix [25]. Because Si zeolite has poor electrical conductivity, the working electrode used for the electrochemical measurements was fabricated by mixing the synthesized Ni–Si with carbon black. The CV measurements revealed that Ni–Zeolite–Carbon was not active for the methanol oxidation reaction (MOR). The Ni–Zeolite–Carbon only displays a catalytic activity for methanol when it was soaked in $NiSO_4$ solution. Figure 8.2 shows the illustrative structure of Ni–Si–C. As can be observed in the non-soaked sample (Fig. 8.2a), the Ni particles have been embedded into the Si zeolite structure and carbon nanoparticles make the contact between the Ni particles. The inactivity of this material was due to the Ni sites being into de Si matrix and C nanoparticles cover their surface. Meanwhile, when the working electrode was soaked in $NiSO_4$ solvent, NiOH groups formed over the Ni–C surface (Fig. 8.2b). These NiOH groups are active sites for the adsorption and the subsequent oxidation of methanol.

Thus, Ni has been electrodeposited on graphite electrode in a solution of 1 mol L^{-1} $NiSO_4$ + 1 mol L^{-1} H_2SO_4 and was used as anode for methanol oxidation in alkaline medium [26]. C/Ni catalyst displays tremendous

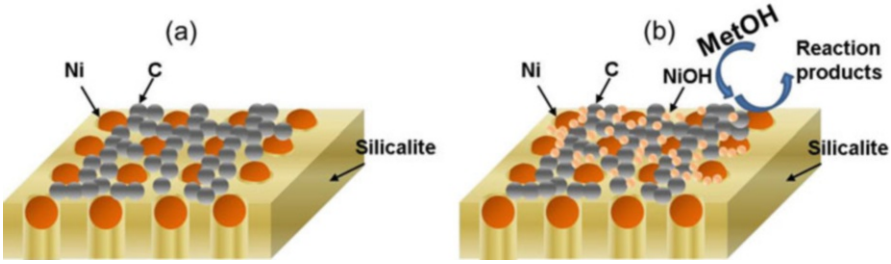

Fig. 8.2 Schematic diagram of silicalite–Ni–C structure: (**a**) without $NiSO_4$, and (**b**) presoaked in $NiSO_4$ solution

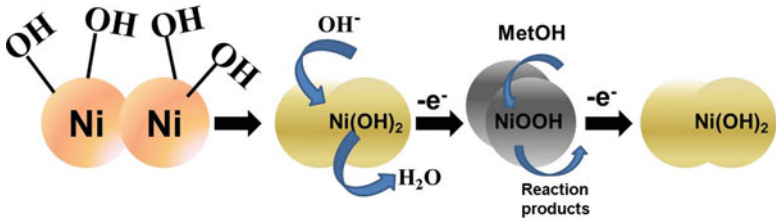

Fig. 8.3 Mechanism of reaction for methanol in Ni electrode in alkaline media

improvement for methanol oxidation and the current density and potential of methanol oxidation were highly dependent on the scan rate. From the earliest studies, it appears that the MOR occurs only under specific conditions.

Based on the earliest results, different mechanism has been proposed for the methanol oxidation at Ni-based electrodes. Equations (8.4) and (8.5) show the one proposed by Fleischman et al. [20]:

$$\mathrm{Ni(OH)2} \overset{\text{fast}}{\rightarrow} \mathrm{NiO(OH)} + \mathrm{e-} + \mathrm{H+} \tag{8.4}$$

$$\mathrm{NiO(OH)} + \text{organic compound} \overset{\text{slow}}{\rightarrow} \mathrm{NiO(OH)2} + \text{product} \tag{8.5}$$

The reactions suggest that the active sites in the Ni catalyst are oxy/hydroxide species. Figure 8.3 displays the schematic diagram for the proposed mechanism of reaction onto Ni-based electrodes.

The effect of oxy/hydroxide species for MOR has been studied in detail by Chen's group [27]. They studied the effect of different $NiCl_2$–cysteine ratio in the electrodeposition of Ni onto glassy carbon electrode in 0.01 mol L^{-1} $NiCl_2$ + 0.1 mol L^{-1} NaOH at a scan rate of 50 mV s^{-1} without cysteine precursor and with 0.05 mol L^{-1} cysteine precursor. The CVs conducted by this group show an anodic peak near 0.41 V vs Hg/HgO (1 mol L^{-1} NaOH) and another at 0.51 V vs Hg/HgO due to the $Ni(OH)_2$/NiOOH redox pair [28].

The increase of anodic and cathodic peaks is attributed to the growth of hydroxide film at the electrode. Moreover, it is reported that increasing the number of potential

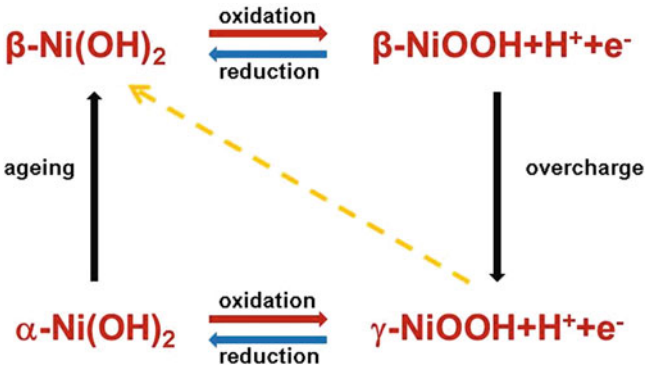

Fig. 8.4 Diagram scheme of the phase transformation of nickel hydroxides under electrochemical process

sweep results in an increase of current densities in the redox pair peaks due to the incorporation of OH^- species into the hydroxide layer, which later is oxidized to NiOOH [26]. On the other hand, the authors found that the presence of cysteine in the mixture results in an increase in the peak intensities related to redox pair of Nickel hydroxide; in other words, cysteine enhanced the formation of $Ni(OH)_2$ and NiOOH.

A detailed study of Nickel electrodeposition was conducted by Do Jin and coworkers [29]. Their studies demonstrate that two different phases of Ni hydroxide were grown onto the electrode. The existence of two Ni hydroxide phases was first reported by Bode et al. [30]. Figure 8.4 depicts the diagram scheme of the phase transformation of nickel hydroxide during chemical and electrochemical processes. As can be seen, the diagram proposes two Ni hydroxide phases, α-Ni $(OH)_2$ and β-$Ni(OH)_2$ and also two phases due to the oxidation β-NiOOH and γ-NiOOH. As is proposed by the diagram, the γ-NiOOH phase can be produced by oxidizing α-$Ni(OH)_2$ and in this process the oxidation state of Ni changes from +2 to +3 and ≈ +3.75 [31]. Also, γ-NiOOH phase can be obtained by overcharging the β-NiOOH+H^++e^-.

Regarding the crystal structure, two pseudo-polymorphs of $Ni(OH)_2$ have been identified, α-$Ni(OH)_2$ and β-$Ni(OH)_2$ [32]. The α-$Ni(OH)_2$ phase has lattice parameters $a_0 = 0.542$ and $c_0 = 0.806$ nm. The oxidation of α-$Ni(OH)_2$ produces γ-NiOOH that possesses an open structure with a c-axis about 2 nm that favors diffusion of metal ions or water molecules [29]. Meanwhile, β-$Ni(OH)_2$ has lattice parameters $a_0 = 0.307$ and $c_0 = 0.461$ nm and its product is β-NiOOH, with a c-axis about 0.5 nm. Therefore, it is desirable that Ni films used for the MOR oxidation have preferentially the γ-NiOOH structure [29].

Figure 8.5 shows the CV of the methanol oxidation in 1 mol L^{-1} KOH + 0.5 mol L^{-1} MetOH in the potential range from −900 to 1600 mV vs $Hg/HgSO_4$/1 mol L^{-1} H_2SO_4 (MMO), at a scan rate of 50 mV s^{-1}. In the forward scan, a broad peak near 1 V vs MMO is observed, due to the current density

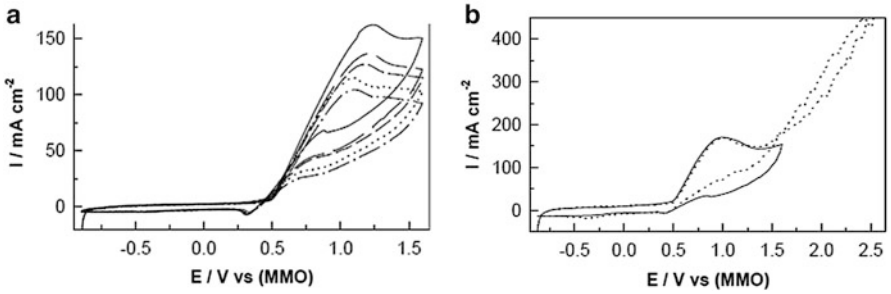

Fig. 8.5 (**a**) Cyclic voltammogram of the MOR on C/Ni electrode at 50 mV s^{-1}, and (**b**) effect of the extended potential on the MOR. Scan rate: 50 mV s^{-1}. Adapted with permission from Ref. [26]. Copyright 2004 Elsevier

generated from the MOR. The reaction at the Ni-based electrodes occurs at high potentials, since NiOOH (the active sites) is formed at potentials close to 0.5 V vs MMO. At higher potentials, competitive reaction occurs between the methanol oxidation and the oxygen evolution reactions [26]. Figure 8.5b displays the CV for MetOH at extended potentials and can be observed that the methanol oxidation reaction delays the oxygen evolution reaction.

Furthermore, in the backward scan a cathodic peak is observed at 0.51 V vs MMO related to the NiOOH species. The current density of this cathodic peak is considerably less intense due to the consumption of NiOOH during the MOR (see Eq. (8.5)) [25].

8.2.1 Effect of Methanol Concentration

Different studies have been conducted to elucidate the effect of methanol concentration on the behavior of fuel cell catalysts. For example, Abdel et al. carried out electrochemical measurements of the MOR with methanol concentrations from 0.1 to 1.5 mol L^{-1} [26]. Figure 8.6 illustrates the behavior of the peak current density and the potential as a function of the methanol concentration. As it can be observed from Fig. 8.6a, the peak of current density increases linearly as methanol concentration increases from 0.1 to 0.5 mol L^{-1}, but at concentrations higher than 0.5 mol L^{-1} a plateau of current density is observed.

8.2.2 Binary and Ternary Nickel-Based Catalyst for Methanol Oxidation

In 1992, Ramasamy and coworkers proposed NiTi alloys as catalysts for the MOR in acid media [33]. They found that NiTi alloys are stable in acid media due to the

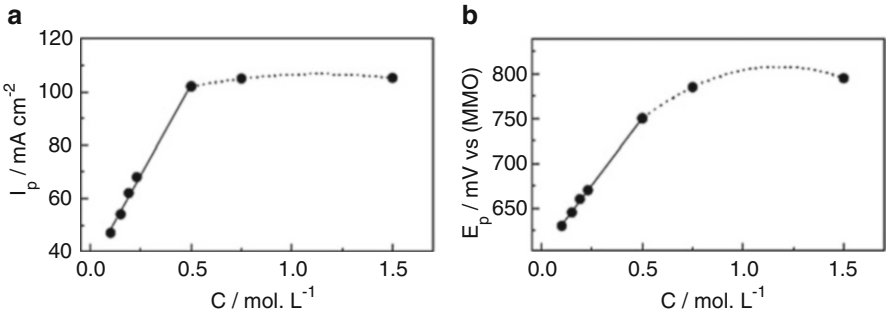

Fig. 8.6 Effect of methanol concentration at Ni/C electrode: (**a**) variation of the peak current density value, and (**b**) variation of the peak potential value. Adapted from ref. [26]. Copyright 2004 Elsevier

passive oxyhydroxide layer formation. On this context, Chellasamy et al. synthesized rhombohedral $NiTiO_3$ nanostructure by sol gel method [34] with an average particle size of 90 nm. They used $NiTiO_3$ nanostructure mixed with activated carbon to obtain the modified glassy carbon electrode for the electrochemical measurements in 1 mol L^{-1} H_2SO_4 and 1 mol L^{-1} H_2SO_4 with methanol. A current density of 4.9 mA cm^{-2} was obtained when the test was performed at 60 °C while no activity for the MOR was observed at room temperature.

The surface properties of NiTi nanostructure play a key role in the MOR. For example, NiTi materials present a hydroxide/oxide film that grows onto the surface of the material. This layer is composed by OH groups and Ni, Ti ions that act as reactive sites for the methanol adsorption and subsequently its oxidation.

NiTi nanostructures were also evaluated in alkaline media by Hou and coworkers [35]. They obtained NiTi nanotubes by electrochemical anodization of NiTi alloy followed by thermal treatment. The surface properties of the NiTi nanotubes were evaluated for the MOR in 1 mol L^{-1} of KOH. The non-thermally treated NiTi nanotubes showed poor performance (1.26 mA cm^{-2}) for the alcohol oxidation while the thermally treated NiTi displayed a peak current density of 8.52 mA cm^{-2} due to the methanol oxidation. The latter was attributed to changes in Ni ions that modify the binding energy of Ti species. The authors also conducted measurements at different temperatures and found an enhancement for the MOR when temperature was increased.

The enhancement of MOR in the electrodes has been discussed considering two points of view. First, higher temperatures can change the surface properties of the electrode that may result in the presence of more hydroxide/oxide groups. On the other hand, the methanol oxidation reaction follows the Arrhenius relationship as is expressed by Eq. (8.6) [36]:

$$k = \mathrm{Ae}^{(\mathrm{Ea}/\mathrm{RT})} \tag{8.6}$$

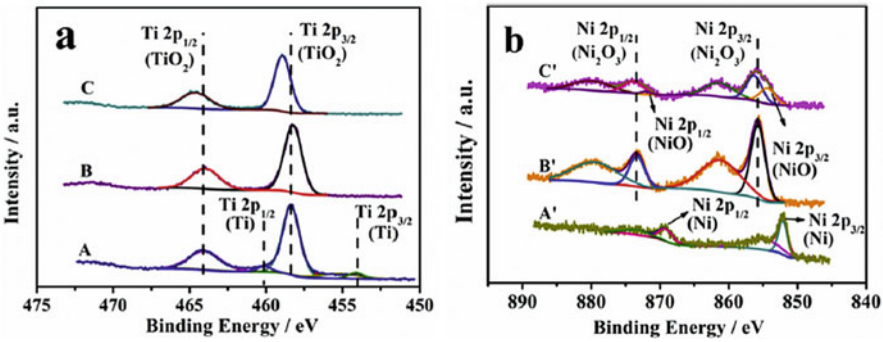

Fig. 8.7 XPS spectra of the NiTiO electrode. (**a**) Ti 2p spectra; (**b**) Ni 2p spectra; for Ni–Ti alloy (labeled as A), NiTiO before annealing (labeled as B), and NiTiO after annealing at 500 °C for 2 h (labeled as C). Copyright 2016 Elsevier [35]

where k is the rate constant, A is a constant, E_a the activation energy (kJ mol^{-1}), R the universal gas constant (8.314×10^{-3} kJ mol^{-1} K^{-1}), and T the temperature in Kelvin.

It is well known that the oxidation state of Ni plays a key role in the MOR. Hou et al. studied the electrocatalytic performance of NiTiO nanotubes for the reaction [35]. They treated NiTiO under hydrogen atmosphere at different temperatures and time of reaction. Figure 8.7 shows the XPS spectra of Ti 2p and Ni 2p. The materials were labeled as A, B, and C for NiTi alloy, NiTiO NTS, and treated NiTiO NTS, respectively. As can be seen, the signal due to Ti^0 disappears at the NiTiO NTS sample, which suggests a phase transformation. Meanwhile, it is observed that when the NiTi alloy is treated under H_2 atmosphere, an NiO phase emerges, indicating that Ni^{3+} is reduced to Ni^{2+}. This reaction produced a positive displacement of the Ti-2p binding energy, due to the oxygen vacancies. Regarding the MOR, the authors found that NiTiO NTs treated at 500 °C for 2 h delivers the highest current density. Furthermore, it has been observed that the second or third element in the compound might improve the stability of Ni-based electrodes. For example, the effect of the electrodeposited Ni onto TiO_2 nanotubes has been investigated [37]. Ni/TiO^2 has demonstrated higher stability (170 mA cm^{-1} for 30 min) than flat Ni electrode (around 1 mA cm^{-1} during 30 min).

The high current density from the MOR in Ni-based materials has been attributed to Ni^{2+} and Ni^{3+} species. It has been observed that Ni-based materials might be improved by incorporating chemical elements with low oxidation potentials that assist the Ni^{2+}/Ni^{3+} redox reaction [38]. Yi and coworkers found that Sn enhanced the MOR on Ni/Ti electrodes [38]. The enhanced catalytic activity of this material has been explained by the well-known bifunctional mechanism, where Sn promotes the adsorption of OH^- at low potentials that facilitates the formation of the NiOOH active sites. Sn electrons also modify the Ni d-band vacancies [39].

Another promising bimetallic catalyst for the MOR is Ni–Cr. Yingying and coworkers synthesized Ni–Cr by thermal decomposition at temperatures in the

range of 500–900 °C [40]. They reported that at temperatures below to 800 °C a bimetallic Ni–Cr is obtained while at higher temperatures a phase transformation occurs and the $NiCr_2O_4$ alloy is obtained. The Ni–Cr sample calcined at 700 °C showed the better performance for the MOR in alkaline media, with current densities close to 12 mA cm^{-2} at 0.7 V vs SCE. The authors attributed the differences in current density from the methanol oxidation to the particles size. They found that at 500, 600, and 700 °C particle sizes of 28.9, 31.4, and 38.5 nm were obtained, respectively; meanwhile at temperatures higher than 800 °C, the alloys showed a particle size in the range of 200 nm. High temperatures normally result in larger crystal sizes [40]. On the other hand, the analysis of the peak current density in the forward (J_f) and backward scans (J_b), revealed that these materials are efficient in the removal of reaction products and intermediates from the catalytic surface due to the presence of Cr.

NiO_x and MnO_x nanocomposites on glassy carbon (i.e., GC/MnO_x/NiO_x) were tested for the MOR [41]. It was found that these anodes possess an excellent catalytic activity for the reaction. However, in order to promote a higher catalytic activity, NiO_x must be placed on top of the MnO_x surface, and not the other way around (i.e., GC/MnO_x/NiO_x) (Fig. 8.8). The enhanced electroactivity of GC/MnO_x/NiO_x for the MOR was ascribed to the improvement of the adsorbability of MeOH on the MnO_x surface.

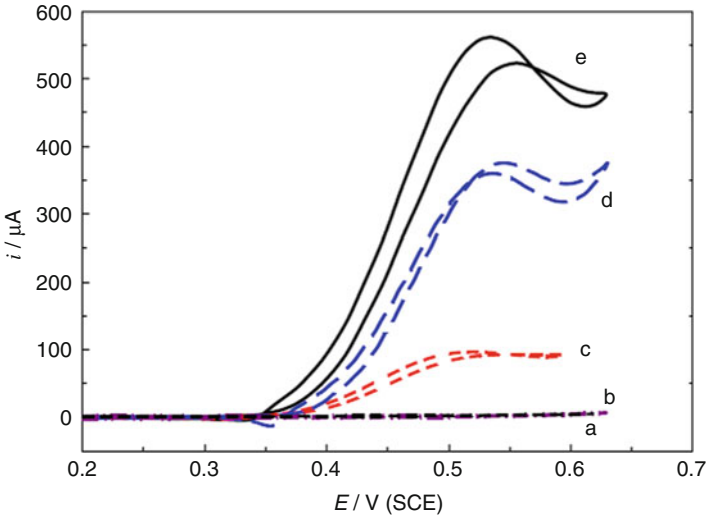

Fig. 8.8 CVs of the MOR at (**a**) GC, (**b**) GC/MnO_x, (**c**) GC/NiO_x/MnO_x, (**d**) GC/NiO_x, and (**e**) GC/MnO_x/NiO_x electrodes in 0.5 mol L^{-1} NaOH containing 0.5 mol L^{-1} methanol, at a scan rate of 10 mV s^{-1}. Copyright 2015 Elsevier [41]

8.2.3 *Effect of Method of Synthesis*

Since thermal treatments result in larger crystal sizes, different methods of synthesis have been proposed to obtain Ni–Cr in nanoscale range. Cheng et al. developed an NiCr binary alloy by using the cathode plasma electrolytic deposition and obtained a crystal size of 30–50 nm [42]. Moreover, Ni–Cr has been successfully developed by radio frequency magnetron sputtering process [43].

The authors obtained a tetragonal structure of Ni–Cr alloy with a thin film of 25 nm. Another easy and cost-effective method to fabricate Ni–Cr alloy films is electrodeposition. Tharamani's group [44] developed Ni–Cr thin films and evaluated their performance for the MOR in acid media. From XRD measurements, they calculated the crystallite size of the coatings around 7.2 nm. The electrochemical test revealed that Ni–Cr has higher catalytic activity for the MOR in acid media with currents of 4 mA in 1 mol L^{-1} of MetOH +0.5 mol L^{-1} H_2SO_4 at a scan rate of 25 mV s^{-1} and temperature of 29 °C. They attributed the better performance of the Ni–Cr to the smaller crystal size that correlated with the results obtained by Yingying and coworkers [40]. The Ni–Cr structure not only showed high performance for the MOR but it also prensented a higher corrosion resistance in 1 mol L^{-1} MetOH +0.5 mol L^{-1} H_2SO_4.

8.2.4 *Methanol Oxidation Reaction on Other Non-Noble Metal-Based Catalysts*

In the literature, other non-precious metal oxides such as porous Cu/PPy/SnO_x, SnO_2/m-ZSM-5, Co_3O_4/NiO core–shell nanowire array, hydrated iridium oxides, and transition metal carbides (TMCs) have been reported as viable nanocatalysts for the MOR. Asghari and coworkers have studied hierarchical nanostructured tin-oxide-decorated polypyrrole on nanoporous copper (porous Cu/PPy/SnO_x) prepared by the galvanostatic method [45]. This anode material showed good catalytic activity for the MOR in acidic media when compared to smooth Cu/PPy/SnO_x and porous Cu/PPy (Fig. 8.9).

This improved performance was attributed to the presence of SnO_x which increases surface area of the electrode material, and has the ability to promote the adsorption and oxidation of reaction intermediates such as CO, while allowing the dehydrogenation of the alcohol according to the following equations:

$$CH_3OH \rightarrow (HCO)_{ads} + 3H^+ + 3e^- \tag{8.7}$$

$$(HCO)_{ads} + {}^{ads}SnX_4(OH)_2^{2-} \rightarrow CO_2 + SnX_4^{2-} + H_2O + H^+ + e^- \tag{8.8}$$

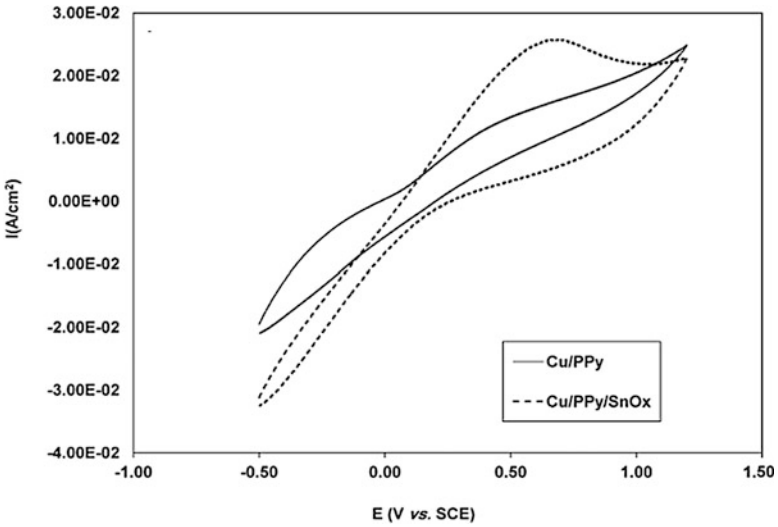

Fig. 8.9 Cyclic voltammograms (tenth scan) of (**a**) bare Cu and Cu/SnO_x, and (**b**) Cu/PPy electrodes in an acidic solution of methanol in the absence and presence of SnO_x nanoparticles synthesized at 4.00 mA cm^{-2}, and the scan rate is 100 mV s^{-1}. Copyright 2016 Elsevier [45]

$$2H_2O^2 \rightarrow 2(OH)_{ads} + 2H^+ + 2e^- \tag{8.9}$$

$$2(OH)_{ads} + SnX_4(OH)_2^{2-} \rightarrow SnX_4(OH)_2^{2-} \tag{8.10}$$

Shi et al. [46] worked on nanocomposites of tin oxide nanocrystals (3 nm) homogenously decorated on the surface of mesoporous zeolite (SnO_2/m-ZSM-5) synthesized by hydrothermal method. It was shown that this material exhibits high electroactivity for the MOR, comparable to that of Pt/C. It was also shown that this catalyst material was stable (Fig. 8.10a). The performance of this electrocatalyst was related to the excellent tolerance of CO poisoning, holding from the synergistic interaction between SnO_2 and m-ZS M-5 (Fig. 8.10b). Elsewhere, Co_3O_4/NiO core–shell nanowire array (with mesoporous nanowire core and branched nanoflake shell) was reported by Wu's group [47].

This material was obtained by combined hydrothermal and electrodeposition methods. It displays excellent electrocatalytic activity towards the MOR compared to its single Co_3O_4 nanowire array. The electroactivity of Co_3O_4/NiO was due to the synergy between the core and the shell structures, which allowed fast kinetics and lowered the overpotential (Fig. 8.11).

Works regarding the MOR using Ir as electrocatalyst have been reported previously. The catalytic activity of Ir for the MOR is considerably lower than that of Pt, Pd, or even Rh [48], even though the mechanism of the MOR on Ir is the same as that on Pt [49]. Consequently, beside those preliminary works, no other relevant reports have been carried out on Ir metal as anode catalyst. Rather, hydrated iridium oxide has been studied, showing appreciable activity for the reaction. It has been reported

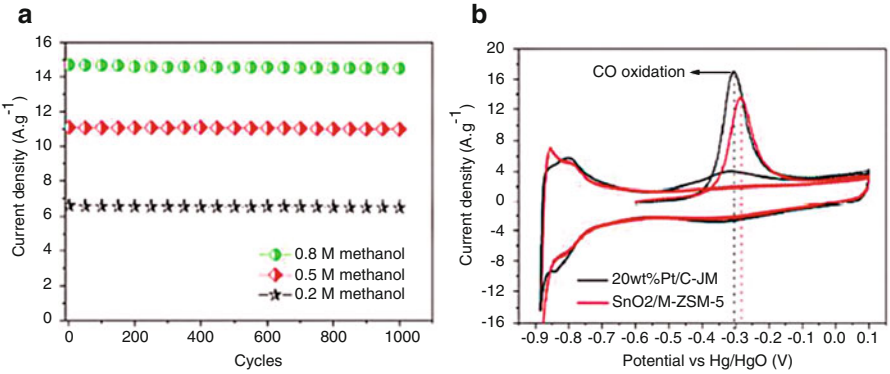

Fig. 8.10 (**a**) Current vs. cycling time of the SnO_2/m-ZSM-5 nanocomposite for methanol oxidation at a constant scan rate of 0.05 V s^{-1}, and (**b**) CO stripping curves of the samples in 0.5 mol L^{-1} NaOH solution at 20 °C. Copyright 2015 Royal Society of Chemistry [46]

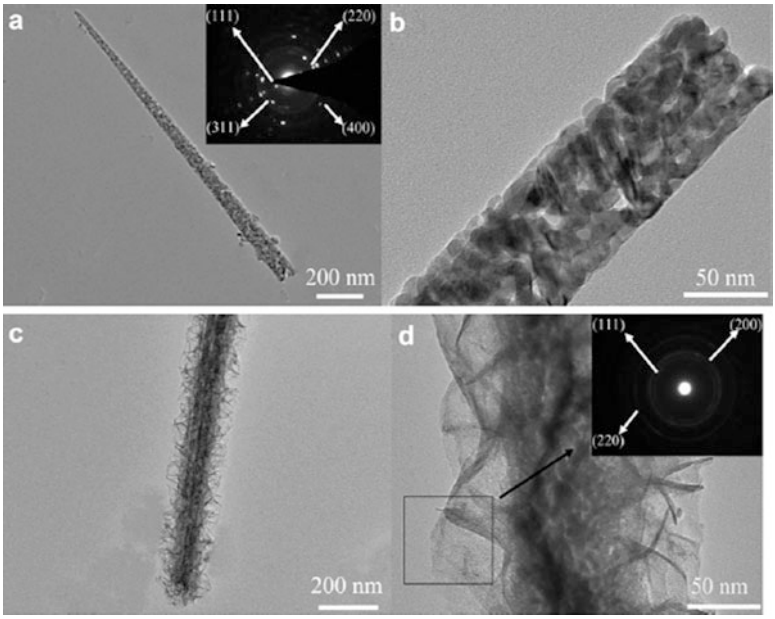

Fig. 8.11 TEM images of (**a**, **b**) Co_3O_4 nanowire (SAED pattern in inset) and (**c, d**) Co_3O_4/NiO core/shell nanowire (SAED pattern in inset). Copyright 2013 Elsevier [47]

that the active Ir oxygenated species promotes the MOR, and it is stable with respect to temperature and pH changes within DMFC operating conditions (Fig. 8.12) [50, 51]. However, an activation process is necessary because of the presence of metallic Ir within the surface. The activation process consists of cycling the electrode in the electrolyte support (H_2SO_4), generating active sites. As reported by Conway

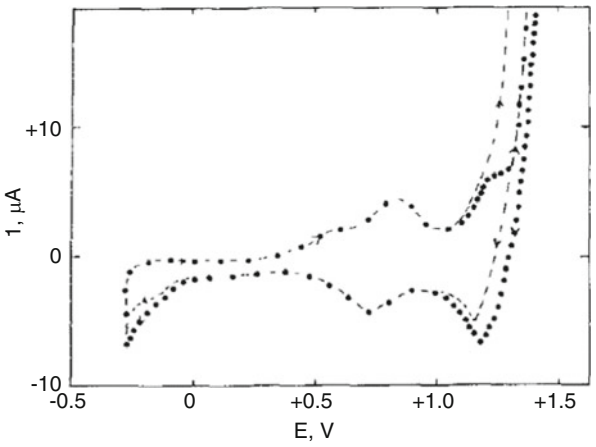

Fig. 8.12 Voltammogram of hydrated iridium oxide film after 500 cycles in pure 0.50 mol L^{-1} H_2SO_4, (dotted line) and in the presence of 0.10 mol L^{-1} CH_3OH (dashed line) measured at a rate of 25 mV s^{-1}. Copyright 1996 Elsevier [50]

and Mozota, in the initial stage the oxide thickness almost linearly increases with the number of cycles [52].

Attention was also paid to TMCs as promising electrocatalysts that could replace noble metals. It displays good mechanical and chemical stability and good corrosion resistance under reaction conditions. TMCs also show several advantages over their single metal counterparts in terms of catalytic activity, selectivity, and resistance to poisoning. TMCs, specially tungsten carbide, have been found to be good catalysts for a number of reactions which used to be catalyzed by noble metals [53]. It can be produced having different phases such as tungsten mono-carbide (WC), tungsten semi-carbide (W_2C), and cubic tungsten carbide (WC_{1-X}). Among them, WC is known to be the most stable [53, 54]. It was found that tungsten carbide performs like noble metals for some electrochemical reactions such as hydrogen, Co, and alcohols oxidation, as well as the oxygen reduction reaction. Tungsten carbides have been widely applied in electrochemical systems, including electrocatalyst for low-temperature fuel cells, for example, as anodes for the MOR where the electrocatalytic activity observed on pure WC was rather low [55]. Chen et al. have studied molybdenum carbides [56]. The product selectivity on the carbide-modified Mo (110) surface was 63%, with the remaining methanol (37%) dissociating to produce CO and H_2.

Comparative studies of methanol oxidation reaction on carbide-modified V(110) and Ti(0001) have been performed [57]. TPD and HREELS techniques showed that C/V (110) and C/Ti (0001) surfaces may produce the methoxy intermediate followed by its decomposition to CH_4 gas, reactions that take place at 465 and 333 K, respectively.

8.3 Ethanol Oxidation Reaction (EOR) on Non-noble Metals

Over the past few decades, ethanol has been extensively studied as fuel for direct ethanol fuel cells (DEFC), due to its high mass energy density (8.01 kWh kg^{-1}) and because is environmentally friendly if produced from biomass [23, 58, 59]. The EOR has been performed on Pt-based electrodes; however, nowadays there are still relevant issues to be solved in order to make DEFCs suitable candidates for the generation of electric energy. First, Pt is a scarce and expensive metal. Second, it has been demonstrated that Pt-based electrocatalysts are poisoned by CO species generated from the EOR, decreasing the number of active sites available to carry out the adsorption and oxidation of ethanol and reaction intermediates.

8.3.1 Nickel-Based Anodes

In order to overcome the issues related to Pt-based electrocatalysts, non-noble metals have been proposed as electrocatalyst for the EOR. The oxidation of low molecular alcohols on metal oxides has been proposed by Fleischmann et al. [20] and after that numerous studies have been reported, aiming to generate knowledge on the reaction mechanism of the EOR on such oxides.

In 1994, Motheo and coworkers evaluated the EOR on Ni electrodes in 0.1 mol L^{-1} KOH without and with 0.1 mol L^{-1} ethanol [60]. The authors observed that Ni electrode showed a peak current of 2.1 mA close to 0.9 V due to the $Ni(OH)_2$/NiOOH redox pair. Meanwhile, the first cycle of the EOR on Ni electrode showed a current of 3.13 mA at 1.14 V. The authors stated that the increase in current and the shift in the peak potential was due to two reactions that occur at overlapping potentials: the oxidation of ethanol and the formation of NiOOH species [61]. On the one hand, the already formed oxide film adsorbs ethanol, being subsequently oxidized to higher valence species. On the other, the EOR may be enhanced by the formation of superoxides on the Ni electrode.

This phenomenon was investigated by conducting studies of Ni electrodeposition at Cu foil coated with Pd in the presence of various alcohols by Neuróhr's group [62]. They electrodeposited Ni in methanol, ethanol, and glycerol in the potential range of 1.0 to −1.5 V vs SCE. In the case of methanol, they observed a shift in the anodic peak current density, from 0.25 to 0.6 V vs SCE when the CV is conducted at the range of −1 to 1 and − 1.5 to 1 V vs SCE, respectively. Furthermore, Jae et al. studied the electrodeposition of Ni oxide at graphite substrates by using a mixture of water–ethanol 50:50 (V/V) as electrolyte [63]. They found that ethanol plays a key role in the process because of a change in the dielectric constant is observed that results in a better adhesion of Ni onto the substrate.

A complete study of Ni-based electrodes in KOH solution was published by Jao-Woo and coworkers by electrochemical impedance spectroscopy (EIS)

measurements at different potentials [63]. At potential of 0.24 and 0.28 V, the equivalent electronic circuit was composed of 2 resistive elements namely R_s, R_1 due to the solution resistance and the polarization resistance, respectively. Meanwhile, Q_1, Q_2, Q_3, Q_4, and Q_5 represented the outer and inner pores of the film, the kinetics of the oxidation process, the absorbed intermediated species, and the diffusion of the intermediated species, respectively. At low potentials (0.24–0.28 V), the involved mechanism was the reaction and transformation of NiOOH. Moreover, studies were conducted at potentials from 0.32 to 0.42 V. It is worth mentioning that the R_1 value had a significant change at 0.37 V (660.2 Ω) and then it became larger at 0.38 V (1666.3 Ω). The author suggested that a passive layer is formed at this point. The EOR follows the same mechanism proposed above for the MOR at Ni-based electrodes (see Eq. (8.5)), where ethanol is absorbed at NiOOH species that is oxidized to form acetaldehyde and finally oxidized to acetic acid [63, 64].

On the other hand, the EIS studies for EOR were conducted in 1 mol L^{-1} KOH + 0.2 mol L^{-1} ethanol in the potential range from 0.26 to 0.48 V vs Ag/AgCl. Herein, R_s, R_1 and R_2 represent the solution resistance and the polarization resistances, respectively. While, Q_1 and Q_2 are due to the diffusion and adsorption of intermediates, respectively. At 0.3 V, the value of polarization resistance was 11448.0 Ω and at 0.35 V a drastic drop was observed (4527.0 Ω) probably due to the start of the EOR at the Ni electrode, in good agreement with other studies reported elsewhere [60].

The byproducts from the EOR at Ni electrodes have been investigated by using in situ infrared spectra (FTIR) [61]. It has been seen that the onset potential for the EOR occurs at 1.37 V vs RHE. Afterwards, a signal is observed at 1550 and 1415 cm^{-1} due the presence of symmetric and asymmetric vibrations bands characteristic of acetate ions [15], and this perturbation increases with the applied potential. Also, a consumption of the OH^- species is observed, with an alteration between 2500 and 3000 cm^{-1} [9].

This latter information confirms that at high potentials the OH^- species have been consumed by two possible mechanisms: (a) to form fresh $Ni(OH)_2$ species that was further oxidized to NiOOH, and (b) to oxidize ethanol to acetic acid. It is important to note that no peaks related to CO and CO_2 (perturbations normally located at 1840 cm^{-1} and 2345 cm^{-1} [9]) have been detected, suggesting that the mechanism of the EOR at Ni electrodes in alkaline media is:

$$CH_3CH_2OH + 4OH^- \rightarrow CH_3COOH + 3H_2O + 4e^- \tag{8.11}$$

8.3.2 *Iridium-Based Anodes*

Another cheap catalyst materials for the EOR was developed by Cao et al. based on the use of Iridium (Ir) [65], starting from the observations by Fujiwara's group

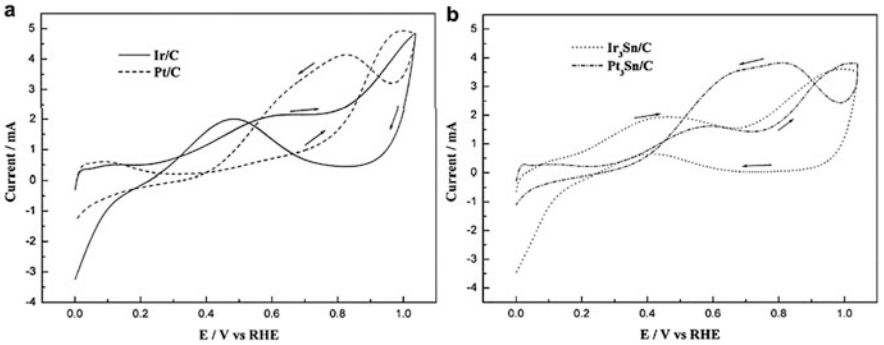

Fig. 8.13 Cyclic voltammograms of ethanol oxidation on Ir/C (solid line), Pt/C (dashed line), Ir_3Sn/C (dotted line), and Pt_3Sn/C (dashed-dotted line) catalysts in 0.5 mol L^{-1} H_2SO_4 with 1 mol L^{-1} ethanol at room temperature with a scan rate of 50 mV s^{-1}. (**a**) Ir/C and Pt/C; (**b**) Ir_3Sn/C and Pt_3Sn/C. Copyright 2007 Elsevier [65]

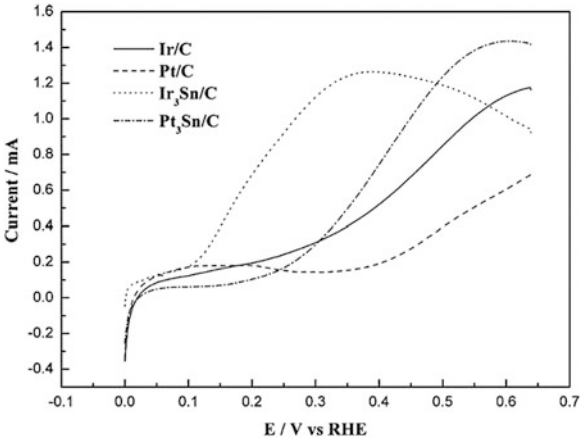

Fig. 8.14 Linear sweep voltammograms of ethanol oxidation of Ir/C (solid line), Pt/C (dashed line), Ir_3Sn/C (dotted line), and Pt_3Sn/C (dashed-dotted line) catalysts in 0.5 M H_2SO_4 with 1 mol L^{-1} ethanol at room temperature with a scan rate of 10 mV s^{-1}. Copyright 2007 Elsevier [65]

[66]. The authors reported that the peak current of the EOR in the positive scan on the Ir/C catalyst was lower compared to Pt/C. Nevertheless, the onset potential of the reaction on Ir/C was more negative than that of Pt/C (Fig. 8.13).

In the negative scan, the current value is also lower on Ir/C than that on Pt/C. Meanwhile, using Ir_3Sn/C and Pt_3Sn/C cases, two oxidation peaks were observed. Although the peak current at Ir_3Sn/C catalyst in the high potential region was lower than that of Pt_3Sn/C catalyst, in the low potential region the oxidation peak on Ir_3Sn/C catalyst appeared at more negative onset potential, indicating a superior electrocatalytic activity towards the EOR (Fig. 8.14). In such potential range, which correlates with single-cell operation conditions, Lamy's group reported the presence of acetaldehyde, acetic acid, and CO_2 on Ir electrodes [67], which is in agreement with the results for Pt electrodes [68].

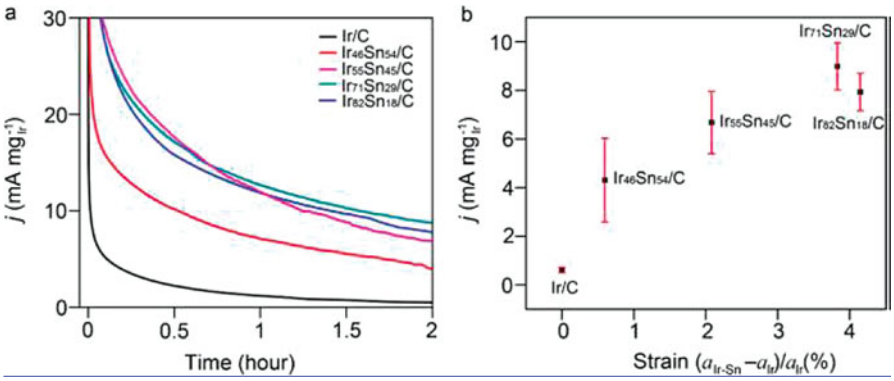

Fig. 8.15 (**a**) Current density vs time measurements of Ir/C, $Ir_{46}Sn_{54}$/C, $Ir_{55}Sn_{45}$/C, $Ir_{71}Sn_{29}$/C, and $Ir_{82}Sn_{18}$/C at 0.10 V in 0.5 mol L^{-1} of H_2SO_4/ 0.5 M of ethanol electrolyte, and (**b**) plot of current density vs time activity vs strain (*aIr-Sn-aIr*)/*aIr*(%). Specifically, *aIr_Sn* is denoted as the lattice constant of each electrocatalyst, while *aIr* represents the lattice constant of homemade carbon-supported Ir nanoparticles. Copyright 2011 American Chemical Society [69]

It was found that on Ir electrode, acetaldehyde could be formed at low potentials, where the surface was partially covered by CO_{ads} and H_{ads}. The addition of Sn as cocatalyst resulted in a significant improvement of catalytic activity at the Ir-based electrode. Cao et al. found that Ir–Sn has comparable catalytic activity to that of Pt–Sn. Ir–Sn was also susceptible to poisoning. Du et al. [69] also showed that the $Ir_{71}Sn_{29}$/C catalyst has high catalytic activity for the EOR due to the formation of acetic acid at low potentials (0.07 V vs Ag/AgCl) without breaking of the C–C bond. They studied different Ir/Sn ratio, all showing larger lattice parameters than pure Ir nanoparticles. The authors also noticed that the lattice parameter and mass current density of the EOR increased with increasing amount of Sn alloyed with Ir (Fig. 8.15).

Among the various Ir–Sn catalysts, Ir–Sn/C (71:29) and (82:18) showed the larger lattice parameter and higher catalytic activity. The high performance was explained by the electronic back donation from Sn to Ir in the Ir–Sn alloy phase, which changed the electronic structure of Ir, allowing for the weakening of the Ir–CO bond and therefore improving the catalytic performance of the carbon-supported IrSn alloys. The authors explained the correlation between the Ir–Sn/C heterogeneous structure and the high catalytic activity for the EOR from several characterization techniques, including DFT calculations and electrochemical measurements [69].

Their findings involved that: (1) the $Ir_{71}Sn_{29}$/C catalyst consists of a core–shell-like structure with an Ir core-rich, Ir–Sn alloy shell-rich, and the presence of SnO_2 on the surface, indicating an Ir/Ir–Sn/SnO_2 heterogeneous structure with a maximum metallic Sn content alloyed with Ir of around 20%; (2) both the Ir–Sn alloy and SnO_2 on the surface are important to promote the EOR. DFT calculations modeling (Fig. 8.16) showed that the presence of Sn, either through a pure Sn surface or Sn in the Ir–Sn alloy, destabilizes the reaction intermediates which become unstable on

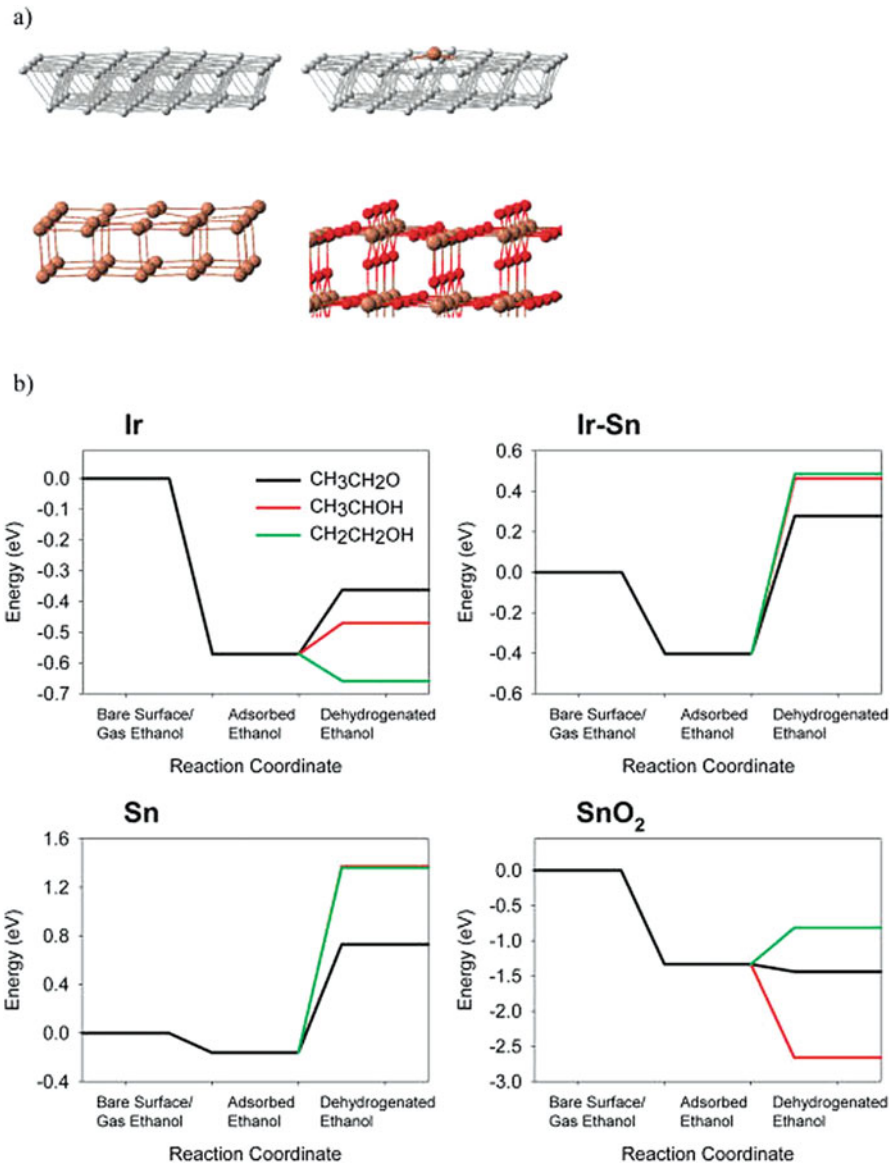

Fig. 8.16 (**a**) Surface cluster models used in the current work for modeling ethanol dehydrogenation. Gray spheres represent Ir atoms, brown spheres represent Sn atoms, and red spheres represent O atoms. Ir(111), Ir–Sn(111), Sn(100), and SnO_2(110) surfaces are shown, and (**b**) calculated energies for adsorption of ethanol and reaction (H removal). Note that for Sn, CH_2CH_2OH and CH_3CHOH have similar reaction energies. Copyright 2011 American Chemical Society [69]

the surface. On the other hand, both Ir and SnO_2 display reaction energies that are reasonably exothermic, with the dehydrogenation reaction over SnO_2 being highly exothermic.

8.3.3 Cobalt-Based Anodes

Cobalt was used as electrocatalyst for the EOR by Barakat and coworkers [70]. It was found that Co alone has a low electrocatalytic activity, but when doped with cadmium its performance increased. It was found that Cd was the key component in the catalyst that adsorbed/desorbed and oxidized the CO_{ads} species [70].

Meanwhile, Co acts as other cocatalysts, enhancing the electrocatalytic reaction through synergetic effect which involves reducing the bond energy of the intermediates formed on the surface of the active sites. Comparing the CVs of the Cd–Co and Pt catalysts (Fig. 8.17), it was found that the former performed better as it has lower onset potential, as well as a higher peak current density. Barakat strongly suggested that the research on this bimetallic catalyst was performed more thoroughly, since the cost for the transition metal catalysts is much lower than Pt and Pd itself, thus making it one low-cost catalyst for the EOR. Cobalt was also used in three metallic alloys with Ni and Fe to form Ni–Fe–Co, that were synthesized starting with the condensation polymerization of phenol-hydrazones, substituted phenols, and

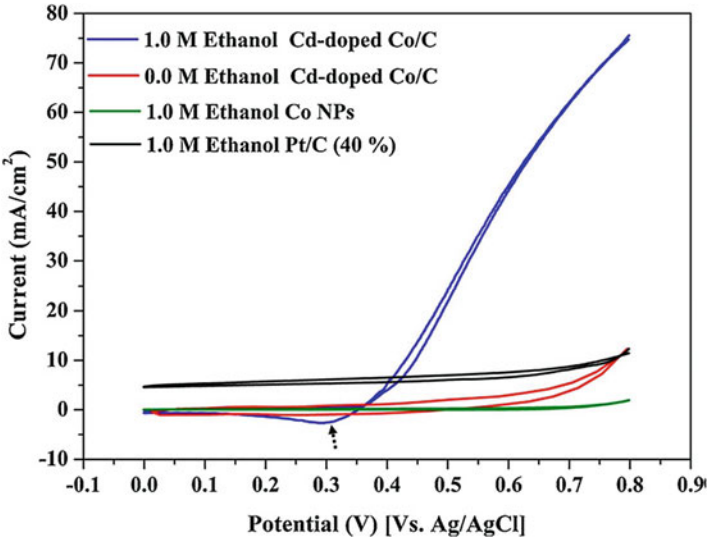

Fig. 8.17 Cyclic voltammograms at a scan rate of 50 mV s^{-1} and 25 °C for the introduced electrocatalyst, Pt/C (40%) and pristine cobalt nanoparticles in 1 mol L^{-1} KOH and in the presence of 1 mol L^{-1} ethanol. The arrow points to the oxidation peak of ethanol in the reverse scanning. Copyright 2013 Elsevier [70]

formaldehyde [71]. The resulting resin is reacted with a mixture of Ni, Fe, and Co salts followed by reduction and pyrolysis in a H_2 atmosphere at 360 °C. The alloys were tested for the oxidation of alcohols such as ethanol, methanol, ethylene glycol, and glycerol. Good electroactivity was observed for the EOR in alkaline media using these catalysts.

Although Pt is known to have good activity for the EOR in alkaline media, the preponderance of partial oxidation to acetaldehyde and acetate [72, 73] stops the reaction with only four electrons transferred, out of 12 that theoretically should be exchanged (Eq. (8.12)). This limitation of the Pt-based catalyst can be considered as one of the reasons alternative catalysts are being developed.

$$CH_3CH_2OH + 5NaOH \rightarrow CH_3COONa + 4Na + 4e^- + 4H_2O + 2CO_2 \quad (8.12)$$

A company called ACTA has recently reported a good catalytic activity for the EOR, with complete oxidation of the alcohol to CO_2 or carbonate, by using Ni–Fe–Co catalysts. These anode materials showed small nanoparticles deposited in a matrix of hydrazone-based polymer, and have the trade name of HYPERMEC [74–77]. During the studies of the EOR at this catalyst, no acetate was detected. Acetaldehyde was observed as an intermediate of the EOR, and further oxidized to carbonate [74, 75]. Probably, the relevance of the performance of HYPERMEC is the complete oxidation of ethanol to CO_2.

Moreover, the peak current density of the EOR at this catalyst was higher than that obtained on Pt catalysts. Also, the performance of HYPERMEC catalysts in a commercial anion exchange membrane was high, showing stability during the test (less than 10% performance degradation over 1800 h at 25 mW cm^{-2}) [75]. One of the reasons of the good performance of HYPERMEC catalysts for the EOR was the lack of CO poisoning as shown by DRIFT analysis. The spectra indicated that CO readily desorbs from HYPERMEC [75], in contrast to the negative effect of CO on Pt-based catalysts. Mechanistic studies of the EOR on HYPERMEC catalysts have not been reported to date, to the best of our knowledge.

8.4 Ethylene Glycol Oxidation (EGOR) in Alkaline Media

As an attractive source of energy, ethylene glycol has a good potential for fuel cell applications due to its high reactivity in electrooxidation, inflammability, low toxicity, and high boiling point that enables easy handling and storage [78]. Another advantage of using ethylene glycol as the fuel in alcohol fuel cells is that its theoretical energy density is close to that of methanol and ethanol (5.2, 6.1 and 8.6 kWh kg^{-1} for ethylene glycol, methanol, and ethanol, respectively) [79]. Furthermore, studies have shown that ethylene glycol can be directly produced from the catalytic conversion of biomass-related cellulose [80]. Some studies have been performed in order to use noble metal-free catalyst as anodes for the EGOR.

8.4.1 HYPERMEC (Fe–Co–Ni/C)

As mentioned above, HYPERMEC has been tested as anode catalyst for the oxidation of different alcohols, especially for its high performance during the EOR. Abe et al. [81] studied the electrooxidation of ethylene glycol in a fuel cell composed of $LaSr_3Fe_3O_{10}$ (7) electrolyte and of HYPERMEC (Fe–Co–Ni/C) anode material, and its performance compared to those of Pt/C, PtRu/C, and Pd/C. The direct ethylene glycol solid alkaline inorganic fuel cell using Pt/C anode and $LaSr_3Fe_3O_{10}$ electrolyte delivered the highest output power density of 32 mW cm^{-2} at a current density of 80 mA cm^{-2}, while the Fe–Co–Ni/C anode generated an output power density of 27 mW cm^{-2} at a current density of 90 mA cm^{-2}. As it was presented, the Fe–Co–Ni/C anode material provided a performance comparable to that of Pt/C.

8.5 Conclusions

Non-noble metal electrocatalysts have shown good physicochemical and electrochemical characteristics that make them suitable to be used in fuel cell technologies for electrical energy generation. The use of these electrocatalysts not only can improve the overall efficiency of the fuel cell but also reduce its cost. Nowadays, significant efforts have been made for the development of highly active electrocatalysts. However, it is necessary to solve some issues related to corrosion, stability, and electroactivity. We are convinced that in the future the non-precious materials will play a key role for the development and improvement of sustainable technologies that have a positive effect in daily life and in the reduction of pollution.

References

1. Speight JG (2011) Fuels for fuel cells. In: Shekhawat D, Spivey JJ, Berry DA (eds) Fuel cells: technologies for fuel processing, 1st edn. Elsevier, New York, NY, pp 29–48
2. Spellman FR (2016) Energy basics. In: The science of renewable energy, 2nd edn. CRC Press, Boca Raton, FL, pp 15–34
3. Shekhawat D, Berry DA, Spivey JJ (2011) Introduction to fuel processing. In: Shekhawat D, Spivey JJ, Berry DA (eds) Fuel cells: technologies for fuel processing, 1st edn. Elsevier, New York, NY, pp 1–9
4. Solorza-Feria O, Varela FJR (2014) Pt and Pd-based electrocatalysts for ethanol and ethylene glycol fuel cells. In: Direct alcohol fuel cells. Springer, Dordrecht, pp 63–78
5. Albarbar A, Alrweq M (2018) Introduction and background. In: Proton exchange membrane fuel cells. Springer, Cham, pp 1–8
6. Edlund D (2011) Methanol fuel cell systems: advancing towards commercialization. Pan Stanford, Singapore
7. Williams MC (2011) Fuel cells. In: Shekhawat D, Spivey JJ, Berry DA (eds) Fuel cells: technologies for fuel processing, 1st edn. Elsevier, New York, NY, pp 11–27

8. Corti HR, Gonzalez ER (2014) Introduction to direct alcohol fuel cells. In: Direct alcohol fuel cells. Springer, Dordrecht, pp 1–32
9. Pech-Rodríguez WJ, Calles-Arriaga C, González-Quijano D, Vargas-Gutiérrez G, Morais C, Napporn TW, Rodríguez-Varela FJ (2018) Electrocatalysis of the ethylene glycol oxidation reaction and in situ fourier-transform infrared study on PtMo/C electrocatalysts in alkaline and acid media. J Power Sources 375:335–344. https://doi.org/10.1016/j.jpowsour.2017.07.081
10. Gonzalez ER, Mota-Lima A (2014) Catalysts for methanol oxidation. In: Direct alcohol fuel cells. Springer, Dordrecht, pp 33–62
11. Zhou W, Zhou Z, Song S, Li W, Sun G, Tsiakaras P, Xin Q (2003) Pt based anode catalysts for direct ethanol fuel cells. Appl Catal B Environ 46:273–285. https://doi.org/10.1016/S0926-3373(03)00218-2
12. Sullivan JA, Keane O, Dulgheru P, O'Callaghan N (2015) Environmental applications of multifunctional nanocomposite catalytic materials: issues with catalyst combinations. In: Tiwari A, Titinchi S (eds) Advanced catalytic materials. Wiley, Hoboken, NJ, pp 1–36
13. Wang H, Jusys Z, Behm RJ (2009) Adsorption and electrooxidation of ethylene glycol and its C2 oxidation products on a carbon-supported Pt catalyst: a quantitative DEMS study. Electrochim Acta 54:6484–6498. https://doi.org/10.1016/j.electacta.2009.05.097
14. Perry ML, Fuller TF (2002) A historical perspective of fuel cell technology in the 20th century. J Electrochem Soc 149:S59. https://doi.org/10.1149/1.1488651
15. Pech-Rodríguez WJ, González-Quijano D, Vargas-Gutiérrez G, Morais C, Napporn TW, Rodríguez-Varela FJ (2017) Electrochemical and in situ FTIR study of the ethanol oxidation reaction on PtMo/C nanomaterials in alkaline media. Appl Catal B Environ 203:654–662. https://doi.org/10.1016/j.apcatb.2016.10.058
16. González-Quijano D, Pech-Rodríguez WJ, Escalante-García JI, Vargas-Gutiérrez G, Rodríguez-Varela FJ (2014) Electrocatalysts for ethanol and ethylene glycol oxidation reactions. Part I: effects of the polyol synthesis conditions on the characteristics and catalytic activity of Pt–Sn/C anodes. Int J Hydrog Energy 39:16676–16685. https://doi.org/10.1016/j.ijhydene.2014.04.125
17. González-Quijano D, Pech-Rodríguez WJ, González-Quijano JA, Escalante-García JI, Vargas-Gutiérrez G, Alonso-Lemus I, Rodríguez-Varela FJ (2015) Electrocatalysts for ethanol and ethylene glycol oxidation reactions. Part II: effects of the polyol synthesis conditions on the characteristics and catalytic activity of Pt–Ru/C anodes. Int J Hydrog Energy 40:17291–17299. https://doi.org/10.1016/j.ijhydene.2015.06.154
18. Cunha EM, Ribeiro J, Kokoh KB, de Andrade AR (2011) Preparation, characterization and application of Pt–Ru–Sn/C trimetallic electrocatalysts for ethanol oxidation in direct fuel cell. Int J Hydrog Energy 36:11034–11042. https://doi.org/10.1016/j.ijhydene.2011.06.011
19. Beyhan S, Léger JM, Kadirgan F (2014) Understanding the influence of Ni, Co, Rh and Pd addition to PtSn/C catalyst for the oxidation of ethanol by in situ Fourier transform infrared spectroscopy. Appl Catal B Environ 144:66–74. https://doi.org/10.1016/j.apcatb.2013.07.020
20. Fleischmann M, Korinek K, Pletcher D (1971) The oxidation of organic compounds at a nickel anode in alkaline solution. J Electroanal Chem Interfacial Electrochem 31:39–49. https://doi.org/10.1016/S0022-0728(71)80040-2
21. Maximovitch S, Bronoel G (1981) Oxidation of methanol on nickel—zinc catalysts. Electrochim Acta 26:1331–1338. https://doi.org/10.1016/0013-4686(81)85118-3
22. Fleischmann M, Korinek K, Pletcher D (1972) The oxidation of hydrazine at a nickel anode in alkaline solution. J Electroanal Chem Interfacial Electrochem 34:499–503. https://doi.org/10.1016/S0022-0728(72)80425-X
23. Zhou WJ, Song SQ, Li WZ, Sun GQ, Xin Q, Kontou S, Poulianitis K, Tsiakaras P (2004) Pt-based anode catalysts for direct ethanol fuel cells. Solid State Ionics 175:797–803. https://doi.org/10.1016/j.ssi.2004.09.055
24. Taraszewska J, Rosłonek G (1994) Electrocatalytic oxidation of methanol on a glassy carbon electrode modified by nickel hydroxide formed by ex situ chemical precipitation. J Electroanal Chem 364:209–213. https://doi.org/10.1016/0022-0728(93)02919-9

25. Khalil MW, Abdel Rahim MA, Zimmer A, Hassan HB, Abdel Hameed RM (2005) Nickel impregnated silicalite-1 as an electro-catalyst for methanol oxidation. J Power Sources 144:35–41. https://doi.org/10.1016/j.jpowsour.2004.12.014
26. Abdel Rahim MA, Abdel Hameed RM, Khalil MW (2004) Nickel as a catalyst for the electro-oxidation of methanol in alkaline medium. J Power Sources 134:160–169. https://doi.org/10.1016/j.jpowsour.2004.02.034
27. Chen D, Giroud F, Minteer SD (2014) Nickel cysteine complexes as anodic electrocatalysts for fuel cells. J Electrochem Soc 161:F933–F939. https://doi.org/10.1149/2.0811409jes
28. Zhao Y, Liu J, Wu Y, Wang F (2017) Proton conductive Pt-Co nanoparticles anchoring on citric acid functionalized graphene for efficient oxygen reduction reaction. J Power Sources 360:528–537. https://doi.org/10.1016/j.jpowsour.2017.06.046
29. Jeong DJ, Kim W-S, Choi Y-K, Sung Y-E (2001) Intercalation/deintercalation characteristics of electrodeposited and anodized nickel thin film on ITO electrode in aqueous and nonaqueous electrolytes. J Electroanal Chem 511:79–87. https://doi.org/10.1016/S0022-0728(01)00563-0
30. Bode H, Dehmelt K, Witte J (1966) Zur kenntnis der nickelhydroxidelektrode—I.Über das nickel (II)-hydroxidhydrat. Electrochim Acta 11:1079–1IN1. https://doi.org/10.1016/0013-4686(66)80045-2
31. Oliva P, Leonardi J, Laurent JF, Delmas C, Braconnier JJ, Figlarz M, Fievet F, Guibert A d. (1982) Review of the structure and the electrochemistry of nickel hydroxides and oxy-hydroxides. J Power Sources 8:229–255. https://doi.org/10.1016/0378-7753(82)80057-8
32. Hall DS, Lockwood DJ, Bock C, MacDougall BR (2014) Nickel hydroxides and related materials: a review of their structures, synthesis and properties. Proc Math Phys Eng Sci 471:20140792–20140792. https://doi.org/10.1098/rspa.2014.0792
33. Mancharan R, Goodenough JB (1992) Methanol oxidation in acid on ordered NiTi. J Mater Chem 2:875–887. https://doi.org/10.1039/jm9920200875
34. Chellasamy V, Thangadurai P (2017) Structural and electrochemical investigations of nano-structured NiTiO3 in acidic environment. Front Mater Sci 11:162–170. https://doi.org/10.1007/s11706-017-0380-1
35. Hou G-Y, Xie Y-Y, Wu L-K, Cao H-Z, Tang Y-P, Zheng G-Q (2016) Electrocatalytic performance of Ni-Ti-O nanotube arrays/NiTi alloy electrode annealed under H_2 atmosphere for electro-oxidation of methanol. Int J Hydrog Energy 41:9295–9302. https://doi.org/10.1016/j.ijhydene.2016.04.054
36. Guczi L, Erdôhelyi A (2012) Catalysis for alternative energy generation. Springer, New York, NY. https://doi.org/10.1007/978-1-4614-0344-9
37. Hosseini MG, Momeni MM, Faraji M (2010) Highly active nickel nanoparticles supported on TiO_2 nanotube electrodes for methanol electrooxidation. Electroanalysis 22:2620–2625. https://doi.org/10.1002/elan.200900620
38. Yi Q-F, Huang W, Yu W-Q, Li L, Liu X-P (2008) Fabrication of novel titanium-supported Ni-Sn catalysts for methanol electro-oxidation. Chinese J Chem 26:1367–1372. https://doi.org/10.1002/cjoc.200890249
39. Jafarian M, Moghaddam RB, Mahjani MG, Gobal F (2006) Electro-catalytic oxidation of methanol on a Ni–Cu alloy in alkaline medium. J Appl Electrochem 36:913–918. https://doi.org/10.1007/s10800-006-9155-6
40. Gu Y, Luo J, Liu Y, Yang H, Ouyang R, Miao Y (2015) Synthesis of bimetallic Ni–Cr nano-oxides as catalysts for methanol oxidation in NaOH solution. J Nanosci Nanotechnol 15:3743–3749. https://doi.org/10.1166/jnn.2015.9528
41. Tammam RH, Fekry AM, Saleh MM (2015) Electrocatalytic oxidation of methanol on ordered binary catalyst of manganese and nickel oxide nanoparticles. Int J Hydrog Energy 40:275–283. https://doi.org/10.1016/j.ijhydene.2014.03.109
42. Quan C, He Y, Zhang J (2016) High temperature oxidation behavior of a novel Ni−Cr binary alloy coating prepared by cathode plasma electrolytic deposition. Surf Coatings Technol 292:11–19. https://doi.org/10.1016/j.surfcoat.2016.03.012

43. Patil A, Patil V, Choi J-W, Kim H-J, Cho B-H, Yoon S-J (2009) Structural and electrochemical properties of Nichrome anode thin films for lithium battery. J Electroceram 23:230–235. https://doi.org/10.1007/s10832-007-9405-y
44. Tharamani CN, Mayanna SM (2006) Studies on the development and characterization of Ni–Cr alloys for fuel cell applications. Electrochem Solid-State Lett 9:A412–A414. https://doi.org/10.1149/1.2216591
45. Asghari E, Ashassi-Sorkhabi H, Vahed A, Rezaei-Moghadam B, Charmi GR (2016) The use of a hierarchically platinum-free electrode composed of tin oxide decorated polypyrrole on nanoporous copper in catalysis of methanol electrooxidation. Thin Solid Films 598:6–15. https://doi.org/10.1016/j.tsf.2015.12.005
46. Cui X, Zhu Y, Hua Z, Feng J, Liu Z, Chen L, Shi J (2015) SnO_2 nanocrystal-decorated mesoporous ZSM-5 as a precious metal-free electrode catalyst for methanol oxidation. Energy Environ Sci 8:1261–1266. https://doi.org/10.1039/C5EE00240K
47. Wu JB, Li ZG, Huang XH, Lin Y (2013) Porous Co3O4/NiO core/shell nanowire array with enhanced catalytic activity for methanol electro-oxidation. J Power Sources 224:1–5. https://doi.org/10.1016/j.jpowsour.2012.09.085
48. Breiter MW (1963) Comparative voltammetric study of methanol oxidation and adsorption on noble metal electrodes in perchloric acid solutions. Electrochim Acta 8:973–983. https://doi.org/10.1016/0013-4686(62)87051-0
49. Bagotzky VS, Vassiliev YB, Khazova OA, Sedova SS (1971) Adsorption and anodic oxidation of methanol on iridium and rhodium electrodes. Electrochim Acta 16:913–938. https://doi.org/10.1016/0013-4686(71)85057-0
50. Hefny MM, Abdel-Wanees S (1996) Electro-oxidation at a coated iridium electrode. Electrochim Acta 41:1419–1422. https://doi.org/10.1016/0013-4686(95)00376-2
51. Mousty C, Fóti G, Comninellis C, Reid V (1999) Electrochemical behaviour of DSA type electrodes prepared by induction heating. Electrochim Acta 45:451–456. https://doi.org/10.1016/S0013-4686(99)00273-X
52. Conway BE, Mozota J (1983) Surface and bulk processes at oxidized iridium electrodes—II. Conductivity-switched behaviour of thick oxide films. Electrochim Acta 28:9–16. https://doi.org/10.1016/0013-4686(83)85080-4
53. Zellner MB, Chen JG (2005) Surface science and electrochemical studies of WC and W_2C PVD films as potential electrocatalysts. Catal Today 99:299–307. https://doi.org/10.1016/j.cattod.2004.10.004
54. Brady CDA, Rees EJ, Burstein GT (2008) Electrocatalysis by nanocrystalline tungsten carbides and the effects of codeposited silver. J Power Sources 179:17–26. https://doi.org/10.1016/j.jpowsour.2008.01.002
55. Hwu HH, Chen JG, Kourtakis K, Lavin JG (2001) Potential application of tungsten carbides as electrocatalysts. 1. Decomposition of methanol over carbide-modified W(111). J Phys Chem B 105:10037–10044. https://doi.org/10.1021/jp0116196
56. Hwu HH, Chen JG (2003) Reactions of methanol and water over carbide-modified Mo(110). Surf Sci 536:75–87. https://doi.org/10.1016/S0039-6028(03)00607-1
57. Zellner MB, Hwu HH, Chen JG (2005) Comparative studies of methanol decomposition on carbide-modified V(110) and Ti(0001). Surf Sci 598:185–199. https://doi.org/10.1016/j.susc.2005.09.027
58. Colmenares L, Wang H, Jusys Z, Jiang L, Yan S, Sun GQ, Behm RJ (2006) Ethanol oxidation on novel, carbon supported Pt alloy catalysts—model studies under defined diffusion conditions. Electrochim Acta 52:221–233. https://doi.org/10.1016/j.electacta.2006.04.063
59. Rousseau S, Coutanceau C, Lamy C, Léger J-M (2006) Direct ethanol fuel cell (DEFC): electrical performances and reaction products distribution under operating conditions with different platinum-based anodes. J Power Sources 158:18–24. https://doi.org/10.1016/j.jpowsour.2005.08.027

60. Motheo AJ, Machado SAS, Rabelo FJB, Santos JR Jr (1994) Electrochemical study of ethanol oxidation on nickel in alkaline media. J Braz Chem Soc 5:161–165. https://doi.org/10.5935/0103-5053.19940028
61. Barbosa AFB, Oliveira VL, van Drunen J, Tremiliosi-Filho G (2015) Ethanol electro-oxidation reaction using a polycrystalline nickel electrode in alkaline media: temperature influence and reaction mechanism. J Electroanal Chem 746:31–38. https://doi.org/10.1016/j.jelechem.2015.03.024
62. Neuróhr K, Pogány L, Tóth BG, Révész Á, Bakonyi I, Péter L (2015) Electrodeposition of Ni from various non-aqueous media: the case of alcoholic solutions. J Electrochem Soc 162:D256–D264. https://doi.org/10.1149/2.0381507jes
63. Kim J-W, Park S-M (2003) In situ XANES studies of electrodeposited nickel oxide films with metal additives for the electro-oxidation of ethanol. J Electrochem Soc 150:E560. https://doi.org/10.1149/1.1613671
64. Kim J-W, Park S-M (1999) Electrochemical oxidation of ethanol at thermally prepared RuO_2-modified electrodes in alkaline media. J Electrochem Soc 146:1075–1080. https://doi.org/10.1149/1.1391723
65. Cao L, Sun G, Li H, Xin Q (2007) Carbon-supported IrSn catalysts for a direct ethanol fuel cell. Electrochem Commun 9:2541–2546. https://doi.org/10.1016/j.elecom.2007.07.031
66. Fujiwara N, Siroma Z, Ioroi T, Yasuda K (2007) Rapid evaluation of the electrooxidation of fuel compounds with a multiple-electrode setup for direct polymer electrolyte fuel cells. J Power Sources 164:457–463. https://doi.org/10.1016/j.jpowsour.2006.10.085
67. de Tacconi NR, Lezna RO, Beden B, Hahn F, Lamy C (1994) In-situ FTIR study of the electrocatalytic oxidation of ethanol at iridium and rhodium electrodes. J Electroanal Chem 379:329–337. https://doi.org/10.1016/0022-0728(94)87155-8
68. Akhairi MAF, Kamarudin SK (2016) Catalysts in direct ethanol fuel cell (DEFC): an overview. Int J Hydrog Energy 41:4214–4228. https://doi.org/10.1016/j.ijhydene.2015.12.145
69. Du W, Wang Q, Saxner D, Deskins NA, Su D, Krzanowski JE, Frenkel AI, Teng X (2011) Highly active iridium/iridium–tin/tin oxide heterogeneous nanoparticles as alternative electrocatalysts for the ethanol oxidation reaction. J Am Chem Soc 133:15172–15183. https://doi.org/10.1021/ja205649z
70. Barakat NAM, Abdelkareem MA, Kim HY (2013) Ethanol electro-oxidation using cadmium-doped cobalt/carbon nanoparticles as novel non precious electrocatalyst. Appl Catal A Gen 455:193–198. https://doi.org/10.1016/j.apcata.2013.02.004
71. Spendelow JS, Wieckowski A (2007) Electrocatalysis of oxygen reduction and small alcohol oxidation in alkaline media. Phys Chem Chem Phys 9:2654. https://doi.org/10.1039/b703315j
72. López-Atalaya M, Morallón E, Cases F, Vázquez JL, Pérez JM (1994) Electrochemical oxidation of ethanol on Pt(hkl) basal surfaces in NaOH and Na2CO3 media. J Power Sources 52:109–117. https://doi.org/10.1016/0378-7753(94)01950-9
73. Wang H, Jusys Z, Behm RJ (2004) Ethanol electrooxidation on a carbon-supported Pt catalyst: reaction kinetics and product yields. J Phys Chem B 108:19413–19424. https://doi.org/10.1021/jp046561k
74. Bianchini C (2006) Taiwan small fuel cells symposium. Taiwan
75. Bianchini C (2006) Small fuel cells for portable applications, 7th edn. Knowledge Foundation, Brookline, pp 227–251
76. Bianchini C, Bert P, Giambastiani G, Catanorchi C, Filpi A, Piani M, Santiccioli S, Tampucci A, Vizza F, Scaffidi A (2006) Fuel cell seminar and energy exposition. Honolulu
77. Ren X (2006) Alkaline membrane fuel cell workshop. Phoenix
78. Lin Q, Wei Y, Liu W, Yu Y, Hu J (2017) Electrocatalytic oxidation of ethylene glycol and glycerol on nickel ion implanted-modified indium tin oxide electrode. Int J Hydrog Energy 42:1403–1411. https://doi.org/10.1016/j.ijhydene.2016.10.011
79. Xin L, Zhang Z, Qi J, Chadderdon D, Li W (2012) Electrocatalytic oxidation of ethylene glycol (EG) on supported Pt and Au catalysts in alkaline media: reaction pathway investigation in

three-electrode cell and fuel cell reactors. Appl Catal B Environ 125:85–94. https://doi.org/10.1016/j.apcatb.2012.05.024
80. Qi J, Xin L, Chadderdon DJ, Qiu Y, Jiang Y, Benipal N, Liang C, Li W (2014) Electrocatalytic selective oxidation of glycerol to tartronate on Au/C anode catalysts in anion exchange membrane fuel cells with electricity cogeneration. Appl Catal B Environ 154–155:360–368. https://doi.org/10.1016/j.apcatb.2014.02.040
81. Takeguchi T, Arikawa H, Yamauchi M, Abe R (2011) Selective ethylene glycol oxidation reaction for carbon neutral energy cycle system. ECS Trans 41:1755–1759

Index

A
Acid media
  TMC, 242, 243
  TMeC, 244, 245
  TMeN, 244, 245
  TMM, 240–242
Active DFAFCs, 115
Active site, 54, 55, 63
Active μDEFCs, 146, 148–150
Active μDMFC, 143–145
Air breathing DFAFCs, 115
Alkaline anion exchange membrane micro-direct methanol fuel cells (AEM-μDMFCs), 132
Alkaline fuel cells (AFCs), 2, 5, 26, 228
Alkaline media
  EGOR, 284
  heteroatom-doped carbon materials
    biomass, 253
    carbon nanotubes doped, 250
    C-C bonds, 251
    chemical structure, 252
    DFT, 251
    4-electron pathway, 251
    N-C type bond, 251
    N-doped carbons, 251
    Pt/C, 250
    XPS, 250
  perovskite-type oxides
    ABO3, 245
    AMnO3, 247
    electrocatalytic measurements, 248
    Goldschmidt tolerance factor, 246
    hexagonal perovskite, 246
    oxygen stoichiometry, 247
    structure, 246
  spinel-type oxides, 248–250
Alkaline membrane fuel cells (AMFCs), 3
Alloys
  Ir–Sn, 281
  Ni–Cr, 274
  $NiCr_2O_4$, 273
  NiTi, 270, 272
Alternative liquid fuel
  direct oxidation (*see* Direct oxidation fuel cells)
Anchoring, 218
Anion exchange membrane fuel cells (AEMFCs), 236
  advantages, 9
  AFCs, 2
  AMFCs, 3
  CH_4, 3
  characteristics, 3
  commercialization, 54
  components, 3, 4
  DB, 8
  DE, 5, 6, 11
  DEG, 6, 7, 11
  DF, 8
  DG, 7, 8
  disadvantages, 9
  DM, 5, 11
  H_2/O_2, 3–5
  higher power densities, 9
  HOR, 3
  non-noble Fe-N-C catalyst, 11
  nanostructured anodes and cathodes, 9–11, 13
  non-PGM catalysts, 14

F. J. Rodríguez-Varela, T. W. Napporn (eds.), *Advanced Electrocatalysts for Low-Temperature Fuel Cells*, https://doi.org/10.1007/978-3-319-99019-4

Anion exchange membrane fuel cells (AEMFCs) (*cont.*)
non-Pt cathode catalysts, 10
operating conditions, 10
ORR, 3
and PEM (*see* Proton exchange membrane fuel cells (PEMFCs))
power density, 9, 10
Pt/C cathode, 9
Pt-Ru/C anode, 9
renewable hydrogen, 9
types, 11–13
xQAPS type, 11
Anion exchange membranes (AEMs)
advantages, 25
alkaline stability, 26
cationic functional-group chemistries, 26
electrolytes transport different ions, 14
fuel cells (*see* Anion exchange membrane fuel cells (AEMFCs))
functionalized/non-functionalized inorganic fillers, 28
ionomers, 28
mechanical properties, 25
OH^- ions, 25
performance and stability data, 27, 28
phosphonium/sulfonium groups, 26
poly(arylene ethers), 26
polymer blending, 29
preparation methods, 26
QA functional groups, 25–27
solid polymer, 25
synthesized, 26
Anode material, 98, 107
Anode overpotentials, 97, 107
Attenuated total reflection Fourier-transform infrared (ATR-FTIR) spectroscopy, 56

B
Bacterial cellulose (BC), 197
BAM3G membranes, 20
Bifunctional effect, 54
Bifunctional mechanism, 33
Biomass
BC, 197
carbon and heteroatom source, 253
cellulose, 197
CS, 197
food, 253
HTC, 196
human hairs, 199
lignocellulose, 196
NCS, 198
N-doped porous carbon, 198
oxysalt, 196
poultry-based bio-waste, 198
sucrose, 196
Bowl-like carbons (BLCs), 200, 201

C
Carbonaceous support materials, 182, 203
Carbon black (CB), 176, 200, 201, 218
Carbon molecular sieves (CMS) layer, 104
Carbon nanofibers (CNFs), 219
Carbon nanotubes (CNTs), 146
Carbon support electrocatalysts
carbon blacks, 218
characteristics, 217
CNTs, 218
PEMFCs, 216, 217
Pt dispersion, 218
Carboxylic, 218, 225
Carnot efficiency, 216
Catalyst layers (CL), 216
Catalysts
abiotic FCs, 157
acid media, 136
alkaline media, 136, 137
EGOR, 109–110
EOR, 104–106
FAO, 113–115
methanol-based FCs, 133
MNT, 131
MOR, 99
Pt-based, 142, 146, 151
Pt-based alloys, 134
Raney-type, 158
support, 74
Catalyst support, 74
Cathode material, 92–95, 101, 103, 104, 106, 108, 111, 112, 115, 116, 118, 119
CH_3CH_2OH, 33
Chemical reduction, 180, 183, 184
Chemical vapor deposition (CVD), 178, 179, 195
Chevrel phase, 242, 243
Chitosan (CS), 197
CH_3OH, 32, 33
Climate change, 92
CO
adsorption, 55, 56
and CO_2, 57
concentrations, 60

electrooxidation, 54, 56, 61
H_2SO_4 solutions, 60
hydrogen streams, 54
oxidation, 56
poisoning, 58
Pt/C, 58
PtMo/C, 57
PtRu/C, 58
Pt_3Sn alloys, 57
Pt/WC electrodes, 62
$PtWO_3$/C, 58
room temperature, 59
tolerance, 54
tolerant Pt-based catalysts, 55
Cobalt-base anodes, 283, 284
Core–shell, 275, 281
Core–shell structures
HOR
anodic catalysts, PEMFCs, 60
CO/H_2 electrooxidation, 60, 61
CO-tolerant catalysts, 59
MoO_x@Pt, 60
nanoarchitectures, 59, 61
nitrides, 61
$Pt_{0.8}Mo_{0.2}$, 60
Pt shells, 59
PtSn, 60, 61
Pt/TiWN, 61
RDE measurements, 60
Ru@Pt, 59
shell thickness, 61
ORR, 71, 72
Covalent functionalization
carbon nanofibers, 219
carbon supports, 221
CB, 220
C–C bonds, 220
CNTs, 219
C-O, 220
ECSA, 220
metal/Pt NPs, 219
MWCNTs, 219, 222
nitrogen functionalization, 221, 223, 224
Critical micelle concentration (CMC), 189
Cumulative fluoride loss (CFL), 20
Current-voltage characteristics, 101
Cyclic voltammetry (CV), 267

D
D-band occupancy, 67
Dealloying, 69, 70
Defects, 218, 223, 225
Degradation mechanisms
catalyst support, 74
and durability, 73
electrocatalyst, 73
metal dissolution, 74
metal nanoparticles
agglomeration, 74
detachment, 74
operation of LTFC, 73
Ostwald ripening, 74
Dehydration mechanism, 112
Dehydrogenation mechanism, 112
Density functional theory (DFT), 251
Density of states (DOS), 244
Desorption–re-adsorption–further oxidation mechanism, 108
Diffusion layers (GDL), 216
Direct alcohol fuel cells (DAFCs), 194, 265
Direct borohydride-AEMFCs (DB-AEMFCs), 8
Direct ethanol AEMFCs (DE-AEMFCs), 5, 6, 11
Direct ethanol fuel cell (DEFC), 33
anode chamber, 101
electrons travels, 101
electro-oxidation, 101
energy density, 101
EOR (*see* Ethanol oxidation reaction (EOR))
ethanol crossover, 104
fermentation, agricultural products, 101
performance, 106–108
steam reforming process, Naphtha, 101
Direct ethylene glycol AEMFCs (DEG-AEMFCs), 6, 7
Direct ethylene glycol fuel cell (DEGFC)
EGOR (*see* Ethylene glycol oxidation reaction (EGOR))
energy density, 107
performance, 110–112
shale gas, 108
Direct formate-AEMFCs (DF-AEMFCs), 8
Direct formic acid fuel cell (DFAFC)
catalysts, 113–115
cell configuration, 115, 116
dehydration, 112
dehydrogenation, 112
electro-oxidation, 111–113
fuel crossover, 111
$HCOO^-$ group, 111
OCV, 111
PEMFC, 111
performance, 115, 116

Direct glucose fuel cell (DGFC), 156
Direct glycerol AEMFCs
(DG-AEMFCs), 7, 8, 11
Direct glycerol fuel cell (DGEFC), 117
Direct liquid fuel cells (DLFCs)
MF-DLFC, 133
MR-DLFC, 133
PEM-DLFC, 133
Direct methanol AEMFCs
(DM-AEMFCs), 5, 11
Direct methanol fuel cells (DMFCs), 135, 176, 236, 265, 267
advantages, 94
characterization, 93
commercialization, 94
deployment, 94
feedstock, 94
formation
intermediate products, 93
nanostructures catalysts, 94
methanol crossover, 94, 95
MOR (*see* Methanol oxidation reaction (MOR))
on-board storage constraints, 94
oxidation, 93
PEM, 93
performance, 98, 100, 101
renewable energy sources, 94
Direct oxidation fuel cells
advantages, 92
binary and ternary catalysts, 118
catalysts, 120
commercialization, 118
DEFC (*see* Direct ethanol fuel cell (DEFC))
DEGFC (*see* Direct ethylene glycol fuel cell (DEGFC))
DFAFC (*see* Direct formic acid fuel cell (DFAFC))
DGEFC (*see* Direct glycerol fuel cell (DGEFC))
DMFCs (*see* Direct methanol fuel cells (DMFCs))
EGOR, 119
fuel oxidation mechanism, 118
gravimetric energy densities, 92
HOR, 92
KIST, 119
liquid fuels, 92
low operating temperature, 92
metal oxide framework, 120
Nafion®, 119
nanoporous proton conducting membrane, 119
NDCP Power, 119
OCV, 92
ORR, 92
PEM, 118
PEMFCs, 92
performance, 119
power back-up system, 118
Pt, 92
PtSn/C, 119
PtSnNi/C, 119
μDLFC power density output, 142
Dodecyl-benzene sodium sulfonate (NaDDBS), 227
Doped binary alloys, 68
Dual pathway mechanism, 151

E

Electrocatalysis, 53, 62
Electrochemical active surface area (ECSA), 113, 137, 220
Electrochemical surface area (ESA), 176
Electro-deposited PdNPs, 114
Electrodes
DMFCs, 135
micro-fuel cell devices, 131
Nafion®, 159
Pt and Au, 158
Pt-Cu, 158
Electronic (ligand/promoted) effect, 55
2-Electron pathway, 241
4-Electron pathway, 237, 242, 247, 251
Electro-oxidation
DFAFC, 112, 113
Ethanol, 265, 266
Ethanol oxidation reaction (EOR)
acetaldehyde, 103
acidic electrolyte, 102
AEM, 146
anodic half-cell reaction, 102
C1/C2 pathway, 103
catalysts, 104–106
cathodic half-cell reaction, 102
cobalt-based anodes, 283, 284
ethane, 103
iridium-based anodes, 279, 281
MEA, 146
vs. methanol, 145
μDEFCs
active, 146, 148–150
passive, 147
nickel-based anodes, 278, 279
Ethylene glycol (EG), 220, 266

Ethylene glycol oxidation reaction (EGOR), 154, 155, 284
  catalysts, 109–110
  cathode, 108
  CO_2 formation, 109
  C2 products, 108
  DEGFC, 108
  desorption–re-adsorption–further oxidation mechanism, 108
  electron transfer rate, 108
Evaporation induced self-assembly (EISA), 190, 191
Expandable graphene oxide (EGO), 183
Expandable graphene sheet (EGS), 184

F
Fermi level, 66
Fluorine-free ion exchange membranes, 22
Formic acid oxidation (FAO), 113–115
Formic acid oxidation reaction (FAOR), 151, 153
Formyl-like species $-(CHO)_{ads}$, 32
Fossil fuel based energy source, 92
Fuel cells
  clean energy source, 92
  conventional, 92
  direct oxidation fuel cells (*see* Direct oxidation fuel cells)
Fuel cross over
  ethanol, 104
  methanol, 94, 95
Functionalised MWCNT (f-MWCNT), 106

G
Glucose oxidation reaction (GOR)
  abiotic FCs, 157, 160
  enzymatic FCs, 157
  microbial FCs, 157
  μDGFC, 157, 158
  Nafion®, 159
  PBS, 159
  power density, 161
  Pt and tailored graphene, 158
  Pt-Cu electrodes, 158
Glycerol electro-oxidation reaction (GEOR), 116–118
Glycerol oxidation reaction (GlyOR), 119, 156, 157
Graphene
  2D planar structure, 177
  NPs
    EGS, 184
    electrochemical techniques, 183
    G-P-G catalyst, 183
    hybrid electrocatalysts, 182
    MW, 182
    MWCNT, 185
    Pt, 182, 183
    TP-BNGN, 184
  synthesis techniques
    CVD, 178, 179
    electrochemical reduction, 180
    electrolytic exfoliation, 181
    GO, 180
    green tea, 180
    HOPG, 178
    Hummers method, 179
    Raman spectrum, 179, 181
    scotch tape method, 177
    thermal exfoliation route, 180
    TP, 180
    TRG, 179
    XPS analysis, 180
Graphitic carbon nanostructure (GCN), 202
Gravimetric energy densities, 92
Green carbons
  AC, 203
  biomass
    BC, 197
    cellulose, 197
    CS, 197
    HTC, 196
    human hairs, 199
    lignocellulose, 196
    NCS, 198
    N-doped porous carbon, 198
    oxysalt, 196
    poultry based bio-waste, 198
    sucrose, 196
  BLCs, 200, 201
  carbonaceous, 195
  CS, 199
  Cu–Ru@Pt core-shell NPs, 203
  3D N-doped porous microspherical cavities, 202
  GCN, 202
  HCS, 202
  HPC, 201
  ODC, 200
  Pt/BLC, 200
  Pt/UTCL-C catalyst, 201
Grubb–Niedrach FC, 20

H
Hard carbon spherules (HCS), 202
Hard template
  CKM-3, 187
  3D pore structure, 186
  HMCSs, 188
  HMS, 186
  in-situ self-assembly approach, 188
  MCM, 186
  nanocasting, 186
  SBA, 186
  SBA-15, 187
  SCCs, 188
  silica templates, 187
  TEOS, 187
Heteroatom-doped carbon materials
  biomass, 253
  carbon nanotubes doped, 250
  C-C bonds, 251
  chemical structure, 252
  DFT, 251
  4-electron pathway, 251
  N-C type bond, 251
  N-doped carbons, 251
  Pt/C, 250
  XPS, 250
Heteroatom precursor, *see* Heteroatom-doped carbon materials
Heterocyclic azole molecules, 19
Heyrovsky reaction, 53
Heyrovsky–Volmer pathway, 30
Heyrovsky–Volmer route, 53
Hierarchical porous carbon (HPC), 201
Highly ordered pyrolytic graphite (HOPG), 178
H_2/O_2 AEMFCs, 3–5
Hollow mesoporous aluminosilicate spheres (HMASs), 188
Hollow mesoporous carbon spheres (HMCSs), 188
Hummers method, 179
Hydrocarbon PEMs
  aromatic polymers and copolymers, 23
  characteristics, 23
  chemical durability, 25
  chemical structure, 24
  decomposition, 23
  fluorine-free ion exchange membranes, 22
  mechanical durability, 25
  membranes manufacturing process, 25
  polyarylene polymers, 23
  polystyrenes, 23
  SPK, 24
  SPP semiblock copolymers, 24
  sulfonated polymers, 22, 23
  synthetic routes, 23
  types, 24
Hydrogen binding energy (HBE) *vs.* HOR, 53, 54
Hydrogen oxidation reaction (HOR), 216
  in acidic media
    core-shell architectures (*see* Core-shell structures)
    Pt (*see* Pt)
  anodic reaction, 52
  behavior, 31
  bifunctional effect, 54
  CO, 54
  CO_{ads}, 9
  core-shell architectures, 54
  dissociation/ionization, 53
  electrochemical, 52
  electrode material nature, 53
  electronic (ligand/promoted) effect, 55
  H_2, 52
  vs. HBE, 53, 54
  kinetics, 54
  LH mechanism, 54
  mechanism, 53
  molecular hydrogen diffusion, 53
  morphological and structural effects, 55
  non-PGM catalysts, 4
  and ORR, 3
  oxygenated species and cations, 54
  platinum electrode, 30
  product desorption, 53
  RDE measurements, 30
  RDS, 54
  surface metallic arrangement, 53
Hydrothermal carbonization (HTC), 196
Hydroxyl (–OH), 219
HYPERMEC (Fe–Co–Ni/C), 285

I
Implanted μDGFCs, 159
In-situ FTIR analysis, 5
Ion exchange capacity (IEC), 25
Iridium-based anodes, 281
  Ir/C catalyst, 279
  Ir_3Sn/C catalyst, 280, 281
  surface cluster models, 282

J
Julius Tafel model, 237

K
Kinetics
  cathode side, PEMFC, 62
  electrode, 53
  HOR, 54, 60
  ORR, 62, 73
Koutecky–Levich equation, 34
Koutecky–Levich method, 238, 239
Koutecky–Levich plots, 34, 35

L
Langmuir–Hinshelwood (LH) mechanism, 54
Levich law, 34
Low-temperature fuel cells (LTFCs), 176, 177, 182, 185, 195, 196, 203
  AEMFCs (*see* Anion exchange membrane fuel cells (AEMFCs))
  high-power density, 2
  PEMFCs (*see* Proton exchange membrane fuel cells (PEMFCs))

M
Membrane-electrode-assemblies (MEAs), 11, 15, 19, 22, 29, 37, 146, 216
Membraneless, 131, 151, 154, 156, 159, 161
Membraneless microfluidic direct liquid fuel cell (MF-DLFC), 133
Membranes, 141, 146, 151, 158, 161
Mesoporous carbon nitrides (MCN), 106
Mesoscale models, 15
Metal alloys
  Pt-early transition, 70, 71
  Pt-lanthanide alloys, 70, 71
  Pt-late transition
    bimetallic nanoparticles, 68
    dealloying, 69, 70
    3-d metal series, 68
    doped binary alloys, 68
    monometallic nanoparticles, 68
    non-noble metals, 68
    ORR electrocatalytic activity, 68
    platinum-skin, 68–70
    Pt:Ni ratio values, 68
    ternary/quaternary alloys, 68
    volcano plots, 68
Metal carbides, 62
Metal dispersion, 218
Metal-free electrocatalysts, 251–254
Metal oxides in Pt, 58, 59
Methanol, 265
Methanol oxidation reaction (MOR), 5, 176, 182
  catalysts
    acid media, 136
    alkaline media, 136, 137
    binary, 97
    Cu, 97
    CV experiments, 99
    density functional theory, 97
    high-throughput screening method, 97, 98
    metal oxides, 98
    Pd, 96
    $Pd_{73}Pt_{27}$, 96
    Pt, 96
    PtCoW/C, 98
    Pt–M, 96
    Ru, 96
    Sn, 96
    ternary, 97, 98
    Ti, 97
  dissociation, 95
  electrosorption, 95
  formation, 95
  mesoporous zeolite, 275
  μDMFC, 141
    active, 143–145
    control unit, 142, 145
    $CoSe_2$/C, 141
    passive, 138, 139
    Pt/C, 141
    Pt-Ru and Pt catalysts, 141, 142
    spray-coating technique, 142
    SU-8 photoresist, 142
  Ni-based materials (*see* Nickel-base anodes)
  sluggish kinetics, 95
  SnO_2/m-ZSM-5, 276
  SnO_x, 274
  TMCs, 277
  water adsorption and activation, 95
Micro and nano technologies (MNT), 131
Micro-direct ethanol fuel cells (μDEFCs)
  active, 146, 148–150
  passive, 147
  Pd-based anode catalysts, 146
Micro-direct ethylene glycol fuel cells (μDEGFCs), 154
Micro-direct glycerol fuel cells (μDGlyFC), 156
Micro-direct liquid fuel cells (μDLFC)

Micro-direct liquid fuel cells (μDLFC) (*cont.*)
electro-catalysts, 131
MNT, 131
PDMS, 132
principle, 131
Micro-direct methanol fuel cells (μDMFC), 141
active, 143–145
control unit, 142, 145
$CoSe_2$/C, 141
passive, 138, 139
Pt/C, 141
Pt-Ru and Pt catalysts, 141, 142
spray-coating technique, 142
SU-8 photoresist, 142
Microwave (MW), 182
Mixed-reactant fuel cell (MR-FC), 134
Mixed-reactant membraneless direct liquid fuel cell (MR-DLFC), 133
Molecular dynamics (MD) simulations, 15
Multiwall carbon nanotube (MWCNT), 106, 114, 115

N

Nafion® membranes, 2, 6, 11, 15–18, 21, 25, 38
Nanoparticles
bimetallic, 68
core–shell, 60, 71
definition, 71
dispersion, 182, 183, 192, 195, 200, 202
hollow, 71
intermetallic, 60
metal, 74
monometallic platinum, 68
ORR, 67
Pt (*see* Pt)
PtNi octahedral, 68
Pt/TiWN, 61
spherical, 67
Nanoporous proton conducting membrane (NP-PCM), 110, 111
Naphtha, 101
N-doped carbon nanofiber (CNF), 223
N-doped graphene nanosheets (NDGN), 223
N-doped highly oriented pyrolytic graphite (HOPG), 224
N-doped nanoporous carbon nanosheets (NCS), 198
Nickel-base anodes
CV, 267, 269
cyclic voltammogram, 270
electrodeposition, 269
EOR, 278, 279
methanol concentration, 270
method of synthesis, 274
MOR
Arrhenius relationship, 271
bimetallic catalyst, 272
CVs, 273
Ni^{2+}/Ni^{3+} redox reaction, 272
NiO phase, 272
NiO_x and MnO_x, 273
NiTi, 270, 271
NiTiO NTS, 272
NiOOH, 269
oxy/hydroxide species, 268
planar nickel electrodes, 267
Silicate Zeolite structure, 267, 268
Nitrogen doped carbons (NDC), 224, 250
Nitrogen doped graphene (NDG), 224
Nitrogen functionalization
catalyst–support system, 221
C–N containing materials, 223
CNF, 223
HOPG, 224
NDC, 224
NDG, 224
NDGN, 223
pyridinic N, 223
Nitrogen precursor, *see* Nitrogen-doped carbon
Non-covalent functionalization
carbon support, 225, 226, 229
CNTs, 225, 226
MWCNT, 227, 228
NaDDBS, 227
polymer based, 228, 230
SDS, 227
surface defects, 225
SWCNTs, 228
Non-fluorinated polystyrene sulfonic acid (PSSA) membranes, 20
Non-noble catalysts, 266
Non-noble metal catalysts, 3
Non-noble metal electrocatalysts
TMC, 242, 243
TMM (*see* Transition metals macrocycles (TMM))
Non-platinum electrocatalysts
materials, 72
Pd, 72, 73
Non-platinum group metal (PGM), 3, 4, 9, 14

O

Okara-derived carbon (ODC), 199
Open circuit voltage (OCV), 92, 111

Ordered mesoporous carbons (OMCs)
and CB support materials, 193
DAFCs, 194
EISA, 193
MCM-48, 185
MEA, 194
MWCNT, 195
PEMFC, 194
Pt-BOMC, 195
Pt/CB, 193
Pt/MC, 193
Pt-M NPs, 195
Pt-OMC-SAM-800/3, 193
surface functionalization, 192, 193
synthesis
hard-templating, 186–188
soft template, 189–191
Ordered mesoporous carbon sphere (OMCS), 193
Ostwald ripening, 74
Oxygen reduction reaction (ORR), 3, 92, 102, 116, 134, 135, 176
acid media (*see* Acid media)
in alkaline media, 9, 62, 63 (*see also* Alkaline media)
associative mechanism, 64
cathode, 30, 63
chemical adsorption of oxygen, 63
degradation, 73–74
dissociative pathway, 63
DoE, 62
drawbacks, 62
electrolytes, 237
electron and proton transfer, 63
electron transfer, 63, 237
fuel cells, 62
$HOOH_{ads}$, 64
and HOR, 3
Koutecky–Levich slope, 238
mass transport, 237
non-PGM catalysts, 4
non-platinum electrocatalysts, 72, 73
O–O cleavage, 63
OOH_{ads}, 64
pathways, 236
PEMFCs
acid medium, 33
hydrodynamic voltammograms, 34, 36
Koutecky–Levich equation, 34
Koutecky–Levich plots, 34, 35
Levich law, 34
molecular oxygen in water, 34
multi-electron transfer process, 34
polarization curves, 34, 35
RDE, 34, 35
RRDE, 34, 36
peroxo intermediate, 64
proton transfer, 63
Pt (*see* Pt)
Pt-based catalysts, 236
RDE, 238
RRDE, 238, 239
Sabatier principle, 64
scaling relationships, 64, 65
thermodynamic potential, 237
volcano plot, 65

P
Palladium (Pd), 71–73
Palladium (Pd)-alloy catalysts, 72, 73
Partially fluorinated PEMs
BAM3G membranes, 20
Grubb–Niedrach FC, 20
membrane lifetime, 20
non-fluorinated PSSA membranes, 20
PFCB, 21, 22
PFEP-TFE-g-SSA membranes, 21
polymer blending, 21
radiation-induced grafting, 21
SPFCB/PVDF blend membranes, 22
SSA, 21
Passive μDEFCs, 147
Passive μDMFC, 138, 139
Perfluorinated PEMs
advantages, 17
complex viscosity, 19
extrusion by melt-casting, 18
extrusion process, 19
lower EW PFSAs, 16
manufacturing process, 17
MD simulations, 15
MEAs, 15
melt processes, 17–19
mesoscale models, 15
Nafion®, 15, 16, 19
PFSA ionomers, 16–18
phase separation, 15
SSC ionomers, 16
SSC-PFSA ionomers, 16
TFE repeat units, 16
volume change, 19, 20
water transport, 15
Perfluorosulfonic-acid membranes (PFSA)
BPVE, 21
cost, 17

Perfluorosulfonic-acid membranes (PFSA) (*cont.*)
development, 15
electrolytes, 14
EW, 16
ionomers, 16–19
LSC, 18
Nafion®, 15
PEMs, 25
semi-crystallinity, 16
SSC, 19
Perovskite-type oxides
ABO_3, 245
$AMnO_3$, 247
electrocatalytic measurements, 248
Goldschmidt tolerance factor, 246
hexagonal perovskite, 246
oxygen stoichiometry, 247
structure, 246
PFEP-TFE-$_g$-SSA membranes, 21
Pluri-metallic, 266
Polaron theory, 237
Poly(arylene ethers), 26
Poly(arylene perfluorocyclobutane) (PFCB), 21, 22
Polydimethylsiloxane (PDMS), 132
Polyelectrolytes, 228, 230
Polymer blending, 21, 29
Polymer electrolyte membrane fuel cells (PEMFCs), 2
Polystyrenes, 23
Porous Pt electrodes, 158
Portable devices, 130
Power density, 94, 96, 100, 104, 106, 107, 110, 111, 114–116, 119
Proton exchange membrane direct liquid fuel cell (PEM-DLFC), 133
Proton exchange membrane fuel cells (PEMFCs), 176, 236
advantages, 14
alkaline media, 14
at the anode
CH_3CH_2OH, 33
CH_3OH, 32, 33
compounds, 29
H_2, 30, 31
automotive applications, 216
catalytic layer-electrolyte, 29
at the cathode
ORR, 33–36
cell voltage, 29
challenges, 14
commercialization, 54
domains, 29
electric efficiency, 29
electrode materials, 37, 38
electrodes, 264
elements, 264
high-power densities, 14
hydrogen, 265
MEA, 29
NPs, 217
ORR kinetics, 14
perfluorosulfonic acid membranes, 2
PFSA, 14
PGM, 14
Pt-based anode and cathode, 217
types of carbon, 29
and water, 14
Proton exchange membranes (PEMs)
applications, 14
direct oxidation fuel cells (*see* Direct oxidation fuel cells)
electrolytes transport different ions, 14
fuel cell (*see* Proton exchange membrane fuel cells (PEMFCs))
hydrocarbon, 22–25
partially fluorinated, 20–22
perfluorinated, 15–20
sulfonic acid (SO3-), 15
Pseudobinary compounds, 242
Pt
HOR
alloys, 56–58
bifunctional mechanism, 55
disadvantages, 55
electrocatalysts, 56
ligand effects, 55
at low pH values, 55
metal oxide, 58, 59
nitrides, 62
structure, 55
transition metal carbides, 62
0.0 V *vs.* RHE, 55
ORR
advantages, 67
core-shell structures, 71, 72
d-band occupancy, 67
early transition metal alloys, 70, 71
Fermi level, 66
lanthanide alloys, 70, 71
late transition metal alloys, 68–70
morphological effects, electrocatalysts, 66, 67
pure electronic effect, 67
Pt-based alloys

bimetallic, 56, 57
CO-poisoning, 56
FEFF8 code calculations, 57
PtMo, 57
PtRu, 56
PtSn, 56, 57
quaternary, 58
ternary, 57, 58
XAS measurements, 57
Pt electrocatalysts, 193, 201
Pt on nitrogen-doped carbon nanocapsules (Pt/NCNC), 223
Pt-Sn electrode oxidizes CO, 31

Q
Quaternary ammonia poly (2, 6-dimethyl-1, 4-phenylene oxide) (QAPPO), 228
Quaternary ammonium (QA) functional groups, 25–27

R
Rate-determining step (RDS), 54
Renewable energy, 94, 107, 118
Renewable hydrogen, 9
Reversible hydrogen electrode (RHE), 55, 252
Rotating disk electrode (RDE), 30, 34, 35, 57, 193, 238
Rotating ring disk electrode (RRDE), 34, 238

S
Sabatier principle, 64
Scaling relationships, 64, 65
Scotch tape method, 178
Shale gas, 108
Short side chain (SSC) ionomers, 16
Silica colloidal crystals (SCCs), 188
Sodium dodecyl sulfate (SDS), 227
Soft template
carbon precursor and surfactants, 189
CMC, 189
EISA, 190, 191
Pluronic F127, 191
pore size, 191
Solid alkaline fuel cells, 285
SPEEK membrane, 104
SPFCB/PVDF blend membranes, 22
Spinel-type oxides, 248–250
Spray-coating technique, 142
Stability
in acidic media, 68
anodic PEM, 57
binary systems, 57
CO-tolerance, 59
cycles test, 71
degradation, 73–74
Pt-Mo/C, 57
PtRu/C, 56
PtSn alloy, 60
Styrene sulfonic acid (SSA), 21
SU-8 photoresist technology, 142
Sulfonated benzophenone poly(arylene ether ketone) (SPK), 24
Sulfonated phenylene poly(arylene ether ketone) (SPP) semiblock copolymers, 24
Sulfonated polymers, 22, 23
Surface functionalization, 192, 193
Surface modification, 219
Surfactants, 225–228
Synthesis techniques, 274
CVD, 178, 179
electrochemical reduction, 180
GO, 180
HOPG, 178
Hummers method, 179
Raman spectrum, 179, 181
scotch tape method, 177
thermal exfoliation route, 180
TP, 180
TRG, 179
XPS analysis, 180

T
Tafel reaction, 53
Tafel slopes, 34
Tafel–Volmer pathway, 30
Tafel–Volmer sequence, 53
Ternary electro-catalyst, 118
Tetraethylorthosilicate (TEOS), 187
Thermally reduced graphene (TRG), 179
Transition metal carbides (TMeC), 244, 245
Transition metal chalcogenides (TMC)
Chevrel phase, 242, 243
Me_6X_8 and $MoM^2{}_xX_8$ pseudobinary, 242
VASP, 243
Transition metal nitrides (TMeN), 244, 245
Transition metals macrocycles (TMM)
2 and 4 electrons pathway, 240

Transition metals macrocycles (TMM) (*cont.*)
N_4 chelate complexes, 241
ORR activity, 242
Pc and PP ligands, 240
Triple phase boundary (TPB), 113
Tungsten mono-carbide (WC), 277

U
Underpotential deposition (UPD), 71
US Department of Energy (DoE), 62

V
Vienna ab initio simulation package (VASP), 243
Vinylbenzyl chloride (VBC) radiation, 27
Volcano-shaped curves, 53
Volmer reaction, 53

X
X-ray photoelectron spectroscopy (XPS), 250